ΠΑΝΕΠΙΣΤΗΜΙΟ ΚΡΗΤΗΣ
ΣΧΟΛΗ ΕΠΙΣΤΗΜΩΝ ΥΓΕΙΑΣ-
ΤΜΗΜΑ ΙΑΤΡΙΚΗΣ
ΤΟΜΕΑΣ ΒΑΣΙΚΩΝ ΕΠΙΣΤΗΜΩΝ
ΕΡΓΑΣΤΗΡΙΟ ΒΙΟΧΗΜΕΙΑΣ

Διδακτορική διατριβή

Πρωτεΐνες που ρυθμίζουν τα επίπεδα και τις λειτουργίες της HDL: Νέες προοπικές για τη θεραπεία της καρδιαγγειακής νόσου

Παναγιώτης Φωτάκης

Επιβλέπων Καθηγητής: Δ. Καρδάσης

Φλεβάρης, 2014

Ευρωπαϊκή Ένωση
Ευρωπαϊκό Κοινωνικό Ταμείο
ΕΠΙΧΕΙΡΗΣΙΑΚΟ ΠΡΟΓΡΑΜΜΑ
ΕΚΠΑΙΔΕΥΣΗ ΚΑΙ ΔΙΑ ΒΙΟΥ ΜΑΘΗΣΗ
επένδυση στην κοινωνία της γνώσης
ΥΠΟΥΡΓΕΙΟ ΠΑΙΔΕΙΑΣ & ΘΡΗΣΚΕΥΜΑΤΩΝ, ΠΟΛΙΤΙΣΜΟΥ & ΑΘΛΗΤΙΣΜΟΥ
ΕΙΔΙΚΗ ΥΠΗΡΕΣΙΑ ΔΙΑΧΕΙΡΙΣΗΣ
ΕΣΠΑ 2007-2013
πρόγραμμα για την ανάπτυξη
ΕΥΡΩΠΑΪΚΟ ΚΟΙΝΩΝΙΚΟ ΤΑΜΕΙΟ
Με τη συγχρηματοδότηση της Ελλάδας και της Ευρωπαϊκής Ένωσης

UNIVERSITY OF CRETE

SCHOOL HEALTH SCIENCES-DEPARTMENT OF MEDICINE

BASIC SCIENCES-BIOCHEMISTRY

Ph.D. thesis

Proteins that regulate the levels and functions of HDL: New perspectives for the treatment of cardiovascular disease

Panagiotis Fotakis

Supervisor: Prof. D. Kardassis

Submitted in fulfilment of the requirements for the PhD degree in the graduate program

"Molecular basis of human disease"

February, 2014

European Union
European Social Fund

OPERATIONAL PROGRAMME
EDUCATION AND LIFELONG LEARNING
investing in knowledge society
MINISTRY OF EDUCATION & RELIGIOUS AFFAIRS, CULTURE & SPORTS
MANAGING AUTHORITY

NSRF 2007-2013
programme for development
EUROPEAN SOCIAL FUND

Co-financed by Greece and the European Union

ACKNOWLEDGMENTS

As I complete my PhD thesis I would like to thank Professor Vassilis I. Zannis for all his mentorship and support during the last 6 years. He taught me valuable lessons both about Science and Life.

I am also grateful to Professor Dimitris Kardassis, who gave me the opportunity to start my PhD in his lab and helped me throughout my studies in the graduate program "The Molecular Basis of Human Disease" and also for the financial support. I would also like to thank the members of my committee Dr. Papakonstanti, Dr. Eliopoulos, Dr. Thermos, Dr. Tsatsanis and Dr. Kokkinidis.

Many thanks to all the members of Dr. Zannis' lab, especially to Andreas Kateifides who trained me well when I first moved into Boston, as well as Adelina Duka and Gayle Forbes. I would also like to thank the members of Dr. Kardassis; lab, Veta Papakosta, Ioanna Tinikaou, Efi Thymiakou, Eleftheria Vasilaki, Sofia Mavridou and Ioanna Mosialou.

My thanks also go to Angelika Chroni and Efstratios Stratikos. Their contribution made it possible for this work to become more complete and provided meaningful contributions to my studies.

Finally, I would like to erxpress my deepest graditute to my parent, Georgios and Maria, for their continuous support and to Maria Chronopoulou, who made me realize that nothing in Life make sense except in the light of Love.

Η παρούσα έρευνα έχει συγχρηματοδοτηθεί από την Ευρωπαϊκή Ένωση (Ευρωπαϊκό Κοινωνικό Ταμείο - ΕΚΤ) και από εθνικούς πόρους μέσω του Επιχειρησιακού Προγράμματος «Εκπαίδευση και Δια Βίου Μάθηση» του Εθνικού Στρατηγικού Πλαισίου Αναφοράς (ΕΣΠΑ) – Ερευνητικό Χρηματοδοτούμενο Έργο: Ηράκλειτος ΙΙ. Επένδυση στην κοινωνία της γνώσης μέσω του Ευρωπαϊκού Κοινωνικού Ταμείου».

This research has been co-financed by the European Union (European Social Fund – ESF) and Greek national funds through the Operational Program "Education and Lifelong Learning" of the National Strategic Reference Framework (NSRF) - Research Funding Program: Heracleitus II. Investing in knowledge society through the European Social Fund»

CONTENTS

ABSTRACT

Many studies have shown that HDL has a plethora of functions that may contribute to the protection from cardiovascular disease. The pathway of the biogenesis and catabolism of HDL is a complex process and involves several membrane bound and plasma proteins. Using adenoviruses mediated gene transfer in various mouse models, the studies described in this thesis explore the pathway of the biogenesis of HDL and more specifically the following:

1. The importance of the hydrophobic residues in the 218-230 region of apoA-I in the biogenesis of HDL.
2. The effects of LCAT mutations on the biogenesis of HDL.
3. The effects of CTα on the biogenesis of HDL.
4. The contribution of dominant mutations in apoE to lipid homeostasis and the biogenesis of HDL.
5. The synergy of apoA-IV and LCAT on the biogenesis of apoA-IV containing HDL.
6. The effect of reconsituted HDL containing apoE and apoA-I on endothelial gene expression.

The importance of the hydrophobic residues in the 218-230 region of apoA-I in the biogenesis of HDL

We have investigated the significance of hydrophobic residues 218-230 on the structure and functions of apoA-I and their contribution to the biogenesis of HDL. We introduced three sets of point mutations in the 218-230 region of apoA-I substituting hydrophobic residues with

Alanies. Adenovirus-mediated gene transfer of apoA-I[L218A/L219A/V221A/L222A] in apoA-I$^{-/-}$ mice decreased plasma cholesterol and apoA-I levels to 15% of WT control, and generated preβ and α4 HDL particles. In apoA-I$^{-/-}$ x apoE$^{-/-}$ mice the same mutant formed few discoidal and preβ HDL particles that could not be converted to mature α-HDL particles by excess Lecithin cholesterol acyltransferase (LCAT). Adenovirus-mediated gene transfer of the apoA-I[F225A/V227A/F229A/L230A] mutant in apoA-I$^{-/-}$ mice decreased plasma cholesterol, HDL cholesterol and apoA-I levels. When expressed in apoA-I$^{-/-}$ x apoE$^{-/-}$ mice, approximately 40% of the mutant apoA-I as well as mouse apoA-IV and apoB-48 appear in the VLDL/IDL/LDL. In both mouse models the apoA-I mutant generated small spherical particles of preβ and α4 HDL mobility. Co-expression of the apoA-I mutant and human LCAT increased and shifted the HDL cholesterol peak towards lower densities, created normal α-HDL subpopulations and generated spherical HDL particles. The apoA-I[218-222] and apoA-I[225-230] mutants had 20% and 31% respectively to promote ABCA1-mediated cholesterol efflux as compared to WT apoA-I. Both mutants had ~65% of normal capacity to activate LCAT *in vitro*. Biophysical analyses suggested that both mutants affected the structural integrity and plasticity of apoA-I that is necessary for normal functions. Adenovirus mediated gene transfer of apoA-I[L218A/L219A/V221A/L222A/F225A/V227A/F229A/L230A] in apoA-I$^{-/-}$ had a similar phenotype to apoA-I[L218A/L219A/V221A/L222A] that could not be corrected by excess LCAT. We conclude that the alteration of the hydrophobic 218-222 residues of apoA-I disrupts apoA-I/ABCA1 interactions and promotes the generation of defective preβ particles that fail to mature into α-HDL subpopulations, thus resulting in low plasma apoA-I and HDL. Alterations of the hydrophobic residues 225-230 also inhibited the biogenesis of HDL and led to the

accumulation of immature preβ and α4 HDL particles, a phenotype that could be corrected by administration of LCAT.

The effects of LCAT mutations and CTα on the biogenesis of HDL

We have investigated the effect of overexpression of CTP:phosphocholine cytidylyltransferase (CTα) as well as LCAT mutants on the biogenesis of HDL in different mouse models. Adenovirus-mediated gene transfer of human apoA-I along with CTα in apoA-$I^{-/-}$ mice increased plasma cholesterol and phospholipid levels, mainly due to an increase in the HDL fraction, increased the large size HDL subpopulations and formed spherical HDL particles. Gene transfer of WT LCAT in $LCAT^{-/-}$ mice greatly increased total plasma cholesterol levels mainly due to increase in HDL cholesterol. In contrast gene transfer of human LCAT carrying the natural mutations LCAT[T123I] and LCAT[P250S] affected moderately plasma cholesterol levels. Fractionation of plasma by density gradient ultracentrifugation showed that WT LCAT increased the plasma apoE and apoA-IV levels and shifted the distribution of apoA-I to lower densities. The LCAT[T123I] and LCAT[P250S] mutants restored partially the presence of apoA-I in the HDL2/HDL3 fraction and in the case of the LCAT[T123I] mutant increased apoE in the VLD/IDL/LDL fractions. The LCAT[T123I] caused a biphasic and LCAT[P250S] a monophasic distribution of the HDL cholesterol. Deficiency in LCAT is associated with formation of two preβ HDL subpopulations and small size α-HDL particles. Gene transfer of the LCAT[T123I] and LCAT[P250S] mutants in $LCAT^{-/-}$ mice generated preβ and α-HDL subpopulations with similar size whereas treatment with WT LCAT generated α-HDL subpopulations. Co-expression of the the apoA-I[L159R]Fin or the apoA-I[225-230] with LCAT restored the defective HDL phenotype

casued by the mutant apoA-I forms. In contrast, co-expression of LCAT[T123I] and LCAT[P250S] with either of the apoA-I[L159R]Fin or the apoA-I[225-230] only moderately restored the HDL phenotype. We conclude that overexpression of CTα and LCAT promotes the biogenesis of HDL and the mutations in LCAT affect differently the biogenesis of HDL.

The contribution of dominant mutations in apoE to lipid homeostasis and the biogenesis of HDL

The K146N/R147W substitutions in human apoE3 were first described in patients with a dominant form of type III hyperlipoproteinemia. The effects of these mutations on the *in vivo* functions of apoE were studied by adenovirus mediated gene transfer of the full length and a truncated apoE3[K146N/R147W]-202 mutant using different mouse models. A low dose of adenovirus expressing the apoE3[K146N/R147W] mutant in apoE$^{-/-}$ or apoA-I$^{-/-}$ x apoE$^{-/-}$ mice exacerbated the hypercholesterolemia and increased greatly plasma apoE and triglycerides levels. In apoE$^{-/-}$ mice the apoE3[K146N/R147W] mutant displaced apoA-I from the VLDL/LDL/ HDL region and resulted in the accumulation of discoidal apoE containing HDL particles in plasma. Similar doses of WT apoE3 cleared the cholesterol of apoE$^{-/-}$ mice without induction of hypertriglyceridemia and promoted formation of spherical HDL particles. A unique feature of the truncated apoE3[K146N/R147W]-202 mutant is that it prevented the induction of hypertriglyceridemia but did not correct the hypercholesterolemia. Other apoE-202 truncated mutants tested previously did not induce hypertriglyceridemia but corrected hypercholesterolemia. Treatment of apoE$^{-/-}$ mice with apoE3[K146N/R147W] and lipoprotein lipase corrected the hypertriglyceridemia but did not prevent the formation of discoidal HDL.

Treatment with LCAT also corrected hypertriglyceridemia normalized the CE/TC ratio of plasma and generated spherical HDL. The combined data indicate that the K146N/R147W substitutions in the full length and the truncated apoE3[K146N/R147W] mutant prevent receptor-mediated remnant clearance. The accumulation in plasma of lipoprotein remnants that contain the full length apoE3[K146N/R147W] mutant suggests that this mutant acts as a dominant negative ligand that exacerbates the dyslipidemia and also affects the activity of LCAT thus inhibiting the biogenesis of HDL.

The synergy of apoA-IV and LCAT on the biogenesis of apoA-IV containing HDL

We studied the contribution of LCAT on the biogenesis of apoA-IV containing HDL. Adenovirus-mediated gene transfer of apoA-IV in $LCAT^{-/-}$ failed to show the formation of spherical and α-migrating HDL particles. Adenovirus-mediated gene transfer of apoA-IV in $apoA\text{-}I^{-/-}$ mice did not change plasma lipid levels. ApoA-IV floated predominantly in the HDL3 region. Co-expression of apoA-IV and LCAT in $apoA\text{-}I^{-/-}$ mice restored the formation of HDL-A-IV. The findings are consistent with a novel function of apoA-IV in the biogenesis of discrete HDL-A-IV particles with the participation of LCAT, and may explain previously reported anti-inflammatory and atheroprotective properties of apoA-IV.

The effect of reconsituted HDL containing apoE and apoA-I on endothelial gene expression

We performed reliminary microarray experimetns in human aortic endothelial cells (HAECs) following treatment of reconstituted HDL containing apoA-I (using phospholipids and

cholesterol, designated as rHDLAI+, or phospholipids alone, designated as rHDLAI-) or apoE (rHDLE+ and rHDL-). The bioinformatics analyses showed that the rHDLAI- and rHDLAI+ treatments caused the differential expression (over 2-fold change and≤ 0.05 FDR) in 137 and 190 genes respectively. The differentially expressed genes in response to rHDLE3- and rHDLE3+ were 198 and 272 respectively. The microarrays data were validated with high throughput qRT-PCR based screening using the dynamic array chips. Pathways of highly interconnected genes were tentatively identified based the Ingenuity Pathway Analysis (IPA) program and pubmed literature searches.

ΠΕΡΙΛΗΨΗ

Πολυάριθμες επιδημιολογικές και γενετικές μελέτες καθώς και μελέτες σε μοντέλα ζώων έχουν δείξει ότι HDL έχει έναν μεγάλο αριθμό λειτουργιών που μπορεί να συμβάλουν στην προστασία από την καρδιαγγειακή νόσο. Ο μεταβολισμός της HDL είναι μια σύνθετη διαδικασία και περιλαμβάνει τη δράση πρωτεϊνών της κυτταρική μεμβράνης καθώς και πρωτεϊνών του πλάσματος. Στη διατριβή αυτή περιγράφονται πειράματα που διερευνούν το μονοπάτι του σχηματισμού της HDL χρησιμοποιώντας γονιδιακή μεταφορά μέσω αδενοϊών σε διάφορα ζωικά μοντέλα ποντικο. Πιό συγκεκριμένα μελετήσαμε τα εξής:

1. Τη σημασία των υδρόφοβων αμινοξέων στην περιοχή 218-230 της apoA-I στο σχηματισμό της HDL.
2. Την επίδραση μεταλλάξεων στην LCAT στο σχηματισμό της HDL.
3. Την επίδραση του ενζύμου CTα στο σχηματισμό της HDL.
4. Η συμβολή των επικρατουσών μεταλλάξεων της apoE στην ομοιόσταση των λιπιδίων και στο σχηματισμό της HDL.
5. Η σύμπραξη της apoA-IV και της LCAT στο σχηματισμό της HDL που περιέχει apoA-IV.
6. Η επίδραση της HDL που περιέχει apoE ή apoA-I στην έκφραση γονιδίων των ενδοθηλιακών κυττάρων.

Η σημασία των υδρόφοβων αμινοξέων στην περιοχή 218-230 της apoA-I στο σχηματισμό της HDL

Μελετήσαμε τη σημασία των υδρόφοβων αμινοξέων στο καρβοξυτελικό άκρο της apoA-I στη δομή και τις λειτουργίες της καθώς και τη συμβολή τους στο σχηματισμό της HDL. Συγκεκριμένα, εισαγάγαμε τρία σετ σημειακών μεταλλάξεων στην περιοχή 218-230 της apoA-I, αντικαθιστώντας τα υδρόφοβα αμινοξέα με Αλανίνες. Γονιδιακή μεταφορά μέσω αδενοϊών της μεταλλαγμένης μορφής apoA-I[L218A/L219A/V221A/L222A] σε apoA-$I^{-/-}$ ποντίκια μείωσε τη χοληστερόλη του πλάσματος και τα επίπεδα της apoA-I στο 15% σε σχέση με την αγρίου τύπου apoA-I και οδήγησε στι σχηματισμό preβ και α4 HDL. Στα apoA-$I^{-/-}$ x $apoE^{-/-}$ ποντίκια η ίδια μετάλλαξη οδήγησε στο σχηματισμό δισκοειδών σωματιδίων HDL και preβ HDL που δεν μπορούν να μετατραπούν σε ώριμους α-HDL υποπληθυσμούς με υπερέκφραση της LCAT. Γονιδιακή μεταφορά μέσω αδενοϊών της μεταλλαγμένης μορφής apoA-I[F225A/V227A/F229A/L230A] σε apoA-$I^{-/-}$ ποντίκια μείωσε τη χοληστερόλη του πλάσματος, τη χοληστερόλη της HDL και τα επίπεδα της apoA-I. Όταν αυτη η μεταλλαγμένη μορφής της apoA-I εκφράστηκε σε apoA-$I^{-/-}$ x $apoE^{-/-}$ ποντίκια, περίπου το 40% της μεταλλαγμένης apoA-I καθώς επίσης η ποντικίσια apoA-IV και apoB-48 εντοπίστηκε στα κλάσματα των VLDL/IDL/LDL. Και στα δύο μοντέλα ποντικιών, η apoA-I[F225A/V227A/F229A/L230A] οδήγησε στο σχηματισμό μικρών σφαιρικών preβ και α4-HDL σωματιδίων. Συνέκφραση της apoA-I[F225A/V227A/F229A/L230A] και της LCAT αύξησε και μετατόπισε την καμπύλη της χοληστερόλη της HDL προς τα κλάσματα χαμηλότερης πυκνότητας, και οδήγησε στο σχηματισμό των φυσιολογικών υποπληθυσμών της HDL. Οι μεταλλάξεις apoA-I[218-222] και apoA-I[225-230] είχαν το 20% και 31% αντίστοιχα της ικανότητας της αγρίου τύπου apoA-I να

προάγουν την εκροή χοληστερόλη μέσω της ABCA1. Επίσης και οι δύο μεταλλάξεις είχαν το ~65% της ικανότητας της αγρίου τύπου apoA-I να ενεργοποιήσουν την LCAT in vitro. Οι βιοφυσικές αναλύσεις έδειξαν ότι και οι δύο μεταλλάξεις είχαν επιπτώσεις στη δομή και την πλαστικότητα της apoA-I που είναι απαραίτητη για τις κανονικές της λειτουργίες. Γονιδιακή μεταφορά μέσω αδενοϊών της μεταλλαγμένης μορφής apoA-I[L218A/L219A/V221A/L222A/F225A/V227A/F229A/L230A] σε apoA-I$^{-/-}$ ποντίκια δημιούργησε παρόμοιο φαινότυπο με την apoA-I[L218A/L219A/V221A/L222A] ο οποίος δεν μπορούσε να διορθωθεί με την υπερέκφραση της LCAT. Συμπερασματικά, η αλλαγή των υδρόφοβων αμινοξέων στη περιοχή 218-222 της apoA-I διαταράσσει την αλληλεπίδραση μεταξύ της apoA-I και της ABCA1 και οδηγεί στο σχηματισμό ελαττωματικών preβ υποπληθυσμών που αποτυγχάνουν να ωριμάσουν σε ώριμη α-HDL με αποτέλεσμα τα χαμηλά επίπεδα της apoA-I και της HDL στο πλάσμα. Οι μεταλλάξεις των υδρόφοβων αμινοξέων στην περιοχή 225-230 της apoA-I επίσης εμπόδισαν τη βιογένεση της HDL και οδήγησαν στη συσσώρευση ανώριμων preβ και α4-HDL υποπληθυσμών μόρια, ένας φαινότυπος που μπορεί να διορθωθεί με την υπερέκφραση της LCAT.

Η επίδραση των μεταλλαγών της LCAT και της υπερέκφρασης της CTα στη βιογένση της HDL

Μελετήσαμε την επίδραση της υπερέκφρασης του ενζύμου cytidylyltransferase CTP:phosphocholine (CTα) καθώς επίσης και μεταλλάξεων της LCAT στη βιογένεση της HDL σε διάφορα μοντέλα ποντικών. Γονιδιακή μεταφορά μέσω αδενοϊών της apoA-I μαζί με την CTα σε apoA-I$^{-/-}$ ποντίκια αύξησε τη χοληστερόλη του πλάσματος, τα επίπεδα των φωσφολιπιδίων, τους μεγάλου μεγέθους α1-HDL υποπληθυσμούς και οδήγησε στη διαμόρφωση σφαιρικών σωματιδίων HDL. Γονιδιακή μεταφορά μέσω αδενοϊών της αγρίου τύπου LCAT σε LCAT$^{-/-}$

ποντίκια αύξησε πολύ τα συνολικά επίπεδα χοληστερόλης πλάσματος που οφείλονται κυρίως στην αύξηση στη χοληστερόλη της HDL. Αντίθετα η γονιδιακή μεταφορά μέσω αδενοϊών της LCAT που φέρει τις φυσικές μεταλλαξεις LCAT[T123I] και LCAT[P250S] επηρέασε σε μικρότερο βαθμό τα επίπεδα της χοληστερόλης του πλάσματος. Κλασμάτωση του πλάσματος με υπερφυγοκέντριση σε διαβάθμιση KBr έδειξε ότι η αγρίου τύπου LCAT αύξησε τα επίπεδα της apoE και apoA-IV του πλάσματος και μετατόπισε την apoA-I στα κλάσματα χαμηλότερης πυκνότητας. Οι μεταλλάξεις LCAT[T123I] και LCAT[P250S] αποκατέστησαν μερικώς την παρουσία της apoA-I στα κλάσματα της HDL2/HDL3 και στην περίπτωση της μετάλλαξης LCAT[T123I] αύξησε την apoE στα κλασματα της VLD/IDL/LDL. Τα $LCAT^{-/-}$ ποντίκια σχγματίζουν δύο υποπληθυσμούς preβ HDL και έναν α4-HDL. Οι μεταλλάξεις LCAT[T123I] και LCAT[P250S] παρήγαγαν preβ και α4,α3,α2-HDL υποπληθυσμούς ενώ η αγρίου τύπου LCAT παρήγαγε μόνο α-HDL μεγάλου μεγέθους. Συνέκφραση της apoA-I[L159R]Fin ή της apoA-I[225-230] με την LCAT αποκατέστησε τον ελαττωματικό φαινότυπο της HDL που δημιουργούν οι μεταλλάξεις apoA-I[L159R]Fin και apoA-I[225-230]. Αντίθετα, η συνέκφραση οποιασδήποτε από τις μεταλλάξεις LCAT[T123I] και LCAT[P250S] είτε με την apoA-I[L159R]Fin ή την apoA-I[225-230] δεν αποκατήστησε πλήρως το φαινότυπο της HDL. Συμπέρασματικά η υπερέκφραση της CTα και της LCAT προάγει τη βιογένεση της HDL ενώ οι μεταλλάξεις στην LCAT επιδρούν αρνητικά στην βιογένεση της HDL.

Η συμβολή επικρατουσών μεταλλάξεων της apoE στην ομοιόσταση των λιπιδίων και στην βιογένεση της HDL

Οι σημειακές μεταλλάξεις K146N/R147W στην ανθρώπινη apoE3 περιγράφηκαν για πρώτη φορά σε ασθενείς με μια κυρίαρχη μορφή της υπερλιποπρωτεϊναιμίας τύπου III. Οι επιδράσεις των μεταλλάξεων αυτών στις *in vivo* λειτουργίες της apoE μελετήθηκαν με γονιδιακή μεταφορά μέσω αδενοϊών των apoE3[K146N/R147W] και apoE3[K146N/R147W]-202 σε διάφορα μοντέλα ποντικών. Η έκφραση της apoE3[K146N/R147W] σε χαμηλά επίπεδα σε apoE$^{-/-}$ ή apoA-I$^{-/-}$ x apoE$^{-/-}$ ποντίκια επιδείνωσε την υπερχοληστερολαιμία και αύξησε σημαντικά την συγκέντρωση της apoE και των τριγλυκεριδίων. Στα apoE$^{-/-}$ ποντίκια η μετταλεγμένη μορφή apoE3[K146N/R147W] εκτόπισε την apoA-I από όλα τα κλάσματα των VLDL/LDL/HDL και οδήγησε στη συσσώρευση στο πλάσμα δισκοειδών σωματιδίων HDL που περιέχουν apoE. Παρόμοιες δόσεις αγρίου τύπου apoE3 σε apoE$^{-/-}$ ποντίκια οδήγησαν στο καθαρισμό της χοληστερόλης από το πλάσμα, χωρίς την επαγωγή υπερτριγλυκεριδαιμίας, και στον σχηματισμό σφαιρικών σωματιδίων HDL. Ένα μοναδικό χαρακτηριστικό της μεταλλαγμένης μορφής apoE3[K146N/R147W]-202 είναι ότι εμπόδισε την επαγωγή υπερτριγλυκεριδαιμίας, αλλά δεν διόρθωσε την υπερχοληστερολαιμία. Συνέκφραση της apoE3[K146N/R147W] και της LPL σε apoE$^{-/-}$ ποντίκια διόρθωσε την υπερτριγλυκεριδαιμία, αλλά δεν εμπόδισε τον σχηματισμό της δισκοειδούς HDL. Συνέκφραση της apoE3[K146N/R147W] και της LCAT επίσης διόρθωσε την υπερτριγλυκεριδαιμία, τα επίπεδα των εστέρων της χοληστερόλης του πλάσματος και οδήγησε στη παραγωγή σφαιρικής HDL. Συμπερασματικά, οι αντικαταστάσεις K146N/R147W αποτρέπουν τον καθαρισμό της χοληστερόλης, επιδεινώνουν

την δυσλιπιδαιμία και επηρεάζουν την λειτουργία της LCAT αναστέλλοντας έτσι την βιογένεση της HDL .

Η σύμπραξη της apoA-IV και της LCAT στη βιογένεση της HDL που περιέχει apoA-IV

Μελετήσαμε τη συμβολή LCAT στη βιογένεση της HDL που περιέχει apoA-IV. Γονιδιακή μεταφορά μέσω αδενοϊών της apoA-IV σε $LCAT^{-/-}$ ποντίκια απέτυχε να σχηματίσει HDL. Μεταφορά της apoA-IV σε $apoA\text{-}I^{-/-}$ ποντίκια δεν επηρέασε τα επίπεδα των λιπιδίων του πλάσματος ενώ η apoA-IV εντοπιστηκε στα κλάσματα της HDL3. Συνέκφραση της apoA-IV και της LCAT σε $apoA\text{-}I^{-/-}$ ποντίκια αποκατέστησε το σχηματισμό της HDL που περιέχει apoA-IV. Τα αποτελέσματα υποδεικνύουν ότι η apoA-IV μπορεί να σχηματίσει μοναδικους πληθυσμούς HDL που περιέχουν apoA-IV με τη συμμετοχή της LCAT, και δίνουν μια πιθανή εξηγήση για τις αντιφλεγμονώδεις και αθηρωπροστατευτικές ιδιότητες της apoA-IV.

Η επίδραση της τεχνητής HDL που περιέχει apoE και apoA-I στην γονιδιακή έκφραση των ενδοθηλιακών κυττάρων

Προκαταρτικά πειράματα μικροσυστοιχιών RNA από ανθρώπινα ενδοθηλιακά κύτταρα της αορτής μετά από την έκθεσή τους σε τεχνητή HDL που περιέχει apoA-I [χρησιμοποιώντας φωσφολιπίδια και χοληστερόλη (rHDLAI+) ή μόνο φωσφολιπίδια (rHDLAI-)] ή apoE (rHDLE+ και rHDL-). Οι αναλύσεις βιοπληροφορικής έδειξαν ότι η rHDLAI– και η rHDLAI+ προκάλεσαν τη διαφορική έκφραση σε 137 και 190 γονίδια αντίστοιχα. Ομοίως στην περίπτωση των rHDLE3- και rHDLE3+ παρατηρήθηκαν διαφορές σε 198 και 272 γονίδια αντίστοιχα. Οι μικροσυστοιχίες RNA επιβεβαιώθηκαν με qPRT-PCR. Χρησιμοποιώντας το λογισμικό IPA analysis καθώς και

εκτεταμένη έρευνα στη βιβλιογραφία σχηματίσαμε προτακαρτικά σηματοδοτικά μονοπάτια στα οποία συμμετέχουν τα διαφορικά εκφραζόμενα γονίδια που εντοπίστηκαν.

1. INTRODUCTION

1.1 Classification of lipoproteins and their function

Lipoproteins are macromolecular structures formed by the association of proteins and lipids, whose main function is to facilitate the transport of lipids, such as free cholesterol, cholesterol esters, phospholipids and triglycerides in the blood. The basic structure of the lipoproteins involves a hydrophobic core and a hydrophilic surface, forming and envelope around the core. The hydrophobic core is formed mainly by cholesterol esters and triglycerides. The envelope is formed mainly by proteins, free cholesterol and amphipathic lipids of the kind of phospholipids, like phosphatidylcholine, lysolecithin, sphingomyelin and others (1).

The phospholipids have their polar part oriented to the aqueous surface, while the apolar part interacts with the hydrophobic core of the lipoprotein. Free Cholesterol also forms part of the lipoprotein envelope, with the carbon 3 hydroxyl oriented to the polar environment, and the apolar side of the molecule embedded in the hydrophobic portion of the monolayer formed by the phospholipids. The proteins that form the lipoproteins are called apolipoproteins. The hydrophilic amino acids of these apolipoproteins are oriented to the outside, while the hydrophobic amino acids interact with the apolar part of the lipoprotein structure (1).

There are five major classes and various subclasses of lipoprotein. Based on their buoyant density, the major lipoproteins are chylomicrons, very low density lipoproteins (VLDL), intermediate-density lipoproteins (IDL), low-density lipoproteins (LDL), and high-density lipoproteins (HDL) (2) (Table 1.I).

Table 1.I: Lipoprotein classification, lipid and protein content (modified from (3))

Class	Density (g/ml)	Diam. (nm)	Mol.mass (kDa)	Prot. (%)	FC (%)	EC (%)	PL (%)	TG (%)	Apoproteins (major/minor)	source
HDL	1.063-1.21	5-12	175-360	45-55	3-5	15-20	26-32	2-7	**A-I, A-II/** CI,CII,CIII,D,E,J,AV	Liver & intestine
LDL	1.019-1.063	18-30	2300	18-20	6-8	45-50	18-24	4-8	**B-100** CI,CII,CIII,E	VLDL
IDL	1.006-1.019	25-50		18	29		22	31		VLDL
VLDL	0.94-1.006	30-80	10-80000	6-10	4-8	16-22	15-20	45-65	**B-100,E,CI,CII,CIII/**A-I,A-II,A-IV,CIV,AV	liver
Chylo microns	<0.94	75-1200	~400000	1-2	1-3	2-4	3-6	80-95	**A-I,A-IV,B-48,CI,CIII,E /**A-II,CII	intestine

The three major pathways of the lipoprotein metabolism are the chylomicron pathway, the VLDL/IDL/LDL pathway and the HDL pathway, all of which are metabolically interrelated. Several different proteins, including apolipoproteins, plasma enzymes, lipid transfer proteins, lipoprotein receptors, and lipid transporters, participate in these pathways and contribute to lipid homeostasis (3).

Chylomicrons are lipoprotein particles that consist of triglycerides (80-95%), phospholipids (3-6%), cholesterol (1-5%), and proteins (1-2%). They transport dietary lipids from the intestine to other locations in the body, such as the liver, adipose, cardiac, and skeletal muscle tissue, where their triglyceride components are hydrolyzed and unloaded and the remaining chylomicron remnants are taken up by the liver (4).

VLDL is secreted from the liver and carries mostly triglycerides and some cholesterol (5). Similarly to chylomicrons, the triglycerides on VLDL are hydrolyzed by various lipases resulting in the formation of IDL. Further hydrolysis of the triglycerides on IDL result in the formation of particles, which are poor in triglycerides but enriched in cholesterol, called LDL. The role of the

VLDL/IDL/LDL pathway is to transport triglycerides and cholesterol from the liver to where is needed in the peripheral tissues (5).

HDL is formed extracellularly mostly in the liver through the lipidation of its major apolipoprotein component, apolipoprotein A-I (apoA-I) and undergoes many steps of maturation. Its main role is to facilitate the delivery of the cholesterol from the peripheral tissues back to the liver (6), but it exhibits other functions too (7). The details of the HDL metabolism and its functions are discussed extensively in the following sections.

There are many diseases associated with defects in the three lipoprotein pathways and are reviewed in detail in (3). Furthermore, epidemiological studies have shown that, generally, increased plasma levels of LDL and decreased plasma levels of HDL are associated with an increased risk of coronary heart disease (8;9).

In the context of this thesis we will focus on the biogenesis and remodeling of HDL, perturbations of the pathway of HDL metabolism caused by the mutations in apoA-I, LCAT and apoE as well as on the function of HDL.

1.2 Overview of thepathway of the biogenesis and remodeling of HDL

High-density lipoproteins (HDL) are a heterogeneous group of macromolecules in the plasma of 7-12 nm diameter that float in the 1.063-1.21 g/ml density range and are composed of a core of cholesterol esters and triglycerides surrounded by an amphipathic layer of free cholesterol, phospholipids and apolipoproteins (mainly apolipoprotein A-I) (10). HDL has several functions that contribute to cholesterol homeostasis and protection from a variety of human

diseases. Thus HDL promotes cholesterol efflux from macrophages and other tissues, prevents oxidation of LDL, and inhibits expression of pro-inflammatory cytokines by macrophages as well as expression of adhesion molecules by endothelial cells (11). HDL inhibits cell apoptosis and promotes endothelial cell proliferation and migration, stimulates release of nitric oxide (NO) from endothelial cells thus promoting vasodilation, inhibits platelet aggregation and thrombosis and has antibacterial, antiparasitic and antiviral activities (11). Furthermore, Interaction of HDL with SR-BI receptor can also provide cholesteryl esters to steroidogenic tissues for steroid hormone synthesis (6).

The biogenesis and catabolism of HDL is a complex process and involves several membrane bound and plasma proteins (12). The HDL synthesis is initiated by the secretion of apoA-I mainly by the liver and to a lesser extent by the intestine (13). Secreted lipid-free apoA-I or minimally lipidated apoA-I interacts with the ABCA1 transporter (ATP-binding cassette transporter A1), which transfers the cellular phospholipids and cholesterol to apoA-I. The initial, poorly lipidated, apoA-I acquires more lipids and gradually forms the discoidal-shaped HDL particles which are enriched with unesterified cholesterol. Through the action of LCAT (Lecithin: cholesterol acyltransferase), which esterifies the free cholesterol on the surface of HDL, the discoidal particles are converted to spherical HDL particles (14) (Figure1.1). The esterified cholesterol moves to the HDL core, thus creating spherical HDL particles. Mutations in apoA-I, ABCA1 and LCAT prevent the formation of apoA-I containing HDL (15). Following a similar pathway apoE and apoA-IV can also synthesize HDL particles that contain these proteins (16;17) (Figure1.1).

Furthermore, HDL is remodeled by the action of many proteins. HDL acquires more cholesterol from ABCG1 (ATP binding cassette transporter G1) (18) and phospholipids from the VLDL/LDL by the action of PLTP (Phospholipid transfer protein) (19). The continuous action of LCAT and PLTP enzymes contribute to the formation of mature spherical cholesterol-ester-enriched HDL. Other proteins that participate in HDL remodeling are CETP (Cholesterol ester transfer protein), which catalyzes the exchange of cholesterol esters from HDL with triglycerides from VLDL (20), and SR-B1 (Scavenger receptor B1), which mediates the bidirectional movement of free cholesterol from tissues to HDL and cholesterol esters from HDL to tissues (21). Finally, HL (hepatic lipase), EL (endothelial lipase) and LPL (lipoprotein lipase) hydrolyze the phospholipids and triglycerides of HDL resulting in lipid-poor apoA-I (22-25). Lipid-poor apoA-I is catabolized by the kidney or is reutilized for HDL synthesis (10).

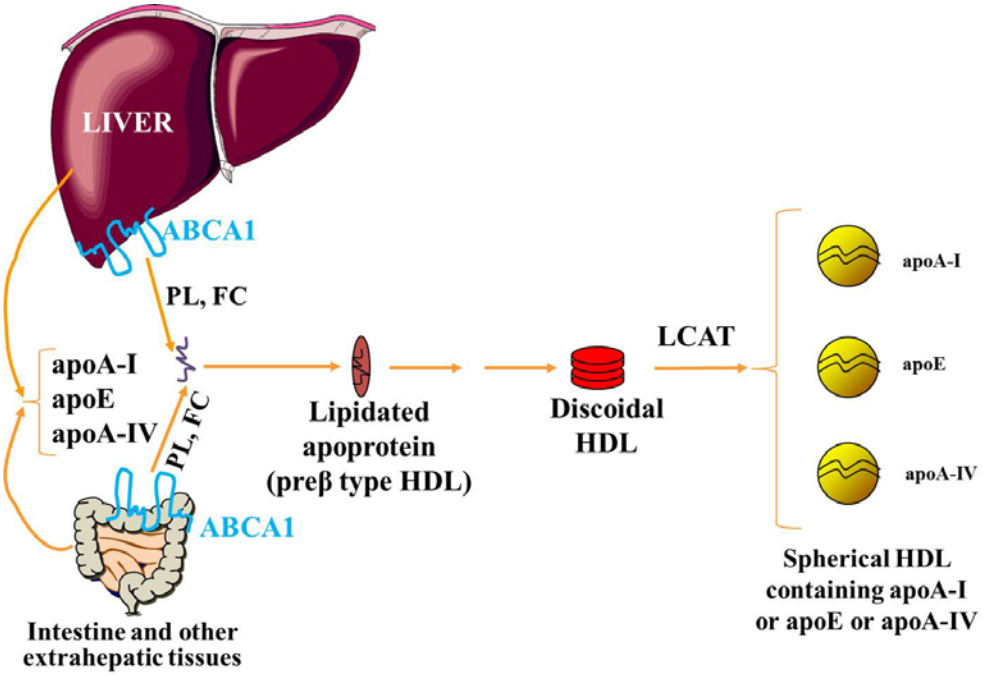

Figure 1.1: Schematic representation of the pathway of the biogenesis of HDL containing apoA-I or apoE or apoA-IV.

Numerous epidemiological studies as well as animal studies have shown that high levels of HDL in the plasma are inversely correlated with the risk of coronary artery disease (26;27). Furthermore, mutations in genes encoding proteins that are related to the HDL particle, such as apoA-I, LCAT and Paraoxanase1, have been shown to be associated with acceleration of atherosclerosis (28-30).

1.3 HDL subpopulations

The HDL particles can vary in shape, size, apolipoprotein composition and electrophoretic mobility which reflect their functionality. As mentioned in the previous section, the HDL can take a discoidal shape during its initial steps of its biogenesis or after extensive remodeling. Most of the HDL particles, though, are presented in their mature spherical shape under normal conditions (31). Additionally, the HDL can be distinguished according to their density into two subpopulations, HDL2 (1.063-1.125 g/ml) and HDL3 (1.125-1.21 g/ml) and according to the particle size into five subpopulations, HDL2b (~10.6 nm diameter), HDL2a (~9.2 nm), HDL3a (~8.4 nm), HDL3b (~8.0 nm) and HDL3c (~7.6 nm) (32) (Figure 1.2).

Another way to separate the HDL is depending on its main apolipoprotein content. The main apolipoproteins of HDL are apoA-I (~70% of total HDL protein) and apoA-II (~20% of total HDL protein) (33). One kind of subpopulations may contain apoA-I but not apoA-II, whereas the other can contain both apoA-I and apoA-II (34) (Figure 1.2).

HDL can also be separated depending on their mobility (alpha, preβeta and gamma) in agarose gel electrophoresis which reflects differences in the surface charge. Alpha-migrating particles (α-HDL) include HDL2, HDL3 as well as apoA-I-containing HDL and apoA-I/A-II-

containing HDL subpopulations. Preβeta HDL (preβ HDL) is either discoidal or lipid poor apoA-I and gamma HDL contains apoE but no apoA-I (35;36) (Figure 1.2). Furthermore, native-native 2D gel electrophoresis of HDL has shown the existence of 13 distinct HDL subpopulations preβ1a,b-, preβ2a,b,c-, α1-4-, and pre-α1-4-HDL (37-39) (Figure 1.3). The α1-4 HDL and pre-α1-4 HDL subpopulations are may also be referred altogether as α-1-4 HDL subpopulations.

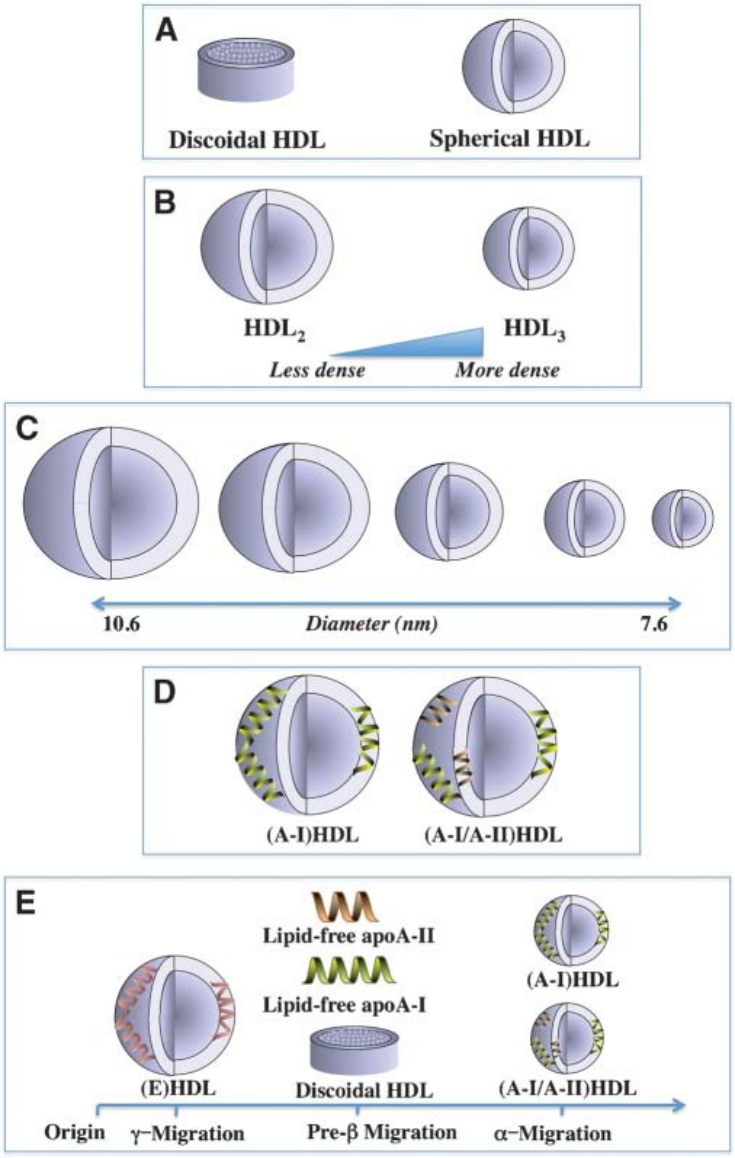

Figure 1.2: HDL heterogeneity. The HDL in human plasma consist of several subpopulations of particles that vary widely in shape (A), density (B), size (C), composition (D), and surface charge (E). Picture taken from (31).

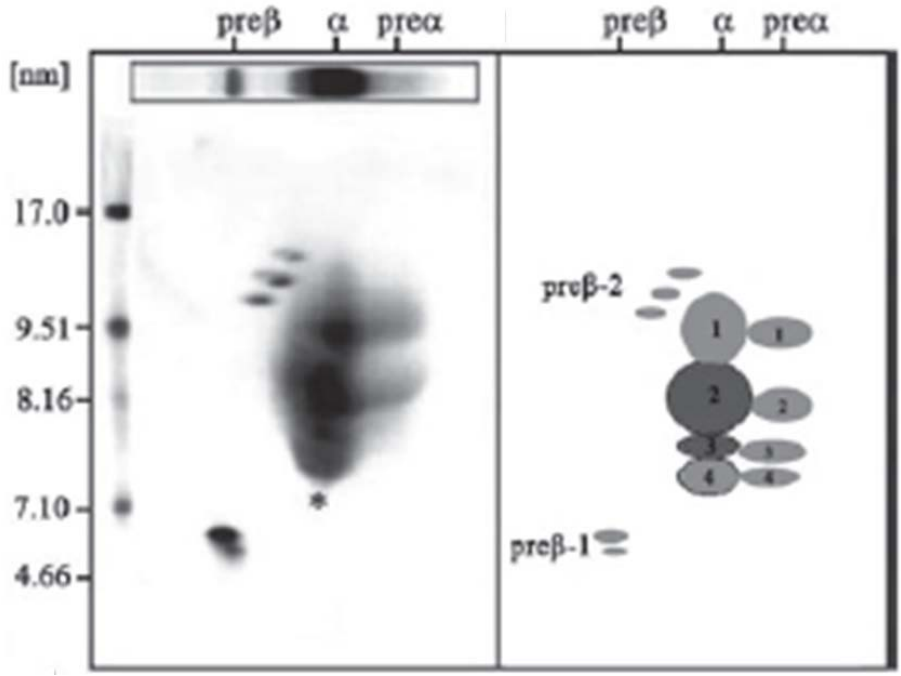

Figure 1.3: Two dimensional separation of apoA-I subpopulations of plasma and schematic representation of the resulting subpopulations. The plasma has been electrophoresed in the first dimension in 0.7 % agarose, followed by application of the agarose strip to the top of the non-denaturing polyacrylamide gel (2-36%) and subsequently electrophoresed. Picture modified from (37).

1.4 ApoA-I: Synthesis, regulation and genetics

ApoA-I is one of the main players in the formation of the HDL particles functioning as the protein scaffold that accepts the lipids through the action of ABCA1 and also by activating LCAT for the maturation of HDL. The apoA-I human gene is about 2.2kb and lies on

chromosome 11 (40) and is closely linked near the apoC-III and apoA-IV genes (41;42). The apoA-I cDNA is 878 bp long and encodes for a 267 precursor apoA-I (prepoapoA-I) that contains an 18 amino acid signal peptide and a 6 amino acid long pro-peptide. The 249 amino acid long proapoA-I is secreted into the plasma and is converted to the mature 243 amino acid apoA-I form by extracellular hydrolysis of the pro-peptide (43). The apoA-I gene is mostly expressed in the liver and the intestine, and to a lesser extent in other tissues (13).

The apoA-I promoter contains Hormone Response Elements (HREs) that bind members of the hormone nuclear receptor superfamily that bind orphan nuclear receptors, such as Hepatocyte Nuclear Factor-4 (HNF-4), Regulatory Protein 1 (ARP-1) and Liver Receptor Homologue 1 (LRH-1) (44-46) and ligand dependent receptors such as RXR (Retinoid X Receptor), RAR (Retinoic Acid Receptor) and TR (Thyroid Hormone Receptor) (44). The activity of the apoA-I promoter is greatly enhanced by the proximal apoC-III enhancer, which contains two HREs as well as three SP1 binding sites (47;48), and coordinates the expression of the genes in the apoA-I/apoC-III/apoA-IV cluster. In vitro mutagenesis of either the HREs or the SP1 sites reduced significantly the activity of the apoA-I promoter/C-III enhancer (49). The importance of these sites in the transcription of apoA-I was also confirmed in transgenic mice carrying the mutations in the HREs of the apoA-I promoter/C-III enhancer (50;51). It has also been shown that fibrates activate the mouse apoA-I promoter through the action of PPARa (44;52;53) but have no effect on human apoA-I promoter (54). Many other factors such as dietary habits, cytokines, hormonal, and pharmacological factors are known to influence apoA-I transcription and are reviewed in (55-59).

Fifty-five apoA-I mutations have reported in humans (Human Gene Mutations Database http://www.hgmd.cf.ac.uk/ac/gene.php?gene=APOA1). These mutations have been associated with low HDL-C levels or hereditary amyloidosis (60). Seventeen mutations, associated with low plasma HDL levels, are found in the N-terminal region of apoA-I or within the central helices 5-7 and result in diminished capacity of the apoA-I mutants to activate LCAT (60). Few cases of apoA-I mutations have been reported to be associated with premature CAD (28;61;62). An interesting case is the apoA-I[R173C] Milano mutation which has been reported to confer atheroprotection despite the low HDL levels (63;64). Eleven apoA-I mutations in the N-terminal region and in helix 7 of apoA-I have been associated with amyloidosis. These mutations cause the formation of amyloid fibrils that contain a ~10kDa N-terminal apoA-I peptide as the major component (60;65) .

1.5 Structural features of apoA-I that promote HDL formation

ApoA-I contains 22 or 11 amino acid repeats which, according to the models of Nolte & Atkinson (66), are organized in amphipathic a-helices (67). X-ray crystallography of the N-terminal deletion mutant of apoA-I, apoA-I[Δ(1-43)] provided a 3.2 Å resolution structure where apoA-I appears to have a continuous amphipathic α-helical conformation that is punctuated by small or pronounced kinks (68;69). Overall, the apoA-I molecule appears to adopt a horseshoe shape with dimensions of 125x80x40 Å (70-75). In this structure two apoA-I molecules form an antiparallel dimer that registers at the central helices 5-5 and terminal helices 10-10 (69) (Figure 1.4 A). Based on the crystal structure of apoA-I in solution, a belt model was proposed to explain the structure of apoA-I on discoidal HDL particles. In this model, two antiparallel

molecules of apoA-I consisting of continuous amphipathic α-helices with 3.67 residues per turn (designated 11/3 helices) are parallel to the plane of the disc (70). The apoA-I dimer is wrapped beltwise around a discoidal bilayer and shields the hydrophobic fatty acid chains of the phospholipids (Figure 1.4 B). It has been proposed that the optimal arrangements of the dimers are those that maximize intermolecular salt bridge interactions (72). In this alignment two anti-parallel apoA-I molecules have overlays of the central helixes 5-5 and terminal helixes 10-10 that match the overlay pattern of the crystal structure of lipid-free apoA-I (69).

Analysis of the 93 Å spherical HDL in solution by small angle neutron scattering (SANS) showed that apoA-I folds around a central lipid core that has 88.4 Å x 68.2 Å dimensions to form a spheroidal HDL (sHDL) particle (Figure 1.4 C). Three possible arrangements of apoA-I on the sHDL particle were considered: a) A model designated HdHp (heterodimer and a hairpin) where two apoA-I molecules were arranged in anti-parallel planar orientation and a third molecule assumed a hairpin structure; b) A model designated 3Hp (3 hairpins) where three apoA-I molecules were folded as hairpins; and c) A model designated integrated trimer (iT) where three apoA-I molecules interact with each other on the HDL surface (76). Based on cross-linking of the K residues Wu *et al.* suggested that spherical HDL may be compatible with the HdHp model (76). This model retains the predominant anti-parallel orientation of the two apoA-I molecules and a 5-5 helix registry proposed for the crystal structure of apoA-I for the apoA-I dimer (69).

Silva *et al.* identified fourteen intra-chain and seven inter-chain cross-links in reconstituted spherical 93 Å particles and proposed three models to explain the arrangement of apoA-I on the HDL particles: a) a planar circular belt containing three apoA-I molecules in anti-

parallel orientation; b) two apoA-I molecules arranged in planar circular anti-parallel double belt and a third molecule in the form of hairpin; c) a “trefoil” model where the right hand half of two anti-parallel apoA-I molecules of the double belt model were displaced by 60^{o} out of their planar position of the disc and were aligned in anti-parallel orientation with a third molecule bent at 60^{o} angle (77).

A recent study examined the structure of nascent HDL after incubation of apoA-I with ABCA1-expressing HEK293 cells. These studies showed that the largest 9-14 nm diameter HDL particles contained three apoA-I molecules whereas the smaller 7.5 nm diameter spheroidal nascent HDL particles carried two molecules of apoA-I. In both cases the apoA-I molecules adopted an antiparallel belt-like configuration (78).

Negative staining electron microscopy showed contiguous high densities originating from the protein moieties near the centers and the edges of the HDL particles (79). Combination of cross-linking and mass spectrometry showed that HDL subpopulations of different sizes, containing predominantly apoA-I, assume the structures that are similar to that found in reconstituted HDL. The size of HDL is achieved by twisting of the resident apoA-I molecules on the HDL particles resulting in a symmetrical cage-like structure (80). Moreover, it has been suggested by hydrogen exchange and mass spectrometry methods that the secondary structure of apoA-I remains relatively unchanged between the discoidal and spherical HDL particles (81).

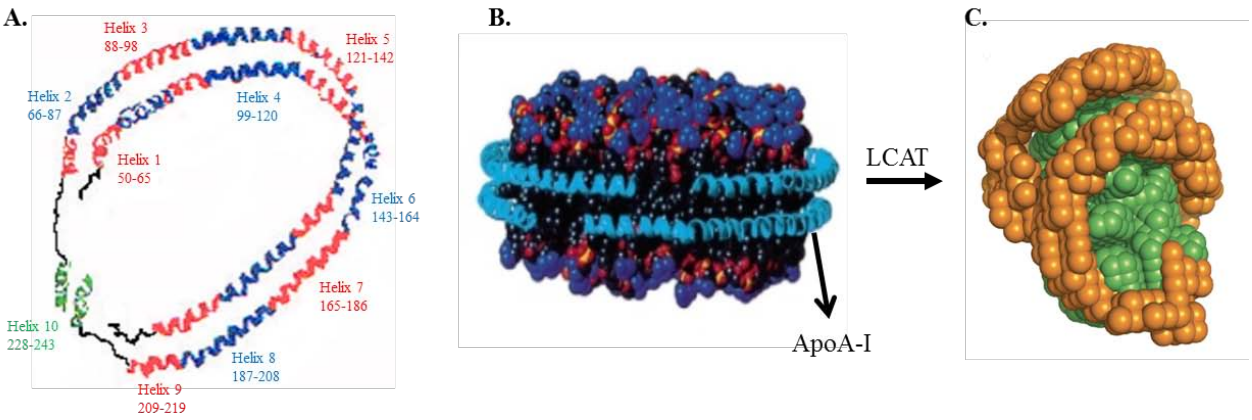

Figure 1.4: Summary of structure of apoA-I. (A) Model of the crystal structure of apoA-I [Δ(1-43)]. The figure is based on the protein Databank 1AVI.PDB (69). (B) "Belt" model of apoA-I on discoidal HDL particles adapted from (70;72). C. Low resolution structure of spheroid HDL (sHDL particle) showing the position of the lipid moieties in green and the protein moiety in yellow(76)**.**

Another study, using cross linking of cystein residues introduced by *in vitro* mutagenesis as well as cross linking of lysine and tyrosine residues and mass spectrometry, examined the configuration of lipid-free apoA-I in solution. The authors suggested that apoA-I in solution is a squat, oblate spheroid with the helices 1 through 7 forming a four-helix bundle. The N-terminal region and the C-terminal amphipathic helices 8-10 were associated with the helix bundle and located in close proximity to each other (82).

A recent study by Mei & Atkinson shed light on the role of apoA-I in the formation of discoidal HDL particles and its interactions with LCAT (83). The high 2.2-Å resolution crystal structure of apoA-I[Δ(185–243)] showed the formation of a half-circle dimer which consists of two elongated antiparallel helices with proline kinks. The N-terminal domain of each of the apoA-I molecules lay close to the C-terminal domain of the symmetry-related partner forming a

four-helix bundle. The central region of the structure is more flexible and connects the two ends of the bundle. This structure is in agreement with many of the conformational features of apoA-I discoidal HDL proposed previously using modeling and Molecular Dynamics simulations (84). The importance of this model lies in the fact that it offers an explanation of how the apoA-I double belt undergoes continuous conformational changes enabling it to accept lipids, from the discoidal HDL to the large spherical HDL. According to this model, during the HDL maturation minimal changes happen in the variable constant region whereas the variable region undergoes large quantized re-arrangements enabling the expansion of the double-belt (85). Furthermore, this model has been used to explain the atheroprotective functions of apoA-I$[R173C]_{Milano}$ and apoA-I$[R151C]_{Paris}$ (86) as well as the amyloid formation of N-terminal fragments of apoA-I in hereditary amyloidosis (87).

Unique insights into structure-function relationships of apoA-I were obtained by bioinformatics analysis of the apoA-I residues conserved throughout evolution in 31 species. It was found that strong conservation exists in the first 30 salt-bridge forming residues of apoA-I and in the central domains (helix 2/3 to helix 7/8). The most conserved residues are on helix 7 and the least conserved in helix 10. Furthermore, eight residues were fully conserved (88). In this study the location of the conserved residues on the helical wheel model suggested interactions with phospholipids, oxidized lipids and antioxidant enzymes.

1.6 ABCA1

The ABCA1 gene is located on human chromosome 9 at the gene locus 9q31.1. It expands along 149 kb, includes 50 exons and encodes a 2261 amino acid protein. The ABCA1 is a ubiquitous protein that belongs to the ABC family of transporters and is expressed abundantly in the liver, macrophages, brain and various other tissues (89;90). The superfamily of ABC transporters utilizes ATP as a source of energy for the transportation of various molecules across plasma membranes. There are two types of ABC transporters. The first includes whole transporters having two similar structural units joined covalently, such as ABCA1 and ABCA7 while the second includes half transporters of single structural units that form hetero- or homodimers, such as ABCG1 and ABCG4 (91).

The protein structure of ABCA1 (Figure 1.5) is characterized by two transmembrane domains with six helices each and two cytoplasmic nucleotide binding domains (NBD) containing two conserved peptide motifs, named Walker A and B, which are present in all ATP-binding proteins. The NBD also contain a motif unique in ABC transporters called Walker C. Very important regions of ABCA1 are the two extracellular loops that are highly glycosylated, are linked by cystein bonds and are thought to bind ApoA-I (92). The ATP binding and hydrolysis in both NBD regions cause conformational changes in the extracellular domains of ABCA1 that allow the binding of apoA-I (93).

ABCA1 is localized only on the basolateral surface of the hepatocytes (94); it is also found on endocytic vesicles and was shown to travel between late endocytic vesicles and the cell surface (95).

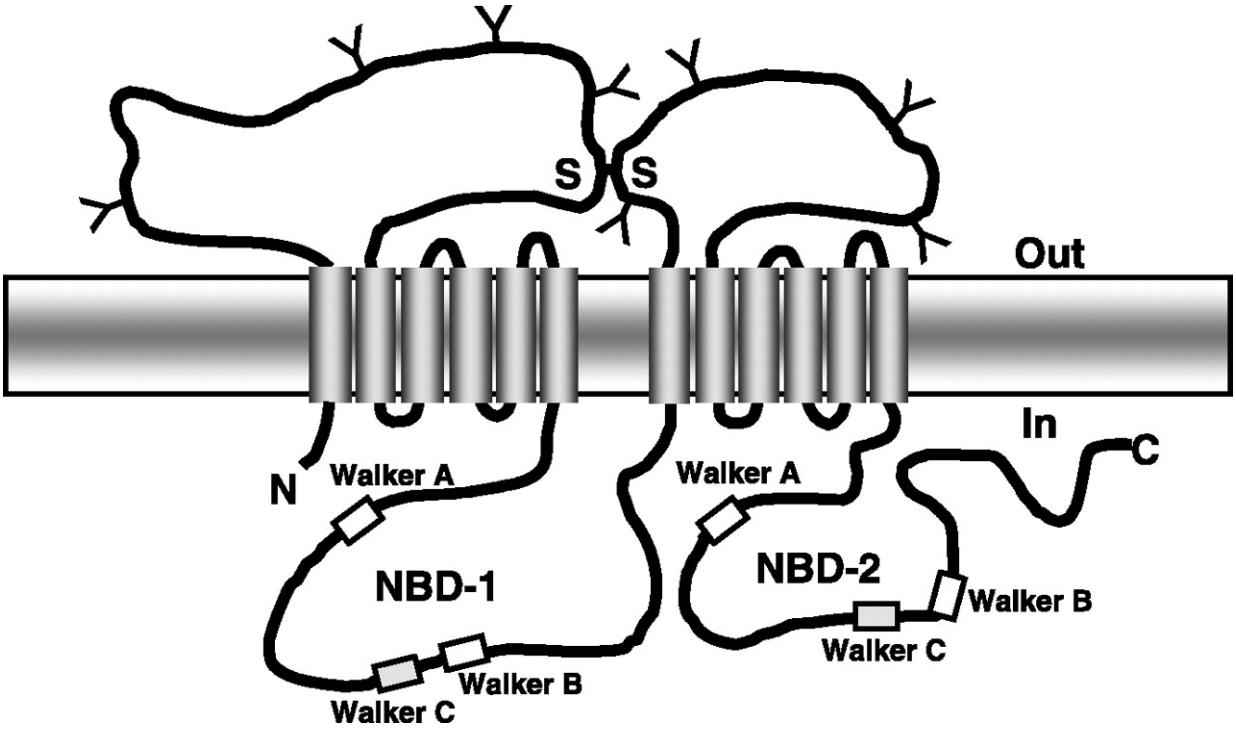

Figure 1.5: Topological model of ABCA1. Y indicates approximate glycosylation sites, and S-S indicates one predicted disulfide bond. NBD-1 and NBD-2 are the nucleotide binding domains that contain the highly conserved Walker A and Walker B domains and the Walker C signature motif (92).

1.7 Interactions of apoA-I with ABCA1 *in vitro*

ABCA1 binds directly to apoA-I (96;97) and promotes efflux of cellular phospholipids and cholesterol to lipid free or minimally lipidated apoA-I and other apolipoproteins, but not to spherical HDL particles (98;99). It has been shown that although apoA-I does not alter ABCA1 mRNA abundance; it increases the content of ABCA1 protein markedly, suggesting the effect of apoA-I on ABCA1 degradation (100). The transfer of lipids to apoA-I by ABCA1 stabilizes apoA-I, thus Tangier disease that is characterized by defects in the ABCA1 gene can result in increased

catabolism of apoA-I (101), and ABCA1 single nucleotide polymorphisms were reported to change the fasting and postprandial values of apoA-I (102).

Studies in HeLa cells that expressed an ABCA1 green fluorescence fusion protein showed the intracellular trafficking of ABCA1 complexed to apoA-I (94;95). Other studies showed that in macrophages ABCA1 associates with apoA-I in the coated pits, it is internalized, interacts with intracellular lipid pools and is re-secreted as a lipidated particle (103-105). A similar pathway that leads to transcytosis has been described in endothelial cells (106;107).

A series of cell culture and *in vitro* experiments investigated the ability of apoA-I mutants to promote ABCA1 mediated efflux of cholesterol and phospholipids and to crosslink to ABCA1. These mutants had amino terminal deletions, carboxy terminal deletions that removed the 220-231 region, carboxy terminal deletions that maintained the 220-231 region and double deletions of the amino- and carboxy- terminal regions (108). These studies reviewed in (108) showed that wild type (WT) ABCA1-mediated cholesterol and phospholipid efflux was not affected by amino-terminal apoA-I deletions, but it was diminished by carboxy-terminal deletions in which residues 220-231 were removed. Efflux was not affected by deletion of the carboxy-terminal 232-243 region and it was restored to 80% of WT control by double deletions of both the amino- and carboxy-termini (12;14;108;109). Lipid efflux was either unaffected or moderately reduced by a variety of point mutations or deletions of internal helices 2-7 and indicated that different combinations of central helices can promote lipid efflux (96;110). Chemical cross-linking/immunoprecipitation studies showed that the ability of apoA-I mutants to promote ABCA1-depended lipid efflux is correlated with the ability of these mutants to be cross-linked efficiently to ABCA1 (96).

Cross-linking between apoA-I and ABCA1 and cholesterol efflux was also affected by mutations in ABCA1 found in human subjects. The majority of the ABCA1 mutations cross link poorly to WT apoA-I and have diminished capacity to promote cholesterol efflux (111;112). A notable exemption is the ABCA1[W590S] mutant which can cross-link stronger to apoA-I than to WT ABCA1 but has diminished capacity to promote cholesterol efflux and to promote formation of HDL (111-113). It was suggested that this ABCA1 mutation may have altered the environment of the binding site of ABCA1 in such a way that the binding of apoA-I is strong but not productive and prevents efficient lipid efflux (96).

Although a monomeric forms of ABCA1 can promote cholesterol efflux (114), it has been reported that a tetrameric or oligomeric form of ABCA1 is required for the efficient efflux of phospholipids (115). In a recent study, using single-molecule fluorescent imaging in living cells, it was shown that ABCA1 is associated with lipids on the plasma membrane and forms immobilized dimers (116). Functional interaction between apoA-I and the ABCA1 dimer results in the transfer of lipids to apoA-I and the dissociation of ABCA1 into monomers. Mobilization of new lipids converts the monomer of ABCA1 into dimers (116).

Additionally, to investigate how the nascent HDL is formed, Wang et al. compared the ability of WT ABCA1 and ABCA1 mutants associated with Tangier disease to bind apoA-I, efflux cholesterol as well as cause conformational changes in apoA-I (117). Using an apoA-I[L38C/M112C] mutant labeled with a proximity self-quenching fluorophore at the cystein residues 38 and 112, they showed that the WT ABCA1 caused the unfolding of the N-terminus of apoA-I before lipidation. The ability of the ABCA1 mutants to cause the apoA-I unfolding was directly correlated to their ability to bind apoA-I (117). The study also showed the presence of

an intermediate conformation of apoA-I after binding to ABCA1 and before lipidation and release of the apoA-I molecule.

Other studies examined the importance of cystein residues of ABCA1 in apoA-I binding and HDL formation. These studies showed that substitution of Cys75 or Cys309 by serines impaired apoA-I binding. Simultaneous substitution of both Cys1463 and Cys1465 by serines impaired apoA-I binding and HDL formation and substitution of Cys1477 impaired HDL formation, suggesting that these residues are essential for the functionality of ABCA1 (118). Chemical modification of the lysine residues in the extracellular domain of ABCA1 abolished the ABCA1/apoA-I interactions, indicating the importance of these residues for the functions of ABCA1 that lead to the formation of HDL (119).

Finally, it has been shown that the interaction of apoA-I with ABCA1 activates signaling mechanisms, involving protein kinase A (PKA), protein kinase C (PKC), Janus kinase 2 (JAK2), Cdc42 and Ca^{2+}, that modulate ABCA1 levels or its mediated lipid transport activity by a posttranslational mechanism (120).

1.8 Interactions of apoA-I with ABCA1 *in vivo*

Inactivating mutations in ABCA1 found in patients with Tangier disease are associated with very low levels of total plasma and HDL cholesterol levels, diminished capacity to promote cholesterol efflux, formation of preβ-migrating particles and abnormal lipid deposition in various tissues (15;121-124).

Analysis of the serum of carriers with ABCA1 mutations by two dimensional gel electrophoresis and western blotting using anti-human apoA-I antibody showed that subjects homozygous or compound mutant heterozygous for ABCA1 fail to form α-HDL particles but instead they form preβ and other small size particles (15) (Figure 1.6).

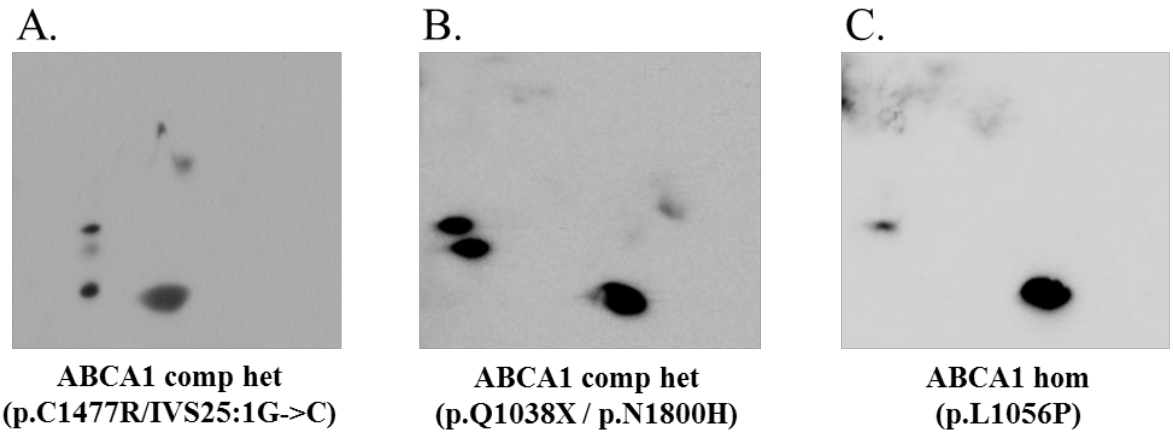

Figure 1.6: Two dimensional gel electrophoresis of plasma obtained from homozygotes or compound heterozygotes ABCA1 deficient human subjects with Tangier disease as indicated. Adapted from reference (15).

Previous studies using adenovirus-mediated gene transfer of apoA-I C-terminal deletion mutant in apoA-I$^{-/-}$ mice established that the elimination of the 220-231 region of apoA-I prevents the synthesis of α-HDL but allow the synthesis of preβ HDL particles (125). As discussed later, part of the studies performed for this thesis included the investigation of the significance of the hydrophobic and charged residues in the 218-230 region of apoA-I for the biogenesis of HDL (126;127). The HDL particles found in these studies resembled those found in

the human subjects carrying ABCA1 mutations (15) and may be created by mechanisms that involve non-productive interactions between ABCA1 and apoA-I.

Several ABCA1 mutations in humans that alter the functions of ABCA1 are associated with increased susceptibility to atherosclerosis (128). Specific amino acid substitutions found in the Danish general population were associated with increased risk for ischemic heart disease and reduced life expectancy through unknown mechanisms (129). Inactivation of the ABCA1 gene in mice leads to low total serum cholesterol levels, lipid deposition in various tissues, impaired growth and neuronal development and mimics the phenotype described in patients with Tangier disease (122). In addition ABCA1 deficient mice exhibit moderate increase in cholesterol absorption in response to high cholesterol diet (130;131). The role of ABCA1 on the lipid content of bile salts and cholesterol secretion is not clear (132;133). Transgenic mice overexpressing ABCA1 are more resistant to atherosclerosis in the C57BL/6 background but less resistant when crossed with $apoE^{-/-}$ mice under western-diet (134). Total ABCA1 deficiency in the atherosclerotic-prone $LDLr^{-/-}$ or $apoE^{-/-}$ backgrounds was not associated with increased atherosclerosis (131). Similar results were observed in $LDLr^{-/-}$ mice lacking expression of ABCA1 in the liver (135). In contrast, ablation of the macrophage ABCA1 caused increased atherosclerosis in $apoE^{-/-}$ mice indicating the importance of macrophage cholesterol efflux in atheroprotection (131). Bone marrow transplantation experiments indicated that ABCA1 plays an important role in the control of macrophage recruitment to the tissues and that its overexpression in macrophages inhibits the progression of atherosclerosis (136;137). Furthermore, endothelial cell-specific overexpression of ABCA1 in C57Bl/6N mice increase HDL levels and decreased atherosclerosis in response to an atherogenic diet. The atheroprotective

effect of endothelial expression of ABCA1 was lost when these transgenic mice were crossed with apoE$^{-/-}$ or ABCA1$^{-/-}$ mice (138). Under normal diet, the ABCA1-overexpressing endothelial cells also exhibited an atheroprotective gene expression profile such as increased eNOS, Rhob and Tfpi and reduced Caspase, Ripk1, Tnfsf10, Cxcl1 and Pecam1 (138).

In mice, the majority of HDL is produced by the liver (139). When the liver and intestinal ABCA1 genes were inactivated in mice HDL was not found in plasma, indicating that the liver and the intestine are the only sites that contribute to the production of HDL (124). Following intestinal-specific inactivation of the ABCA1 gene in mice, the HDL that was generated by the liver accounted for 70% of the HDL found in WT mice (139). In mice that do not express hepatic ABCA1, the HDL concentration in the lymph was greatly diminished despite the fact that the intestine contributes 30% to the synthesis of HDL. This implies that the HDL that is produced in the intestine is secreted directly into the plasma (139). This is further supported by the finding that in mice that do not express intestinal ABCA1, the apoA-I and cholesterol concentration of lymph was not affected (139).

In liver-specific or whole body ABCA1 knock-out mice, the plasma HDL catabolism and the fractional catabolic rate of HDL by the liver and to a lesser extent by the kidney and the adrenal is increased (124;140). In ABCA1$^{-/-}$ mice poorly lipidated apoA-I particles or preβ HDL failed to mature and are rapidly catabolized by the kidney (124).

1.9 LCAT: Structure, enzymatic activity and role of LCAT in the biogenesis of HDL

LCAT (lecithin cholesterol acyltransferase) is a plasma enzyme playing an important role in maintaining plasma and HDL cholesterol homeostasis and regulating its transport in the bloodstream. The LCAT gene is on locus 16q22.1 and contains 4200bp (141). It encodes a 416 amino acid polypeptide chain with molecular mass of 49 kDa or 67 kDa after glycosylation (142). LCAT mRNA is found predominantly in the liver and to a much lesser extent in the brain and the testis (143;144). Following secretion the LCAT protein circulates in blood reversibly bound to lipoproteins. The plasma concentration of LCAT is 6 mg/L and remains relatively steady with only slight changes depending on age, gender, use of hormones, smoking and alcohol (145).

Following activation by apoA-I, LCAT interacts with discoidal and spherical HDL and catalyzes the transfer of the 2-acyl group of lecithin or phosphatidylethanolamine to the free hydroxyl residue of cholesterol to form cholesteryl ester (146;147). It also catalyzes the reverse reaction of esterification of lysolecithin to lecithin (148).

Although its preferred substrate is HDL, LCAT has also been reported to esterify cholesterol on LDL particles where apoE is the activator of LCAT (149). The esterification of cholesterol within HDL by LCAT is known as α-LCAT activity whereas within LDL is called β-LCAT activity.

Insight on the potential functional interactions between apoA-I and LCAT have been gained from a computer-derived 3D structure of LCAT based on the amino acid and functional homology with the human pancreatic lipase and *Candita antarctica* lipase. This analysis predicted that LCAT belongs to the α/β hydrolase fold family and contains seven conserved

parallel β strands and four α-helices that are connected by loops (150) (Figure 1.7 A,B). Two of the helices located between residues 153 to 171 and 182 to 202 are close to the active site of the enzyme which contains the catalytic residues S181, D345 and H377. The residues F103 and L182 are predicted to participate in the formation of the oxyanion hole. Residues 50 to 74 are predicted to form a potential lid domain that may participate in enzyme substrate interactions. W61 residue within this domain is important for the enzymatic activity and may interact with the Sn-2 fatty acyl chain of the phospholipid (150). It has been suggested that electrostatic interactions between one or more of the helices of LCAT and putative apoA-I helices may position apoA-I close to the active site of LCAT and thus contribute to the LCAT activation (150). Charge-charge interactions between LCAT and apoA-I have also been implied by the quantitative dissociation of LCAT from HDL in concentrated salt solutions (151). Based on the proposed 3D model of LCAT, it was found that the mutations associated with LCAT deficiency are in the vicinity of the catalytic residues of the enzyme; in contrast, most mutations associated with FED are found on the hydrophobic surface of the amphipathic helices of the enzyme and may affect its interactions with apoA-I and HDL (152;153).

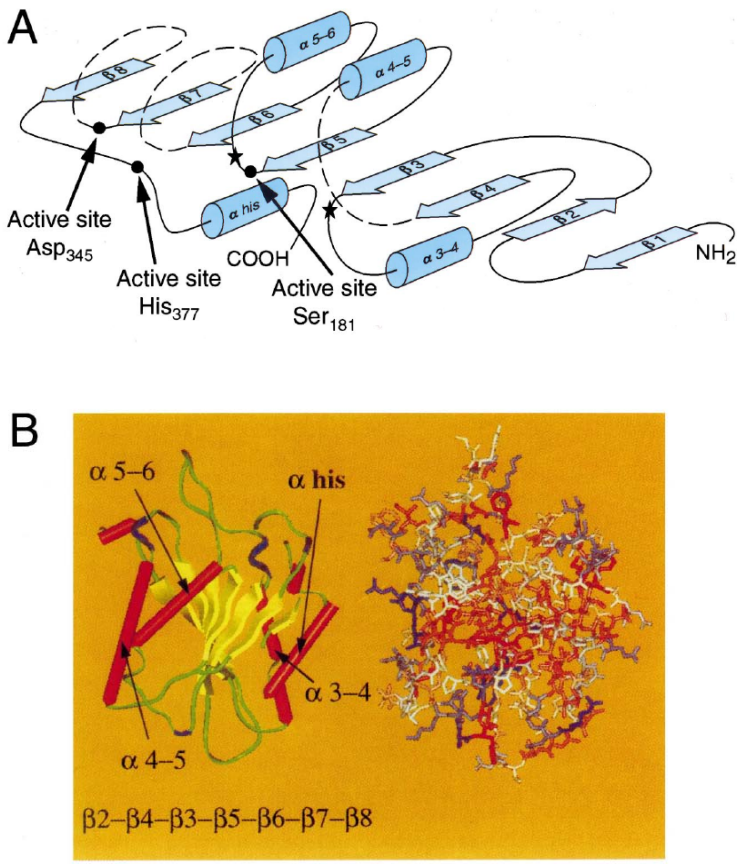

Figure 1.7: Topology of the general α/β hydrolase fold. The human LCAT lacks the β1 strand. The dots indicate the catalytic triad residues and the stars other active site residues (A). 3D-model of the core structure of LCAT. The β-strands are indicated with yellow, the α-helices by red and the loops by green. On the right is the same model showing hydrophilic residues in blue and hydrophobic residues in red. Here the catalytic residues would be located in the loops at the top and center of the structure (B). Taken from (150;154).

The enzymatic reaction catalyzed by LCAT can be separated in distinct steps such as the binding of LCAT to HDL, the activation by apoA-I, binding of PC, formation of acyl-enzyme, release of lysoPC, cholesterol binding to the active site and finally release of CE and

regeneration of free enzyme. The enzymatic reaction can be summarized in the hydrolysis and transfer of sn-2 fatty acid from PC to the 3-hydroxyl group of cholesterol (Figure 1.8 A,B). The rate limiting step is probably the binding of PC to the active site of LCAT and this is supported by the observation that the activation energy for the formation of CE products depends on acyl chain length and the unsaturation of the PC substrate (155). The esterified cholesterol is very hydrophobic and segregates into the core of HDL and the lysoPC diffuses into the aqueous medium and binds to serum albumin. The initial binding of LCAT to HDL is determined by the lipid surface and not by apoA-I although the activation by apoA-I is needed for catalysis. Also, the much higher affinity of LCAT to HDL than LDL is attributed to the stabilization of the enzyme by apoA-I (156;157). On the other hand sphingomyelin inhibits the binding of LCAT to HDL (158;159). The knowledge about each distinct step of the enzymatic reaction of LCAT is limited and most of it involves the activation by apoA-I.

A

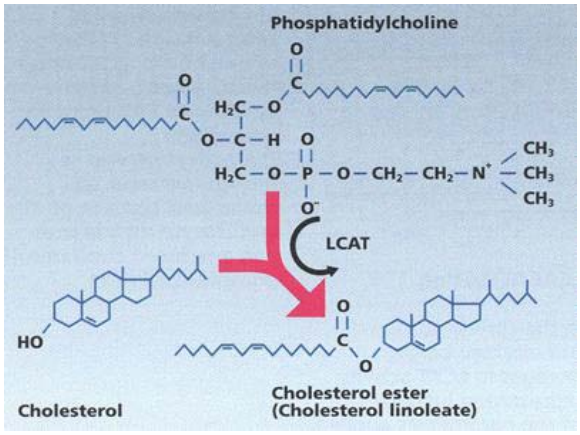

B

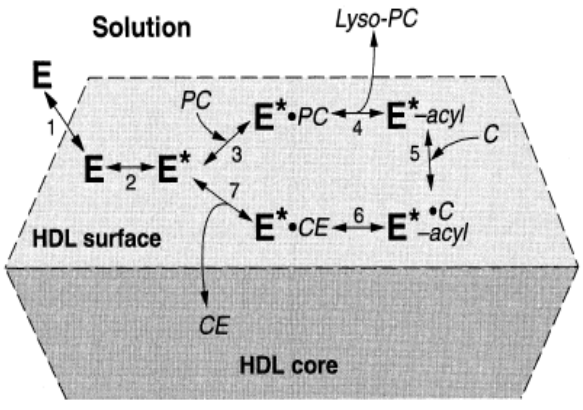

Figure 1.8: (A) The enzymatic reaction catalyzed by LCAT. (B) The reaction steps of LCAT on the surface of HDL. **E** represents LCAT in solution and bound to HDL, **E*** is the activated LCAT by apoA-I and **E***-acyl is

the acylated form of the enzyme. PC and C are the lipid substrates of LCAT and lyso-PC and CE are the products of the reaction. The CE are more hydrophobic than free cholesterol and move to the core of the HDL particle (154).

1.10 Contribution of LCAT in HDL biogenesis and atherosclerosis

Several of LCAT mutations have been found and characterized in humans (160;161). The recognized syndromes caused by mutations in LCAT are Familial LCAT deficiency (FLD), characterized by total abolishment of LCAT activity, and fish eye disease (FED), characterized by partial loss of α-LCAT activity but not β-LCAT activity (160). FLD is characterized by very low LCAT mass or LCAT activity in the plasma, low HDL-C, apoA-I, apoA-II and apoB levels but increased triglycerides. The HDL particles are small, lipid-poor, disc-shaped belonging to preβ and α4-HDL subpopulations (Figure 1.9) (15;162). The preβ particles of subjects carrying LCAT mutations in homozygosity or heterozygosity have been shown to carry apoA-II (162). The clinical manifestation of FLD is corneal opacity, anemia and sometimes proteinuria and renal disease (160;163). FED is a milder situation in which only corneal opacity is present and the cholesterol esterification rates are not altered due to the retention of β-LCAT activity of the enzyme. The plasma HDL levels in FED are low and the LCAT mass partially reduced. Despite the atherogenic lipid/lipoprotein profile of the above syndromes, they are only a few cases of FED patients which were associated with increased intima media thickness, atherosclerosis and premature CAD (29;164-167). Furthermore, epidemiological studies have shown controversial results either failing or succeeding to show correlation between the LCAT concentration and the risk of cardiovascular (167-173).

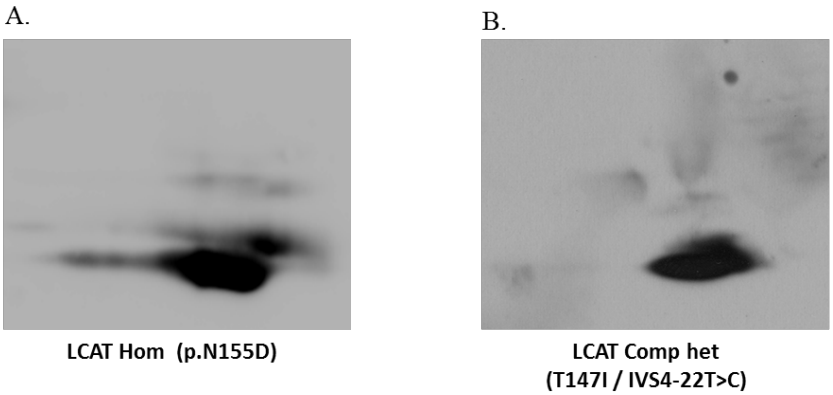

Figure 1.9 (A,B): Two-dimensional gel electrophoresis from plasma obtained from one homozygote and one compound heterozygote for LCAT deficiency as indicated (A,B) showing the presence of mostly small α-HDL subpopulations. Data obtained from (15).

A possible reason for the lack of association of LCAT mutations with cardiovascular disease maybe the increase of preβ HDL in plasma, which may be sufficient to efflux cholesterol from tissues, macrophages and the aortic intima (174-177). In support of this it has been shown that sera obtained from LCAT heterozygotes had increased capacity to promote ABCA1 mediated cholesterol efflux and decreased capacity to promote ABCG1 and SR-BI mediated cholesterol efflux from macrophages as compared with sera obtained from normal subjects (178). These properties were attributed to the increased preβ and decreased α-HDL subpopulations in the sera of the LCAT heterozygotes (178). Heterozygosity for LCAT mutations in the Italian population was not associated with increased preclinical atherosclerosis despite the lower HDL-C levels as compared to normal subjects (179). In addition, homozygous and heterozygous carriers of LCAT mutations had only mild lipid oxidation compared to normal controls despite the fact that they had decreased LCAT activity, HDL cholesterol, apoA-I,

platelet-activating factor-acetylhydrolase activity and Paraoxanase 1 activity, all of which have anti-oxidant potential (180). This offers another explanation as to why atherosclerosis is rare in LCAT deficiency.

In FED patients the β-LCAT activity may be enough to protect from CVD. In addition, apoE and apoA-IV HDL may compensate for the loss of apoA-I HDL (16;17). In most LCAT deficiency cases the apoB and LDL levels are reduced so this may offset the risk associated with low HDL. The reduced LDL levels may result from rapid catabolism of LDL by LDL-R rather than decreased synthesis of LDL (181). There have been reported few cases of FED patients with premature CVD who exhibit increased plasma apoB and LDL-C levels (165;166). An interesting study showed that the presence of the apoE2 allele in total LCAT deficiency is associated with increased LDL cholesterol and triglycerides as opposed to apoE3 or apoE4 alleles, indicating that apoE may act as a modifier for the FLD phenotype (182).

The role of LCAT in the pathogenesis of atherosclerosis was studied in $LCAT^{-/-}$ and LCAT transgenic animal models. LCAT KO mice have similar lipid/lipoprotein profile to that of FLD patients and include decreased HDL-C, apoA-I and apoA-II and mature α-HDL but increased preβ HDL levels (174;175;183). The overexpression of human LCAT in transgenic rabbits and mice showed increased levels of total cholesterol, cholesterol esters, phospholipids and HDL-C and decreased preβ HDL (184-187). In the human LCAT transgenic mice that were generated by Vaisman et al (184), it was observed an accumulation of large apoE and apoA-I containing HDL particles and small HDL particles containing apoA-I/apoA-II probably due to the marked overexpression of LCAT.

$LCAT^{-/-}$ mice do no suffer from atherosclerosis but a subset of $LCAT^{-/-}$ mice accumulate lipoprotein X and develop proteinuria and glomerulosclerosis (183). LCAT deficiency in control,

apoE$^{-/-}$, LDLr$^{-/-}$ or CETP transgenic mouse background were protected from atherosclerosis. It was suggested that the protective effect of LCAT deficiency resulted from low levels of apoB-containing lipoproteins and the increased LDLr activity (183). In contrast, Furbee et al. showed that LCAT deficiency in the LDLr$^{-/-}$ or apoE$^{-/-}$ background enhanced atherosclerosis (188). In the latter study no change in the apoB lipoproteins was observed. The reason for the different observations in the two studies is not clear but it may be attributed to the different composition of the atherogenic diet (183;188).

Unexpectedly, the human LCAT transgenic mice are not protected from diet-induced atherosclerosis or have enhanced development of aortic lesions when LCAT is highly overexpressed (189;190) but not when LCAT is overexpressed at lower levels (191). In contrast, human LCAT transgenic rabbits have decreased apoB levels and are protected from atherosclerosis in response to atherogenic diet in normal but not in LDLr$^{-/-}$ background (192;193). Furthermore, adenovirus-mediated gene transfer of human LCAT in non-human primates increased HDL and decreased LDL thus generating a highly antiatherogenic lipid/lipoprotein profile (194).

The striking difference between LCAT transgenic mice and rabbits in atheroprotection can be explained by the absence of significant CETP activity in mice compared to rabbits and humans. CETP possibly modulates the remodeling of apoB-containing lipoproteins leading to efficient clearance from the plasma. The expression of CETP in LCAT transgenic mice appears to improve the HDL properties, increase the uptake of HDL by the liver and thus inhibit the development of atherosclerosis (195).

While atherosclerosis is not a major issue in LCAT deficiency, both FLD patients and LCAT KO mice under western diet are characterized by renal disease. Studies in these mice and

FLD patients show that lipoprotein X (LpX), a large molecular weight LDL which consists of FC-, PC-rich but triglyceride poor residues may be the possible cause of neuphropathy (183;196).

Despite the unclear role of LCAT in the development of cardiovascular disease a number of recent studies have shown promise for the use of LCAT as a pharmacological agent against atherosclerosis or FLD-induced renal disease. Infusion of human recombinant LCAT in $LCAT^{-/-}$ mice increased the HDL-C levels and cholesterol efflux and lowered the LpX levels which suggest a potential treatment for both cardiovascular disease as well as LCAT-deficiency-associated glomerulopathy (197). Adeno-associated AAV8-mediated gene transfer of human LCAT in heterozygous LDLr knock-out mice expressing CETP increased HDL and decrease LDL leading to a favorable lipid/lipoprotein profile (198). Adenoviral gene transfer and long term expression of apoA-I and LCAT in New Zealand rabbits fed an atherogenic diet promoted cholesterol removal from complex atherosclerotic lesions and reduced atherosclerosis (199). Intraperitoneal administration of a small molecule, named compound A, that activates LCAT in mice and hamsters fed an atherogenic diet resulted in increased HDL-C levels and decreased VLDL-C levels and enhanced the RCT (200). Finally, a phase 1 clinical trial has been completed by Alphacore Pharma LLc in order to evaluate the effects of intravenous infusion of recombinant human LCAT (ACP-501) in subjects with coronary artery disease (201). The results of these studies are expected soon.

1.11 Interactions of apoA-I with LCAT

The specific residues or the regions of LCAT that participate in the activation by apoA-I are unknown. Nevertheless, it is speculated that the Glutamic acid residues of the amphipathic

helix between residues 154-171 are involved in this interaction (202-204). Another study has examined the effect of FED mutations of LCAT which cause loss of α-LCAT activity only, possibly due to defective interactions with apoA-I. Mutations in the residues T123, N131, F382 and N391 of LCAT cause loss of α-LCAT activity and this makes them candidate residues that are involved in the interactions between apoA-I and LCAT (153). Furthermore, according to the 3D-model of the structure of LCAT, described previously, it has been suggested that LCAT mutations causing FLD are near the active site of LCAT while FED mutations are clustered in a different more hydrophilic side that may participate in the activation of LCAT by apoA-I (152;154).

Francone et al. studied the interactions of LCAT with apoA-II (185). When human apoA-I or apoA-I/apoA-II was co-expressed with LCAT in mice, the HDL-C and CE levels were much greater as compared to mice expressing LCAT alone. Co-expression of apoA-II with LCAT did not change the HDL levels indicating that apoA-I is the major activator of LCAT *in vivo*. Another study has shown that modification of the arginine, lysine and tryptophan residues by methylglyoxal changed the conformation of apoA-I which could no longer activate LCAT efficiently (205).

Extensive studies have also been made to identify the regions and residues of apoA-I that are responsible for LCAT activation. It has been proposed that residues R130 and K133 of apoA-I play an important role in the formation of an amphipathic presentation tunnel located between helices 5-5 of apoA-I in the double belt model of HDL. Such a tunnel could allow migration of the hydrophobic acyl chains of phospholipids and the amphipathic unesterified cholesterol from the bilayer to the active site of LCAT that contains sites for phospholipase activity and esterification activity (206). The esterification of the cholesterol converts the 3.67 residues per turn helices to an idealized 3.6 residues per turn helix (69).

Several naturally occurring apoA-I mutations that produce pathological phenotypes have been described (60;207;208). It has been estimated that structural mutations of apoA-I occur in 0.3% of the Japanese population and may affect the plasma HDL levels (209). Twenty-five apoA-I mutations are associated with low HDL levels and seventeen of these mutants reduce the capacity of apoA-I to activate LCAT (60;207). These mutations are clustered predominantly in or at the vicinity of helix 6 of apoA-I and some of them predispose to atherosclerosis (208;210-212). Below are described some representative mutations of this category that affect the biogenesis and maturation of HDL by disrupting LCAT activation.

Previous studies showed that hemizygotes (compound heterozygotes for an apoA-I null allele and an apoA-I(L141R)$_{Pisa}$ allele) had greatly decreased plasma apoA-I levels and near absence of HDL cholesterol. Plasma from hemizygotes contained preβ1-HDL and low concentration of small particles with alpha electrophoretic mobility (213). Heterozygotes for apoA-I(L141R)$_{Pisa}$ had approximately half-normal values for HDL cholesterol and plasma apoA-I (212;214). Three male hemizygote patients and one heterozygote patient developed coronary stenosis (212).

Other studies also showed that heterozygotes for apoA-I(L159R)$_{FIN}$ mutation had greatly reduced plasma levels of HDL cholesterol and apoA-I (215), that was mainly distributed in the HDL3 region and had abnormal electrophoretic mobility (208;216). They also had small size (8-9 nm) HDL particles and decreased plasma and HDL cholesteryl ester levels (208;216). Human HDL containing apoA-I(L159R)$_{FIN}$ had increased fractional catabolic rate compared to normal HDL, indicating increased catabolism of the mutant apoA-I protein (208;215). Only one affected patient with this mutation had clinically manifested atherosclerosis (208).

To explain the etiology and potential therapy of genetically determined low levels of HDL resulting from natural apoA-I mutations, the *in vitro* and *in vivo* properties of two naturally occurring mutants, the apoA-I[L141A]$_{Pisa}$ and apoA-I[L159R]$_{FIN}$ have been studied in our laboratory. *In vitro* studies showed that both mutants were secreted efficiently from cells, had normal ability to promote ABCA1-mediated cholesterol efflux but greatly diminished capacity to activate LCAT (0.4-2% of WT apoA-I). Adenovirus-mediated gene transfer showed that compared to WT apoA-I, expression of either of the two mutants in apoA-I$^{-/-}$ mice greatly decreased total plasma cholesterol and apoA-I levels as well as the CE/TC ratio compared to WT apoA-I (Table 1.II). Another change that was associated with differences between the WT apoA-I and either of the two mutants was the greatly decreased HDL cholesterol peak as determined by FPLC fractionation of the plasma (Figure 1.10 A). Density gradient ultracentrifugation of plasma showed great reduction of the amount of apoA-I that floated in the HDL region of the apoA-I[L141A]$_{Pisa}$ mutant as compared to WT apoA-I (Figures 1.10 C, F). EM analysis of the HDL fractions obtained by density gradient ultracentrifugation showed the presence of large number of spherical HDL for WT apoA-I but only a few spherical HDL particles for the apoA-I[L141A]$_{Pisa}$ mutant (Figures 1.10 D, G). Two-dimensional gel electrophoresis of the plasma showed the formation of small amount of preβ HDL and large amount of α1, α2, α3, α4 HDL subpopulations for the WT apoA-I and only preβ and small size α4-HDL subpopulations for the apoA-I[L141A]$_{Pisa}$ mutant (Figure 1.10 E, H). Similar results were observed for apoA-I[L159R]$_{FIN}$ (217).

Co-infection of apoA-I$^{-/-}$ mice with adenoviruses expressing either of the two mutants and human LCAT normalized the plasma apoA-I, the total plasma cholesterol levels and the

CE/TC ratio (Table 1.II), increased the HDL cholesterol peak (Figure 1.10 A) and the amount of apoA-I that floated in the HDL region (Figure 1.10 I). It also generated large amount of spherical HDL (Figure 1.10 J) and restored the normal preβ- and α-HDL subpopulations (Figure 1.10 K). Similar results were observed for apoA-I[L159R]$_{FIN}$ (217).

Another interesting naturally occurring apoA-I mutation is the apoA-I[R160L]$_{Oslo}$. Previous studies showed that heterozygotes of apoA-I[R160L]$_{Oslo}$ have approximately 60% and 70% of normal HDL and apoA-I levels respectively, form preβ1 and small size α-HDL particles and have a 30% reduction in their plasma LCAT activity (218). Gene transfer of the apoA-I[R160L]$_{Oslo}$ mutant in apoA-I-/- mice produced an aberrant HDL phenotype characterized by decreased total plasma cholesterol and apoA-I levels (Table 1.II) and decrease in the HDL cholesterol peak as determined by FPLC (Figure 1.10 B) (219). Density gradient ultracentrifugation of plasma followed by SDS-PAGE analysis of the resulting fractions showed that compared to WT apoA-I, the amount of apoA-I that floats in the HDL3 and HDL2 region was decreased (Figure 1.10 L). Electron microscopy of HDL obtained from mice expressing the apoA-I[R160L]$_{Oslo}$ mutant showed the presence of a mixture of discoidal and spherical HDL particles (Figure 1.10 M) and two-dimensional gel electrophoresis of plasma showed the presence of preβ1 and α4-HDL subpopulations (Figure 1.10 N) (219). Co-expression of the apoA-I[R160L]$_{Oslo}$ mutant and human LCAT increased plasma cholesterol and apoA-I levels, increased the CE/TC ratio of HDL as well as the HDL cholesterol peak (Table 1.II & Figure 1.10 B). It also increased the amount of apoA-I that floats in the HDL region (Figure 1.10 O) promoted the formation of spherical HDL particles (Figure 1.10 P) and restored the formation normal preβ and α-HDL subpopulations of larger size (Figure 1.10 Q) (219).

A similar phenotype produced by expressing the apoA-I[R160V/H162A] mutant in apoA-$I^{-/-}$ mice (220). This double mutation resulted in diminished HDL cholesterol peak, decreased amount of apoA-I that floated in the HDL region as well as a shift of the apoA-I towards the HDL3 region. The mutant apoA-I formed predominantly discoidal particles that had preβ and α4-HDL electrophoretic mobility. The low plasma apoA-I levels associated with this mutant and the abnormal HDL phenotype was completely corrected by co-expession of this mutant and human LCAT (220). The apoA-I[R160V/H162A] mutations also inhibited SR-BI mediated cholesterol efflux and are discussed in a later section.

Similar but not identical phenotypes were obtained by the bioengineered mutations apoA-I[R149A] and the naturally occurring mutations apoA-$I[R151C]_{Paris}$ (219) and apoA-$I[L144R]_{Zaragosa}$ (62). The last two mutations have not been associated with incidence of atherosclerosis in humans.

The apoA-I mutations discussed here offer a valuable tool to dissect the molecular events which lead to the biogenesis of HDL and possibly to understand the types of molecular interactions between apoA-I and LCAT which lead to the activation of the enzyme.

In our case residues R149, R153 and R160 were reported to create a positive electrostatic potential around apoA-I. Mutations in these residues reduced drastically the ability of rHDL particles containing these apoA-I mutants to activate LCAT *in vitro* (221). Based on the "belt" model for discoidal rHDL, these residues are located on the hydrophilic face of the apoA-I helices and do not form intramolecular salt bridges in the antiparallel apoA-I dimer that covers the fatty acyl chain of the discoidal particle. This arrangement allows in principle these apoA-I

residues to form salt bridges or hydrogen bonds with appropriate residues of LCAT and thus contribute to LCAT activation.

Table 1.II: Plasma lipids and hepatic mRNA levels of apoA-I$^{-/-}$ mice expressing WT and the mutant forms of apoA-I in the presence and absence of LCAT as indicated.

Protein Expressed	Cholesterol (mg/dl)	CE/TC	Triglycerides (mg/dl)	Relative ApoA-I mRNA (%)	ApoA-I Protein (mg/dl)
apoA-I WT	148 ± 11	0.78±0.01	63 ± 1	100 ± 32	186 ± 34
apoA-I $(L141R)_{Pisa}$	23 ± 0.4	0.44±0.03	11 ± 2.8	88 ± 9	17 ± 4
apoA-I $(L141R)_{Pisa}$ + LCAT	184±53	0.68±0.01	41±0.3	91±2	224±7
apoA-I $(L159R)_{FIN}$	16±5	0.13±0.04	25±4	216±32	25±9
apoA-I $(L159R)_{FIN}$ + LCAT	224±22	0.73±0.01	53±15	63±9	190±20
apoA-I $(R159L)_{Oslo}$	43±13	0.23±0.01	36±4	117±30	66±31
apoA-I $(R160L)_{Oslo}$ + LCAT	250±47	0.082±0.01	62±11	60±1	127±26

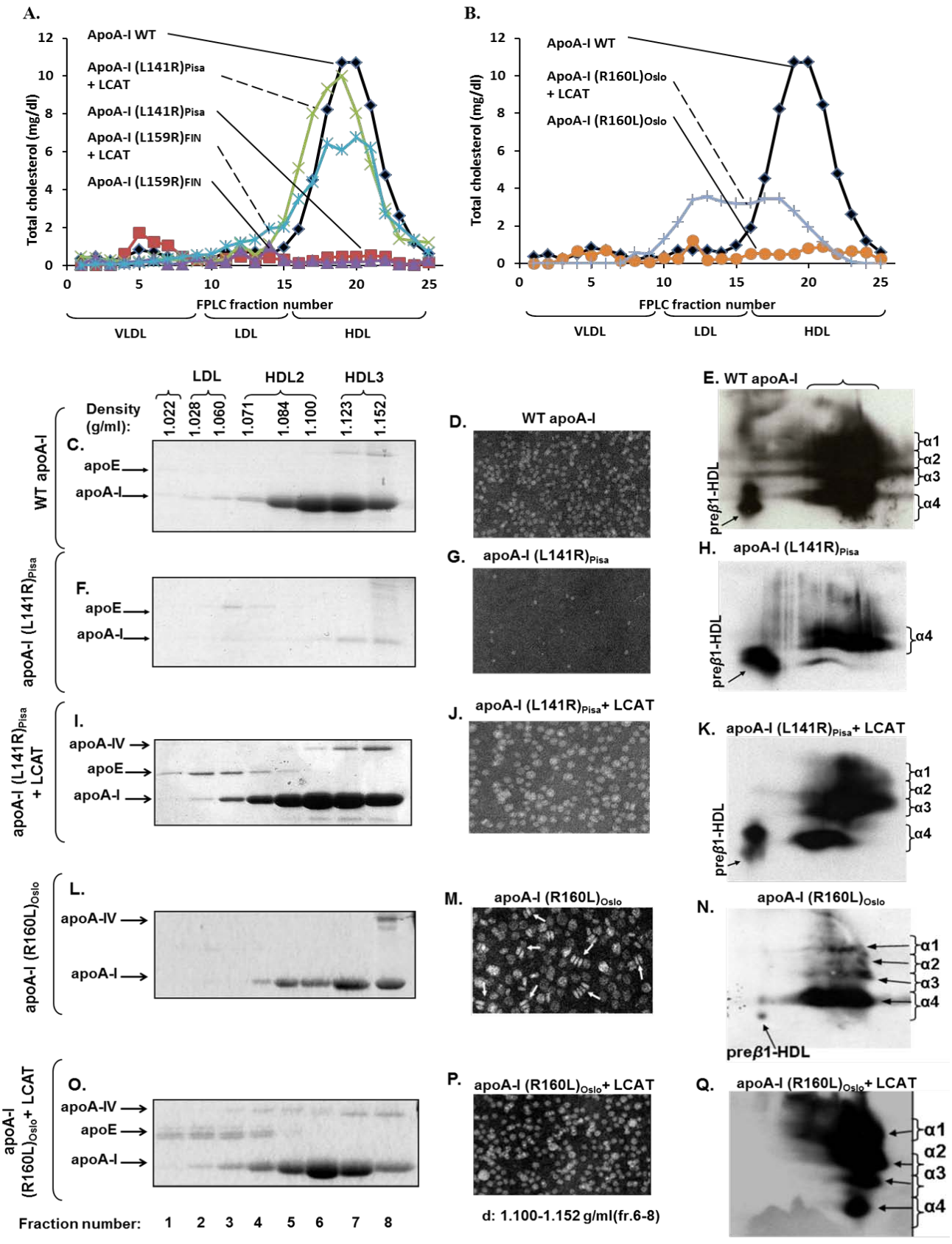
A.
ApoA-I WT
ApoA-I (L141R)Pisa + LCAT
ApoA-I (L141R)Pisa
ApoA-I (L159R)FIN + LCAT
ApoA-I (L159R)FIN
Total cholesterol (mg/dl)
FPLC fraction number
VLDL
LDL
HDL
B.
ApoA-I WT
ApoA-I (R160L)Oslo + LCAT
ApoA-I (R160L)Oslo
Total cholesterol (mg/dl)
FPLC fraction number
VLDL
LDL
HDL
LDL
HDL2
HDL3
Density (g/ml):
1.022
1.028
1.060
1.071
1.084
1.100
1.123
1.152
WT apoA-I
C.
apoE
apoA-I
apoA-I (L141R)Pisa
F.
apoE
apoA-I
apoA-I (L141R)Pisa + LCAT
I.
apoA-IV
apoE
apoA-I
apoA-I (R160L)Oslo
L.
apoA-IV
apoA-I
apoA-I (R160L)Oslo + LCAT
O.
apoA-IV
apoE
apoA-I
Fraction number: 1 2 3 4 5 6 7 8
D.
WT apoA-I
G.
apoA-I (L141R)Pisa
J.
apoA-I (L141R)Pisa + LCAT
M.
apoA-I (R160L)Oslo
P.
apoA-I (R160L)Oslo + LCAT
d: 1.100-1.152 g/ml(fr.6-8)
E. WT apoA-I
preβ1-HDL
α1
α2
α3
α4
H.
apoA-I (L141R)Pisa
preβ1-HDL
α4
K.
apoA-I (L141R)Pisa + LCAT
preβ1-HDL
α1
α2
α3
α4
N.
apoA-I (R160L)Oslo
α1
α2
α3
α4
preβ1-HDL
Q.
apoA-I (R160L)Oslo + LCAT
α1
α2
α3
α4

Figure 1.10 (A-Q): The effect of apoA-I[L141]$_{Pisa}$ and the apoA-I[L159R]$_{FIN}$ mutations on the biogenesis of HDL. Plasma FPLC profiles of apoA-I$^{-/-}$ mice expressing WT apoA-I or the apoA-I[L141]$_{Pisa}$ or the apoA-I[L159R]$_{FIN}$ mutant alone or in combination with LCAT as indicated (A). Plasma FPLC profiles of apoA-I$^{-/-}$ mice expressing WT apoA-I or the apoA-I[R160L]$_{Oslo}$ mutant alone or in combination with LCAT as indicated (B). Analysis of plasma of apoA-I$^{-/-}$ mice infected with adenoviruses expressing the WT apoA-I or the apoA-I[L141]$_{Pisa}$ or the apoA-I[R160L]$_{Oslo}$ mutants alone or in combination with human LCAT by density gradient ultracentrifugation and SDS-PAGE (C, F, I, L, O) as indicated. EM analysis of HDL fractions 6-7 obtained from apoA-I$^{-/-}$ mice expressing the WT apoA-I or the apoA-I[L141]$_{Pisa}$ or the apoA-I[R160L]$_{Oslo}$ mutants alone or in combination with human LCAT, following density gradient ultracentrifugation of plasma, as indicated (D, G, J, M, P). Two dimensional gel electrophoresis of plasma of apoA-I$^{-/-}$ mice infected with adenoviruses expressing WT apoA-I or the apoA-I[L141]$_{Pisa}$ or the apoA-I[R160L]$_{Oslo}$ mutants alone or in combination with human LCAT, as indicated (E, H, K, N, Q).

To explain the low HDL levels and the abnormal HDL phenotype of the apoA-I$^{-/-}$ mice expressing the apoA-I(L141R)$_{Pisa}$, we analyzed the relative abundance of the endogenous mouse LCAT following gene transfer of the apoA-I(L141R)$_{Pisa}$ mutant alone or in the presence of LCAT. This analysis showed a dramatic increase of the mouse LCAT in mice expressing the apoA-I(L141R)$_{Pisa}$ mutant as compared to mice expressing the WT apoA-I. Co-infection of apoA-I$^{-/-}$ mice with the apoA-I(L141R)$_{Pisa}$ mutant and human LCAT restored the mouse LCAT to normal levels (those observed in the presence of WT apoA-I) (Figure 1.11 A). The depletion of the endogenous LCAT in mice expressing the mutant forms of apoA-I could be the result of rapid

degradation of endogenous mouse LCAT bound to minimally lipidated apoA-I mutants possibly by the kidney.

The ability of the apoA-I[L141R]$_{Pisa}$ and apoA-I(L159R)$_{FIN}$ mutants to be secreted efficiently from cells and to promote ABCA1-mediated cholesterol efflux suggests that the functional interactions between apoA-I and ABCA1 that lead to the lipidation of apoA-I are normal and the low apoA-I and HDL levels caused by these two mutants are the result of fast removal of the lipidated nascent HDL particles from the plasma compartment. This interpretation is supported by the increased catabolic rate of HDL containing apoA-I(L159R)$_{FIN}$ (208) and the accumulation of proapoA-I in the plasma of hemizygotes for apoA-I(L141R)$_{Pisa}$ (212). Accumulation of proapoA-I has been previously observed in patients with Tangier disease (222) that are characterized by increased catabolic rate of HDL (123). It has been also shown previously that cubulin, a 600 KDa membrane protein, binds both apoA-I and HDL and promotes their catabolism by the kidney (223;224).

Previous studies showed that preβ-HDL is an efficient substrate of LCAT (176). In the presence of excess LCAT, the esterification of the cholesterol of the newly formed preβ-particles appears to prevent their fast catabolism and allows them to proceed in the formation of discoidal and spherical HDL. In the case of the apoA-I[R160L]$_{Oslo}$, the HDL pathway appears to be inhibited in the step of the conversion of the discoidal to spherical HDL particles. Figures 1.11 B-D depicts the normal pathway of the biogenesis of HDL (B) and the disruption of this pathway by the apoA-I(L141R)$_{Pisa}$ and apoA-I(L159R)$_{FIN}$ (C) and apoA-I[R160L]$_{Oslo}$ mutants (D).

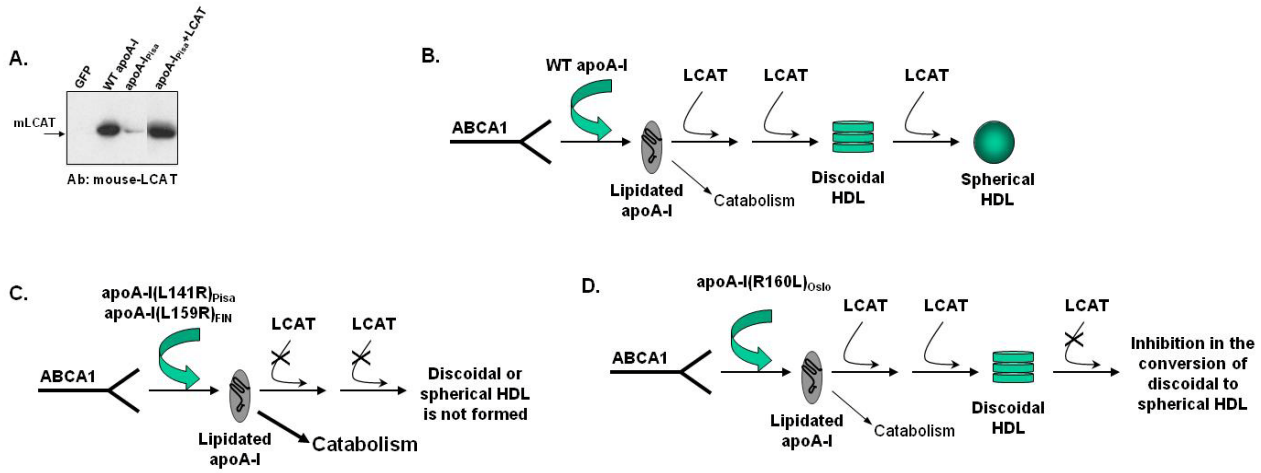

Figure 1.11 (A-D). Western blot analysis of plasma from apoA-I$^{-/-}$ mice infected with adenoviruses expressing either the control protein, GFP, or the WT apoA-I or the apoA-I(L141R)$_{Pisa}$ alone or in combination with human LCAT, as indicated at the top of the figure (A). Schematic representation showing the pathway of biogenesis of HDL (B) and how the apoA-I(L141R)$_{Pisa}$ and apoA-I(L159R)$_{FIN}$ mutants affect the esterification of cholesterol of the pre-HDL particles and prevent their conversion to discoidal and spherical HDL, thus promoting their catabolism (C). Schematic representation showing the inability of the apoA-I(R160L)$_{Oslo}$ mutant to convert the discoidal to spherical HDL particles (D).

Apart from the central region of apoA-I there are also a C-terminal and an N-terminal domain that may participate in LCAT activation. Adenovirus mediated gene transfer in apoA-I$^{-/-}$ mice of specific apoA-I mutants showed that the substitution of the hydrophobic residues in the 211-229 region of apoA-I with either charged or less bulky hydrophobic residues resulted in low HDL levels and formation of discoidal HDL (109). In contrast, substitution of charged residues E234, E235, K238 and K239 with Alanines led to formation of normal HDL (109). Impairment of LCAT activation and accumulation of discoidal HDL have also been

observed following gene transfer experiments with mutants of apoA-I that lack the N-terminal 7-65 or 89-99 regions (225;226).

1.12 ApoA-I mutations causing dyslipidemia

A series of apoA-I mutations, shown in Figure 1.12 A, resulted in severe hypertriglyceridemia (110;226). The most recently studied case was apoA-I[D89A/E91A/E92A] mutant where the charged residues were substituted by Alanines. The capacity of the apoA-I[D89A/E91A/E92A] mutant to promote ABCA1-mediated cholesterol efflux and activate LCAT *in vitro* was approximately 2/3 of that of WT apoA-I (227).

In vivo studies using adenovirus-mediated gene transfer in apoA-I deficient mice showed that compared to WT apoA-I, the apoA-I[D89A/E91A/E92A] mutant increased plasma cholesterol, reduced the CE/TC ratio and caused severe hypertriglyceridemia (Table 1.III) (227). The HDL cholesterol peak was greatly reduced as determined by FPLC fractionation of plasma and most of the cholesterol was distributed predominantly in the VLDL/IDL/LDL region (Figure 1.12 B). The triglycerides were distributed in the VLDL/IDL region. Following density gradient ultracentrifugation of plasma, approximately 40% of the apoA-I mutant was distributed in VLDL/IDL region, in contrast to the WT apoA-I that was distributed in the HDL2/HDL3 region (Figure 1.12 C,F). The WT apoA-I formed spherical HDL whereas the apoA-I[D89A/E91A/E92A] mutant formed mostly spherical and few discoidal HDL particles as determined by EM (Figures 1.12 D,G). Two-dimensional gel electrophoresis showed that WT apoA-I formed normal preβ and α-HDL subpopulations whereas the apoA-I[D89A/E91A/E92A] mutants formed and α4-HDL subpopulations (Figure 1.12 E,H) (227).

Co-expression of apoA-I[D89A/E91A/E92A] mutants and human lipoprotein lipase in apoA-I deficient mice abolished hypertriglyceridemia (Table 1.III), redistributed apoA-I in the HDL2/HDL3 regions (Figure 1.12 I), restored in part the α1,2,3,4 HDL subpopulations (Figure 1.12 K), but did not change significantly the cholesterol ester to total cholesterol ratio (Table 1.III) or the formation of discoidal HDL particles (Figure 1.12 J) (227).

The findings indicate that residues D89, E91 and E92 of apoA-I are important for plasma cholesterol and triglyceride homeostasis as well as for the maturation of HDL.

The lipid, lipoprotein and HDL profiles generated by another mutant, in the vicinity of the residues D89, E91 and E92, where residues K94 and K96 were changed to Alanines were similar to those of WT apoA-I indicating that the observed changes on the HDL phenotype were unique for the charged residues D89, E91 and E92 (227). Expression of a deletion mutant, apoA-I[Δ89-99], in apoA-I deficient mice, increased plasma cholesterol levels, increased the plasma preβ HDL subpopulation, generated discoidal HDL particles but did not induce hypertriglyceridemia (226).

The apoA-I[D89A/E91A/E92A] mutant has two similar characteristics with two other mutants in different regions of apoA-I, the apoA-I[Δ(61-78)] and the apoA-I [E110A/E111A] (110;226) (Table 1.III). The first characteristic is that all three mutants caused accumulation of apoA-I in the VLDL/IDL region. As shown previously, the accumulation of apoA-I in the lower densities affects the *in vitro* lipolysis of the VLDL/IDL fraction by exogenous lipoprotein lipase (110;226). The second characteristic is that the three apoA-I mutants have lost negative charged residues that are present in the WT sequence. The E78, D89 and E111 residues have the ability to form solvent inaccessible salt bridges with positively charged residues present in

the antiparallel apoA-I molecule of a discoidal HDL particle (70) (Figure 1.12 L).

In these arrangements of the apoA-I molecules on the sHDL particle residues E78 in helix 2, D89 in helix 3 and E111 in helix 4, can form solvent inaccessible salt bridges with residues R188 in helix 8, R177 in helix 7 and H155 in helix 6 respectively of the antiparallel strand. The affinity of all three mutants for triglyceride rich lipoprotein particles is further supported by binding studies to triglyceride-rich emulsion particles (228).

It is interesting that in the 11/3 α-helical wheel residues E78, D89 and E111 are all located in wheel position 2. With the exception of R188 all other five residues involved in salt bridges are conserved in mammals.

The lipid and lipoprotein abnormalities observed in this mutant suggest that the increased abundance of apoA-I in the VLDL/IDL region may create lipoprotein lipase insufficiency that is responsible for the induction of hypertriglyceridemia.

The persistence of discoidal particle following the lipoprotein lipase treatment indicates a direct effect of the [D89A/E91A/E92A] mutation in the activation of LCAT *in vivo*. Previous studies showed that discoidal and small size HDL particles and LCAT associated with them may be catabolized fast by the kidney and thus lead to LCAT insufficiency and reduced plasma HDL levels (124;215;217).

It is conceivable that loosening of the structure of apoA-I around the D89 or E92 area due to the substitution of the original residues by Alanines (A), may provide new surfaces for interaction of HDL with other proteins or lipoprotein particles such as VLDL in ways that inhibit triglyceride hydrolysis. Furthermore, the accumulation of discoidal HDL as well as the formation

of preβ and small α4-HDL particles as shown by the *in vivo* experiments indicates that replacement of D89, E91 and E92 by A has a direct impact on the activation of LCAT.

Table 1.III: Plasma lipids and hepatic mRNA levels of apoA-I$^{-/-}$ mice expressing WT and the mutant forms of apoA-I as indicated.

Protein expressed	Cholesterol (mg/dL)	CE/TC	Triglycerides (mg/dL)	Relative apoA-I mRNA (%)	Plasma apoA-I (mg/dL)
apoA-I$^{-/-}$	33±6	-	42±7	-	-
WT apoA-I	268±55	0.72±0.06	70±11	100±32	283±84
apoA-I [D89A/E91A/E92A]	497±139	0.36±0.31	2106±1629	101±24	235±106
apoA-I [D89A/E91A/ E92A] + hLPL	122±56	0.44±0.14	49±16	41±6	99±18
apoA-I [Δ(62-78)]	220±16	-	986±289	130±5	265±36
apoA-I [E110A/E111A]	520±45	-	1510±590	69±23	204±27

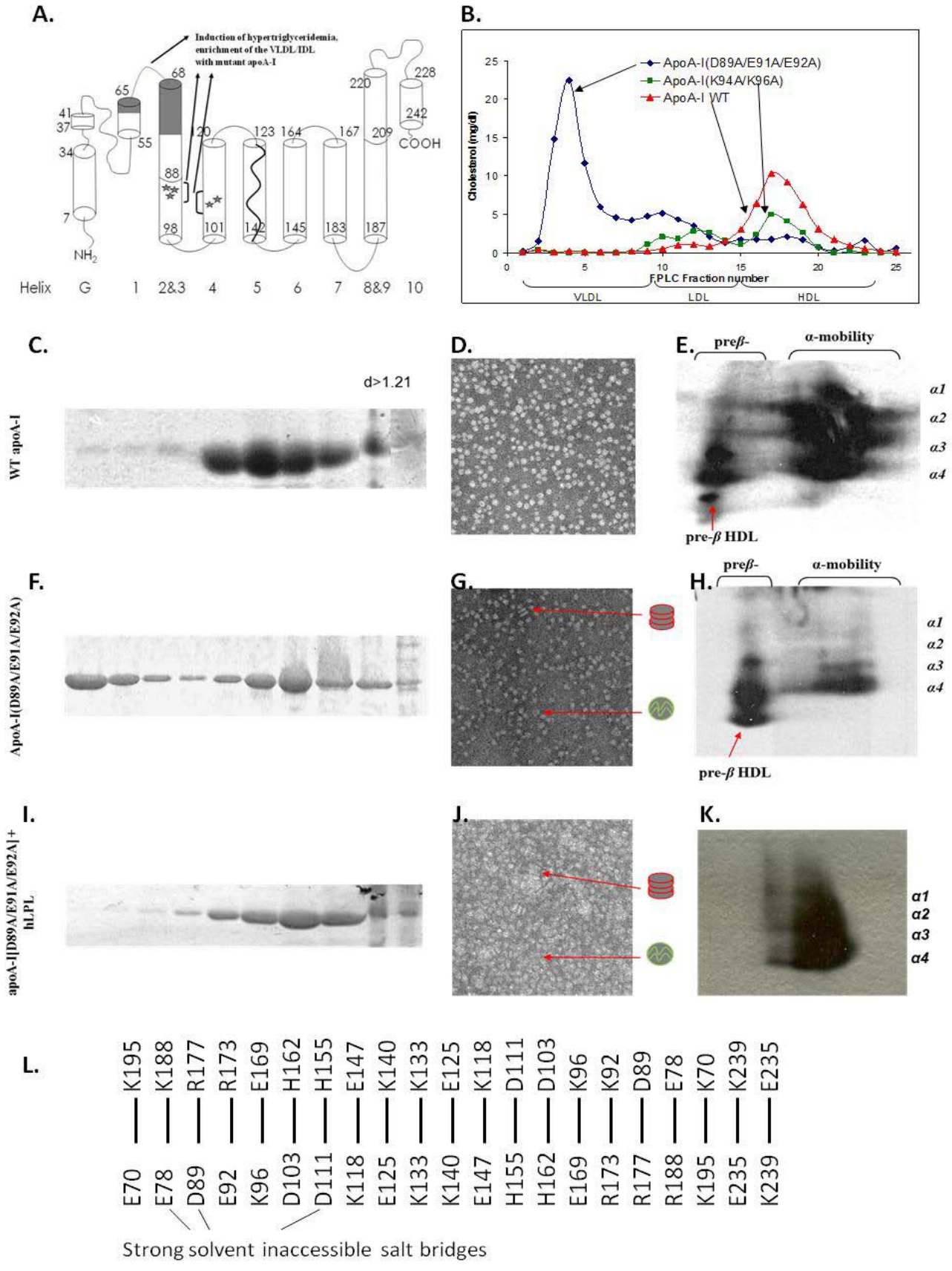
A.
Induction of hypertriglyceridemia, enrichment of the VLDL/IDL with mutant apoA-I
41
37
34
7
NH2
65
55
68
88
98
120
101
123
142
164
145
167
183
209
187
220
228
242
COOH
Helix G 1 2&3 4 5 6 7 8&9 10
B.
ApoA-I(D89A/E91A/E92A)
ApoA-I(K94A/K96A)
ApoA-I WT
Cholesterol (mg/dl)
FPLC Fraction number
VLDL
LDL
HDL
C.
d>1.21
WT apoA-I
D.
E.
preβ-
α-mobility
α1
α2
α3
α4
pre-β HDL
F.
ApoA-I(D89A/E91A/E92A)
G.
H.
preβ-
α-mobility
α1
α2
α3
α4
pre-β HDL
I.
apoA-I[D89A/E91A/E92A]+ hLPL
J.
K.
α1
α2
α3
α4
L.
K195 — E70
K188 — E78
R177 — D89
R173 — E92
E169 — K96
H162 — D103
H155 — D111
E147 — K118
K140 — E125
K133 — K133
E125 — K140
K118 — E147
D111 — H155
D103 — H162
K96 — E169
K92 — R173
D89 — R177
E78 — R188
K70 — K195
K239 — E235
E235 — K239
Strong solvent inaccessible salt bridges

Figure 1.12 (A-L). Effects of apoA-I mutations on the induction of dyslipidemia. Location of the apoA-I mutations that cause hypertriglyceridemia as indicated. The model of the secondary structure of apoA-I is based on references (66;83;229) (A). Plasma FPLC profiles of apoA-I$^{-/-}$ mice expressing WT apoA-I or the apoA-I[D89A/E91A/E92A] or the apoA-I[K94A/K96A] mutant as indicated (B). Analysis of plasma of apoA-I$^{-/-}$ mice infected with adenoviruses expressing the WT apoA-I or the apoA-I[D89A/E91A/E92A] mutant alone or in combination with human LPL, as indicated, by density gradient ultracentrifugation and SDS-PAGE (C, F, I). EM analysis of HDL fractions 6-7 obtained from apoA-I$^{-/-}$ mice expressing the WT apoA-I or the apoA-I[D89A/E91A/E92A] mutant alone or in combination with LPL, as indicated, following density gradient ultracentrifugation of plasma (D, G, J). Two dimensional gel electrophoresis of plasma of apoA-I$^{-/-}$ mice infected with adenoviruses expressing WT apoA-I or the apoA-I[D89A/E91A/E92A] mutant alone or in combination with LPL, as indicated (E, H, K). Schematic representation of the solvent inaccessible interhelical charged interactions of apoA-I dimers arranged in an antiparallel orientation in the belt model of rHDL (L).

1.13 ApoE: Genetics, Biosynthesis, Structure and functions

Apolipoprotein E (ApoE), initially known as Arginine-rich apolipoprotein was identified as a component of triglyceride-rich lipoproteins (230). Subsequent studies showed that it plays a crucial role in the clearance of lipoprotein remnants from the circulation by interacting with the LDL receptor (231-233). ApoE is also a minor component of HDL (3).

The apoE gene is located on human chromosome 9 at the gene locus 19q13.2, spans in about 3.6 kbp and encodes for a 35 kDa, 299 amino acid protein (234). It is expressed predominantly in the liver but also in other tissues such as the brain, adrenal glands, testis, spleen, kidney as well as the macrophages (13).

In humans there have been detected three major alleles, ε2 (cys112, cys158), ε3 (cys112, arg158), and ε4 (arg112, arg158) (235). The apoE alleles give rise to three homozygous (E2/E2, E3/E3, E4/E4) apoE phenotypes (235;236).The most common allele is ε3 which is found in about the 78.6% of the population (237). The ε4 allele is found in the 13.4% and ε2 is found in the 7.5% of the population (237). As explained later the apoE2, apoE4 isoforms as well as specific mutations of apoE are associated with various diseases (238;239).

The apoE has two major structural domains separated by a hinge (240) and similarly to apoA-I contains amphipathic helices that allow its association with lipids and the formation of lipoproteins (241). The N-terminal domain (amino acids 1–191) contains the receptor binding region (amino acids 134–150 and Arg-172) (242;243) and forms a four-helix antiparallel bundle (241;242). Based on computer modelling, the C-terminal domain (amino acids 225–299) consists of 3 amphipathic helices and contains domains (amino acids 244–272) that contribute to binding of lipids and lipoproteins (242;244;245). Based on a 10 Å crystal structure of apoE bound to dipalmitoylphosphatidylcholine (DMPC) and biochemical evidence, it has been proposed that two molecules of apoE folds into an α-helical hairpin like structure (246). In the apex of the structure is the receptor binding domain that allows its interaction with the LDL receptor.

1.14 Recessive and dominat forms of type III hyperlipoproteinemia

Type III hyperlipoproteinemia (type III HPL) is a genetic disorder characterized by increased plasma cholesterol, triglycerides and apoE levels, accumulation of remnant lipoproteins, xanthomas and premature atherosclerosis (1;247).

The great majority of the patients with type III HLP have the E2/2 phenotype (247) which results from the substitution of Cys for Arg-158 (247). This mutation combined with other genetic or environmental factors affects the catabolism of apoE containing lipoproteins and results in the accumulation in plasma of remnants of lipoprotein metabolism enriched in cholesteryl esters and apoE (248;249).

The form of type III HLP that is associated with the E2/2 phenotype is inherited in an autosomal recessive mode (238). A variety of rare apoE mutations have also been described that are associated with a dominant mode of inheritance of type III HLP which is expressed at an early age. These include the substitutions Arg-136→Glu, Arg-142→Cys, Arg-142→Leu, Arg-145→Cys, Lys-146→Gln, Lys-146→Glu, Lys-146→Asn, Arg-147→Trp and an insertion of seven amino acids (duplication of residues 121-127) (1;238). Most of the apoE mutations which are associated with dominant forms of type III HLP are between residues 136 to 152. The importance of the 136 to 152 region of apoE for receptor binding was also assessed by *in vitro* mutagenesis (1;250;251). Receptor binding and competition experiments showed that some apoE mutants within the 136 to 152 region had 10 to 50% of the normal receptor binding activity (250-254). It is noteworthy that the receptor binding defect *in vitro* does not correlate with the severity of dyslipidemia, and can be influenced by other secondary factors (250-254). In addition, the degree of penetrance varies depending on the mutation (238). It has been suggested that other factors such as the natural apoE polymorphism which affects the distribution of apoE to different lipoprotein classes (255;256) or interaction of apoE with heparan sulfate proteoglycans (257) may affect the severity of dyslipidemia in these patients (238).

1.15 The role of apoE in lipid homeostasis and atherosclerosis

The importance of apoE in lipid homeostasis is evident in human and mice deficient in apoE or with increased apoE levels in plasma (3). Subjects, who carry loss-of-function mutations in apoE, are characterized by very high cholesterol levels in the circulation (258). Similarly, $apoE^{-/-}$ mice have very high total cholesterol levels and accumulate chylomicron and VLDL remnants (233). Overexpression of apoE in mice result in hypertriglyceridemia (12;259) and the plasma apoE levels correlate with the extend of hypertriglyceridemia (231). The hypertriglyceridemia induced by the apoE overexpression has been attributed to inhibition of LPL (260;261) as well as the stimulation of the secretion of hepatic triglycerides in the VLDL (262). The hyperlipoproteinemia, induced by the overexpression of apoE, was prevented by truncation of the C-terminus of apoE (263;264). Furthermore, mutations of the hydrophobic residues between amino acids 261-265 of apoE into Alanines prevented hypertriglyceridemia (265;266). These studies clearly show that apoE is very important for both the cholesterol and triglyceride homeostasis. Overall, at low levels apoE clears lipoprotein remnants and does not affect plasma triglycerides, whereas at high levels induces hypertriglyceridemia (12;259).

The $apoE^{-/-}$ mice on normal diet spontaneously develop atherosclerosis at age 8-10 weeks (233;267). As described later, subjects with apoE mutations causing type III HPL are also susceptible to atherosclerosis (268). Adenovirus- or helper dependent adenovirus-mediated gene transfer of apoE prevented or reduced significantly the progression of atherosclerosis (269-271). Similarly, apoE transgenic mice expressing low levels of apoE are also protected from atherosclerosis (272). Mice lacking macrophage apoE have increased atherosclerosis when fed

an atherogenic diet (273) whereas expression of apoE in macrophages confers atheroprotection to mice without correction of the plasma cholesterol levels (274). Additional bone marrow transplantation experiments have shown reduction of atherosclerosis when apoE$^{-/-}$ mice received bone marrow from normal mice (275) but increase atherosclerosis when normal mice receive bone marrow from apoE$^{-/-}$ mice (276).

1.16 The role of apoE in Alzheimer's disease

Epidemiological, genetic and biochemical data have linked the ε4 allele to familial late-onset Alzheimer's disease (AD) (277). ApoE binds to Aβ and is found in amyloid plaques (278;279). Overexpression of apoE4 in AD-prone mice results in greater plaque deposition and increased oligomeric Aβ formation as compared to mice overexpressing apoE3 or apoE2 (280-282). Furthermore, apoE4 cannot facilitate Aβ trafficking and degradation as efficiently as apoE3 (283) and is associated with increased susceptibility to inflammation as compared to apoE and apoE2 (284), both of which may explained the increased risk for AD in the presence of the ε4 allele.

ApoE-deficient mice do not form mature amyloid, indicating that lipid-free apoE participates in amyloid deposition (285-288). It appears that this is the reason that ABCA1$^{-/-}$ deficiency increases Aβ deposits in the brain parenchyma and/or the vasculature of APP-over-expressing mice despite the low apoE levels (289-291). This indicates that poorly lipidated apoE may be recruited to amyloid plaques (278;292) or is unable to clear amyloid deposits. In this regard removal of Aβ from brain slices of mice that express ABCA1 requires apoE synthesis by astrocytes (293). The fact that delipidated apoE is a poor ligand for the LDL receptor and LRP

(294;295), it is possible that receptor-mediated Aβ clearance will require formation of apoE-containing HDL via the HDL biosynthesis pathway.

1.17 Formation of apoE- and apoA-IV containing HDL

As mentioned previously, apoE is also a minor components of HDL (3). Using adenovirus-mediated gene transfer in apoA-I$^{-/-}$ or ABCA1$^{-/-}$ mice, we obtained unequivocal evidence that apoE of any phenotype participates in the biogenesis of apoE-containing HDL particles (HDL-E) using a similar pathway that is used for the biogenesis of apoA-I containing HDL particles (17). In the initial experiments gene transfer of an apoE4-expressing adenovirus increased both HDL and the triglyceride-rich VLDL/IDL/LDL fraction and generated discoidal HDL particles (compare Figure 1.13 A with Figure 1. 13 B). Control experiments showed the absence of discoidal or spherical HDL size particles in the plasma of apoA-I deficient mice (Figure 1. 13 B). Co-infection of apoA-I$^{-/-}$ mice with a mixture of adenoviruses expressing both apoE4 and human LCAT converted the discoidal to spherical HDL (Figure 1. 13 C), suggesting that LCAT is essential for the maturation of the discoidal apoE-containing HDL to spherical particles (17). The LCAT treatment also cleared the triglyceride-rich lipoproteins and increased the HDL cholesterol peak as determined by FPLC (Figure 1. 13 D). The involvement of ABCA1 was established by gene transfer of apoE in ABCA1$^{-/-}$ mice prior to and after treatment with apoE4 indicated that apoE4 could not promote formation of HDL particles in ABCA1$^{-/-}$ mice (Figure 1. 13 E, F). Other experiments in apoA-I$^{-/-}$ x apoE$^{-/-}$ mice established that residues 1-202 of apoE are sufficient to promote biogenesis of apoE containing HDL (296).

These findings suggest that in contrast to apoA-I where the C-terminal domain is required for the biogenesis of HDL (125), the carboxy-terminal domain of apoE is not required for HDL formation. Overall, the findings indicate that apoE has a dual functionality. In addition to its documented role in the clearance of triglyceride-rich lipoproteins, it participates in the biogenesis of HDL-E in a process that is similar to that of apoA-I.

HDL-E thus formed may have antioxidant and anti-inflammatory functions similar to those described for apoA-I-containing HDL, which may contribute to the atheroprotective properties of apoE (232;233;297;298). ApoE-containing HDL may also have important biological functions in the brain (299).

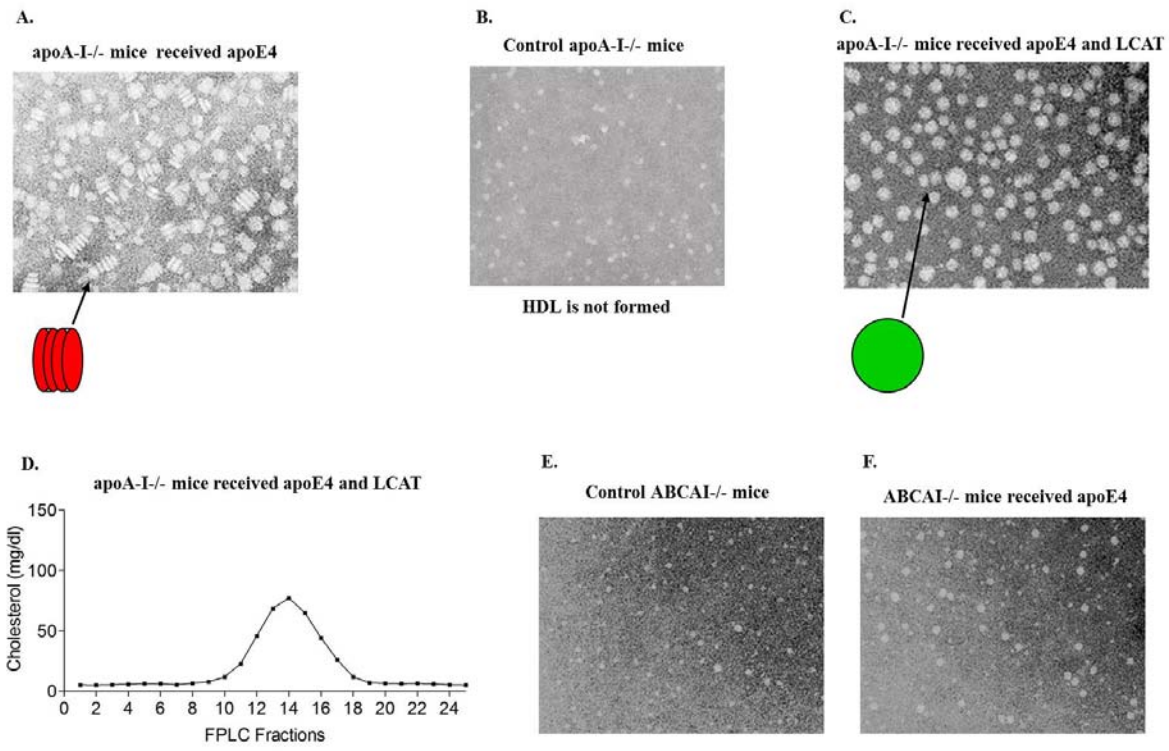

Figure 1.13 (A-F). EM analysis of apoA-I$^{-/-}$ and ABCA1$^{-/-}$ mice prior to and following infection with adenovirus expressing human apoE4 as indicated (A-C,E,F) and FPLC profile of apoA-I$^{-/-}$ mice expressing

apoE4 and LCAT (D). Plasma for the analyses described in panels A,C,D,F was obtained 4 days following adenovirus infection.

Using adenovirus-mediated gene transfer in apoA-I$^{-/-}$ and apoA-I$^{-/-}$ x apoE$^{-/-}$ mice we established that similar to apoE, apoA-IV also participates in the biogenesis of apoA-IV containing HDL (HDL-A-IV) and requires for this purpose the activity of ABCA1 and LCAT (16).

Gene transfer of apoA-IV in apoA-I$^{-/-}$ mice did not change plasma lipid levels. Density gradient ultracentrifugation showed that apoA-IV floated in the HDL2/HDL3 region (Figure 1.14 A), promoted the formation of spherical HDL particles as determined by electron microscopy (Figure 1.14 B), and generated mostly α- and a few preβ HDL subpopulations as determined by two dimensional gel electrophoresis (Figure 1.14 C). When expressed in apoA-I$^{-/-}$ × apoE$^{-/-}$ mice, apoA-IV increased plasma cholesterol and triglyceride levels and shifted the distribution of the apoA-IV protein in the lower density fractions. This treatment likewise generated spherical particles and α- and preβ-like HDL subpopulations. Co-expression of apoA-IV and LCAT in apoA-I$^{-/-}$ mice restored the formation of HDL-A-IV. Spherical and α-migrating HDL particles were not detectable following gene transfer of apoA-IV in ABCA1$^{-/-}$ or LCAT$^{-/-}$ mice (16). The ability of apoA-IV to promote biogenesis of HDL may explain previously reported anti-inflammatory and atheroprotective properties of apoA-IV.

In vitro studies showed that lipid-free apoA-IV and reconstituted HDL-A-IV promoted ABCA1- and scavenger receptor BI (SR-BI)-mediated cholesterol efflux, with the same efficiency as apoA-I and apoE (16;300).

My contribution in the studies of involved the investigation of the formation of apoA-IV-containing HDL in LCAT$^{-/-}$ mice following adenovirus mediated gene transfer of apoA-I as well as the co-expression experiments of apoA-IV and LCAT in the apoA-I$^{-/-}$ mice. These studies are described extensively in the results of this thesis.

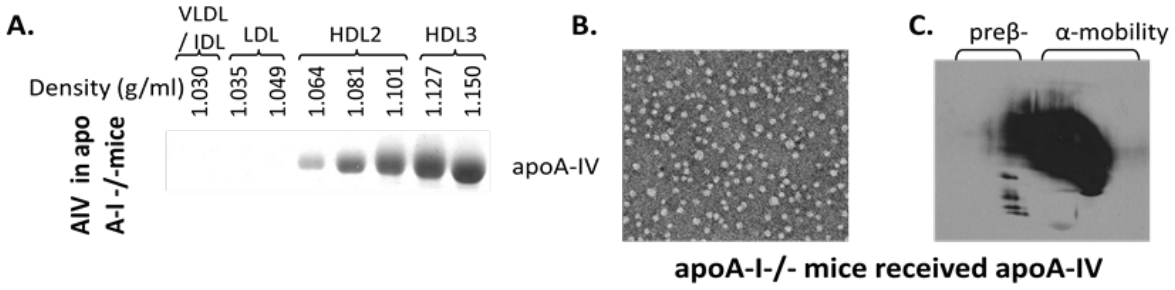

Figure 1.14 (A-H). Analyses of the plasma of apoA-I$^{-/-}$ mice following infection with adenovirus expressing human apoA-IV and control mice as indicated. Density gradient ultracentrifugation and SDS-PAGE (A), EM (B) and two-dimensional gel electrophoresis (C) of plasma of apoA-I$^{-/-}$ mice 4 days post infection with an adenovirus expressing human apoA-IV. The role of LCAT in the formation of apoA-IV containing HDL is presented in the results.

1.18 Proteins involved in HDL remodeling and catabolism

Following synthesis by the liver and the intestine, HDL is subsequently remodeled and catabolized in the plasma via interactions with cell receptors and plasma proteins. Remodeling of HDL generates a dynamic mixture of discrete HDL subfractions that vary in size, shape, apolipoprotein and lipid composition and functions. HDL remodeling affects the structure and metabolic turnover of HDL (301-304).

Remodelling of HDL by the action of hepatic lipase (HL) and endothelial lipase (EL) involves hydrolysis of residual triglycerides and some phospholipids of HDL (305;306), leads to the conversion of HDL2 to HDL3 and preβ-HDL (22-25) and accelerates the catabolism of HDL. Preβ-HDL formation also requires the functions of apolipoprotein M (apoM) (307).

Portion of the cholesteryl esters formed by the actions of LCAT can be transferred to VLDL/IDL/LDL by the cholesteryl ester transfer protein (CETP) (20;308) The phospholipid transfer protein (PLTP) can transfer the phospholipids from VLDL/IDL to the HDL particle during lipolysis to generate HDL2 and can also convert HDL3 particles to HDL2 and preβ-HDL (19;309). HDL binding proteins/receptors have been documented at all steps of HDL metabolism and involve: the SR-BI, that is mostly expressed in hepatocytes, macrophages and steroidogenic tissues and mediates selective CE uptake by the cells and tissues and cholesterol efflux (310-313), the ABCG1, which mediates cholesterol efflux (314), the ecto-F_1 – ATPase subunit which mediates HDL holo-particle uptake by the liver (315;316) and the cubilin/megalin receptors for removal of apoA-I and preβ-HDL by the kidney (315).

1.19 Metabolism of preβ HDL subpopulations

In section 1.3 we presented the different HDL subpopulation that exist on the basis of size, shape, density and apoproteins content. The precursor product relationship between preβ and α-HDL particles as well as the precise origin and functions of the preβ HDL particles is still a matter of investigation.

It has been reported earlier that preβ HDL comprises approximately 5% of total plasma HDL. It is heterogeneous in size and contains several species of 5–6 nm in diameter (202;317).

The best characterized species are preβ1 and preβ2 (202). The concentration of preβ1 HDL is increased in large lymph vessels (318) and in aortic intima (319)

Preβ-HDL particles can be formed by two different routes. The first is de novo synthesis by the HDL biogenesis pathway Figure 1.1. The second is generation of preβ HDL particles from α-HDL particles by reactions catalyzed by CETP, PLTP, HL and apoM (320-324).

Cell culture studies showed that lipid-free apoA-I added to a culture medium of CHO cells can recruit phospholipids and cholesterol, initially to form small 73Å particles, and subsequently larger apoA-I-containing particles by the action of LCAT that have a precursor product relationship (325;326).

Subsequent studies showed that a large proportion of apoA-I is secreted from HepG-2, CaCo-2 or apoA-I expressing CHO cells in lipid-free monomeric form, with a Stokes radius of 2.6 nm and preα electrophoretic mobility that is unable to promote efflux of phospholipids and cholesterol. It was suggested that in a reaction dependent on ABCA1 the 2.6 nm form was converted into a 3.6 nm monomeric apoA-I form with preβ electrophoretic mobility that was able to promote efflux of phospholipids and cholesterol from cells and thus increase its size (327). Expression of apoM in cells transfected with ABCA1 can also increase the size of preβ HDL (328). Other studies have shown that some types of preβ HDL particles can be formed independently of apoA-I/ABCA1 interactions in the plasma of humans with Tangier disease and the plasma of apoA-I-deficient mice expressing mutant apoA-I forms (125;127;329). Furthermore, inhibition of ABCA1 in HepG2 cells and macrophage cultures by glyburide inhibited the formation of α-HDL particles but did not affect the formation of preβ HDL particles (330).

The presence of increased concentrations of preβ1 HDL in the vascular bed suggests that these particles may be generated locally by gradual lipidation of lipid-poor apoA-I (177;319). It has been proposed that lipid-free or lipid-poor apoA-I secreted by cells or dissociating from lipoprotein particles may enter the interstitial fluid from the plasma compartment and via interactions with ABCA1, form preβ1 HDL. Preβ1 HDL particles formed in plasma may also enter the interstitial fluid (202;331). These particles may be enlarged further by recruitment of phospholipids and cholesterol from cell membranes (302). In addition, esterification of the cholesterol of preβ1 HDL by LCAT contributes to their gradual conversion into spherical HDL without prior formation of discoidal HDL particles (176;302).

1.20 CTα and its role in HDL metabolism

CT (CTP:phosphocholine citidyl transferase) is an enzyme produced by the liver and other tissues in two isoforms, CTα and CTβ and plays a crucial role in the biosynthesis of phosphatidylcholine (PC) through the CDP-choline or "Kennendy pathway" (332;333). The absence of the CT in mice causes early embryonic lethality, indicating the importance of this enzyme (334). Transcriptionally, the CTα expression is upregulated by Sp1, Sp3, Rb, TEF4, Ets-1 and E2F and repressed by Net (335)

Liver-specific inactivation of CTα resulted in a 50% decrease of the HDL levels, including HDL-PC, HDL-C and apoA-I as well as reduction of the apoB100 and triglycerides (336). It is possible that the PC insufficiency may have led to the formation of immature HDL particles that were rapidly catabolized. Alternatively, the livers deficient in CTα might counteract the

impaired PC biosynthesis by limiting the amount of PC and cholesterol available for HDL formation (336). Isolation of hepatocytes from the liver-specific CTα knock-out mice showed that the expression of ABCA1 was reduced and the PC efflux was impaired (337). Adenovirus-mediated gene transfer of CTα restored the PC efflux in the isolated hepatocytes and normalized the plasma HDL and VLDL levels in the knock-out mice (337). These findings suggest that the CTα-PC biosynthetic pathway may be an important player for the maintenance of the plasma HDL and VLDL homeostasis.

1.21 Complexity of HDL

Genome wide association (GWA) studies showed that new genes and the corresponding proteins affect plasma HDL levels by unknown mechanisms (338-347). In parallel, proteomic analysis showed that a large number of plasma proteins can associate with HDL and this may affect the HDL structure and functions (348).

The proteins associated with HDL can be classified in six major categories, and include: proteins involved in lipid, lipoprotein and HDL biogenesis and metabolism, acute phage proteins, protease inhibitors, complement regulatory proteins and few others (albumin fibrinogen a chain platelet basic protein) (349;350) (Figure 1.15). Differences were observed in the proteomic composition of HDL subpopulations derived from HDL particles of different sizes (351). Furthermore the HDL proteome could be altered by pharmacological treatments (352).

Another level in the complexity of HDL was added by the finding that a number of microRNAs (miRNA) are transported and delivered to cells by HDL (353). The delivery of miR-223 to cells and downregulation of targets genes is SR-BI-dependent. Additionally, The HDL

miRNA cargo is different in normal subjects and subjects with familial hypercholesterolemia (353).

Finally, HDL carries a variety of other molecules such as the bioactive lipids sphingosine-1-phosphate and sphingomyelin, which are implicated in cell signaling, as well as vitamins, retinol, steroids, bile acids and carotenoids (reviewed in (354)).

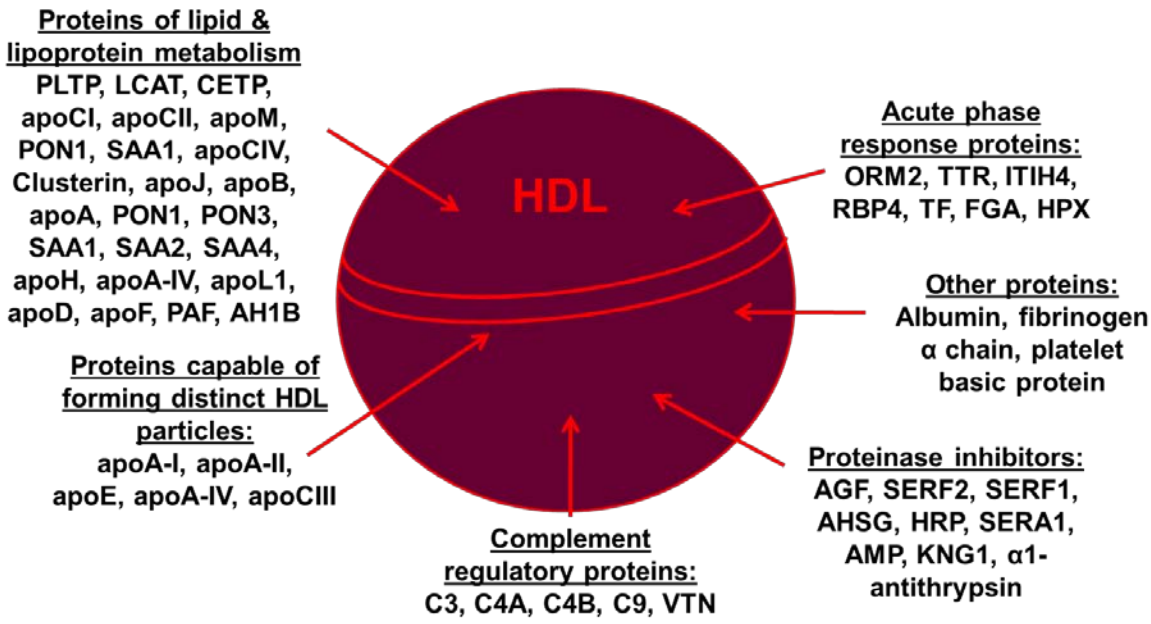

Figure 1.15: The proteomic composition of HDL. Based on (349;350).

1.22 Evidence that increased HDL cholesterol protects from coronary artery disease

Numerous epidemiological studies have shown an inverse correlation between HDL cholesterol levels and the risk for CAD. In the Framingham Heart study, which was the first major epidemiological study examined the relation between HDL cholesterol (HDL-C) levels and coronary artery disease, it was found that people whose HDL-C was less that 35 mg/dL at the beginning of the study had a future coronary risk more than eight fold as compared to subjects

whose HDL-C was greater than 65 mg/dL (355;356). Since then, many more epidemiological studies have established this relationship (26;357-362).

Many animal models support the inverse correlation of the HDL-C levels and cardiovascular disease. For example, mice and rabbits overexpressing apoA-I are more resistant to atherosclerosis (363;364). Furthermore, hepatic overexpression of the apoA-I gene in the background of apoE$^{-/-}$ or LDLr$^{-/-}$ mice reduced the atherosclerosis burden of these mice following an atherogenic diet (365-367). In contrast, mice lacking apoA-I but overexpressing human apoB at the same time had more severe atherosclerotic lesions compared to mice expressing apoB alone (368). This showed that HDL deficiency increased the atherosclerosis susceptibility when accompanied by other risk factors, such as elevated LDL. In another study, rabbits fed an atherogenic diet showed regression of the atheromatic plaques after injection of HDL from healthy rabbits (369). Furthermore, double deficient mice for apoA-I and the LDL receptor fed an atherogenic diet developed atherosclerosis and had increased circulating auto-antibodies, increased T-cells, B-cells, dendritic cells and macrophages and dispalyed increase T-cell proliferation and activation. The abnormal phenotype was corrected by adenovirus mediated gene expression of apoA-I (370). These findings demonstrated the importance of apoA-I and HDL for atheroprotection.

In light of this evidence, the National Cholesterol Education Program (NCEP) in the US has recommended many lifestyle modifications such as weight reduction, increased physical activity, reduction in alcohol consumption and smoking cessation, some of which may increase the HDL-C levels (371). Moreover, HDL-C levels are increased by treatment with several classes of currently available lipid-modifying agents. Statins, although used to mainly lower LDL-C, can also increase HDL-C by 5-10% and have been shown to reduce CAD progression. Patient with

low HDL levels benefit more compared to patient with higher HDL levels (372;373). Fibrates increase HDL-C by 20% and decrease triglycerides by 50% and have been associated with reductions in cardiovascular morbidity and mortality (374;375). Niacin increase HDL-C by 30% and lower triglycerides and LDL-C by 50% and 20% respectively. Niacin in combination with a statin can greatly reduce CAD events (376). Finally, torcetrapib, a CETP inhibitor, increased HDL-C by 50% and lower LDL-C by 20%. Despite the favorable lipoprotein profile, torectrapib resulted in increased cardiovascular and non-cardiovascular mortality in a randomized phase III clinical trial (377).

Despite the very large evidence that HDL-C is a powerful negative risk factor in humans, there are very few intervention studies that have put this position directly to the test. The aforementioned intervention studies in which drug induced elevation of HDL-C are associated with reduction in atherosclerosis were not designed to specifically test the benefits of raising HDL-C. Two direct studies in humans provided strong support that HDL may have therapeutic value. In the first study, reconstituted HDL containing the apoA-I Milano variant and phospholipid was infused intravenously in patients with acute coronary syndrome. This resulted in significant reduction in the atheroma burden in the coronary arteries as assessed by intravascular ultrasound (378;379). Despite the fact that the limitation of this study was the small number of subjects, it provided a powerful incentive to conduct further research on HDL. A larger study, using the same methodology, assessed the effect of reconstituted HDL containing normal apoA-I on atheroma burden. In this study, infusion of rHDL did not change coronary atheroma volume, but improved the plaque characteristic and coronary score as assessed by quantitative coronary angiography (380).

1.23 Atheroprotective and other functions of apoA-I and HDL

In order to understand how HDL protects against atherosclerosis, it is first necessary to understand the mechanism that causes it. In principle, atherosclerosis is an inflammatory disease caused by the accumulation of atherogenic lipoproteins, such as LDL, in the arterial wall when their concentration is very high in the plasma, for example in hypercholesterolemia. The LDL cholesterol reacts with free radicals and gets oxidized (ox-LDL) which triggers a series of events leading to atherosclerosis. Oxidized LDL, as well as the pro-inflammatory cytokines TNF-α and IL1β, stimulate the expression of cell adhesion protein-1 (VCAM-1), intracellular adhesion molecule-1 (ICAM-1) and E-selectin by the endothelial cells which bind blood monocytes. Oxidized LDL also induces the expression of chemotactic protein-1 (MCP-1) by endothelial cells, smooth muscle cells, and monocytes which attracts the monocytes into the artery wall, and promotes their differentiation to macrophages. The macrophages take up the ox-LDL, accumulate excessive cholesterol and transform to foam cells, which create the initial atherosclerotic lesion, called the fatty streak. Macrophages and other blood borne cells as well as activated endothelial cells promote the migration of smooth muscle cells from the media to the intima. The smooth muscle cells proliferate and produce matrix components, such as collagens and proteoglycans, which are incorporated in the lesion. As the disease progresses the advanced lesion is formed where the cholesterol-laden foam cells die and form the necrotic core of the lesion and the smooth muscle cells along with the matrix components form the fibrous cup (3;381).

1.24 The macrophage Reverse Cholesterol Transport

The ability of HDL to efflux cholesterol from macrophages in the intima relieves the macrophage foam cells from their cholesterol burden and has been suggested to inhibit the progression or even promoting the regression of atherosclerosis (382) (Figure 1.16).

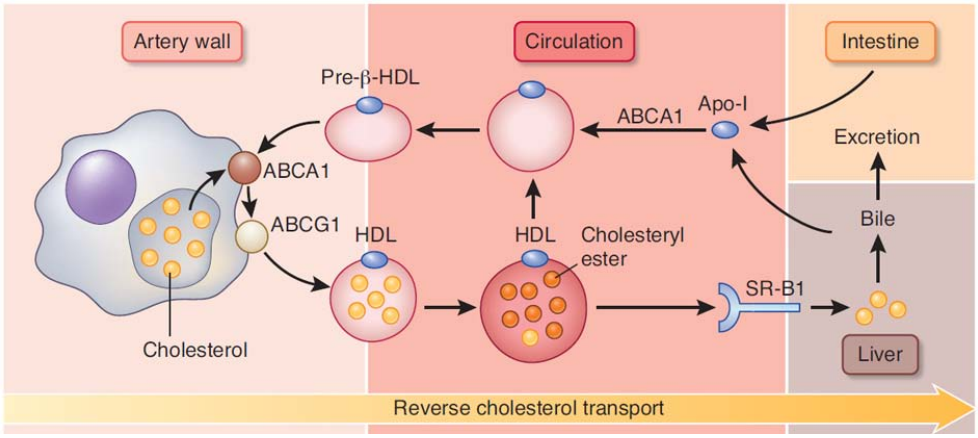

Figure 1.16: The macrophage reverse cholesterol transport (383).

The cholesterol efflux from the macrophages is mediated both by ABCA1 and ABCG1. Knock-down of both ABCA1 and ABCG1 in macrophages reduced cholesterol efflux *ex vivo* and RCT *in vivo* to a greater extent than loss of either transporter alone (384). Khera et al. showed that the macrophage cholesterol efflux capacity is a better predictor for cardiovascular disease than the HDL cholesterol levels (385). There is plenty of evidence in mouse models supporting that macrophage RCT is important for atheroprotection. Transplantation of bone marrow from ABCA1$^{-/-}$ mice in wild type mice increased atherosclerotic lesion development while maintaining normal plasma HDL-C levels (136). In contrast, mice that were transplanted with bone marrow from ABCA1 overexpressing mice have reduced atherosclerosis (137). Furthermore, transplantation of ABCA1/ABCG1 double knockout bone marrow into LDLr$^{-/-}$ mice resulted in

substantially greater atherosclerosis than bone marrow from either single knockout alone (386). Similarly, experiments showed increased inflammation, increased monocyte count and enhanced atherosclerosis in $LDLr^{-/-}$ mice transplanted with of ABCA1/ABCG1 double knockout macrophages (387). LXR agonists and PPARα and PPARγ agonists upregulate ABCA1 and have reported to enhance the macrophage RCT and to inhibit atherosclerosis (388-392). Recent studies have shown that miR-33 deficient mice have increased ABCA1 and HDL levels and the peritoneal macrophages from these mice exhibit increased cholesterol efflux (393;394). It has also been reported that silencing miR-33a results in a reduction of atherosclerosis in mice (393). Silencing of miR-33 also increases HDL and lowers VLDL triglycerides in non-human primates (395). The above studies indicate that inhibition of miR-33 may protect from atherosclerosis by increasing the expression of ABCA1 and thus facilitating the enhancement of the macrophage RCT. Other microRNAs, such as miR-26, miR-106b and miR-758, have also been shown to decrease cholesterol efflux by suppressing ABCA1 expression (396-398).

Using an *in vivo* model that measures the reverse transport of ^{3}[H]-cholesterol from cholesterol-loaded J774 macrophages via the plasma to the liver and its incorporation to the bile and excretion to the feces, Rader et al. have determined how over- or under-expression of genes of the HDL pathway affect this type of RCT. He showed that apoA-I overexpression promotes and apoA-I deficiency impairs macrophage RCT, consistent with the atheroprotective functions of apoA-I (399;400). Additionally, the atheroprotective variant of apoA-I, apoA-I Milano, as well as apoA-I mimetic peptides D-4F, 5A, ATI-5261 and FAMP in mice stimulated the macrophage RCT and reduced atherosclerosis (401-405).

Overexpression of hepatic SR-BI promoted macrophage RCT whereas ablation of SR-BI reduced macrophage RCT (406). This is consistent with the protective effect of SR-BI against atherosclerosis (407-409).

Other studies have also shown that macrophage apoE (410) as well as hepatic CETP (411) are important for the RCT, whereas hepatic LCAT does not have any significant effect (178).

1.25 Anti-inflammatory properties of HDL

As we described earlier, ox-LDL is a crucial factor in the development of atherosclerosis since it signals the initiation of the inflammatory responses that ultimately triggers the formation of the atheromatic plaques (3). ApoA-I renders LDL resistant to oxidation by lipoxigenase, an enzyme which participates in the oxidation of fatty acids (298). Furthermore, HDL carries several antioxidant enzymes, such as paraoxonase 1 (PON1), platelet-activating factor acetylhydrolase (PAF-AH), LCAT and reduced glutathione selenoperoxidase (298;412). Gene transfer of apoA-I in rats with diabetes mellitus increased HDL-C levels and inhibited angiotensin II type 1 receptor mediated NAD(P)H oxidase activation and the generation of reactive oxygen species (413). In healthy subjects, HDL is able to inhibit the formation of mildly oxidized LDL (oxLDL). On the other hand, lipid hydroperoxides can be transferred from ox-LDL to HDL by CETP (414) resulting in the rapid clearance of ox-LDL (415).

There is evidence of several mechanisms that may be involved in the anti-inflammatory functions of HDL. Many studies have shown that HDL inhibits the expression of endothelial

adhesion molecules, such as VCAM-1, ICAM-1, and E-selectin as well as pro-inflammatory cytokines and chemokines, such as MCP-1 (416-419). Nicholls *et al*. inserted a non-occlusive collar around carotid arteries in rabbits to imitate carotid stenosis and infused reconstituted HDL (rHDL). The treatment with rHDL resulted in the inhibition of VCAM-1, ICAM-1 and MCP-1 production, as well as in inhibition of leukocyte infiltration and the abolishment of reactive oxygen species production in the artery wall (420). The carotid vascular inflammation and neutrophil infiltration could be inhibited by rHDL containing normal apoA-I but not by apoA-I obtained from diabetic patients (418).

The inhibition of the expression of adhesion molecules may be mediated by SR-BI and PI3K and eNOS, and in some studies, also by S1P receptors, in the latter case implicating the involvement of HDL-associated S1P (421). HDL may also decrease inflammation by inducing the activation of PI3 kinase, Akt and ERK1/2 though upregulation of the expression of 3β-hydroxysteriod-Δ24 reductase (DHCR24) and heme oxygenase-1 (HO-1) (422) and TGF-β2 (416;423). Other studies have indicated that HDL, through S1P receptor and SR-BI receptor, activates PI3K/Akt and eNOS that leads to the inhibition of the expression of adhesion molecules on endothelial cells and promotes cell migration (424). The mechanisms involve calcium/calmodulin-dependent protein kinase (CaMKK), liver kinase B1 (LKB1) and AMP-activated protein kinase (AMPK) as upstream regulators of PI3K/Akt (424).

Lipid free apoA-I and HDL may inhibit activation of NF-κB through mechanisms that involve Toll-Like Receptor 4 and chemokine receptors respectively and thus inhibit inflammation (417;425;426). It has also been shown that HDL prevents the formation of granulins, which induce the expression of the pro-inflammatory TNFa and IL1β in macrophages

(427). HDL also inhibits the binding of T-cell microparticles to monocytes, thus inhibiting the production of proinflammatory cytokine (428). Lipid-free apoA-I and HDL attenuated neutrophil activation as determined by the levels of leukocyte adhesion molecule CD11b through mechanisms that involve ABCA1 and SR-BI and thus inhibited inflammation (429). Earlier studies have shown that apoA-I and HDL inhibit the PMA-mediated activation of the CD11b (430).

There are two kinds of macrophage subpopulations, M1, which cause tissue damage through different mechanisms, and M2, which are involved in wound healing and tissue repair (431). HDL has been implicated in the macrophage polarization into the M1 or M2 macrophage subpopulations. HDL inhibits the M1 polarization of macrophages by downregulating genes such as TNF-α, IL-1β and MCP-1 (432) whereas it promotes the M2 polarization by signaling via STAT-6 signaling mechanism (433).

Recent studies have explored how PON1 contributes to the anti-inflammatory activity of HDL. It has been shown that PON1 directly suppresses the macrophage M1 phenotype and reduces the production of reactive oxygen species as well as phagocystosis and necrotic macrophage death (434). Additionally, PON1 reduced the cholesterol burden of macrophages by enhancing the cholesterol efflux ability of HDL (435) and by inhibiting the differentiation of monocytes to macrophages (436). The activity of PON1 was significantly reduced in the presence of high levels of VLDL-triglycerides (437). These studies support the atheroprotective functions of HDL via PON1 and imply that high triglycerides levels may promote the formation of dysfunctional HDL.

The beneficial effects of apoA-I has also been reinforced by the use of mimetic apoA-I peptides, such as 5A, L-4F, L37pA and D37pA, which have been shown to reduce vascular inflammation in *in vivo* models by inhibiting the lipid oxidation and the expression of adhesion molecules (425;438;439). Furthermore, infusion of rHDL in patients with type 2 diabetes mellitus reduced the expression of CD11b, which promotes cell adhesion. Moreover, plasma HDL isolated 4 to 72 hours post rHDL infusion suppressed the expression of VCAM-1 in cultures of HAECs and had increased ability to promote cholesterol efflux from THP-1 macrophages (440).

A series of studies have also implicated cholesterol efflux and HDL in hematopoietic stem cell (HSPC) proliferation and leukocytosis (441-443). It has been shown that $ABCA1^{-/-}$ x $ABCG1^{-/-}$ mice have severe leukocytosis. This phenotype was corrected when bone marrow from the $ABCA1^{-/-}$ x $ABCG1^{-/-}$ mice was transplanted to apoA-I transgenic mice but not in WT mice, indicating that increased levels of HDL suppress HSPC proliferation (443). Recent studies have shown that apoE bound to heparan sulfate proteoglycans is a critical mediator of the cholesterol efflux via ABCA1/ABCG1 and contributes to the decrease of cell proliferation (442). Other studies showed that $LDLr^{-/-}$ x apoA-$I^{+/-}$ mice, which have lower HDL-C levels as compared to LDLr-/- mice, exhibited expansions of hematopoietic stem cell, monocytosis and neutrophilia (441). Parallel studies in children with familial hypercholesterolemia showed that the HDL-C levels were inversely correlated with the monocyte count (441). The findings indicated a close link between high LDL levels and low HDL levels with leukocytosis and may explain the increased atherosclerosis when high LDL levels are combined with low HDL levels.

1.26 Effects of HDL on endothelial cell apoptosis, proliferation and migration

HDL has been shown to protect the ox-LDL- and TNFa-induced endothelial cell apoptosis (444-446). Smaller size HDL3 has been shown to have a higher anti-apoptotic capability than larger HDL, which was attributed to its capacity to accept through its methionine residues the phospholipid hydroperoxides (PLOOH) of oxLDL (447). In patients with the metabolic syndrome, the anti-apoptotic properties of HDL3 were reduced possibly due to the higher triglyceride content of the HDL particles (448). HDL obtained from patients with CAD has altered proteomic composition and triggered proapoptotic pathways, suggesting that the presence of CAD altered the functionality of HDL (449).

ABCG1 was shown to promote efflux of 7-ketocholesterol and related oxysterols from macrophages and endothelial cells to HDL, thus protecting cells from apoptosis (450;451). It has also been shown that the ABCG1-mediated cholesterol efflux reduces the inhibitory interaction of eNOS with caveolin-1 and restores eNOs activity in endothelial cells (452).

The most common mechanisms, though, that have been proposed to explain the anti-apoptotic function of HDL include interactions of HDL with SR-BI, interactions of S1P with S1P1 and S1P3 receptors and interactions of lipid-free apoA-I with F1-ATPase. Interactions of apoA-I with cell surface F1-ATPase inhibited apoptosis of HUVEC and stimulated cell proliferation (453). Down-regulation of the ABCA1 by siRNA did not affect the anti-apoptotic and proliferative functions of apoA-I whereas inhibition of SR-BI by a specific antibody diminished the anti-apoptotic and proliferative functions of HDL_3 (453). The findings suggest that interactions of lipid free apoA-I with F1-ATPase and of HDL with SR-BI contribute to their anti-apoptotic and proliferative effects on endothelial cells. The anti-apoptotic effects of HDL on

endothelial cells could be mimicked by the lysosphingolipid components of HDL (446). In addition, the lysophospholipid sphingosine-1-phosphate (S1P) enhanced endothelial cell survival with effects comparable to those of native HDL, and these responses are inhibited by knockdown of the S1P receptor EDG-1/$S1P_1$, by pertussis toxin, and by PI3 kinase and Erk pathway antagonists (454). Tumor necrosis factor-α (TNF-α)-induced endothelial cell apoptosis is also inhibited by HDL, and this is associated with diminished induction of caspase 3, which is a component of all primary apoptotic pathways (445). Although the vast majority of evidence for antiapoptotic action of HDL on endothelium comes from cell culture work, in studies of the apoA-I mimetic D-4F in a rat model of diabetes, the mimetic improved vascular reactivity and decreased endothelial cell fragmentation and sloughing (455), suggesting that the antiapoptotic actions of HDL may be operative in vivo.

In addition to its anti-apoptotic actions on endothelial cells, HDL can directly stimulate endothelial cell proliferation and repair the endothelium damage that is induced in vascular disease (456). It has been shown that HDL promotes proliferation of HUVEC through calcium-dependent processes (457) and migration of endothelial cells through S1P-dedaited signalling cascades, leading to the activation of PI3 kinase, p38MAP kinase and Rho kinases (454). Other studies show that HDL can activate the MAPK pathway either through processes that involve protein kinase C (PKC), Raf-1, MEK and ERK1/2 or PKC independent pathways (458). The data suggest that interactions of HDL with SR-BI activate Ras in a PKC independent manner and this leads to subsequent activation of MAPK signalling cascade (458). Capillary tube formation stimulated by HDL in vitro has been found to be pertussis toxin-sensitive but independent of p38 MAP kinase, alternatively requiring p42/44 MAP kinase activity residing downstream of Ras

(459). It has also been observed that HDL stimulates endothelial cell migration *in vitro* via the activation of Rac GTPase; this process does not require HDL cargo molecules, and it is dependent on SR-BI and the activation of Src kinases, PI3-kinase, and p44/42 MAP kinases. Rapid initial stimulation of lamellipodia formation by the HDL/SR-BI tandem via Src kinases and Rac also occurs in cultured endothelial cells (460). *In vivo* experiments have also shown that re-endothelialization of carotid artery following injury is promoted by apoA-I expression and is inhibited in apoA-I deficient in mice (460). Along with promoting growth and migration and tube formation by differentiated endothelial cells, HDL action via SR-BI activates the same processes in endothelial progenitor cells (EPC). The responses in EPC are dependent on PI3 kinase, Akt, p42/44 MAP kinase, and endothelial nitric-oxide synthase (eNOS) (461;462).

Reconstituted HDL-mediated signaling through SR-BI has been shown to inhibit NF-κB activation and chemokine expression in smooth muscle cell (SMC) and it also inhibited SMC proliferation by affecting the ERK1/2 phosphorylation (463). This study suggests a possible treatment for the occlusion of the veins after a bypass surgery.

1.27 HDL and eNOS activation

The ability of HDL to activate endothelial nitric oxide synthase (eNOS) (464), which regulates vascular function, is implicated in most of the beneficial functions of HDL on the endothelial cells, such as the anti-apoptotic, the anti-inflammatory functions as well as the endothelial cell proliferation, migration and blood vessel vasodilation (465).

Various studies have shown that increased HDL levels are associated with greater vasodilator effects in humans and this effect is impaired in patients with CAD (466;467). The stimulation of eNOS enzymatic activity by HDL entails eNOS phosphorylation at Ser1179 via Akt, and this is mediated by Src family kinases and PI3 kinase. Enzyme activation by HDL also requires Src- and PI3 kinase-dependent activation of Erk1/2 MAP kinases (297). Studies in endothelial cells and Chinese hamster ovary (CHO) cells that express SR-BI, showed that SR-BI-HDL interactions lead to the phosphorylation and activation of eNOS. The HDL-induced eNOS activation occurs in the caveolae. The HDL-mediated NO-dependent relaxation is lost in aortic rings of SR-BI$^{-/-}$ mice (468). More studies established that the C-terminal cytoplasmic PDZ-interacting domain and the transmembrane domain of SR-BI were both required for eNOS activation (469). The cytoplasmic PDZK1 interacting domain of SR-BI binds adaptor proteins such as PDZK1 that may participate in cell signalling (470). The S1P component of HDL cause eNOS dependent relaxation of mouse aortic rings via intracellular Ca^{2+} mobilization and eNOS phosphorylation mediated by Akt (471). Another that may be involved in the HDL-induced activation of eNOS may be 5' AMP-activated protein kinase (AMPK) through the phosphorylation of eNOS at multiple sites (Ser116, Ser635, and Ser1179) (472). It was suggested that activation by AMPK may involve physical interactions between the apoA-I component of HDL and eNOS. Such interactions may be accomplished following SR-BI mediated endocytosis of HDL (473).

The SR-BI mediated signalling that leads to activation of eNOS, promotes cell growth and migration and protects cells from apoptosis (474;475). Activation of eNOS required its localization in the caveolae, where caveolin SR-BI and CD36 are also found (476). It has been

proposed that oxLDL acting through CD36 depletes the cholesterol content of caveolae and leads to eNOS redistribution to intracellular sites and resulting in decreased eNOS activity (476;477). HDL acting through SR-BI maintains the concentration of caveolae-associated cholesterol, inhibits the actions of oxLDL and maintains eNOS in the caveolae (476). This interpretation implies that strong interactions between eNOS and Cav-1 stimulate eNOS activity. It has been shown that oxidized phospholipids uncouple eNOS activity and lead to the generation of oxygen radicals which induces the expression of sterol regulatory element binding protein (SREBP) and IL-8 (478;479). ApoA-I mimetic peptides also prevent LDL from uncoupling eNOS activity to favour $O_2^{\cdot -}$ anion production as opposed to normal production of NO (480). Finally it has been shown that SR-BI via a highly conserved redox motif CXXS between residues 323-326 can promote a ligand independed apoptosis via a caspase 8 pathway and this effect could be reversed by HDL and eNOS (481). It was proposed that at low HDL levels oxitative stress causes relocation of eNOS away from the caveolae and this results in SR-BI induced apoptosis (481).

1.28 Effects on thrombosis

Increased HDL cholesterol levels are associated with decreased risk of venous thrombosis (482). In contrast low HDL levels are associated with increased risk of venous thrombosis (483). Infusion of rHDL in volunteers that received low levels of endotoxin limited the prothrombotic and procoagulant effect of endotoxin (484). Infusion of rHDL in subjects with type 2 diabetes reduced significantly the platelet activation and aggregation by reducing the cholesterol content of the platelet membranes (485). In animal models, infusion of apoA-I_{MILANO}

in a rat model of acute arterial thrombosis increased the time of thrombus formation and decreased the weight of the thrombus (486). Recently it was shown that transplantation of ABCG4$^{-/-}$ bone marrow in LDLr$^{-/-}$ mice resulted in increased thrombosis and atherosclerosis. Infusion of rHDL in LDLr$^{-/-}$ mice and in a mouse model of myeloproliferative neoplasm decreased the platelet count in an ABCG4-dependant manner (487).

Studies have shown that the HDL-induced anti-thrombotic may involve increased synthesis of prostacyclin (PGI2) in cultured endothelial cells (457;488), increased expression of cyclooxygenase-2 (Cox-2) by smooth muscle cells and release of PGI2 via a signalling pathway that involves p38MAP kinase and N terminal kinase c-Jun (JNK-1) (489;490). It has been shown that the interaction of apoA-I with ABCA1 in endothelial cells, induced the expression of Cox-2 and the production of PGI2 through the p38 MAPK, ERK1/2 and JAK2 signaling pathways (491). Other studies have shown that the HDL-induced Cox-2 expression and PGI2 release in endothelial cells involves the SR-BI-mediated PI3K-Akt-eNOS signaling pathway (492).

It has been shown that there is a positive correlation between plasma HDL and anticoagulant response to activated protein C (APC)/protein S *in vitro*, which downregulates thrombin formation (493;494), and negative correlation with the plasma thrombin activation markers such as prothrombin fragments F1.2 and D-dimer (495). Shpingosine, another molecule present in HDL, has been shown to inhibit prothrombin activation on platelets' surface by disrupting procoagulant interactions between factors Xa and Va (496). HDL also downregulated expression of plasminogen activator inhibitor-I (PAI-1) and upregulated tissue plasminogen activator (t-PA) in endothelial cell cultures (497). Transgenic mice expressing the human PAI-1 developed age-dependent coronary arterial thrombosis (497). In contrast oxidized HDL3

induced the expression of PAI-I in endothelial cells through signalling mechanisms that involve activation of ERK1/2 and p38MAPK and mRNA stabilization (498).

Recent studies have shown that SR-BI$^{-/-}$ mice as well as transgenic mice expressing SR-BI in the liver, developed deep vein thrombosis. A pro-thrombotic phenotype was also observed in apoA-I$^{-/-}$ or eNOS$^{-/-}$ mice. The prothrombotic phenotype was corrected by infusion of apoA-I suggesting that suppression of platelet activation is mediated by an apoA-I (HDL)/SR-BI/eNOS signaling pathway (499). Cell-signaling mediated by interaction of HDL3 with SR-BI inhibits platelet activation. The high content of negatively charged phospholipids (phosphatidylserine and phosphatidylinositol) of HDL3 appears to be important for each anti-thrombotic activity of HDL (500).

1.29 Heterogeneity of HDL and coronary artery disease

As discussed previously, the HDL particles are heterogeneous in size, shape, density as well as protein content and this may contribute to the diverse functions of HDL including its atheroprotective properties.

It has been shown SR-BI has increased capacity to promote selective cholesteryl ester uptake by cells in the presence of LpA-I as compared to LpA-I/LpA-II (501). Patients with coronary heart disease have decreased concentration of the largest size HDL subpopulations which are considered to be atheroprotective (502-505). Other studies suggest that less mature subpopulations such as discoidal and preβ HDL particles are more efficient than spherical, α-HDL in their ability to protect from atherosclerosis, largely due to their ability to promote

ABCA1-mediated cholesterol efflux (506). There are also studies indicating that HDL3 has anti-inflammatory and anti-oxidant properties *in vitro* (414;507;508). Another study showed that infusion of discoidal rHDL in rabbits inhibited the endothelial expression of VCAM-1 and ICAM-1 (420). A recent study examined the antioxidant and anti-inflammatory properties of HDL as well as the HDL subpopulations of samples obtained from subjects carrying mutations in the apoA-I, ABCA1 and LCAT genes. These subjects had different lipid and lipoprotein profiles and the presence of absence of clinically reported CAD (15). The subjects carrying the mutations in heterozygosity lacked the larger α1-HDL subpopulation but have the preβ and the other α-HDL subpopulations. A more severe phenotype was observed in homozygotes or compound heterozygotes who had either preβ or preβ and α4-HDL subpopulation. In all instances, the aberrant HDL phenotype was associated with to a reduced anti-oxidant and anti-inflammatory capacity of HDL. This offers strong evidence that the presence of larger, mature HDL subpopulation is needed for HDL to exert its anti-oxidant and anti-inflammatory properties.

Other studies have shown that the HDL of subjects with cardiovascular disease has a distinct proteomic signature as compared to normolipidemic subjects (349;509). However it is unclear how these changes contribute to the pathogenesis of CAD. Nevertheless, these changes are valuable biomarkers for the cardiovascular disease and can facilitate evaluation of the treatment regimen. To this end, a study showed that a combined treatment of statins and niacin partially corrected the HDL proteomic profile of subjects with stenotic lesions towards that of the normal control subjects (352).

Overall, the evidence linking protection against cardiovascular disease to specific HDL subpopulations and proteomic cargo is still unclear. Thus, it remains unknown how the cardioprotective effects of HDL are influenced by the HDL heterogeneity.

1.30 Dysfunctional HDL

High levels of HDL cholesterol are not always correlated with atheroprotection. Human subjects have been identified with high HDL levels and coronary artery disease, thus suggesting that the HDL in these subjects may have pro-atherogenic properties (510). A similar situation exists in SR-BI$^{-/-}$ mice and LCAT transgenic mice that have increased levels of HDL but are not protected from diet induced atherosclerosis (190;409;511;512). Furthermore, there is evidence of dysfunctional HDL in many diseases such as diabetes, rheumatoid arthritis, chronic kidney disease and CAD, where HDL has reduced anti-oxidant, anti-inflammatory and cholesterol efflux activity as well as altered protein cargo (513-519). Recent clinical intervention studies failed to show that increasing HDL cholesterol levels reduces the risk for cardiovascular events (520;521). The presence of dysfunctional HDL was also suggested to explain the increased mortality caused by the CETP inhibitor torcetrapib despite the high HDL levels, although this still remains a speculation (522).

Myeloperoxidase (MPO) is very well known to modify the Tyrosine residues of apoA-I, resulting in dysfunctional HDL (523). Subjects with CAD have increased modification of apoA-I in specific Tyrosine residues both in plasma and atherosclerotic lesions (524). Furthermore, these modifications have been associated with impaired ABCA1-mediated cholesterol efflux from

macrophages (525) and impaired binding of LCAT to HDL (526;527). In a recent study it was shown that 20% of the apoA-I recovered from human atherosclerotic lesion was oxidized in residue Trp72 by MPO (528). This modified form of apoA-I was in a lipid-poor state, had diminished capacity to promote ABCA1-mediated cholesterol efflux and had pro-inflammatory properties (528).

Another study showed that atherosclerotic plaque-laden aortas are highly enriched in apoA-I as compared to normal aortas (529). Both in lesion and normal aortas the apoA-I was predominantly lipid-poor and highly cross-linked. Furthermore, apoA-I from atherosclerotic lesions had impaired ability to promote ABCA1-mediated cholesterol efflux and activate LCAT as compared to plasma apoA-I from normal subjects (529).

Finally, Kar *et al*. demonstrated the ability of oxidized phospholipids (Ox-PL) to destabilize rHDL particles and alter their function (530). Furthermore, they showed that reconstituted HDL particles with high amounts of Ox-PL reduced the activity of PON1 HDL (530). PON1 plays an important role in the stimulation of reverse cholesterol transport from macrophages to HDL particles and in the anti-oxidant activity of HDL (531;532).

1.31 Clinical significance

Despite this remarkable progress on HDL biology and genetics, there is a lack of important pieces of information that will make possible the translation of basic research finding on HDL into effective pharmaceuticals for the treatment of heart disease and possible other diseases. There is evidence suggesting that the HDL cholesterol levels are inversely correlated

with the risk of cardiovascular disease. On other hand the HDL cholesterol levels alone are not sufficient to predict the risk for atherosclerosis. It has been established that HDL has a plethora of other functions that may contribute to the protection from cardiovascular disease. These include the capacity to remove cholesterol from the macrophages, the documented anti-inflammatory, anti-oxidant, anti-thrombotic and anti-apoptotic properties, the protection of the endothelium as well as the inhibition of the hematopoietic stem cell proliferation. Changes in the HDL proteomic and lipidomic composition or modifications of its protein and lipid moieties may alter the functionality of HDL. Understanding the complexity, the functions and the signaling pathways mediated by HDL may facilitate in the near future the discovery of new biomarkers to predict cardiovascular disease as well as the development of new HDL-based therapies to prevent or treat atherosclerosis and other human diseases.

1.32 Chapters

The objectives of my thesis are to explore the biogenesis of HDL by gene mutations in various key players of the HDL biosynthetic pathway. This thesis contains the following chapters:

I. Generation and characterization of recombinant adenoviruses expressing wild type and mutants proteins involved in the HDL biogenesis

II. Importance of the hydrophobic residues in the 218-230 region of apoA-I in the biogenesis of HDL.

III. Effects of LCAT mutations on the biogenesis of HDL.

IV. Effects of CTα on the biogenesis of HDL.

V. Contributions of dominant mutations in apoE to lipid homeostasis and the biogenesis of HDL

VI. Synergy of apoA-IV and LCAT on the biogenesis of apoA-IV containing HDL

VII. Effect of reconsituted HDL containing apoE and apoA-I on endothelial gene expression

2. MATERIALS AND METHODS

2.1. Materials

The restriction enzymes, the ligase, the buffers and the DNA polymerases that were used for the construction of plasmids were purchased from New England Biolabs (Ipswich, MA). The dideoxynucleotides (dNTPs) that were used for the polymerase chain reactions (PCR) were purchased from Promega (Madison, WI) and the primers were constructed by Invitrogen (Carlsbad, CA). The following plasmid vectors were used in this project: pENTER221 (Invitrogen), pAdTrack-CMV (Addgene), pCDNA3.1 (Invitrogen) and pGEM (Promega). The molecular weight marker "1 kb DNA Ladder" for DNA and the Presteained Protein Marker, Broad Range (6-175kDa) for proteins were bought from New England Biolabs. The Hybond ECL nitrocellulose membranes were bought from GE Healthcare (Piscataway, NJ) and the Immobilon™-P polyvinylidene fluoride (PVDF) membranes were bought from Millipore (Billerica, MA). For the detection of proteins by Western the enhanced chemiluminescence (ECL) system of GE Healthcare was used. The acrylamide gels with gradient concentration 4-20% Tris-HCL, IPR COMB were bought from BIO-RAD (Hercules, CA). The column Superose 6 PC 3.2/30 was bought from GE Healthcare. For the Western blotting analyses there were used the X-Omat LS films (Kodak; Rochester, NY). The [^{3}H]-cholesterol was purchased from Perkin Elmer (Boston, MA). Various chemical compounds and glassware were bought from Fisher Scientific and Sigma Aldrich. The rest of the materials and chemical compounds that were used are described in the following sections or were obtained from common commercial sources in the clearest possible form.

2.2 DNA/RNA and Molecular cloning techniques

2.2.1 Generation of mutations on apoA-I, apoE and LCAT gene

The plasmid pCDNA3.1-apoAIg-ΔBglII was used as template for the generation of the mutations on apoA-I gene that we investigated in this study. For this purpose it was used the QuickChange® II XL system that was bought from Agilent Technologies. The template plasmid was generated as it is described in (219). Briefly the pUC19-apoAIg plasmid (533) was digested with BglII and treated with the Klenow fragment of the DNA polymerase I to fill the recessed 3'end and ligated in order to eliminate the BglII restricting site. The derivative plasmid, designated pUC19-apoAIg(ΔBglII), was used as a template to amplify by PCR the human apoA-I genomic sequence with two primers carrying the XbaI/BglII recognition sites and the EcoRV recognition sites incorporating them to the 5' and 3' of the apoA-I genomic sequence, respectively. The product of the PCR was cloned into the pCDNA3.1 vector, resulting in the generation of the vector pCDNA3.1-apoAIg(ΔBglII). The template DNA was incubated with the appropriate primers which are shown in Table 2.I. The primers harbor mutations at the center of their sequence and on either side they have the sequence of the nucleotides of the wild type gene. The changes were done in order to obtain the desired amino acid changes in the final protein. The mutagenic primers were constructed according to the guidelines provided by Stratagene.

The mixture of template plasmid and primers was incubated with PfuUltra® polymerase that was provided with the QuickChange® II XL system and dNTPs in a PCR program as described by the manufacturer. After 18 amplification cycles the PCR product was incubated with the restriction enzyme DpnI in order to digest the template plasmid which is methylated or semi-

methylated DNA. After the incubation, the newly synthesized DNA which carries the apoA-I mutations was used for the transformation of XL10-Gold® (Agilent Technologies) competent cells. Colonies resistant to ampicillin were selected and grown in mini cultures. DNA was extracted and purified from these cultures, and was sequenced in order to confirm the introduction of the desired mutations. Colonies having the mutation of interest were then used to produce large quantities of the plasmid.

The apoE mutants were similarly generated with the QuickChange® II XL system using the pGEM-7Zf(+)-apoE vector containing exons II, III, IV of the human gene as a template (534) and the appropriate mutagenic primers (Table 2.I).

The human WT LCAT cDNA and the mutant LCAT cDNAs in the pENTR221 vector was a gift of Dr. Kuivenhoven (Medical Center of Groningen).

2.2.2 DNA electrophoresis in agarose gel

For the nucleic acid electrophoresis agarose gels of 0.5% to 1% concentration were used. The procedure that was used is the following: In a conical 250 ml flask, 120 ml of TAE 1x (50x TAE; 2M Tris-HCL pH 7.5, 2mM EDTA, acetic acid for pH equilibration) and 1 g (Ultrapure Agarose®, Invitrogen) are added. The mixture is heated up to boiling point until the agarose is dissolved. When the temperature of the mixture goes down to around 50^{O}C, 7.5 ul of ethidium bromide (10 mg/ml) are added, then the mixture is poured in an appropriate apparatus (cast) and the combs that will form the sample loading wells are placed. When the gel sets it is transferred to a tank that contains 1x TAE buffer. Usually the electrophoresis is performed at 80

Volt (V) and for the isolation of DNA fragments from gel it is performed at 50 V until the samples are efficiently separated

Table 2.I: The mutagenic primers used in PCR amplifications

Name	Sequence	Location of sequence
apoA-I [L218A/L219A/ V221A/L222A]-F	5′- G GAC CTC CGC CAA GGC **GC**[a]G **GC**G CCC G**C**G **GC**G GAG AGC TTC AAG GTC -3′	nt 743-788[b] (sense) (aminoacids +212 to +227)[c]
apoA-I [L218A/L219A/ V221A/L222A]-R	5′- GAC CTT GAA GCT CTC C**GC** C**G**C GGG C**GC** C**GC** GCC TTG GCG GAG GTC C -3′	nt 788-743 (antisense) (aminoacids +227 to +212)
apoA-I [F225A/V227A/ V229A/L230A]-F	5′- G CCC GTG CTG GAG AGC **GC**C AAG G**C**C AGC **GC**C **GC**G AGC GCT CTC GAG GAG -3′	nt 764-812 (sense) (aminoacids +219 to +235)
apoA-I [F225A/V227A/ V229A/L230A]-R	5′- CTC CTC GAG AGC GCT C**GC** G**GC** GCT G**G**C CTT G**GC** GCT CTC CAG CAC GGG C -3′	nt 812-764 (antisense) (aminoacids +235 to +219)
[d]apoA-I [L218A/L219A/ V221A/L222A/F225A/ V227A/F229A/L230A]-F	5’- CCC GCG GCG GAG AGC **GC**C AAG G**C**C AGC **GC**C **GC**G AGC GCT CTC GAG GA -3’	nt 765-811 (sense) (aminoacids +220 to +235)
apoA-I [L218A/L219A/ V221A/L222A/F225A/ V227A/F229A/L230A]-R	5’- TC CTC GAG AGC GCT C**GC** G**GC** GCT G**G**C CTT G**GC** GCT CTC CAG CAC GGG -3’	nt 811-765 (antisense) (aminoacids +235 to +220)
apoE3[K146N/R147W]-F	5’- CTG CGC AAG CTG CGT AA**T** **T**GG CTC CTC CGC GAT -3'	nt 477-507 (sense) (aminoacids +141 to +151)
apoE3[K146N/R147W]-R	5’- ATC GCG GAG GAG CC**A** **A**TT ACG CAG CTT GCG CAG -3'	nt 507-477 (antisense) (aminoacids +151 to +141)
[e]apoE3[L203Stop]-F	5’- CTG GCC GGC CAG CCG **TG**A CAG GAG CGG GCC CA -3'	nt 648-678 (sense) (aminoacids +198 to +208)
apoE3[L203Stop]-R	5’- TGG GCC CGC TCC TGT **CA**C GGC TGG CCG GCC AG -3'	nt 678-648 (antisense) (aminoacids +198 to +208)

[a]Mutagenized residues are marked in boldface type and are underlined.

[b]Nucleotide number of the human apoA-I cDNA sequence, oligonucleotide position relative to the translation initiation ATG condon.

[c]Aminoacid position (+) refers to the mature plasma apoA-I sequence.

[d]For the generation of this mutant the template used was pCDNA3.1apoA-IWTΔBglII containing the L218A/L219A/V221A/L222A substitutions in the apoA-I gene.

[e]These primers were used for the generation of apoE3[K146N/R147W]-202 using as a template the apoE3[K146N/R147W] construct.

2.2.3 Extraction of DNA from agarose gel

For the extraction of DNA from agarose gel the Gel extraction system (Origene) was used. The band that contained the desired DNA fragment was cut using a clean blade and excised from the agarose gel. The piece of gel was weighted and up to 400 mg was placed in an eppendorf tube. Then for every 10 mg of gel 30 ug of Gel Solubilization Buffer (L1) were added. The gel was solubilized by incubation at 50°C for 15 min. Subsequently the dissolved gel was transferred in a cartilage (provided by the kit) and was centrifuged at 12,000 x g for 1 min. The flowthrough was discarded and the cartilage was washed with an additional 500 ul of L1. The next step was to wash the cartilage with 700 ul of Wash Buffer (L2). The cartilage was further centrifuged an additional minute and then 50 ul of warm TE Buffer were added at the center of the cartilage. It was incubated at RT for 1 min and then collected in a clean eppendorf tube by centrifuging at 12,000 x g for 2 min.

2.2.4 Digestion with restriction enzymes

The plasmids and the products of the PCRs that were used for cloning were incubated with restriction enzymes according to the instructions of the manufacturer (New England Biolabs; Ipswich, MA). Most digestions were performed using 15 ug of nucleic acid at 37°C, for 1-3 hours.

The BglII/EcoRV restriction sites were used to introduce the apoA-I cDNAs and the apoA-IV cDNA to the pAdTrack-CMV vector. The LCAT cDNA was amplified using 5'- 3' primers that contained restriction sites for BglII and EcoRV respectively (Forward: 5'-GA**A GAT CTA** CCA TGG

GGC CGC CCG GCT CCC CA-3', Reverse: 5'-GCG **GAT ATC** CTA TTC AGG AGG CGG GGG CTC TGG-3', Intermediate for sequencing: 5'-CCT CGG CTG TCT ACA CTT GC-3' and 5'-CCT TGG GGT AGA CTG CTG GAT CG – 5') for insertion to the pAdTrack-CMV vector. The CTα cDNA was amplified with primers containing the BglII and NotI restriction sites (Forward: 5'-GA**A GAT CTA** CCA TGG ATG CAC AGT GTT CAG C -3', Reverse: 5'- TTT **GCG GCC GC**T TAG TCT TCT TCA TCC TCA C -3') which were used for insertion to the pAdTrack-CMV vector. ApoE was introduced to the pAdTrack-CMV vector with the HindIII and XbaI restriction enzymes whereas for the LPL we used KpnI and HindIII. The apoA-IV cDNA was generated by RT-PCR of human DNA using as primers 5'- 3' that contained restriction sites for Bgl-II and EcoRV respectively and cloned into these restriction sites of the pAdTrack-CMV vector.

2.2.5 Ligation reaction

The ligation reactions were performed at 16°C, for 16 hours in total volume of 20 ul. The amount of DNA that was used was approximately 200 ng. The reaction had plasmid DNA and DNA of the insert in a ratio of 1:100, T4 DNA ligase and the appropriate buffer according to the manufacturer's (New England Biolabs; Ipswich, MA) instructions.

2.2.6 Transformation of E.coli DH5α by heat shock

For the transformation of bacterial cells, 50 ul of DH5α bacterial competent cells (Invitrogen; Carlsbad, CA) were thawed in ice and 20 ul of the ligation reaction or 20-100 ng of the plasmid were mixed with the cells. The cells were then incubated on ice for 30 min followed

by heat-shock for 30 seconds in a 42^{o}C water bath. The reaction was then placed on ice for 5 minutes. Subsequently, 0.95 ml of S.O.C. medium (Invitrogen; Carlsbad, CA) was added in the cells and they were incubated in shaker at 225 rpm at 37^{o}C for 1 hour. Then 100 ul of the transformed cells were spread on LB plates with the appropriate antibiotic. The plates were incubated at 37^{o}C for 16-18 hours.

2.2.7 Transformation of E.coli BJ5183-AD1 by electroporation

The adenovirus plasmid was generated in BJ-5183-AD1 (Agilent Technologies; Santa Clara, CA) bacterial cells after electroporation in the presence of the pAdTrack-CMV-X vector (where X is the gene of interest) that was previously digested with PmeI, according to the instructions of the manufacturer. For the electroporation, 40 ul of BJ-5183-AD1 cells were used for each reaction. These cells have already the pAdEasy-1 plasmid that encodes the genome of adenovirus type 5 except for transcription units E1 and E3 and they also promote the homologous recombination of plasmids. The recombination with the shuttle vector pAdTrack-CMV-X formed finally a plasmid that has the adenoviral genes and the gene of interest. The electroporation was performed under these conditions: 200 Ω, 2.5 kV, 25 μF using the Bio-Rad Gene Pulser II electroporation machine in 0.2 cm Gene Pulser Cuvettes (Bio-Rad). The cells were plated in agar plates and the correct clones were selected based on their resistance to kanamycin. DNA was purified from the resistant clones and was analyzed on agarose gel. The clones that had the correct recombination gave a 3 or a 4.5 kb band and also had a band at 32 kb after being digested with the restriction enzyme PacI. The positive clones were amplified

(DH5a transformation) and were isolated using the High Purity Plasmid Maxiprep System (Origene).

2.2.8 Small scale preparation for plasmid purification (miniprep)

After bacteria have grown on LB agar plates (American Bioanalytical, Natick, MA) overnight, a single colony of bacterial clone was picked and transferred in 2 ml of LB broth (American Bioanalytical, Natick, MA) containing Kanamycin (10 ug/ml) or Ampicillin (100 ug/ml), respectively. The culture was incubated overnight at 37^{o}C in a shaking incubator. The bacteria were transferred in eppendorf tubes and were centrifuged at 13000 rpm for 1 min. The "High Purity Plasmid Miniprep System" by Origene was used for the plasmid extraction and purification as follows. The supernatant was removed and the pellet was resuspended in 150 ul of Cell Suspension Buffer [50 mM Tris-HCl (pH 8.0), 10 mM EDTA, 2 mg RNase A]. Then 150 ul of Cell Lysis Solution [200 mM NaOH, 1% SDS w/v] were added and the cells were mixed gently and then incubated on ice for 5 min. The next step was to add the Neutralization Buffer [3.1 M potassium acetate (pH5.5)] and the cells were mixed well. The lysed cells were centrifuged at 13000 rpm for 15 minutes and 500 ul of the supernatant was transferred in to a new tube. Then 2/3 volume of chloroform was added and the contents of the tube were mixed vigorously. The mixture was centrifuged again at 13000 rpm for 30 min and the supernatant was discarded. The pellet was washed by adding 500 ul of 70% EtOH and centrifuged at 13000 rpm for 5 min. The supernatant was then removed and the pellet is left to dry. Finally it was resuspended in 20 ul ~30-50 ul of T.E. [10 mM Tris-HCl (pH 8.0), 0.1 mM EDTA] or ddH_2O and stored at -20 ^{0}C.

2.2.9 Large scale preparation for plasmid purification (maxiprep)

The "High Purity Plasmid Maxiprep System" produced by Origene was used for the plasmid purification, and the directions provided by the manufacturer were followed. After the transformation of DNA in DH5β, a single colony was amplified in 400 ml LB/antibiotic overnight at 37^0C in shaker. The bacterial cells were then pelleted by centrifugation at 4000 rpm for 10 min at 4^0C. The bacterial pellet was resuspended in 10 ml of Cell Suspension Buffer [50 mM Tris-HCl (pH 8.0), 10 mM EDTA, 2 mg RNase A], and lysed by the addition of 10 ml Cell Lysis Solution [200 mM NaOH, 1% SDS w/v]. Precipitation of the bacterial proteins was achieved by adding 10 ml of Neutralization Buffer [3.1 M potassium acetate (pH5.5)]. The mixture was centrifuged at 4000 rpm for 10 minutes at 4^0C and the supernatant was removed and applied on a Marligen column that was previously equilibrated with 30 ml of Equilibration Buffer [600 mM NaCl, 100 mM sodium acetate (pH 5.0), 0.15% Triton® X-100 (v/v)]. The column was washed with 60 ml of Wash Buffer [800 mM NaCl, 100 mM sodium acetate (pH 5.0)], and the DNA was eluted with 15 ml of Elution Buffer [1.25 M NaCl, 100 mM Tris-HCl (pH 8.5)]. The DNA was precipitated by adding 10.5 ml of isopropanol, mixed well and centrifuged at 9000 rpm for 30 minutes at 4^0C. The supernatant was discarded and the DNA was diluted in 300 ul of ddH_2O and transferred to a 1.5 ml microcentrifuge tube. It was finally precipitated with 750 ul of cold (-80°C) ethanol and 30 ul of CH_3COOH 3M (pH 5.5), mixed well and centrifuged at 13000 rpm for 30 minutes. The supernatant was discarded and the pellet was let to dry. The DNA was then resuspended in 200 ul of T.E. Buffer [10 mM Tris-HCl (pH 8.0), 0.1 mM EDTA].

2.2.10 DNA/RNA quantification by UV spectroscopy

To quantify DNA or RNA concentration in solution, ultraviolet spectrophotometry using the Beckman DU530 UV/Vis Spectrophotometer (Beckman; Fullerton, CA) was employed. The following options were selected: nucleic acids, double stranded DNA or RNA. A baseline "blank" measurement was made of only water in the quartz optical cuvette of 1 cm path length (Fisher; Agawam, MA) and the program used this value to subtract baseline for further calculations. A known dilution of DNA or RNA of unknown concentration was made, usually 5 ul in 1 ml water, and put in the quartz cuvette and read. The program automatically subtracts the baseline value and multiplies by the dilution factor, returning a concentration value. The cuvette was rinsed with water in preparation for the next sample.

2.2.11 RNA isolation from HACAT cells

The CTα (CTP:phosphocholine citidyl transferase) cDNA was isolated from HACAT cells (human keratinocyte). Briefly, 500.000 HACAT cells were plated and incubated for 4 days. Then, the cells were washed once with PBS and 1 ml Trizol (Invitrogen; Carlsbad, CA) was added to the plate. The cells were collected along with the Trizol by pipetting and transferred in an eppedorf tube. 200 ul of chloroform were added and the sample was vortexed for 10 min followed by a spin for 15 min at 12000 rpm at 4^{o}C. The upper phase of the mixture was transferred in a new eppedorf tube and 0.5 ml isopropanol were added. The sample was centrifuged for 15 min at 12000 rpm at 4^{o}C and the supernatant was discarded. The pellet was washed with 75% EtOH and centrifuged at for 15 min at 12000 rpm at 4^{o}C. After discarding the supernatant we allowed the

pellet to dry and then it was resuspended in 30 ul DEPC-water (American Bioanalytical, Natick, MA) and stores at -80^{o}C.

The RNA from the HACAT cells was used to synthesize cDNA by reverse transcription. For the reverse transcription all materials, including dNTPs, random primers, first strand primers, DTT and reverse transcriptase were purchased from Applied biosystems (Foster City, CA). Finally, a large scale PCR using the appropriate primers for CTα (see section 2.2.4) was performed to isolate the CTα cDNA. The CTα cDNA was subcloned to the pAdTrack-CMV vector, using the BglII and NotI restriction enzymes, for adenovirus production.

2.2.12 Liver RNA isolation with Trizol

To purify total hepatic RNA, mouse livers were homogenized in Trizol (Invitrogen; Carlsbad, CA) followed by extraction of RNA from the homogenate using chloroform. A small piece of liver from mouse necropsy was stored in a 2-mL screw-cap tube at -80^{o}C. 1 ml of cold Trizol reagent was added to the sample and the tube's contents were homogenized in a Mini-Beadbeater-1 (BioSpec; Bartlesville, OK) at 3000 rpm for 30 seconds. Another 30 seconds of homogenization was used if liver pieces were still visible. The homogenate was stored on ice until all samples were homogenized as above. To separate aqueous and organic phases, 100 ul of chloroform was added to the homogenate, with shaking to mix, and the phases were formed by centrifugation at 13000 rpm for 15 minutes. After centrifugation, 350 ul of the upper aqueous phase, which contains RNA, was transferred to a sterile 1.5 ml microfuge tube. The interphase and the bottom organic phase, which contain genomic DNA and protein,

respectively, were discarded. To precipitate RNA, an equal volume (350 ul) of isopropanol was added to aqueous phase aliquot. The tube was end-over mixed several times to fully precipitate the RNA, and the RNA was pelleted by centrifugation at 13000 rpm for 15 minutes. After centrifugation, the pellet was washed with 500 ul of 75% ethanol:DEPC-treated water. The tube was end-over mixed several times and the RNA was re-pelleted by centrifugation at 13000 rpm for 5 minutes. After centrifugation, the pellet was left to dry and then was reconstituted in 150 ul of DEPC-treated water. To help RNA dissolution the samples were heated at 65^{o}C for 5 minutes. The RNA was quantified using the Beckman DU530 UV/Vis Spectrophotometer and was then stored at -80^{o}C.

2.2.13 Synthesis of cDNA from RNA and Quantitative real time PCR using TaqMan probes

RNA was reverse transcribed to cDNA, using the ABI High Capacity Reverse Transcriptase Kit (Applied Biosystems; Foster City, CA), for analysis with quantitative PCR. Each reverse transcription reaction was prepared on ice and composed according to the manufacturer's instructions. The reaction was thermal cycled according to the following program: 25^{o}C for 10 minutes, 37^{o}C for 120 minutes, 85^{o}C for 5 seconds and 4^{o}C hold.

Quantitation of RNA, after reverse transcription to cDNA, was accomplished using quantitative PCR with TaqMan probes and primers. The human LCAT (#Hs00173415_m1), human CTα (#Hs00192339_m1), human apoA-I (#Hs00985000_g1), human apoE (#Hs00171168_m1), human apoA-IV (Hs00166636_m1), mouse ABCA1 (# Mm00442646_m1) and 18S rRNA (#4319413E) probe/primer sets were purchased pre-optimized from Applied

Biosystems, as was the Gene Expression Master Mix (#4369016) containing the polymerase. The reactions was multiplexed to detect for the human gene of interest and 18S rRNA at the same time by using different fluorophores for each probe (FAM for the human gene of interest and VIC for 18S). Each reaction contained 1 ul cDNA (of a 1:500 dilution in water), 0.5 ul of the human gene probe/primer mix, 0.5 ul of the 18S probe/primer mix, 10 ul of the Gene Expression Master Mix, and 8 ul of DEPC-treated water. The reactions were composed in a frosted 96-well optical PCR plate and the plate was sealed with optical adhesive membrane (Bioplastics no: AB17500). A thermal cycling program was used in an ABI 7300 Real Time PCR machine as follows: 1 cycle at 50^{o}C, 20 minutes for UDG incubation, 1 cycle at 95^{o}C ,10 minutes for enzyme activation, 40 cycles at 95^{o}C, 15 sec for denaturation and 1 cycle at 60^{o}C, 1 min for Annealing, extension and reading. The 96-well plate was set up as a “ddCt" plate. After running, the threshold cycles were used to calculate relative values based upon the ddCt method using the program SDS v2.3 supplied by ABI.

2.3 Construction and analyses of adenoviruses

2.3.1 Transfection of adenoviral genome into HEK911 cells

The recombinant vectors for each gene of interest were incubated with the restriction enzyme PacI in order to get linearized and 10 ug of DNA were used to transfect 911 cells. For the transfection the Lipofectamin™2000 reagent (Invitrogen; Carlsbad, CA) was used according to the manufacturer’s instructions. Ten to twelve days post-transfection the viral particles that were formed caused lysis of the cells and the cell lysate was used for infection of a larger scale

culture in a T175 flask. The infections were performed in DMEM culture medium with 2% Heat Inactivated Horse Serum (HIHS) and 1% P/S. Two to three days after the new infection the cells were lysed and the new lysate was used for the infection of HEK-293 cells in a larger scale.

2.3.2 Large scale growth and purification of recombinant adenoviruses in HEK293 cells

For large scale growth of recombinant adenoviruses, HEK-293 cells were plated in T175 triple flasks and let to grow until the monolayer was confluent. The infection with either the previously mentioned lysate or 20 ul of purified virus was done using L-15 medium with 2% HIHS and 1% P/S. Three days after the infection and before the cells get lysed; large amounts of recombinant viral particles were produced. The cells that carry the produced viral particles were collected with centrifugation at 1000 rpm for 10 minutes. The collected pellet was resuspended in 2 ml of medium and stored at -80^{o}C. Then the suspension was frozen and thawed (-80^{o}C/37^{o}C) three times so the cells would lyse and the viral particles would be released in the medium. The suspension was then centrifuged at 3000 rpm for 10 min. The supernatant that contained the viral particles was subsequently centrifuged in $CsCl_2$ gradient twice in order to isolate the viral particles. For the first centrifugation 2 ml of $CsCl_2$ I (0.619 g/ml in TE) were transferred in a centrifuge tube, they were overlaid with 5 ml of $CsCl_2$ II (0.277 g/ml in TE) and 2-3 ml of the viral particles were placed on top. They were centrifuged at 30000 rpm for 90 minutes at 4^{o}C. The viral particles were concentrated in a region between the two dilutions. This region was collected with the help of a syringe and was transferred in 12 ml of dilution $CsCl_2$ III (0.450 g/ml in TE). It was centrifuged again at 55000 rpm at 4^{o}C for 16-20 hours. The viral particles were concentrated in a small ~2 mm zone. This zone was collected and

was dialyzed against sucrose buffer [10 mM Tris-HCL, 2 mM $MgCl_2$, 5% Sucrose, pH; 8] in a Slide-A-Lyzer® molecular weight cut-off (MWCO) 10000 (PIERCE; Rockfor, IL) dialysis cassette. The viral dilution was separated in 50 ul aliquots in 1.5 ml tubes and stored at -80^{o}C.

2.3.3 Plaque assay

911 cells were plated and grown to a monolayer, and subsequently were infected with serial dilutions of the virus. More specifically the viral particles were diluted $5x10^4$ to $5x10^7$ times in L-15 culture medium supplemented with 2 % HIHS and 1% P/S, and then were used to infect 911 cells that were seeded the previous day in 6-well plates at a concentration of $1.5x10^6$ cells per well. The cells after 30 minutes of incubation with the virus were fixed with culture medium [2x MEM, 4% HIHS, and 25 mM $MgCl_2$] diluted with agar [1.5% agar 40 mM Hepes, pH: 7.4]. The cells were incubated at 37^{o}C for 10 to 12 days. The plaques of lysis/infection of the cells were visual with naked eye and formed characteristic gray regions, in the case of the viruses we studied there was also expression of green fluorescence protein (GFP) and the plaques could be visualized under an optical microscope with the help of ultraviolet light. The plaques were counted for each dilution and the title of the virus was calculated.

2.3.4 Protein expression by adenoviruses

To estimate the expression of the various genes of interest that were generated in the adenoviruses, HTB-13 cells were cultured in 80% confluence in 6-well plates using 2 ml of L-15 medium supplemented with 2% HIHS and 1% P/S. The cells were infected with adenoviruses

that express the gene of interest with multiplicity of infection (MOI) 10, 15, and 20. As MOI we define the number of viral particles per cell. Twenty four hours post infection the cells were washed with 1x PBS and were incubated for 2 hours in medium that did not have any serum. Then new serum-free medium was added. The cells were incubated for 24 hours at 37^{o}C and then the medium as well as the cell extract was collected. The medium was collected to confirm the presence of secreted proteins like apoA-I, apoE and LCAT while the cell extract was collected for cellular proteins like CTα. An aliquot of the medium or the cell extract (100 ul) was analyzed by SDS-PAGE to estimate the expression/secretion of the protein of interest. The amount of protein was roughly estimated by analyzing on the same gel a known amount of BSA protein.

2.4 Cell culture and protein techniques

2.4.1 Cell cultures

The materials that were used in the cell cultures and specifically the culture media Dulbecco's Modified Eagles Medium (DMEM), DMEM high glucose and Leibovitz's L-15 (L-15) and HamsF12 medium, the buffer dilution Phosphate Buffered Saline (PBS), the enzyme Trypsin-EDTA as well as the antibiotics Penicillin-Streptomycin 9P/S) were bought from Cellgro (Manassas, VA) whereas the Fetal Bovine Serum (FBS) and Heat-Inactivated Horse Serum from Biomeda (Foster City, CA).

The cell lines used in these studies were HTB-13 (SW1783, human astrocytes), 911 (human embryonic retinoblasts), HEK-293 (human embryonic kidney) and HEK293 EBNA-T. The

stocks of the cultures are kept at -80^{o}C. The cells were placed in 37^{o}C water bath to thaw and then transferred in flasks with culture medium which was replaced the next day. The cells were grown in 25 or 175 cm^{2} flasks or 6 or 24-well plates in a HeraCell, Heraeus incubator (ThermoFisher Scientific; Waltham, MA) in 5% CO_2 at 37^{o}C. The cells were grown in L15 medium for HTB-13 and HEK-293 cell lines, DMEM for 911 cell line or high glucose DMEM for the HEK293 EBNA-T cell line supplemented with 10% FBS and 1% P/S. The medium in the flasks was replaced every 72 hours. The cells were split when the monolayer is confluent, with the use of trypsin-EDTA, to the desired concentration with the addition of culture medium.

2.4.2 Large scale production of apoA-I and apoE in HTB-13 cells

HTB-13 cells in roller bottles were used to secrete large amounts of apoA-I, apoE and their mutant forms after infection with adenoviruses expressing the respective cDNAs. Cells were seeded into six roller bottles (Fisher; Agawam, MA) at a concentration of 1.2x10^{8} cells per bottle, and kept in a roller incubator at 37^{o}C. Each cell was infected with a dose of 20 plaque forming units of virus (multiplicity of infection= 20), in 50 ml L-15 medium + 2% HTHS + 1% P-S. Medium was harvested and replaced every day for six days. 100 ul aliquots of media from each harvest were stored to assess for protein production by running 20 ul on SDS-PAGE and staining with Coomassie blue. Medium was centrifuged at 2000 rpm to pellet cellular debris and the supernatants were filtered through 0.45 micron PVDF and stored at -80^{o}C until purified.

For the purification the medium was frozen in Labconco® fast freeze flasks, placed on the lyophilizer and concentrated 5-fold. Then the concentrated media was placed in a 15000

MWCO dialysis tube and dialyzed against 25 mM ammonium bicarbonate at 4^{o}C. The dialysis media was changed three times and each time the protein was left to dialyze for at least 4 hours. After dialysis the protein was dried by lyophylization.

2.4.3 Purification of apoA-I and apoE that was produced in HTB-13 cells

For the purification the medium was frozen in Labconco® fast freeze flasks, placed on the lyophilizer and concentrated 5-fold. Then the concentrated media was placed in a 15000 MWCO dialysis tube and dialyzed against 25 mM ammonium bicarbonate at 4^{o}C. The dialysis media was changed three times and each time the protein was left to dialyze for at least 4 hours. After dialysis the protein was dried by lyophylization.

The lyophilized medium, containing the protein, was resuspended in 0.01M Tris, pH 8, filtered and passed through a 5 mL HiTrap Q HP column (GE Healthcare). The proteins were eluted with linear gradient of 0.15M NH_4CO_3 in the Tris buffer as described previously (108). The purity of the apoA-I preparation was assessed by SDS-PAGE and fractions greater than 95% pure were pooled.

2.4.4 LCAT production and concentration

HTB-13 cells were plated in T175 flasks and infected with the adenoviruses expressing LCAT or LCAT mutants at 20 MOI. After 1 day of incubation with the adenoviruses, the medium was changed (L-15, 2% HIHS, 1% PS) and after 2 days the medium was collected for 3

consecutive days. The total medium was concentrated up to 15 ml using 10000 Da molecular weight cut-off centriplus filters (Amicon) by centrifugation at 6500 rpm for 2 hours at 4^0C using a JA-20 rotor. The medium was further concentrated up to 1 ml using 10000 Da molecular weight cut-off microcon filters (Amicon) by centrifugation at 13000 rpm for 5 minutes at 4^0C. The volume of the concentrated medium was adjusted to 10% glycerol by adding 100% glycerol and to 1xStorage buffer (50 mM sodium phosphate, pH 7.4, 50 mM EDTA). The concentrated medium was divided into single use aliquots of 2 ul and stored at -80°C. The LCAT was assessed by western blotting.

2.4.5 Protein extraction from cell cultures

For protein extraction from cells grown in 6-well or p60 plates, the medium was removed and the cells were rinsed in cold PBS. The cells were scraped and collected in 1 ml PBS in eppedorf tubes and then centrifuged at 5000 rpm for 5 minutes at 4^oC. The supernatant was discarded and 150 ul of lysis buffer (20 mM Tris–HCl, pH 7.5, 150 mM NaCl, 10% glycerol, 1% Triton X-100) with protease inhibitor cocktail (Roche) were added to the pellet. The samples underwent a 30 minute rotation and centrifuged at 13000 rpm for 5 minutes at 4^oC. The supernatant containing the protein was stored in -80^{o}C.

2.4.6 Protein extraction from mouse livers

100 ug of mouse liver was placed in a glass tube along with 350-450 ul RIPA buffer (1xPBS, 0.5% sodium deoxycholate, 1%NP-40, 0.1% SDS) containing a protease inhibitor

cocktail (Roche). The tissue was homogenized for 20 seconds and the tube was transferred on ice. After two freeze/thaw cycles in liquid nitrogen and a 37^{o}C waterbath, the samples were vortexed for 15 minutes in the cold room. Finally, they were placed on ice for 30 minutes and were centrifuged at 13000 rpm for 10 minutes at 4^{o}C. The supernatant containing the protein was stored in -80^{o}C. In some samples there was an abundance if triglycerides in the supernatant. To remove them, the samples were centrifuges 3 times at max speed and each time the lipids were removed by pipetting as much as possible. Additionally, for the extraction of large proteins such as ABCA1, the final centrifugation was at 5000 rpm since large proteins form aggregates in high speed.

2.4.7 Quantification of protein using DC protein assay

Protein was quantified with a microplate reader using the Bio-Rad DC Protein Assay (Bio-Rad; Hercules, CA), which is based on the procedure of Lowry. 20 ul of Reagent S were mixed with 1 ml of reagent A in a 1.5 ml microcentrifuge tube to make the working reagent A'. 25 ul of working reagent A' was pipetted into each well of a 96-well plate with 5 ul of samples or standard BSA amounts per well. 200 ul of reagent B was added to each well and the plate was mixed briefly. The plate was assayed at 750 nm wavelength. The standards used were dilutions of BSA at concentrations 1.5 mg/ml, 1 mg/ml, 0.6 mg/ml, 0.2 mg/ml and 0 mg/ml (PBS only). A regression of the standards was made and used to calculate concentration of unknown samples from absorbance at 750 nm.

2.4.8 SDS-polyacrylamide gel electrophoresis (SDS-PAGE)

For the analysis of proteins by SDS-PAGE there was used the appropriate amount of 4x SDS Loading Buffer [2.5 ml 1M Tris-HCl pH 8, 1.6 ml β-mercaptoethanol, 8 ml 20% SDS, 4 ml glycerol, 8 mg bromophenol blue], 12.5% polyacrylamide gels for the running gel [3.2 ml ddH_2O, 4.2 ml 30% bis-acrylamide, 2.5 ml running buffer (Tris-HCl 1.5 M, SDS 0.4%, pH 8.8), 160 ul 10% ammonium persulfate (APS), 8 ul TEMED] and 4% for the stacking gel [3.6 ml ddH_2O, 0.9 ml 30% bis-acrylamide, 1.5 ml stacking buffer (0.5M Tris-HCL, 0.4% SDS, pH 6.8, 60 ul 10% APS, 6 ul TEMED]. The electrophoreses were performed in 500 ml of 1x TGS dilution [1L 10x TGS : 30.2 g Tris-HCl, 144 g Glycine, 10 g SDS, pH 8.3], at 120 V with the use of Bio-Rad Protean electroblot.

The gels were stained and fixed with Coomasie Brilliant Blue [2.5 g Coomasie Brilliant Blue R, 50 % methanol and 10% acetic acid] for 30 minutes and then destained in destaining solution [50% methanol, 10% acetic acid] for 60 minutes or more in order to obtain a clear image of the protein bands. The gels were dried in a Bio-Rad gel dryer under vacuum at 80^{o}C for 1 hour.

2.4.9 Western blotting

The proteins analyzed by SDS-PAGE were transferred to nylon PVDF membranes. Prior to transfer the membranes were incubated first in methanol for 15 s, then in water for 2 min, and finally in transfer buffer [700 ml H_2O, 100 ml 10x TGS and 200 ml methanol] to equilibrate for at least 5 min.

The transfer was performed using Bio-Rad Protean electroblot apparatus in 1L transfer buffer with electrophoresis at 35 V, at 4^{o}C for 16 hours. After the transfer, the membranes were washed with TBS-T [1x TBS, 0.05% Tween-20], (1L 10x TBS: 90 g NaCl, 0.5M Tris-HCl, pH 7.3) for 10 minutes at room temperature. The membranes were incubated with blocking buffer [1x TBS-T, 5% non-fat milk] for 1 hour at room temperature and were incubated for 1 hour at 37^{o}C with primary antibody specific for the protein we want to detect in the appropriate dilution in blocking buffer (Table 2.II). The membranes were washed three times for 10 minutes with TBS-T at room temperature. The secondary antibody was applied in the appropriate dilution in blocking buffer (Table 2.II) for 1 hour at 37^{o}C. The secondary antibody recognizes the primary antibody and it has also attached to it the enzyme horse radish peroxidase (HRP). The membranes were washed three times for 10 minutes with TBS-T followed by an additional wash for 5 minutes with TBS at room temperature. The detection of the proteins was accomplished with the ECL system and by exposing the films for different time intervals.

Table 2.II: Antibodies used for western blots

Protein	Primary antibody	Secondary antibody
LCAT (human)	rabbit anti-human, polyclonal 1:1000 (gift from Dr. Parks JS)	goat anti-rabbit IgG, HRP 1:5000 sc-2004 (Santa Cruz)
PCYT1A or CTα (human)	mouse anti-human, monoclonal 1:1000 WH0005130M3 (Sigma)	goat anti-mouse IgG, HRP 1:10000 sc-2005 (Santa Cruz)
ApoA-I (human)	goat anti-human, polyclonal 1:2000 AB740 (EMD Millipore)	rabbit anti-goat IgG, HRP 1:5000 sc-2768 (Santa Cruz)
ApoA-I (mouse)	rabbit anti-mouse, polyclonal 1:5000 K23500R (Biodesign)	goat anti-rabbit IgG, HRP 1:5000 sc-2004 (Santa cruz)
ApoA-IV (human)	goat anti-human, polyclonal 1:1000 (gift from Dr. K. Weisgraber)	rabbit anti-goat IgG, HRP 1:5000 sc-2768 (Santa Cruz)
ApoE (human)	goat anti-human, polyclonal 1:5000 K74190G (Biodesign)	rabbit anti-goat IgG, HRP 1:5000 sc-2768 (Santa Cruz)
LPL (human)	goat anti-human polyclonal 1:1000 (Santa Cruz)	rabbit anti-goat IgG, HRP 1:5000 sc-2768 (Santa Cruz)
ABCA1	rabbit anti-human, polyclonal	goat anti-rabbit IgG, HRP

(human/mouse)	1:1000 NB400-105 (Novus Bio)	1:5000 sc-2004 (Santa cruz)
GAPDH (human/mouse)	rabbit anti-human polyclonal 1:1000 sc-25778 (Santa Cruz)	goat anti-rabbit IgG, HRP 1:5000 sc-2004 (Santa cruz)

2.4.10 Preparation of recombinant HDL (rHDL) containing apoA-I or apoE

Proteoliposomes containing apoA-I or apoE, cholesterol, sodium cholate, and POPC phospholipids were prepared as previously described (535). Stock solutions of lipids were made as follows: 2 mg/ml cholesterol (Sigma; St. Louis, MO) in chloroform: methanol, 30 mg/ml sodium cholate in salt buffer, 20 mg/ml 1-palmitoyl-2-oleoyl-sn-glycero-3-phosphocholine (POPC; Avanti; Alabaster, AL) in chloroform: methanol, 2 mg/ml apoa-I or apoE in salt buffer. Salt buffer contained 10 mM Tris HCl pH 8, 150 mM NaCl, and 0.01% EDTA. Chloroform: methanol was a mixture of 2 parts chloroform and 1 part methanol.

The proteoliposomes were prepared with a molar ratio of POPC/cholesterol/apoE/cholate of 100:10:1:100. First, 135.5 ul (111 ul for apoE) POPC stock and 70 ul (50 ul for apoE) of cholesterol stock were put in a glass tube and evaporated under a stream of nitrogen gas until dry. Lipids were resuspended in salt buffer on ice for an hour (250 ul for apoA-I and 246 ul for apoE). 51 ul (42 ul for apoE) of sodium cholate solution was added to the tube and the mixture was incubated on ice for an hour to form micelles. 500 ul of 2 mg/ml apoA-I or apoE was added to the mixture, which was incubated on ice for an hour to form proteoliposomes. The proteoliposomes were dialyzed against salt buffer overnight at 4^{O}C with stirring.

2.4.11 α-LCAT assay

For LCAT analysis on HDL (α-LCAT activity), the rHDL particles used as substrate contained cholesterol + [^{3}C]cholesterol ([^{3}C]cholesterol; 0.04 mCi/ml, specific activity 45 mCi/mmol -Perkin Elmer Life Sciences, Inc.; Boston, MA), β-oleoyl-γ-palmitoyl-L-α-phosphatidylcholine (POPC) (Avanti; Alabaster, AL) and apoA-I and were prepared by the sodium cholate dialysis method as described in section 2.4.10. The main difference was the amount of the reagents used. The molar ratio of POPC/Cholesterol and [^{3}H]Cholesterol/apoA-I/Na-Cholate was 100/10/1/100. The ratio of cholesterol to [^{3}H]cholesterol was around 5:2 and the goal was to obtain 5000-7000 counts per minute per 1 nmole of cholesterol. For the reactions a series of apoA-I amounts (ranging from 1.5 to 32 ng) were combined with 50 ul fatty acid free BSA at 40 mg/ml concentration, 20 ul β-mercapto-ethanol 100 mM, and salt buffer to a final volume of 450 ul. The reactions were placed at 37^{o}C and after 10 minutes 50 ul of LCAT was added. The LCAT used was a dilution of the concentrated purified enzyme. Usually a 1:1000 – 1:5000 dilution was used. This was calculated by adjusting the dilution so that at 30 minutes, 15 % of the cholesterol of rHDL containing 4 ug of WT apoA-I was converted to cholesterol esters. The reactions were carried on for 30 minutes and then they were terminated by adding 5 ml chloroform: methanol 2:1 containing 0.2 mg cholesterol and 0.2 mg cholesteryl oleate. The reactions were let to settle down so that the two phases could separate. The upper, aqueous phase was carefully removed with a glass pipette and discarded and the lower, non-polar phase that contained the cholesterol was dried under N_2. The dried lipids were solubilized in chloroform and were spotted on ITLC (Pall) paper. They were then developed for 1.5 min in a TLC tank that was presaturated with petroleum ether: ethyl ether: acetic acid at a volume ratio

of 85:15:1. The cholesterol was visualized under iodine and the ITLC was cut. The upper band contained the cholesteryl esters that moved faster and the middle the free cholesterol. These two pieces were placed in two scintillation vials containing 10 ml scintillation cocktail ECONOMICAL biodegenerable counting cocktail (Econo-Safe™; Canton, MA) and their radioactivity was measured. The lower band was the oxidized cholesterol that moved even slower and its radioactivity was not assessed. The cholesterol esterification rate was expressed as nanomoles of cholesteryl ester formed per hour. To convert the counts per minute that were recorded by the Beckman LS6500 scintillator to nanomoles the following formula was used:

$$nmol\,CE/hour = CPM_{CE} \times \frac{nmol_{TC}}{CPM_{TC}} \times \frac{1}{0.5\ hours}$$

where $nmol_{TC}$ represents the nanomoles of proteoliposomes cholesterol in the 500 ul reaction, CPM_{CE} the counts per minute of cholesteryl esters and CPM_{TC} represents the combined counts per minute of cholesterol and cholesteryl esters. To calculate the apparent $Vmax_{app}$ and Km_{app}, the rate of cholesteryl ester formation was plotted versus the concentration of apoA-I. The data were fitted to Michaelis-Menten kinetics, using the Prism software (GraphPad Software, Inc.).

1.2.1 β-LCAT assay

For LCAT analysis on IDL/LDL (β-LCAT activity), the lipoproteins from human plasma (IRB protocol number: H-32538) were isolated by sequential ultracentrifugation at densities between 1.007 and 1.063 g/ml (IDL+LDL) and dialyzed in the dialysis buffer (10 mM Tris-HCl, pH 7.4, 0.15 M NaCl, 5 mM EDTA) at 4^0C for 16-24 hours. The amount of the free cholesterol in the

fractions was the determined using the free cholesterol C kit by Wako (Wako Chemicals USA, Inc.). The fraction were heat inactivated at 56^{o}C for 30 min and the radiolabeled lipoproteins were prepared by equilibration with [^{3}C]cholesterol at 4°C as described by Dobiasova and Schutzova (536).

Briefly, 5 ul [^{3}C]cholesterol in a glass tube was dried under N2 and then dissolved in 200 ul absolute ethanol. Using a perforator, Whatmann paper discs were cut and put on parafilm. 6 ul of the [^{3}C]cholesterol dissolved in ethanol were pipetted on each disc, let air dry for 10 minutes and stored at 4^{0}C in eppedorf tubes (for up to 3 months). For IDL/LDL labeling, an amount of the IDL/LDL fractions that contain 18 nmol FC (MW of FC: 386.65 g/mol) (537) was added to a tube with the disc containing the [^{3}C]cholesterol for 20 hours at 4^{0}C. The samples were then dialyzed against dialysis buffer to remove [^{3}C]cholesterol that is unbound to IDL/LDL.

An aliquot of 4.5 ul of concentrated cell culture medium containing the WT LCAT or the mutant LCAT proteins [the equal quantity was estimated by western blot and using the ImageJ software (Rasband WS. ImageJ, U.S. National Institutes of Health, Bethesda, Maryland, USA)] were added to the mixture containing the labeled IDL/LDL, 5mM β-mercaptoethanol, and 1.5% bovine serum albumin (essentially fatty acid free) to a final volume of 0.4 ml (in dialysis buffer). The reaction mixture was incubated at 37^{o}C for 24 hours and the reaction was terminated by adding 2 ml of ethanol. The mixture was centrifuged at 2000 rpm for 10 minutes and the supernatant containing the cholesterol and the cholesteryl ester was transferred to a new glass tube. The samples were dried under N2 and resuspended 75 µl of chloroform. The spotting of cholesterol and cholesteryl esters was performed using ITLC paper and 25:15:1 (v/v/v) Petroleum ether:Ethyl ether:acetic acid as described in section 2.3.11. The results were

expressed as the percentage of free cholesterol esterification which refers to the rate of cholesteryl ester formation in isolated lipoprotein fraction catalyzed by the recombinant enzyme.

2.4.13 ABCA1 efflux assay

For the ABCA1-mediated cholesterol efflux assay, HEL293-EBNA-T cells were plated in a 24 well plate that was precoated with poly-D-lysine at a $2x10^5$ cells/well concentration. The cells were cultured in antibiotic free high glucose DMEM medium supplemented with 10% FBS. The next day the medium was removed and fresh medium was added (0.5 ml/well). The cells were then transfected with a pcDNA3.1 plasmid expressing ABCA1 or a Mock plasmid. Briefly for each well 1 ug of plasmid DNA was diluted in 50 ul of opti-MEM I (Invitrogen) and 2.5 ul of Lipofectamine 2000 (Invitrogen) was diluted in 50 ul of opti-MEM I. After a 5 min incubation the diluted DNA was combined with the Lipofectamin 2000. Following a 20 min incubation at RT the liposome complexes were added to the cells. The next day the medium was switched to high glucose DMEM/10% heat inactivated FBS supplement with 0.5 µCi [^{3}H]cholesterol/ml. The cells were allowed to load [^{3}H]cholesterol for 24 h. Then the cells were washed twice with warm PBS. Subsequently they were incubated in 0.5 ml of 2 mg/ml fatty-acid free BSA in high glucose DMEM for 1 h. The medium was removed and 0.5 ml of medium containing 2 mg/ml fatty-acid free BSA in high glucose DMEM supplemented with 1 µM apoA-I WT (28 ug/ml) or mutants was added.

Following incubation at 37°C for 4 h, the medium was collected in eppendorf tubes and was centrifuged at 8000prm for 5 min. The next step was to transfer 300 ul of the efflux medium into a scintillation vial containing 10 ml of scintillation fluid, mix and count the radioactivity. As for the calculation of the total cholesterol present in the cells 1 ml of 0.1 M NaOH was added in each well and after incubation for 1 h the lysate was transferred in 10 ml of scintillation fluid and radioactivity was measured. The percentage of efflux was calculated as the counts in the efflux medium divided by the combined counts of the lysate and the efflux medium. The ABCA1-mediated efflux was calculated after subtracting from the ABCA1 transfected cells the efflux of the Mock-transfected cells.

2.4.14 Human arterial endothelial cell preparation and incubation with rHDL

Human aortic endothelial cells (HAECs) purchased from Lonza Walkersville Inc (CC-2535) were plated in p100 plates in EGM-2 Bullet kit (EBM-2 Basal medium with singlequot kit supplementary and growth factors) (Lonza) and 10% FBS. The medium was changed the next day and then after every other day. When the cells reached 90% confluency, they were splitted using trypsin-EDTA and plated in three p100 plates. The cells were splitted again at 90% confluency, plated in p60 plates and maintained for 48 hours. When they reached at 90% confluency the medium with the growth factors were removed and substituted by EBM-2 (without growth factors) containing 0.5% FBS and 5% lipoprotein-deficient serum (LDS) for 4 hours and then with EBM-2 containing 5% lipoprotein-deficient serum (LDS) for 12 hours in the presence or absence of rHDL, HDL or PBS. The treatments included 250 ug of rHDL containing apoA-I or apoE with or without cholesterol (section 2.4.10), free apoA-I, free apoE, HDL isolated

from human or mice plasma and PBS. Total RNA and protein were extracted (see sections 2.2.11 and 2.4.5) and 1 ug RNA was used for microarray analysis (Affymetrix). Functional annotation of the significantly changed genes based on selected Gene Ontology categories was performed using the Gene Tools software (Scieplas Ltd, UK). Microarray data were validated with high-throughput qRT-PCR based screening using the dynamic array chips (Fluidigm, Biomark).

2.5 Mouse manipulations (adenoviral injections, liver and mouse plasma collection)

ApoA-I$^{-/-}$ (ApoA-I^{tm1Unc}) C57BL/6J mice (538) were purchased from Jackson Laboratories (Bar Harbor, ME), mice deficient for apoA-I and apoE were a gift of Dr. Fayanne Thorngate and Dr. David Williams (539), mice deficient in ABCA1 (130) (purchased from Jackson Laboratories) were provided by Dr. Mike Filtzerald. Mice deficient for LCAT were a gift of Dr. Santa- Marina Fojo (174).

The mice were maintained on a 12 h light/dark cycle and standard rodent chow diet. All procedures performed on the mice were in accordance with National Institutes of Health and institutional guidelines. 6-8 weeks old mice were injected via tail vein with recombinant adenovirus in an appropriate dose per animal and the animals were sacrificed 4 days post-injection following a 4 h fast.

For the collection of blood sample and the subsequent plasma isolation from the mouse vein there were used the Microvette CB 300 K2E (STARSTEDT) tubes. For the collection of larger volume of blood before the sacrifice of the animals we used Microtube 1.3 ml KE

microcentrifuge tubes. From each mouse around 750 ul of blood were collected. Then the samples were centrifuged at 3500 rpm for 10 min and the plasma was separated. The plasma was transferred in a new microcentrifuge tube and was stored at $4^{o}C$ until further analyses were performed.

2.6 Lipid/lipoprotein analyses

2.6.1 Lipid and apoA-I measurement in plasma

The concentration of total cholesterol, free cholesterol, triglycerides, phospholipids and apoA-I of plasma drawn 4 days post-infection was determined using the cholesterol E, free cholesterol C, Phospholipids C reagents, apoA-I (Wako Chemicals USA, Inc.) and Infinity^{TM} Triglycerides (ThermoScientific; Middletown, VA) respectively, according to the manufacturer's instructions. The concentration of cholesteryl esters was determined by subtracting the concentration of free cholesterol from the concentration of total cholesterol. The concentration of apoA-I was measured using the AutoKit-AI (Wako Chemicals USA, Inc.).

2.6.2 ApoE measurement in plasma

Plasma apoE concentration was determined using a sandwich ELISA employing HRP-mediated cleavage of TMB substrate. Anti-human-apoE antibody (Biodesign K74190G) was used to capture the measured ligand. The antibody was diluted 1:1000 in PBS, and 100 ul of this

dilution was added to each well of a Nunc MaxiSorp 96-well plate. The plates were covered with film and incubated at 4^{o}C overnight or up to one week.

Plates were then emptied, washed five times with 200 ul per well of wash solution (PBS + 0.05% Tween-20), and blocked with 200 ul per well of blocking solution (PBS + 0.1% Casein) for at least two hours at 37^{o}C. In the meantime, plasma samples were serially diluted in blocking solution. Plasma samples that were high in cholesterol or triglycerides were diluted up to 4 million times, and the dilutions between 100 thousand and 4 million times were applied to the plate. Plasma samples that were low in cholesterol or triglycerides were diluted up to 400 thousand times, and the dilutions between 50 thousand and 400 thousand times were applied to the plate. Standard human serum (Wako Control Serum II; Wako Diagnostics; Richmond, VA) of 1.8 mg/dl apoE concentration was serial diluted with blocking buffer (dilutions in ug/dL were 1800, 18, 9, 4.5, 2.25, 1.125, 0.56, 0.28, 0.14 and 0.07) and applied to the plate. 100 ul of each sample dilution, as well as duplicates of 100 ul of each standard dilution, were applied to the plate. Plates were covered with adhesive film and incubated overnight at 4^{o}C.

The following day, the plates were washed five times with 200 ul per well of wash solution. 100 ul of detection antibody solution [10 ml blocking buffer, 100 ul normal goat serum (Sigma-aldrich; St. Louis, MO), 50 ul 10% Tween-20, 10 ul secondary antibody (Biodesign; Saco, ME, K34002G)] was added to each well, and the plates were covered with adhesive film and incubated for 2 hours at 37^{o}C. After incubation, the plates were washed five times with 200 ul per well of wash solution. 100 ul of 1-Step Slow TMB (Pierce; Rockford, IL; 34024) was added per well and incubated at room temperature for 10 minutes or until a linear standard curve developed. The TMB reaction was stopped by the addition of 200 ul per well of

0.1M H2SO4. Plates were read at 450 nm in a plate reader (Dynex MRX II; Dynex; Chantilly, VA).

From the standard dilutions, a standard curve of concentration versus absorbance at 450 nm was calculated using the five dilutions of lowest concentration, as the dilutions of higher concentration are generally beyond linear range. Concentration of the experimental samples was calculated by comparing to the standard curve and multiplying by the sample dilution factor.

2.6.3 Fast Protein Liquid Chromatography (FPLC)

For the analysis of plasma with FPLC 20 ul of plasma (diluted in 40 ul of PBS for a total volume of 60 ul) were used. The plasma obtained from mice infected with adenovirus-expressing WT or mutant apoA-I forms was loaded onto a Sepharose 6 PC column in a SMART microFPLC system (Amersham Biosciences) and eluted with PBS. A total of 25 fractions of 50 ul volume each were collected for further analysis using the following program.

```
0.00 FLOW                50.0
0.00 CON_B               100.0
0.00 LOOP                1
0.00 FILL                B, 2, 10, 15000
0.20 INJECT
0.90 NEEDLE_POSITION     DOWN
0.90 GOTO_TUBE           1
0.90 FRACTION_SIZE       50
2.15 FRAC_STOP
2.15 FLOW                75
3.15 LOAD
3.15 NEW_CHROMATOGRAM
3.15 END_LOOP
```

The concentration of lipids in the FPLC fractions was determined as described in section 2.6.1.

2.6.4 Fractionation of plasma by density gradient ultracentrifugation

For this analysis, 240 ul of plasma obtained from adenovirus-infected mice was diluted with saline to a total volume of 0.4 ml. The mixture was adjusted to a density of 1.23 g/ml with KBr and overlaid with 0.8 ml of KBr solution of *d* = 1.21 g/ml, 2 ml of KBr solution of *d* = 1.063 g/ml, 0.4 ml of KBr solution of *d* = 1.019 g/ml, and 0.4 ml of normal saline. The mixture was centrifuged for 22 h in SW60 rotor at 28500 rpm. Following ultracentrifugation, 0.4 ml fractions were collected from the top for further analyses. The refractive index of the fractions was measured using a refractometer (American Optical Corp.) and it was converted to density for each sample based on a standard curve derived from solutions of known densities. The fractions were dialyzed against ammonium acetate and carbonate buffer (126 mM ammonium acetate, 2.6 mM ammonium carbonate, 0.26 mM EDTA, pH 7.4). Aliquots of the fractions were dialysed in ddH_2O and subjected to SDS-PAGE, and the protein bands were visualized by staining with Coomassie Brilliant Blue.

2.6.5 Electron Microscopy

For EM analysis, fractions that float in the VLDL/IDL/LDL or HDL region were dialyzed against ammonium acetate and carbonate buffer. The samples were applied on carbon-coated grids, were stained with sodium phosphotungstate, were visualized in the Philips CM-120

electron microscope (Philips Electron Optics, Eindhoven, Netherlands) and photographed; these procedures were performed by Dr. Donald Gantz at the Department of Biophysics of Boston University. The photographs have been magnified 225,000 times.

2.6.6 Non-denaturing two-dimensional (2D) gel electrophoresis

The distribution of HDL subfractions in plasma was analysed by 2D electrophoresis as described by Fielding and Fielding 1996 (540) with some modifications. In the first dimension, an appropriate amount of plasma sample was separated by electrophoresis at 4^{o}C in a 0.75% agarose gel using a 50 mM barbital buffer (pH 8.6, Sigma, St Louis, MO) until the bromophenol blue marker had migrated 5.5 cm. Agarose gel strips containing the separated lipoproteins were then transferred to a 4-20% polyacrylamide gradient gel. Separation in the second dimension was performed at 90 V for 2-3 h at 4^{o}C using non-denaturing 1x TGS buffer [1l 10x TGS: 30.2g Tris-HCl, 144g Glycine]. The proteins were transferred to a nitrocellulose membrane and apoA-I was detected by using the goat polyclonal anti-human apoA-I antibody AB740 (Chemicon International) in a 1:2000 dilution.

2.7 Biophysical studies

2.7.1 ApoA-I preparation for biophysical analyses

Before all analyses, lyophilized wild-type or mutant apoA-I forms were dissolved at a final concentration of 0.2mg/mL in 8M guanidine hydrochloride in DPBS. The protein samples

were incubated for 1h at room temperature and then dialyzed extensively against DPBS pH 7.4. The samples were centrifuged at 12000g for 10 min to remove any precipitated protein. The supernatant solutions were quantitated by measuring their absorbance at 280nm. The proteins were kept at low concentrations (~0.1mg/mL) on ice to avoid aggregation. All analyses were performed on freshly refolded protein.

2.7.2 Circular dichroism measurements

A Jasco-715 spectropolarimeter connected to a Jasco PTC-348 WI Peltier temperature controller was used to record the far-UV CD spectra of the ApoA-I samples from 190 to 260nm at 25°C using a quartz cuvette with an optical path of 1nm. The protein samples were at 0.1mg/mL in DPBS (pH 7.4). The measurement parameters were as follows: bandwidth 1nm, response 8sec, step size 0.2nm and scan speed 50nm/min. Each spectrum was the average of 5 accumulations. The results were corrected by subtracting the buffer baseline.

Helical content was calculated based on the molar ellipticity at 222nm as described by Greenfield et al. (541) using the equation: $\%\alpha\text{-helix}_{222nm}=([\Theta]_{222}+3000)/(36000+3000)\times100$.

To record the thermal denaturation profile of the protein, we monitored the change in molar ellipticity at 222nm, while the temperature was raised from 20 to 80°C, at a rate of 1°C/min. The curve was fitted to a Boltzman sigmoidal model curve using the Graphpad Prism™ software.

2.7.3 Chemical denaturation

To record the chemical denaturation profile of ApoA-I, 0.1 mg/mL of freshly refolded protein was added to a 4 mL quartz fluorimeter cuvette and the intrinsic tryptophan protein fluorescence was measured after excitation at 295 nm. Small amounts of an 8.0 M guanidine hydrochloride (Applichem) solution were gradually added in the cuvette. The contents were continuously mixed using a magnetic stirrer. After each addition of guanidine hydrochloride, the sample was incubated in the dark for 2 min before measuring the fluorescence signal.

2.7.4 8-anilino-1-naphthalene-sulfonate (ANS) fluorescence

1,8 ANS (1-anilinonaphthalene-8-sulfonic acid, Sigma-Aldrich) was dissolved in dimethylsulfoxide (DMSO) to a final concentration of 50 mM (ANS stock solution). Freshly refolded ApoA-I at 0.05mg/ml in DPBS pH 7.4 was placed in a 4 mL quartz fluorimeter cuvette (Hellma, Germany). Fluorescence measurements were performed in a Quantamaster 4 fluorescence spectrometer (Photon Technology International, New Jersey). The scan rate was 1 nm/s with excitation at 395 nm and emission range from 420 to 550 nm. After measuring the background protein fluorescence, 7.5 *ul* of ANS stock solution were added in the cuvette and mixed so that the final ANS concentration was 250 μM. A control ANS spectrum in the absence of protein was also recorded.

2.8 Statistical analysis

Dependent variables were assessed for difference between experimental groups using Student's t-test with unequal variance. Student's t-test was calculated using Microsoft Excel (Microsoft, Inc.). Differences of $p \leq 0.05$ were considered statistically significant.

3. RESULTS-DISCUSSION

The results-discussion section includes chapters I-VII. In chapter I is described the generation and characterization of recombinant adenoviruses expressing wild type and mutants proteins involved in the HDL biogenesis. In chapter II is described the importance of the hydrophobic residues in the 218-230 region of apoA-I in the biogenesis of HDL. This project includes the *in vivo* experiments, functional analyses and physicochemical studies of the following apoA-I mutants:

1. apoA-I[L218A/L219A/V221A/L222A]
2. apoA-I[F225A/V227A/F229A/L230A]
3. apoA-I[L218A/L219A/V221A/L222A/F225A/V227A/F229A/L230A]

The mutants will be abbreviated from now on as apoA-I[218-222], apoA-I[225-230] and apoA-I[218-230] respectively.

In chapter III and chapter IV are described experiments where we study the effect of naturally occurring human LCAT mutations and CTα respectively on the biogenesis of HDL.

In chapter V are described the *in vivo* experiments designed to assess the molecular etiology of a dominant form of type III hyperlipoproteinemia that results from the natural apoE mutations K146N/R147W in humans.

In chapter VI is described my contribution is studies to assess the role of apoA-IV in the biogenesis of apoA-IV-containing HDL and in chapter VII my contribution in studies designed to assess the effect of reconstituted HDLs in endothelial gene expression.

Chapter I: Generation and characterization of recombinant adenoviruses expressing wild type and mutants proteins involved in the HDL biogenesis

For this thesis I used adenoviruses expressing the WT apoA-I, the apoA-I mutants, the WT apoE3, the apoE3 mutants, the WT LCAT, the LCAT mutants, LPL and GFP in gene transfer studies in different mouse models. For a detailed list of the adenoviruses see Table 3.I.

Adenoviruses expressing the WT apoA-I and the apoA-I mutants, apoA-I[218-222], apoA-I[225-230] and apoA-I[218-230] have been generated as described previously (542). Briefly, the apoA-I mutants were generated by site-directed mutagenesis using the primers described in Table 2.I and the method described in 2.2.1 of the Materials and Methods. In the case of apoA-I[218-230] mutant the template was pCDNA3.1apoA-I[218-222]. The mutated apoA-I cDNA was cloned in the shuttle vector pAdTrack-CMV and the recombinant viruses were constructed using the Ad-Easy-1 system where the recombinant adenovirus construct is generated in bacteria BJ-5183 that harbor the required adenoviral genes (543).

The adenoviral constructs containing the apoE3 mutants had been similarly generated (544) (Table 3.I) using the appropriate mutagenic primers (Table 2.I). The truncated apoE3[K146N/R147W]-202 was generated using the pGEM7-apoE3[K146N/R147W] vector as a template and the mutagenic primers apoE3[L203Stop]-F and apoE3[L203Stop]-R (Table 2.I).

The LPL cDNA cloned in the pCMV-Sport6 vector was excised using the KpnI and HindIII restrictions enzymes and subcloned into the corresponding sites of the pAdTrack-CMV vector (544). The apoA-IV cDNA was generated by RT-PCR of human DNA using as primers 5'- 3' that

contained restriction sites for Bgl-II and EcoRV respectively. The apoA-IV cDNA was digested with Bgl-II and EcoRV and cloned into the correspondence sites of the pAdTrack-CMV vector (16).

Table 3.I: Adenoviruses produced

Name of adenovirus	Titer (pfu/μl)	Rationale
WT apoA-I	3.3×10^7	Control WT virus for the apoA-I mutants
apoA-I[218A/L219A/ V221A/L222A]	5.5×10^7	Conserved residues among species. Deletion of 220-231 region of apoA-I inhibited apoA-I-ABCA1 interaction. The 218-230 area is unstructured and is not organized in amphipathic helices similar to the rest of apoA-I.
apoA-I[F225A/V227A /F229A/L230A]	4×10^7	
apoA-I[L218A/L219A/ V221A/L222A/F225A/V 227A /F229A/L230A][a]	2×10^7	
WT apoE3	4.5×10^7	Control WT virus for the apoE3 mutants
apoE3[K146N/R147W]	4.3×10^7	Dominant form of type III hyperlipoproteinemia in humans (545)
apoE3[K146N/R147W]-202	1.1×10^8	To assess the contribution of the C-terminal 203-229 domain to clear plasma cholesterol and triglycerides
apoE4-202	5.8×10^7	Used as control since these truncated forms clear plasma cholesterol and triglycerides
apoE4[R142C]-202	1.2×10^8	
WT CTα [WT]	3.5×10^7	Used to examine the effects of CTα on HDL formation
WT LCAT	3×10^7	Control WT virus for the LCAT mutants. Also used to rescue the defective lipid/lipoprotein phenotype caused by the apoA-I mutants or apoE3 mutants
LCAT[E110D][c]	-[b]	Half normal HDL-C levels in heterozygosity in humans (161)
LCAT[Y111N[c]	-[b]	Half normal HDL-C levels in heterozygosity in humans (161)
LCAT[E110D/Y111N][c]	-[b]	Half normal HDL-C levels in heterozygosity in humans (161)
LCAT[T123I][c]	8×10^7	Fish Eye Disease syndrome in humans (164)
LCAT[N131D][c]	-[b]	Intermediate LCAT deficiency phenotype in humans (165)
LCAT[R135Q][c]	-[b]	Fish Eye Disease syndrome in humans (166)
LCAT[V222F][c]	-[b]	Familial LCAT Deficiency syndrome in humans (161)
LCAT[P250S][c]	1.2×10^8	Familial LCAT Deficiency syndrome in humans (unpublished)[d]
LCAT[R298C][c]	-[b]	Half normal HDL-C levels in heterozygosity in humans (161)
LCAT[C313Y][c]	1.1×10^8	Familial LCAT Deficiency syndrome in humans (546)
WT apoA-IV	2.4×10^8	Used in the
WT LPL	6.7×10^7	Used to rescue the defective lipid/lipoprotein phenotype caused by the apoE3 mutants
GFP	1.3×10^8	Used as control

[a] The mutagenic pCDNA3.1apoA-I[L 218A/L219A/V221A/L222A/F225A/V227A/F229A/L230A] construct was generated by Ioanna Tiniakou.

[b] For these mutants I constructed the recombinant adenoviral plasmids but not the recombinant adenoviruses

[c] The position of the mutations is based on LCAT sequence without the precursor 24 amino acids. The nomenclature of the mutations based on the guidelines of the Human Genome Variation Society should include the 24 aa leader sequence and becomes LCAT[E134D], LCAT[Y135N], LCAT[E134D/Y135N], LCAT[T147I], LCAT[N155D], LCAT[R159Q], LCAT[V246F], LCAT[P274S], LCAT[R322C] and LCAT[C337Y] respectively.

[d] A natural mutation of LCAT has been published in which Proline is substituted by Arginine (547).

The human WT LCAT cDNA and the mutant LCAT cDNAs were initially cloned in the pENTR221 vector. Using the appropriate primers carrying the Bgl-II and EcoRV restriction sites in the 5'- and 3'- prime end respectively (see section 2.2.4), the WT and the mutant LCAT cDNAs were generated with PCR using the pENTR221-LCAT vector as a template. These cDNAs were subsequently cloned in the pAdTrack-CMV vector using the Bgl-II and EcoRV restriction sites. The recombinant pAdTrack-CMV-LCAT plasmids containing either the WT LCAT or the mutant LCAT cDNAs were sequenced (in the region that contained the LCAT transgenes) to verify the presence of the desired mutations and the absence of new mutations. Restriction digestion analysis confirmed the presence of the Bgl-II/EcoRV and PacI restriction sites (data not shown). Furthermore, transient transfection of HEK293 confirmed the expression of the WT LCAT and the LCAT mutants in the cells as well as the presence or absence of the LCAT protein in the medium with western blot (data not shown).

The CTα cDNA was isolated from HACAT cells with primers containing the Bgl-II and NotI restriction sites and was subcloned in the pAdTrack-CMV vector. Similar experiments as

described for the LCAT mutants were performed to confirm the cDNA sequence of the construct and the expression of CTα (data not shown).

Recombinant adenoviruses were generated using the pAdEasy system (543;548) (Figure 3.1). Briefly, the pAdTrack-CMV vectors containing the desired cDNAs (or genes) were linearized with PmeI and were used to transform by electroporation BJ-5183-AD1 cells. Within the cells the pAdTrack-CMV vectors recombine with the pAdEasy-1 shuttle vector to form the adenoviral plasmid. The recombinant adenoviral DNA was extracted as described in materials and methods and digested with PacI to find positive clones that produce a 3 or 4.5 kb insert (Figure 3.2).

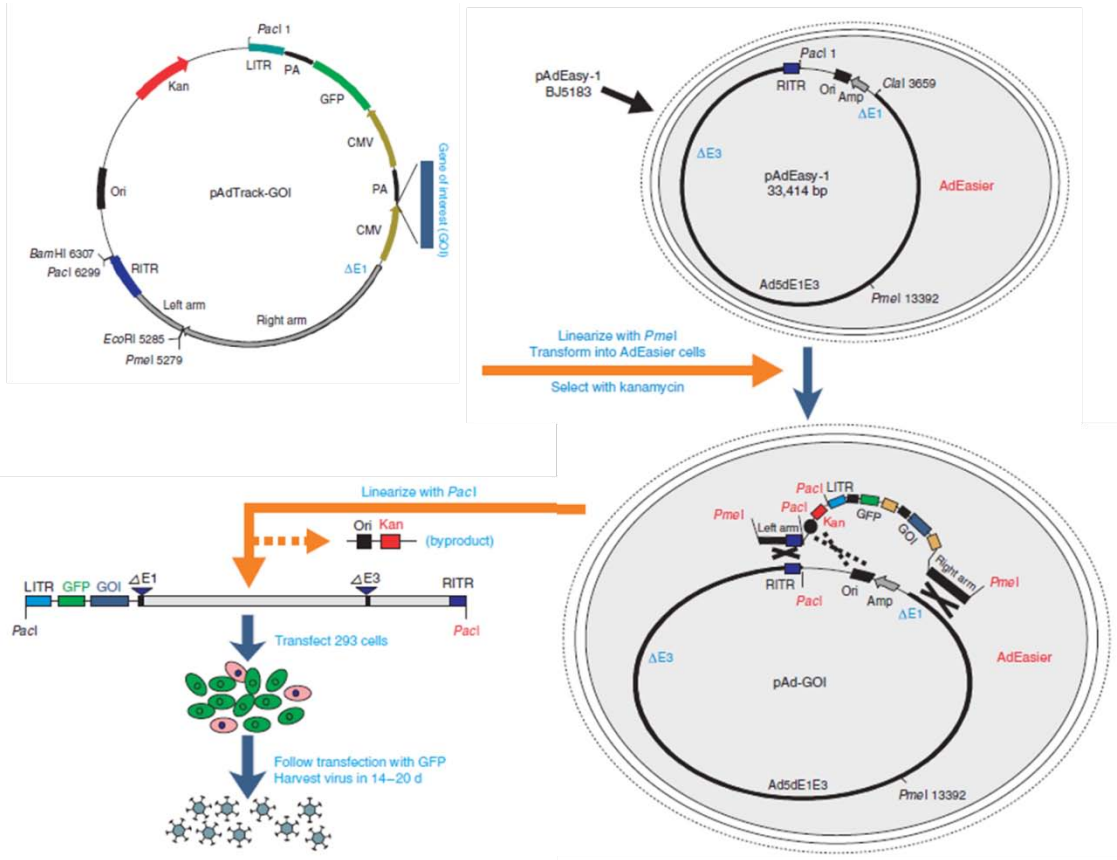

Figure 3.1. Schematic representation of the steps that lead to the generation of the recombinant adenoviruses expressing the gene of interest. Obtained from (543).

The recombinant adenoviral plasmid obtained from positive clones was then transformed to DH5a competent cells and large amount of recombinant adenoviral plasmid was isolated and purified, linearized with PacI and used to transfect 911 cells in a T25 flask by lipofectamine. Cells were lysed after 9 to 10 days and the lysate was used to infect HEK293 cells grown in T175 flasks. Lysates obtained from theses flasks five to six days post-infection were used to infect HEK293 grown in ten triple T175 flasks. Cell extracts obtained from the triple flasks were then purified by two consecutive CsCl gradient ultracentrifugations. The titres of the viruses were estimated with plaque assay as described in materials and methods (Table 3.I). Three LCAT mutants were used in adenovirus-mediated gene transfer experiments, a Fish Eye Disease LCAT mutation (LCAT[T123I]) and two Familial LCAT Deficiency mutations (LCAT[P250S] and LCAT[C313Y]), to study their effect on the biogenesis of HDL.

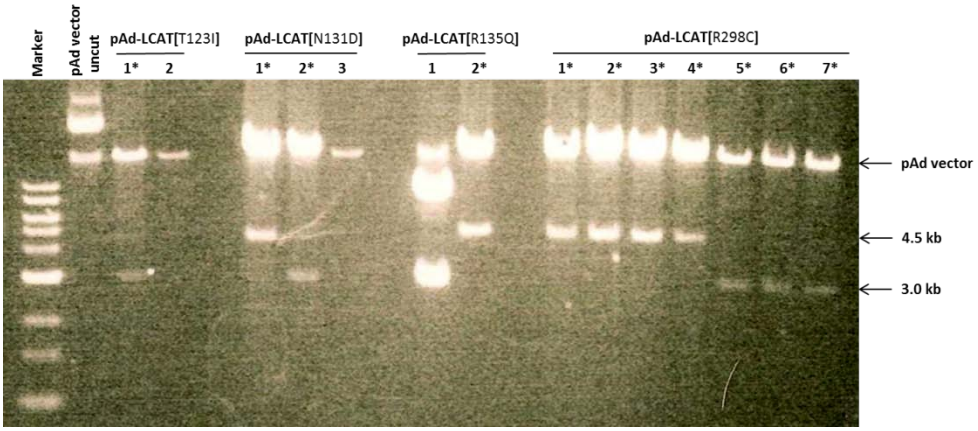

Figure 3.2: PacI digestion of recombinant pAd plasmids. Digestion of the recombinant pAd-LCAT[T123I], pAd-LCAT[N131D], pAd-LCAT[R135Q] and pAd-LCAT[R298C]with PacI, to assess the formation of two fragments, a 4.5 or 3 kB fragment containing the bacterial origin of replication and the ampicillin

resistance gene and an approximately 30 kB fragment consisting of the remaining recombinant adenovirus. The positive clones are denoted with an *. Similar results were obtained for recombinant plasmids containing WT LCAT, the rest of LCAT mutants and CTα (described in Table 3.I).

To evaluate the expression of the various transgenes after their packaging in the adenoviruses, HTB-13 cells were infected with adenoviruses expressing the gene of interest. Figure 3.3 shows an example of the expression of CTα, WT LCAT, LCAT[T123I], LCAT[P250S], LCAT[C313Y], WT apoA-I, apoA-I[218-230] and WT apoE3 at various MOI (multiplicity of infection) as indicated. Cell extract or medium collected from the HTB-13 cultures was dissolved in SDS-sample buffer and were analysed by SDS-PAGE and western blotting. The analyses showed that the infected cells produced and secreted efficiently WT LCAT, LCAT[T123I] and LCAT[P250S]. In contrast, LCAT[C313Y] was present in the cell extract but not in the medium (Figure 3.3A). This signifies that although LCAT[C313Y] is expressed, the mutation on residue 313 hinders its secretion into the cultured media. The molecular mass of the WT LCAT and the LCAT mutants was as expected, approximately 46 kDa in the cell extract and 65kDa in the medium due to known post-translational modifications (549;550) (Figure 3.3A). Expression of CTα, which is an intracellular protein, WT apoA-I, apoA-I[218-230] and WT apoE3 were also confirmed in HTB-13 cells following infection with the corresponding recombinant adenoviruses (Figure 3.3B,C). Similar experiments had been performed for the rest of the apoA-I and apoE mutants to examine their normal production and secretion (542;544).

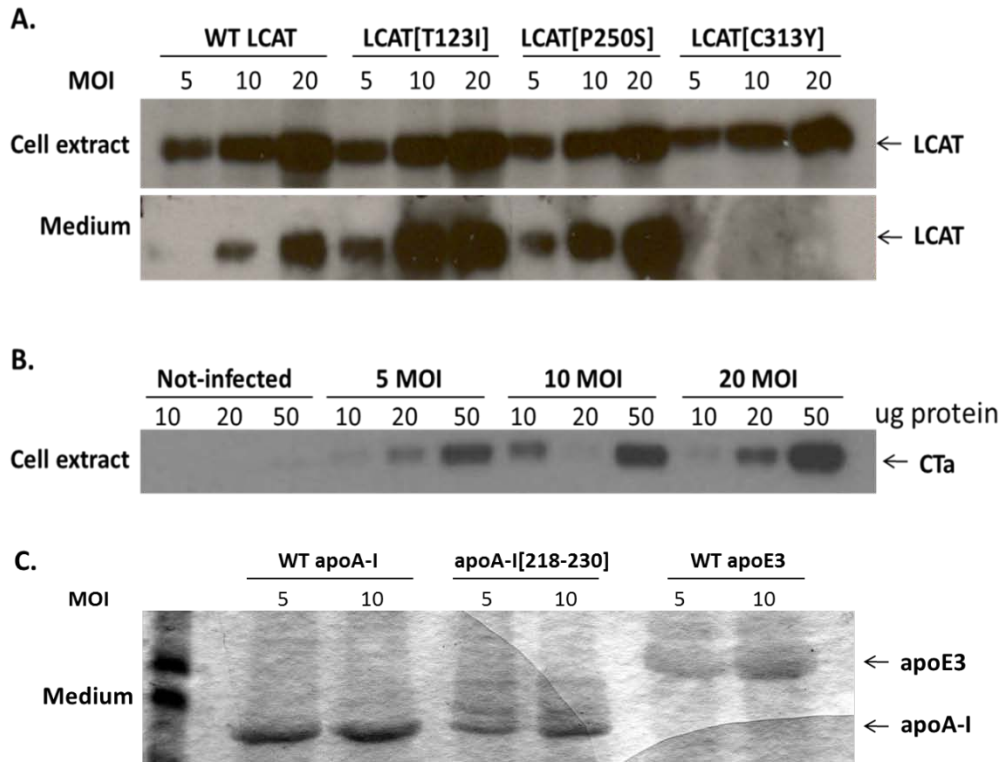

Figure 3.3 (A,B): Expression of WT LCAT, LCAT mutants, CTα, WT apoA-I, apoA-I[218-230] and WT apoE3 following infection of HTB-13 cells with the corresponding adenoviruses. SDS-PAGE and western blot of 45 ug of total cell extract and 600 ul of culture medium concentrated to 25 ul from HTB-13 cells infected with adenoviruses expressing the WT and mutant LCAT forms at a MOI of 5,10 and 20 viruses per cell as indicated (A). SDS-PAGE and western blot of 10, 20 and 50 ug of total cell extract from HTB-13 cells uninfected or infected with adenoviruses expressing the CTα at a MOI of 5, 10 and 20 as indicated (B). SDS-PAGE of culture medium from HTB-13 cells expressing WT apoA-I, apoA-I[218-230] and WT apoE3at MOI of 5 and 10 viruses per cell as indicated (C).

Chapter II. Importance of the hydrophobic residues in the 218-230 region of apoA-I for the biogenesis of HDL.

RESULTS

The objective of these studies was to investigate the role of hydrophobic and charged amino acid residues within the 218-230 residues of the C-terminal region of apoA-I. This area is conserved among animal species and previous studies have shown that deletions that eliminate the 220-231 region of apoA-I have reduced capacity to promote ABCA1-mediated cholesterol efflux and thus fail to form mature HDL (108;125). Our aim was to identify the specific C-terminal residues of apoA-I that are required for correct interactions with ABCA1 and/or LCAT that lead to the formation of mature α-HDL particles. For this reason we introduced three sets of point mutations in the 218-230 region of apoA-I (Figure 3.4) where we substituted hydrophobic by Alanines. The apoA-I mutant generated were:

1. apoA-I[L218A/L219A/V221A/L222]

2. apoA-I[F225A/V227A/F229A/L230A]

3. apoA-I[L218A/L219A/V221/L222A/F225A/V227A/F229A/L230A]

These apoA-I variants were used to study the effects of the mutations on the biogenesis of HDL *in vivo* using adenovirus-mediated gene transfer in apoA-I$^{-/-}$ and apoA-I$^{-/-}$ x apoE$^{-/-}$ mice and the structural integrity and the functions of apoA-I *in vitro*. Some results The results from these studies have been published recently (127;551).

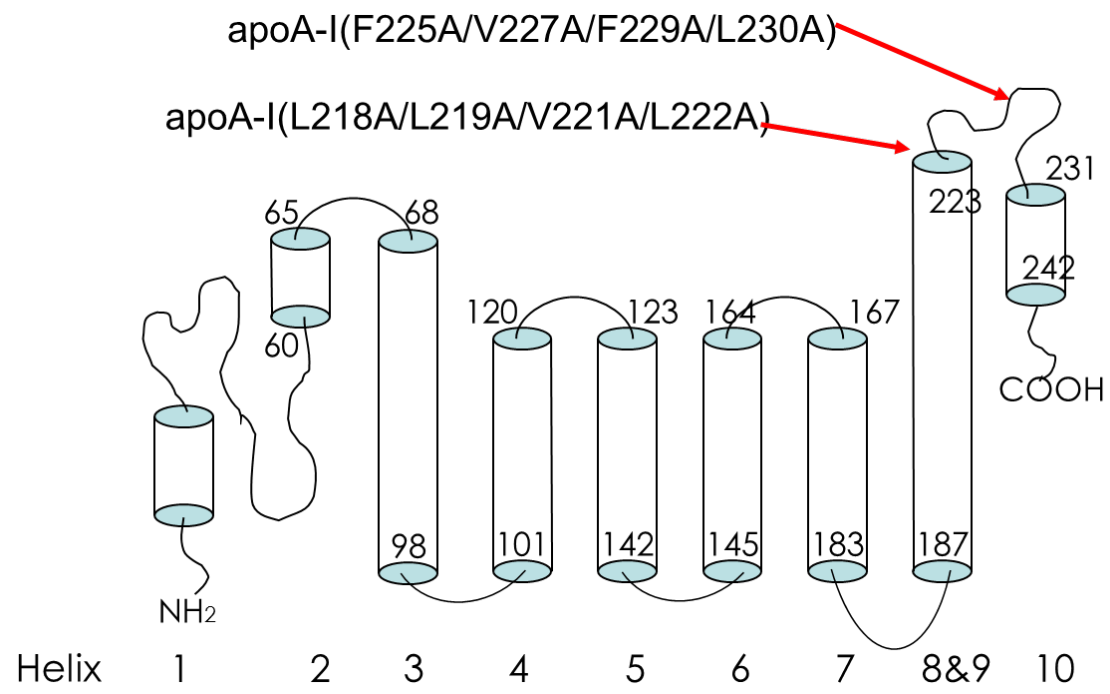

Figure 3.4: Position of the apoA-I[218-222] and apoA-I[225-230] mutations in the secinsary structure of apoA-I as indicated.

Expression of the apoA-I transgenes following adenovirus infection of mice

Total hepatic RNA was isolated from the livers of apoA-I$^{-/-}$ mice four days post infection with adenoviruses expressing the WT apoA-I and the apoA-I mutants, apoA-I[218-222], apoA-I[225-230] and apoA-I[218-230]. The relative expression of the WT and the mutant apoA-I transgenes was determined by qPCR as described in the experimental procedures. This analysis showed that the expression of WT and the apoA-I[218-222], apoA-I[225-230], apoA-I[218-230] mutants were comparable to WT apoA-I (Table 3.II A-C).

Table 3.II (A-C): Plasma lipids and hepatic mRNA levels of apoA-I$^{-/-}$ mice expressing WT and the mutant forms of apoA-I in the presence and absence of LCAT as indicated.

A.

Protein Expressed	Total Cholesterol (mg/dL)	Triglycerides (mg/dL)	Relative apoA-I mRNA (%)	apoA-I plasma levels (mg/dL)
GFP	25 ± 9	45 ± 10	-	-
WT apoA-I	278 ± 74$^{\wedge}$	78 ± 24	100 ± 26*	260 ± 40
apoA-I[218-222]	45 ± 14$^{\wedge +}$	50 ± 20	95 ± 24	41 ± 5^{+}

B.

Protein Expressed	Total Cholesterol (mg/dL)	Triglycerides (mg/dL)	Relative apoA-I mRNA (%)	apoA-I plasma levels (mg/dL)
GFP	27 ± 8	34 ± 14	-	-
WT apoA-I	182 ± 82$^{\wedge}$	39 ± 15	100 ± 15*****	173±63
apoA-I[225-230]	41 ± 12$^{\wedge +}$	42 ± 14	130 ± 10^{+}	59±17^{+}
apoA-I[225-230] + LCAT	297 ± 69$^{\wedge}$	48 ± 21	80 ± 10	149±43

C.

Protein Expressed	Total Cholesterol (mg/dL)	Triglycerides (mg/dL)	Relative apoA-I mRNA (%)	apoA-I plasma levels (mg/dL)
GFP	21 ± 2	36 ± 13	-	-
WT apoA-I	230 ± 89$^{\wedge}$	50 ± 21	90 ± 15*****	148 ± 34
apoA-I[218-230]	34 ± 7$^{\wedge +}$	40 ± 13	70 ± 36	-
apoA-I[218-230] + LCAT	109 ± 22$^{\wedge +}$	44 ± 15	140 ± 36	-

Values are means ± standard deviation based on analysis of 4-6 mice per experiment. Expression of apoA-I is relative to the expression of apoA-I WT in the apoA-I$^{-/-}$ mouse group and is indicated by a (*). Expression of LCAT was also confirmed by RT-PCR. Statistical significant differences in cholesterol, triglyceride, mRNA and protein levels at $p<0.05$ between mice expressing the WT apoA-I and the apoA-I mutants are indicated by a **+** symbol and between mice expressing GFP and the apoA-I transgenes are indicated by a $^{\wedge}$ symbol. The measurements of Table 3.II A pertinent to the expression of the apoA-I[218-222] in apoA-I$^{-/-}$ have been performed by Andreas Kateifides (542).

Plasma lipids, apoA-I levels and FPLC profiles

Plasma lipids and apoA-I were determined four days post infection of apoA-I$^{-/-}$ mice with adenoviruses expressing the WT and the four apoA-I mutants. It was found that the apoA-I[218-222], apoA-I[225-230] and apoA-I[218-230] mutant decreased plasma cholesterol levels to approximately 16 %, 22% and 15% respectively as compared to WT apoA-I. The apoA-I[218-222] and apoA-I[225-230] mutants also decreased apoA-I protein levels to 16 % and 34% respectively as compared to WT apoA-I while the protein levels of apoA-I[218-230] were not detectable by our method (Table 3.II A-C). Plasma triglyceride levels were not significantly altered in any of the mutants (Table 3.II A-C).

FPLC analysis of plasma from apoA-I$^{-/-}$ mice infected with the recombinant adenovirus expressing either WT apoA-I or the four apoA-I mutants showed that in all cases cholesterol was distributed in the HDL region and the HDL cholesterol peaks of the apoA-I[218-222], apoA-I[225-230] and apoA-I[218-230] mutants were greatly diminished (Figure 3.5).

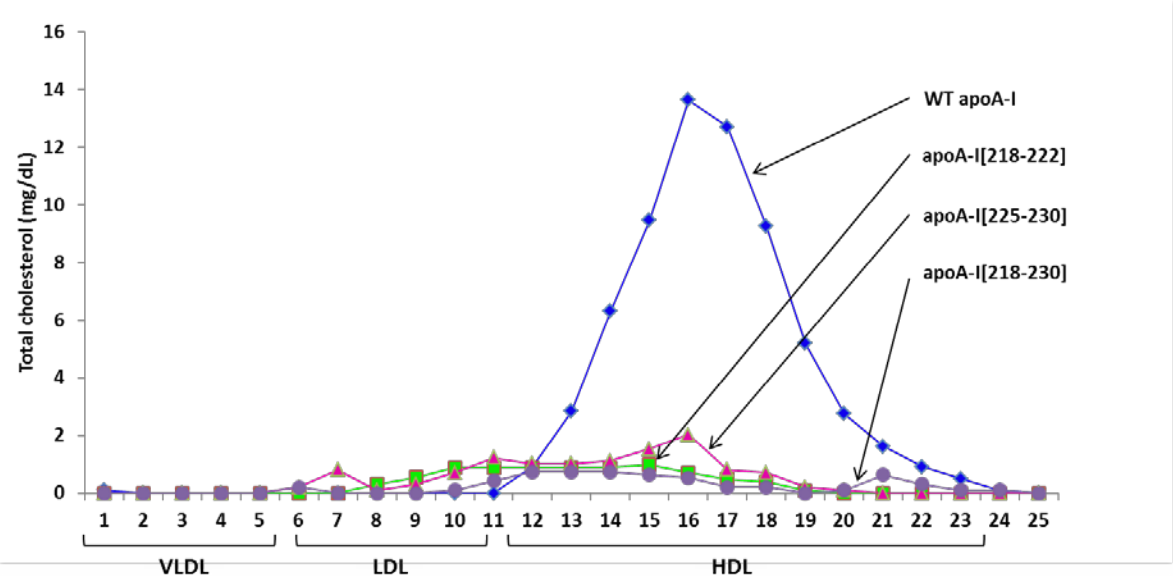

Figure 3.5: FPLC cholesterol profiles four days post infection of apoA-I$^{-/-}$ mice infected with adenovirus expressing WT apoA-I and the apoA-I[218-222], apoA-I[225-230] or apoA-I[218-230] mutants as indicated.

Fractionation of plasma of mice expressing the WT apoA-I and the apoA-I mutants by density gradient ultracentrifugation and analysis of the fraction by SDS-PAGE

Fractionation of plasma by density gradient ultracentrifugation and subsequent analysis of the resulting fractions by SDS-PAGE showed that the WT apoA-I was equally distributed in the HDL2 and HDL3 region whereas the apoA-I[218-222] and apoA-I[225-230] mutants were predominantly distributed in the HDL3 and to a lesser extend the HDL2 region (Figure 3.6 A-C). Both mutants were characterized by low levels of apoA-I and also in the case of the apoA-I[218-222] mutant there were observed increased levels of mouse apoE that floated in the HDL2/HDL3, but also in the VLDL/IDL/LDL region (Figure 3.6 B). Flotation of other apolipoproteins in the VLDL/LDL/IDL/HDL region was not observed when the WT apoA-I and the apoA-I[225-230] mutant were expressed in apoA-I$^{-/-}$ mice (Figure 3.6 A,C). Flotation of the apoA-I[218-230] showed traces of apoA-I protein in the d>1.251 g/ml fraction along with mouse apoE in the HDL region (Figure 3.6 D).

Electron Microscopy analysis of the HDL fractions

Analysis of the HDL fractions 6 and 7 obtained following density gradient ultracentrifugation by EM showed that the WT apoA-I as well as all apoA-I mutants generated spherical particles (Figure 3.6 E-H). The diameter of the particles were 10±1.7 nm for the WT

apoA-I, 10±2 nm for the apoA-I[218-222], 8±1.3 nm for the apoA-I[225-230] mutant and 8±1.4 nm for the apoA-I[218-230] mutant.

Two-dimensional gel electrophoresis of the plasma

Two-dimensional gel electrophoresis of plasma showed that WT apoA-I formed normal preβ- and α1-, α2-, α3-, α4-HDL subpopulations (Figure 3.6 I). The apoA-I[218-222] formed increased amounts of preβ- and of α4- and α3-HDL subpopulations (Figure 3.5 J). ApoA-I[225-230] mutant formed predominantly preβ-, small amounts of α4-HDL and traces of α3-HDL subpopulations (Figure 3.6 K). The apoA-I[218-230] mutant formed only preβ-HDL subpopulations and traces of α-HDL (Figure 3.6 L).

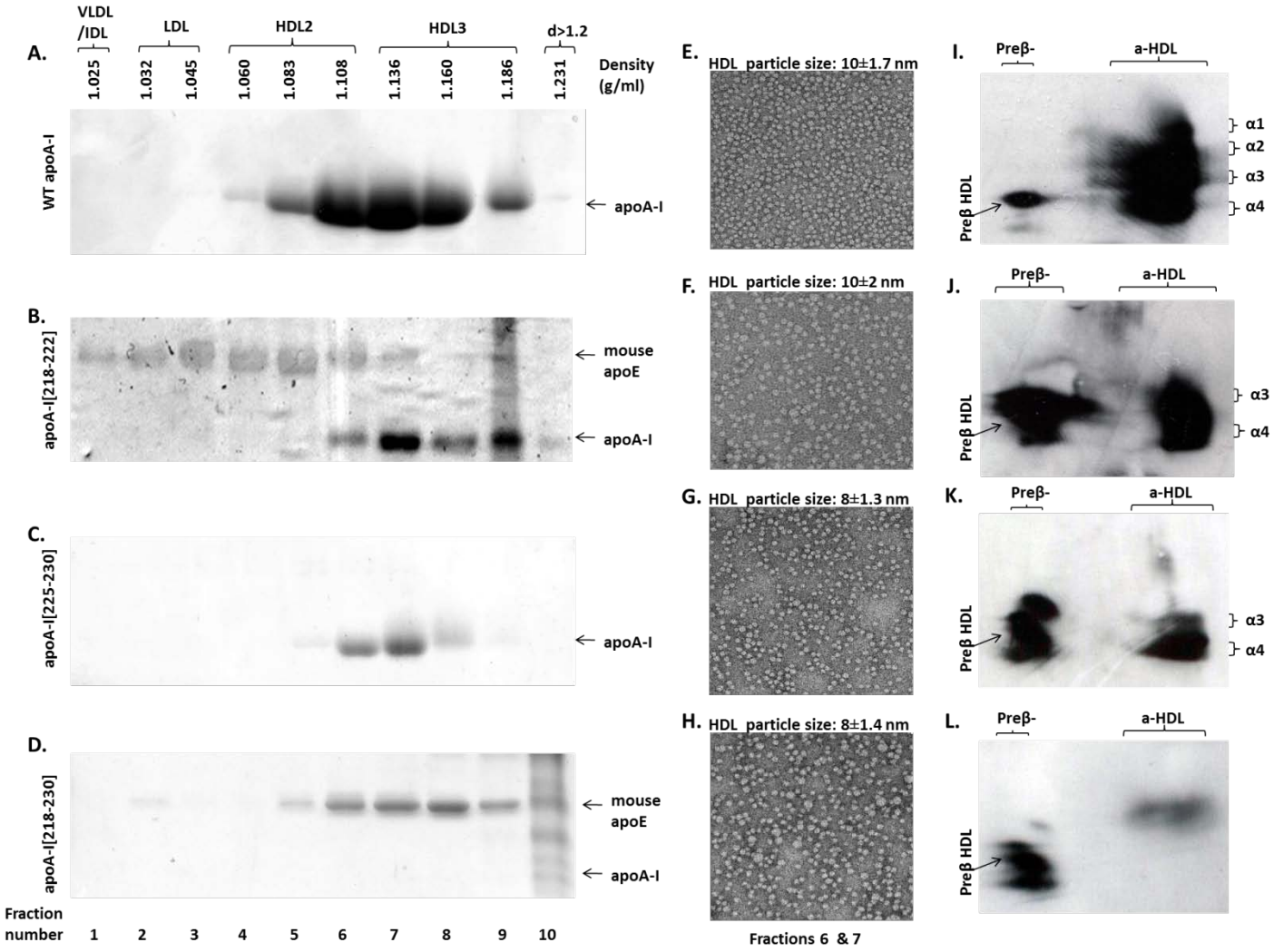

Figure 3.6 (A-L): Analysis of plasma of apoA-I$^{-/-}$ mice infected with adenoviruses expressing the WT apoA-I (A), the apoA-I[218-222]mutant (B), the apoA-I[225-230]mutant (C), or the apoA-I[218-230] mutant (D), by density gradient ultracentrifugation and SDS-PAGE. EM analysis of HDL fractions 6-7 obtained from apoA-I$^{-/-}$ mice expressing the WT apoA-I (E), the apoA-I[218-222]mutant (F), the apoA-I[225-230]mutant (G), or the apoA-I[218-230] mutant (H) following density gradient ultracentrifugation of plasma as indicated. The photomicrographs were taken at 75,000× magnification and enlarged 3 times. Two dimensional gel electrophoresis of plasma of apoA-I$^{-/-}$ mice infected with adenoviruses expressing the WT apoA-I (I), the apoA-I[218-222]mutant (J), the apoA-I[225-230]mutant (K), or the

apoA-I[218-230] mutant (L). Preliminary experiments of apoA-I[218-222] in apoA-I-/- mice had been performed by Andreas Kateifides and here were repeated.

Assessment of the contribution of mouse apoE in the formation of HDL in mice expressing the mutant forms of apoA-I

A question raised from the previous results is what is the contribution of apoA-I[218-222] and mouse apoE in the formation of HDL. To address this question, initially we confirmed by western blot the presence of mouse apoE in apoA-$I^{-/-}$ mice expressing the apoA-I[218-222] mutant. The majority of apoE floated in the HDL2/HDL3 region and to a lesser extent in the VLDL/IDL/LDL region (Figure 3.7 B). In mice expressing WT apoA-I, mouse apoE was found only in the VLDL/IDL/LDL region (Figure 3.7 A). Two-dimensional gel electrophoresis of plasma and immunodetection by anti-mouse apoE showed the presence of apoE-containing HDL in plasma only in mice expressing the apoA-I[218-222] mutant (Figure 3.7 C,D).

In order to clarify whether the HDL particles observed in Figure 3.6 F originate from the apoA-I[218-222] mutant or mouse apoE that float in the HDL region (Figure 3.6 B) we performed adenovirus mediated gene transfer in apoA-$I^{-/-}$ x $apoE^{-/-}$ mice which lack both apoA-I and apoE. Analysis of relative expression of the WT and the mutant apoA-I transgenes by qPCR showed that the expression of WT apoA-I and apoA-I[218-222] mutant were comparable (Table 3.III A). The plasma cholesterol and triglyceride levels of mice expressing the apoA-I[218-222] mutant were increased compared to those of the non-infected apoA-$I^{-/-}$ x $apoE^{-/-}$ mice but decreased compared to WT apoA-I (Table 3.III A). The mice expressing WT apoA-I presented with very high plasma cholesterol levels and also developed hypertriglyceridemia (Table 3.III A).

The FPLC profiles of plasma obtained from mice expressing WT apoA-I, the apoA-I[218-222] mutant shown in Figure 3.8. This comparative analysis showed that the great majority of cholesterol was distributed in the VLDL/IDL region in both WT apoA-I and the mutant. In the case of WT apoA-I an amount of cholesterol was distributed in the HDL region whereas the apoA-I[218-222] mutant did not have an HDL cholesterol peak (Figure 3.8).

Separation of the plasma by density gradient ultracentrifugation and SDS-PAGE analysis of the fractions showed that WT apoA-I was distributed predominantly in the HDL2/HDL3 region (Figure 3.9 A). EM analysis of the fractions 6 & 7 obtained by density gradient ultracentrifugation of the plasma showed that WT apoA-I generated spherical particles (Figure 3.9 B). Two dimensional gel electrophoresis showed that the plasma of mice expressing WT apoA-I contained the normal preβ- and α-HDL subpopulations (Figure 3.9 C). SDS-PAGE analysis of plasma fractions obtained from mice expressing the apoA-I[218-222] mutant showed the presence of small amounts of the mutant protein in the HDL3 region (Figure 3.9 D). The L218A/L219A/V221A/L222A mutations in apoA-I resulted in a great increase in plasma apoA-IV that floated in the IDL/LDL/HDL2/HDL3 region (Figure 3.9 D) as well as the presence of apoB-48 in the HDL region (Figure 3.9 E). The presence of apoA-IV was also confirmed by western blot (Figure 3.10 A,B). The apoA-I[218-222] mutant generated few discoidal particles as well as particles corresponding in size to VLDL (48.5±15 nm), IDL (28.8±3 nm) and LDL (20.2±2.5 nm) (Figure 3.9 F). The appearance of the LDL and IDL size particles is also supported by the presence of apoB-48 in fractions 6 & 7 used for the EM analysis (Figure 3.9 E). The plasma of mice expressing the apoA-I[218-222] mutant contained only preβ-HDL particles (Figure 3.9 G). The relative migration of the particles generated by WT apoA-I and the apoA-I[218-222] mutant

was established by two dimensional gel electrophoresis of mixtures of the plasmas containing these two apoA-I forms (Figure 3.9 H).

Similar analyses was performed for the apoA-I[225-230] mutant in apoA-I$^{-/-}$ x apoE$^{-/-}$ mice. The plasma cholesterol and triglyceride levels of mice expressing the apoA-I[225-230] mutant were comparable to those of the non-infected apoA-I$^{-/-}$ x apoE$^{-/-}$ mice (Table 3.III B). In contrast, the plasma cholesterol levels of the mice expressing the WT apoA-I was increased 1.5-fold as compared to the apoA-I$^{-/-}$ x apoE$^{-/-}$ mice and the mice had high triglycerides. The difference in the plasma cholesterol levels between apoA-I$^{-/-}$ x apoE$^{-/-}$ mice expressing WT apoA-I and the apoA-I[225-230] mutant can be explained by the corresponding FPLC analyses of the plasmas. This analysis showed that in apoA-I$^{-/-}$ x apoE$^{-/-}$ mice expressing the WT apoA-I, approximately two thirds of the cholesterol is found in the VLDL/IDL region and the remaining in the HDL region. In contrast, in mice expressing the apoA-I[225-230] mutant the great majority of the cholesterol (>90%) is found in the VLDL/IDL region and the remaining in the LDL region. There is no appreciable HDL cholesterol peak in the HDL region (Figure 3.11 A). All triglycerides are found in the VLDL/IDL region (Figure 3.11 B).

Fractionation of the plasma by density gradient ultracentrifugation showed that WT apoA-I was distributed predominantly in the HDL2/HDL3 region with small amounts in the VLDL/IDL/LDL region (Figure 3.11 C). Similar analysis for the apoA-I[225-230] mutant showed that apoA-I and mouse apoA-IV are distributed in all lipoprotein fractions and the VLDL/IDL/LDL/HDL2 fractions were enriched with mouse apoB-48 (Figure 3.11 D). EM analysis of the fractions 6 & 7 obtained by density gradient ultracentrifugation of the plasma showed that both the WT apoA-I and the apoA-I mutant generated spherical particles that differed in

size (Figure 3.11 E,F). The diameter of the particles were 9.2±1.9 nm for the WT apoA-I and 7±2.3 nm for the apoA-I[225-230] mutant. Larger spherical particles corresponding in size to IDL and LDL were observed in the HDL density fractions of apoA-I$^{-/-}$ x apoE$^{-/-}$ mice expressing the apoA-I[225-230] mutant. The appearance of the IDL and LDL size particles coincides with the presence of apoB-48 in fractions 6 & 7 used for the EM analysis (Figure 3.11 D). Two dimensional gel electrophoresis showed that the plasma of mice expressing WT apoA-I contained the normal preβ- and α-HDL subpopulations (Figure 3.11 G), whereas the plasma of mice expressing the apoA-I[225-230] mutant contained predominantly (~70%) preβ, smaller amounts (~30%) of α4-HDL and few α3-HDL particles (Figure 3.11 H). The relative migration of the particles generated by WT apoA-I and the apoA-I[225-230] mutant in apoA-I$^{-/-}$ and apoA-I$^{-/-}$ x apoE$^{-/-}$ mice were established by two dimensional gel electrophoresis of mixtures of the plasmas containing these two apoA-I forms (Figure 3.12 A,B).

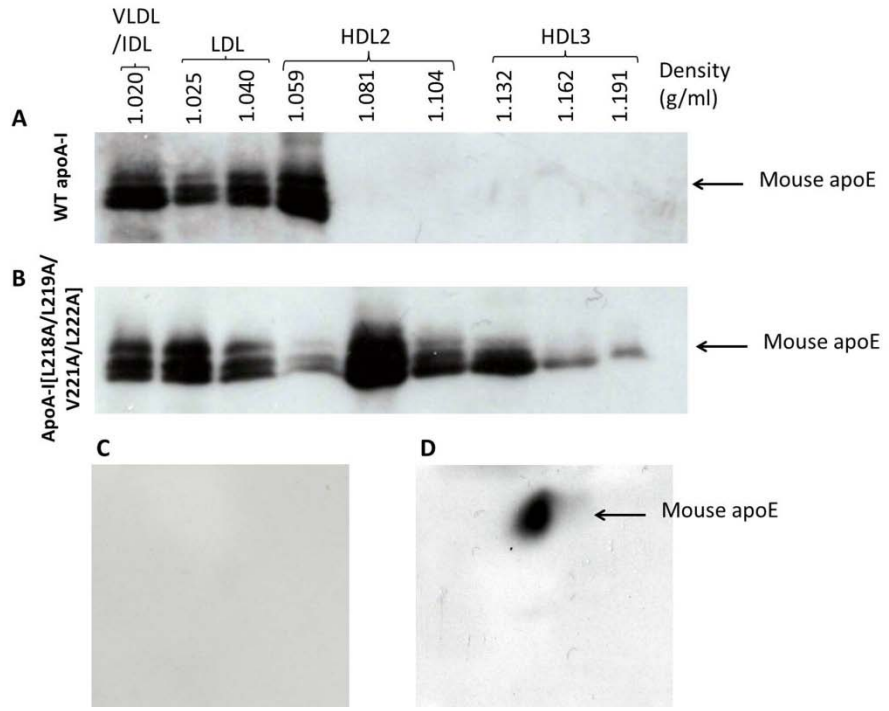

Figure 3.7 (A-D): Western blot analyses of plasma fractions obtained from apoA-I$^{-/-}$ mice expressing the WT apoA-I or the apoA-I[218-222] mutant following density gradient ultracentrifugation (A, B). The figure shows the absence of apoE in the HDL fractions of apoA-I$^{-/-}$ mice expressing the WT apoA-I (A) and strong presence of apoE in the HDL fractions of apoA-I$^{-/-}$ mice expressing the apoA-I[218-L222] mutant (B). Two dimensional gels of plasma obtained from apoA-I$^{-/-}$ mice expressing the WT apoA-I or the apoA-I[218-222] mutant and detection of apoE with anti-mouse apoE antibody (C, D). The figure shows the absence of apoE-containing HDL in apoA-I$^{-/-}$ mice expressing the WT apoA-I (C) and the presence of apoE in apoA-I$^{-/-}$ mice expressing the apoA-I[218-222] mutant (D). The presence of mouse apoE in panels A-D was probed using a goat polyclonal anti-mouse apoE antibody.

Table 3.III (A,B): Plasma lipids and hepatic mRNA levels of apoA-I$^{-/-}$ x apoE$^{-/-}$ mice expressing WT and the mutant forms of apoA-I[218-222] or apoA-I[225-230] in the presence and absence of LCAT as indicated.

A.

Protein Expressed	Total Cholesterol (mg/dL)	Triglycerides (mg/dL)	Relative apoA-I mRNA (%)
GFP	350 ± 85	52 ± 13	Non detect
WT apoA-I	1343 ± 104$^{\wedge}$	294 ± 129$^{\wedge}$	100 ± 13*
apoA-I[218-222]	778 ± 52$^{\wedge +}$	18 ± 2$^{\wedge +}$	92 ± 23
apoA-I[218-222] + LCAT	754 ± 122$^{\wedge +}$	37 ± 10^{+}	90 ± 30

B.

Protein Expressed	Total Cholesterol (mg/dL)	Triglycerides (mg/dL)	Relative apoA-I mRNA (%)
GFP	337 ± 107	58 ± 23	Non detect
WT apoA-I	520 ± 85	680 ± 290$^{\wedge}$	100 ± 21*****
apoA-I[225-230]	337 ± 90	35 ± 22^{+}	140 ± 50
apoA-I[225-230] + LCAT	778 ± 103$^{\wedge +}$	87 ± 65^{+}	90 ± 30

Values are means ± standard deviation based on analysis of 5-8 mice per experiment. Expression of apoA-I is relative to the expression of apoA-I WT in the apoA-I$^{-/-}$ mouse group and is indicated by a (*). Expression of LCAT was also confirmed by RT-PCR. Statistical significant differences in cholesterol, triglyceride, mRNA and protein levels at $p<0.05$ between mice expressing the WT apoA-I and the apoA-I mutants are indicated by a (**+**) and between mice expressing GFP and the apoA-I transgenes are indicated by ($^{\wedge}$).

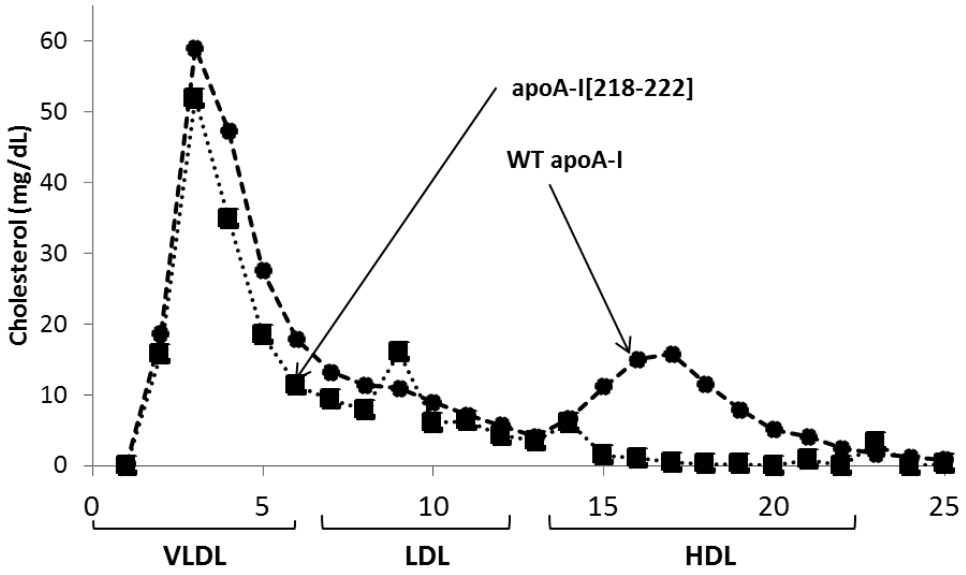

Figure 3.8: FPLC cholesterol profiles four days post infection of apoA-I$^{-/-}$ x apoE$^{-/-}$ mice infected with adenovirus expressing WT apoA-I and the apoA-I[218-222] mutant as indicated.

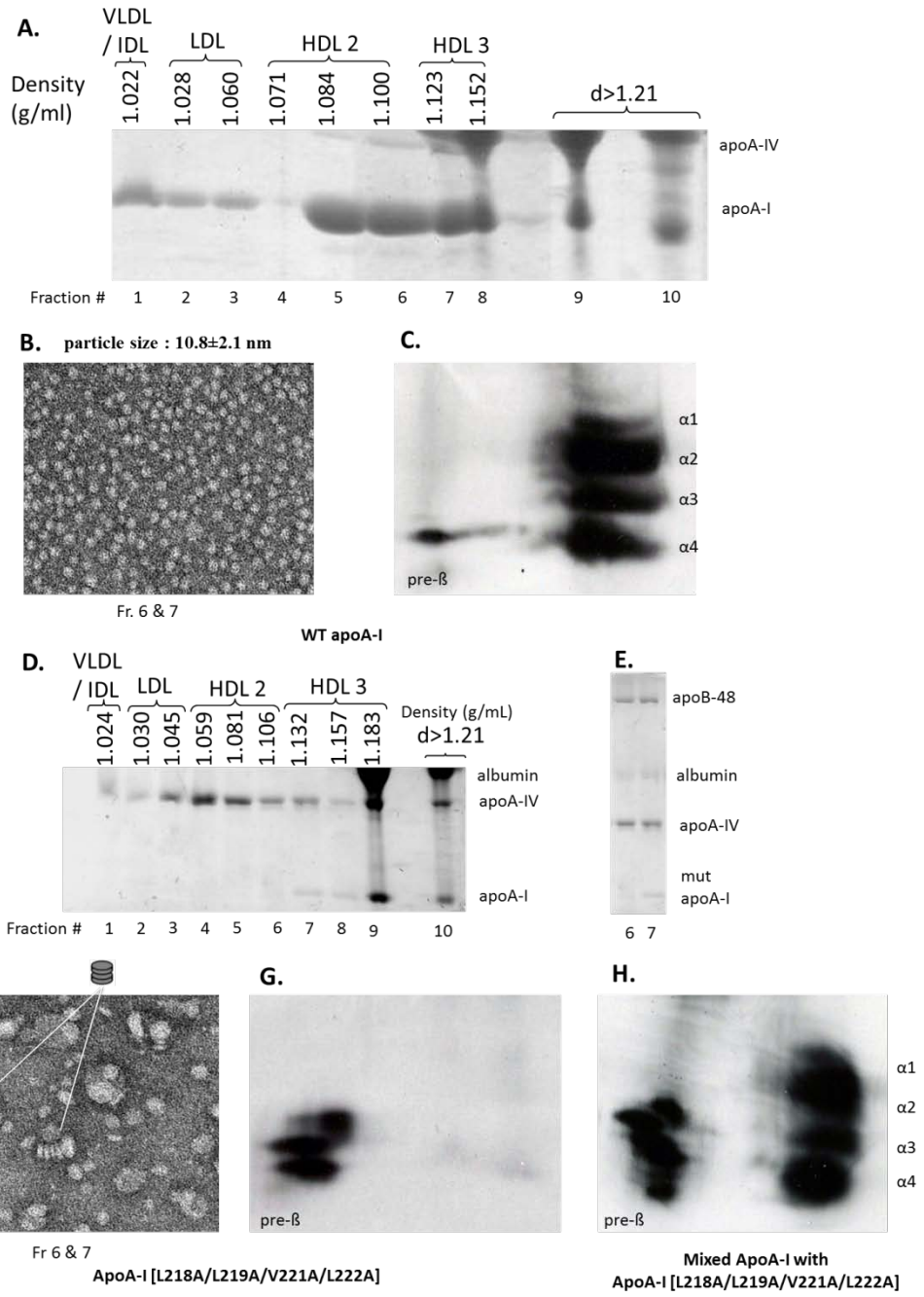

Figure 3.9 (A-H): Analysis of plasma of apoA-I$^{-/-}$ x apoE$^{-/-}$ mice infected with adenoviruses expressing the WT apoA-I (*A*) or the apoA-I[218-222] mutant (*D*) by density gradient ultracentrifugation and SDS-PAGE. EM analysis of HDL fractions 6-7 obtained from apoA-I$^{-/-}$ x apoE$^{-/-}$ mice expressing the WT apoA-I (*B)* or the apoA-I[218-222] mutant *(F)* following density gradient ultracentrifugation of plasma as indicated. The photomicrographs were taken at 75,000× magnification and enlarged 3 times. SDS gel

electrophoresis showing lipoprotein composition of fractions 6 & 7 (*E*). These fractions were used for EM analysis in panel F. Two dimensional gel electrophoresis of plasma of apoA-I$^{-/-}$ x apoE$^{-/-}$ mice infected with adenoviruses expressing WT apoA-I *(C)* or the apoA-I[L218-222] mutant *(G)* or a mixture of samples obtained from mice expressing the WT apoA-I and the apoA-I[218-222] mutant *(H).*

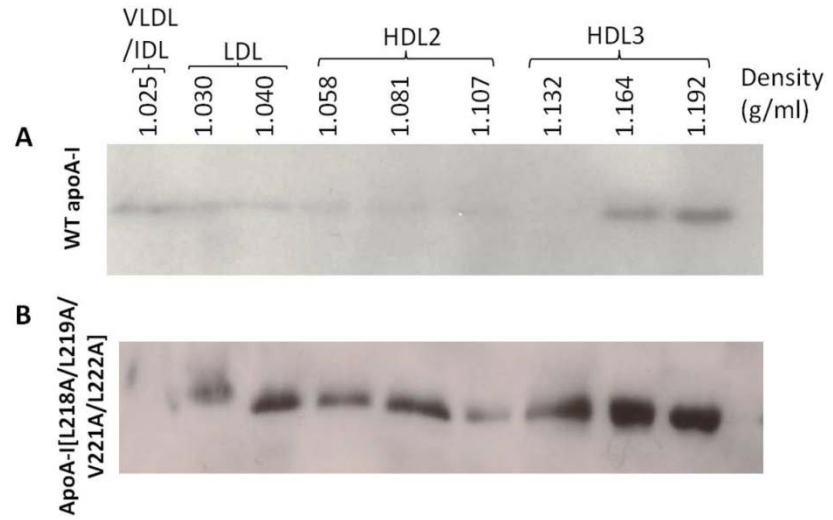

Figure 3.10 (A,B): Western blotting in apoA-I$^{-/-}$ x apoE$^{-/-}$ double deficient mice expressing the WT apoA-I or the apoA-I[218-222] mutant (A, B). The figure shows low levels of apoA-IV in mice expressing the WT apoA-I (A) and high levels of apoA-IV in mice expressing the apoA-I[218-222] mutant that float in al density fractions (B). The presence of mouse apoA-IV in panels A, B was probed using a goat polyclonal anti-mouse apoA-IV antibody.

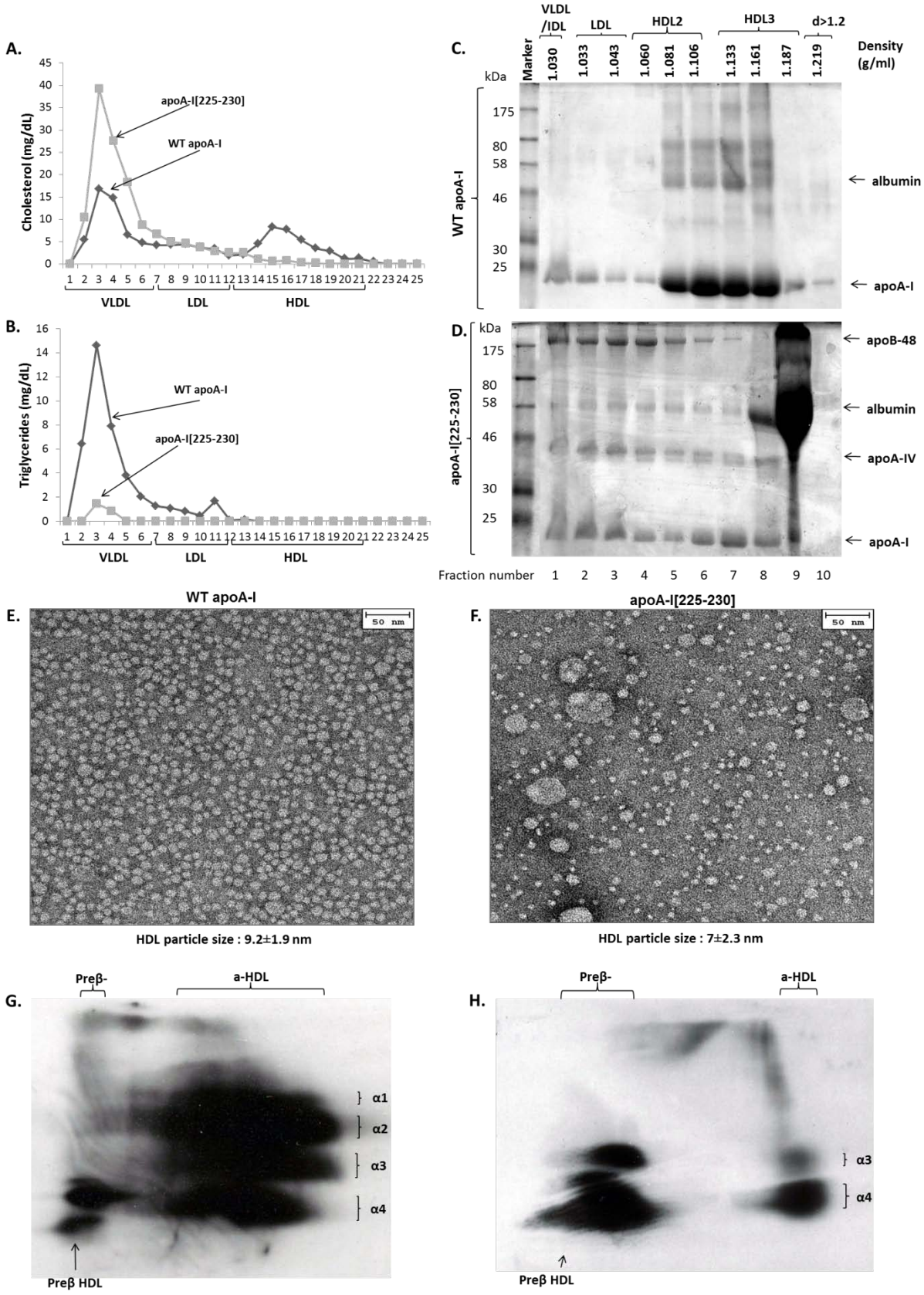
A.
Cholesterol (mg/dL)
apoA-I[225-230]
WT apoA-I
VLDL
LDL
HDL
B.
Triglycerides (mg/dL)
WT apoA-I
apoA-I[225-230]
VLDL
LDL
HDL
C.
VLDL /IDL
LDL
HDL2
HDL3
d>1.2
Marker
1.030
1.033
1.043
1.060
1.081
1.106
1.133
1.161
1.187
1.219
Density (g/ml)
kDa
WT apoA-I
albumin
apoA-I
D.
kDa
apoA-I[225-230]
apoB-48
albumin
apoA-IV
apoA-I
Fraction number 1 2 3 4 5 6 7 8 9 10
E.
WT apoA-I
50 nm
HDL particle size : 9.2±1.9 nm
F.
apoA-I[225-230]
50 nm
HDL particle size : 7±2.3 nm
G.
Preβ-
a-HDL
α1
α2
α3
α4
Preβ HDL
H.
Preβ-
a-HDL
α3
α4
Preβ HDL

Figure 3.11 (A-H): Analysis of plasma of apoA-I$^{-/-}$ x apoE$^{-/-}$ mice infected with adenoviruses expressing the WT apoA-I or apoA-I[225-230] mutant by FPLC (*A, B*) and by density gradient ultracentrifugation and SDS-PAGE (*C*, *D*). EM analysis of HDL fractions 6-7 obtained from apoA-I$^{-/-}$ x apoE$^{-/-}$ mice expressing the WT apoA-I (*E)* or apoA-I[225-230] mutant (*F*) following density gradient ultracentrifugation of plasma as indicated. Two dimensional gel electrophoresis of plasma of apoA-I$^{-/-}$ x apoE$^{-/-}$ mice infected with adenoviruses expressing WT apoA-I *(G)* or apoA-I[225-230] mutant *(H).*

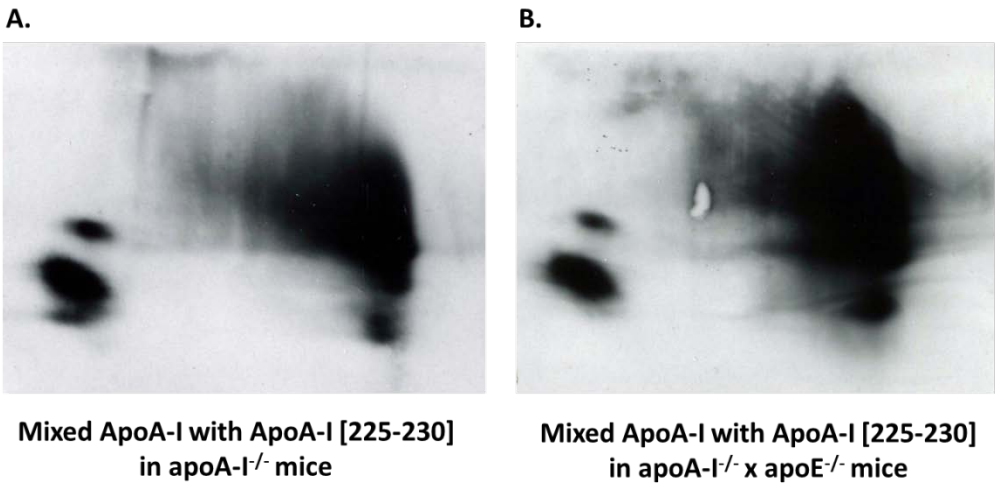

Figure 3.12 (A, B)*:* Two dimensional gel electrophoresis of a mixture of samples obtained from plasma of apoA-I$^{-/-}$ (A) or apoA-I$^{-/-}$ x apoE$^{-/-}$ (B) mice expressing the either the WT apoA-I or the apoA-I[225-230] mutant.

Ability of LCAT to correct the defective HDL phenotype caused by the apoA-I mutants

Previous studies have shown that the low HDL levels and the abnormal HDL phenotypes of some natural apoA-I mutants could be corrected by excess LCAT (217;219;220). To assess the potential insufficiency of LCAT that resulted in the generation of the discoidal particles

observed in Figure 3.9 F, we carried out gene transfer of both the apoA-I[218-222] mutant and LCAT in apoA-$I^{-/-}$ x $apoE^{-/-}$ mice. The lipid parameters and the expression levels of the transgene are shown in Table 3.III A. The FPLC profiles of plasma obtained from mice expressing WT apoA-I, the apoA-I[218-222] mutant alone or the apoA-I[218-222] mutant in the presence of LCAT are shown in Figure 3.13 A. This analysis showed that co-expression of the apoA-I[218-222] mutant and LCAT had a small effect on the HDL cholesterol peak compared to apoA-I[218-222] mutant alone, but generated a pronounced cholesterol shoulder in the VLDL/IDL/LDL region (Figure 3.13 A). Density gradient ultracentrifugation of plasma followed by SDS-PAGE analysis of the fractions showed that small amount of the mutant apoA-I was found in the HDL3. In addition, the plasma concentration of mouse apoA-IV increased and the protein had shifted towards the VLDL/IDL/LDL region (Figure 3.13 B). EM analysis of the HDL fraction obtained by density gradient ultracentrifugation showed the presence of small number of spherical HDL particles along with larger particles corresponding in size to LDL and IDL (Figure 3.13 C). The appearance of the LDL and IDL sized particles is also supported by the presence of apoB-48 in fractions 6 & 7 used for the EM analysis (Figure 3.13 D). It is possible that the LDL and IDL size particles may arise by initial formation of apoA-IV containing HDL (16) and subsequent fusion of such HDL particles with apoB containing lipoproteins (Figure 3.13 C, D). Two dimensional gel electrophoresis showed that the plasma of mice co-expressing the apoA-I[218-222] mutant and LCAT contained only small amount of preβ- and α4-HDL particles (Figure 3.13 E).

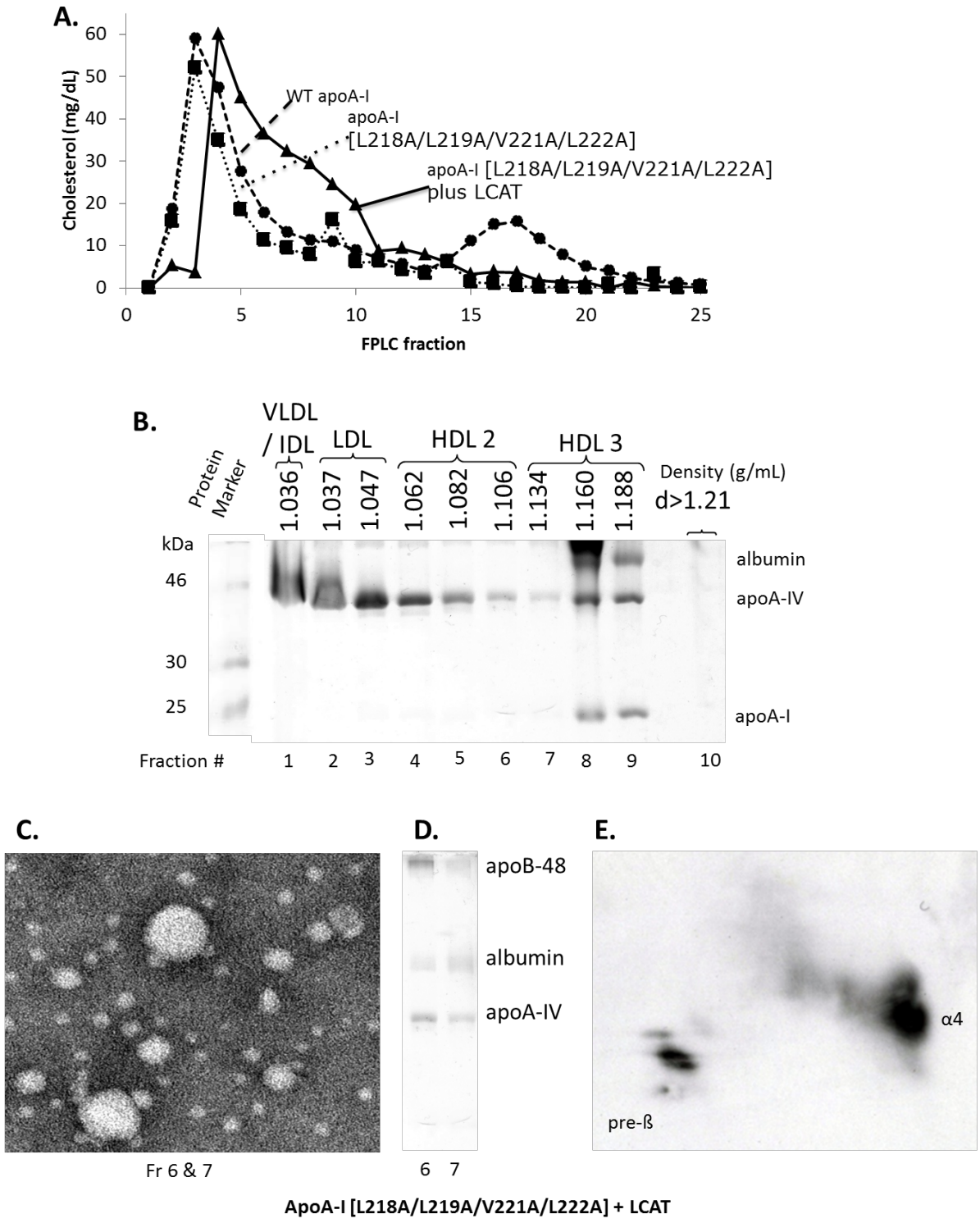

Figure 3.13 (A-E): Analyses of plasma of apoA-I$^{-/-}$ x apoE$^{-/-}$ mice infected with adenoviruses expressing the WT apoA-I or the apoA-I[218-222] mutant alone or in combination with human LCAT. Plasma FPLC profiles of mice expressing WT apoA-I or the apoA-I[218-222] mutant alone or in combination with LCAT

as indicated (*A*). SDS-PAGE of fractions obtained by density gradient ultracentrifugation from mice expressing the apoA-I[218-222] mutant and LCAT (*B*). EM analysis of the HDL corresponding to fractions 6 and 7 of panel B *(C).* The photomicrograph was taken at 75,000× magnification and enlarged 3 times. SDS gel electrophoresis showing apolipoprotein composition of fractions 6 & 7 used for EM analysis in panel C *(D).* Two dimensional gel electrophoresis of plasma of apoA-I$^{-/-}$ x apoE$^{-/-}$ mice infected with adenoviruses expressing the apoA-I[218-222] mutant and LCAT *(E).*

In the case of the apoA-I[225-230] mutant we assessed whether the defective phenotype can be corrected by LCAT in both apoA-I$^{-/-}$ and apoA-I$^{-/-}$ x apoE$^{-/-}$ mice. In apoA-I$^{-/-}$ mice co-expression of the apoA-I[225-230] mutant and LCAT increased plasma cholesterol without changing the plasma triglyceride levels (Table 3.II B). The FPLC analysis of the plasma showed that the increase in plasma cholesterol was accompanied by a dramatic increase in the HDL cholesterol peak that was shifted towards the lower densities (Figure 3.14 A). In double deficient mice the co-expression of the apoA-I[225-230] mutant with LCAT caused an 2.3-fold increase in plasma cholesterol, as compared to non-infected mice, without any significant change in plasma triglycerides (Table 3.III B). The FPLC analysis showed that the increase in plasma cholesterol was associated with the generation of a cholesterol shoulder that extended from VLDL to HDL (Figure 3.14 B).

Density gradient ultracentrifugation of plasma in apoA-I$^{-/-}$ mice co-expressing the apoA-I[225-230] mutant and LCAT showed that the major proportion of apoA-I was distributed mainly in the HDL2 region and a smaller amount in the VLDL/IDL/LDL and HDL3 regions. Mouse apoE was distributed predominantly in the VLDL/IDL/LDL region and to a lesser extend in the

HDL2 region. ApoA-IV floated in all lipoprotein fractions (Figure 3.14 C). The identity of the apoA-IV and apoE bands was confirmed by western blotting (data not shown). In apoA-$I^{-/-}$ x $apoE^{-/-}$ mice expressing both the apoA-I[225-230] mutant and LCAT, both apoA-I and apoA-IV were distributed in all lipoprotein fractions. ApoB-48 was present predominantly in the VLDL/IDL/LDL and HDL2 region and to a lesser extent in the HDL3 region (Figure 3.14 D).

Electron microscopy of the HDL fractions 6 and 7 obtained from the plasma of apoA-$I^{-/-}$ mice co-expressing the apoA-I[225-230] mutant and LCAT showed the presence of spherical particles of 11±3.1 nm diameter (Figure 3.14 E). Similar analysis of the HDL fractions 6 and 7 of plasma of apoA-$I^{-/-}$ x $apoE^{-/-}$ mice co-expressing the apoA-I[225-230] mutant and LCAT also showed the presence of spherical particles of 10.3±2.8 nm diameter as well as a greater proportion of the larger particles that correspond in size to VLDL/IDL/LDL size (Figure 3.14 F).

Two-dimensional gel electrophoresis of plasma of both apoA-$I^{-/-}$ and apoA-$I^{-/-}$ x $apoE^{-/-}$ mice showed that the co-expression of the apoA-I[225-230] mutant with LCAT restored the normal preβ and α-HDL subpopulations and generated α-HDL size subpopulations with larger size (Figure 3.14 G, H).

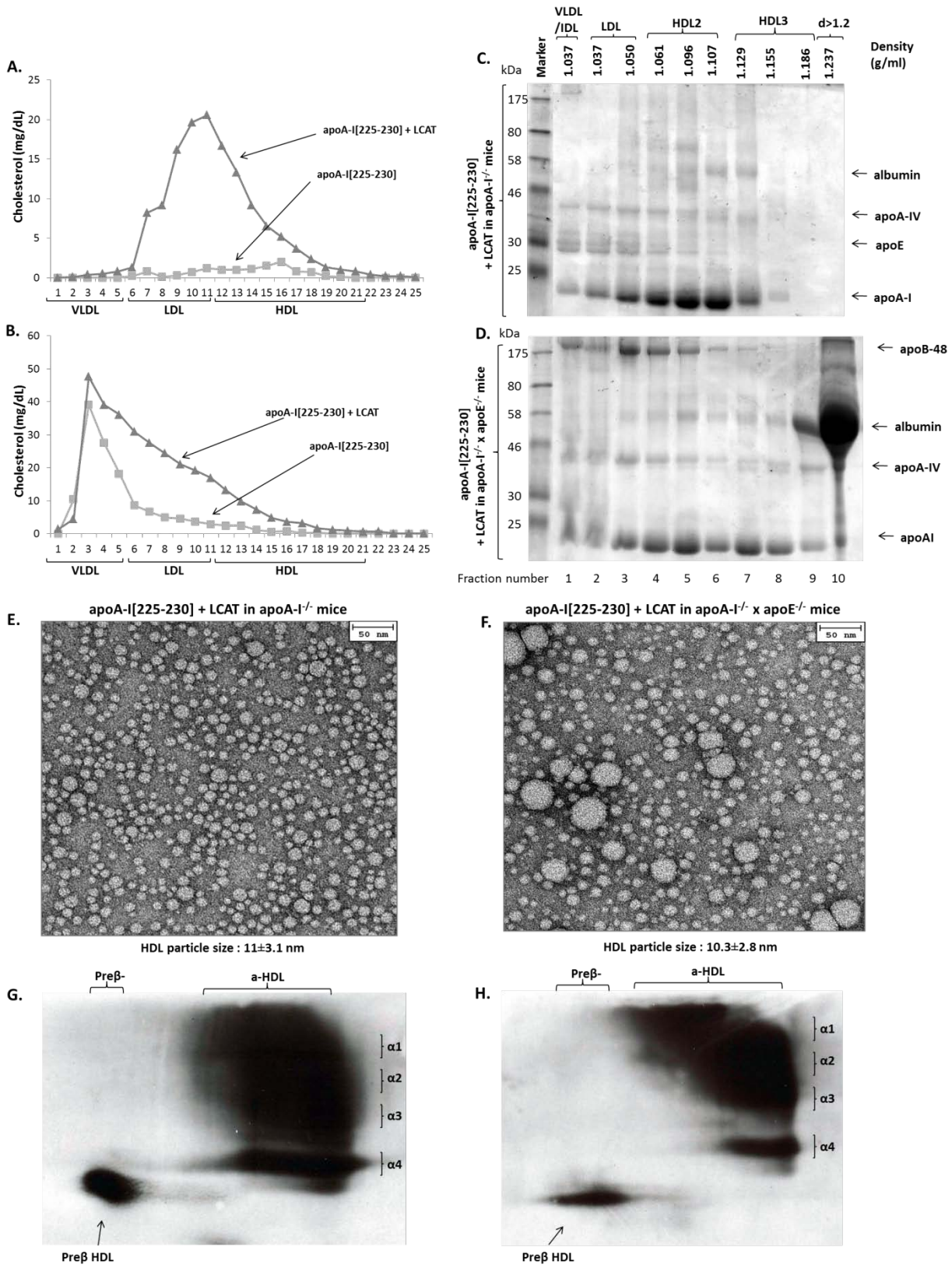
A.
Cholesterol (mg/dL)
apoA-I[225-230] + LCAT
apoA-I[225-230]
VLDL
LDL
HDL
B.
Cholesterol (mg/dL)
apoA-I[225-230] + LCAT
apoA-I[225-230]
VLDL
LDL
HDL
C.
kDa
Marker
VLDL /IDL
LDL
HDL2
HDL3
d>1.2
Density (g/ml)
1.037
1.037
1.050
1.061
1.096
1.107
1.129
1.155
1.186
1.237
apoA-I[225-230] + LCAT in apoA-I-/- mice
albumin
apoA-IV
apoE
apoA-I
D.
kDa
apoA-I[225-230] + LCAT in apoA-I-/- x apoE-/- mice
apoB-48
albumin
apoA-IV
apoAI
Fraction number
E.
apoA-I[225-230] + LCAT in apoA-I-/- mice
50 nm
HDL particle size : 11±3.1 nm
F.
apoA-I[225-230] + LCAT in apoA-I-/- x apoE-/- mice
50 nm
HDL particle size : 10.3±2.8 nm
G.
Preβ-
a-HDL
α1
α2
α3
α4
Preβ HDL
H.
Preβ-
a-HDL
α1
α2
α3
α4
Preβ HDL

Figure 3.14 (A-H): Analyses of plasma of apoA-I$^{-/-}$ *(A,C,E,G)* or apoA-I$^{-/-}$ x apoE$^{-/-}$ mice *(B,D,F,H)* infected with adenoviruses expressing the apoA-I[225-230] mutant in combination with human LCAT. Plasma FPLC profiles of apoA-I[225-230] mutant alone or the apoA-I[225-230] mutant in combination with human LCAT in apoA-I$^{-/-}$ *(A)* or apoA-I$^{-/-}$ x apoE$^{-/-}$ mice *(B)*. SDS-PAGE of fractions obtained by density gradient ultracentrifugation of plasma obtained from apoA-I$^{-/-}$ *(C)* or apoA-I$^{-/-}$ x apoE$^{-/-}$ mice *(D)* mice expressing the apoA-I[225-230] mutant and human LCAT. EM analysis of HDL fractions 6-7 obtained from apoA-I$^{-/-}$ *(E)* or apoA-I$^{-/-}$ x apoE$^{-/-}$ *(F)* mice expressing the apoA-I[225-230] mutant and human LCAT following density gradient ultracentrifugation of plasma as indicated. Two dimensional gel electrophoresis of plasma of apoA-I$^{-/-}$ *(G)* or apoA-I$^{-/-}$ x apoE$^{-/-}$ *(H)* mice expressing the apoA-I[225-230] mutant and human LCAT .

Co-expression of the apoA-I[218-230] mutant and human LCAT in apoA-I$^{-/-}$ mice increase total cholesterol levels as compared to the expression of apoA-I[218-230] mutant alone but it did not affect the triglycerides (Table 3.II C). The FPLC analysis of the plasma showed small increase in plasma cholesterol of mice expressing the apoA-I[218-230] mutant and LCAT as compared to the mice exrpessing the apoA-I[218-230] mutant alone. The HDL cholesterol peak was considerably smaller as comapred that of mice expressing WT apoA-I and was slightly shifted towards the LDL region (Figure 3.15 A). Density gradient ultracentrifugation of plasma in apoA-I$^{-/-}$ mice co-expressing the apoA-I[218-230] mutant and LCAT showed very small amounts of the apoA-I[218-230] mutant that was distributed in the HDL2/HDL3 region. Mouse apoE and mouse apoA-IV also appear and were distributed predominantly in the HDL2 region and to a lesser extent in the other lipoprotein fractions (Figure 3.15 B). Electron microscopy of the HDL fractions 6 and 7 showed the presence of spherical particles of 10.6±2.1 nm diameter (Figure

3.15 C). Two-dimensional gel electrophoresis of plasma showed the formation of predominantly preβ-HDL particles and traces of α-HDL (Figure 3.15 D).

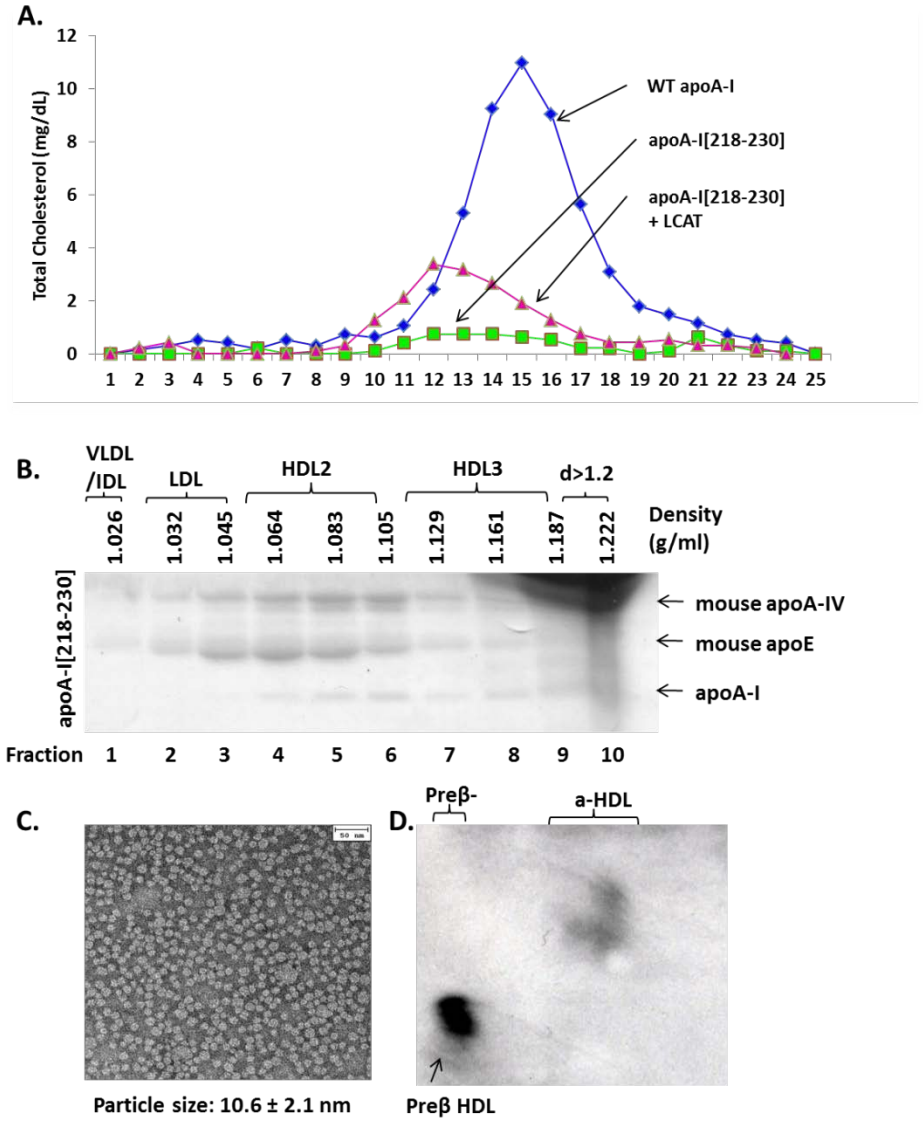

Figure 3.15 (A-D): Analyses of plasma of apoA-I$^{-/-}$ mice infected with adenoviruses expressing the WT apoA-I or the apoA-I[218-230] mutant in combination with human LCAT. Plasma FPLC profiles of mice expressing WT apoA-I or the apoA-I[218-230] mutant alone or in combination with LCAT as indicated (A). SDS-PAGE of fractions obtained by density gradient ultracentrifugation from mice expressing the apoA-I[218-230] mutant and LCAT (B). EM analysis of the HDL corresponding to fractions 6 and 7 of panel B

(C). The photomicrograph was taken at 75,000× magnification and enlarged 3 times. Two dimensional gel electrophoresis of plasma of apoA-I$^{-/-}$ mice infected with adenoviruses expressing the apoA-I[218-230] mutant and LCAT (D).

To explain why α4-HDL particles are formed in the apoA-I$^{-/-}$ deficient mice expressing the apoA-I[218-222] mutant, we explored the possibility of changes in ABCA1 protein or mRNA levels in these mouse models. Previous in vitro experiments had shown that in THP-1 cells, apoA-I protects ABCA1 from proteasome mediated degradation (552). However, the *in vivo* animal experiments in the present study did not show significant changes in ABCA1 mRNA or protein levels in apoA-I$^{-/-}$ or apoA-I$^{-/-}$ x apoE$^{-/-}$ mice without any treatment or following gene transfer of either the WT apoA-I or the apoA-I[218-222] mutant (Figure 3.16).

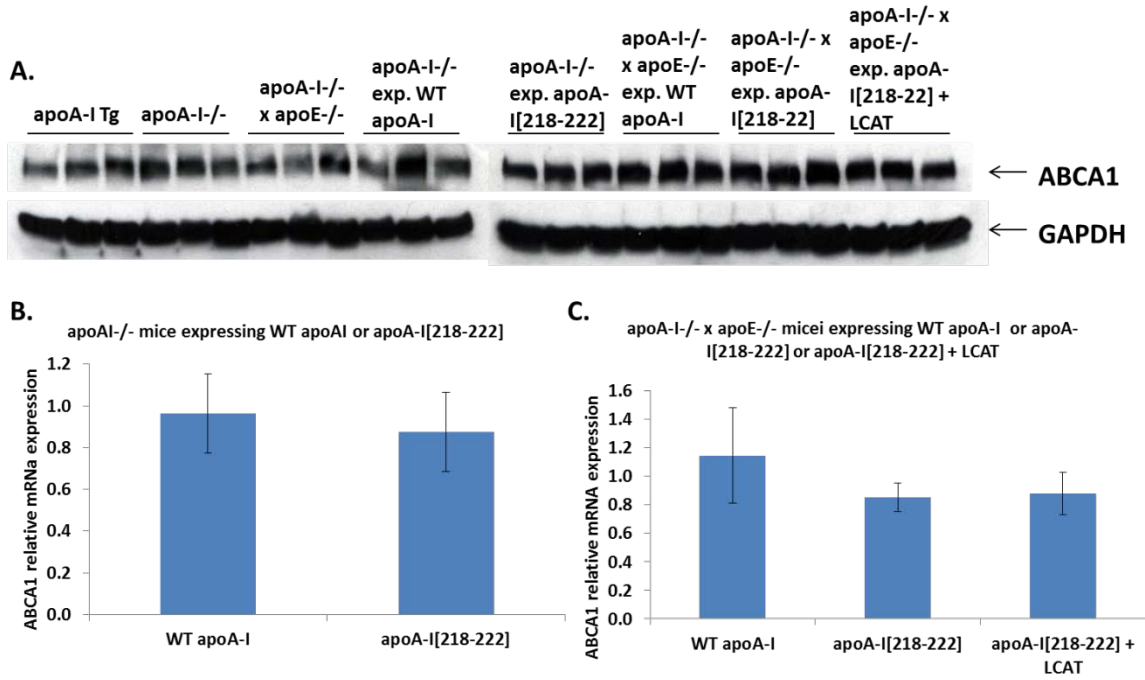

Figure 3.16 (A-C): Western blotting of hepatic extracts derived from apoA-I transgenic or apoA-I$^{-/-}$ or apoA-I$^{-/-}$ x apoE$^{-/-}$ double deficient mice without treatment or following adenovirus-mediated gene

transfer of the WT apoA-I or the apoA-I[218-222] mutant (A). Hepatic ABCA1 mRNA levels of apoA-$I^{-/-}$ or apoA-$I^{-/-}$ x $apoE^{-/-}$ double deficient mice following adenovirus-mediated gene transfer of the WT apoA-I or the apoA-I[218-222] mutant (B, C). The differences in protein and mRNA levels between the groups were not statistically significant.

Large scale production and purification of apoA-I

Large quantities of apoA-I were produced by adenovirus infection of cultures of HTB13 cells grown on a large scale roller bottles as described in experimental procedures. Serum-free media were collected up to six days post infection and analysed by SDS-PAGE to assess the levels of secreted apoA-I (Figure 3.17). Each harvest was 250 ml and the protein concentration was approximately 0.5-1.5 mg/ml. The harvested medium was dialysed in 25 mM ammonium bicarbonate or EDTA and lyophilized. For subsequent use the lyophilized powder was resuspendedn in 0.01M Tris, pH 8 in a smaller volume (30-60 ml). The protein was then purified as described in the materials and methods and used for *in vitro* functional and physicochemical studies.

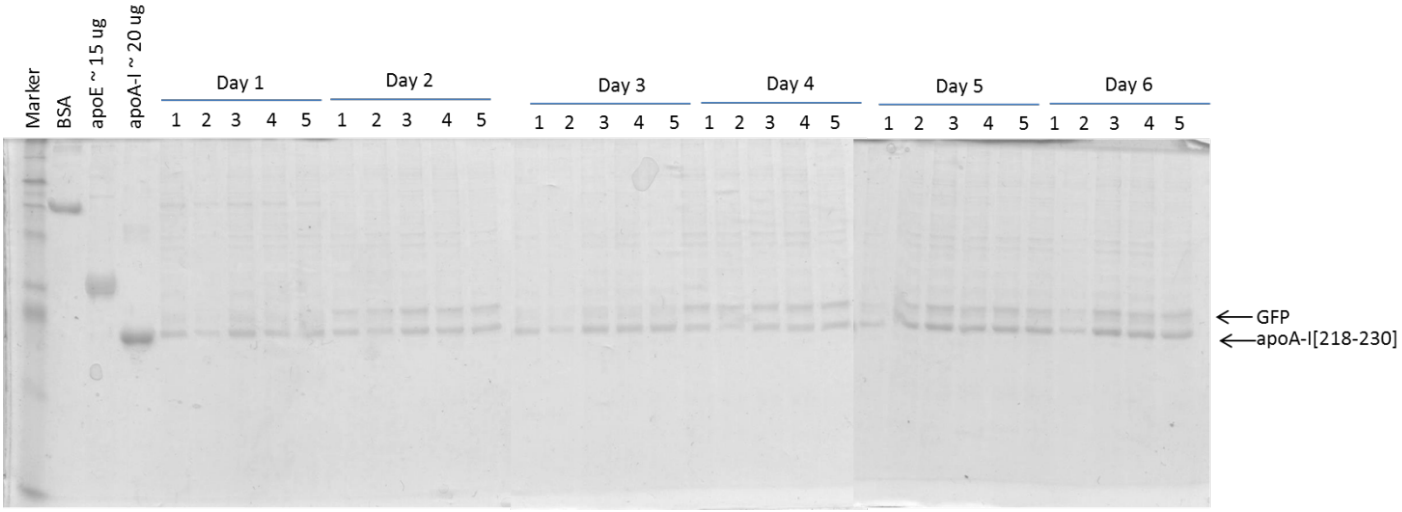

Figure 3.17: Analysis of production of apoA-I[218-230] by SDS PAGE. SDS PAGE analysis of apoA-I[218-230] secreted into the culture medium of HTB-13 cells infected with an adenovirus expressing apoA-I[218-230]. The cells were grown in roller bottles as described in experimental procedures and serum free medium was collected on days 1-6 post infection. From each harvest an aliquot of 20 ul was analysed by SDS-PAGE. The position of BSA, the apoA-I, apoE and the molecular markers are indicated.

Comparative analysis of the in vitro functions of the WT and the mutant forms of apoA-I

To interpret the observed defects in HDL biogenesis that result from the apoA-I[218-222] and apoA-I[225-230] mutations, the purified protein was used to perform functional *in vitro* studies. It was found that the ability of the apoA-I[218-222] mutant to promote ABCA1-mediated cholesterol efflux and to activate LCAT, were 20% and 66% respectively as compared to the WT control (Figure 3.18 A,B). The ability of the apoA-I[225-230] mutant to promote ABCA1-mediated cholesterol efflux and to activate LCAT was 31% and 66% respectively as compared to the WT control (Figure 3.18 C,D).

Sschematic representations of the putative defects in the biogenesis of HDL that originates from the diminished functional interactions between ABCA1 and the apoA-I[218-222] or the apoA-I[225-230] mutant as well as and the inability of the endogenous LCAT to convert the defective preβ HDL to mature α-HDL particles as well the are illustrated in Figure 3.19 A,B.

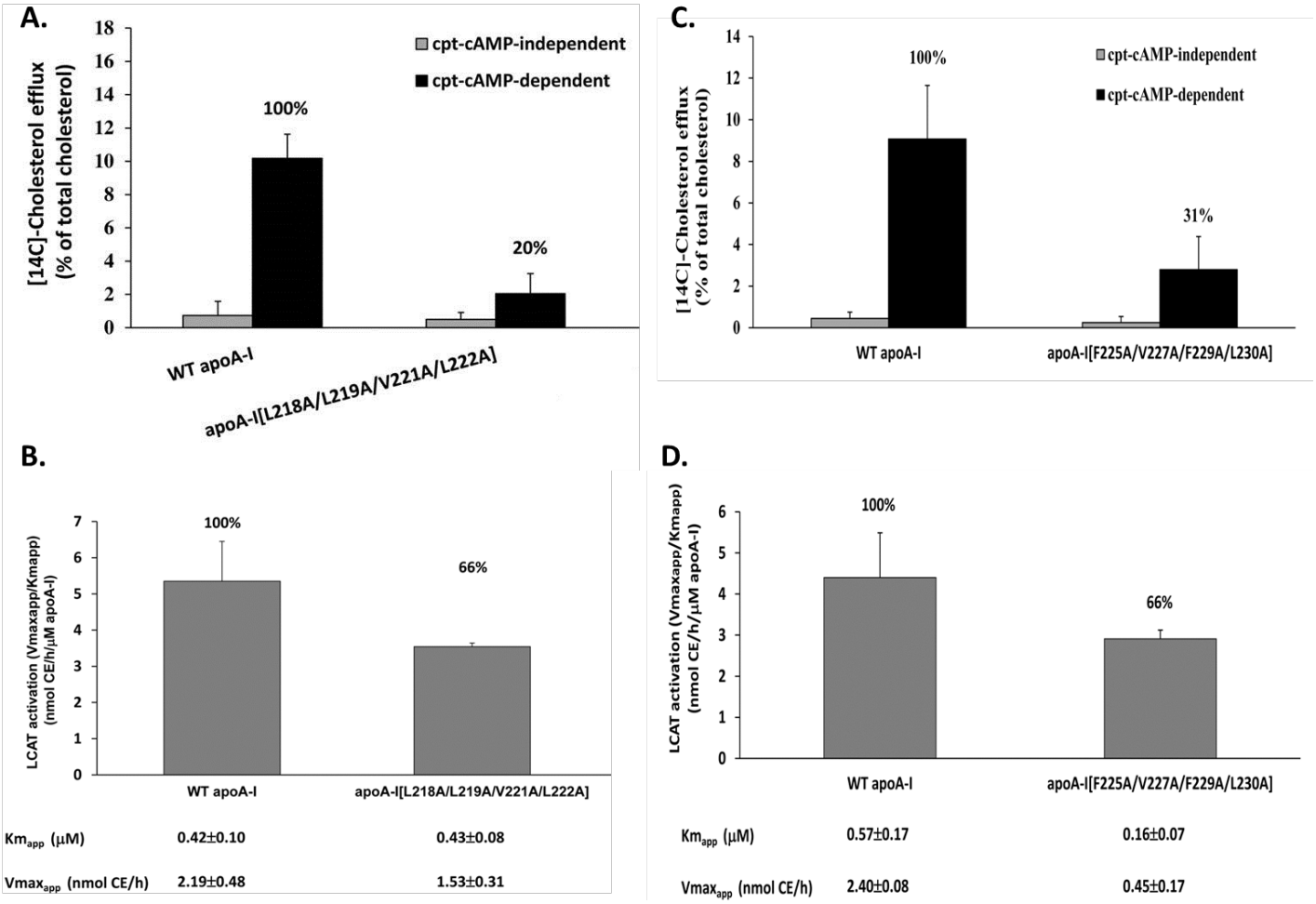

Figure 3.18 (A-D): ABCA1-mediated cholesterol efflux from J774 mouse macrophages treated with cpt-cAMP using WT apoA-I or the apoA-I[218-222] mutant as cholesterol acceptors *(A).* The ABCA1 independent and ABCA1 mediated efflux is shown. The ABCA1 mediated cholesterol efflux by WT apoA-I is set to 100%. LCAT activation capacity of WT apoA-I or the apoA-I[218-222] (B). Similar data were ontained for the apoA-I[225-230] mutant (C,D) Experiments were performed as described in the experimental procedures. The data represent the average from two independent experiments performed in triplicate.

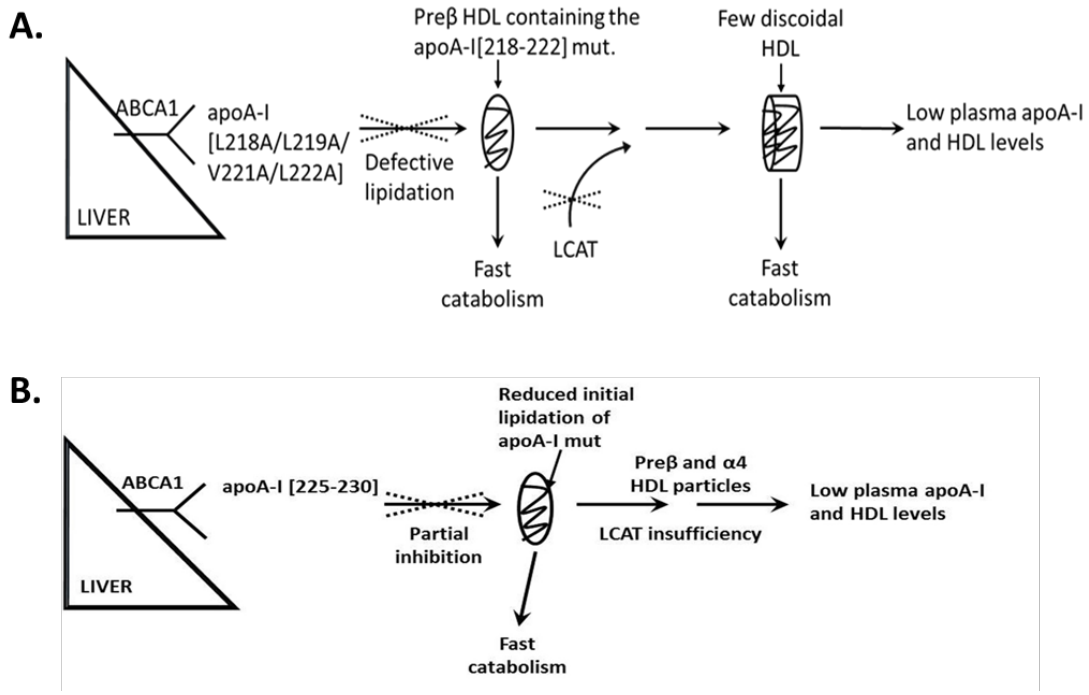

Figure 3.19: Schematic representation of the affect of the (L218A/L219A/V221A/L222A) (A) and the (F225A/V227A/F229A/L230A) mutations (B) on the biogenesis of HDL.

Effect the apoA-I mutants on the α-helical content, thermal unfolding, chemical unfolding and hydrophobic surface exposure of apoA-I

To test whether the functional changes of the apoA-I[218-222] mutant is accompanied by changes in the structure and conformation of the protein as determined by biophysical assays. Circular dichroism measurements indicated 7% loss of helical content for the apoA-I[218-222] mutant (Table 3.IV A). Thermal unfolding of apoA-I followed by CD measurements showed that the apoA-I[218-222] mutant had a much more cooperative unfolding transition indicating a more compact structure for the this mutant protein (Table 3.IV A). The chemical unfolding profile of the apoA-I[218-222] mutant, probed by intrinsic tryptophan fluorescence, was identical to that of the WT apoA-I (Table 3.IV A). Finally, the ANS fluorescence

measurements indicated that the apoA-I[218-222] mutant had a 40% reduction of hydrophobic surface exposure to the solvent (Table 3.IV A).

Table 3.IV (A,B): Calculated biophysical parameters for WT and mutant apoA-I[218-222], apoA-I[E223A/K226A] (A) and apoA-I[225-230] (B) forms.

A.

Mutation	**Helicity***	**Thermal Denaturation***			**Chemical Denaturation***	**ANS binding***
apoA-I	α-helix	T_m (^oC)	Slope*[1]	Cooperativity index (n)	$D_{1/2}$ (M)	Fold-increase[#]
apoA-I WT	60±1.5	55.6±0.4	8.3±0.4	6.4±0.2	1.01±0.02	6.0±0.4
L218A/L219A/V221A/L222A	52.7±1.6[1]	56.1±0.8	4.6±0.2[1]	9.7±0.6[1]	1.00±0.03	3.5±0.2[1]

B.

Mutation	**Helicity***	**Thermal Denaturation***			**Chemical Denaturation***	**ANS binding***
apoA-I	α-helix	T_m (^oC)	Slope*[1]	Cooperativity index (n)	$D_{1/2}$ (M)	Fold-increase[#]
WT	59.3±0.5	56.0±0.5	7.8±0.1	6.3±0.4	1.02±0.06	10.2±0.5
F225A/V227A/F229A/L230A	51.7±0.3[1]	57.8±0.2[3]	4.0±0.0[1]	11.4±0.4[5]	1.01±0.03	6.0±0.4[1]

Values are means ± SD from three to four experiments.

[1]p<0.0001; [2]p<0.005; [3]p<0.05; [4]p<0.0005; [5]p<0.001. [#] Fold-increase in signal compared to unbound ANS.

*[1] Slope is calculated from the fit of thermal denaturation curve to a Boltzman sigmoidal model curve using the equation $[\Theta]_{222}$= Bottom + ((Top-Bottom)/(1 =exp((Tm-X)/Slope))). X describes the temperature and slope describes the steepness of the curve, with a larger value denoting a shallow curve.

*Parameters obtained from the indicated measurements are as follows: α-helix, is the % α-helical content of the protein as calculated from the molecular ellipticity of the protein sample at 222nm. $T_{m,}$ is middle point of the thermal denaturation transition (melting temperature). Slope, is the calculated slope of the linear component of the thermal denaturation transition, around the melting temperature. The cooperativity index n, is an indicator of the cooperativity of the thermal unfolding transition and is

calculated using the Hill equation the Hill equation n=(log 81)/log($T_{0.9}$ /$T_{0.1}$), where $T_{0.9}$ and $T_{0.1}$ are the temperatures where the unfolding transition has reached a fractional completion of 0.9 and 0.1. $D_{1/2}$ is the Guanidine HCl concentration at which the mid-point of the chemical denaturation is achieved. Fold-increase is the increase in ANS fluorescence in the presence of the protein relative to free ANS in the same buffer.

Physicochemical analyses were also performed for the apoA-I[225-230] mutant. Circular dichroism measurements indicated 7.6% loss of helical content in the apoA-I[225-230] mutant (Table 3.IV B). Thermal unfolding followed by the CD signal showed that the F225A/V227A/F229A/L230A mutations caused a more cooperative unfolding transition as compared to WT apoA-I (Table 3.IV B). In contrast, the chemical unfolding profile of the mutant, probed by the intrinsic tryptophan fluorescence, was similar to that of the wild-type apoA-I (Table 3.IV B). Finally, the ANS fluorescence measurements show that the F225A/V227A/F229A/L230A mutations caused a 41% reduction of hydrophobic surface exposure to the solvent (Table 3.IV B).

DISCUSSION

Significance of the hydrophobic residues L218, L219, V221, L222 of apoA-I in the biogenesis of HDL

Rationale for selection of the mutations. Lipid-free or minimally lipidated apoA-I promote ABCA1-mediated cholesterol efflux and thus serve as acceptors of cellular

phospholipid and cholesterol (108;553;554). Lipid-bound apoA-I is a physiological activator of LCAT (554). The functional interactions between apoA-I and ABCA1 are important for cholesterol efflux and also initiate the biogenesis of HDL (98;99;108). To identify the specific C-terminal residues of apoA-I that are required for correct interactions with ABCA1 and/or LCAT that lead to the formation of mature α-HDL particles we have introduced two sets of mutations that span the 218-226 region of apoA-I. The properties of the apoA-I[218-222] mutant thus generated were studied by in vitro experiments and adenovirus mediated gene transfer.

The L218A/L219A/V221A/L222A mutations alter the functional and physicochemical properties of apoA-I. The in vitro experiments showed that compared to WT apoA-I, the capacity of the apoA-I[218-222] mutant to promote ABCA1 mediated cholesterol efflux and to activate LCAT was 20 and 66% respectively. The changes in the physicochemical properties of the apoA-I[218-222] mutant included a 7% decrease in its α-helical content, a more cooperative thermal unfolding transition yet an identical chemical unfolding transition, and a 40% reduction of hydrophobic surfaces exposed to the solvent. The higher cooperativity observed during the thermal denaturation of this mutant suggests a more compact and stable structure something that may appear at odds with the lack of any observed stabilization during the chemical denaturation. The two methods, however, report on different aspects of the conformational change that follows protein denaturation (overall secondary structure versus the immediate environment of the tryptophan residues). In apoA-I all of the tryptophan residues are located in the N-terminal moiety of the molecule and therefore the lack of changes during chemical denaturation suggest that the thermodynamic stability of this domain is not affected by the mutation. Conversely, the altered thermal denaturation profile can be explained by localized

changes in the folding and stability of the C-terminal moiety of the protein only, where the mutated residues are, or to changes in the interactions between the C-terminal and N-terminal domain that primarily affect the stability of the C-terminal domain. However, since the two methods of denaturation also use different mechanisms to unfold the protein, the possibility that the stabilization seen during the thermal denaturation is dependent on the particular unfolding pathway utilized during heat denaturation should not be ruled out.

Finally, although the four mutated amino acids in the apoA-I[218-222] mutants correspond to ~5% of total hydrophobic amino acids of the protein, introduction of the mutations resulted in a 40% reduction of hydrophobic surface exposure, indicating that the residues L218/L219/V221/L222 give rise to almost half of the exposed hydrophobic sites of apoA-I. Taken as a whole, these findings suggest that the apoA-I[218-222] mutant greatly affect the structural integrity and conformational plasticity of apoA-I, effects that may at least partially underlie the observed changes in its *in vitro* and *in vivo* functions.

Ability of the apoA-I[218-222] mutant to promote biogenesis of HDL. Adenovirus mediated gene transfer of the WT apoA-I and apoA-I[218-222] mutant in apoA-I$^{-/-}$ mice showed that at comparable levels of gene expression the plasma cholesterol and apoA-I levels of mice expressing apoA-I[218-222] mutant were greatly reduced as compared to WT apoA-I. The plasma cholesterol reduction was due to the great decrease in the HDL cholesterol levels as determined by FPLC fractionation. Density gradient ultracentrifugation of plasma showed that compared to WT apoA-I the apoA-I[218-222] mutant was mainly distributed in the HDL3 fraction and its quantity was greatly reduced. The HDL fraction contained also substantial amount of mouse apoE and some apoA-IV.

A sensitive analysis that can detect abnormalities in the pathway of HDL biogenesis is the two-dimensional gel electrophoresis of plasma. This analysis showed that the apoA-I[218-222] mutant when expressed in apoA-I$^{-/-}$ mice generated preβ and α4 HDL particles. Such particles were shown previously to undergo fast catabolism by the kidney (124;219). The ability of the apoA-I[218-222] mutant to form HDL particles was also assessed by EM analysis of the HDL fractions obtained by density gradient ultracentrifugation of plasma. This analysis showed the presence of spherical HDL particles.

We have shown recently that apoE or apoA-IV containing HDL particles can be formed following a pathway similar to that used for the generation of apoA-I containing HDL particles (16;17). Since the HDL fraction 6 & 7 analyzed by EM contained both apoA-I[218-222] mutant and mouse apoE we considered the possibility that the observed spherical HDL particles in Figure 3.6 F may represent a mixture of apoA-I and apoE containing HDL.

To address this question we performed gene transfer of the apoA-I[218-222] mutant in double deficient (apoA-I$^{-/-}$ x apoE$^{-/-}$) mice that lack the two endogenous mouse apolipoproteins. Density gradient ultracentrifugation showed that the plasma of these mice contained only small amounts of apoA-I in the HDL3 and the lipoprotein-free (d≥1.21 g/ml) fractions. EM analysis showed the presence of few discoidal HDL as well as spherical particles correspondent in size to LDL and IDL. This is compatible with the presence of apoB-48 and apoA-IV in the HDL density range. Two-dimensional gel electrophoresis of plasma showed that it contained only preβ HDL. These data indicated that in apoA-I$^{-/-}$ x apoE$^{-/-}$ mice the apoA-I[218-222] mutant caused a defective lipidation of apoA-I, possibly due to defective apoA-I/ABCA1 interactions. This resulted in the generation of only preβ HDL particles that could not be converted to mature α-

HDL particles. Previous studies showed that C-terminal deletion mutants that remove the 220-231 region of apoA-I prevented the biogenesis of normal α-HDL particles but allowed the formation of preβ HDL particles (108;125). Similar preβ HDL particles have been found in the plasma of ABCA1 deficient mice and humans carrying ABCA1 mutations that are characterized by HDL deficiency (15;329;555).

It appears that in apoA-I$^{-/-}$ mice the diminished interactions between ABCA1 and the apoA-I[218-222] mutant, observed in vitro give the opportunity to the mouse apoE to compete more effectively for the ABCA1 binding site (556) and thus be lipidated. This will lead to the formation of spherical apoE containing HDL particles which float in the HDL2/HDL3 regions (Figure 3.6 B,F and Figure 3.7). Through unknown mechanisms the formation of apoE containing HDL appears to partially stabilize the limited number of nascent HDL particles that contain the apoA-I[218-222] mutant. In the absence of both apoA-I and apoE in the double deficient mice, there is limited lipidation of the apoA-I[218-222] mutant as evidenced by the low amount of apoA-I which floats in the HDL region and the formation of few discoidal HDL particles (Figure 3.9 F,G). The absence of apoE in this case appears to have a major destabilizing effect on any nascent HDL particle formed that contain the apoA-I[218-222] mutant. This explains the low apoA-I and HDL levels and the formation of few discoidal HDL particles associated with this mutant. Furthermore the absence of apoE allows formation of apoA-IV containing HDL particles in mice expressing the apoA-I[218-222] mutant which appear to interact with apoB containing lipoproteins and shift their flotation in the HDL density range.

To explain why α4-HDL particles are formed in the apoA-I$^{-/-}$ deficient mice expressing the apoA-I[218-222] mutant, we explored the possibility of changes in ABCA1 protein or mRNA

levels in these mouse models. Previous in vitro experiments had shown that in THP-1 cells apoA-I protects ABCA1 from proteasome mediated degradation (552). However, the in vivo animal experiments in the present study did not show significant changes in ABCA1 mRNA or protein levels in apoA-$I^{-/-}$ or apoA-$I^{-/-}$ x $apoE^{-/-}$ mice without any treatment or following gene transfer of either the WT apoA-I or the apoA-I[218-222] mutant (Figure 3.16).

In previous studies we have shown that naturally occurring point mutations in apoA-I when expressed in mouse models, activate insufficiently LCAT and lead to the accumulation of discoidal HDL particles in plasma. In this category belongs the apoA-I variants apoA-$I[R151C]_{Paris}$ and apoA-$I[R160L]_{Oslo}$ as well as the bioengineered mutants apoA-I[R149A] and apoA-I[R160V/H162A] (219;220). Other naturally occurring apoA-I variants such as apoA-$I[L141R]_{Piza}$ and apoA-$I[L159R]_{Finland}$ mutants, when expressed in mouse models, were characterized by very low levels of HDL cholesterol, few HDL particles and the presence of preβ and α4 HDL particles in plasma (217). A characteristic feature of these two categories of mutants, that are associated with low plasma HDL levels, is that the abnormal HDL phenotype could be corrected in vivo by gene transfer of human LCAT (217;219;220). The phenotype produced by the apoA-I[218-222] mutant is distinct from all previously described phenotypes and cannot be corrected by overexpression of LCAT. In addition the mutant protein had reduced capability to promote the ABCA1 mediated cholesterol efflux. Although other interpretations are possible, the in vivo and in vitro data suggest that the interaction of the apoA-I[218-222] mutant with ABCA1 results in defective lipidation that leads to the generation of preβ HDL particles that are not a good substrate for LCAT. If this interpretation is correct one can envision a very precise initial orientation of the apoA-I ligand within the binding site of ABCA1 (556) similar to that described

before for enzyme substrate interactions. A precise fit of the apoA-I ligand into the ABCA1 binding site will allow its correct lipidation. The nascent particle thus formed can then undergo cholesterol esterification by LCAT that leads to the formation of mature α-HDL particles. In contrast, incorrectly lipidated apoA-I becomes a poor substrate of LCAT.

Clinical implications. The apoA-I[218-222] mutant generated a unique aberrant HDL phenotype that has not been observed previously. The hallmark of this phenotype is low HDL levels, formation of preβ and discoidal HDL that does not mature further to spherical α-HDL particles and presence of IDL, LDL size particles in the HDL region that are enriched in apoA-IV and apoB-48. Phenotypes generated by mutagenesis of apoA-I can facilitate the identification of similar phenotypes that may exist in the human population. Such phenotypes may serve in the diagnosis, prognosis and potential treatment of a specific dyslipidemias.

Significance of the hydrophobic residues 225 to 230 of apoA-I for the biogenesis of HDL

The F225A/V227A/F229A/L230A mutations alter the functional and physicochemical properties of apoA-I. The functional assays probed two well characterized properties of lipid free and lipoprotein bound apoA-I, which are its ability to promote ABCA1 mediated cholesterol efflux and to activate LCAT respectively (108;146;553). The decreased capacity of the apoA-I[225-230] mutant to promote ABCA1 mediated cholesterol efflux (31% of the WT control) is expected to influence its capacity to form HDL *in vivo*. The reduction in the ability of the apoA-I mutant to activate LCAT was modest (65% of WT control). However, previous studies showed

that the capacity of reconstituted HDL containing an apoA-I mutant to activate LCAT in vitro does not always predict their ability to affect LCAT activation *in vivo* (226;331).

The physicochemical analysis of the apoA-I[225-230] mutant suggested that the mutations lead to a more compact folding that may limit the conformational flexibility of the protein. The observed 7.6% decrease in the protein's α-helical content indicates that the structural changes brought about by the mutations extend beyond the limited area of the location of the mutations. Thermodynamic stability analysis indicated that the mutation also resulted to a protein that is thermodynamically stabilized and presents a more cooperative unfolding transition and compact structure. This was only evident during thermal unfolding and not during chemical denaturation. Since, however, the chemical denaturation reports only on the local environment of the tryptophan residues of the protein, which are all located on the N-terminal region of ApoA-I, this observation suggests that the structural repercussions brought about by the mutations may be limited to the C-terminal region of apoA-I where the mutation resides. In either case, a more cooperative thermal transition signifies a more compact structure with reduced conformational flexibility, a property that is necessary for lipid association. A recent related study involving different amino acid substitutions within the 225-236 region of apoA-I explored the effects of the aromatic and hydrophobic residues F225, F229, A232 and Y236 on the cholesterol efflux capacity and the ability of apoA-I to solubilize phospholipids and form HDL particles by cell cultures. It was concluded that both functions were similar to those of WT apoA-I when the overall hydrophobicity of apoA-I was not affected by the mutations in residues F225, F229, A232 and Y236. However both functions were impeded by a factor of three by substitution of the aromatic amino acids that decreased the

hydrophobicity of apoA-I (557). Another important finding of the present study is that although F225/V227/F229/L230 represent ~5% of total hydrophobic amino acids of apoA-I, their substitution by Alanines resulted in a 41% reduction in the ANS fluorescence, indicating that these residues constitute a major solvent-exposed hydrophobic patch on the surface of apoA-I. Overall, our findings suggest that the F225A/V227A/F229A/L230A mutations greatly affect the structural integrity and conformational flexibility of apoA-I, effects that may at least partially underlie the observed changes in its *in vitro* and *in vivo* functions.

The 225-230 mutations are associated with abnormalities in the biogenesis and maturation of HDL. In previous studies, systematic mutagenesis and gene transfer of human apoA-I mutants in apoA-I deficient mice disrupted specific steps along the pathway of the biogenesis of HDL and generated discrete HDL phenotypes (331). These phenotypes were characterized by low HDL levels, preponderance of immature HDL subpopulations or accumulation of discoidal HDL particles in plasma (108;110;217;219;220;226).

To obtain a clearer picture how the apoA-I mutations affected different steps of the biogenesis and maturation of HDL in the presence or the absence of the endogenous mouse apoE, the gene transfer studies were carried out in apoA-I$^{-/-}$ mice that lack mouse apoA-I and the apoA-I$^{-/-}$ x apoE$^{-/-}$ mice that lack both mouse apoA-I and apoE.

The studies in apoA-I$^{-/-}$ mice showed that the expression of the apoA-I[225-230] mutant was associated with great reduction in the plasma cholesterol and apoA-I levels despite the fact that the expression of the mutant transgene was higher than that of the WT apoA-I transgene.

The reduction in plasma apoA-I was associated with a great decrease in the HDL cholesterol levels as determined by FPLC fractionation of the plasma and was further confirmed by density gradient ultracentrifugation of plasma which showed reduction in the quantity of the apoA-I[225-230] mutant.

Potential abnormalities in the HDL phenotype in apoA-$I^{-/-}$ mice, resulting from the expression of the apoA-I[225-230] mutant, were verified by two-dimensional gel electrophoresis of plasma that showed the formation of preβ and α4-HDL particles. Accumulation of such particles is indicative of defective maturation of HDL due to insufficiency of mouse LCAT (217;219). The LCAT insufficiency may originate from fast catabolism of the nascent HDL particles along with the endogenous LCAT bound to them (217). Fast catabolism of the nascent HDL particles by the kidney has been described previously (124;219).

The plasma of both of apoA-$I^{-/-}$ and apoA-$I^{-/-}$ x apo$E^{-/-}$ mice expressing the apoA-I[225-230] mutant contained predominantly preβ and to a lesser extent α4 HDL particles, thus reaffirming the concept that the apoA-I[225-230] mutations affected the biogenesis of HDL. An unexpected finding was that the expression of the apoA-I[225-230] mutant in apoA-$I^{-/-}$ x apo$E^{-/-}$ mice resulted in the flotation of the mutant protein in all density fractions, along with mouse apoA-IV and apoB-48. The presence of apoB-48 in the higher density fractions affected the particle composition of the HDL fraction, by enriching it with larger particles corresponding in size to VLDL, IDL and LDL. Previous studies showed that apoA-IV can also generate apoA-IV containing HDL particles (16). It is thus possible that apoA-IV containing HDL may fuse with apoB-48 containing particles and pull them towards the higher density regions.

LCAT corrects the aberrant HDL phenotype caused by the apoA-I[225-230] mutations. In previous studies we have shown that naturally occurring or bioengineered point mutations in apoA-I when expressed in mouse models, activate LCAT insufficiently and in some instances may lead to the accumulation of discoidal HDL particles in plasma (219;220). Other mutations lead to very low levels of HDL cholesterol levels and accumulation of premature preβ and α4-HDL particles in plasma (217). A characteristic feature of these mutations is that the low HDL levels and the abnormal HDL phenotype could be corrected in vivo by gene transfer of LCAT (217;219;220). The preceding article showed that substitutions of residues L218, L219, V221, L222 by Alanines led to the generation of a unique and previously undetected low HDL phenotype that was characterized by the formation of only preβ HDL particles and could not be converted to spherical particles by excess LCAT (127). Since the changes in the structure and the functions of the apoA-I[225-230] and the apoA-I[218-222] mutant had several similarities, we carried out experiments to determine whether the aberrant HDL phenotype generated by the apoA-I[225-230] mutations could be corrected by LCAT. These experiments showed that co-expression of the LCAT and the apoA-I[225-230] mutant in apoA-$I^{-/-}$mice restored the HDL cholesterol peak of the FPLC profile and shifted it towards lower densities (compare Figure 3.5 with Figure 3.14 A). It also increased apoA-I levels and shifted its distribution to lower densities (compare Figure 3.6 A with Figure 3.14 C). Finally, it promoted the appearance of mouse apoE predominantly in the lower densities and of apoA-IV in all lipoprotein fractions (compare Figure 3.6 A with Figure 3.14 C).

Similar experiments in double deficient mice, showed that the co-expression of the LCAT and the apoA-I[225-230] mutant created a cholesterol shoulder that extended from VLDL to HDL as determined by FPLC analysis (Figure 3.14 B). The distribution of the mutant apoA-I,

apoA-IV and apoB-48 in different densities was similar to that observed in mice expressing the apoA-I mutant alone (Figure 3.14 D). In both mouse models the LCAT treatment created normal preβ and α-HDL subpopulations and generated spherical HDL particles of larger size. Thus, the observed LCAT insufficiency caused by the apoA-I[225-230] mutations could be reversed by treatment with LCAT.

The ability of LCAT to restore aberrant HDL phenotype caused by genetic or environmental factors may have important clinical implications for the correction of HDL abnormalities in humans. An abnormality that persisted in apoA-$I^{-/-}$ x apo$E^{-/-}$ mice expressing the apoA-I[225-230] mutant was the presence of VLDL, IDL and LDL size particles in the HDL fractions.

The present study in combination with the preceding study (127) shows the essential role of eight hydrophobic residues present in the 218-230 region of apoA-I for the structure and functions of apoA-I and its ability to form HDL. The two studies enhance our understanding of the complex factors that contribute to the correct extracellular assembly, maturation and proteomic composition of HDL. Future studies are required to identify by existing and new assays how the aberrant forms of HDL identified in these and previous studies (108;110;125;217;219;220;226) affect different functions of HDL that are required for protection from atherosclerosis and other diseases.

Significance of all the hydrophobic residues in the region 218-230 of apoA-I for the biogenesis of HDL

The purpose of this study was to determine whether the phenotype generated by the 218-230 mutations was more severe than the phenotypes generated by either the 218-222 or the 225-230 mutations. The double mutant 218-230 has many of the characteristics of the 218-222 mutant. It is characterized by low plasma apoA-I and HDL levels and formation of preβ particles that cannot be converted to α-HDL particles by excess LCAT.

Previous studies showed that mutations within these regions inhibited the ability of lipid-free apoA-I to promote transendothelial transport (107), as well as its bactericidal activity against Gram-negative bacteria (558), indicating the importance of the 218-222 residues for the functions of apoA-I.

The present study in combination with the two previous studies (126;127) shows the essential role of eight hydrophobic residues present in the 218-230 region of apoA-I for the structure and functions of apoA-I and its ability to form HDL. Overall, these studies enhance our understanding of the complex factors that contribute to the correct extracellular assembly, maturation and proteomic composition of HDL as well as the functions of apoA-I. Future studies are required to identify by existing and new assays how the aberrant forms of HDL identified in these and previous studies (108;110;125;217;219;220;226) affect different functions of HDL that are required for protection from atherosclerosis and other diseases.

Chapter III. Effects of LCAT mutations on the biogenesis of HDL.

RESULTS

Lecithin cholesterol acyltransferase (LCAT) is one of the key modulators of plasma high-density lipoprotein cholesterol (HDL-C) (29;160;382). In this study we explored the role of naturally occurring LCAT mutations on the biogenesis of HDL. These mutations are LCAT[E110D], LCAT[Y111N], LCAT[E110D], LCAT[Y111N], LCAT[T123I], LCAT[N131D], LCAT[R135Q], LCAT[V222F], LCAT[P250S], LCAT[R298C] and LCAT[C313Y]. The LCAT[E110D], LCAT[Y111N], LCAT[E110D/Y111N], LCAT[V222F], LCAT[R298C]. The LCAT[E110D], LCAT[Y111N], LCAT[V222F] and LCAT[R298C] mutations have been found in subjects with low HDL levels after screening a Dutch population for low HDL levels (161). The LCAT[T123I], LCAT[N131D] and LCAT[R135Q] mutations have been reported in probands and mebers of the affected families with Fish Eye Disease syndrome (164-166). The clinical manifestations were very low HDL-C levels, corneal opacification and in some cases coronary heart disease (164-166). The LCAT[C313Y] mutation was detected in a family of Moroccan origin with low HDL-C levels, total absence of LCAT activity in the plasma, corneal opacification, proteinuria and nephropathy at a very early age (546). The LCAT[P250S] mutation was detected in a subject from Greece who is suffering from familial LCAT deficiency (unpublished).

The cDNAs of the mutant forms of LCAT were provided by Dr. J.A, Kuivenhoven (Medical Center of Cronigen) and were subcloned in the pAd-Track-CMV vector in order to make adenoviruses expressing these mutants. Recombinant adenoviral plasmids were generated for all the mutations as described in methods. Detailed adenovirus mediated gene transfer studies were performed for the LCAT[T123I], which is representative of the Fish Eye Disease syndrome,

and the other two LCAT[P250S] and LCAT[C313Y], which are representative of Familial LCAT Deficiency.

The initial gene transfer experiments in HTB-13 cells showed that the LCAT[C313Y] mutant was not secreted into the culture medium (Figure 3.3 A). This finding explains the total absence of plasma LCAT activity and the very low HDL levels in the subjects carrying the LCAT[C313Y] mutation and therefore this mutant was not studied further. LCAT secreted by HTB-13 cells expressing infected with the LCAT[T123I] and LCAT[P250S] mutants as well as WT LCAT were used to measure their α- and β-LCAT activity. The LCAT[T123I] and LCAT[P250S] mutants were used in gene transfer experiments in LCAT deficient mice. To assess how the LCAT mutations affect the biogenesis of HDL, in one set of gene transfer experiments we evaluated the ability of the LCAT[T123I] and the LCAT[P250S] mutants to restore the HDL and apoA-I levels in apoA-$I^{-/-}$ mice following co-expression of these mutants with either apoA-$I[L159R]_{FIN}$ or apoA-I[225-230] that were shown previously to have defective biogenesis of HDL (126;217). Following gene transfer we measured hepatic mRNA levels, plasma lipids and the formation of HDL particles.

Determination of the α- and β-LCAT activity of WT LCAT and the LCAT mutant forms

The esterification of cholesterol of HDL by LCAT is known as α-LCAT activity whereas the esterification of IDL/LDL is called β-LCAT activity (160). Familial LCAT deficiency is characterized by loss of both α-LCAT and β-LCAT activity whereas Fish Eye Disease is characterized by only loss of α-LCAT activity (160). The α- and the β-activity of WT and the LCAT[T123I] and LCAT[P250S] mutants was assayed using reconstituted HDL (rHDL) and plasma human IDL/LDL

respectievly as substrate. The experiments were performed as described in sections 2.4.11 and 2.4.12 of materials and methods. The α-LCAT activity of the two mutatns was greatly diminished as compared to WT LCAT (1.5% and 3.5% for LCAT[T123I] and LCAT[P250S] respectively) (Figure 3.20 A). In contrast, the β-LCAT activity of the LCAT[T123I] mutant (ability to esterify the cholesterol on IDL/LDL) was 139% of the WT LCAT whereas the β-LCAT activity of LCAT[P250S] mutant was only 22% of the WT LCAT (Figure 3.20 B). These results are consistent with the classification of the LCAT[T123I] and LCAT[P250S] mutants as FED and FLD mutations respectievly.

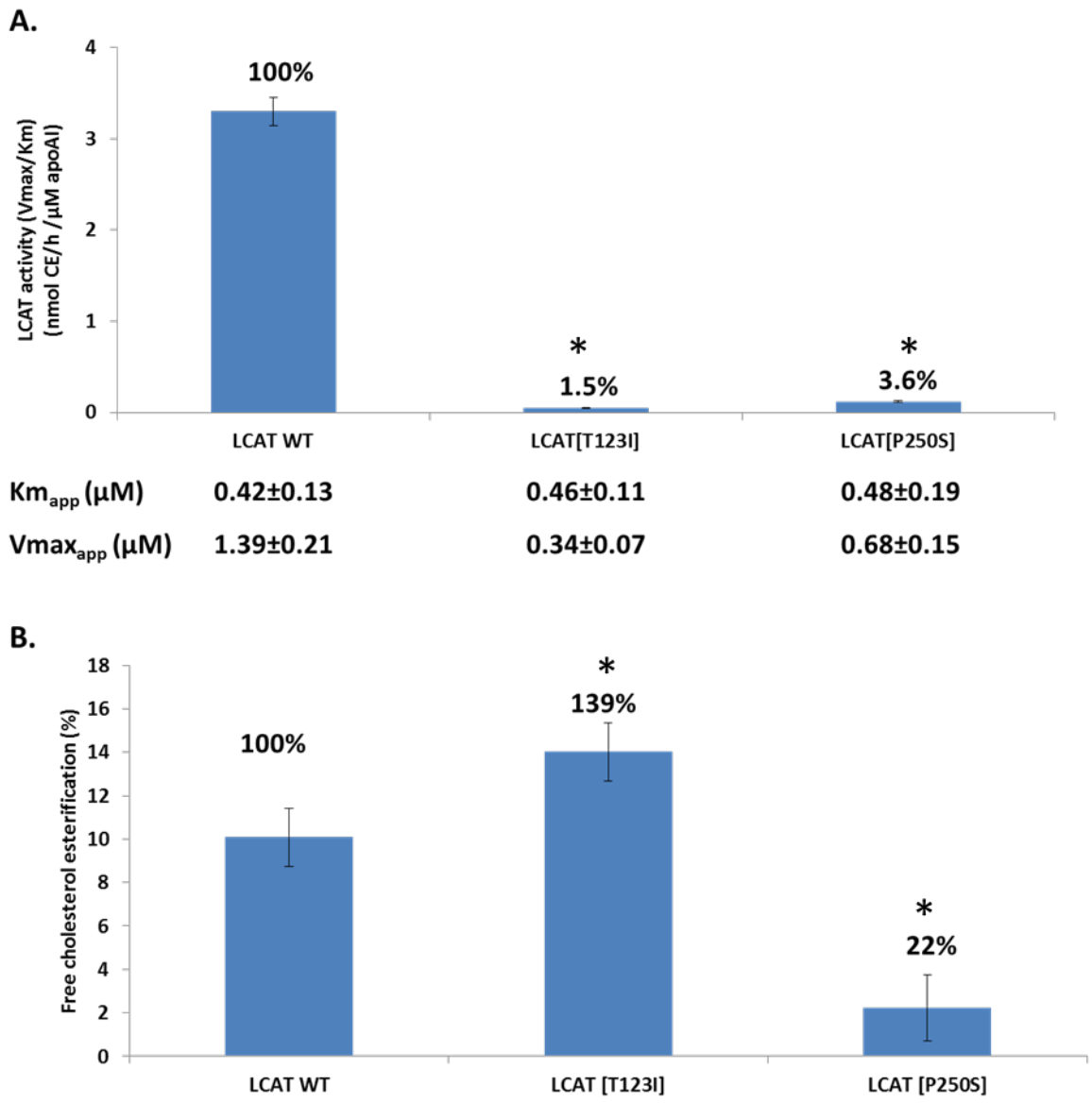

Figure 3.20 (A,B): Determination of the α-LCAT activity (ability to esterify cholesterol on rHDL) in panel A and the β-LCAT activity (ability to esterify cholesterol on IDL/LDL) in panel B of WT LCAT and the two mutant forms of LCAT (LCAT[T123I] and LCAT[P250S]). The data represent the average from three independent experiments performed in duplicates. P<0.05 for both mutants as compared to WT LCAT (indicated with and *).

Plasma lipids, apoA-I mRNA levels and FPLC profiles

To examine the effect of the LCAT mutations of the biogenesis of HDL, $LCAT^{-/-}$ mice were injected with adenoviruses expressing GFP as control, the WT LCAT or either of the LCAT[T123I] and LCAT[P250S] mutants at $8x10^8$ pfu. Total plasma cholesterol, free cholesterol, triglycerides, phospholipids and hepatic apoA-I mRNA levels were determined four days post-infection. The $LCAT^{-/-}$ mice had low total cholesterol, trilgycerides and phospholipids and CE/TC ratio (Table 3.V). Gene transfer of WT human LCAT in $LCAT^{-/-}$ mice increased significantly total plasma cholesterol and phospholipid levels as well the CE/TC ratio. Expression of the LCAT[T123I] increased the total plasma cholesterol and phospholipids to levels corresponding to 44% and 50% of WT LCAT and normalized the CE/TC to a ratio of 0.8. (Table 3.V). Expression of the LCAT[P250S] increased the total plasma cholesterol and phospholipids to levels corresponding to 25% and 57% of WT LCAT and partially corrected the CE/TC to a ratio of 0.6. The triglycerides in mice expressing the WT LCAT and the two mutant forms of LCAT were normal (60-65 mg/dL) (Table 3.V).

Fractionation of the plasma with FPLC and analysis of the distribution of the cholesterol showed that in mice expressing the WT LCAT there was a large peak of cholesterol extending in the HDL to LDL fraction. The cholesterol peak in mice expressing the LCAT[P250S] mutant was significantly decreased as compared to that of mice expressing the WT LCAT and the cholesterol was distributed predominantly in the HDL fractions. In mice expressing the LCAT[T123I] mutant there were two discrete cholesterol peaks covering the HDL and the LDL regions (Figure 3.21).

Table 3.V: Plasma lipids and hepatic mRNA levels of $LCAT^{-/-}$ mice expressing GFP, the WT human LCAT and the mutant forms of LCAT[T123I] or LCAT[P250S].

Protein expressed	Cholesterol (mg/dL)	CE/TC	Phospholipids (mg/dL)	Triglycerides (mg/dL)	Relative LCAT mRNA (%)
LCAT -/-	31±6	0.3±0.1	44±14	30±21	-
WT LCAT	368±47^	0.8±0.1^	263±34^	65±20	100±33*
LCAT[T123I]	162±20+^	0.8±0.1^	132±58+^	60±17	100±38
LCAT[P250S]	91±13+^	0.6±0.2+^	151±21+^	65±17	110±26

Values are means ± standard deviation based on analysis of 10 mice per experiment. Expression of LCAT mRNA is relative to the expression of WT LCAT and is indicated by a (*). Statistical significant differences in cholesterol, triglyceride and LCAT mRNA levels at $p<0.05$ between mice expressing the WT LCAT and the LCAT mutants are indicated by a (**+**) andbetween mice expressing GFP and WT LCAT or the mutant form of LCAT are indicated by a (**^**).

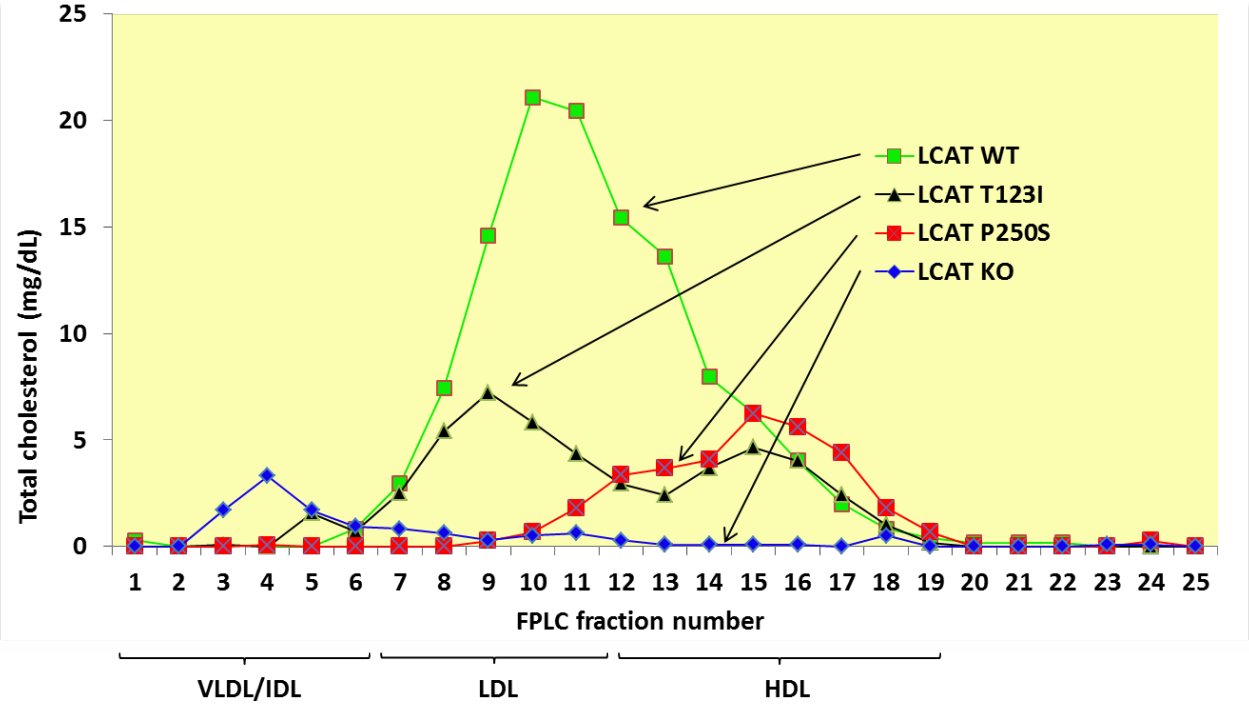

Figure 3.21: Plasma FPLC cholesterol profile of LCAT$^{-/-}$ mice expressing WT LCAT or the LCAT[T123I] or the LCAT[P25S] mutants as indicated.

Fractionation of plasma by density gradient ultracentrifugation and analysis of the fraction by SDS-PAGE, electron microscopy analysis of the HDL fractions and two-dimensional gel electrophoresis of the plasma

Fractionation of plasma by density gradient ultracentrifugation and subsequent analysis of the resulting fractions by SDS-PAGE served two purposes: it gave important information of the distribution of apoA-I and other apoproteins in different lipoprotein fractions, and it provided the HDL fractions that were used for EM analysis. In $LCAT^{-/-}$ mice, we could not detect any apoA-I or apoA-IV in any of the fractions and were only traces of apoE in the HDL2 and LDL fractions (Figure 3.22 A). In $LCAT^{-/-}$ mice expressing the WT LCAT, apoA-I was predominantly distributed in the HDL2/HDL3 fractions and to a lesser extent in the LDL fraction (Figure 3.22 B). ApoE and apoA-IV were present in all liporpotein fractions but predominantly in the LDL and HDL2 fraction. ApoB-48 was present in the in the VLDL/IDL/LDL region and to a lesser extent in the HDL2 fractions (Figure 3.22 B). In $LCAT^{-/-}$ mice expressing the LCAT[T123I] mutant, apoA-I was predominatly distributed in the HDL3 region and to a lesser extend in the LDL fraction (Figure 3.22 C). A small amount of apoE and apoB-48 was found in the VLDL/IDL region and traces of apoA-IV in the HDL3 region (Figure 3.22 C). In $LCAT^{-/-}$ mice expressing the LCAT[P250S] mutant, apoA-I was predominatly distributed in the HDL3 region and to a lesser extend in the HDL2 region (Figure 3.22 D)

Analysis of the HDL fractions 6 and 7 obtained following density gradient ultracentrifugation by EM showed the $LCAT^{-/-}$ mice expressing GFP contained very few small size spherical particles (6.1±1.3 nm dimeter) (Figure 3.22 E). The HDL from $LCAT^{-/-}$ mice expressing the WT LCAT contained spherical HDL particles (9.1±2 nm dimeter) (Figure 3.22 F). In

cotrnast, the HDL in LCAT$^{-/-}$ mice expressing the LCAT[T123I] or LCAT[P250S] mutant contained numerous small size particels of approximatly 7 nm diameter. (Figures 3.22 G,H).

Two dimensional gel electrophoresis of plasma showed that LCAT$^{-/-}$ mice formed predominantly two preβ HDL subpopulations and small size α4-HDL (Figure 3.22 I). LCAT$^{-/-}$ mice expressing the WT LCAT formed α2-,α3-and larger size α1-HDL subpopulations (Figure 3.22 J). LCAT$^{-/-}$ mice expressing the LCAT[T123I] mutant contained α2- and α3-HDL subpopulations, superimposed on the preβ and α4-HDL subpopulation seen in LCAT$^{-/-}$ mice (Figure 3.22 K). LCAT$^{-/-}$ mice expressing the LCAT[P250S] mutant also contained α2-, α3-HDL subpopulation as well as α4- and numerous preβ HDL subpopulations (Figures 3.22 L).

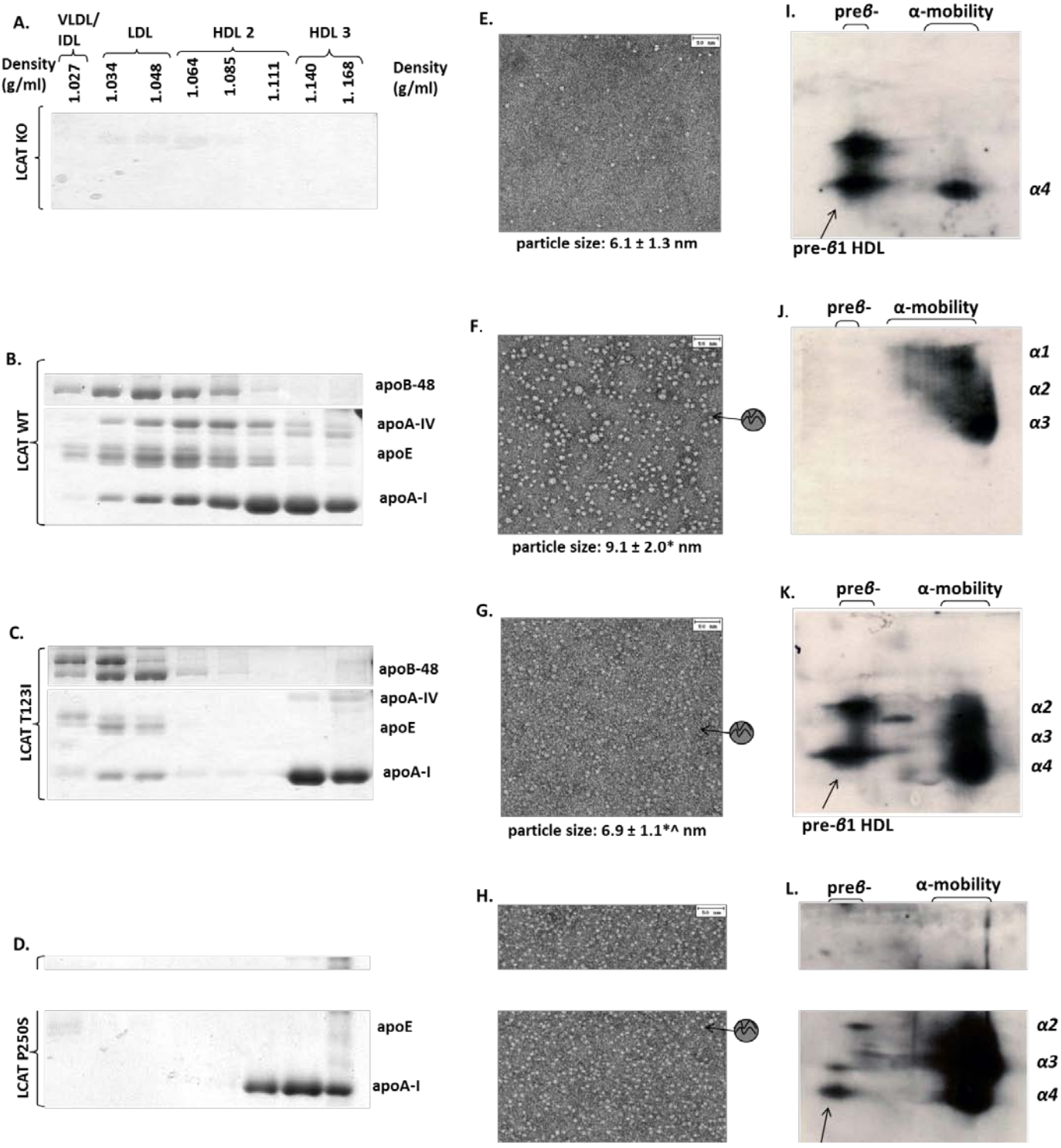

Figure 3.22 (A-L): Analysis of plasma of LCAT$^{-/-}$ mice infected with adenoviruses expressing GFP, the WT LCAT or the LCAT[T123I] and LCAT[P250S] mutants by: density gradient ultracentrifugation and SDS-PAGE (A-D), EM analysis of HDL fractions 6-7 (E-H), two dimensional gel electrophoresis of plasma of (I-L).

Ability of LCAT mutants to correct the defective HDL phenotype caused by the apoA-I[L159R]Fin and the apoA-I[F225A/V227A/F229A/L230A] mutants

We investigated the ability of the LCAT mutants to correct the aberrant HDL phenotypes of mice expressing the apoA-I[L159R]$_{FIN}$ or apoA-I[225-230] mutants in apoA-I$^{-/-}$ background. In this set of experiments, apoA-I$^{-/-}$ mice were separated in groups of 4-5 mice. One group was injected with 1.5x10^{9} pfu GFP. Three groups were injected with either WT apoA-I or apoA-I[L159R]$_{FIN}$ or apoA-I[225-230] at 1x10^{9} pfu and 5x10^{8} pfu GFP. Six groups were injected with a combination of 1x10^{9} pfu of the apoA-I[L159R]$_{FIN}$ or apoA-I[225-230] mutanta and 5x10^{8} pfu of either the WT LCAT or each of the LCAT[T13I] and LCAT[P250S] mutants (Table 3.VI).

Plasma total cholesterol, CE/TC ratio, triglycerides, apoA-I protein levels and hepatic human LCAT and apoA-I mRNA levels were determined four days post infection of apoA-I$^{-/-}$ mice. In all cases the apoA-I and LCAT mRNA levels were comparable. ApoA-I$^{-/-}$ mice expressing GFP had very low total cholesterol levels. Expression of WT apoA-I increased 9-fold the total cholesterol levels, expression of apoA-I[225-230] increase only 2-fold the total cholesterol levels and expression of apoA-I[L159R]$_{FIN}$ did not increase cholesterol levels as compared to mice expressing GFP (Table 3.VI). Similarly, in mice expressing the apoA-I[225-230] and apoA-I[L159R]$_{FIN}$ mutants, the apoA-I protein levels of were very low as compared to mice expressing the WT apoA-I (Table 3.VI). The co-expression of either the apoA-I[225-230] or apoA-I[L159R]$_{FIN}$, with WT LCAT increased significantly the total cholesterol and plasma apoA-I levels as compared to mice expressing each apoA-I mutants alone (Table 3.VI). In contrast, the co-expression of either of the apoA-I[225-230] or apoA-I[L159R]$_{FIN}$ mutants with either of the LCAT[T123I] or LCAT[P250S] mutant forms showed a moderate increase in total cholesterol and

apoA-I plasma levels as compared to mice expressing each of the apoA-I mutants alone (Table 3.VI). The incrase in plasma cholesterol levels caused by the co-expression of the apoA-I mutants with the LCAT mutatns was higher for the apoA-I[225-230] as compared to apoA-I[L159R]$_{FIN}$ (Table 3.VI). In all cases, the changes in plasma triglyceride levels and the CE/TC ratio were not significant (Table 3.VI).

FPLC analysis showed that in apoA-I$^{-/-}$ mice expressing the WT apoA-I formed a large cholesterol peak in the HDL region (Figures 3.23 A). In mice expressing apoA-I[L159R]$_{FIN}$ mutant the cholesterol peak was barely detectable but it increased dramatically when the apoA-I[L159R]$_{FIN}$ mutant was co-expressed with WT LCAT and shifted to lower densities as compared to the HDL peak of mice expressing the WT apoA-I (Figures 3.23 A). In mice co-expressing the apoA-I[L159R]$_{FIN}$ mutant and LCAT[T123I] there was a modest increase in HDL cholesterol and its distribution was biphasic covering the HDL and LDL regions (Figures 3.23 A). In mice co-expressing the apoA-I[L159R]$_{FIN}$ mutant and LCAT[P250S] there was a modest increase in HDL cholesterol that was distributed predominantly in the HDL and to a lesser extent in the LDL region (Figures 3.23 A).

FPLC analysis showed that in apoA-I$^{-/-}$ mice expressing apoA-I[225-230] mutant the cholesterol peak was low and it was distributed in the HDL region (Figures 3.23 B). When the apoA-I[225-230] mutant was co-expressed with WT LCAT, the cholesterol was greatly increased nad it was shifted to lower densities as compared to the HDL peak of mice expressing the WT apoA-I (Figures 3.23 B). In mice co-expressing the apoA-I[225-230] mutant and LCAT[T123I] there was a modest increase in HDL cholesterol and its distribution was biphasic covering the HDL and LDL regions (Figures 3.23 B). In mice co-expressing the apoA-I[225-230] mutant and

LCAT[P250S] there was a modest increase in HDL cholesterol that was distributed predominantly in the HDL and to a lesser extent in the LDL region (Figures 3.23 B).

Table 3.VI: Plasma lipids, apoA-I protein levels and hepatic mRNA levels of apoA-I and LCAT of apoA-I$^{-/-}$ mice expressing GFP, the WT apoA-I and apoA-I[225-230] or apoA-I[L159R]$_{FIN}$ alone or in combination with the WT human LCAT or the mutant forms of LCAT[T123I] and LCAT[P250S] as indicated.

Protein expressed	Cholesterol (mg/dL)	CE/TC	Triglycerides (mg/dL)	apoA-I protein (mg/dL)	Relative apoA-I mRNA (%)	Relative LCAT mRNA (%)
apoA-I$^{-/-}$	27.5±6.5	0.68±0.04	37.3±11.1	-	-	-
apoA-I WT	251.7±70.6	0.85±0.12	41.6±12.1	191±88	100±32*	-
apoA-I[225-230]	58.2±17.3^{+}	0.78±0.05	45.1±15.5	59±17^{+}	77±39	-
apoA-I[225-230] + LCAT	247.4±90.6	0.79±0.01	48.1±18.7	149±43	91±41	90±17*
apoA-I[225-230] + LCAT[T123I]	108.5±37.3^{+}^	0.82±0.02	38.3±10.8	90±14^{+}^	104±42	100±14
apoA-I[225-230] + LCAT[P250S]	109.3±76.3^{+}^	0.81±0.07	42.2±4.2	85±5^{+}^	97±45	100±14
apoA-I[L159R]FIN	26.4±3^{+}	0.75±0.1	26.5±13	25±4^{+}	100±50	-
apoA-I[L159R]FIN + LCAT	380.5±76^{+}	0.79±0.04	44.5±5	381±93^{+}	120±37	115±21*
apoA-I[L159R]FIN + LCAT[T123I]	46.3±6^{+}^	0.85±0.04	28.6±7	107±21^{+}^	116±52	98±29
apoA-I[L159R]FIN + LCAT[P250S]	45.1±21^{+}^	0.70±0.09	38.7±16	136±19^	130±17	100±40

Values are means ± standard deviation based on analysis of 4-5 mice per experiment. Expression of apoA-I and LCAT are relative to the expression of WT apoA-I and WT LCAT respectively and is indicated by a (*). Statistical significant differences in cholesterol, triglyceride, mRNA and protein levels at $p<0.05$ between mice expressing the WT apoA-I and the apoA-I mutants are indicated by a (**+**)and between mice expressing the mutant form of apoA-I along with WT LCAT and the mice expressing the mutant forms of apoA-I along with the mutant forms of LCAT are indicated by a (^). No significant differences in mRNA expressions of apoA-I or LCAT were observed as compared to their respective WT forms.

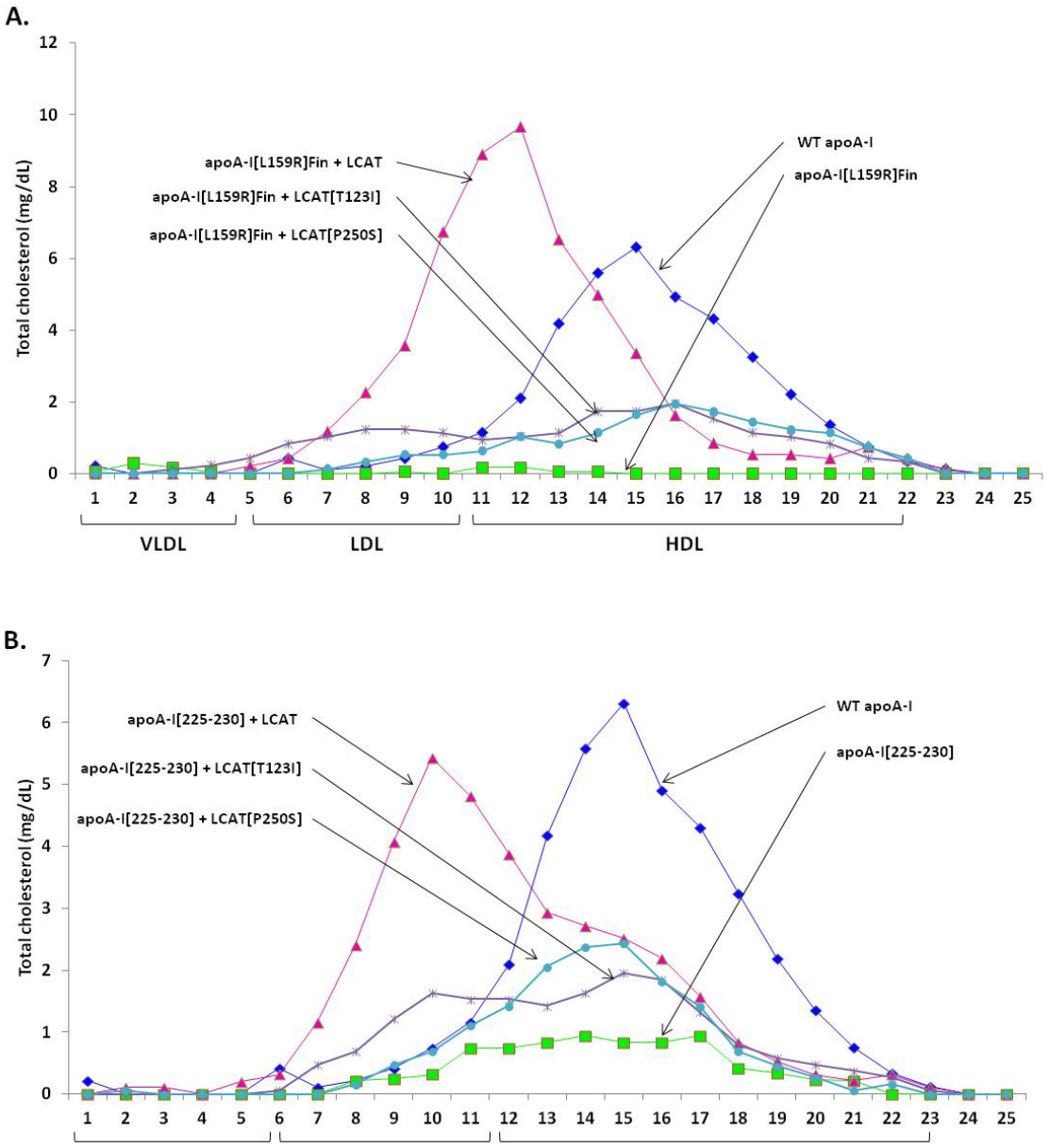

Figure 3.23 (A,B): Plasma FPLC cholesterol profile of apoA$^{-/-}$ mice expressing WT apoA-I and apoA-I[L159R]$_{FIN}$ alone or in combination with either WT LCAT or the LCAT[T123I] and the LCAT[P250S] mutants as indicated (A). Plasma FPLC profiles for apoA$^{-/-}$ mice expressing the apoA-I[225-230] alone or in combination with the WT LCAT, LCAT[T123I] or LCAT[P250S] (B) as indicated.

Fractionation of plasma obtained following gene transfer by density gradient ultracentrifugation showed that the WT apoA-I was equally distributed in the HDL2 and HDL3 region (Figure 3.24 A) whereas the apoA-I[L159R]$_{FIN}$ mutant was predominantly distributed in the HDL3 region (Figure 3.24 B). In mice co-expressing the apoA-I[L159R]$_{FIN}$ mutant and LCAT, most of apoA-I was distributed in the HDL2/HDL3 region and to a lesser extend in the VLDL/IDL/LDL regions. Mouse apoE was also distributed predominantly in the VLDL/IDL/LDL region and to a lesser extent in the HDL2 region (Figure 3.24 C). In mice co-expressing the apoA-I[L159R]$_{FIN}$ mutant and either LCAT[T123I] or LCAT[P250S] the apoA-I was predominantly in the HDL3 region (Figures 3.24 D,E). Traces of apoE were also detected in the LDL region of mice co-expressing the apoA-I[L159R]$_{FIN}$ mutant and the LCAT[T123I] (Figures 3.24 D).

EM analysis of the HDL fractions 6 and 7 obtained by density gradient ultracentrifugation showed the presence of spherical particles of size 9±1.1 nm in diameter in mice expressing apoA-I WT and fewer number of smallel HDL spherical particles of average diameter 5.8 nm in diametery in mice expressing the apoA-I[L159R]$_{FIN}$ (Figures 3.24 F,G). Co-expression of the apoA-I[L159R]$_{FIN}$ mutant and WT LCAT generated spherical particle of average diameter 9.9±1.8 nm (Figures 3.24 H). Smaller size spherical particles of average diameter 7.5 nm and fewer in numbers were generated in mice co-expressing the apoA-I[L159R]$_{FIN}$ and with either of the LCAT[T123I] or LCAT[P250S] mutants (Figures 3.24 I,J).

Analysis of the plasma obtained following gene transfer by two dimensional electrophoresis showed the presence of small amounts of preβ HDL and all the a-HDL subpopulations in mice expressing WT apoA-I (Figure 3.24 K).The plasma of the mice expressing the apoA-I[L159R]$_{FIN}$ contained predominantly preβ HDL subpopulations and small amount of α4- and α3-HDL subpopulations (Figure 3.24 L). Co-expression of the apoA-I[L159R]$_{FIN}$ mutant

with WT LCAT restored the α-HDL subpopulations and increased the levels of the larger α1-HDL subpopulation (Figure 3.24 M).Co-expression of the apoA-I[L159R]$_{FIN}$ and either LCAT[T123I] or LCAT[P250S] mutants generated preβ subpopulation along with α3,α4-HDL subpopulations (Figures 3.24 N,O).

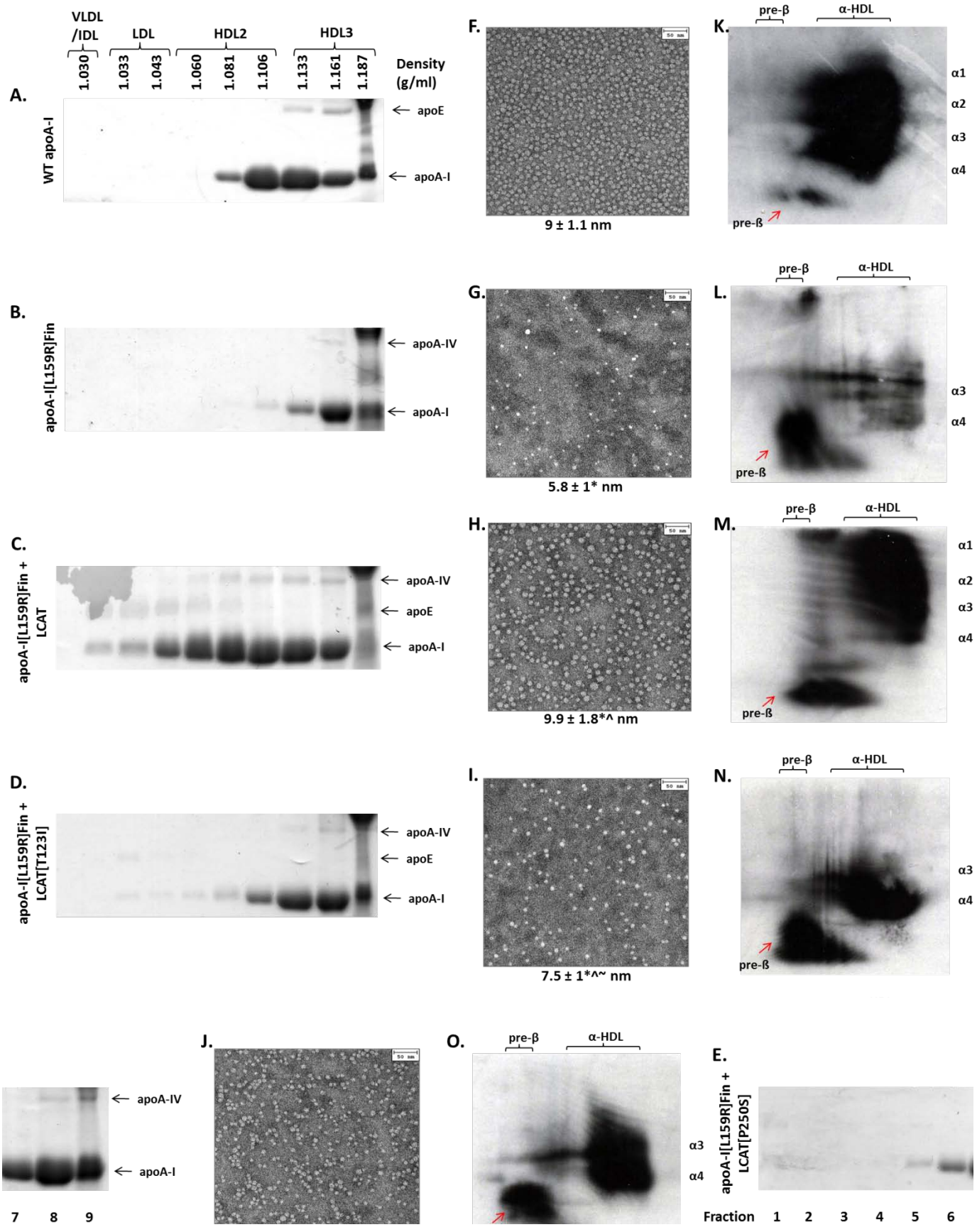
A.
VLDL /IDL
LDL
HDL2
HDL3
1.030
1.033
1.043
1.060
1.081
1.106
1.133
1.161
1.187
Density (g/ml)
WT apoA-I
apoE
apoA-I
B.
apoA-I[L159R]Fin
apoA-IV
apoA-I
C.
apoA-I[L159R]Fin + LCAT
apoA-IV
apoE
apoA-I
D.
apoA-I[L159R]Fin + LCAT[T123I]
apoA-IV
apoE
apoA-I
7 8 9
apoA-IV
apoA-I
F.
9 ± 1.1 nm
G.
5.8 ± 1* nm
H.
9.9 ± 1.8*^ nm
I.
7.5 ± 1*^~ nm
J.
K.
pre-β
α-HDL
α1
α2
α3
α4
pre-ß
L.
pre-β
α-HDL
α3
α4
pre-ß
M.
pre-β
α-HDL
α1
α2
α3
α4
pre-ß
N.
pre-β
α-HDL
α3
α4
pre-ß
O.
pre-β
α-HDL
α3
α4
E.
apoA-I[L159R]Fin + LCAT[P250S]
Fraction 1 2 3 4 5 6

Figure 3.24 (A-O): Analysis of the plasma of apoA-I$^{-/-}$ mice infected with adenoviruses expressing the WT apoA-I, the apoA-I[L159R]$_{FIN}$ alone or in combination with either WT LCAT or the LCAT[T123I] and LCAT[P250S] mutants by: density gradient ultracentrifugation and SDS-PAGE (A-E), EM of HDL fractions 6-7 (F-J) and two dimensional gel electrophoresis of plasma (K-O).

We have also tested the ability of the LCAT mutant forms to correct the aberrant phenotype caused by the apoA-I[225-230] mutant shown in Figure 3.6 C,G,K employing the same approacehd and methodologies described for the apoA-I[L159R]$_{FIN.}$

Fractionation of plasma obtained following gene transfer by density gradient ultracentrifugation showed that in mice co-expressing the apoA-I[225-230] mutant and either LCAT[T123I] or LCAT[P250S] the apoA-I was predominantly in the HDL3 region (Figures 3.25 A,B). In the case of LCAT[T123I], large amounts of apoE were present in the HDL2/HDL3 region (Figures 3.25 A).

Analysis of the HDL fractions 6 and 7 obtained following density gradient ultracentrifugation by EM showed presence of spherical HDL particles of average diameter 8 nm in mice expressing the apoA-I[225-230] mutant in comination with either LCAT[T123I] or LCAT[P250S] (Figures 3.25 C,D).

Analysis of the plasma by two dimensional gele electrophoresis showed that the co-expression of the apoA-I[225-230] with either the LCAT[T123I] or LCAT[P250S] mutants generated preβ subpopulations and α3,α4-HDL subpopulations (Figures 3.25 E,F).

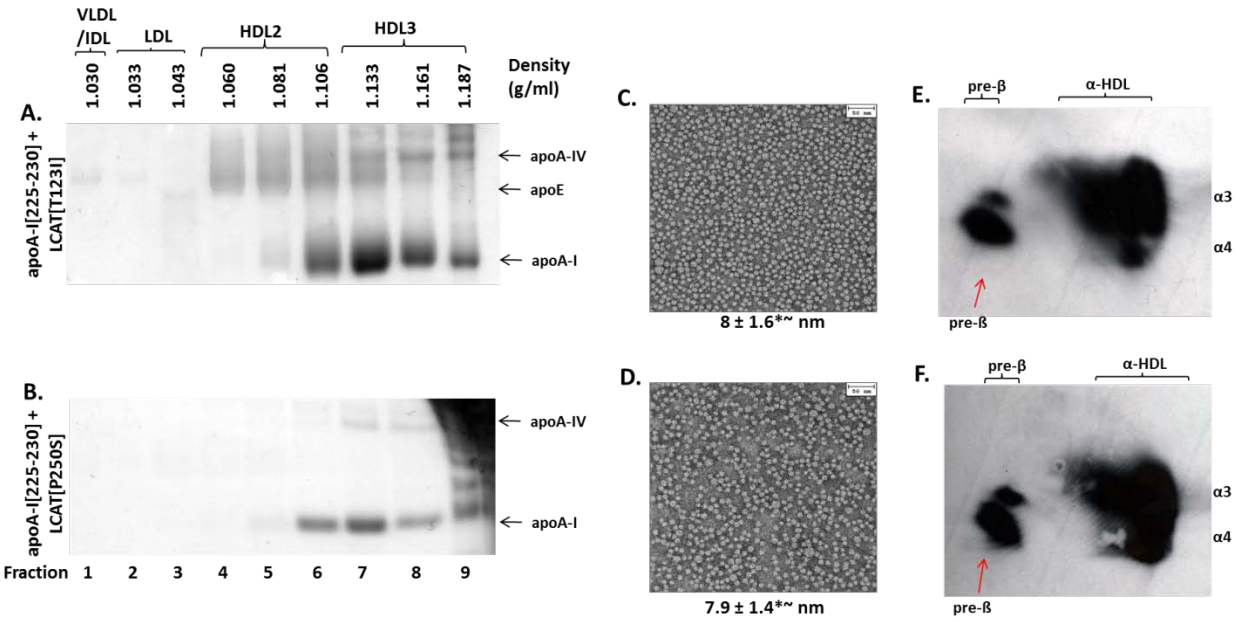

Figure 3.25 (A-F): Analysis of plasma of apoA-I$^{-/-}$ mice infected with adenoviruses expressing the apoA-I[225-230] with either LCAT[T123I] or LCAT[P250S] mutants by: density gradient ultracentrifugation and SDS-PAGE (A,B), EM of the HDL fractions 6-7 (C,D) and two dimensional gel electrophoresis (E,F).

DISCUSSION

Background:

Lecithin cholesterol acyltransferase (LCAT) is a key enzyme that regulates biogenesis and plasma levels of high-density lipoprotein (HDL) (29;160;382).

Following activation by apoA-I, LCAT interacts with discoidal and spherical HDL and catalyzes the transfer of the 2-acyl group of lecithin or phosphatidylethanolamine to the free hydroxyl residue of cholesterol to form cholesteryl esters (146;147). It also catalyzes the reverse reaction of esterification of lysolecithin to lecithin (148).

Although the preferred substrate of LCAT is HDL cholesterol, this enzyme also catalyzes the esterification of cholesterol of LDL where apoE is the activator of LCAT (149). The esterification of cholesterol of HDL by LCAT is known as α-LCAT activity whereas of LDL is called β-LCAT activity.

A computer-derived 3D structure of LCAT predicted that it belongs to the α/β hydrolase fold family and contains seven conserved parallel β strands and four α-helices that are connected by loops (150)

The active site of the enzyme contains the catalytic triad Ser181, Asp345, His377 that is found in proteolytic enzymes.

Based on the proposed 3D model of LCAT, it was found that the mutations associated with LCAT deficiency are in the vicinity of the catalytic residues of the enzyme and the mutations associated with FED are on the hydrophobic surface of the amphipathic helices of the enzyme and may interact with apoA-I and HDL (152;153).

Several of LCAT mutations have been found in humans (160;161). These mutations are associated with two clinical syndromes. Familial LCAT deficiency (FLD) is characterized by total loss of LCAT activity, and fish eye disease (FED) is characterized by loss of α-LCAT activity and preservation of β-LCAT activity (160).

FLD is characterized by very low LCAT mass or LCAT activity in the plasma, low HDL-C, apoA-I, apoA-II and apoB levels, increased triglyceride levels, formation of discoidal particles with preβ and α4-HDL electrophoretic mobility (15;162). The clinical manifestation of FLD is corneal opacity, anemia, proteinuria and renal disease (160;163). FED is a milder condition characterized by corneal opacity, decreased plasma HDL levels and LCAT mass.

Despite the atherogenic lipid/lipoprotein profile of the LCAT syndromes, there are only a few cases of FED patients which were associated with increased intima media thickness, atherosclerosis and premature CAD (29;164-167).

In the present study we have investigated the phenoypes the impact of two FLD (LCAT[P250S] and LCAT[C313Y]) and one FED (LCAT[T123I]) mutation on the formation of HDL as well as the *in vivo* interaction of the mutant LCAT enzymes with the mutant apoA-I forms (apoA-I[L159R]$_{FIN}$ and apoA-I[F225A/V227A /F229A/L230A]).

The C313Y mutations in LCAT prevent the secretion of the mutant enzyme

We employed gene transfer of WT and mutant LCAT forms in HTB-13 cells in order to determine the secretion of LCAT into the medium and also in order to produce WT and mutant forms of LCAT for *in vitro* experiments. The observation that the WT LCAT and the two mutants, LCAT[T123I] and LCAT[P250S], are secreted efficiently by the cells whereas the LCAT[C313Y] is not secreted explains the total absence of plasma LCAT activity and the very low HDL levels in the subjects carrying the LCAT[C313Y] mutation and therefore this mutant was not studied further.

The LCAT[P250S] has diminished α- and β-LCAT activity whereas the LCAT[T123I] has diminished α- and slighltly increase β-LCAT activity

LCAT secreted by HTB-13 cells, grown in a large scale in roller bottles was used to measure the α-LCAT activity using reconstituted HDL (rHDL) containing apoA-I, phospholipids and cholesterol and β-LCAT activity using plasma human IDL/LDL respectively as substrates.

The finding that the LCAT[P250S] mutant had dimished α- and β-LCAT activity and the LCAT[T123I] mutant had diminished α-LCAT activity but maintained the β-LCAT activity is consistent with the classification of the LCAT[T123I] and LCAT[P250S] mutants as FED and FLD mutations respectievly.

Effect of LCAT mutations on the biogenesis of HDL

The effect of LCAT mutants in the biogenesis of HDL was tested by adenovirus gene transfer in $LCAT^{-/-}$ mice. The LCAT deficiecy was associated with lack of HDL cholesterol peak, the loss of apoA-I from all lipoprotein fractions, presence of very small HDL particles and formation of predominantly preβ and α-4 HDL particles. This abberant HDL phenotype was completely corrected by gene transfer of WT LCAT but only partially with gene transfer of LCAT[T123I] and LCAT[P250S]. The low apoA-I and HDL levels produced by expression of the LCAT mutants in combination with the small HDL particles formed is consistent with accelerated catabolism of the lipoprotein particles formed by these two mutants (215).

Defective functional interactions of the LCAT mutatns with mutant apoA-I forms

Previous studies have shown that apoA-I mutants that have diminished capacity to activate LCAT in vitro when expressed in mouse models have low HDL levels and aberrant HDL phenotypes. These phenotypes could be corrected by overeexpression of WT LCAT. We performed gene transfer experiments to asses the ability of the two mutant LCAT forms to correct the aberrat phenotypes of apoA-I$[L159R]_{FIN}$ and apoA-I[F225A/V227A /F229A/L230A]. We consider it was possible that some apoA-I mutations may restore the interactions of apoA-I with a specific LCAT mutant and thus restore the normal HDL phenotype. Although this scenario

may be rare we have been able previously to correct the efflux capacity of mutant forms of SR-BI with a mutant apoA-I form (559).

Our studies showed that although WT LCAT corrected completely the aberrant HDL phenotype of apoA-I[L159R]$_{FIN,}$ the mutant forms produced similar results to those obtained be gene transfer of the LCAT mutants in the LCAT$^{-/-}$ mice.

Overall, our findings are consistent with the hypothesis that defective interactions of the mutant LCAT froms with WT and mutant apoA-I forms generate unstable HDL particles that are cleared rapidly by the kidney (560). The accelerated katabolism of the aberrant HDL particles by the kideny is consistent with the renal disease observed in the LCAT deficient patients (160;163).

Chapter IV: The effect of CTα on the biogenesis of HDL

RESULTS

CTP:phosphocholine cytidylyltransferase (CT) is a key enzyme in the biosynthetic pathway of phosphatidylcholine. Hepatic cells express two isoforms of CT (α and β) (337). Liver-specific CT knock-out mice have decreased levels of HDL-C, HDL phosphatidylcholine and apoA-I as compared to WT mice indicating that phosphatidylcholine generated by CT controbutes to the HDL homeostasis (337). Our aim was to assess the role of CTα on the biogenesis of HDL by adenoviruses-mediated gene transfer of CTα and human apoA-I in apoA-$I^{-/-}$ mice.

For this set of experiments, apoA-$I^{-/-}$ mice were injected with $8x10^8$ pfu WT apoA-I in combination with $5x10^8$ pfu GFP or $5x10^8$ pfu CTα. Plasma total cholesterol, CE/TC ratio, phospholipids, triglycerides, apoA-I protein and hepatic mRNA levels were determined four days post infection. Mice expressing CTα exhibited a significant increase in total plasma cholesterol, phospholipids as well as apoA-I protein levels as compared to mice expressing apoA-I alone (Table 3.VII).

FPLC analysis of the plasma of apoA-$I^{-/-}$ mice coexpressing apoA-I and CTα showed the presence of a cholesterol peak in the HDL region that was significantly icreased as compared to the HDL pak of mice expressing WT apoA-I in combination with GFP (Figures 3.26 A). Fractionation of plasma by density gradient ultracentrifugation and subsequent analysis of the resulting fractions by SDS-PAGE showed that in mice co-expressing apoA-I and CTα, apoA-I was predominantly distributed in the HDL2/HDL3 fractions and to a lesser extend in the VLDL/IDL/LDL fractions. In mice expressing the apoA-I in combination with GFP, apoA-I was present only in the HDL2/HDL3 fractions (Figures 3.26 B,C). EM analysis of the HDL fractions 6

and 7 obtained by density gradient ultracentrifugation showed presence of a homogenous populaton of spherical HDL particles 8.5±1 nm in diameter in mice co-expressing apoA-I in combination with GFP. The HDL obtained from mice co-expressing apoA-I and CTα, the patricles were also spherical but heterogenous in size with an average diameter 11.2±3.8 nm (Figures 3.26 D,E). Two dimensional gel electrophoresis of the plasma showed the formation of preβ and α-HDL subpopulations in both cases. Hoever co-expression of apoA-I and CTα resulted in incrreased amount of the larger α1-HDL subpopulation (Figures 3.26 F,G).

Table 3.VII (A,B): Plasma lipids, apoA-I protein levels and hepatic mRNA levels of apoA-I of apoA-I$^{-/-}$ mice expressing GFP and the WT apoA-I alone or in combination with CTα as indicated.

Protein expressed	Cholesterol (mg/dL)	CE/TC	Phospholipids (mg/dL)	Triglycerides (mg/dL)	ApoA-I protein levels (mg/dL)	Relative apoA-I mRNA (%)
apoA-I$^{-/-}$	34±5	0.6±0.1	28±13	11±6	-	-
apoA-I	104±20	0.7±0.1	142±65	32±8	65±22	1±0.01
apoA-I + CTα	291±37^{+}	0.6±0.1	349±97^{+}	52±22	170±23^{+}	0.99±0.06*

Values are means ± standard deviation based on analysis of 6-8 mice per experiment. * indicates the apoA-I mRNA levels of mice expressing apoA-I and CTα as compared to the mice expressing CTα alone. + indicates statistical significant differences in plasma cholesterol, triglycerides, phospholipids, apoA-I levels and hepatic apoA-I mRNA levels at $p<0.05$ between mice expressing the WT apoA-I and combination of apoA-I and CTα. The expression of CTα was confirmed by qRT-PCR.

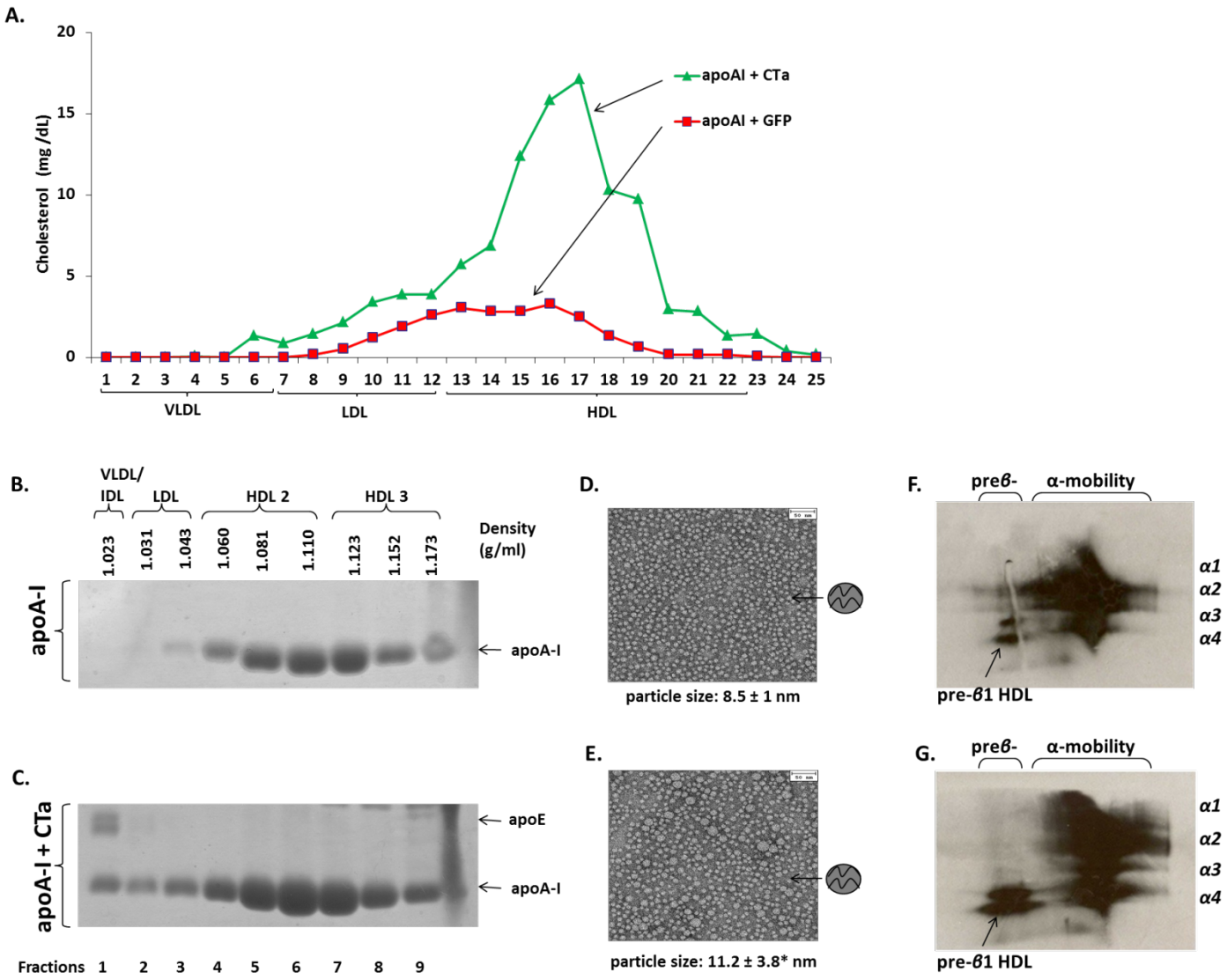

Figure 3.26 (A-G): FPLC cholesterol profiles of apoA-I$^{-/-}$ mice infected with adenoviruses expressing the WT apoA-I in combination with GFP or in combination with CTα (A). Density gradient ultracentrifugation and SDS-PAGE analysis of apoA-I$^{-/-}$ mice expressing the WT apoA-I in combination with GFP (B) or in combination with CTα (C). EM analysis of HDL fractions 6-7 obtained from apoA-I$^{-/-}$ mice expressing the WT apoA-I in combination with GFP (D) or in combination with CTα (E) following density gradient ultracentrifugation of plasma as indicated. The photomicrographs were taken at 75,000× magnification and enlarged 3 times. Two dimensional gel electrophoresis of plasma of apoA-I$^{-/-}$ mice expressing the WT apoA-I alone (F) or in combination with CTα (G).

DISCUSSION

Previous studies showed that inactivation of CTα in the liver decreased levels of HDL-C, HDL phosphatidylcholine and apoA-I as compare to WT mice indicating that phosphatidylcholine generated by CT contributes to the HDL homeostasis (337). Our experiments complimentary to those reported previously with the liver speceific knock-out mice. Gene transfer of low doses of adenovirus expressing CTα increased total plasma cholesterol, phospholipids and apoA-I protein and HDL levels as compared to mice expressing apoA-I alone.

High doses of CTα expressing adenovirus (greater that $5x10^8$ pfu) were toxic. Further studies are required to determine weather increase moderate increases in CTα levels will contribute to elevation in plasma HDL levels without causeing any toxicity.

Chapter V. Contributions of dominant mutations in apoE to lipid homeostasis and the biogenesis of HDL

RESULTS

The apoE3[K146N/R147W] variant, which was initially designated apoE1-Hammersmith (561), had been found in heterozygosity in three members of a family, two of which exhibited tubero-eruptive xanthomas, high plasma cholesterol and triglyceride levels and the appearance of a broad β band following electrophoresis of plasma (561).

The purpose of this study was to examine the molecular etiology of the dominant form of type III hyperlipoproteinemia that is associated with these mutations. We used adenovirus-mediated gene transfer in both apoE$^{-/-}$ and apoA-I$^{-/-}$ x apoE$^{-/-}$ mice of the full length apoE3[K146N/R147W] and a truncated apoE3[K146N/R147W]-202 form. The deletion of the C-terminal region of apoE, 203-299, has been shown to prevent hyperlipidemia for other apoE variants (263;264;562). Furthermore, we evaluated the contribution of LCAT and LPL in the induction of the hyperlipoproteinemic phenotype.

Induction of dyslipidemia by the apoE3[K146N/R147W] mutant and the contribution of the C-terminal domain of apoE3[K146N/R147W] in the induction of dyslipidemia: lipids, mRNA and protein levels of apoE3 and FPLC profile.

To elucidate how the K146N/R147W substitutions in human apoE3 induces dyslipidemia, we have assessed the ability of wild-type apoE3 as well as the full length apoE3[K146N/R147W] and various truncated apoE forms extending from residue 1 to 202, to clear the high plasma cholesterol levels of the apoE deficient mice and to affect the plasma

triglycerides following gene transfer. The experiments with the truncated apoE forms were designed to assess the contribution of the C-terminal 203-229 domain to clear plasma cholesterol and to induce hypertriglyceridemia.

We have found that a low dose ($5x10^8$ pfu) of an adenovirus expressing apoE3[K146N/R147W] increased plasma cholesterol in $apoE^{-/-}$ mice over a four day period and induced severe hypertriglyceridemia (Figure 3.27 A,B). The increase in plasma triglyceride levels caused by the apoE3[K146N/R147W] mutant correlated with a parallel increase in plasma apoE levels (Figure 3.27 C). In contrast, infection of $apoE^{-/-}$ mice with a similar dose ($5x10^8$ pfu) of adenovirus expressing wild-type apoE3 decreased plasma cholesterol, did not affect plasma triglycerides levels and caused only small increase in plasma apoE levels (Figure 3.27 A-C). Finally, a high dose (2x10*9 pfu) of the truncated apoE3[K146N/R147W]-202 did not clear cholesterols but also did not induce hypertriglyceridemia (Figure 3.27 A-C). Real-time qPCR analysis showed that the mRNA levels of the WT apoE3 and the apoE3[K146N/R147W] mutant were comparable whereas the mRNA of the truncated apoE3[K146N/R147W]-202 mutant were much higher reflecting the higher dose of the recombinant adenovirus selected for this experiment (Table 3.VIII A). Two other truncated apoE forms studied previously that were used as controls, the apoE4-202 and apoE4[R142C]-202 (534;563) cleared (with different kinetics) the plasma cholesterol but did not induce hypertriglyceridemia (Figure 3.27 A,B). The expression of wild-type apoE3 and the full length and truncated apoE3[K146N/R147W] mutant, affected differently the cholesteryl ester to total cholesterol (CE/TC) ratio of plasma. The apoE3[K146N/R147W] mutant decreased it, whereas the truncated apoE3[K146N/R147W]-202 did not have a significant effect, as compared to the wild-type apoE3 (Table 3.VIII B).

Table 3.VIII (A,B): Hepatic apoE mRNA levels of mice infected with adenoviruses expressing expression the wild-type apoE3 (A) and plasma cholesterol esters to total cholesterol ratio of wild-type and mutant apoE forms prior to and on days 1-4 post-infection in apoE$^{-/-}$ mice (B).

A.

Protein Expressed	Relative apoE3 mRNA (*%*)
WT apoE3 in apoE$^{-/-}$ mice	130 ± 60*
apoE3[K146N/R147W] in apoE$^{-/-}$ mice	110 ±40
apoE3[K146N/R147W]-202 in apoE$^{-/-}$ mice	480 ± 60^{+}
apoE3[K146N/R147W] in apoE$^{-/-}$ mice co-expressing LPL	146±59
apoE3[K146N/R147W] in apoE$^{-/-}$ mice co-expressing LCAT	57±54
WT apoE3 in apoA-I$^{-/-}$ x apoE$^{-/-}$ mice	100 ± 30*
apoE3[K146N/R147W] in apoA-I$^{-/-}$ x apoE$^{-/-}$ mice	110 ± 50
apoE3[K146N/R147W]-202 in apoA-I$^{-/-}$ x apoE$^{-/-}$ mice	300 ± 110^{+}

Values are means ± standard deviation based on analysis of 4-6 mice per experiment. (*) Expression of apoE3 is relative to the expression of WT apoE3 in the apoE$^{-/-}$ or apoA-I$^{-/-}$ x apoE$^{-/-}$ mouse groups. Statistical significant differences in cholesterol and triglyceride levels at $p<0.05$ was calculated between mice expressing the WT apoE and the apoE3[K146N/R147W] or apoE3[K146N/R147W]-202 mutant in either the apoE$^{-/-}$ or apoA-I$^{-/-}$ x apoE$^{-/-}$ mouse background and are indicated by a ($^{+}$).

B.

	WT apoE3	apoE3[K146N/ R147W]	apoE3[K146N/ R147W]-202	apoE3[K146N/ R147W]+LPL	apoE3[K146N/ R147W]+LCAT
DAY 0	0.61±0.09				
DAY 1	0.80±0.04	0.48±0.12*	0.60±0.17	0.33±0.07	0.54±0.08$^{\#}$
DAY 2	0.77±0.03	0.49±0.18*	0.59±0.19	0.33±0.11	0.57±0.03$^{\#}$
DAY 3	0.74±0.12	0.43±0.14*	0.53±0.21	0.41±0.10	0.51±0.03
DAY 4	0.72±0.21	0.34±0.11*	0.55±0.13~	0.43±0.07	0.56±0.07^$^{\#}$

* $P<0.05$ as compared to WT apoE3, ~$P<0.05$ as compared to apoE3[K146N/R147W], **^** $P<0.05$ as compared to apoE3[K146N/R147W], # $P<0.05$ as compared to apoE3[K146N/R147W] + LPL

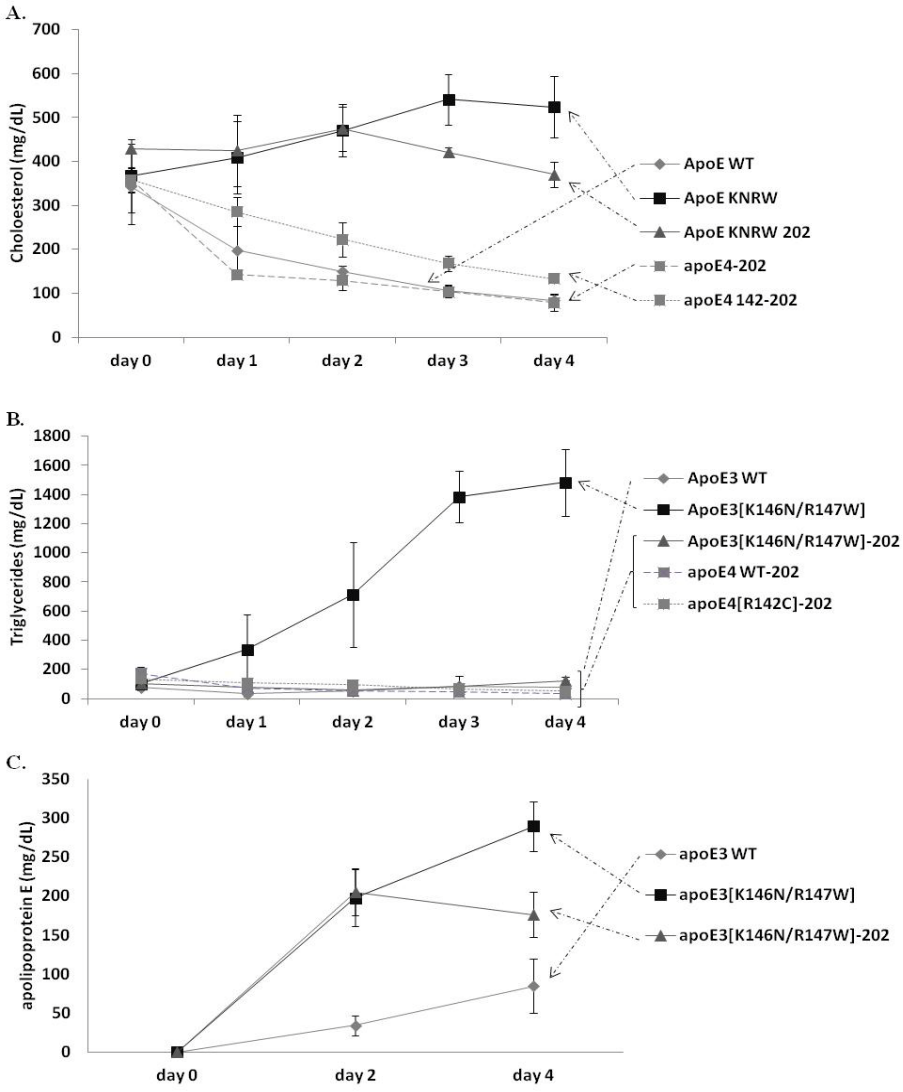

Figure 3.27 (A-C): Plasma cholesterol, triglycerides and apoE plasma protein levels of apoE$^{-/-}$ mice in different days post-infection with recombinant adenoviruses expressing the wild-type apoE3, the full length apoE3[K146N/R147W] and the truncated apoE3[K146N/R147W]-202 mutants and control truncated apoE4-202 and apoE4[R142C]-202 forms as indicated. Plasma cholesterol (A), plasma triglycerides (B), plasma apoE (C). The plasma cholesterol ester to total cholesterol ratio in different days post-infection are shown in supplemental table 2. The doses of the adenoviruses used were 5x10*8 pfu for the full length forms and 2x10*9 pfu for the truncated forms. The apoE mRNA levels of the different apoE forms used are shown in Table 3.VIII A. Parameters reported mean ± standard deviation.

FPLC fractionation of plasma showed that mice expressing wild-type apoE3 had an HDL cholesterol peak as described previously (17). Mice expressing the apoE[K146N/R147W]-202 mutant likewise contained a smaller HDL cholesterol peak along with a cholesterol shoulder extending in the LDL and IDL region. Mice expressing the apoE[K146N/R147W] mutant had a negligible HDL cholesterol peak but also contained a shoulder extending in the VLDL and LDL region (Figure 3.28 A). The majority of the triglycerides in mice expressing the apoE3[K146N/R147W] mutant were found in the VLDL region and to a much lesser extend to the IDL and LDL region (Figure 3.28 B). The FPLC profiles are compatible with the distribution of the apoA-I and apoE in HDL and other lipoprotein fractions as determined by density gradient ultracentrifugation of plasma (Figure 3.29 A-C).

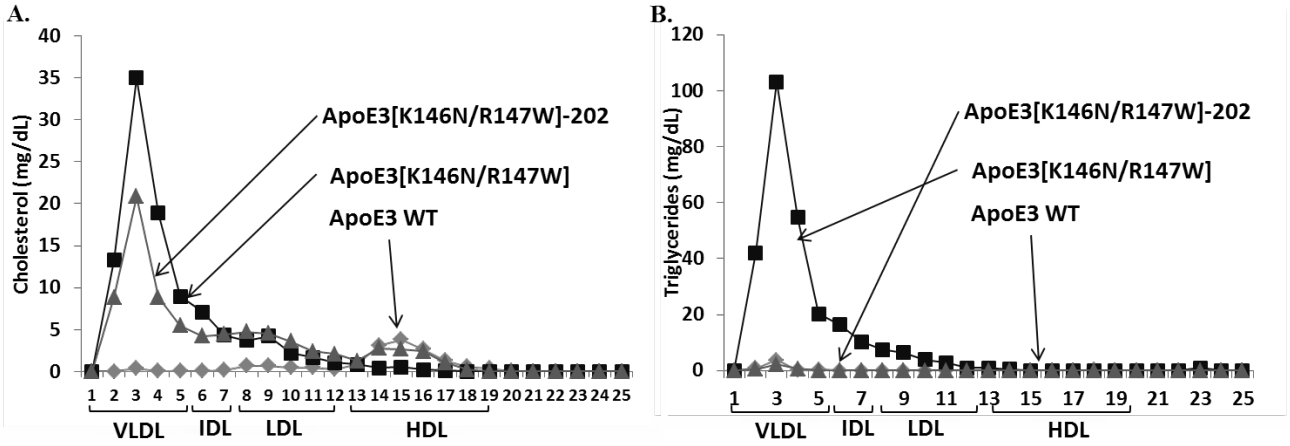

Figure 3.28 (A,B): FPLC profiles of plasma cholesterol and triglycerides four days post infection of apoE$^{-/-}$ mice expressing the wild-type apoE3, the full length apoE3[K146N/R147W] and the truncated apoE3[K146N/R147W]-202 mutants as indicated. FPLC cholesterol profiles (A) and FPLC triglycerides profile (B).

Evaluation of the distribution of apoE3 by density gradient ultracentrifugation and analysis of the fraction by electron microscopy

The proteomic composition of HDL and other lipoprotein fractions were assessed by density gradient ultracentrifugation of plasma obtained four days post adenovirus infection and analysis of the fractions by SDS-PAGE. When the apoE$^{-/-}$ mice were infected with a low dose ($5x10^8$ pfu) of apoE3-expressing adenovirus, the majority of the apoE was found in the HDL3 region where mouse apoA-I also resides. This apoprotein distribution indicated that the HDL fraction of mice expressing apoE3 described in Figure 3.28 A, contains mostly apoA-I and to a lesser extend apoE-containing HDL. Smaller amounts of apoE along with apoB-48 were found in the VLDL/IDL/LDL region (Figure 3.29 A).

When the apoE$^{-/-}$ mice were infected with a similar dose ($5x10^8$) pfu of adenovirus expressing apoE3[K146N/R147W] approximately 60% of apoE along with apoB-48 was found in the VLDL/IDL/LDL region and the remaining in the HDL2/HDL3 region. Unexpectedly, the expression of mutant apoE was associated with complete absence of the apoA-I in the HDL region and the other lipoprotein fractions (Figure 3.29 B). In apoA-I transgenic mice that express high levels of human apoA-I, expression of the apoE[K146N/R147W] mutant decreased but did not eliminate the amount of apoA-I that floats in the HDL region (Figure 3.30).

In apoE$^{-/-}$ mice expressing the truncated apoE3[K146N/R147W]-202 mutant, the majority of apoE, along with apoA-I was distributed in the HDL2/HDL3 region and the remaining in the VLDL/IDL/LDL region (Figure 3.29 C).

Analysis of fraction 6 and 7 obtained by density gradient ultracentrifugation by electron microscopy showed that the wild-type apoE3 and the truncated apoE3[K146N/R147W]-202 mutant formed spherical particles (Figures 3.29 D, F) and the apoE3[K146N/R147W] mutant

formed discoidal HDL and larger size particles corresponding in size to IDL/LDL (Figure 3.29 E). Based on the apoprotein composition observed in Figures 3.29 A-C, the spherical particles observed in panels 3.29 D,F represent apoA-I and to a lesser extend apoE containing HDL particles whereas the discoidal particles observed in Figure 3.29 E represent apoE-containing HDL. Electron microscopy of fractions 4 and 5 showed the presence of discoidal particles in both apoE3[K146N/R147W] and apoE3[K146N/R147W]-202 mutants, but only spherical particles in mice expressing WT apoE (Figure 3.29 G-I).

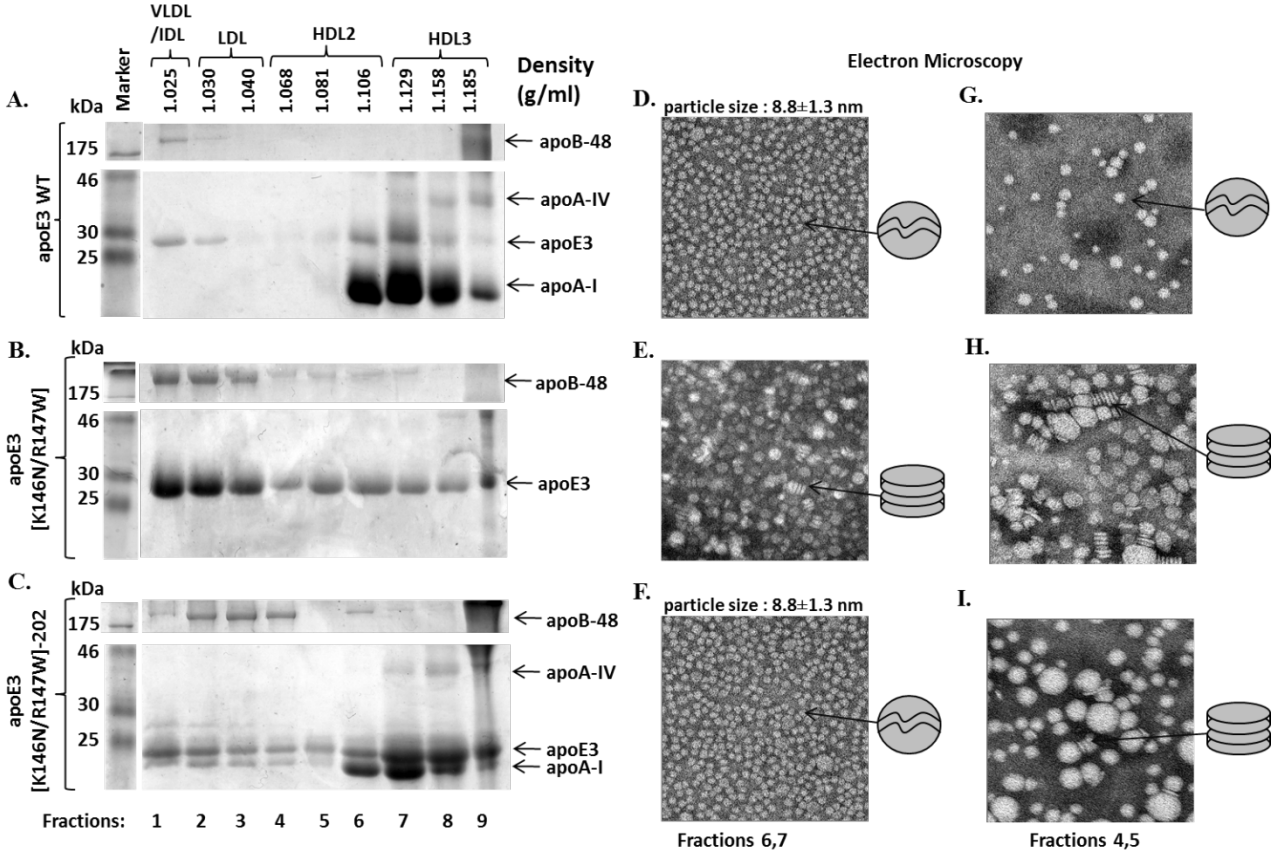

Figure 3.29 (A-I): Analysis of the plasma of apoE$^{-/-}$ mice infected with adenoviruses expressing the wild-type apoE3 (A), the full length apoE3[K146N/R147W] mutant (B) and the truncated apoE3[K146N/R147W]-202 mutant (C) by density gradient ultracentrifugation and SDS-PAGE of the

resulting fractions. EM analysis of HDL fractions 6-7 obtained from apoE$^{-/-}$ mice expressing the wild-type apoE3 (D), the full length apoE3[K146N/R147W] mutant (E) and the truncated apoE3[K146N/R147W]-202 mutant (F). The photomicrographs were taken at 75,000× magnification and enlarged 3 times. EM analysis of fractions 4-5 of the WT and the mutant apoE forms are also shown in panels G-I.

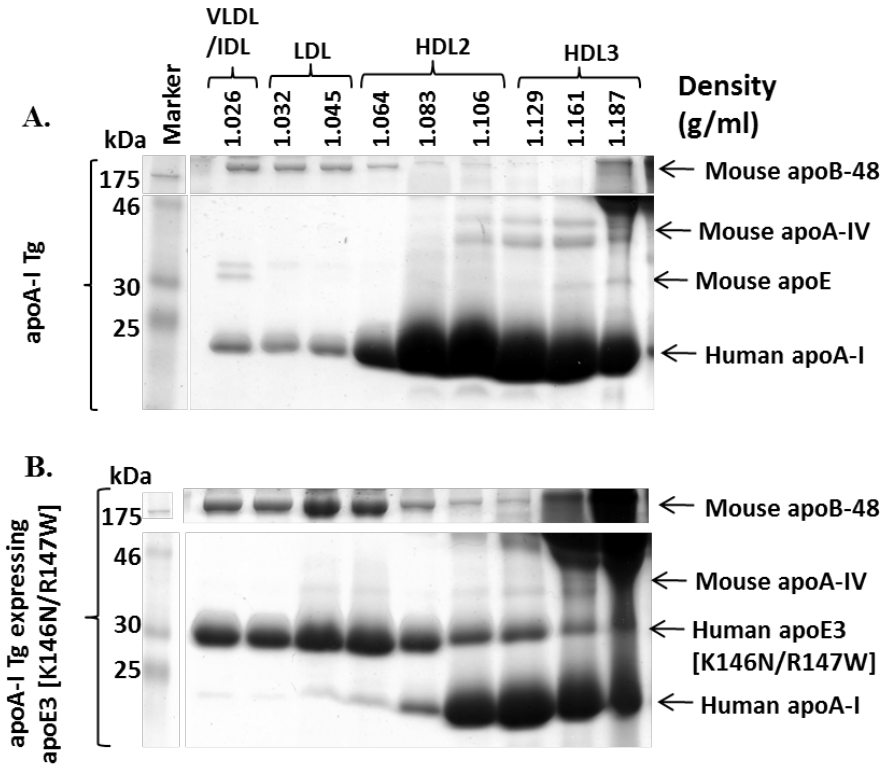

Figure 3.30 (A,B): Density gradient ultracentrifugation analysis of the plasma of apoA-I transgenic mice prior to (A) and four days post-infection (B) with adenoviruses expressing the full length apoE3[K146N/R147W] mutant.

Two dimensional gel electrophoresis of plasma followed by probing of the blots with human apoE antibody showed similar but not identical broad patterns of particles both for the wild-type apoE3 and the apoE3[K146N/R147W] mutant (Figure 3.31 A,B) whereas the truncated

apoE3[K146N/R147W]-202 mutant gave a more discrete set of particles (Figure 3.31 C). The relationship between the different particles was investigated by two dimensional gel electrophoresis of mixture of plasma obtained from mice expressing the apoE3[K146N/R147W]-202 mutant and either the wild-type apoE3 or the apoE3[K146N/R147W] mutant. The particles of the apoE3[K146N/R147W]-202 mutants were slightly shifted towards the cathode in relationship to the particles of the wild-type apoE3 (Figure 3.31 D) whereas the particles of the full length apoE3[K146N/R147W] and the truncated apoE3[K146N/R147W]-202 mutant merged (Figure 3.31 E).

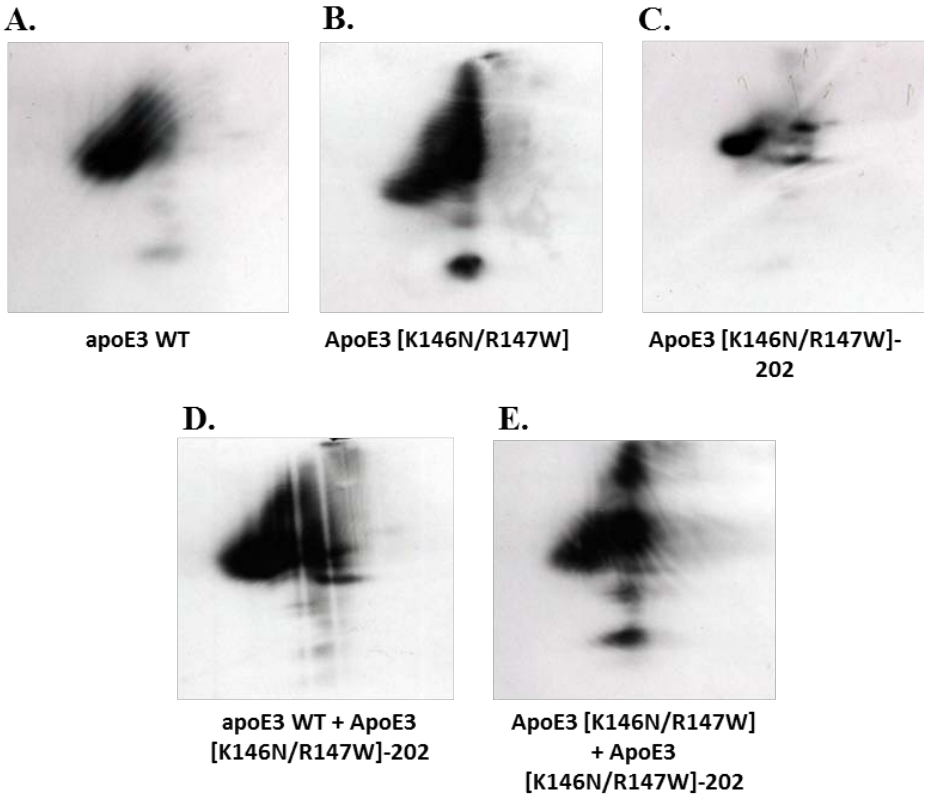

Figure 3.31 (A-E): Two dimensional gel electrophoresis of plasma of apoE$^{-/-}$ mice infected with adenoviruses expressing the wild-type apoE3 (a), the full length apoE3[K146N/R147W] mutant (B) and the truncated apoE3[K146N/R147W]-202 mutant (C). The relationship between the two dimensional patterns of the wild-type apoE3 and the apoE3[K146N/R147W]-202 mutant and the apoE3[K146N/R147W] and apoE3[K146N/R147W]-202 mutants were established by mixing experiments shown in panels D and F.

Assessment of the contribution of apoE in the formation of HDL in mice expressing the apoE3[K146N/R147W] mutant

The effects of the apoE3[K146N/R147W] mutations were also studied by gene transfer in apoA-I$^{-/-}$ x apoE$^{-/-}$ mice in order to obtain a clearer picture of the mechanism by which the apoE mutations affect HDL particle formation. This information could not be unambiguously obtained by the experiments described in Figure 3.29 A, C, D, F because the HDL fraction used for EM analysis contained both apoA-I and apoE.

The experiments showed that the patterns of clearance of plasma cholesterol and the induction (or lack of induction) of hypertriglyceridemia following gene transfer of the wild-type apoE3 and the full length and truncated apoE3[K146N/R147W] mutants in apoA-I$^{-/-}$ x apoE$^{-/-}$ mice was similar to that observed in the experiments involving apoE$^{-/-}$ mice shown in Figure 3.27 A-C. Specifically, we found that wild-type apoE3 cleared gradually cholesterol 1-4 days post infection, caused a moderate increase in plasma apoE levels and did not induce hypertriglyceridemia. The full length apoE3[K146N/R147W] mutant did not clear cholesterol and induced severe hypertriglyceridemia. The truncated apoE3[K146N/R147W]-202 mutant did not clear cholesterol, increased plasma apoE levels but also did not induce hypertriglyceridemia

(Figure 3.32 A-C). The difference between the wild-type and the truncated apoE forms was that the full length apoE3[K146N/R147W] mutant induced hypertriglyceridemia whereas the truncated apoE3[K146N/R147W]-202 did not (Figure 3.32 B).

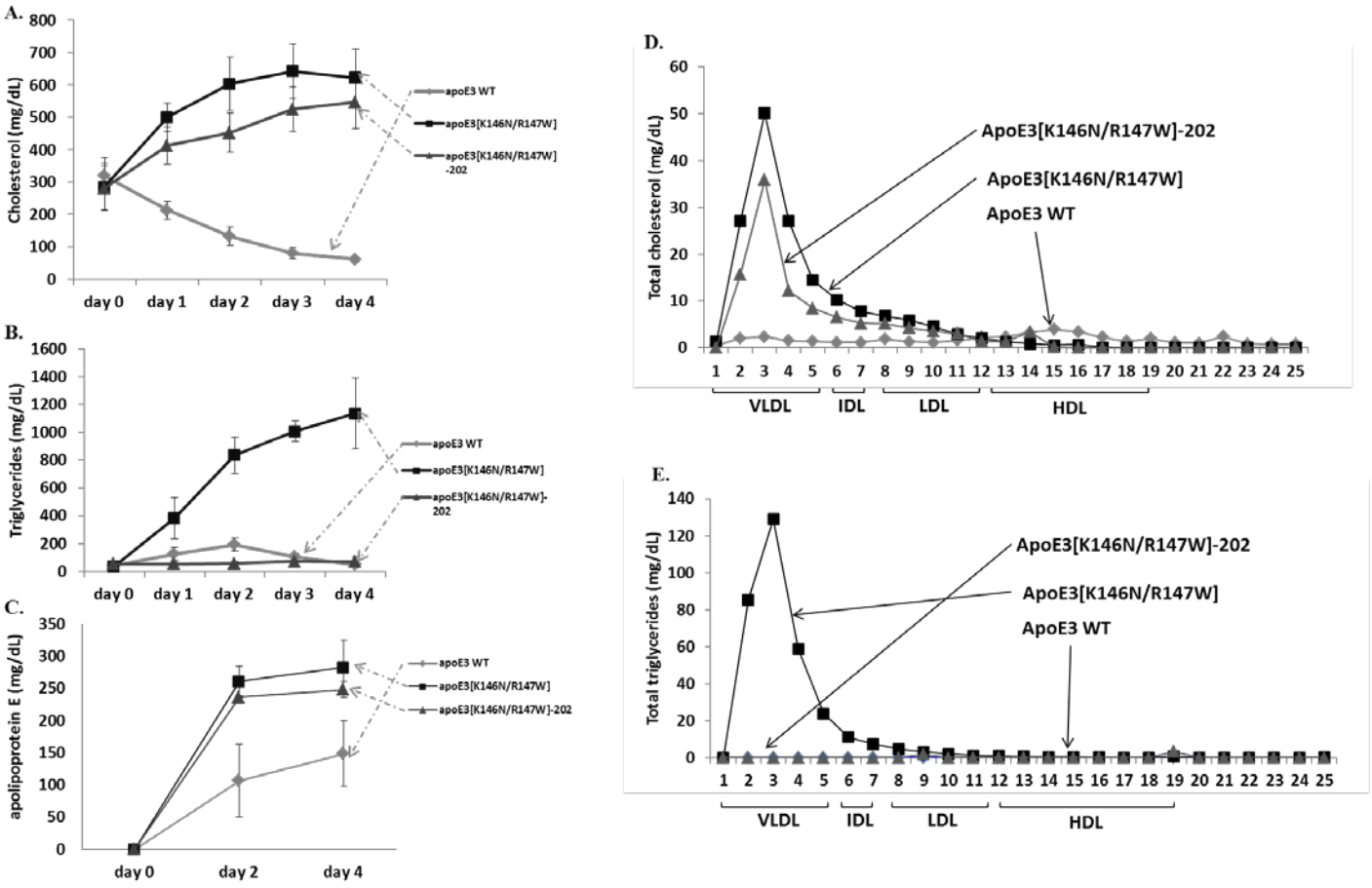

Figure 3.32 (A-E): Plasma cholesterol, triglycerides, apoE levels and FPLC profiles of apoA-I$^{-/-}$ x apoE$^{-/-}$ mice infected with recombinant adenoviruses expressing the wild-type apoE3, the full length apoE3[K146N/R147W] mutant and the truncated apoE3[K146N/R147W]-202 mutant as indicated. Plasma cholesterol (A), plasma triglycerides (B), plasma apoE (C), FPLC cholesterol (D) and FPLC triglycerides (E).

FPLC analysis of plasma from mice expressing the wild-type apoE3 showed the presence of a small cholesterol peak in the HDL region but also smaller amounts in all other lipoprotein fractions (Figure 3.32 D). In mice expressing the full length and the truncated apoE3[K146N/R147W] mutant the FPLC analysis of the plasma showed a cholesterol shoulder in the LDL/IDL region (Figure 3.32 D). The majority of the triglycerides in mice expressing the apoE3[K146N/R147W] mutant where found in the VLDL region and to a much lesser extend to the IDL and LDL region (Figure 3.32 E). The patterns of cholesterol distribution are compatible with the distribution of apoE following density ultracentrifugation of the plasma and analysis of the fractions by SDS-PAGE (compare Figure 3.32 D with Figures 3.33 A-C).

This latter analysis showed that in apoA-$I^{-/-}$ x $apoE^{-/-}$ expressing apoE3, the majority of apoE was in the HDL2/HDL3 fraction but a considerable portion was also found in the VLDL/IDL/LDL fraction (Figures 3.33 A). In mice expressing the apoE3[K146N/R147W] mutant, the great majority of apoE is shifted towards the VLDL/IDL/LDL region and smaller amount remained in the HDL region (Figures 3.33 B). A similar distribution in apoE was observed in apoA-$I^{-/-}$ x $apoE^{-/-}$ mice expressing the truncated apoE3[K146N/R147W]-202 mutant (Figures 3.33 C).

Electron microscopy of fractions 6 and 7 obtained by density ultracentrifugation of the plasma showed that wild-type apoE3 generated spherical particles and the full length and truncated apoE3[K146N/R147W] forms generated discoidal particles (Figures 3.33 D-F). Small amount of discoidal particles along with larger particles corresponding in size to LDL/IDL were also found in fractions 4 and 5 in mice expressing the full length and truncated apoE3[K146N/R147W] forms (data not shown). Since the double deficient mice do not contain

mouse apoE or apoA-I, the spherical and discoidal particles observed represent apoE-containing HDL.

The experiments described in Figures 3.33 E, F made it clear that the expression of both the full length and the truncated apoE3[K146N/R147W] form promoted the formation of discoidal apoE containing HDL particles whereas the WT apoE3 promoted the formation of spherical apoE containing HDL (Figures 3.33 D).

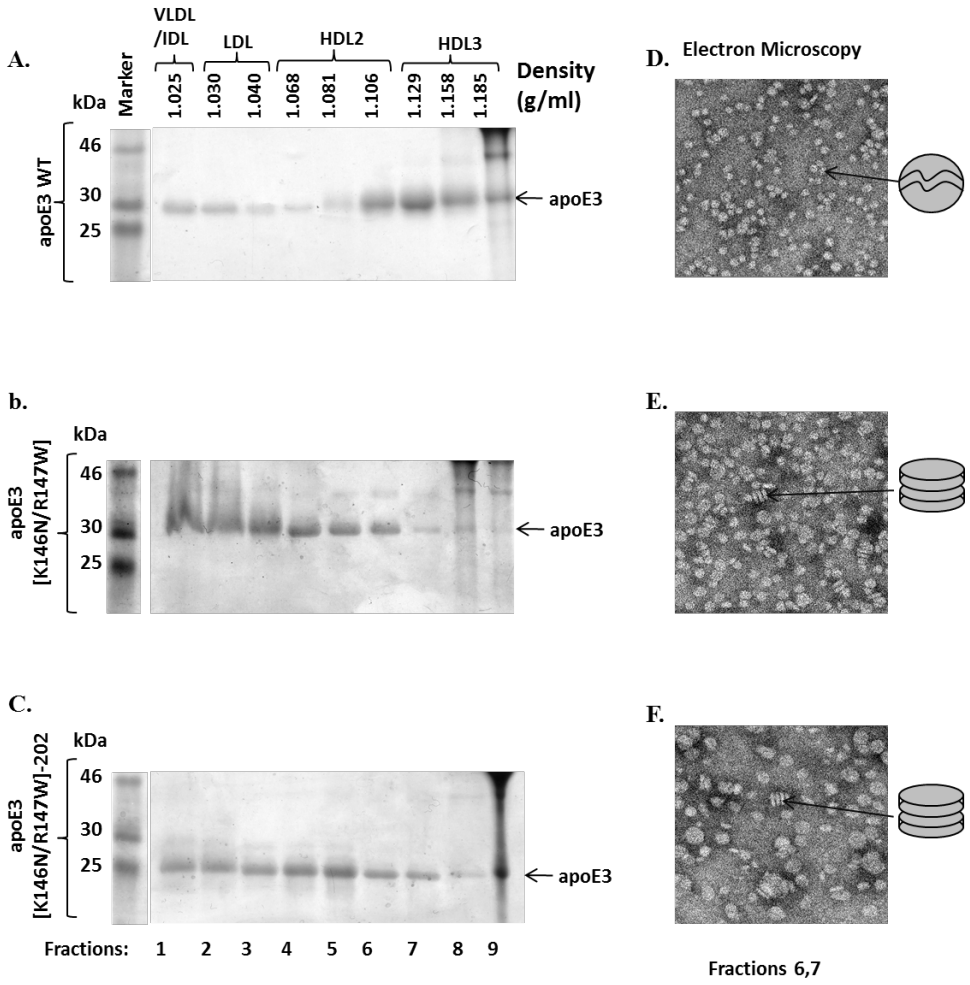

Figure 3.33 (A-F): Density gradient ultracentrifugation and SDS-PAGE analysis of plasma obtained from wild-type apoE3 (A), apoE3[K146N/R147W] (B) and apoE3[K146N/R147W]-202 (C), EM analysis of HDL

fractions 6-7 obtained by density gradient ultracentrifugation of plasma of wild-type apoE3 (D), apoE3[K146N/R147W] (E) and apoE3[K146N/R147W]-202 (F).

The role of LCAT and LPL in the induction of dyslipidemia in mice expressing the apoE3[K146N/R147W]

The accumulation of triglycerides and apoE in apoE$^{-/-}$ mice that received the adenovirus expressing apoE3[K146N/R147W] (Figure 3.27 A-C) indicated that the endogenous lipoprotein lipase was insufficient to hydrolyze the triglycerides of VLDL. For this reason, we used co-expression experiments in apoE$^{-/-}$ mice to assess the ability of increased LPL levels to correct the hypertriglyceridemia and the HDL abnormalities caused by the apoE3[K146N/R147W] mutant.

Co-infection of apoE$^{-/-}$ mice with 7x10^{8} pfu of adenovirus expressing apoE3[K146N/R147W] and 5x10^{8} pfu of adenovirus expressing human LPL, gradually increased the plasma cholesterol levels 2-4 days post-infection. The increase in plasma cholesterol was not statistically different to that observed following infection of apoE$^{-/-}$ mice with adenovirus expressing apoE3[K146N/R147W] alone (Figure 3.34 A). Importantly, co-infection with the two viruses caused only a moderate increase of plasma triglycerides 3 to 4 days post-infection (Figure 3.34 B). Furthermore, the LPL overexpression increased slightly the plasma apoE levels 2-4 days post infection (Figure 3.34 C). FPLC analysis of plasma from mice expressing the apoE3[K146N/R147W] mutant and LPL showed the presence of a small HDL cholesterol peak along with a large shoulder in the LDL/IDL region (Figure 3.34 D). Residual triglycerides were distributed in the VLDL region (Figure 3.34 E).

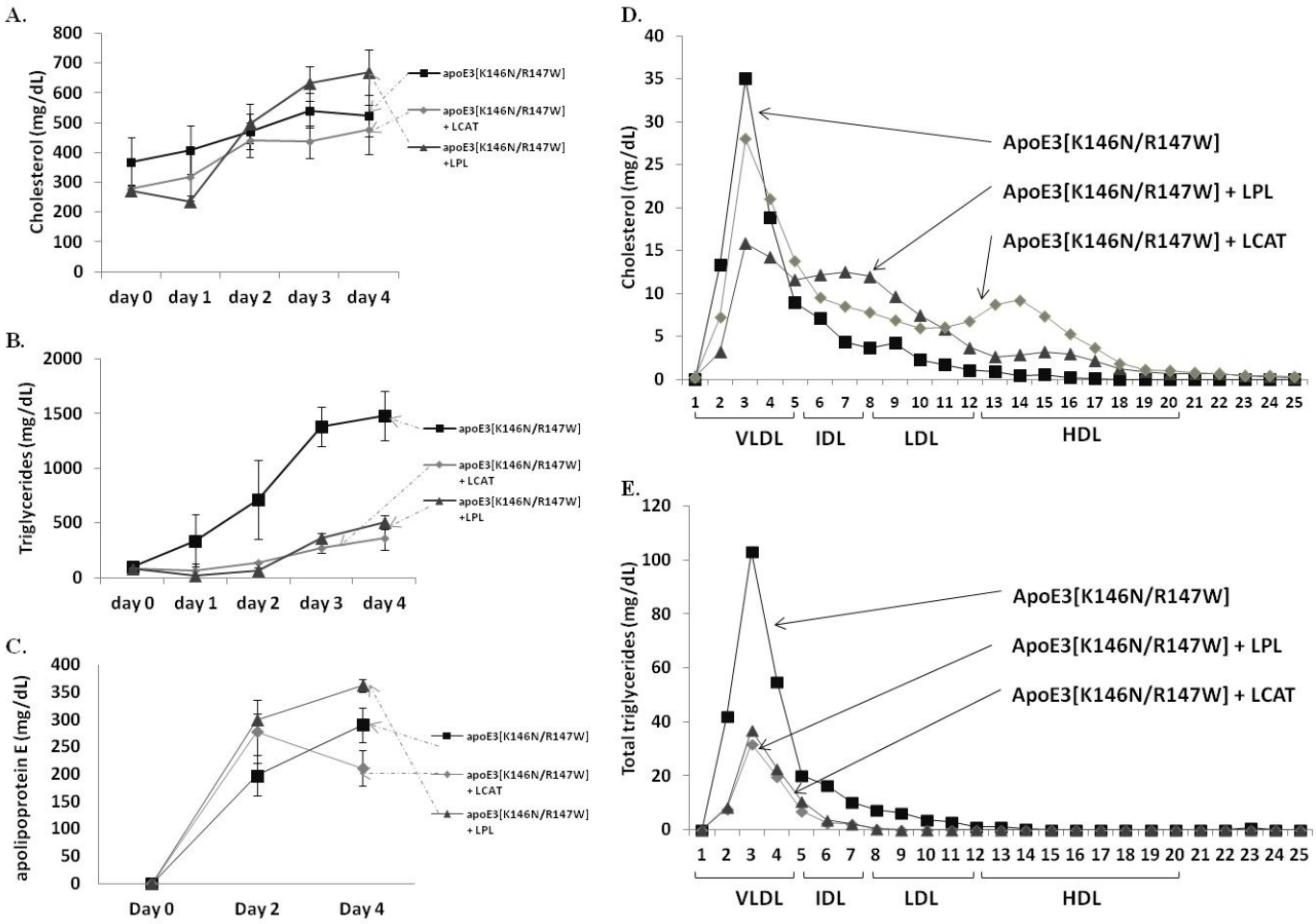

Figure 3.34 (A-E): Plasma cholesterol, triglycerides, apoE levels and FPLC profiles of apoE$^{-/-}$ mice infected with recombinant adenoviruses expressing the full length apoE3[K146N/R147W] alone or in combination with LCAT or LPL as indicated. Plasma cholesterol (A), plasma triglycerides (B), plasma apoE (C), FPLC cholesterol profiles (D) and FPLC triglycerides profile (E) of plasma of apoE$^{-/-}$ mice infected with the indicated adenoviruses. The doses of the adenoviruses used were 7x10*8 pfu for the apoE3[K146N/R147W] mutant and 5x10*8 pfu for LCAT and LPL. Parameters reported mean ± standard deviation.

Density gradient ultracentrifugation of the plasma also supported the increase in plasma apoE and showed that apoE was distributed primarily in the HDL2/HDL3 region (Figure 3.35 A). The increased apoE levels in the HDL region were associated with the loss of plasma apoA-I that otherwise floats in the same region (compare figures 3.29 B and 3.35 A). Electron Microscopy of HDL corresponding to fractions 6 and 7 of Figure 3.35 A showed the presence of predominantly discoidal particles (Figure 3.35 B), indicating that correction of hypertriglyceridemia did not correct the defective maturation of HDL. Few discoidal particles along with larger size particles corresponding in size to LDL/IDL particles were also observed in fractions 4 and 5 (Figure 3.35 C). The persistence of discoidal HDL particles following LPL treatment is consistent with the observed decrease of the CE/TC ratio in plasma (Table 3.VIII B).

The presence of discoidal particles (Figure 3.29 E) and the decrease of the CE/TC ratio in the plasma of apoE$^{-/-}$ mice expressing the apoE3[K146N/R147W] mutant (Table 3. VIII B) suggested inability of LCAT to esterify the cholesterol of HDL and possible other lipoproteins. This prompted us to assess whether the apoE3[K146N/R147W] mutant induced dyslipidemia could be corrected by co-infection of apoE$^{-/-}$ mice with a mixture of adenoviruses expressing apoE3[K146N/R147W] and human LCAT. The experiments showed that the LCAT treatment gradually increased the plasma cholesterol levels 2-4 days post-infection and caused only a moderate increase of plasma triglycerides 3 to 4 days post-infection (Figure 3.34 A,B). The increase in plasma cholesterol was not statistically different to that observed by treatment of apoE$^{-/-}$ mice with adenovirus expressing apoE3[K146N/R147W] mutant alone or in the presence of LPL. Furthermore, the LCAT overexpression increased plasma apoE 2-4 days post infection to levels that were slightly lower to those observed in apoE$^{-/-}$ mice treated with apoE3[K146N/R147W] alone (Figure 3.34 C). The increase in plasma apoE levels are also

supported by density gradient ultracentrifugation of the plasma and SDS-PAGE analysis of the resulting fractions as described below. FPLC analysis from plasma of mice expressing the apoE[K146N/R147W] mutant and LCAT showed the presence of a large HDL cholesterol peak along with a shoulder extended in the LDL/IDL region (Figure 3.34 D). Residual triglycerides were distributed in the VLDL region (Figure 3.34 E).

Density gradient ultracentrifugation of the plasma and SDS-PAGE analysis of the resulting fractions showed that the LCAT treatment shifted apoE to the VLDL/IDL/LDL region and restored apoA-I in the HDL region (Figure 3.35 D). Electron microscopy of the HDL fractions 6 and 7 of Figure 3.35 D showed that apoE$^{-/-}$ mice infected with adenovirus expressing apoE3[K146N/R147W] and LCAT formed spherical particles (Figure 3.35 E). Formation of spherical particle is consistent with the normalization of the CE/TC ratio of plasma and the reappearance of apoA-I in the HDL region following LCAT treatment (Figure 3.35 D) (Table 3.VIII B).

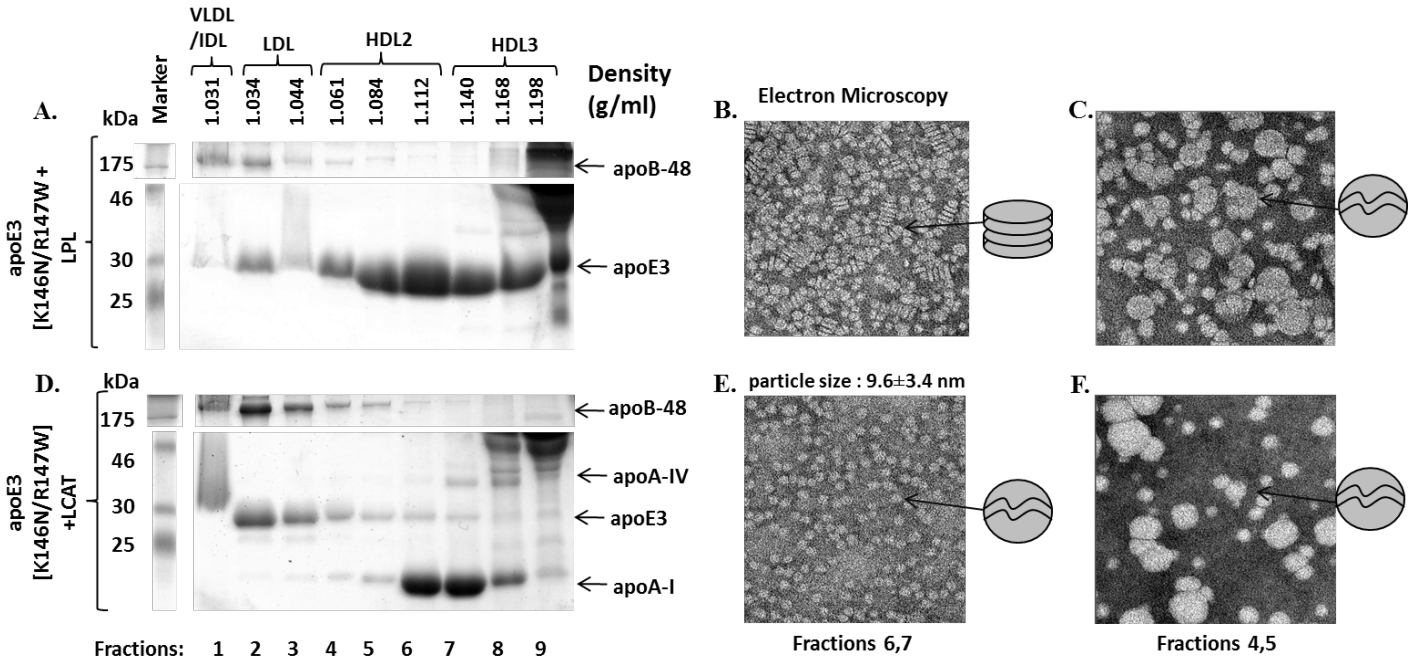

Figure 3.35 (A-F): Analysis of the plasma of apoE$^{-/-}$ mice infected with adenoviruses expressing the full length apoE3[K146N/R147W] in combination with LPL (A) or LCAT (D) as indicated by density gradient ultracentrifugation and SDS-PAGE of the resulting fractions. EM analysis of HDL fractions 6-7 obtained from apoE$^{-/-}$ mice expressing the full length apoE3[K146N/R147W] in combination with LPL (B) or LCAT (E). The photomicrographs were taken at 75,000× magnification and enlarged 3 times. EM analysis of fractions 4-5 of the apoE3[K146N/R147W] in combination with LPL or LCAT are shown in panels C, F.

Large scale production of WT apoE3 and the apoE3 mutants

The WT apoE3 and the apoE3 mutant proteins were produced in large scale in HTB-13 cells in order to be used in the future for ABCA1-mediated efflux and LCAT activation functional assays, as well as for physicochemical analyses. The method was similar to that described in section 3.3.8 for the apoA-I mutants. In Figure 3.36 is shown an example of apoE3[K146N/R147W] after harvesting the medium and after the lyophilisation of the medium.

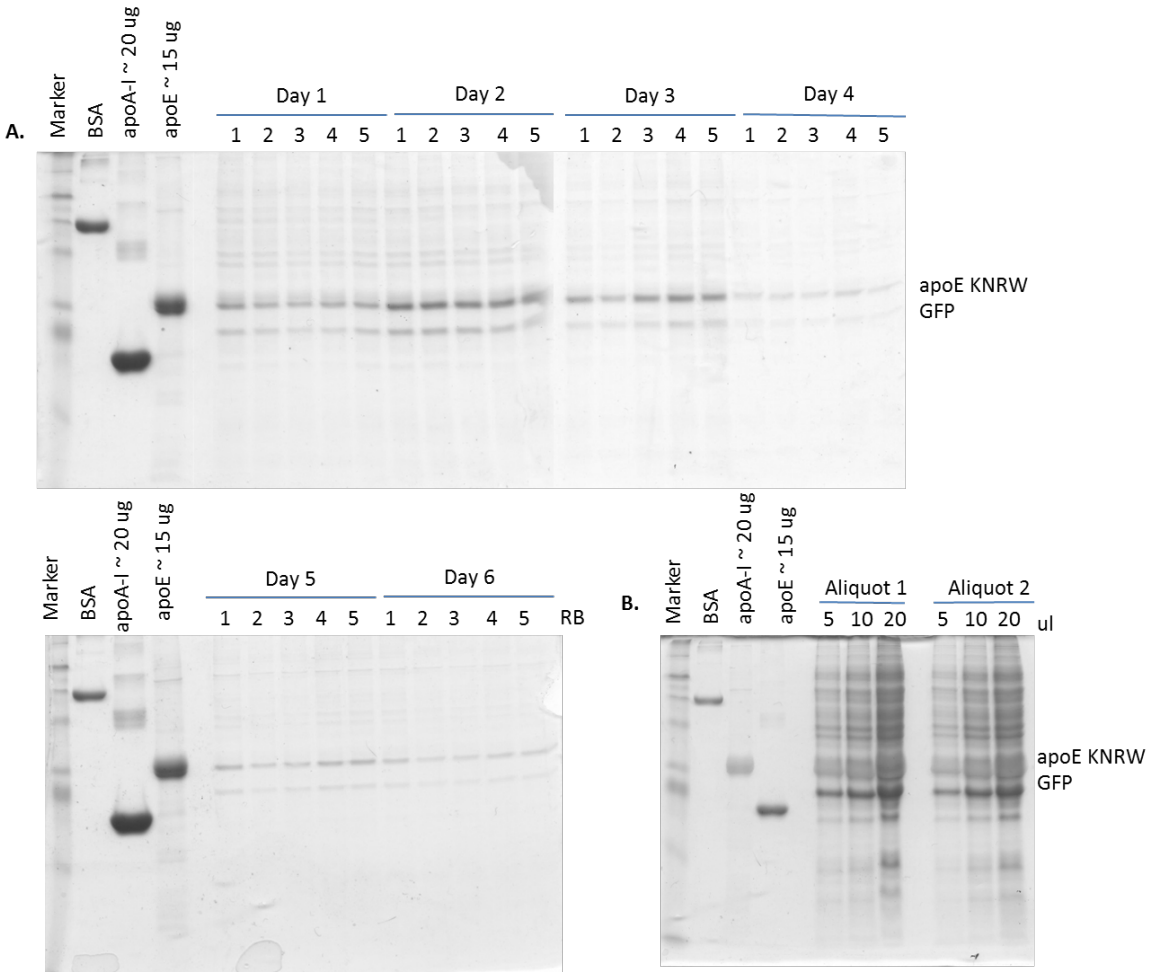

Figure 3.36: Analysis of production of apoE3[K146N/R147W] **by SDS PAGE.** SDS PAGE analysis of apoE3[K146N/R147W] secreted into the culture medium of HTB-13 cells infected with an adenovirus expressing apoE3[K146N/R147W] (A). SDS PAGE analysis of apoE3[K146N/R147W] after the lyophilisation of the medium and the resuspension in 0.001% EDTS into two aliquots of 30 ml each (B). The cells were grown in roller bottles as described in experimental procedures and serum free medium was collected on days 1-6 post infection. The position of the apoE and the molecular markers are indicated.

DISCUSSION

Molecular etiology of a dominant form of type III hyperlipoproteinemia caused by the natural apoE3[K146N/R147W] mutations

A variety of rare apoE mutations between residues 136-147 have been described in humans that are associated with dominant inheritance of type III hyperlipoproteinemia (type III HLP) that is manifested at an early age (238).

The importance of the 136-152 region of apoE for binding to the LDL receptor was assessed by *in vitro* mutagenesis (250-252). It has been recognized that the binding affinity of reconstituted HDL containing these apoE mutants for the LDL receptor determined in vitro did not always correlate with the severity of the dyslipidemia observed in vivo. Thus it was suggested that the occurrence of the disease can be influenced by other secondary factors including the apoE phenotype or the affinity of the specific mutants for heparan sulfate proteoglycans (238;251-254;257;564).

The apoE3[K146N/R147W] variant studied here was initially designated apoE1-Hammersmith (561). This apoE variant contains two additional negative charges as compared to apoE3 due to substitution of two positively charged residues by neutral residues. Two family members heterozygous for the apoE1 allele exhibited the clinical markers of type III HLP at very early age, including tubero-eruptive xanthomas, high plasma cholesterol and triglyceride levels and the appearance of a broad β band following electrophoresis of plasma (561).

Lipid and lipoprotein phenotype of apoE$^{-/-}$ mice expressing the apoE3[K146N/R147W] mutant. Initially we used adenovirus mediated gene transfer in apoE$^{-/-}$ mice to study the lipid and lipoprotein phenotype that results from the expression of the apoE3[K146N/R147W] mutant. The advantage of the adenovirus system is that when the mutant protein is expressed in apoE$^{-/-}$ mice, it creates within a few days the phenotype expected of subjects with homozygous defect in the corresponding ε allele. Human subjects or experimental animals homozygous for the apoE3[K146N/R147W] mutations have not been studied previously. The phenotype that was generated following the gene transfer is characterized by severe hypercholesterolemia and hypertriglyceridemia, reduced CE/TC ratio in plasma, formation of discoidal apoE-containing HDL, very high plasma apoE levels and accumulation of apoE in the VLDL/IDL/LDL region. It is expected that a similar phenotype in humans homozygous for the mutations will have severe clinical consequences that may lead to cardiovascular disease. Abnormal lipid and lipoprotein phenotypes have been observed in mice as a result of overexpression of the endogenous mouse apoE (565). Thus the observed dyslipidemia in this study cannot be attributed to abnormal interactions of the human apoE with the mouse apolipoproteins.

Potential etiology of the apoE3[K146N/R147W]-induced hypertriglyceridemia. The accumulation of apoE in the VLDL/IDL/LDL region appears to create insufficiency for both lipoprotein lipase and LCAT activity. As reported previously (260;261) the insufficiency of lipoprotein lipase appears to result from inhibition of this enzyme by the apoE which accumulates in VLDL/IDL/LDL size lipoprotein particles. The lipoprotein lipase treatment corrected the hypertriglyceridemia but did not affect the hypercholesterolemia or the plasma

CE/TC ratio and did not reverse the formation of discoidal HDL particles. The increased levels of lipoprotein lipase in the circulation following gene transfer could in principle promote lipoprotein clearance both by increasing the rate of lipolysis and exposing the receptor-binding domain of apoE, as well as by direct receptor-mediated clearance mechanisms involving LPL (566;567). Other studies have suggested that excess of secreted apoE may partially displace the lipoprotein lipase and/or apoCII and thus reduce the rate of lipoprotein triglyceride lipolysis (259). The ability of excess lipoprotein lipase to correct the hypertriglyceridemia induced by apoE3[K146N/R147W], observed in this study, suggests that the activity of lipoprotein lipase rather than apoCII may be rate-limiting for the clearance of VLDL/IDL/LDL triglycerides. Consistently with our finding a previous study also showed that defective recognition of apoE-containing lipoproteins, either due to mutations in apoE or deficiency in the LDL receptor, may increase the sensitivity and severity of hypertriglyceridemia (231). The same study also showed that the LDL receptor alone can account for the clearance of apoE-containing lipoprotein remnants in mice, and that the contribution of the other members of the LDL-receptor family and heparan sulfate proteoglycans (HSPGs) may be limited (231).

Potential etiology of the apoE3[K146N/R147W]-induced defective maturation of HDL that results in the accumulation of discoidal HDL particles in plasma. A common property of the full length as well as of the truncated apoE3[K146N/R147W]-202 mutant is that they inhibited the esterification of the cholesterol as evidenced by the decrease of the CE/TC ratio of plasma and promoted the formation of discoidal HDL particles. The LCAT treatment corrected the hypertriglyceridemia, normalized the plasma CE/TC ratio, restored the apoA-I in

the HDL fractions and generated spherical HDL particles, but did not correct the hypercholesterolemia. The insufficiency in LCAT may be the result of fast catabolism of LCAT bound to discoidal HDL particles that are formed in the plasma of mice expressing apoE3[K146N/R147W] by the kidney. Accelerated catabolism of discoidal particles and reduction in LCAT activity has been observed in subjects with apoA-I mutations (215;217).

It is unclear whether the defective maturation of discoidal into spherical particles is a direct consequence of the K146N/R147W mutation and its impact on the maturation of HDL or is the result of the increased plasma apoE levels that may affect LCAT activity. Accumulation of discoidal HDL particles was observed previously in apoA-I mutants (220).

Deletion of the C terminal residues 293-299 of apoE3[K146N/R147W] prevented induction of hypertriglyceridemia but exacerbated the hypercholesterolemia. Previous studies showed that proteoliposomes containing truncated apoE-184 or apoE-191 that lack the C-terminal apoE region can bind to the LDL receptor (250). The combined data established that the amino terminal 1 to 202 or 1 to 184 domain of apoE is an efficient ligand for the LDL receptor (12;250;563).

ApoE contains an N-terminal and a C-terminal domain which fold independently (568). It has been proposed that apoE inter-domain interactions affect the structure of apoE isoforms (241;569;570), their different affinity for VLDL (244;569;570) as well as the contribution of apoE4 in Alzheimer's disease (571).

In the present study, the truncated apoE3[K146N/R147W]-202 mutant prevented the induction of hypertriglyceridemia in apoE$^{-/-}$ or apoA-I$^{-/-}$ x apoE$^{-/-}$ mice. This finding is consistent with previous studies involving other truncated apoE forms, including the truncated form of apoE4[R142C] that is also associated with a dominant form of type III HPL (563).

Potential mechanism of hypercholesterolemia induced by the full length and the truncated apoE3[K146N/R147W] mutant. ApoE3[K146N/R147W] induced an increase in plasma cholesterol levels in apoE$^{-/-}$ or apoA-I$^{-/-}$ x apoE$^{-/-}$mice could be the result of altered recognition of the receptor binding domain of the mutant protein by the LDL receptor. Alternatively it could be the result of unfavorable interactions between the N- and C-terminal domains that shield the receptor binding domain of apoE as suggested previously (264), or a combination of both factors. It has been proposed that apoE inter-domain interactions may be at least partially responsible for the subtle differences in the structural and the functional properties of different apoE isoforms (241;244;569-571). These two possibilities were tested by adenovirus gene transfer experiments using the truncated apoE[K146N/R147W]-202 form that extend from residue 1 to 202. The expectation was that if the cholesterol clearance defect was the result of unfavorable N and C-terminal domain interactions that shield the receptor binding domain then deletion of the C-terminal domain would be expected to correct the cholesterol clearance defect.

The present study showed that similar to the full length apoE3[K146N/R147W] mutant protein, high levels of expression of the truncated apoE3[K146N/R147W]-202 form increased further the high cholesterol levels of apoE$^{-/-}$ mice despite the fact that it did not induce

hypertriglyceridemia. This property of the truncated apoE3[K146N/R147W]-202 differentiated this mutant from all previously studied truncated apoE forms which cleared cholesterol without induction of hypertriglyceridemia (263;534;563). These findings indicate that the amino terminal 1 to 202 domain of the mutant protein does not inhibit lipolysis but is not capable of clearing the high cholesterol levels of the apoE$^{-/-}$ mice.

The fact that gene transfer of the full length apoE3[K146N/R147W] and the truncated apoE3[K146N/R147W]-202 form increased the plasma cholesterol levels of the apoE$^{-/-}$ or apoA-I$^{-/-}$ x apoE$^{-/-}$ mice, indicates that both proteins act as dominant negative ligands that prevent receptor-mediated remnant clearance. The fact that the defective clearance of lipoprotein remnants persists following treatment with LPL or LCAT indicates that the apoE mutations are the primary cause of the dyslipidemia and the insufficiently of LPL and LCAT.

Taken together with previous studies (263;534;563), our data indicate that the dyslipidemia induced by the apoE3[K146N/R147W] in mice and possibly human patients carrying these mutations most likely is brought about due to the ability of this mutant to act as a dominant negative ligand that upon binding blocks the LDL receptor and prevents the catabolism of triglyceride rich apoE-containing lipoprotein particles. The accumulation of apoE in VLDL/LDL/IDL appears to inhibit the functions of lipoprotein lipase and causes hypertriglyceridemia. It also inhibits the functions of LCAT and causes accumulation of discoidal HDL particles in plasma. The hypertriglyceridemia can be corrected by co-expression of apoE3[K146N/R147W] with LPL or LCAT. However, the HDL maturation defect which is demonstrated by the accumulation of discoidal particles persists following LPL treatment and can only be corrected by excess LCAT.

In addition to its functions in remnant clearance and the biogenesis of HDL (17;231;238), lipid free or lipoprotein associated apoE has been reported to affect various other biological processes, including smooth muscle cell (SMC) migration and proliferation, neointima hyperplasia, inflammation, diet-induced obesity and hyperinsulinemia, endoplasmic reticulum stress leading to apoptosis and glucose tolerance (572-579). Inhibition of SMC migration requires binding of apoE to the LRP1 that leads to cyclic AMP accumulation and activation of protein kinase A (578;580). ApoE peptides 141-145 or receptor blocking monoclonal antibodies prevented inhibition of SMC migration (578).

Other studies showed that endothelial cell derived apoE stimulates endothelial nitric oxide synthase (eNOS) through interactions of lipid free or lipid bound apoE with apoE receptor-2 (apoER2) (581;582).

The inhibition of SMC proliferation requires binding of apoE to proteoglycans that led to activation of inducible nitric oxide synthase (iNOS) (578;580;583). ApoE is also required for development of neointima hyperplasia (584) and its binding to the denuded artery inhibits hyperplasia by activating iNOS and thus affecting cell migration and proliferation (572-577).

Furthermore, lipid free apoE suppresses inflammatory responses in macrophages by inhibiting activation of TLR4 and TLR3 in response to extracellular agonists through mechanisms that involve LRP1 and heparin sulfate proteoglycans binding respectively that leads to the suppression of JNK and c-Jun activation (585).

Given that several apoE mediated signaling pathways involve interactions of apoE with its receptors, it is possible that the severe proatherogenic phenotype generated by the

apoE3[K146N/R147W] mutant may result partially from aberrant signaling mechanism following binding of this mutant to different apoE receptors. Future studies are required to address this question.

Chapter VI. Synergy of apoA-IV and LCAT on the biogenesis of apoA-IV containing HDL

RESULTS

We have described recently a novel function of apoA-IV in the biogenesis of discrete HDL-A-IV particles with the participation of ABCA1 and LCAT (16). In this study we employed adenovirus-mediated gene transfer of human apoA-IV in different mouse models, such as apoA-$I^{-/-}$, apoA-$I^{-/-}$ x $apoE^{-/-}$, $ABCA1^{-/-}$ and $LCAT^{-/-}$ mice to investigate the role of apoA-IV in the biogenesis of apoA-IV containing HDL. Adenovirus-mediated gene transfer of apoA-IV in apoA-$I^{-/-}$ mice did not change significantly plasma lipid levels as compared to the GFP-expressing apoA-$I^{-/-}$ mice. ApoA-IV floated in the HDL2/HDL3 region, promoted the formation of spherical HDL particles as determined by electron microscopy and generated mostly α- and few preβ-like HDL subpopulations (16). Gene transfer of apoA-IV in apoA-$I^{-/-}$ x $apoE^{-/-}$ mice increased plasma cholesterol and triglyceride levels and 80% of the protein was distributed in the VLDL/IDL/LDL region. This treatment likewise generated α- and preβ-like HDL subpopulations. Spherical and α-migrating HDL particles were not detectable following gene transfer of apoA-IV in $ABCA1^{-/-}$ mice (16).

My contribution to this work has been the determination of the FPLC cholesterol profiles of apoA-$I^{-/-}$ and apoA-$I^{-/-}$ x $apoE^{-/-}$ mice expressing the human apoA-IV, study of the biogenesis of apoA-IV containing HDL in $LCAT^{-/-}$ mice and study of the effect of co-expression of LCAT and apoA-IV on the biogenesis of apoA-I-containing HDL in apoA-$I^{-/-}$ mice. The experiments perforemd are described below.

FPLC analysis of the distribution of the cholesterol and triglycerides in apoA-$I^{-/-}$ mice expressing the human apoA-IV showed the presence of a very small HDL cholesterol peak in the

HDL region and no triglyceride peak (Figure 3.37 A,B). In contrast, in apoA-I$^{-/-}$ x apoE$^{-/-}$ mice expressing apoA-IV, FPLC analysis showed that all the cholesterol and triglycerides were found in the VLDL/IDL region (Figure 3.37 A,B).

To determine the role of LCAT in the biogenesis of HDL-A-IV, I used adenovirus-mediated gene transfer of apoA-IV in LCAT$^{-/-}$ mice. It was found that similarly to ABCA1$^{-/-}$ mice, expression of apoA-IV in LCAT$^{-/-}$ mice failed to form HDL particles as determined by density gradient ultracentrifugation of the plasma and EM analysis of the HDL fractions (Figure 3.38 A,B). Two-dimensional gel electrophoresis of the plasma showed the formation of two particles with preβ-like mobility (Figure 3.38 C). The relationship of these particles with α-HDL particles formed in apoA-I$^{-/-}$ mice expressing apoA-IV was established by mixing experiments (Figure 3.38 D).

The role of LCAT in the biogenesis of apoA-IV containing HDL was also explored by co-expression of apoA-IV and LCAT in apoA-I$^{-/-}$ mice. This treatment increased the plasma HDL cholesterol levels as determined by FPLC (Figure 3.39 A). It also promoted the flotation of apoA-IV in the HDL2 and HDL3 region (Figure 3.39 B) and generated spherical HDL-A-IV particles (Figure 3.39 C). The LCAT treatment also increased the concentration of the mouse apoE in the HDL2 fraction (Figure 3.39 B). These experiments showed that the co-expression of apoA-IV and LCAT in apoA-I$^{-/-}$ mice restored the formation of HDL-A-IV.

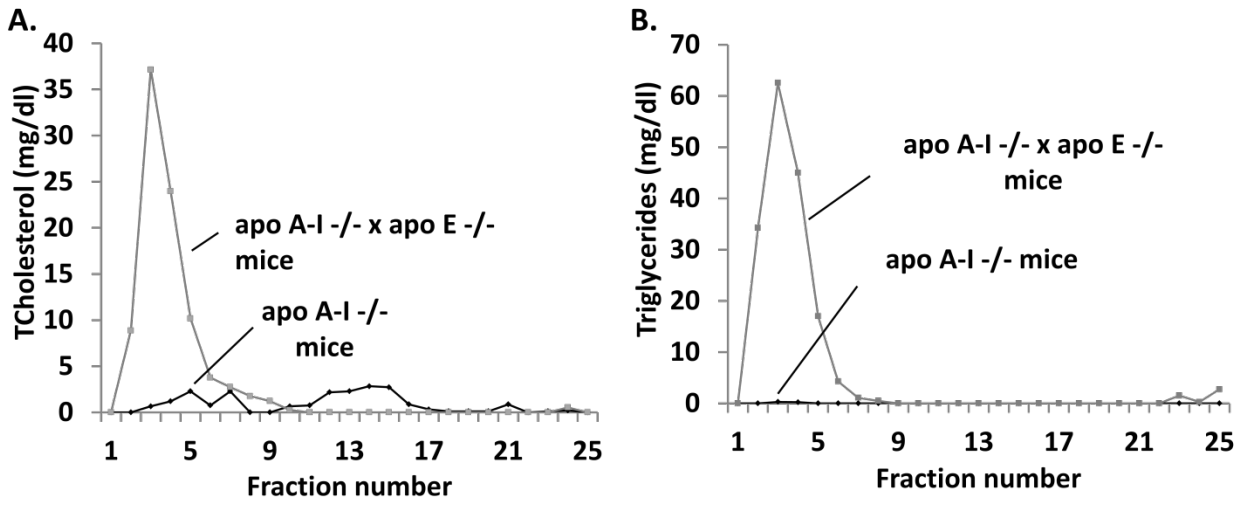

Figure 3.37 (A,B): Plasma FPLC cholesterol (A) and triglyceride (B) profiles of apoA-I$^{-/-}$ and apoA-I$^{-/-}$ x apoE$^{-/-}$ mice expressing the human apoA-IV as indicated.

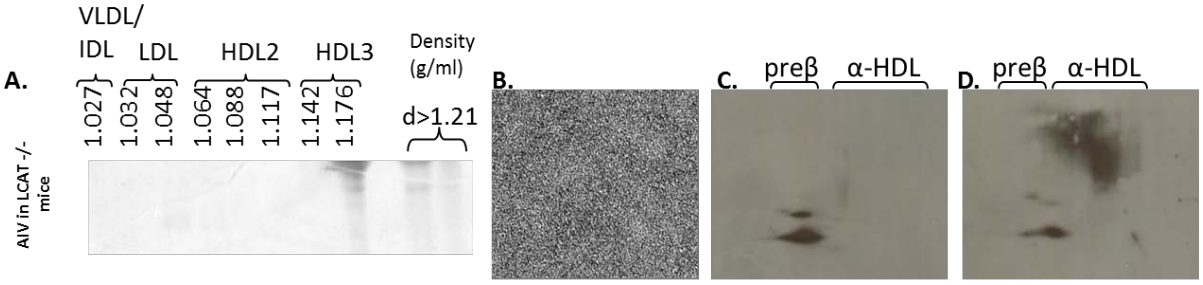

Figure 3.38 (A-D): Analysis of plasma of LCAT$^{-/-}$ mice infected with adenoviruses expressing the human apoA-IV by density gradient ultracentrifugation and SDS-PAGE (A). EM analysis of HDL fractions 6-7 obtained from LCAT$^{-/-}$ mice expressing the human apoA-IV (B) following density gradient ultracentrifugation of plasma as indicated. The photomicrographs were taken at 75,000× magnification and enlarged 3 times. Two dimensional gel electrophoresis of plasma of LCAT$^{-/-}$ mice expressing the human apoA-IV (C). The relative electrophoretic migration of the particles in panel C with α-HDL particles formed in apoA-I$^{-/-}$ mice expressing apoA-IV was established by mixing experiments (D).

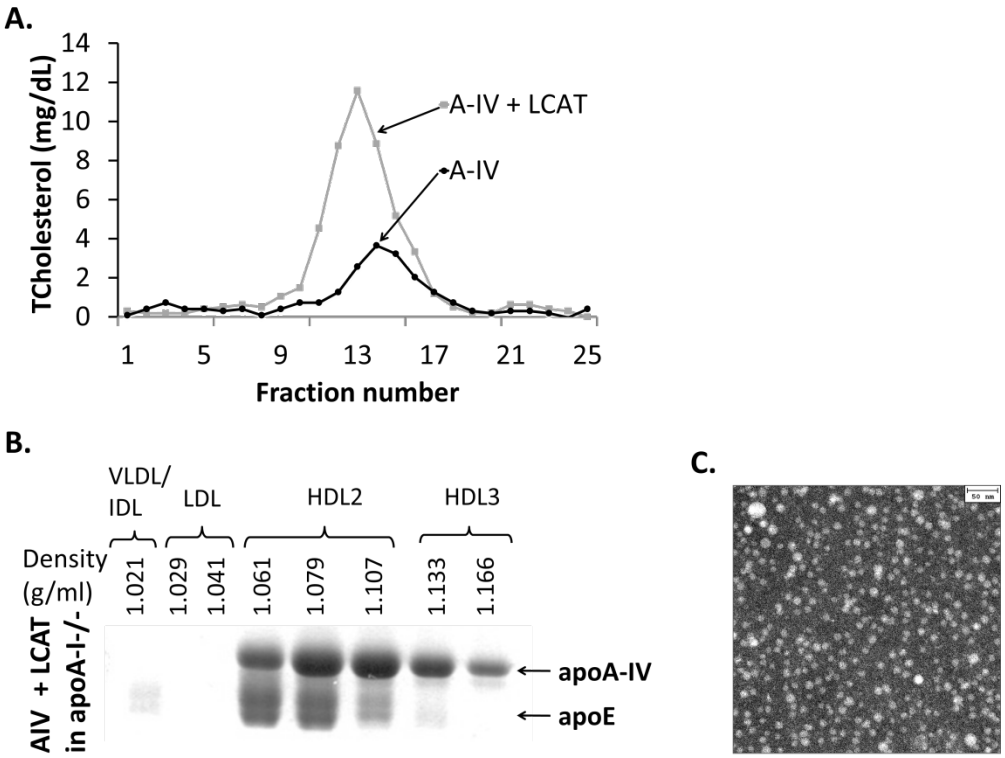

Figure 3.39 (A-C): FPLC cholesterol profiles of apoA-I$^{-/-}$ mice expressing the human apoA-IV alone or in combination with the human LCAT (A). Analysis of plasma of apoA-I$^{-/-}$ mice infected with adenoviruses expressing the human apoA-IV along with the human LCAT by density gradient ultracentrifugation and SDS-PAGE (B). EM analysis of HDL fractions 6-7 obtained from apoA-I$^{-/-}$ mice expressing the human apoA-IV along with the human LCAT (C) following density gradient ultracentrifugation of plasma as indicated. The photomicrographs were taken at 75,000× magnification and enlarged 3 times.

DISCUSSION

Role of apoA-IV, ABCA1, and LCAT in the biogenesis of HDL-A-IV. Although the functions of the intestinally delivered apoA-IV have been extensively studied during the past 35 years there is limited information on the physiological significance and the functions of apoA-IV synthesized by the liver. Earlier studies showed that when apoA-IV is purified from plasma by

immunoprecipitation, immunoaffinity, gel filtration or non-denaturing gradient gel electrophoresis, it is found on the HDL density fraction (586-588) but it dissociates from lipoproteins following ultracentrifugation of plasma (589). This raises the question whether apoA-IV containing HDL particles originate from the transfer of apoA-IV, that is displaced from chylomicrons, to the surface of a preformed HDL molecule that contains apoA-I and in some instances other apolipoproteins. An alternative possibility is that HDL-A-IV particles are synthesized *de novo* by the liver.

Clues pertinent to this question were obtained from studies of transgenic mice expressing the apoA-IV gene under the control of its natural promoter or a heterologous hepatic promoter (590-592). Transgenic mice carrying the apoA-IV gene under the control of the common apoA-I/apoCIII/apoA-IV promoter and enhancer (593) express apoA-IV predominantly in the intestine and to a lesser extend in the liver (590). When the plasma of these transgenic mice was fractionated by gel filtration, the majority of apoA-IV was distributed in the same HDL fractions where apoA-I was also found (590). Such localization of apoA-IV reinforces the concept that lipid-free apoA-IV originating from chylomicrons or secreted by the liver may contribute in the *de novo* synthesis of HDL-A-IV particles.

We have shown previously that *de novo* synthesis of HDL particles containing apoA-I or apoE is initiated by interactions of the lipid-poor apolipoproteins with the ABCA1 lipid transporter. These functional interactions catalyze the transfer of phospholipids and subsequently cholesterol from intracellular membrane pools to lipid-free apoA-I or apoE leading to the formation of minimally lipidated particles which are gradually converted to discoidal particles (14;17;108;296). Subsequent esterification of the cholesterol of the

minimally nascent preβ and discoidal particles by LCAT generates the spherical HDL particles present in the plasma that can be visualized by EM (14;17). In the present study the ability of apoA-IV to promote *de novo* formation of HDL-A-IV particles was established by adenovirus mediated gene transfer in four different mouse models. My responsibility was to examine the contribution of LCAT in the formation of apoA-IV-containing HDL.

The requirement of LCAT for the formation of HDL-A-IV was established by adenovirus-mediated gene transfer of apoA-IV in $LCAT^{-/-}$ mice. In these experiments, the absence of LCAT prevented the formation of nascent or mature HDL-A-IV particles. It is possible that in the absence of LCAT, nascent HDL-A-IV particles formed by initial interactions of lipid-free apoA-IV with ABCA1 are susceptible to fast catabolism. This interpretation is supported by co-expression of apoA-IV and LCAT in $LCAT^{-/-}$ mice. This treatment increased the HDL cholesterol peak and the plasma apoA-IV levels, promoted the formation of spherical HDL-A-IV particles and resulted in the distribution of apoA-IV in the HDL2 and HDL3 regions. Fast catabolism of preβ-apoA-I containing HDL particles by the kidney has been described previously (215).

Overall, my contribution in this study helped to establish that apoA-IV has the capacity to promote the *de novo* biogenesis of discrete HDL-A-IV particles. The formation of these particles requires the functions of LCAT. Further work is required to establish whether the generation of HDL-A-IV by the liver is responsible at least partially for the previously reported anti-inflammatory and atheroprotective functions of apoA-IV (591;592;594-596).

Chapter VII. Effect of reconsituted HDL containing apoE and apoA-I on endothelial gene expression

RESULTS-DISCUSSION

There is increased evidence that atherosclerosis is associated with endothelial dysfunctions in humans and experimental animals and that HDL plays a central role for the preservation of functions of the endothelium that are necessary for atheroprotection (597-599). The beneficial effects of HDL on endothelial cells are discussed in the introduction of this thesis and are reviewed in (7).

We hypothesized that normal and aberrant forms of HDL, such as those discussed in the previous sections, generated during the course of synthesis, or as a result of remodeling and modifications of HDL by other proteins, will positively or negatively affect the functions of the endothelial cells by influencing gene expression. For this purpose, we performed here preliminary microarray experimetns in human aortic endothelial cells (HAECs) following treatment of reconstituted HDL containing apoA-I or apoE. The long-term goal of this ongoing apporach is to obtain comparative gene expression signatures of endothelial cells in response to normal and aberrant forms of HDL. The gene signatures thus obtained may serve as predicitve markes for identifying functionally beneficial HDLs.

As described in section 2.4.14 of materials and methods, we treated HAECs for 12 hours with rHDL containing apoA-I or apoE with or without cholesterol and PBS. rDHLAI- was prepared with apoA-I and phospholipids (ratio 1:100). rHDL+ was prepared with apoA-I, phospholipids, and cholesterol (ratio 1:100:10) and similarly were prepared rHDLE- and rHDLE+ that contain

apoE. Total RNA was extracted and used for microarray analysis to identify differentially expressed genes.

The bioinformatics analyses performed showed that the rHDLAI- and rHDLAI+ treatments caused the differential expression (over 2-fold change and≤ 0.05 FDR) in 137 and 190 genes respectively. The differentially expressed genes in response to rHDLE3- and rHDLE3+ were 198 and 272 respectively. This analysis confirmed the initial findings. The microarrays based on FDR <0.05 and a greater than 2 fold change may provide false positive or negative results. For this reason the microarray data were validated with high throughput qRT-PCR based screening using the dynamic array chips (Fluidigm Biomark) in collaboration with Dr. Jane Freedman and Dr. Kahraman Tanriverdi in the core facility of U. Mass Medical School (Shown in Table 3.IX). The system is designed to analyze simultaneously in a single array up to 96 qRT-PCR reactions on 96 specimens, corresponding to 9216 assays/array.

Pathways of highly interconnected genes were tentatively identified based the Ingenuity Pathway Analysis (IPA) program (600;601) and pubmed literature searches in collaboration with Dr. Despina Sanoudou and Efi Valanti (Bioacademy of Athens). Based on these pilot analyses, the membrane protein FLT1, which is ivolved in the migration of endothelial cells, and the cytoplasmic protein VEGFA, which is upregulated in response to rHDL-AI+, may enhance cell migration by activating the PI3K/Akt signaling pathway (Figure 3.40). It also indicated that three cytoplasmic proteins (ADAMTS1, ANGPTL4, MGP) that are implicated in endothelial cell migration are upregulated and three (DKK1, CXCL1, IL8) are downregulated (Table 3.IX). Similar analysis is in progress for the genes involved in apoptosis/cell survival, lipid metabolism, cell growth, cell development, cell cycle, and cell signaling will be analyzed in a similar way.

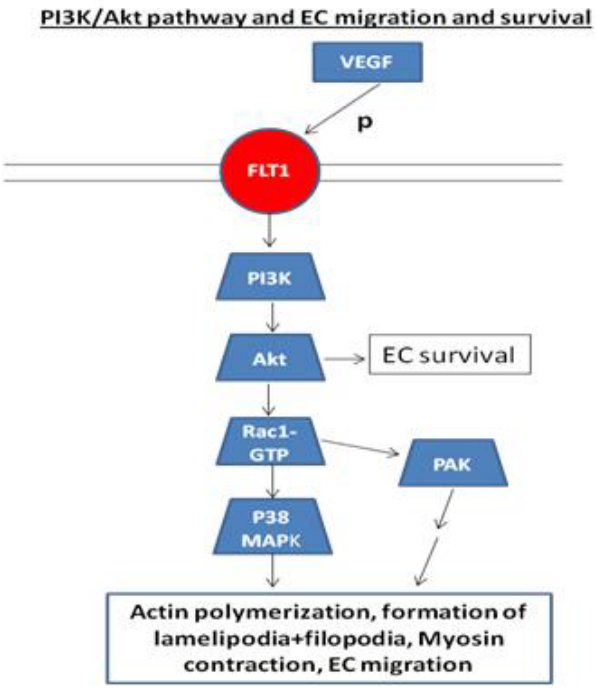

Figure 3.40. Schematic representation of the potential involvement of FLT1 in signaling pathways that promotes endothelial cell migration and survival. Arrows indicate a positive effect in cell signaling.

Table 3.IX: Fold change in endothelial genes expression in response to rHDLAI-, rHDLAI+, rHDLE3- and rHDLE3+

	fold change (5 arrays)						fold change (10 arrays)			fold change (5 arrays)					
	micro rHDLAI-	qPCR rHDLAI-	p-value	micro rHDLAI+	qPCR rHDLAI+	p-value	micro rHDLAI+	qPCR rHDLAI+	p-value	micro rHDLE3-	qPCR rHDLE3-	p-value	micro rHDLE3+	qPCR rHDLE3+	p-value
Secreted Proteins															
ANGPTL4	6.50	15.78	3.2E-02	8.50	17.15	2.9E-02	7.35	8.02	5.8E-05	5.30	9.14	2.6E-02	5.30	8.75	2.5E-02
LIPG	3.40	3.68	2.4E-02	3.60	3.51	2.4E-02	3.50	4.79	9.4E-06	4.60	4.84	1.7E-02	4.60	4.08	1.8E-02
ADAMTS1	2.40	2.31	2.4E-02	2.30	1.85	2.4E-02	2.02	1.93	4.5E-03	3.80	4.16	1.7E-02	3.80	4.69	1.8E-02
IL8	0.27	0.12	2.4E-02	0.27	0.11	2.9E-02	0.33	0.14	1.7E-05	0.23	0.06	1.7E-02	0.27	0.05	1.8E-02
DKK1	0.30	NS	NS	0.33	0.18	4.9E-02	0.25	0.13	1.2E-04	0.27	0.18	4.5E-02	0.24	0.17	4.4E-02
TGF-B2	0.45	0.35	3.2E-02	0.40	0.30	2.4E-02	0.29	0.15	4.6E-05	0.37	NS	NS	0.37	0.44	1.8E-02
VAV3	-	NS	NS	1.43	NS	NS	1.39	NS	NS	3.80	5.95	1.7E-02	4.00	4.12	1.8E-02
PDGFD	-	NS	NS	-	0.66	2.9E-02	-	NS	NS	2.20	2.43	1.7E-02	2.50	2.44	1.8E-02
PTX3	-	NS	NS	-	NS	NS	-	NS	NS	0.13	0.10	4.5E-02	0.11	0.08	2.5E-02
CXCL1	0.51	0.29	2.4E-02	0.47	0.25	2.9E-02	0.45	0.27	3.1E-05	0.40	0.03	1.7E-02	0.43	0.03	2.5E-02
IFI44L	11.60	17.76	2.4E-02	8.40	10.73	2.9E-02	6.90	11.30	2.2E-05	-	NS	NS	-	NS	NS
IFIT1	4.00	4.16	2.4E-02	3.10	NS	NS	2.60	NS	NS	-	0.36	4.6E-02	-	0.19	1.8E-02
VEGFA+	1.80	NS	NS	2.20	2.22	2.4E-02	2.80	4.97	9.4E-06	-	NS	NS	-	NS	NS
TNFSF18+	0.50	0.59	2.4E-02	0.43	0.36	2.4E-02	0.49	0.47	4.2E-02	0.43	0.51	1.7E-02	0.42	0.44	1.8E-02
MAMDC2	0.42	0.38	2.4E-02	0.34	0.28	2.4E-02	0.34	0.29	9.4E-06	0.26	0.31	1.7E-02	0.22	0.23	1.8E-02
PMCH	0.27	0.16	2.4E-02	0.23	0.16	2.4E-02	0.23	NS	NS	0.57	0.46	1.7E-02	-	0.51	4.5E-02
APOL6	1.61	NS	NS	2.00	NS	NS	3.35	6.11	9.4E-05	-	NS	NS	-	NS	NS
TFIP	-	0.48	2.4E-02	-	0.50	2.9E-02	-	NS	NS	2.20	2.95	1.7E-02	2.20	2.45	1.8E-02
CXCL11	1.54	2.18	3.2E-02	1.70	2.03	2.9E-02	1.70	3.53	2.4E-02	0.40	0.60	2.6E-02	0.43	0.43	4.5E-02
MANF	-	NS	NS	-	NS	NS	0.69	NS	NS	1.66	1.91	1.7E-02	1.80	NS	NS
MGP	-	2.15	2.4E-02	-	2.33	2.4E-02	1.25	2.57	9.4E-06	1.87	9.74	1.7E-02	2.00	14.33	1.8E-02
EGR1	1.66	2.95	3.2E-02	-	NS	NS	-	NS	NS	2.36	5.89	2.6E-02	2.25	4.14	2.5E-02
Membrane Proteins															
VIPR1	2.70	4.48	2.4E-02	3.40	5.14	2.4E-02	3.05	4.64	9.4E-06	2.40	3.86	2.6E-02	2.70	4.09	1.8E-02
LDLR	2.20	NS	NS	2.10	NS	NS	2.20	5.61	7.5E-05	1.72	NS	NS	1.71	NS	NS
UNC5B	-	2.39	2.4E-02	-	2.31	2.4E-02	1.40	NS	NS	3.60	9.90	1.7E-02	3.50	10.57	2.5E-02
EFNB2	1.50	1.44	3.2E-02	1.48	NS	NS	1.31	NS	NS	3.00	3.65	1.7E-02	3.10	3.32	1.8E-02
FLT1	1.67	1.62	2.4E-02	1.69	1.62	2.9E-02	1.57	3.02	9.4E-05	2.80	4.03	1.7E-02	2.90	4.04	1.8E-02
ACE	-	NS	NS	-	1.68	2.4E-02	1.41	NS	NS	2.50	3.22	1.7E-02	2.70	3.99	1.8E-02
CLDN11	-	NS	NS	-	0.55	2.4E-02	0.50	NS	NS	0.33	0.20	1.7E-02	0.32	0.17	2.5E-02
CD40	1.40	2.05	3.2E-02	1.50	2.23	2.9E-02	1.80	2.70	1.5E-05	1.80	2.81	1.7E-02	2.00	2.96	2.5E-02
Nuclear Proteins															
RARB	0.34	0.29	2.4E-02	0.26	0.23	2.4E-02	0.18	0.18	9.4E-06	0.26	0.23	1.7E-02	0.24	0.24	2.5E-02
NUPR1	0.37	0.25	2.4E-02	0.37	0.26	2.4E-02	0.37	NS	NS	0.23	0.13	1.7E-02	0.17	0.08	1.8E-02
UHRF1	0.40	0.24	2.4E-02	0.27	0.13	2.4E-02	0.24	0.16	3.1E-05	0.66	0.49	1.7E-02	0.53	0.34	1.8E-02
JUN	0.48	0.34	2.4E-02	0.37	0.24	2.4E-02	0.39	0.37	1.6E-03	-	0.55	4.6E-02	-	0.36	1.8E-02
PRDM1	-	0.58	3.2E-02	0.59	0.34	2.4E-02	0.75	NS	NS	4.80	5.99	1.7E-02	4.50	4.16	1.8E-02
NEDD9	-	NS	NS	-	NS	NS	0.80	NS	NS	2.30	3.70	1.7E-02	2.80	4.09	1.8E-02
FAM111B	0.25	0.23	3.2E-02	0.16	0.09	2.9E-02	0.12	0.15	4.8E-04	0.59	NS	NS	0.43	0.55	4.4E-02
ESCO2	0.28	0.39	2.4E-02	0.23	0.25	2.4E-02	0.16	0.25	3.4E-02	0.37	0.67	2.6E-02	0.30	0.51	1.8E-02
NRC3C1+	-	NS	NS	1.50	NS	NS	1.70	2.54	1.6E-03	-	NS	NS	-	NS	NS
CCND1+	-	NS	NS	0.63	0.38	2.9E-02	0.58	0.46	2.0E-04	-	NS	NS	-	NS	NS
Cytoplasmic Proteins															
PDK4	3.10	3.56	2.4E-02	3.20	3.59	2.4E-02	3.20	4.37	9.4E-06	1.61	1.91	1.7E-02	1.80	1.91	1.8E-02
MT1E	0.29	NS	NS	0.31	0.10	4.9E-02	0.41	0.35	1.9E-02	0.22	NS	NS	0.21	0.04	2.5E-02
DHRS3	0.38	0.42	3.2E-02	0.40	0.38	2.9E-02	0.42	0.56	2.4E-02	0.26	0.19	2.6E-02	0.31	0.26	4.4E-02
ST8SIA4	1.69	1.82	3.2E-02	1.90	NS	NS	1.76	1.53	3.8E-04	3.80	2.08	1.7E-02	4.60	5.34	1.8E-02
FABP4	-	NS	NS	-	NS	NS	0.55	NS	NS	3.40	6.56	1.7E-02	3.30	3.71	2.5E-02
CHST1	-	NS	NS	-	NS	NS	0.62	NS	NS	2.70	4.06	1.7E-02	3.10	3.61	1.8E-02
SULT1E1	-	NS	NS	0.60	NS	NS	0.47	0.49	2.4E-02	0.34	0.24	1.7E-02	0.31	0.26	1.8E-02
ANKRD1	-	0.53	2.4E-02	0.65	0.36	2.4E-02	0.57	0.33	9.4E-06	0.37	0.21	1.7E-02	0.32	0.14	1.8E-02
PRKAA2	-	NS	NS	-	NS	NS	-	NS	NS	0.40	0.52	1.7E-02	0.46	0.45	1.8E-02
PTGIS	0.68	NS	NS	-	NS	NS	-	NS	NS	0.43	0.42	1.7E-02	0.46	0.48	1.8E-02
MX1	4.20	9.28	3.2E-02	3.60	5.19	2.9E-02	3.80	4.53	2.2E-05	0.67	0.42	2.6E-02	-	0.39	2.5E-02
CHAC1	4.00	NS	NS	6.30	NS	NS	8.90	18.68	4.5E-05	-	NS	NS	1.70	NS	NS
EPST11	4.00	3.89	2.4E-02	4.10	3.16	2.4E-02	4.20	4.64	9.4E-06	-	0.25	1.7E-02	0.71	0.18	2.5E-02
IFITM1	3.30	6.41	2.4E-02	2.10	4.21	2.4E-02	2.10	2.79	1.9E-02	0.71	NS	NS	-	NS	NS
IFI44	4.20	NS	NS	3.60	2.93	2.9E-02	3.80	3.70	2.9E-05	-	NS	NS	-	NS	NS
PIK3CG	1.63	1.93	3.2E-02	2.14	2.02	2.4E-02	-	3.37	4.6E-05	2.24	3.37	1.7E-02	2.62	3.15	1.8E-02

ANGPTL4: angiopoietin-like 4;LIPG: lipase, endothelial;ADAMTS1 ADAM metallopeptidase with thrombospondin type 1 motif, 1;IL8: interleukin 8;DKK1: dickkopf homolog 1 (Xenopus laevis);TGF-B2: Tumor Growth Factor B2;VAV3: vav 3 guanine nucleotide exchange factor;PDGFD: platelet derived growth factor D;PTX3: pentraxin 3, long;CXCL1: chemokine (C-X-C motif) ligand 11;IFI44L: interferon-induced protein 44-like;IFIT1: interferon-induced protein with tetratricopeptide repeats 1;VEGFA+: vascular endothelial growth factor A;IL6: interleukin 6;TNFSF18+: tumor necrosis factor (ligand) superfamily, member 18;MAMDC2: MAM domain containing 2;PMCH: pro-melanin-concentrating hormone;APOL6: apolipoprotein L, 6;TFIP: tissue factor pathway inhibitor 2;CXCL11: chemokine (C-X-C motif) ligand 11;MANF: mesencephalic astrocyte-derived neurotrophic factor;MGP: matrix Gla protein; EGR1: early growth response 1; VIPR1: vasoactive intestinal peptide receptor 1;LDLR: low density lipoprotein receptor;UNC5B: unc-5 homolog B (C. elegans);EFNB2: ephrin-B2;FLT1: fms-related tyrosine kinase 1 (vascular endothelial growth factor/vascular permeability factor receptor);ACE: angiotensin I converting enzyme (peptidyl-dipeptidase A) 1;CLDN11: claudin 11;CD40: CD40 antigen (TNF receptor superfamily member 5);RARB: retinoic acid receptor, beta;NUPR1: nuclear protein, transcriptional regulator, 1;UHRF1: ubiquitin-like with PHD and ring finger domains 1;JUN: jun proto-oncogene;PRDM1: PR domain containing 1, with ZNF domain;NEDD9: neural precursor cell expressed, developmentally down-regulated 9;FAM111B: family with sequence similarity 111, member B;ESCO2: establishment of cohesion 1 homolog 2 (S. cerevisiae);NRC3C1+: glucocortoid receptor;CCND1+: cyclin D1;PDK4; pyruvate dehydrogenase kinase, isozyme 4;MT1E: metallothionein 1E;DHRS3: dehydrogenase/reductase (SDR family) member 3;ST8SIA4; ST8 alpha-N-acetyl-neuraminide alpha-2,8-sialyltransferase 4;FABP4: fatty acid binding protein 4, adipocyte;CHST1: carbohydrate (keratan sulfate Gal-6) sulfotransferase 1;SULT1E1: sulfotransferase family 1E, estrogen-preferring, member 1;ANKRD1: ankyrin repeat domain 1 (cardiac muscle);PRKAA2: protein kinase, AMP-activated, alpha 2 catalytic subunit;PTGIS: prostaglandin I2 (prostacyclin) synthase;MX1: myxovirus (influenza virus) resistance 1, interferon-inducible protein p78 (mouse);CHAC1: ChaC, cation transport regulator homolog 1 (E. coli);EPST11: epithelial stromal interaction 1 (breast);IFITM1: interferon-induced protein with tetratricopeptide repeats 1;IFI44: interferon-induced protein 44; PIK3CG:phosphoinositide-3-kinase, catalytic, gamma polypeptide.

FUTURE STUDIES

The studies on the hydrophobic residues in the c-terminal 218-230 region of apoA-I contributes to the clarification of the molecular pathways that are involved in the initial step of the biogenesis of HDL and complemetes previous anlaysis performed in our lab examining the importance of various residues and regions of apoA-I for HDL formation. Overall, these analyses demonstrate that expression of mutant apoA-I forms in different mouse models disrupted specific steps along the pathway of the biogenesis of HDL and generated discrete lipid and HDL phenotypes (331). The phenotypes generated included: inhibition of the formation of HDL (108;126;127); generation of unstable intermediates (217;219); inhibition of the activation of LCAT (220); increase in plasma cholesterol or increase in both plasma cholesterol and triglycerides (110;226)(Figure 3.41).

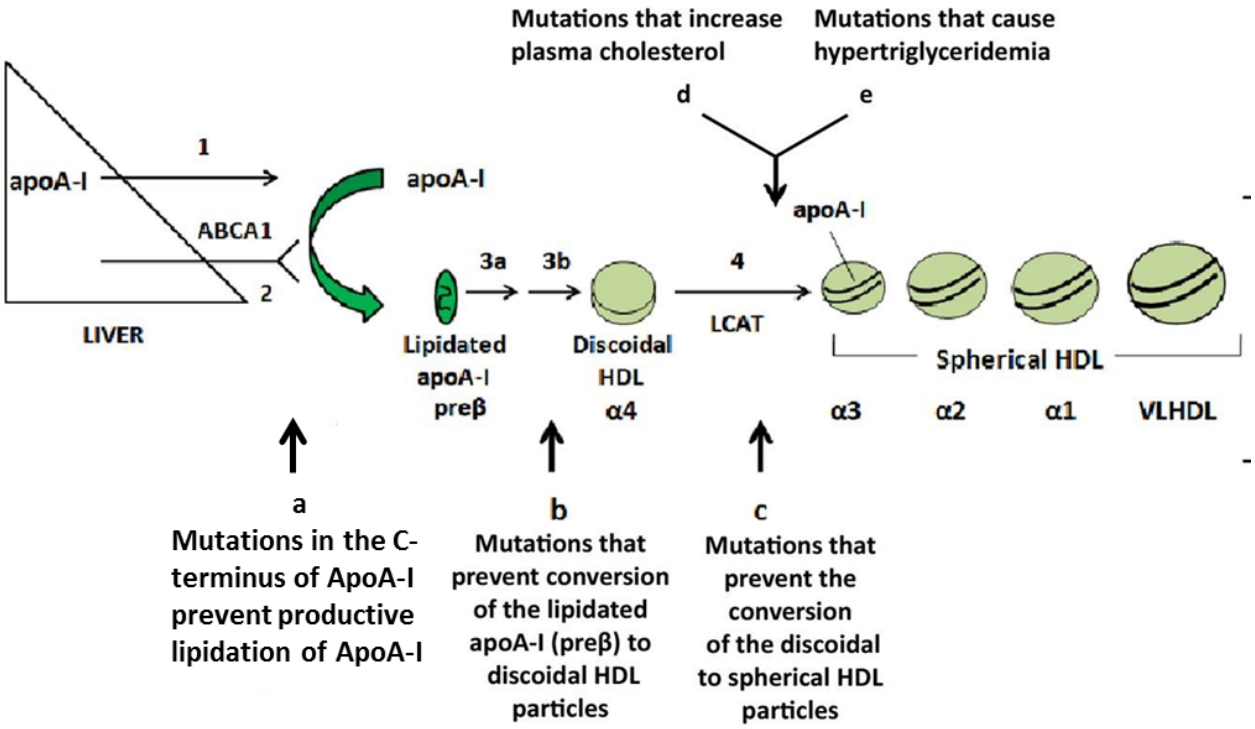

Figure 3.41: The pathway of HDL biogenesis. Superimposed on the pathway are defects that inhibit different steps of this pathway. The mutations in the c-terminus of apoA-I are represented in (a).

It is possible that phenotypes generated by mutagenesis of apoA-I may exist in the human population. The studies described above provide molecular markers that could be used for the diagnosis, prognosis and to monitor improvements in the properties of HDL following treatment of HDL abnormalities or dyslipidemias associated with the biogenesis and remodeling of HDL. The correction or not of the aberrant HDL phenotypes by treatment with LCAT suggests a potential therapeutic intervention for HDL abnormalities that result from specific mutations in apoA-I or conditions that result in low HDL levels.

Future studies to expand the work of this thesis would be to investigate the significance of other conserved residues of apoA-I, taking into consideration their location in the 3D structure and the residues that participate in the formation of solvent-inaccessible salt bridges on the surface of HDL, on the biogenesis of HDL, in the development of hypertriglyceridemia as well as on the properties and functions of apoA-I and HDL. The studies will encompass alanine scanning mutagenesis of apoA-I, gene transfer in mouse models, and analyses of the resulting HDL phenotypes. These analyses may help the understanding of which residues are responsible for the pleiotropic functions of apoA-I.

Additionaly, we could investigate by unbiased high throughput methodologies how HDL containing WT and mutant forms of apoA-I, such as those described here, affect endothelial cell, monocytes or β pancreatic cell gene expression signatures and functions. We will use human genome microarrays and high throughput qRT-PCR screening to obtain comparative gene expression signatures of endothelial cells in response to HDL containing WT and mutant forms of apoA-I produced in mouse models. The functions of most promising candidate genes identified by the microarray studies could be followed up.

Development of adeno-associated virus (AAV) expressing the mutants studied here and gene transfer in mice will allow us to investigate the contribution of the mutations on the development of atherosclerosis.

Other promising studies include the elucidation of the proteomic and lipidomic composition of HDL containing WT and mutant forms of apoA-I and the effect of apoA-II and apoC-III on the biogenesis of HDL.

REFERENCES

1. **Zannis, V. I., D. Kardassis, and E. E. Zanni 1993. Genetic mutations affecting human lipoproteins, their receptors, and their enzymes. *Adv.Hum.Genet.* 21: 145-319**

2. **Havel, J. H. and Kane, J. P. (2001) Introduction: Structure and metabolism of plasma lipoproteins. In Scriver, C. R., Beaudet, A. L., Sly, W. S., and Valle, D., editors. *The Metabolic & Molecular Bases of Inherited Disease*, McGraw-Hill, New York. 2705-2716**

3. **Zannis, V. I., Kypreos, K. E., Chroni, A., Kardassis, D., and Zanni, E. E. (2004) Lipoproteins and atherogenesis. In Loscalzo, J., editor. *Molecular Mechanisms of Atherosclerosis*, Taylor & Francis, New York, NY. 111-174**

4. **Hussain, M. M. 2000. A proposed model for the assembly of chylomicrons. *Atherosclerosis* 148: 1-15**

5. **Blasiole, D. A., R. A. Davis, and A. D. Attie 2007. The physiological and molecular regulation of lipoprotein assembly and secretion. *Mol.Biosyst.* 3: 608-619**

6. **Rader, D. J., E. T. Alexander, G. L. Weibel, J. Billheimer, and G. H. Rothblat 2009. The role of reverse cholesterol transport in animals and humans and relationship to atherosclerosis. *J.Lipid Res.* 50 Suppl: S189-S194**

7. **Zannis, V. I., Kateifides, A. K., Fotakis, P., Zanni, E. E., and Kardassis, D. (2012) Pleiotropic functions of HDL lead to protection from atherosclerosis and other diseases. In Kelishadi, R., editor. *Dyslipidemia - From Prevention to Treatment*, Intech . 173-196**

8. **Anderson, K. M., P. W. Wilson, P. M. Odell, and W. B. Kannel 1991. An updated coronary risk profile. A statement for health professionals. *Circulation* 83: 356-362**

9. **Castelli, W. P., J. T. Doyle, T. Gordon, C. G. Hames, M. C. Hjortland, S. B. Hulley, A. Kagan, and W. J. Zukel 1977. HDL cholesterol and other lipids in coronary heart disease. The cooperative lipoprotein phenotyping study. *Circulation* 55: 767-772**

10. **Zannis, V. I., Zanni, E. E., Papapanagiotou, A., Kardassis, D., Fielding, C. J., and Chroni, A. (2007) ApoA-I functions and synthesis of HDL: Insights from mouse models of human HDL metabolism. In Fielding, C. J., editor. *High-Density Lipoproteins: From basic biology to clinical aspects* , WILEY-VCH Verlag GmbH & Co. KGaA, Weinheim. 267-306**

11. **Zannis, Vassilis I., Kateifides, A., Fotakis, P., Zanni, E. E., and Kardassis, D. Pleiotropic functions of HDL lead to protection from atherosclerosis and other diseases. (In: Dyslipidemias Intech publishing (M. Rebrovic editor) in press). 12-8-2011.**

Ref Type: Generic

12. **Zannis, V. I., A. Chroni, K. E. Kypreos, H. Y. Kan, T. B. Cesar, E. E. Zanni, and D. Kardassis 2004. Probing the pathways of chylomicron and HDL metabolism using adenovirus-mediated gene transfer. *Curr Opin Lipidol.* 15: 151-166**

13. **Zannis, V. I., F. S. Cole, C. L. Jackson, D. M. Kurnit, and S. K. Karathanasis 1985. Distribution of apolipoprotein A-I, C-II, C-III, and E mRNA in fetal human tissues. Time-dependent induction of apolipoprotein E mRNA by cultures of human monocyte-macrophages. *Biochemistry* 24: 4450-4455**

14. **Zannis, V. I., A. Chroni, and M. Krieger 2006. Role of apoA-I, ABCA1, LCAT, and SR-BI in the biogenesis of HDL. *J.Mol.Med.* 84: 276-294**

15. **Daniil, G., A. A. Phedonos, A. G. Holleboom, M. M. Motazacker, L. Argyri, J. A. Kuivenhoven, and A. Chroni 2011. Characterization of antioxidant/anti-inflammatory properties and apoA-**

I-containing subpopulations of HDL from family subjects with monogenic low HDL disorders. *Clin.Chim.Acta* 412: 1213-1220

16. Duka, A., P. Fotakis, D. Georgiadou, A. Kateifides, K. Tzavlaki, E. L. von, E. Stratikos, D. Kardassis, and V. I. Zannis 2013. ApoA-IV promotes the biogenesis of apoA-IV-containing HDL particles with the participation of ABCA1 and LCAT. *J.Lipid Res.* 54: 107-115

17. Kypreos, K. E. and V. I. Zannis 2007. Pathway of biogenesis of apolipoprotein E-containing HDL in vivo with the participation of ABCA1 and LCAT. *Biochem.J.* 403: 359-367

18. Wang, N., D. Lan, W. Chen, F. Matsuura, and A. R. Tall 2004. ATP-binding cassette transporters G1 and G4 mediate cellular cholesterol efflux to high-density lipoproteins. *Proc.Natl.Acad.Sci.U.S.A* 101: 9774-9779

19. Lusa, S., M. Jauhiainen, J. Metso, P. Somerharju, and C. Ehnholm 1996. The mechanism of human plasma phospholipid transfer protein-induced enlargement of high-density lipoprotein particles: evidence for particle fusion. *Biochem.J.* 313 (Pt 1): 275-282

20. Barter, P. J., H. B. Brewer, Jr., M. J. Chapman, C. H. Hennekens, D. J. Rader, and A. R. Tall 2003. Cholesteryl ester transfer protein: a novel target for raising HDL and inhibiting atherosclerosis. *Arterioscler.Thromb.Vasc.Biol.* 23: 160-167

21. Krieger, M. 2001. Scavenger receptor class B type I is a multiligand HDL receptor that influences diverse physiologic systems. *J.Clin.Invest* 108: 793-797

22. Breckenridge, W. C., J. A. Little, P. Alaupovic, C. S. Wang, A. Kuksis, G. Kakis, F. Lindgren, and G. Gardiner 1982. Lipoprotein abnormalities associated with a familial deficiency of hepatic lipase. *Atherosclerosis* 45: 161-179

23. Brunzell, J. D. and Deeb, S. S. (2001) Familial lipoprotein lipase deficiency, apoC-II deficiency, and hepatic lipase deficiency. In Scriver, C. R., Beaudet, A. L., Valle, D., and Sly, W. S., editors. *The Metabolic & Molecular Bases of Inherited Disease*, McGraw-Hill, New York. 2789-2816

24. Ishida, T., S. Choi, R. K. Kundu, K. Hirata, E. M. Rubin, A. D. Cooper, and T. Quertermous 2003. Endothelial lipase is a major determinant of HDL level. *J.Clin.Invest* 111: 347-355

25. Krauss, R. M., R. I. Levy, and D. S. Fredrickson 1974. Selective measurement of two lipase activities in postheparin plasma from normal subjects and patients with hyperlipoproteinemia. *J.Clin.Invest* 54: 1107-1124

26. Barter, P., A. M. Gotto, J. C. LaRosa, J. Maroni, M. Szarek, S. M. Grundy, J. J. Kastelein, V. Bittner, and J. C. Fruchart 2007. HDL cholesterol, very low levels of LDL cholesterol, and cardiovascular events. *N.Engl.J.Med.* 357: 1301-1310

27. Barter, P. and Rye, K. A. (2007) HDL and atherosclerosis. In Fielding, C. J., editor. *High-Density Lipoproteins: From basic biology to clinical aspects*, WILEY-VCH Verlag GmbH & Co. KGaA, Weinheim. 491-506

28. Hovingh, G. K., A. Brownlie, R. J. Bisoendial, M. P. Dube, J. H. Levels, W. Petersen, R. P. Dullaart, E. S. Stroes, A. H. Zwinderman, E. de Groot, M. R. Hayden, J. A. Kuivenhoven, and J. J. Kastelein 2004. A novel apoA-I mutation (L178P) leads to endothelial dysfunction, increased arterial wall thickness, and premature coronary artery disease. *J.Am.Coll.Cardiol.* 44: 1429-1435

29. Hovingh, G. K., B. A. Hutten, A. G. Holleboom, W. Petersen, P. Rol, A. Stalenhoef, A. H. Zwinderman, G. E. De, J. J. Kastelein, and J. A. Kuivenhoven 2005. Compromised LCAT function is associated with increased atherosclerosis. *Circulation* 112: 879-884

30. Leus, F. R., M. E. Wittekoek, J. Prins, J. J. Kastelein, and H. A. Voorbij 2000. Paraoxonase gene polymorphisms are associated with carotid arterial wall thickness in subjects with familial hypercholesterolemia. *Atherosclerosis* 149: 371-377

31. Rye, K. A., C. A. Bursill, G. Lambert, F. Tabet, and P. J. Barter 2009. The metabolism and anti-atherogenic properties of HDL. *J.Lipid Res.* 50 Suppl: S195-S200

32. Blanche, P. J., E. L. Gong, T. M. Forte, and A. V. Nichols 1981. Characterization of human high-density lipoproteins by gradient gel electrophoresis. *Biochim.Biophys.Acta* 665: 408-419

33. Cheung, M. C. and J. J. Albers 1982. Distribution of high density lipoprotein particles with different apoprotein composition: particles with A-I and A-II and particles with A-I but no A-II. *J.Lipid Res.* 23: 747-753

34. Cheung, M. C. and J. J. Albers 1984. Characterization of lipoprotein particles isolated by immunoaffinity chromatography. Particles containing A-I and A-II and particles containing A-I but no A-II. *J.Biol.Chem.* 259: 12201-12209

35. Castro, G. R. and C. J. Fielding 1988. Early incorporation of cell-derived cholesterol into pre-beta-migrating high-density lipoprotein. *Biochemistry* 27: 25-29

36. Huang, Y., A. von Eckardstein, S. Wu, N. Maeda, and G. Assmann 1994. A plasma lipoprotein containing only apolipoprotein E and with gamma mobility on electrophoresis releases cholesterol from cells. *Proc.Natl.Acad.Sci.U.S.A* 91: 1834-1838

37. Asztalos B.F. (2010) High Density Lipoprotein Particles. In Schaefer, E. J., editor. *High Density Lipoproteins, Dyslipidemia, and Coronary Heart Disease*, Springer. 25-32

38. Asztalos, B. F., C. H. Sloop, L. Wong, and P. S. Roheim 1993. Two-dimensional electrophoresis of plasma lipoproteins: recognition of new apo A-I-containing subpopulations. *Biochim.Biophys.Acta* 1169: 291-300

39. Freeman, L. A. 2013. Native-native 2D gel electrophoresis for HDL subpopulation analysis. *Methods Mol.Biol.* 1027: 353-367

40. Arinami, T., T. Hirano, K. Kobayashi, Y. Yamanouchi, and H. Hamaguchi 1990. Assignment of the apolipoprotein A-I gene to 11Q23 based on Rflp in a case with a partial deletion of chromosome-11, Del(11) (Q23.3-]Qter). *Human Genetics* 85: 39-40

41. Cheung, P., F. T. Kao, M. L. Law, C. Jones, T. T. Puck, and L. Chan 1984. Localization of the structural gene for human apolipoprotein A-I on the long arm of human chromosome 11. *Proc.Natl.Acad.Sci.U.S.A* 81: 508-511

42. Karathanasis, S. K., J. McPherson, V. I. Zannis, and J. L. Breslow 1983. Linkage of human apolipoproteins A-I and C-III genes. *Nature* 304: 371-373

43. Zannis, V. I., S. K. Karathanasis, H. T. Keutmann, G. Goldberger, and J. L. Breslow 1983. Intracellular and extracellular processing of human apolipoprotein A-I: secreted apolipoprotein A-I isoprotein 2 is a propeptide. *Proc.Natl.Acad.Sci.U.S.A* 80: 2574-2578

44. Tzameli, I. and V. I. Zannis 1996. Binding specificity and modulation of the ApoA-I promoter activity by homo- and heterodimers of nuclear receptors. *J.Biol.Chem.* 271: 8402-8415

45. Delerive, P., C. M. Galardi, J. E. Bisi, E. Nicodeme, and B. Goodwin 2004. Identification of liver receptor homolog-1 as a novel regulator of apolipoprotein AI gene transcription. *Mol.Endocrinol.* 18: 2378-2387

46. Ladias, J. A. and S. K. Karathanasis 1991. Regulation of the apolipoprotein AI gene by ARP-1, a novel member of the steroid receptor superfamily. *Science* 251: 561-565

47. Talianidis, I., A. Tambakaki, J. Toursounova, and V. I. Zannis 1995. Complex interactions between SP1 bound to multiple distal regulatory sites and HNF-4 bound to the proximal promoter lead to transcriptional activation of liver-specific human APOCIII gene. *Biochemistry* 34: 10298-10309

48. Lavrentiadou, S. N., M. Hadzopoulou-Cladaras, D. Kardassis, and V. I. Zannis 1999. Binding specificity and modulation of the human ApoCIII promoter activity by heterodimers of ligand-dependent nuclear receptors. *Biochemistry* 38: 964-975

49. Kardassis, D., I. Tzameli, M. Hadzopoulou-Cladaras, I. Talianidis, and V. Zannis 1997. Distal apolipoprotein C-III regulatory elements F to J act as a general modular enhancer for proximal promoters that contain hormone response elements. Synergism between hepatic nuclear factor-4 molecules bound to the proximal promoter and distal enhancer sites. *Arterioscler.Thromb.Vasc.Biol.* 17: 222-232

50. Kan, H. Y., S. Georgopoulos, and V. Zannis 2000. A hormone response element in the human apolipoprotein CIII (ApoCIII) enhancer is essential for intestinal expression of the ApoA-I and ApoCIII genes and contributes to the hepatic expression of the two linked genes in transgenic mice. *J.Biol.Chem.* 275: 30423-30431

51. **Georgopoulos, S., H. Y. Kan, C. Reardon-Alulis, and V. Zannis 2000. The SP1 sites of the human apoCIII enhancer are essential for the expression of the apoCIII gene and contribute to the hepatic and intestinal expression of the apoA-I gene in transgenic mice.** ***Nucleic Acids Res.*** **28: 4919-4929**

52. **Staels, B. and J. Auwerx 1998. Regulation of apo A-I gene expression by fibrates.** ***Atherosclerosis*** **137 Suppl: S19-S23**

53. **Duez, H., B. Lefebvre, P. Poulain, I. P. Torra, F. Percevault, G. Luc, J. M. Peters, F. J. Gonzalez, R. Gineste, S. Helleboid, V. Dzavik, J. C. Fruchart, C. Fievet, P. Lefebvre, and B. Staels 2005. Regulation of human apoA-I by gemfibrozil and fenofibrate through selective peroxisome proliferator-activated receptor alpha modulation.** ***Arterioscler.Thromb.Vasc.Biol.*** **25: 585-591**

54. **Sanoudou, D., A. Duka, K. Drosatos, K. C. Hayes, and V. I. Zannis 2009. Role of Esrrg in the fibrate-mediated regulation of lipid metabolism genes in human ApoA-I transgenic mice.** ***Pharmacogenomics.J.*** **10: 165-179**

55. **Haas, M. J. and A. D. Mooradian 2010. Regulation of high-density lipoprotein by inflammatory cytokines: establishing links between immune dysfunction and cardiovascular disease.** ***Diabetes Metab Res.Rev.*** **26: 90-99**

56. **Srivastava, R. and N. Srivastava 2000. High density lipoprotein, apolipoprotein A-I, and coronary artery disease.** ***Molecular and Cellular Biochemistry*** **209: 131-144**

57. **Malik, S. 2003. Transcriptional regulation of the apolipoprotein AI gene.** ***Frontiers in Bioscience*** **8: D360-D368**

58. Haas, M. J. and A. D. Mooradian 2010. Therapeutic interventions to enhance apolipoprotein A-I-mediated cardioprotection. *Drugs* 70: 805-821

59. Mooradian, A. D. (2007) The Effect of Nutrients on Apolipoprotein A-I Gene Expression. In Fielding, C. J., editor. *High-Density Lipoproteins. From basic biology to clinical aspects.*, Wiley-VCH. 399-424

60. Sorci-Thomas, M. G. and M. J. Thomas 2002. The effects of altered apolipoprotein A-I structure on plasma HDL concentration. *Trends Cardiovasc.Med.* 12: 121-128

61. Dastani, Z., C. Dangoisse, B. Boucher, K. Desbiens, L. Krimbou, R. Dufour, R. A. Hegele, P. Pajukanta, J. C. Engert, J. Genest, and M. Marcil 2006. A novel nonsense apolipoprotein A-I mutation (apoA-I(E136X)) causes low HDL cholesterol in French Canadians. *Atherosclerosis* 185: 127-136

62. Haase, C. L., R. Frikke-Schmidt, B. G. Nordestgaard, A. K. Kateifides, D. Kardassis, L. B. Nielsen, C. B. Andersen, L. Kober, A. H. Johnsen, P. Grande, V. I. Zannis, and A. Tybjaerg-Hansen 2011. Mutation in APOA1 predicts increased risk of ischaemic heart disease and total mortality without low HDL cholesterol levels. *J.Intern.Med.*

63. Franceschini, G., C. R. Sirtori, A. Capurso, K. H. Weisgraber, and R. W. Mahley 1980. A-IMilano apoprotein. Decreased high density lipoprotein cholesterol levels with significant lipoprotein modifications and without clinical atherosclerosis in an Italian family. *J.Clin.Invest* 66: 892-900

64. Gomaraschi, M., D. Baldassarre, M. Amato, S. Eligini, P. Conca, C. R. Sirtori, G. Franceschini, and L. Calabresi 2007. Normal vascular function despite low levels of high-density

lipoprotein cholesterol in carriers of the apolipoprotein A-I(Milano) mutant. *Circulation* 116: 2165-2172

65. Obici, L., G. Franceschini, L. Calabresi, S. Giorgetti, M. Stoppini, G. Merlini, and V. Bellotti 2006. Structure, function and amyloidogenic propensity of apolipoprotein A-I. *Amyloid.* 13: 191-205

66. Nolte, R. T. and D. Atkinson 1992. Conformational analysis of apolipoprotein A-I and E-3 based on primary sequence and circular dichroism. *Biophys.J.* 63: 1221-1239

67. Segrest, J. P., R. L. Jackson, J. D. Morrisett, and A. M. Gotto, Jr. 1974. A molecular theory of lipid-protein interactions in the plasma lipoproteins. *FEBS Lett.* 38: 247-258

68. Borhani, D. W., J. A. Engler, and C. G. Brouillette 1999. Crystallization of truncated human apolipoprotein A-I in a novel conformation. *Acta Crystallogr.D.Biol.Crystallogr.* 55 (Pt 9): 1578-1583

69. Borhani, D. W., D. P. Rogers, J. A. Engler, and C. G. Brouillette 1997. Crystal structure of truncated human apolipoprotein A-I suggests a lipid-bound conformation. *Proc.Natl.Acad.Sci.U.S.A* 94: 12291-12296

70. Segrest, J. P., M. K. Jones, A. E. Klon, C. J. Sheldahl, M. Hellinger, H. De Loof, and S. C. Harvey 1999. A detailed molecular belt model for apolipoprotein A-I in discoidal high density lipoprotein. *J.Biol.Chem.* 274: 31755-31758

71. Segrest, J. P. 1977. Amphipathic helixes and plasma lipoproteins: thermodynamic and geometric considerations. *Chem.Phys.Lipids* 18: 7-22

72. Segrest, J. P., L. Li, G. M. Anantharamaiah, S. C. Harvey, K. N. Liadaki, and V. Zannis 2000. Structure and function of apolipoprotein A-I and high-density lipoprotein. *Curr.Opin.Lipidol.* 11: 105-115

73. Panagotopulos, S. E., E. M. Horace, J. N. Maiorano, and W. S. Davidson 2001. Apolipoprotein A-I adopts a belt-like orientation in reconstituted high density lipoproteins. *J.Biol.Chem.* 276: 42965-42970

74. Marcel, Y. L. and R. S. Kiss 2003. Structure-function relationships of apolipoprotein A-I: a flexible protein with dynamic lipid associations. *Curr.Opin.Lipidol.* 14: 151-157

75. Martin, D. D., M. S. Budamagunta, R. O. Ryan, J. C. Voss, and M. N. Oda 2006. Apolipoprotein A-I assumes a looped belt conformation on reconstituted high density lipoprotein. *J.Biol.Chem.*

76. Wu, Z., V. Gogonea, X. Lee, R. P. May, V. Pipich, M. A. Wagner, A. Undurti, T. C. Tallant, C. Baleanu-Gogonea, F. Charlton, A. Ioffe, J. A. Didonato, K. A. Rye, and S. L. Hazen 2011. The low resolution structure of ApoA1 in spherical high density lipoprotein revealed by small angle neutron scattering. *J.Biol.Chem.* 286: 12495-508

77. Silva, R. A., R. Huang, J. Morris, J. Fang, E. O. Gracheva, G. Ren, A. Kontush, W. G. Jerome, K. A. Rye, and W. S. Davidson 2008. Structure of apolipoprotein A-I in spherical high density lipoproteins of different sizes. *Proc.Natl.Acad.Sci.U.S A* 105: 12176-12181

78. Sorci-Thomas, M. G., J. S. Owen, B. Fulp, S. Bhat, X. Zhu, J. S. Parks, D. Shah, W. G. Jerome, M. Gerelus, M. Zabalawi, and M. J. Thomas 2012. Nascent high density lipoproteins formed by ABCA1 resemble lipid rafts and are structurally organized by three apoA-I monomers. *J.Lipid Res.* 53: 1890-1909

79. Zhang, L., J. Song, G. Cavigiolio, B. Y. Ishida, S. Zhang, J. P. Kane, K. H. Weisgraber, M. N. Oda, K. A. Rye, H. J. Pownall, and G. Ren 2011. Morphology and structure of lipoproteins revealed by an optimized negative-staining protocol of electron microscopy. *J.Lipid Res.* 52: 175-184

80. Huang, R., R. A. Silva, W. G. Jerome, A. Kontush, M. J. Chapman, L. K. Curtiss, T. J. Hodges, and W. S. Davidson 2011. Apolipoprotein A-I structural organization in high-density lipoproteins isolated from human plasma. *Nat.Struct.Mol.Biol.* 18: 416-422

81. Chetty, P. S., D. Nguyen, M. Nickel, S. Lund-Katz, L. Mayne, S. W. Englander, and M. C. Phillips 2013. Comparison of apoA-I helical structure and stability in discoidal and spherical HDL particles by HX and mass spectrometry. *J.Lipid Res.* 54: 1589-1597

82. Pollard, R. D., B. Fulp, M. P. Samuel, M. G. Sorci-Thomas, and M. J. Thomas 2013. The conformation of lipid-free human apolipoprotein a-I in solution. *Biochemistry* 52: 9470-9481

83. Mei, X. and D. Atkinson 2011. Crystal structure of C-terminal truncated apolipoprotein A-I reveals the assembly of HDL by dimerization. *J.Biol.Chem.*

84. Segrest, J. P., M. K. Jones, A. Catte, and S. P. Thirumuruganandham 2012. Validation of previous computer models and MD simulations of discoidal HDL by a recent crystal structure of apoA-I. *J.Lipid Res.* 53: 1851-1863

85. Gursky, O. 2013. Crystal structure of Delta(185-243)ApoA-I suggests a mechanistic framework for the protein adaptation to the changing lipid load in good cholesterol: from flatland to sphereland via double belt, belt buckle, double hairpin and trefoil/tetrafoil. *J.Mol.Biol.* 425: 1-16

86. **Gursky, O., M. K. Jones, X. Mei, J. P. Segrest, and D. Atkinson 2013. Structural basis for distinct functions of the naturally occurring Cys mutants of human apolipoprotein A-I.** ***J.Lipid Res.*** **54: 3244-3257**

87. **Gursky, O., X. Mei, and D. Atkinson 2012. The crystal structure of the C-terminal truncated apolipoprotein A-I sheds new light on amyloid formation by the N-terminal fragment.** ***Biochemistry*** **51: 10-18**

88. **Bashtovyy, D., M. K. Jones, G. M. Anantharamaiah, and J. P. Segrest 2011. Sequence conservation of apolipoprotein A-I affords novel insights into HDL structure-function.** ***J.Lipid Res.*** **52: 435-450**

89. **Langmann, T., J. Klucken, M. Reil, G. Liebisch, M. F. Luciani, G. Chimini, W. E. Kaminski, and G. Schmitz 1999. Molecular cloning of the human ATP-binding cassette transporter 1 (hABC1): evidence for sterol-dependent regulation in macrophages.** ***Biochem.Biophys.Res.Commun.*** **257: 29-33**

90. **Kielar, D., W. Dietmaier, T. Langmann, C. Aslanidis, M. Probst, M. Naruszewicz, and G. Schmitz 2001. Rapid quantification of human ABCA1 mRNA in various cell types and tissues by real-time reverse transcription-PCR.** ***Clin.Chem.*** **47: 2089-2097**

91. **Dean, M., Y. Hamon, and G. Chimini 2001. The human ATP-binding cassette (ABC) transporter superfamily.** ***J.Lipid Res.*** **42: 1007-1017**

92. **Oram, J. F. and J. W. Heinecke 2005. ATP-binding cassette transporter A1: a cell cholesterol exporter that protects against cardiovascular disease.** ***Physiol Rev.*** **85: 1343-1372**

93. Nagao, K., K. Takahashi, Y. Azuma, M. Takada, Y. Kimura, M. Matsuo, N. Kioka, and K. Ueda 2012. ATP hydrolysis-dependent conformational changes in the extracellular domain of ABCA1 are associated with apoA-I binding. *J.Lipid Res.* 53: 126-136

94. Neufeld, E. B., S. J. Demosky, Jr., J. A. Stonik, C. Combs, A. T. Remaley, N. Duverger, S. Santamarina-Fojo, and H. B. Brewer, Jr. 2002. The ABCA1 transporter functions on the basolateral surface of hepatocytes. *Biochem.Biophys.Res.Commun.* 297: 974-979

95. Neufeld, E. B., A. T. Remaley, S. J. Demosky, J. A. Stonik, A. M. Cooney, M. Comly, N. K. Dwyer, M. Zhang, J. Blanchette-Mackie, S. Santamarina-Fojo, and H. B. Brewer, Jr. 2001. Cellular localization and trafficking of the human ABCA1 transporter. *J.Biol.Chem.* 276: 27584-27590

96. Chroni, A., T. Liu, M. L. Fitzgerald, M. W. Freeman, and V. I. Zannis 2004. Cross-linking and lipid efflux properties of apoA-I mutants suggest direct association between apoA-I helices and ABCA1. *Biochemistry* 43: 2126-2139

97. Fitzgerald, M. L., A. L. Morris, A. Chroni, A. J. Mendez, V. I. Zannis, and M. W. Freeman 2004. ABCA1 and amphipathic apolipoproteins form high-affinity molecular complexes required for cholesterol efflux. *J.Lipid Res.* 45: 287-294

98. Wang, N., D. L. Silver, P. Costet, and A. R. Tall 2000. Specific binding of ApoA-I, enhanced cholesterol efflux, and altered plasma membrane morphology in cells expressing ABC1. *J.Biol.Chem.* 275: 33053-33058

99. Remaley, A. T., J. A. Stonik, S. J. Demosky, E. B. Neufeld, A. V. Bocharov, T. G. Vishnyakova, T. L. Eggerman, A. P. Patterson, N. J. Duverger, S. Santamarina-Fojo, and H. B. Brewer, Jr.

2001. Apolipoprotein specificity for lipid efflux by the human ABCAI transporter. *Biochem.Biophys.Res.Commun.* 280: 818-823

100. Tang, C. K., G. H. Tang, G. H. Yi, Z. Wang, L. S. Liu, S. Wan, Z. H. Yuan, X. S. He, J. H. Yang, C. G. Ruan, and Y. Z. Yang 2004. Effect of apolipoprotein A-I on ATP binding cassette transporter A1 degradation and cholesterol efflux in THP-1 macrophage-derived foam cells. *Acta Biochim.Biophys.Sin.(Shanghai)* 36: 218-226

101. Francis, G. A., R. H. Knopp, and J. F. Oram 1995. Defective removal of cellular cholesterol and phospholipids by apolipoprotein A-I in Tangier Disease. *J.Clin.Invest* 96: 78-87

102. Delgado-Lista, J., P. Perez-Martinez, F. Perez-Jimenez, A. Garcia-Rios, F. Fuentes, C. Marin, P. Gomez-Luna, A. Camargo, L. D. Parnell, J. M. Ordovas, and J. Lopez-Miranda 2010. ABCA1 gene variants regulate postprandial lipid metabolism in healthy men. *Arterioscler.Thromb.Vasc.Biol.* 30: 1051-1057

103. Takahashi, Y. and J. D. Smith 1999. Cholesterol efflux to apolipoprotein AI involves endocytosis and resecretion in a calcium-dependent pathway. *Proc.Natl.Acad.Sci.U.S.A* 96: 11358-11363

104. Smith, J. D., C. Waelde, A. Horwitz, and P. Zheng 2002. Evaluation of the role of phosphatidylserine translocase activity in ABCA1-mediated lipid efflux. *J.Biol.Chem.* 277: 17797-17803

105. Lorenzi, I., A. von Eckardstein, C. Cavelier, S. Radosavljevic, and L. Rohrer 2008. Apolipoprotein A-I but not high-density lipoproteins are internalised by RAW macrophages: roles of ATP-binding cassette transporter A1 and scavenger receptor BI. *Journal of Molecular Medicine-Jmm* 86: 171-183

106. Cavelier, C., L. Rohrer, and A. von Eckardstein 2006. ATP-binding cassette transporter al modulates apolipoprotein A1 transcytosis through aortic endothelial cells. *Circulation Research* 99: 1060-1066

107. Ohnsorg, P. M., L. Rohrer, D. Perisa, A. Kateifides, A. Chroni, D. Kardassis, V. I. Zannis, and E. A. von 2011. Carboxyl terminus of apolipoprotein A-I (ApoA-I) is necessary for the transport of lipid-free ApoA-I but not prelipidated ApoA-I particles through aortic endothelial cells. *J.Biol.Chem.* 286: 7744-7754

108. Chroni, A., T. Liu, I. Gorshkova, H. Y. Kan, Y. Uehara, A. von Eckardstein, and V. I. Zannis 2003. The central helices of apoA-I can promote ATP-binding cassette transporter A1 (ABCA1)-mediated lipid efflux. Amino acid residues 220-231 of the wild-type apoA-I are required for lipid efflux in vitro and high density lipoprotein formation in vivo. *J.Biol.Chem.* 278: 6719-6730

109. Reardon, C. A., H. Y. Kan, V. Cabana, L. Blachowicz, J. R. Lukens, Q. Wu, K. Liadaki, G. S. Getz, and V. I. Zannis 2001. In vivo studies of HDL assembly and metabolism using adenovirus-mediated transfer of ApoA-I mutants in ApoA-I-deficient mice. *Biochemistry* 40: 13670-13680

110. Chroni, A., H. Y. Kan, K. E. Kypreos, I. N. Gorshkova, A. Shkodrani, and V. I. Zannis 2004. Substitutions of glutamate 110 and 111 in the middle helix 4 of human apolipoprotein A-I (apoA-I) by alanine affect the structure and in vitro functions of apoA-I and induce severe hypertriglyceridemia in apoA-I-deficient mice. *Biochemistry* 43: 10442-10457

111. Bodzioch, M., E. Orso, J. Klucken, T. Langmann, A. Bottcher, W. Diederich, W. Drobnik, S. Barlage, C. Buchler, M. Porsch-Ozcurumez, W. E. Kaminski, H. W. Hahmann, K. Oette, G.

Rothe, C. Aslanidis, K. J. Lackner, and G. Schmitz 1999. The gene encoding ATP-binding cassette transporter 1 is mutated in Tangier disease. *Nat.Genet.* 22: 347-351

112. Fitzgerald, M. L., A. L. Morris, J. S. Rhee, L. P. Andersson, A. J. Mendez, and M. W. Freeman 2002. Naturally occurring mutations in the largest extracellular loops of ABCA1 can disrupt its direct interaction with apolipoprotein A-I. *J.Biol.Chem.* 277: 33178-33187

113. Fitzgerald, M. L., A. J. Mendez, K. J. Moore, L. P. Andersson, H. A. Panjeton, and M. W. Freeman 2001. ATP-binding cassette transporter A1 contains an NH2-terminal signal anchor sequence that translocates the protein's first hydrophilic domain to the exoplasmic space. *J.Biol.Chem.* 276: 15137-15145

114. Ramjeesingh, M., C. Li, I. Kogan, Y. Wang, L. J. Huan, and C. E. Bear 2001. A monomer is the minimum functional unit required for channel and ATPase activity of the cystic fibrosis transmembrane conductance regulator. *Biochemistry* 40: 10700-10706

115. Trompier, D., M. Alibert, S. Davanture, Y. Hamon, M. Pierres, and G. Chimini 2006. Transition from dimers to higher oligomeric forms occurs during the ATPase cycle of the ABCA1 transporter. *J.Biol.Chem.* 281: 20283-20290

116. Nagata, K. O., C. Nakada, R. S. Kasai, A. Kusumi, and K. Ueda 2013. ABCA1 dimer-monomer interconversion during HDL generation revealed by single-molecule imaging. *Proc.Natl.Acad.Sci.U.S.A* 110: 5034-5039

117. Wang, S., K. Gulshan, G. Brubaker, S. L. Hazen, and J. D. Smith 2013. ABCA1 mediates unfolding of apolipoprotein AI N terminus on the cell surface before lipidation and release of nascent high-density lipoprotein. *Arterioscler.Thromb.Vasc.Biol.* 33: 1197-1205

118. Hozoji, M., Y. Kimura, N. Kioka, and K. Ueda 2009. Formation of two intramolecular disulfide bonds is necessary for ApoA-I-dependent cholesterol efflux mediated by ABCA1. *J.Biol.Chem.* 284: 11293-11300

119. Nagao, K., Y. Kimura, and K. Ueda 2012. Lysine residues of ABCA1 are required for the interaction with apoA-I. *Biochim.Biophys.Acta* 1821: 530-535

120. Zhao, G. J., K. Yin, Y. C. Fu, and C. K. Tang 2012. The interaction of ApoA-I and ABCA1 triggers signal transduction pathways to mediate efflux of cellular lipids. *Mol.Med.* 18: 149-158

121. Brunham, L. R., R. R. Singaraja, and M. R. Hayden 2006. Variations on a gene: rare and common variants in ABCA1 and their impact on HDL cholesterol levels and atherosclerosis. *Annu.Rev.Nutr.* 26: 105-129

122. Orso, E., C. Broccardo, W. E. Kaminski, A. Bottcher, G. Liebisch, W. Drobnik, A. Gotz, O. Chambenoit, W. Diederich, T. Langmann, T. Spruss, M. F. Luciani, G. Rothe, K. J. Lackner, G. Chimini, and G. Schmitz 2000. Transport of lipids from golgi to plasma membrane is defective in tangier disease patients and Abc1-deficient mice. *Nat.Genet.* 24: 192-196

123. Assmann, G., von Eckardstein, A., and Brewer, H. B. (2001) Familial analphalipoproteinemia: Tangier disease. In Scriver, C. R., Beaudet, A. L., Sly, W. S., and Valle, D., editors. *The Metabolic and Molecular Basis of Inherited Disease* , McGraw-Hill, New York. 2937-2960

124. Timmins, J. M., J. Y. Lee, E. Boudyguina, K. D. Kluckman, L. R. Brunham, A. Mulya, A. K. Gebre, J. M. Coutinho, P. L. Colvin, T. L. Smith, M. R. Hayden, N. Maeda, and J. S. Parks 2005. Targeted inactivation of hepatic Abca1 causes profound hypoalphalipoproteinemia and kidney hypercatabolism of apoA-I. *J.Clin.Invest* 115: 1333-1342

125. Chroni, A., G. Koukos, A. Duka, and V. I. Zannis 2007. The carboxy-terminal region of apoA-I is required for the ABCA1-dependent formation of alpha-HDL but not prebeta-HDL particles in vivo. *Biochemistry* 46: 5697-5708

126. Fotakis, P., I. Tiniakou, A. K. Kateifides, C. Gkolfinopoulou, A. Chroni, E. Stratikos, V. I. Zannis, and D. Kardassis 2013. Significance of the hydrophobic residues 225 to 230 of apoA-I for the biogenesis of HDL. *J.Lipid Res.*

127. Fotakis, P., A. Kateifides, C. Gkolfinopoulou, D. Georgiadou, M. Beck, K. Grundler, A. Chroni, E. Stratikos, D. Kardassis, and V. I. Zannis 2013. Role of the hydrophobic and charged residues in the 218 to 226 region of apoA-I in the biogenesis of HDL. *J.Lipid Res.*

128. Singaraja, R. R., L. R. Brunham, H. Visscher, J. J. Kastelein, and M. R. Hayden 2003. Efflux and atherosclerosis: the clinical and biochemical impact of variations in the ABCA1 gene. *Arterioscler.Thromb.Vasc.Biol.* 23: 1322-1332

129. Frikke-Schmidt, R., B. G. Nordestgaard, G. B. Jensen, R. Steffensen, and A. Tybjaerg-Hansen 2008. Genetic variation in ABCA1 predicts ischemic heart disease in the general population. *Arterioscler.Thromb.Vasc.Biol.* 28: 180-186

130. McNeish, J., R. J. Aiello, D. Guyot, T. Turi, C. Gabel, C. Aldinger, K. L. Hoppe, M. L. Roach, L. J. Royer, J. de Wet, C. Broccardo, G. Chimini, and O. L. Francone 2000. High density lipoprotein deficiency and foam cell accumulation in mice with targeted disruption of ATP-binding cassette transporter-1. *Proc.Natl.Acad.Sci.U.S.A* 97: 4245-4250

131. Aiello, R. J., D. Brees, P. A. Bourassa, L. Royer, S. Lindsey, T. Coskran, M. Haghpassand, and O. L. Francone 2002. Increased atherosclerosis in hyperlipidemic mice with inactivation of ABCA1 in macrophages. *Arterioscler.Thromb.Vasc.Biol.* 22: 630-637

132. Vaisman, B. L., G. Lambert, M. Amar, C. Joyce, T. Ito, R. D. Shamburek, W. J. Cain, J. Fruchart-Najib, E. D. Neufeld, A. T. Remaley, H. B. Brewer, Jr., and S. Santamarina-Fojo 2001. ABCA1 overexpression leads to hyperalphalipoproteinemia and increased biliary cholesterol excretion in transgenic mice. *J.Clin.Invest* 108: 303-309

133. Groen, A. K., V. W. Bloks, R. H. Bandsma, R. Ottenhoff, G. Chimini, and F. Kuipers 2001. Hepatobiliary cholesterol transport is not impaired in Abca1-null mice lacking HDL. *J.Clin.Invest* 108: 843-850

134. Joyce, C. W., M. J. Amar, G. Lambert, B. L. Vaisman, B. Paigen, J. Najib-Fruchart, R. F. Hoyt, Jr., E. D. Neufeld, A. T. Remaley, D. S. Fredrickson, H. B. Brewer, Jr., and S. Santamarina-Fojo 2002. The ATP binding cassette transporter A1 (ABCA1) modulates the development of aortic atherosclerosis in C57BL/6 and apoE-knockout mice. *Proc.Natl.Acad.Sci.U.S.A* 99: 407-412

135. Bi, X., X. Zhu, M. Duong, E. Y. Boudyguina, M. D. Wilson, A. K. Gebre, and J. S. Parks 2013. Liver ABCA1 deletion in LDLrKO mice does not impair macrophage reverse cholesterol transport or exacerbate atherogenesis. *Arterioscler.Thromb.Vasc.Biol.* 33: 2288-2296

136. Van Eck, M., I. S. Bos, W. E. Kaminski, E. Orso, G. Rothe, J. Twisk, A. Bottcher, E. S. Van Amersfoort, T. A. Christiansen-Weber, W. P. Fung-Leung, T. J. van Berkel, and G. Schmitz 2002. Leukocyte ABCA1 controls susceptibility to atherosclerosis and macrophage recruitment into tissues. *Proc.Natl.Acad.Sci.U.S.A* 99: 6298-6303

137. Van Eck, M., R. R. Singaraja, D. Ye, R. B. Hildebrand, E. R. James, M. R. Hayden, and T. J. van Berkel 2006. Macrophage ATP-binding cassette transporter A1 overexpression inhibits atherosclerotic lesion progression in low-density lipoprotein receptor knockout mice. *Arterioscler.Thromb.Vasc.Biol.* 26: 929-934

138. Vaisman, B. L., S. J. Demosky, J. A. Stonik, M. Ghias, C. L. Knapper, M. L. Sampson, C. Dai, S. J. Levine, and A. T. Remaley 2012. Endothelial expression of human ABCA1 in mice increases plasma HDL cholesterol and reduces diet-induced atherosclerosis. *J.Lipid Res.* 53: 158-167

139. Brunham, L. R., J. K. Kruit, J. Iqbal, C. Fievet, J. M. Timmins, T. D. Pape, B. A. Coburn, N. Bissada, B. Staels, A. K. Groen, M. M. Hussain, J. S. Parks, F. Kuipers, and M. R. Hayden 2006. Intestinal ABCA1 directly contributes to HDL biogenesis in vivo. *J.Clin.Invest* 116: 1052-1062

140. Singaraja, R. R., B. Stahmer, M. Brundert, M. Merkel, J. Heeren, N. Bissada, M. Kang, J. M. Timmins, R. Ramakrishnan, J. S. Parks, M. R. Hayden, and F. Rinninger 2006. Hepatic ATP-binding cassette transporter A1 is a key molecule in high-density lipoprotein cholesteryl ester metabolism in mice. *Arterioscler.Thromb.Vasc.Biol.* 26: 1821-1827

141. McLean, J., K. Wion, D. Drayna, C. Fielding, and R. Lawn 1986. Human lecithin-cholesterol acyltransferase gene: complete gene sequence and sites of expression. *Nucleic Acids Res.* 14: 9397-9406

142. Schindler, P. A., C. A. Settineri, X. Collet, C. J. Fielding, and A. L. Burlingame 1995. Site-specific detection and structural characterization of the glycosylation of human plasma proteins lecithin:cholesterol acyltransferase and apolipoprotein D using HPLC/electrospray mass spectrometry and sequential glycosidase digestion. *Protein Sci.* 4: 791-803

143. Warden, C. H., C. A. Langner, J. I. Gordon, B. A. Taylor, J. W. McLean, and A. J. Lusis 1989. Tissue-specific expression, developmental regulation, and chromosomal mapping of the lecithin: cholesterol acyltransferase gene. Evidence for expression in brain and testes as well as liver. *J.Biol.Chem.* 264: 21573-21581

144. Simon, J. B. and J. L. Boyer 1970. Production of lecithin: cholesterol acyltransferase by the isolated perfused rat liver. *Biochim.Biophys.Acta* 218: 549-551

145. Albers, J. J., C. H. Chen, and J. L. Adolphson 1981. Lecithin:cholesterol acyltransferase (LCAT) mass; its relationship to LCAT activity and cholesterol esterification rate. *J.Lipid Res.* 22: 1206-1213

146. Fielding, C. J., V. G. Shore, and P. E. Fielding 1972. A protein cofactor of lecithin:cholesterol acyltransferase. *Biochem.Biophys.Res.Commun.* 46: 1493-1498

147. Zannis, V. I., Chroni, A., Liu, T., Liadaki, K. N., and Laccotripe, M. (2004) New insights on the roles of apolipoprotein A-I, the ABCA1 lipid transporter, and the HDL receptor SR-BI in the biogenesis and the functions of HDL. In Simionescu, M., editor. 33-72

148. Subbaiah, P. V., J. J. Albers, C. H. Chen, and J. D. Bagdade 1980. Low density lipoprotein-activated lysolecithin acylation by human plasma lecithin-cholesterol acyltransferase. Identity of lysolecithin acyltransferase and lecithin-cholesterol acyltransferase. *J.Biol.Chem.* 255: 9275-9280

149. Zhao, Y., F. E. Thorngate, K. H. Weisgraber, D. L. Williams, and J. S. Parks 2005. Apolipoprotein E is the major physiological activator of lecithin-cholesterol acyltransferase (LCAT) on apolipoprotein B lipoproteins. *Biochemistry* 44: 1013-1025

150. Peelman, F., N. Vinaimont, A. Verhee, B. Vanloo, J. L. Verschelde, C. Labeur, S. Seguret-Mace, N. Duverger, G. Hutchinson, J. Vandekerckhove, J. Tavernier, and M. Rosseneu 1998. A proposed architecture for lecithin cholesterol acyl transferase (LCAT): identification of the catalytic triad and molecular modeling. *Protein Sci.* 7: 587-599

151. Jonas, A. (1987) Lecithin:cholesterol acyltransferase. In A.M.Gotto, editor. *Plasma Lipoproteins*, Elsevier Press, Amsterdam. 299-333

152. Peelman, F., J. L. Verschelde, B. Vanloo, C. Ampe, C. Labeur, J. Tavernier, J. Vandekerckhove, and M. Rosseneu 1999. Effects of natural mutations in lecithin:cholesterol acyltransferase on the enzyme structure and activity. *J.Lipid Res.* 40: 59-69

153. Vanloo, B., F. Peelman, K. Deschuymere, J. Taveirne, A. Verhee, C. Gouyette, C. Labeur, J. Vandekerckhove, J. Tavernier, and M. Rosseneu 2000. Relationship between structure and biochemical phenotype of lecithin:cholesterol acyltransferase (LCAT) mutants causing fish-eye disease. *J.Lipid Res.* 41: 752-761

154. Jonas, A. 2000. Lecithin cholesterol acyltransferase. *Biochim.Biophys.Acta* 1529: 245-256

155. Parks, J. S. and A. K. Gebre 1997. Long-chain polyunsaturated fatty acids in the sn-2 position of phosphatidylcholine decrease the stability of recombinant high density lipoprotein apolipoprotein A-I and the activation energy of the lecithin:cholesterol acyltransferase reaction. *J.Lipid Res.* 38: 266-275

156. Miller, K. R. and J. S. Parks 1997. Influence of vesicle surface composition on the interfacial binding of lecithin:cholesterol acyltransferase and apolipoprotein A-I. *J.Lipid Res.* 38: 1094-1102

157. Kosek, A. B., D. Durbin, and A. Jonas 1999. Binding affinity and reactivity of lecithin cholesterol acyltransferase with native lipoproteins. *Biochem.Biophys.Res.Commun.* 258: 548-551

158. Bolin, D. J. and A. Jonas 1996. Sphingomyelin inhibits the lecithin-cholesterol acyltransferase reaction with reconstituted high density lipoproteins by decreasing enzyme binding. *J.Biol.Chem.* 271: 19152-19158

159. Subbaiah, P. V., P. Horvath, and S. B. Achar 2006. Regulation of the activity and fatty acid specificity of lecithin-cholesterol acyltransferase by sphingomyelin and its metabolites, ceramide and ceramide phosphate. *Biochemistry* 45: 5029-5038

160. Kuivenhoven, J. A., H. Pritchard, J. Hill, J. Frohlich, G. Assmann, and J. Kastelein 1997. The molecular pathology of lecithin:cholesterol acyltransferase (LCAT) deficiency syndromes. *J.Lipid Res.* 38: 191-205

161. Holleboom, A. G., J. A. Kuivenhoven, F. Peelman, A. W. Schimmel, J. Peter, J. C. Defesche, J. J. Kastelein, G. K. Hovingh, E. S. Stroes, and M. M. Motazacker 2011. High prevalence of mutations in LCAT in patients with low HDL cholesterol levels in The Netherlands: identification and characterization of eight novel mutations. *Hum.Mutat.* 32: 1290-1298

162. Asztalos, B. F., E. J. Schaefer, K. V. Horvath, S. Yamashita, M. Miller, G. Franceschini, and L. Calabresi 2007. Role of LCAT in HDL remodeling: investigation of LCAT deficiency states. *J.Lipid Res.* 48: 592-599

163. Holleboom, A. G., J. A. Kuivenhoven, C. C. van Olden, J. Peter, A. W. Schimmel, J. H. Levels, R. M. Valentijn, P. Vos, J. C. Defesche, J. J. Kastelein, G. K. Hovingh, E. S. Stroes, and C. E. Hollak 2011. Proteinuria in early childhood due to familial LCAT deficiency caused by loss of a disulfide bond in lecithin:cholesterol acyl transferase. *Atherosclerosis* 216: 161-165

164. Funke, H., A. von Eckardstein, P. H. Pritchard, J. J. Albers, J. J. Kastelein, C. Droste, and G. Assmann 1991. A molecular defect causing fish eye disease: an amino acid exchange in

lecithin-cholesterol acyltransferase (LCAT) leads to the selective loss of alpha-LCAT activity. *Proc.Natl.Acad.Sci.U.S.A* 88: 4855-4859

165. Kuivenhoven, J. A., van Voorst tot Voorst EJ, H. Wiebusch, S. M. Marcovina, H. Funke, G. Assmann, P. H. Pritchard, and J. J. Kastelein 1995. A unique genetic and biochemical presentation of fish-eye disease. *J.Clin.Invest* 96: 2783-2791

166. Kuivenhoven, J. A., A. F. Stalenhoef, J. S. Hill, P. N. Demacker, A. Errami, J. J. Kastelein, and P. H. Pritchard 1996. Two novel molecular defects in the LCAT gene are associated with fish eye disease. *Arterioscler.Thromb.Vasc.Biol.* 16: 294-303

167. Ayyobi, A. F., S. H. McGladdery, S. Chan, G. B. John Mancini, J. S. Hill, and J. J. Frohlich 2004. Lecithin: cholesterol acyltransferase (LCAT) deficiency and risk of vascular disease: 25 year follow-up. *Atherosclerosis* 177: 361-366

168. Dullaart, R. P., F. Perton, W. J. Sluiter, V. R. de, and T. A. van 2008. Plasma lecithin: cholesterol acyltransferase activity is elevated in metabolic syndrome and is an independent marker of increased carotid artery intima media thickness. *J.Clin.Endocrinol.Metab* 93: 4860-4866

169. Calabresi, L., D. Baldassarre, S. Simonelli, M. Gomaraschi, M. Amato, S. Castelnuovo, B. Frigerio, A. Ravani, D. Sansaro, J. Kauhanen, R. Rauramaa, F. U. de, A. Hamsten, A. J. Smit, E. Mannarino, S. E. Humphries, P. Giral, F. Veglia, C. R. Sirtori, G. Franceschini, and E. Tremoli 2011. Plasma lecithin:cholesterol acyltransferase and carotid intima-media thickness in European individuals at high cardiovascular risk. *J.Lipid Res.* 52: 1569-1574

170. Holleboom, A. G., J. A. Kuivenhoven, M. Vergeer, G. K. Hovingh, J. N. van Miert, N. J. Wareham, J. J. Kastelein, K. T. Khaw, and S. M. Boekholdt 2010. Plasma levels of

lecithin:cholesterol acyltransferase and risk of future coronary artery disease in apparently healthy men and women: a prospective case-control analysis nested in the EPIC-Norfolk population study. *J.Lipid Res.* 51: 416-421

171. Dullaart, R. P., F. Perton, M. M. van der Klauw, H. L. Hillege, and W. J. Sluiter 2010. High plasma lecithin:cholesterol acyltransferase activity does not predict low incidence of cardiovascular events: possible attenuation of cardioprotection associated with high HDL cholesterol. *Atherosclerosis* 208: 537-542

172. Sethi, A. A., M. Sampson, R. Warnick, N. Muniz, B. Vaisman, B. G. Nordestgaard, A. Tybjaerg-Hansen, and A. T. Remaley 2010. High pre-beta1 HDL concentrations and low lecithin: cholesterol acyltransferase activities are strong positive risk markers for ischemic heart disease and independent of HDL-cholesterol. *Clin.Chem.* 56: 1128-1137

173. Duivenvoorden, R., A. G. Holleboom, B. van den Bogaard, A. J. Nederveen, G. E. De, B. A. Hutten, A. W. Schimmel, G. K. Hovingh, J. J. Kastelein, J. A. Kuivenhoven, and E. S. Stroes 2011. Carriers of lecithin cholesterol acyltransferase gene mutations have accelerated atherogenesis as assessed by carotid 3.0-T magnetic resonance imaging [corrected]. *J.Am.Coll.Cardiol.* 58: 2481-2487

174. Sakai, N., B. L. Vaisman, C. A. Koch, R. F. Hoyt, Jr., S. M. Meyn, G. D. Talley, J. A. Paiz, H. B. Brewer, Jr., and S. Santamarina-Fojo 1997. Targeted disruption of the mouse lecithin:cholesterol acyltransferase (LCAT) gene. Generation of a new animal model for human LCAT deficiency. *J.Biol.Chem.* 272: 7506-7510

175. Ng, D. S., O. L. Francone, T. M. Forte, J. Zhang, M. Haghpassand, and E. M. Rubin 1997. Disruption of the murine lecithin:cholesterol acyltransferase gene causes impairment of

adrenal lipid delivery and up-regulation of scavenger receptor class B type I. *J.Biol.Chem.* 272: 15777-15781

176. Nakamura, Y., L. Kotite, Y. Gan, T. A. Spencer, C. J. Fielding, and P. E. Fielding 2004. Molecular mechanism of reverse cholesterol transport: reaction of pre-beta-migrating high-density lipoprotein with plasma lecithin/cholesterol acyltransferase. *Biochemistry* 43: 14811-14820

177. Smith, E. B., C.Ashall, and J.E.Walker. High density lipoprotein (HDL) subfractions in interstitial fluid from human aortic intima and atherosclerostic lesions. Biochem.Soc.Trans. 12, 843-844. 1984.

Ref Type: Generic

178. Calabresi, L., E. Favari, E. Moleri, M. P. Adorni, M. Pedrelli, S. Costa, W. Jessup, I. C. Gelissen, P. T. Kovanen, F. Bernini, and G. Franceschini 2009. Functional LCAT is not required for macrophage cholesterol efflux to human serum. *Atherosclerosis* 204: 141-146

179. Calabresi, L., D. Baldassarre, S. Castelnuovo, P. Conca, L. Bocchi, C. Candini, B. Frigerio, M. Amato, C. R. Sirtori, P. Alessandrini, M. Arca, G. Boscutti, L. Cattin, L. Gesualdo, T. Sampietro, G. Vaudo, F. Veglia, S. Calandra, and G. Franceschini 2009. Functional lecithin: cholesterol acyltransferase is not required for efficient atheroprotection in humans. *Circulation* 120: 628-635

180. Holleboom, A. G., G. Daniil, X. Fu, R. Zhang, G. K. Hovingh, A. W. Schimmel, J. J. Kastelein, E. S. Stroes, J. L. Witztum, B. A. Hutten, S. Tsimikas, S. L. Hazen, A. Chroni, and J. A. Kuivenhoven 2012. Lipid oxidation in carriers of lecithin:cholesterol acyltransferase gene mutations. *Arterioscler.Thromb.Vasc.Biol.* 32: 3066-3075

181. Nishiwaki, M., K. Ikewaki, G. Bader, H. Nazih, M. Hannuksela, A. T. Remaley, R. D. Shamburek, and H. B. Brewer, Jr. 2006. Human lecithin:cholesterol acyltransferase deficiency: in vivo kinetics of low-density lipoprotein and lipoprotein-X. *Arterioscler.Thromb.Vasc.Biol.* 26: 1370-1375

182. Baass, A., H. Wassef, M. Tremblay, L. Bernier, R. Dufour, and J. Davignon 2009. Characterization of a new LCAT mutation causing familial LCAT deficiency (FLD) and the role of APOE as a modifier gene of the FLD phenotype. *Atherosclerosis* 207: 452-457

183. Lambert, G., N. Sakai, B. L. Vaisman, E. B. Neufeld, B. Marteyn, C. C. Chan, B. Paigen, E. Lupia, A. Thomas, L. J. Striker, J. Blanchette-Mackie, G. Csako, J. N. Brady, R. Costello, G. E. Striker, A. T. Remaley, H. B. Brewer, Jr., and S. Santamarina-Fojo 2001. Analysis of glomerulosclerosis and atherosclerosis in lecithin cholesterol acyltransferase-deficient mice. *J.Biol.Chem.* 276: 15090-15098

184. Vaisman, B. L., H. G. Klein, M. Rouis, A. M. Berard, M. R. Kindt, G. D. Talley, S. M. Meyn, R. F. Hoyt, Jr., S. M. Marcovina, J. J. Albers, and . 1995. Overexpression of human lecithin cholesterol acyltransferase leads to hyperalphalipoproteinemia in transgenic mice. *J.Biol.Chem.* 270: 12269-12275

185. Francone, O. L., E. L. Gong, D. S. Ng, C. J. Fielding, and E. M. Rubin 1995. Expression of human lecithin-cholesterol acyltransferase in transgenic mice. Effect of human apolipoprotein AI and human apolipoprotein all on plasma lipoprotein cholesterol metabolism. *J.Clin.Invest* 96: 1440-1448

186. Hoeg, J. M., B. L. Vaisman, S. J. Demosky, Jr., S. M. Meyn, G. D. Talley, R. F. Hoyt, Jr., S. Feldman, A. M. Berard, N. Sakai, D. Wood, M. E. Brousseau, S. Marcovina, H. B. Brewer, Jr., and S. Santamarina-Fojo 1996. Lecithin:cholesterol acyltransferase overexpression

generates hyperalpha-lipoproteinemia and a nonatherogenic lipoprotein pattern in transgenic rabbits. *J.Biol.Chem.* 271: 4396-4402

187. Brousseau, M. E., S. Santamarina-Fojo, B. L. Vaisman, D. Applebaum-Bowden, A. M. Berard, G. D. Talley, H. B. Brewer, Jr., and J. M. Hoeg 1997. Overexpression of human lecithin:cholesterol acyltransferase in cholesterol-fed rabbits: LDL metabolism and HDL metabolism are affected in a gene dose-dependent manner. *J.Lipid Res.* 38: 2537-2547

188. Furbee, J. W., Jr., J. K. Sawyer, and J. S. Parks 2002. Lecithin:cholesterol acyltransferase deficiency increases atherosclerosis in the low density lipoprotein receptor and apolipoprotein E knockout mice. *J.Biol.Chem.* 277: 3511-3519

189. Mehlum, A., M. Muri, T. A. Hagve, L. A. Solberg, and H. Prydz 1997. Mice overexpressing human lecithin: cholesterol acyltransferase are not protected against diet-induced atherosclerosis. *APMIS* 105: 861-868

190. Berard, A. M., B. Foger, A. Remaley, R. Shamburek, B. L. Vaisman, G. Talley, B. Paigen, R. F. Hoyt, Jr., S. Marcovina, H. B. Brewer, Jr., and S. Santamarina-Fojo 1997. High plasma HDL concentrations associated with enhanced atherosclerosis in transgenic mice overexpressing lecithin-cholesteryl acyltransferase. *Nat.Med.* 3: 744-749

191. Furbee, J. W., Jr. and J. S. Parks 2002. Transgenic overexpression of human lecithin: cholesterol acyltransferase (LCAT) in mice does not increase aortic cholesterol deposition. *Atherosclerosis* 165: 89-100

192. Hoeg, J. M., S. Santamarina-Fojo, A. M. Berard, J. F. Cornhill, E. E. Herderick, S. H. Feldman, C. C. Haudenschild, B. L. Vaisman, R. F. Hoyt, Jr., S. J. Demosky, Jr., R. D. Kauffman, C. M. Hazel, S. M. Marcovina, and H. B. Brewer, Jr. 1996. Overexpression of lecithin:cholesterol

acyltransferase in transgenic rabbits prevents diet-induced atherosclerosis. ***Proc.Natl.Acad.Sci.U.S.A*** **93: 11448-11453**

193. Brousseau, M. E., R. D. Kauffman, E. E. Herderick, S. J. Demosky, Jr., W. Evans, S. Marcovina, S. Santamarina-Fojo, H. B. Brewer, Jr., and J. M. Hoeg 2000. LCAT modulates atherogenic plasma lipoproteins and the extent of atherosclerosis only in the presence of normal LDL receptors in transgenic rabbits. ***Arterioscler.Thromb.Vasc.Biol.*** **20: 450-458**

194. Amar, M. J., R. D. Shamburek, B. Vaisman, C. L. Knapper, B. Foger, R. F. Hoyt, Jr., S. Santamarina-Fojo, H. B. Brewer, Jr., and A. T. Remaley 2009. Adenoviral expression of human lecithin-cholesterol acyltransferase in nonhuman primates leads to an antiatherogenic lipoprotein phenotype by increasing high-density lipoprotein and lowering low-density lipoprotein. ***Metabolism*** **58: 568-575**

195. Foger, B., M. Chase, M. J. Amar, B. L. Vaisman, R. D. Shamburek, B. Paigen, J. Fruchart-Najib, J. A. Paiz, C. A. Koch, R. F. Hoyt, H. B. Brewer, Jr., and S. Santamarina-Fojo 1999. Cholesteryl ester transfer protein corrects dysfunctional high density lipoproteins and reduces aortic atherosclerosis in lecithin cholesterol acyltransferase transgenic mice. ***J.Biol.Chem.*** **274: 36912-36920**

196. Lynn, E. G., Y. L. Siow, J. Frohlich, G. T. Cheung, and O K 2001. Lipoprotein-X stimulates monocyte chemoattractant protein-1 expression in mesangial cells via nuclear factor-kappa B. ***Kidney Int.*** **60: 520-532**

197. Rousset, X., B. Vaisman, B. Auerbach, B. R. Krause, R. Homan, J. Stonik, G. Csako, R. Shamburek, and A. T. Remaley 2010. Effect of recombinant human lecithin cholesterol acyltransferase infusion on lipoprotein metabolism in mice. ***J.Pharmacol.Exp.Ther.*** **335: 140-148**

198. Chen, Z., D. Chu, J. M. Castro-Perez, W. Ni, A. Zhang, M. L. Krsmanovic, D. Xie, V. Shah, S. J. Stout, D. G. McLaren, A. C. Stefanni, S. H. Lee, T. P. Roddy, A. S. Plump, B. K. Hubbard, T. F. Vogt, and H. H. Zhou 2011. AAV8-mediated long-term expression of human LCAT significantly improves lipid profiles in hCETP;Ldlr(+/-) mice. *J.Cardiovasc.Transl.Res.* 4: 801-810

199. Van, C. E., J. Lievens, F. Jacobs, Y. Feng, J. Snoeys, and G. B. De 2009. Apolipoprotein A-I and lecithin:cholesterol acyltransferase transfer induce cholesterol unloading in complex atherosclerotic lesions. *Gene Ther.* 16: 757-765

200. Chen, Z., S. P. Wang, M. L. Krsmanovic, J. Castro-Perez, K. Gagen, V. Mendoza, R. Rosa, V. Shah, T. He, S. J. Stout, N. S. Geoghagen, S. H. Lee, D. G. McLaren, L. Wang, T. P. Roddy, A. S. Plump, B. K. Hubbard, C. J. Sinz, and D. G. Johns 2012. Small molecule activation of lecithin cholesterol acyltransferase modulates lipoprotein metabolism in mice and hamsters. *Metabolism* 61: 470-481

201. Alphacore Pharma LLC. Effect of ACP-501 on Safety, Tolerability, Pharmacokinetics and Pharmacodynamics in Subjects With Coronary Artery Disease. 2014.

Ref Type: Online Source

202. Fielding, C. J. and P. E. Fielding 1995. Molecular physiology of reverse cholesterol transport. *J.Lipid Res.* 36: 211-228

203. Wang, J., J. A. DeLozier, A. K. Gebre, P. J. Dolphin, and J. S. Parks 1998. Role of glutamic acid residues 154, 155, and 165 of lecithin:cholesterol acyltransferase in cholesterol esterification and phospholipase A2 activities. *J.Lipid Res.* 39: 51-58

204. Peelman, F., M. Goethals, B. Vanloo, C. Labeur, R. Brasseur, J. Vandekerckhove, and M. Rosseneu 1997. Structural and functional properties of the 154-171 wild-type and variant peptides of human lecithin-cholesterol acyltransferase. *Eur.J.Biochem.* 249: 708-715

205. Nobecourt, E., M. J. Davies, B. E. Brown, L. K. Curtiss, D. J. Bonnet, F. Charlton, A. S. Januszewski, A. J. Jenkins, P. J. Barter, and K. A. Rye 2007. The impact of glycation on apolipoprotein A-I structure and its ability to activate lecithin:cholesterol acyltransferase. *Diabetologia* 50: 643-653

206. Jones, M. K., A. Catte, L. Li, and J. P. Segrest 2009. Dynamics of activation of lecithin:cholesterol acyltransferase by apolipoprotein A-I. *Biochemistry* 48: 11196-11210

207. Zannis, V. I., A. Chroni, and M. Krieger 2006. Role of apoA-I, ABCA1, LCAT, and SR-BI in the biogenesis of HDL. *J.Mol.Med.* 84: 276-294

208. Miettinen, H. E., M. Jauhiainen, H. Gylling, S. Ehnholm, A. Palomaki, T. A. Miettinen, and K. Kontula 1997. Apolipoprotein A-IFIN (Leu159-->Arg) mutation affects lecithin cholesterol acyltransferase activation and subclass distribution of HDL but not cholesterol efflux from fibroblasts. *Arterioscler.Thromb.Vasc.Biol.* 17: 3021-3032

209. Yamakawa-Kobayashi, K., H. Yanagi, H. Fukayama, C. Hirano, Y. Shimakura, N. Yamamoto, T. Arinami, S. Tsuchiya, and H. Hamaguchi 1999. Frequent occurrence of hypoalphalipoproteinemia due to mutant apolipoprotein A-I gene in the population: a population-based survey. *Hum.Mol.Genet.* 8: 331-336

210. Huang, W., J. Sasaki, A. Matsunaga, H. Nanimatsu, K. Moriyama, H. Han, M. Kugi, T. Koga, K. Yamaguchi, and K. Arakawa 1998. A novel homozygous missense mutation in the apo A-I gene with apo A-I deficiency. *Arterioscler.Thromb.Vasc.Biol.* 18: 389-396

211. Miller, M., D. Aiello, H. Pritchard, G. Friel, and K. Zeller 1998. Apolipoprotein A-I(Zavalla) (Leu159-->Pro): HDL cholesterol deficiency in a kindred associated with premature coronary artery disease. *Arterioscler.Thromb.Vasc.Biol.* 18: 1242-1247

212. Miccoli, R., A. Bertolotto, R. Navalesi, L. Odoguardi, A. Boni, J. Wessling, H. Funke, H. Wiebusch, A. Eckardstein, and G. Assmann 1996. Compound heterozygosity for a structural apolipoprotein A-I variant, apo A-I(L141R)Pisa, and an apolipoprotein A-I null allele in patients with absence of HDL cholesterol, corneal opacifications, and coronary heart disease. *Circulation* 94: 1622-1628

213. Miccoli, R., Y. Zhu, U. Daum, J. Wessling, Y. Huang, R. Navalesi, G. Assmann, and A. von Eckardstein 1997. A natural apolipoprotein A-I variant, apoA-I (L141R)Pisa, interferes with the formation of alpha-high density lipoproteins (HDL) but not with the formation of pre beta 1-HDL and influences efflux of cholesterol into plasma. *Journal of Lipid Research* 38: 1242

214. Pisciotta, L., R. Miccoli, A. Cantafora, L. Calabresi, P. Tarugi, P. Alessandrini, B. G. Bittolo, G. Franceschini, C. Cortese, S. Calandra, and S. Bertolini 2003. Recurrent mutations of the apolipoprotein A-I gene in three kindreds with severe HDL deficiency. *Atherosclerosis* 167: 335-345

215. Miettinen, H. E., H. Gylling, T. A. Miettinen, J. Viikari, L. Paulin, and K. Kontula 1997. Apolipoprotein A-IFin. Dominantly inherited hypoalphalipoproteinemia due to a single base substitution in the apolipoprotein A-I gene. *Arterioscler.Thromb.Vasc.Biol.* 17: 83-90

216. McManus, D. C., B. R. Scott, V. Franklin, D. L. Sparks, and Y. L. Marcel 2001. Proteolytic degradation and impaired secretion of an apolipoprotein A-I mutant associated with dominantly inherited hypoalphalipoproteinemia. *J.Biol.Chem.* 276: 21292-21302

217. Koukos, G., A. Chroni, A. Duka, D. Kardassis, and V. I. Zannis 2007. LCAT can rescue the abnormal phenotype produced by the natural ApoA-I mutations (Leu141Arg)Pisa and (Leu159Arg)FIN. *Biochemistry* 46: 10713-10721

218. Leren, T. P., K. S. Bakken, U. Daum, L. Ose, K. Berg, G. Assmann, and A. von Eckardstein 1997. Heterozygosity for apolipoprotein A-I(R160L)Oslo is associated with low levels of high density lipoprotein cholesterol and HDL-subclass LpA-I/A- II but normal levels of HDL-subclass LpA-I. *J.Lipid Res.* 38: 121-131

219. Koukos, G., A. Chroni, A. Duka, D. Kardassis, and V. I. Zannis 2007. Naturally occurring and bioengineered apoA-I mutations that inhibit the conversion of discoidal to spherical HDL: the abnormal HDL phenotypes can be corrected by treatment with LCAT. *Biochem.J.* 406: 167-174

220. Chroni, A., A. Duka, H. Y. Kan, T. Liu, and V. I. Zannis 2005. Point mutations in apolipoprotein a-I mimic the phenotype observed in patients with classical lecithin:cholesterol acyltransferase deficiency. *Biochemistry* 44: 14353-14366

221. Roosbeek, S., B. Vanloo, N. Duverger, H. Caster, J. Breyne, B. De, I, H. Patel, J. Vandekerckhove, C. Shoulders, M. Rosseneu, and F. Peelman 2001. Three arginine residues in apolipoprotein A-I are critical for activation of lecithin:cholesterol acyltransferase. *J.Lipid Res.* 42: 31-40

222. Zannis, V. I., A. M. Lees, R. S. Lees, and J. L. Breslow 1982. Abnormal apoprotein A-I isoprotein composition in patients with Tangier disease. *J.Biol.Chem.* 257: 4978-4986

223. Kozyraki, R., J. Fyfe, M. Kristiansen, C. Gerdes, C. Jacobsen, S. Cui, E. I. Christensen, M. Aminoff, C. A. de la, R. Krahe, P. J. Verroust, and S. K. Moestrup 1999. The intrinsic factor-

vitamin B12 receptor, cubilin, is a high-affinity apolipoprotein A-I receptor facilitating endocytosis of high-density lipoprotein. *Nat.Med.* 5: 656-661

224. Hammad, S. M., S. Stefansson, W. O. Twal, C. J. Drake, P. Fleming, A. Remaley, H. B. Brewer, Jr., and W. S. Argraves 1999. Cubilin, the endocytic receptor for intrinsic factor-vitamin B(12) complex, mediates high-density lipoprotein holoparticle endocytosis. *Proc.Natl.Acad.Sci.U.S.A* 96: 10158-10163

225. Scott, B. R., D. C. McManus, V. Franklin, A. G. McKenzie, T. Neville, D. L. Sparks, and Y. L. Marcel 2001. The N-terminal globular domain and the first class A amphipathic helix of apolipoprotein A-I are important for lecithin:cholesterol acyltransferase activation and the maturation of high density lipoprotein in vivo. *J.Biol.Chem.* 276: 48716-48724

226. Chroni, A., H. Y. Kan, A. Shkodrani, T. Liu, and V. I. Zannis 2005. Deletions of helices 2 and 3 of human apoA-I are associated with severe dyslipidemia following adenovirus-mediated gene transfer in apoA-I-deficient mice. *Biochemistry* 44: 4108-4117

227. Kateifides, A. K., I. N. Gorshkova, A. Duka, A. Chroni, D. Kardassis, and V. I. Zannis 2011. Alteration of negatively charged residues in the 89 to 99 domain of apoA-I affects lipid homeostasis and maturation of HDL. *J.Lipid Res.* 52: 1363-1372

228. Gorshkova, I. N. and D. Atkinson 2011. Enhanced Binding of Apolipoprotein A-I Variants Associated with Hypertriglyceridemia to Triglyceride-Rich Particles. *Biochemistry*

229. Gursky, O. 2013. Crystal structure of Delta(185-243)ApoA-I suggests a mechanistic framework for the protein adaptation to the changing lipid load in good cholesterol: from flatland to sphereland via double belt, belt buckle, double hairpin and trefoil/tetrafoil. *J.Mol.Biol.* 425: 1-16

230. Shore, V. G., B. Shore, and R. G. Hart 1974. Changes in apolipoproteins and properties of rabbit very low density lipoproteins on induction of cholesteremia. *Biochemistry* 13: 1579-1585

231. Kypreos, K. E. and V. I. Zannis 2006. LDL receptor deficiency or apoE mutations prevent remnant clearance and induce hypertriglyceridemia in mice. *J.Lipid Res.* 47: 521-529

232. Schaefer, E. J., R. E. Gregg, G. Ghiselli, T. M. Forte, J. M. Ordovas, L. A. Zech, and H. B. Brewer, Jr. 1986. Familial apolipoprotein E deficiency. *J.Clin.Invest* 78: 1206-1219

233. Plump, A. S., J. D. Smith, T. Hayek, K. Aalto-Setala, A. Walsh, J. G. Verstuyft, E. M. Rubin, and J. L. Breslow 1992. Severe hypercholesterolemia and atherosclerosis in apolipoprotein E-deficient mice created by homologous recombination in ES cells. *Cell* 71: 343-353

234. Rall, S. C., Jr., K. H. Weisgraber, and R. W. Mahley 1982. Human apolipoprotein E. The complete amino acid sequence. *J.Biol.Chem.* 257: 4171-4178

235. Zannis, V. I., J. L. Breslow, G. Utermann, R. W. Mahley, K. H. Weisgraber, R. J. Havel, J. L. Goldstein, M. S. Brown, G. Schonfeld, W. R. Hazzard, and C. Blum 1982. Proposed nomenclature of apoE isoproteins, apoE genotypes, and phenotypes. *J.Lipid Res.* 23: 911-914

236. Zannis, V. I. and J. L. Breslow 1981. Human very low density lipoprotein apolipoprotein E isoprotein polymorphism is explained by genetic variation and posttranslational modification. *Biochemistry* 20: 1033-1041

237. Ordovas, J. M., L. Litwack-Klein, P. W. Wilson, M. M. Schaefer, and E. J. Schaefer 1987. Apolipoprotein E isoform phenotyping methodology and population frequency with identification of apoE1 and apoE5 isoforms. *J.Lipid Res.* 28: 371-380

238. Mahley, R. W. and Rall, S. C., Jr. (2001) Type III hyperlipoproteinemia (dysbetalipoproteinemia): The role of apolipoprotein E in normal and abnormal lipoprotein metabolism. In Scriver, C. R., Beaudet, A. L., Valle, D., and Sly, W. S., editors. *The Metabolic & Molecular Bases of Inherited Disease*, McGraw-Hill, New York. 2835-2862

239. Roses, A. D. 1996. Apolipoprotein E alleles as risk factors in Alzheimer's disease. *Annu.Rev.Med.* 47: 387-400

240. Aggerbeck, L. P., J. R. Wetterau, K. H. Weisgraber, C. S. Wu, and F. T. Lindgren 1988. Human apolipoprotein E3 in aqueous solution. II. Properties of the amino- and carboxyl-terminal domains. *J.Biol.Chem.* 263: 6249-6258

241. Wilson, C., M. R. Wardell, K. H. Weisgraber, R. W. Mahley, and D. A. Agard 1991. Three-dimensional structure of the LDL receptor-binding domain of human apolipoprotein E. *Science* 252: 1817-1822

242. Mahley, R. W. and S. C. Rall, Jr. 2000. Apolipoprotein E: far more than a lipid transport protein. *Annu.Rev.Genomics Hum.Genet.* 1: 507-537

243. Morrow, J. A., K. S. Arnold, J. Dong, M. E. Balestra, T. L. Innerarity, and K. H. Weisgraber 2000. Effect of arginine 172 on the binding of apolipoprotein E to the low density lipoprotein receptor. *J.Biol.Chem.* 275: 2576-2580

244. Weisgraber, K. H. 1994. Apolipoprotein E: structure-function relationships. *Adv.Protein Chem.* 45: 249-302

245. Westerlund, J. A. and K. H. Weisgraber 1993. Discrete carboxyl-terminal segments of apolipoprotein E mediate lipoprotein association and protein oligomerization. *J.Biol.Chem.* 268: 15745-15750

246. Peters-Libeu, C. A., Y. Newhouse, D. M. Hatters, and K. H. Weisgraber 2006. Model of biologically active apolipoprotein E bound to dipalmitoylphosphatidylcholine. *J.Biol.Chem.* 281: 1073-1079

247. Breslow, J. L., V. I. Zannis, T. R. SanGiacomo, J. L. Third, T. Tracy, and C. J. Glueck 1982. Studies of familial type III hyperlipoproteinemia using as a genetic marker the apoE phenotype E2/2. *J.Lipid Res.* 23: 1224-1235

248. Havel, R. J., L. Kotite, J. L. Vigne, J. P. Kane, P. Tun, N. Phillips, and G. C. Chen 1980. Radioimmunoassay of human arginine-rich apolipoprotein, apoprotein E. Concentration in blood plasma and lipoproteins as affected by apoprotein E-3 deficiency. *J.Clin.Invest* 66: 1351-1362

249. Havel, R. J. and J. P. Kane 1973. Primary dysbetalipoproteinemia: predominance of a specific apoprotein species in triglyceride-rich lipoproteins. *Proc.Natl.Acad.Sci.U.S.A* 70: 2015-2019

250. Lalazar, A. and R. W. Mahley 1989. Human apolipoprotein E. Receptor binding activity of truncated variants with carboxyl-terminal deletions. *J.Biol.Chem.* 264: 8447-8450

251. Lalazar, A., K. H. Weisgraber, S. C. Rall, Jr., H. Giladi, T. L. Innerarity, A. Z. Levanon, J. K. Boyles, B. Amit, M. Gorecki, R. W. Mahley, and T. Vogel 1988. Site-specific mutagenesis of human apolipoprotein E. Receptor binding activity of variants with single amino acid substitutions. *J.Biol.Chem.* 263: 3542-3545

252. Rall, S. C., Jr. and R. W. Mahley 1992. The role of apolipoprotein E genetic variants in lipoprotein disorders. *J.Intern Med.* 231: 653-659

253. Chappell, D. A. 1989. High receptor binding affinity of lipoproteins in atypical dysbetalipoproteinemia (type III hyperlipoproteinemia). *J.Clin.Invest* 84: 1906-1915

254. Hui, D. Y., T. L. Innerarity, and R. W. Mahley 1984. Defective hepatic lipoprotein receptor binding of beta-very low density lipoproteins from type III hyperlipoproteinemic patients. Importance of apolipoprotein E. *J.Biol.Chem.* 259: 860-869

255. Steinmetz, A., C. Jakobs, S. Motzny, and H. Kaffarnik 1989. Differential distribution of apolipoprotein E isoforms in human plasma lipoproteins. *Arteriosclerosis* 9: 405-411

256. Weisgraber, K. H. 1990. Apolipoprotein E distribution among human plasma lipoproteins: role of the cysteine-arginine interchange at residue 112. *J.Lipid Res.* 31: 1503-1511

257. Ji, Z. S., S. Fazio, and R. W. Mahley 1994. Variable heparan sulfate proteoglycan binding of apolipoprotein E variants may modulate the expression of type III hyperlipoproteinemia. *J.Biol.Chem.* 269: 13421-13428

258. Ghiselli, G., E. J. Schaefer, P. Gascon, and H. B. Breser, Jr. 1981. Type III hyperlipoproteinemia associated with apolipoprotein E deficiency. *Science* 214: 1239-1241

259. Huang, Y., X. Q. Liu, S. C. Rall, Jr., J. M. Taylor, A. von Eckardstein, G. Assmann, and R. W. Mahley 1998. Overexpression and accumulation of apolipoprotein E as a cause of hypertriglyceridemia. *J.Biol.Chem.* 273: 26388-26393

260. Jong, M. C., V. E. Dahlmans, M. H. Hofker, and L. M. Havekes 1997. Nascent very-low-density lipoprotein triacylglycerol hydrolysis by lipoprotein lipase is inhibited by apolipoprotein E in a dose-dependent manner. *Biochem.J.* 328 (Pt 3): 745-750

261. Rensen, P. C. and T. J. van Berkel 1996. Apolipoprotein E effectively inhibits lipoprotein lipase-mediated lipolysis of chylomicron-like triglyceride-rich lipid emulsions in vitro and in vivo. *J.Biol.Chem.* 271: 14791-14799

262. Mensenkamp, A. R., M. C. Jong, G. H. van, M. J. van Luyn, V. Bloks, R. Havinga, P. J. Voshol, M. H. Hofker, K. W. Van Dijk, L. M. Havekes, and F. Kuipers 1999. Apolipoprotein E participates in the regulation of very low density lipoprotein-triglyceride secretion by the liver. *J.Biol.Chem.* 274: 35711-35718

263. Kypreos, K. E., P. Morani, K. W. Van Dijk, L. M. Havekes, and V. I. Zannis 2001. The amino-terminal 1-185 domain of apoE promotes the clearance of lipoprotein remnants in vivo. The carboxy-terminal domain is required for induction of hyperlipidemia in normal and apoE-deficient mice. *Biochemistry* 40: 6027-6035

264. Kypreos, K. E., X. Li, K. W. Van Dijk, L. M. Havekes, and V. I. Zannis 2003. Molecular mechanisms of type III hyperlipoproteinemia: The contribution of the carboxy-terminal domain of ApoE can account for the dyslipidemia that is associated with the E2/E2 phenotype. *Biochemistry* 42: 9841-9853

265. Kypreos, K. E., K. W. Van Dijk, L. M. Havekes, and V. I. Zannis 2005. Generation of a recombinant apolipoprotein E variant with improved biological functions: hydrophobic residues (LEU-261, TRP-264, PHE-265, LEU-268, VAL-269) of apoE can account for the apoE-induced hypertriglyceridemia. *J.Biol.Chem.* 280: 6276-6284

266. Drosatos, K., K. E. Kypreos, and V. I. Zannis 2007. Residues Leu261, Trp264, and Phe265 account for apolipoprotein E-induced dyslipidemia and affect the formation of apolipoprotein E-containing high-density lipoprotein. *Biochemistry* 46: 9645-9653

267. Rosenfeld, M. E., P. Polinsky, R. Virmani, K. Kauser, G. Rubanyi, and S. M. Schwartz 2000. Advanced atherosclerotic lesions in the innominate artery of the ApoE knockout mouse. *Arterioscler.Thromb.Vasc.Biol.* 20: 2587-2592

268. Mahley, R. W., Y. Huang, and S. C. Rall, Jr. 1999. Pathogenesis of type III hyperlipoproteinemia (dysbetalipoproteinemia). Questions, quandaries, and paradoxes. *J.Lipid Res.* 40: 1933-1949

269. Tsukamoto, K., R. Tangirala, S. H. Chun, E. Pure, and D. J. Rader 1999. Rapid regression of atherosclerosis induced by liver-directed gene transfer of ApoE in ApoE-deficient mice. *Arterioscler.Thromb.Vasc.Biol.* 19: 2162-2170

270. Desurmont, C., J. M. Caillaud, F. Emmanuel, P. Benoit, J. C. Fruchart, G. Castro, D. Branellec, J. M. Heard, and N. Duverger 2000. Complete atherosclerosis regression after human ApoE gene transfer in ApoE-deficient/nude mice. *Arterioscler.Thromb.Vasc.Biol.* 20: 435-442

271. Kim, I. H., A. Jozkowicz, P. A. Piedra, K. Oka, and L. Chan 2001. Lifetime correction of genetic deficiency in mice with a single injection of helper-dependent adenoviral vector. *Proc.Natl.Acad.Sci.U.S.A* 98: 13282-13287

272. Shimano, H., N. Yamada, M. Katsuki, M. Shimada, T. Gotoda, K. Harada, T. Murase, C. Fukazawa, F. Takaku, and Y. Yazaki 1992. Overexpression of apolipoprotein E in transgenic mice: marked reduction in plasma lipoproteins except high density lipoprotein and resistance against diet-induced hypercholesterolemia. *Proc.Natl.Acad.Sci.U.S.A* 89: 1750-1754

273. Bellosta, S., R. W. Mahley, D. A. Sanan, J. Murata, D. L. Newland, J. M. Taylor, and R. E. Pitas 1995. Macrophage-specific expression of human apolipoprotein E reduces atherosclerosis in hypercholesterolemic apolipoprotein E-null mice. *J.Clin.Invest* 96: 2170-2179

274. Fazio, S., V. R. Babaev, A. B. Murray, A. H. Hasty, K. J. Carter, L. A. Gleaves, J. B. Atkinson, and M. F. Linton 1997. Increased atherosclerosis in mice reconstituted with apolipoprotein E null macrophages. *Proc.Natl.Acad.Sci.U.S.A* 94: 4647-4652

275. Linton, M. F. and S. Fazio 1999. Macrophages, lipoprotein metabolism, and atherosclerosis: insights from murine bone marrow transplantation studies. *Curr Opin Lipidol.* 10: 97-105

276. Van Eck, M., N. Herijgers, M. Vidgeon-Hart, N. J. Pearce, P. M. Hoogerbrugge, P. H. Groot, and T. J. van Berkel 2000. Accelerated atherosclerosis in C57Bl/6 mice transplanted with ApoE-deficient bone marrow. *Atherosclerosis* 150: 71-80

277. Corder, E. H., A. M. Saunders, W. J. Strittmatter, D. E. Schmechel, P. C. Gaskell, G. W. Small, A. D. Roses, J. L. Haines, and M. A. Pericak-Vance 1993. Gene dose of apolipoprotein E type 4 allele and the risk of Alzheimer's disease in late onset families. *Science* 261: 921-923

278. Burns, M. P., W. J. Noble, V. Olm, K. Gaynor, E. Casey, J. LaFrancois, L. Wang, and K. Duff 2003. Co-localization of cholesterol, apolipoprotein E and fibrillar Abeta in amyloid plaques. *Brain Res.Mol.Brain Res.* 110: 119-125

279. Aleshkov, S., C. R. Abraham, and V. I. Zannis 1997. Interaction of nascent ApoE2, ApoE3, and ApoE4 isoforms expressed in mammalian cells with amyloid peptide beta (1-40). Relevance to Alzheimer's disease. *Biochemistry* 36: 10571-10580

280. Youmans, K. L., L. M. Tai, E. Nwabuisi-Heath, L. Jungbauer, T. Kanekiyo, M. Gan, J. Kim, W. A. Eimer, S. Estus, G. W. Rebeck, E. J. Weeber, G. Bu, C. Yu, and M. J. LaDu 2012. APOE4-specific changes in Abeta accumulation in a new transgenic mouse model of Alzheimer disease. *J.Biol.Chem.* 287: 41774-41786

281. Tai, L. M., T. Bilousova, L. Jungbauer, S. K. Roeske, K. L. Youmans, C. Yu, W. W. Poon, L. B. Cornwell, C. A. Miller, H. V. Vinters, L. J. Van Eldik, D. W. Fardo, S. Estus, G. Bu, K. H. Gylys, and M. J. LaDu 2013. Levels of soluble apolipoprotein E/amyloid-beta (Abeta) complex are reduced and oligomeric Abeta increased with APOE4 and Alzheimer disease in a transgenic mouse model and human samples. *J.Biol.Chem.* 288: 5914-5926

282. Hudry, E., J. Dashkoff, A. D. Roe, S. Takeda, R. M. Koffie, T. Hashimoto, M. Scheel, T. Spires-Jones, M. Arbel-Ornath, R. Betensky, B. L. Davidson, and B. T. Hyman 2013. Gene transfer of human Apoe isoforms results in differential modulation of amyloid deposition and neurotoxicity in mouse brain. *Sci.Transl.Med.* 5: 212ra161

283. Li, J., T. Kanekiyo, M. Shinohara, Y. Zhang, M. J. LaDu, H. Xu, and G. Bu 2012. Differential regulation of amyloid-beta endocytic trafficking and lysosomal degradation by apolipoprotein E isoforms. *J.Biol.Chem.* 287: 44593-44601

284. Zhu, Y., E. Nwabuisi-Heath, S. B. Dumanis, L. M. Tai, C. Yu, G. W. Rebeck, and M. J. LaDu 2012. APOE genotype alters glial activation and loss of synaptic markers in mice. *Glia* 60: 559-569

285. Bales, K. R., T. Verina, D. J. Cummins, Y. Du, R. C. Dodel, J. Saura, C. E. Fishman, C. A. DeLong, P. Piccardo, V. Petegnief, B. Ghetti, and S. M. Paul 1999. Apolipoprotein E is essential for amyloid deposition in the APP(V717F) transgenic mouse model of Alzheimer's disease. *Proc.Natl.Acad.Sci.U.S.A* 96: 15233-15238

286. Miao, J., M. P. Vitek, F. Xu, M. L. Previti, J. Davis, and W. E. Van Nostrand 2005. Reducing cerebral microvascular amyloid-beta protein deposition diminishes regional neuroinflammation in vasculotropic mutant amyloid precursor protein transgenic mice. *J.Neurosci.* 25: 6271-6277

287. Bales, K. R., T. Verina, R. C. Dodel, Y. Du, L. Altstiel, M. Bender, P. Hyslop, E. M. Johnstone, S. P. Little, D. J. Cummins, P. Piccardo, B. Ghetti, and S. M. Paul 1997. Lack of apolipoprotein E dramatically reduces amyloid beta-peptide deposition. *Nat.Genet.* 17: 263-264

288. Fagan, A. M., M. Watson, M. Parsadanian, K. R. Bales, S. M. Paul, and D. M. Holtzman 2002. Human and murine ApoE markedly alters A beta metabolism before and after plaque formation in a mouse model of Alzheimer's disease. *Neurobiol.Dis.* 9: 305-318

289. Koldamova, R., M. Staufenbiel, and I. Lefterov 2005. Lack of ABCA1 considerably decreases brain ApoE level and increases amyloid deposition in APP23 mice. *J.Biol.Chem.* 280: 43224-43235

290. Wahrle, S. E., H. Jiang, M. Parsadanian, R. E. Hartman, K. R. Bales, S. M. Paul, and D. M. Holtzman 2005. Deletion of Abca1 increases Abeta deposition in the PDAPP transgenic mouse model of Alzheimer disease. *J.Biol.Chem.* 280: 43236-43242

291. Hirsch-Reinshagen, V., L. F. Maia, B. L. Burgess, J. F. Blain, K. E. Naus, S. A. McIsaac, P. F. Parkinson, J. Y. Chan, G. H. Tansley, M. R. Hayden, J. Poirier, W. Van Nostrand, and C. L. Wellington 2005. The absence of ABCA1 decreases soluble ApoE levels but does not diminish amyloid deposition in two murine models of Alzheimer disease. *J.Biol.Chem.* 280: 43243-43256

292. Atwood, C. S., R. N. Martins, M. A. Smith, and G. Perry 2002. Senile plaque composition and posttranslational modification of amyloid-beta peptide and associated proteins. *Peptides* 23: 1343-1350

293. Koistinaho, M., S. Lin, X. Wu, M. Esterman, D. Koger, J. Hanson, R. Higgs, F. Liu, S. Malkani, K. R. Bales, and S. M. Paul 2004. Apolipoprotein E promotes astrocyte colocalization and degradation of deposited amyloid-beta peptides. *Nat.Med.* 10: 719-726

294. Narita, M., D. M. Holtzman, A. M. Fagan, M. J. LaDu, L. Yu, X. Han, R. W. Gross, G. Bu, and A. L. Schwartz 2002. Cellular catabolism of lipid poor apolipoprotein E via cell surface LDL receptor-related protein. *J.Biochem.(Tokyo)* 132: 743-749

295. Ruiz, J., D. Kouiavskaia, M. Migliorini, S. Robinson, E. L. Saenko, N. Gorlatova, D. Li, D. Lawrence, B. T. Hyman, K. H. Weisgraber, and D. K. Strickland 2005. The apoE isoform binding properties of the VLDL receptor reveal marked differences from LRP and the LDL receptor. *J.Lipid Res.* 46: 1721-1731

296. Vezeridis, A. M., A. Chroni, and V. I. Zannis 2011. Domains of apoE4 required for the biogenesis of apoE-containing HDL. *Ann.Med.* 43: 302-311

297. Mineo, C., I. S. Yuhanna, M. J. Quon, and P. W. Shaul 2003. High density lipoprotein-induced endothelial nitric-oxide synthase activation is mediated by Akt and MAP kinases. *J.Biol.Chem.* 278: 9142-9149

298. Navab, M., S. Y. Hama, G. M. Anantharamaiah, K. Hassan, G. P. Hough, A. D. Watson, S. T. Reddy, A. Sevanian, G. C. Fonarow, and A. M. Fogelman 2000. Normal high density lipoprotein inhibits three steps in the formation of mildly oxidized low density lipoprotein: steps 2 and 3. *J.Lipid Res.* 41: 1495-1508

299. Li, X., K. Kypreos, E. E. Zanni, and V. Zannis 2003. Domains of apoE required for binding to apoE receptor 2 and to phospholipids: Implications for the functions of apoE in the brain. *Biochemistry* 42: 10406-10417

300. **Chroni, A., T. J. Nieland, K. E. Kypreos, M. Krieger, and V. I. Zannis 2005. SR-BI mediates cholesterol efflux via its interactions with lipid-bound ApoE. Structural mutations in SR-BI diminish cholesterol efflux.** ***Biochemistry*** **44: 13132-13143**

301. **Sarah Siggins, Kerry-Ann Rye, Vesa M.Olkkonen, Matti Jauhiainen, and Christian Ehnholm (2007) Human Plasma Phospholipid Transfer Protein (PLTP) – Structural and Functional Features . In Fielding, C. J., editor.** ***High-Density lipoproteins.From Basic Biology to Clinical Aspects*****, Wiley-VCH Verlag GmbH & Co. KgaA. 183-206**

302. **Fielding, C. J. and Fielding, P. E. (2007) Reverse Cholesterol Transport – New Roles for Preb1-HDL and Lecithin:Cholesterol Acyltransferase. In Fielding, C. J., editor.** ***High-Density lipoproteins.From Basic Biology to Clinical Aspects*****, Wiley-VCH Verlag GmbH & Co. KgaA. 143-162**

303. **Ning Xu and Peter Nilsson-Ehle (2007) ApoM – A Novel Apolipoprotein with Antiatherogenic Properties . In Fielding, C. J., editor.** ***High-Density lipoproteins.From Basic Biology to Clinical Aspects*****, Wiley-VCH Verlag GmbH & Co. KgaA. 89-110**

304. **Christopher J.Harder and Ruth McPherson (2007) HDL Remodeling by CETP and SR-BI . In Fielding, C. J., editor.** ***High-Density lipoproteins.From Basic Biology to Clinical Aspects*****, Wiley-VCH Verlag GmbH & Co. KgaA. 163-182**

305. **Maugeais, C., U. J. Tietge, U. C. Broedl, D. Marchadier, W. Cain, M. G. McCoy, S. Lund-Katz, J. M. Glick, and D. J. Rader 2003. Dose-dependent acceleration of high-density lipoprotein catabolism by endothelial lipase.** ***Circulation*** **108: 2121-2126**

306. Santamarina-Fojo, S., H. Gonzalez-Navarro, L. Freeman, E. Wagner, and Z. Nong 2004. Hepatic lipase, lipoprotein metabolism, and atherogenesis. *Arterioscler.Thromb.Vasc.Biol.* 24: 1750-1754

307. Wolfrum, C., M. N. Poy, and M. Stoffel 2005. Apolipoprotein M is required for prebeta-HDL formation and cholesterol efflux to HDL and protects against atherosclerosis. *Nat.Med.* 11: 418-422

308. Hopkins, G. J. and P. J. Barter 1980. Transfers of esterified cholesterol and triglyceride between high density and very low density lipoproteins: in vitro studies of rabbits and humans. *Metabolism* 29: 546-550

309. Tall, A. R., L. R. Forester, and G. L. Bongiovanni 1983. Facilitation of phosphatidylcholine transfer into high density lipoproteins by an apolipoprotein in the density 1.20-1.26 g/ml fraction of plasma. *J.Lipid Res.* 24: 277-289

310. Rohrl, C. and H. Stangl 2013. HDL endocytosis and resecretion. *Biochim.Biophys.Acta* 1831: 1626-1633

311. Gu, X., B. Trigatti, S. Xu, S. Acton, J. Babitt, and M. Krieger 1998. The efficient cellular uptake of high density lipoprotein lipids via scavenger receptor class B type I requires not only receptor-mediated surface binding but also receptor-specific lipid transfer mediated by its extracellular domain. *J.Biol.Chem.* 273: 26338-26348

312. Pagler, T. A., S. Rhode, A. Neuhofer, H. Laggner, W. Strobl, C. Hinterndorfer, I. Volf, M. Pavelka, E. R. Eckhardt, D. R. van der Westhuyzen, G. J. Schutz, and H. Stangl 2006. SR-BI-mediated high density lipoprotein (HDL) endocytosis leads to HDL resecretion facilitating cholesterol efflux. *J.Biol.Chem.* 281: 11193-11204

313. Krieger, M. 1999. Charting the fate of the "good cholesterol": identification and characterization of the high-density lipoprotein receptor SR-BI. *Annu.Rev.Biochem.* 68: 523-558

314. Nakamura, K., M. A. Kennedy, A. Baldan, D. D. Bojanic, K. Lyons, and P. A. Edwards 2004. Expression and regulation of multiple murine ATP-binding cassette transporter G1 mRNAs/isoforms that stimulate cellular cholesterol efflux to high density lipoprotein. *J.Biol.Chem.* 279: 45980-45989

315. Martinez, L. O., Perret, B., Barbaras, R., Terce, F., and Collet, X. (2007) Hepatic and renal HDL receptors. In Fielding, C. J., editor. *High-Density lipoproteins. From Basic Biology to Clinical Aspects*, Wiley-VCH Verlag GmbH & Co. KgaA. 307-338

316. Martinez, L. O., S. Jacquet, J. P. Esteve, C. Rolland, E. Cabezon, E. Champagne, T. Pineau, V. Georgeaud, J. E. Walker, F. Terce, X. Collet, B. Perret, and R. Barbaras 2003. Ectopic beta-chain of ATP synthase is an apolipoprotein A-I receptor in hepatic HDL endocytosis. *Nature* 421: 75-79

317. Nanjee, M. N., C. J. Cooke, W. L. Olszewski, and N. E. Miller 2000. Concentrations of electrophoretic and size subclasses of apolipoprotein A-I-containing particles in human peripheral lymph. *Arterioscler.Thromb.Vasc.Biol.* 20: 2148-2155

318. Asztalos, B. F., C. H. Sloop, L. Wong, and P. S. Roheim 1993. Comparison of apo A-I-containing subpopulations of dog plasma and prenodal peripheral lymph: evidence for alteration in subpopulations in the interstitial space. *Biochim.Biophys.Acta* 1169: 301-304

319. Heideman, C. L. and H. F. Hoff 1982. Lipoproteins containing apolipoprotein A-I extracted from human aortas. *Biochim.Biophys.Acta* 711: 431-444

320. Barrans, A., X. Collet, R. Barbaras, B. Jaspard, J. Manent, C. Vieu, H. Chap, and B. Perret 1994. Hepatic lipase induces the formation of pre-beta 1 high density lipoprotein (HDL) from triacylglycerol-rich HDL2. A study comparing liver perfusion to in vitro incubation with lipases. *J.Biol.Chem.* 269: 11572-11577

321. Maugeais, C., U. J. Tietge, U. C. Broedl, D. Marchadier, W. Cain, M. G. McCoy, S. Lund-Katz, J. M. Glick, and D. J. Rader 2003. Dose-dependent acceleration of high-density lipoprotein catabolism by endothelial lipase. *Circulation* 108: 2121-2126

322. Arai, T., T. Tsukada, T. Murase, and K. Matsumoto 2000. Particle size analysis of high density lipoproteins in patients with genetic cholesteryl ester transfer protein deficiency. *Clin.Chim.Acta* 301: 103-117

323. Huuskonen, J., V. M. Olkkonen, M. Jauhiainen, and C. Ehnholm 2001. The impact of phospholipid transfer protein (PLTP) on HDL metabolism. *Atherosclerosis* 155: 269-281

324. Christoffersen, C., M. Jauhiainen, M. Moser, B. Porse, C. Ehnholm, M. Boesl, B. Dahlback, and L. B. Nielsen 2008. Effect of apolipoprotein M on high density lipoprotein metabolism and atherosclerosis in low density lipoprotein receptor knock-out mice. *J.Biol.Chem.* 283: 1839-1847

325. Forte, T. M., R. Goth-Goldstein, R. W. Nordhausen, and M. R. McCall 1993. Apolipoprotein A-I-cell membrane interaction: extracellular assembly of heterogeneous nascent HDL particles. *J.Lipid Res.* 34: 317-324

326. Forte, T. M., J. K. Bielicki, R. Goth-Goldstein, J. Selmek, and M. R. McCall 1995. Recruitment of cell phospholipids and cholesterol by apolipoproteins A-II and A-I: formation of nascent

apolipoprotein-specific HDL that differ in size, phospholipid composition, and reactivity with LCAT. *J.Lipid Res.* 36: 148-157

327. Chau, P., Y. Nakamura, C. J. Fielding, and P. E. Fielding 2006. Mechanism of prebeta-HDL formation and activation. *Biochemistry* 45: 3981-3987

328. Mulya, A., J. Seo, A. L. Brown, A. K. Gebre, E. Boudyguina, G. S. Shelness, and J. S. Parks 2010. Apolipoprotein M expression increases the size of nascent pre beta HDL formed by ATP binding cassette transporter A1. *J.Lipid.Res.* 51: 514-524

329. Asztalos, B. F., M. E. Brousseau, J. R. McNamara, K. V. Horvath, P. S. Roheim, and E. J. Schaefer 2001. Subpopulations of high density lipoproteins in homozygous and heterozygous Tangier disease. *Atherosclerosis* 156: 217-225

330. Krimbou, L., H. H. Hajj, S. Blain, S. Rashid, M. Denis, M. Marcil, and J. Genest 2005. Biogenesis and speciation of nascent apoA-I-containing particles in various cell lines. *J.Lipid Res.* 46: 1668-1677

331. Zannis, V. I., Zanni, E. E., Papapanagiotou, A., Kardassis, D., and Chroni, A. (2006) ApoA-I functions and synthesis of HDL: Insights from mouse models of human HDL metabolism. *High-Density Lipoproteins. From Basic Biology to Clinical Aspects*, Wiley-VCH, Weinheim. 237-265

332. Karim, M., P. Jackson, and S. Jackowski 2003. Gene structure, expression and identification of a new CTP:phosphocholine cytidylyltransferase beta isoform. *Biochim.Biophys.Acta* 1633: 1-12

333. Cole, L. K., J. E. Vance, and D. E. Vance 2012. Phosphatidylcholine biosynthesis and lipoprotein metabolism. *Biochim.Biophys.Acta* 1821: 754-761

334. Wang, L., S. Magdaleno, I. Tabas, and S. Jackowski 2005. Early embryonic lethality in mice with targeted deletion of the CTP:phosphocholine cytidylyltransferase alpha gene (Pcyt1a). *Mol.Cell Biol.* 25: 3357-3363

335. Sugimoto, H., C. Banchio, and D. E. Vance 2008. Transcriptional regulation of phosphatidylcholine biosynthesis. *Prog.Lipid Res.* 47: 204-220

336. Jacobs, R. L., C. Devlin, I. Tabas, and D. E. Vance 2004. Targeted deletion of hepatic CTP:phosphocholine cytidylyltransferase alpha in mice decreases plasma high density and very low density lipoproteins. *J.Biol.Chem.* 279: 47402-47410

337. Jacobs, R. L., S. Lingrell, Y. Zhao, G. A. Francis, and D. E. Vance 2008. Hepatic CTP:phosphocholine cytidylyltransferase-alpha is a critical predictor of plasma high density lipoprotein and very low density lipoprotein. *J.Biol.Chem.* 283: 2147-2155

338. Holleboom, A. G., M. Vergeer, G. K. Hovingh, J. J. Kastelein, and J. A. Kuivenhoven 2008. The value of HDL genetics. *Curr.Opin.Lipidol.* 19: 385-394

339. Kathiresan, S., K. Musunuru, and M. Orho-Melander 2008. Defining the spectrum of alleles that contribute to blood lipid concentrations in humans. *Curr.Opin.Lipidol.* 19: 122-127

340. Sabatti, C., S. K. Service, A. L. Hartikainen, A. Pouta, S. Ripatti, J. Brodsky, C. G. Jones, N. A. Zaitlen, T. Varilo, M. Kaakinen, U. Sovio, A. Ruokonen, J. Laitinen, E. Jakkula, L. Coin, C. Hoggart, A. Collins, H. Turunen, S. Gabriel, P. Elliot, M. I. McCarthy, M. J. Daly, M. R. Jarvelin, N. B. Freimer, and L. Peltonen 2009. Genome-wide association analysis of metabolic traits in a birth cohort from a founder population. *Nat.Genet.* 41: 35-46

341. Aulchenko, Y. S., S. Ripatti, I. Lindqvist, D. Boomsma, I. M. Heid, P. P. Pramstaller, B. W. Penninx, A. C. Janssens, J. F. Wilson, T. Spector, N. G. Martin, N. L. Pedersen, K. O. Kyvik, J.

Kaprio, A. Hofman, N. B. Freimer, M. R. Jarvelin, U. Gyllensten, H. Campbell, I. Rudan, A. Johansson, F. Marroni, C. Hayward, V. Vitart, I. Jonasson, C. Pattaro, A. Wright, N. Hastie, I. Pichler, A. A. Hicks, M. Falchi, G. Willemsen, J. J. Hottenga, E. J. de Geus, G. W. Montgomery, J. Whitfield, P. Magnusson, J. Saharinen, M. Perola, K. Silander, A. Isaacs, E. J. Sijbrands, A. G. Uitterlinden, J. C. Witteman, B. A. Oostra, P. Elliott, A. Ruokonen, C. Sabatti, C. Gieger, T. Meitinger, F. Kronenberg, A. Doring, H. E. Wichmann, J. H. Smit, M. I. McCarthy, C. M. van Duijn, and L. Peltonen 2009. Loci influencing lipid levels and coronary heart disease risk in 16 European population cohorts. *Nat.Genet.* 41: 47-55

342. Teslovich, T. M., K. Musunuru, A. V. Smith, A. C. Edmondson, I. M. Stylianou, M. Koseki, J. P. Pirruccello, S. Ripatti, D. I. Chasman, C. J. Willer, C. T. Johansen, S. W. Fouchier, A. Isaacs, G. M. Peloso, M. Barbalic, S. L. Ricketts, J. C. Bis, Y. S. Aulchenko, G. Thorleifsson, M. F. Feitosa, J. Chambers, M. Orho-Melander, O. Melander, T. Johnson, X. Li, X. Guo, M. Li, C. Y. Shin, G. M. Jin, K. Y. Jin, J. Y. Lee, T. Park, K. Kim, X. Sim, O. R. Twee-Hee, D. C. Croteau-Chonka, L. A. Lange, J. D. Smith, K. Song, Z. J. Hua, X. Yuan, J. Luan, C. Lamina, A. Ziegler, W. Zhang, R. Y. Zee, A. F. Wright, J. C. Witteman, J. F. Wilson, G. Willemsen, H. E. Wichmann, J. B. Whitfield, D. M. Waterworth, N. J. Wareham, G. Waeber, P. Vollenweider, B. F. Voight, V. Vitart, A. G. Uitterlinden, M. Uda, J. Tuomilehto, J. R. Thompson, T. Tanaka, I. Surakka, H. M. Stringham, T. D. Spector, N. Soranzo, J. H. Smit, J. Sinisalo, K. Silander, E. J. Sijbrands, A. Scuteri, J. Scott, D. Schlessinger, S. Sanna, V. Salomaa, J. Saharinen, C. Sabatti, A. Ruokonen, I. Rudan, L. M. Rose, R. Roberts, M. Rieder, B. M. Psaty, P. P. Pramstaller, I. Pichler, M. Perola, B. W. Penninx, N. L. Pedersen, C. Pattaro, A. N. Parker, G. Pare, B. A. Oostra, C. J. O'Donnell, M. S. Nieminen, D. A. Nickerson, G. W. Montgomery, T. Meitinger, R. McPherson, M. I. McCarthy, W. McArdle, D. Masson, N. G. Martin, F. Marroni, M. Mangino, P. K. Magnusson, G. Lucas, R. Luben, R. J. Loos, M. L. Lokki, G. Lettre, C. Langenberg, L. J. Launer, E. G. Lakatta, R.

Laaksonen, K. O. Kyvik, F. Kronenberg, I. R. Konig, K. T. Khaw, J. Kaprio, L. M. Kaplan, A. Johansson, M. R. Jarvelin, J. W. J. Cecile, E. Ingelsson, W. Igl, H. G. Kees, J. J. Hottenga, A. Hofman, A. A. Hicks, C. Hengstenberg, I. M. Heid, C. Hayward, A. S. Havulinna, N. D. Hastie, T. B. Harris, T. Haritunians, A. S. Hall, U. Gyllensten, C. Guiducci, L. C. Groop, E. Gonzalez, C. Gieger, N. B. Freimer, L. Ferrucci, J. Erdmann, P. Elliott, K. G. Ejebe, A. Doring, A. F. Dominiczak, S. Demissie, P. Deloukas, E. J. de Geus, U. de Faire, G. Crawford, F. S. Collins, Y. D. Chen, M. J. Caulfield, H. Campbell, N. P. Burtt, L. L. Bonnycastle, D. I. Boomsma, S. M. Boekholdt, R. N. Bergman, I. Barroso, S. Bandinelli, C. M. Ballantyne, T. L. Assimes, T. Quertermous, D. Altshuler, M. Seielstad, T. Y. Wong, E. S. Tai, A. B. Feranil, C. W. Kuzawa, L. S. Adair, H. A. Taylor, Jr., I. B. Borecki, S. B. Gabriel, J. G. Wilson, H. Holm, U. Thorsteinsdottir, V. Gudnason, R. M. Krauss, K. L. Mohlke, J. M. Ordovas, P. B. Munroe, J. S. Kooner, A. R. Tall, R. A. Hegele, J. J. Kastelein, E. E. Schadt, J. I. Rotter, E. Boerwinkle, D. P. Strachan, V. Mooser, K. Stefansson, M. P. Reilly, N. J. Samani, H. Schunkert, L. A. Cupples, M. S. Sandhu, P. M. Ridker, D. J. Rader, C. M. van Duijn, L. Peltonen, G. R. Abecasis, M. Boehnke, and S. Kathiresan 2010. Biological, clinical and population relevance of 95 loci for blood lipids. *Nature* 466: 707-713

343. Richards, J. B., D. Waterworth, S. O'Rahilly, M. F. Hivert, R. J. Loos, J. R. Perry, T. Tanaka, N. J. Timpson, R. K. Semple, N. Soranzo, K. Song, N. Rocha, E. Grundberg, J. Dupuis, J. C. Florez, C. Langenberg, I. Prokopenko, R. Saxena, R. Sladek, Y. Aulchenko, D. Evans, G. Waeber, J. Erdmann, M. S. Burnett, N. Sattar, J. Devaney, C. Willenborg, A. Hingorani, J. C. Witteman, P. Vollenweider, B. Glaser, C. Hengstenberg, L. Ferrucci, D. Melzer, K. Stark, J. Deanfield, J. Winogradow, M. Grassl, A. S. Hall, J. M. Egan, J. R. Thompson, S. L. Ricketts, I. R. Konig, W. Reinhard, S. Grundy, H. E. Wichmann, P. Barter, R. Mahley, Y. A. Kesaniemi, D. J. Rader, M. P. Reilly, S. E. Epstein, A. F. Stewart, C. M. van Duijn, H. Schunkert, K. Burling, P. Deloukas, T.

Pastinen, N. J. Samani, R. McPherson, S. G. Davey, T. M. Frayling, N. J. Wareham, J. B. Meigs, V. Mooser, and T. D. Spector 2009. A genome-wide association study reveals variants in ARL15 that influence adiponectin levels. *PLoS Genet.* 5: e1000768

344. Willer, C. J., S. Sanna, A. U. Jackson, A. Scuteri, L. L. Bonnycastle, R. Clarke, S. C. Heath, N. J. Timpson, S. S. Najjar, H. M. Stringham, J. Strait, W. L. Duren, A. Maschio, F. Busonero, A. Mulas, G. Albai, A. J. Swift, M. A. Morken, N. Narisu, D. Bennett, S. Parish, H. Shen, P. Galan, P. Meneton, S. Hercberg, D. Zelenika, W. M. Chen, Y. Li, L. J. Scott, P. A. Scheet, J. Sundvall, R. M. Watanabe, R. Nagaraja, S. Ebrahim, D. A. Lawlor, Y. Ben Shlomo, G. Davey-Smith, A. R. Shuldiner, R. Collins, R. N. Bergman, M. Uda, J. Tuomilehto, A. Cao, F. S. Collins, E. Lakatta, G. M. Lathrop, M. Boehnke, D. Schlessinger, K. L. Mohlke, and G. R. Abecasis 2008. Newly identified loci that influence lipid concentrations and risk of coronary artery disease. *Nat.Genet.* 40: 161-169

345. Kathiresan, S., C. J. Willer, G. M. Peloso, S. Demissie, K. Musunuru, E. E. Schadt, L. Kaplan, D. Bennett, Y. Li, T. Tanaka, B. F. Voight, L. L. Bonnycastle, A. U. Jackson, G. Crawford, A. Surti, C. Guiducci, N. P. Burtt, S. Parish, R. Clarke, D. Zelenika, K. A. Kubalanza, M. A. Morken, L. J. Scott, H. M. Stringham, P. Galan, A. J. Swift, J. Kuusisto, R. N. Bergman, J. Sundvall, M. Laakso, L. Ferrucci, P. Scheet, S. Sanna, M. Uda, Q. Yang, K. L. Lunetta, J. Dupuis, P. I. de Bakker, C. J. O'Donnell, J. C. Chambers, J. S. Kooner, S. Hercberg, P. Meneton, E. G. Lakatta, A. Scuteri, D. Schlessinger, J. Tuomilehto, F. S. Collins, L. Groop, D. Altshuler, R. Collins, G. M. Lathrop, O. Melander, V. Salomaa, L. Peltonen, M. Orho-Melander, J. M. Ordovas, M. Boehnke, G. R. Abecasis, K. L. Mohlke, and L. A. Cupples 2009. Common variants at 30 loci contribute to polygenic dyslipidemia. *Nat.Genet.* 41: 56-65

346. Chasman, D. I., G. Pare, S. Mora, J. C. Hopewell, G. Peloso, R. Clarke, L. A. Cupples, A. Hamsten, S. Kathiresan, A. Malarstig, J. M. Ordovas, S. Ripatti, A. N. Parker, J. P. Miletich, and P. M. Ridker 2009. Forty-Three Loci Associated with Plasma Lipoprotein Size, Concentration, and Cholesterol Content in Genome-Wide Analysis. *Plos Genetics* 5:

347. Waterworth, D. M., S. L. Ricketts, K. Song, L. Chen, J. H. Zhao, S. Ripatti, Y. S. Aulchenko, W. Zhang, X. Yuan, N. Lim, J. Luan, S. Ashford, E. Wheeler, E. H. Young, D. Hadley, J. R. Thompson, P. S. Braund, T. Johnson, M. Struchalin, I. Surakka, R. Luben, K. T. Khaw, S. A. Rodwell, R. J. Loos, S. M. Boekholdt, M. Inouye, P. Deloukas, P. Elliott, D. Schlessinger, S. Sanna, A. Scuteri, A. Jackson, K. L. Mohlke, J. Tuomilehto, R. Roberts, A. Stewart, Y. A. Kesaniemi, R. W. Mahley, S. M. Grundy, W. McArdle, L. Cardon, G. Waeber, P. Vollenweider, J. C. Chambers, M. Boehnke, G. R. Abecasis, V. Salomaa, M. R. Jarvelin, A. Ruokonen, I. Barroso, S. E. Epstein, H. H. Hakonarson, D. J. Rader, M. P. Reilly, J. C. Witteman, A. S. Hall, N. J. Samani, D. P. Strachan, P. Barter, C. M. van Duijn, J. S. Kooner, L. Peltonen, N. J. Wareham, R. McPherson, V. Mooser, and M. S. Sandhu 2010. Genetic variants influencing circulating lipid levels and risk of coronary artery disease. *Arterioscler.Thromb.Vasc.Biol.* 30: 2264-2276

348. Gordon, S. M., J. Y. Deng, L. J. Lu, and W. S. Davidson 2010. Proteomic Characterization of Human Plasma High Density Lipoprotein Fractionated by Gel Filtration Chromatography. *Journal of Proteome Research* 9: 5239-5249

349. Vaisar, T., S. Pennathur, P. S. Green, S. A. Gharib, A. N. Hoofnagle, M. C. Cheung, J. Byun, S. Vuletic, S. Kassim, P. Singh, H. Chea, R. H. Knopp, J. Brunzell, R. Geary, A. Chait, X. Q. Zhao, K. Elkon, S. Marcovina, P. Ridker, J. F. Oram, and J. W. Heinecke 2007. Shotgun proteomics

implicates protease inhibition and complement activation in the antiinflammatory properties of HDL. ***J.Clin.Invest*** **117: 746-756**

350. Davidson, W. S., R. A. G. D. Silva, S. Chantepie, W. R. Lagor, M. J. Chapman, and A. Kontush 2009. Proteomic Analysis of Defined HDL Subpopulations Reveals Particle-Specific Protein Clusters Relevance to Antioxidative Function. ***Arteriosclerosis Thrombosis and Vascular Biology*** **29: 870-U234**

351. Davidson, W. S., R. A. Silva, S. Chantepie, W. R. Lagor, M. J. Chapman, and A. Kontush 2009. Proteomic analysis of defined HDL subpopulations reveals particle-specific protein clusters: relevance to antioxidative function. ***Arterioscler.Thromb.Vasc.Biol.*** **29: 870-876**

352. Green, P. S., T. Vaisar, S. Pennathur, J. J. Kulstad, A. B. Moore, S. Marcovina, J. Brunzell, R. H. Knopp, X. Q. Zhao, and J. W. Heinecke 2008. Combined statin and niacin therapy remodels the high-density lipoprotein proteome. ***Circulation*** **118: 1259-1267**

353. Vickers, K. C., B. T. Palmisano, B. M. Shoucri, R. D. Shamburek, and A. T. Remaley 2011. MicroRNAs are transported in plasma and delivered to recipient cells by high-density lipoproteins. ***Nat.Cell Biol.*** **13: 423-433**

354. Vickers, K. C. and A. T. Remaley 2014. HDL and cholesterol: life after the divorce? ***J.Lipid Res.*** **55: 4-12**

355. Abbott, R. D., P. W. Wilson, W. B. Kannel, and W. P. Castelli 1988. High density lipoprotein cholesterol, total cholesterol screening, and myocardial infarction. The Framingham Study. ***Arteriosclerosis*** **8: 207-211**

356. Gordon, T., W. P. Castelli, M. C. Hjortland, W. B. Kannel, and T. R. Dawber 1977. High density lipoprotein as a protective factor against coronary heart disease. The Framingham Study. *Am.J.Med.* 62: 707-714

357. Yusuf, S., S. Hawken, S. Ounpuu, T. Dans, A. Avezum, F. Lanas, M. McQueen, A. Budaj, P. Pais, J. Varigos, and L. Lisheng 2004. Effect of potentially modifiable risk factors associated with myocardial infarction in 52 countries (the INTERHEART study): case-control study. *Lancet* 364: 937-952

358. Rubins, H. B., S. J. Robins, D. Collins, A. Iranmanesh, T. J. Wilt, D. Mann, M. Mayo-Smith, F. H. Faas, M. B. Elam, G. H. Rutan, and . 1995. Distribution of lipids in 8,500 men with coronary artery disease. Department of Veterans Affairs HDL Intervention Trial Study Group. *Am.J.Cardiol.* 75: 1196-1201

359. Assmann, G. and H. Schulte 1992. Relation of high-density lipoprotein cholesterol and triglycerides to incidence of atherosclerotic coronary artery disease (the PROCAM experience). Prospective Cardiovascular Munster study. *Am.J.Cardiol.* 70: 733-737

360. Goldbourt, U., S. Yaari, and J. H. Medalie 1997. Isolated low HDL cholesterol as a risk factor for coronary heart disease mortality. A 21-year follow-up of 8000 men. *Arterioscler.Thromb.Vasc.Biol.* 17: 107-113

361. Lewington, S., G. Whitlock, R. Clarke, P. Sherliker, J. Emberson, J. Halsey, N. Qizilbash, R. Peto, and R. Collins 2007. Blood cholesterol and vascular mortality by age, sex, and blood pressure: a meta-analysis of individual data from 61 prospective studies with 55,000 vascular deaths. *Lancet* 370: 1829-1839

362. Di, A. E., N. Sarwar, P. Perry, S. Kaptoge, K. K. Ray, A. Thompson, A. M. Wood, S. Lewington, N. Sattar, C. J. Packard, R. Collins, S. G. Thompson, and J. Danesh 2009. Major lipids, apolipoproteins, and risk of vascular disease. *JAMA* 302: 1993-2000

363. Duverger, N., H. Kruth, F. Emmanuel, J. M. Caillaud, C. Viglietta, G. Castro, A. Tailleux, C. Fievet, J. C. Fruchart, L. M. Houdebine, and P. Denefle 1996. Inhibition of atherosclerosis development in cholesterol-fed human apolipoprotein A-I-transgenic rabbits. *Circulation* 94: 713-717

364. Rubin, E. M., R. M. Krauss, E. A. Spangler, J. G. Verstuyft, and S. M. Clift 1991. Inhibition of early atherogenesis in transgenic mice by human apolipoprotein AI. *Nature* 353: 265-267

365. Paszty, C., N. Maeda, J. Verstuyft, and E. M. Rubin 1994. Apolipoprotein AI transgene corrects apolipoprotein E deficiency-induced atherosclerosis in mice. *J.Clin.Invest* 94: 899-903

366. Tangirala, R. K., K. Tsukamoto, S. H. Chun, D. Usher, E. Pure, and D. J. Rader 1999. Regression of atherosclerosis induced by liver-directed gene transfer of apolipoprotein A-I in mice. *Circulation* 100: 1816-1822

367. Plump, A. S., C. J. Scott, and J. L. Breslow 1994. Human apolipoprotein A-I gene expression increases high density lipoprotein and suppresses atherosclerosis in the apolipoprotein E-deficient mouse. *Proc.Natl.Acad.Sci.U.S.A* 91: 9607-9611

368. Hughes, S. D., J. Verstuyft, and E. M. Rubin 1997. HDL deficiency in genetically engineered mice requires elevated LDL to accelerate atherogenesis. *Arterioscler.Thromb.Vasc.Biol.* 17: 1725-1729

369. Badimon, J. J., L. Badimon, and V. Fuster 1990. Regression of atherosclerotic lesions by high density lipoprotein plasma fraction in the cholesterol-fed rabbit. *J.Clin.Invest* 85: 1234-1241

370. Wilhelm, A. J., M. Zabalawi, J. S. Owen, D. Shah, J. M. Grayson, A. S. Major, S. Bhat, D. P. Gibbs, Jr., M. J. Thomas, and M. G. Sorci-Thomas 2010. Apolipoprotein A-I modulates regulatory T cells in autoimmune LDLr-/-, ApoA-I-/- mice. *J.Biol.Chem.* 285: 36158-36169

371. 2001. Executive Summary of The Third Report of The National Cholesterol Education Program (NCEP) Expert Panel on Detection, Evaluation, And Treatment of High Blood Cholesterol In Adults (Adult Treatment Panel III). *JAMA* 285: 2486-2497

372. Ballantyne, C. M., J. A. Herd, L. L. Ferlic, J. K. Dunn, J. A. Farmer, P. H. Jones, J. R. Schein, and A. M. Gotto, Jr. 1999. Influence of low HDL on progression of coronary artery disease and response to fluvastatin therapy. *Circulation* 99: 736-743

373. Ishikawa, K., S. Tani, I. Watanabe, M. Matsumoto, K. Furukawa, K. Nomoto, K. Nomoto, T. Kushiro, K. Nagao, and K. Kanmatsuse 2003. Effect of pravastatin on coronary plaque volume. *Am.J.Cardiol.* 92: 975-977

374. Robins, S. J., D. Collins, J. T. Wittes, V. Papademetriou, P. C. Deedwania, E. J. Schaefer, J. R. McNamara, M. L. Kashyap, J. M. Hershman, L. F. Wexler, and H. B. Rubins 2001. Relation of gemfibrozil treatment and lipid levels with major coronary events: VA-HIT: a randomized controlled trial. *JAMA* 285: 1585-1591

375. Manninen, V., M. O. Elo, M. H. Frick, K. Haapa, O. P. Heinonen, P. Heinsalmi, P. Helo, J. K. Huttunen, P. Kaitaniemi, P. Koskinen, and . 1988. Lipid alterations and decline in the incidence of coronary heart disease in the Helsinki Heart Study. *JAMA* 260: 641-651

376. Brown, B. G., X. Q. Zhao, A. Chait, L. D. Fisher, M. C. Cheung, J. S. Morse, A. A. Dowdy, E. K. Marino, E. L. Bolson, P. Alaupovic, J. Frohlich, and J. J. Albers 2001. Simvastatin and niacin, antioxidant vitamins, or the combination for the prevention of coronary disease. *N.Engl.J.Med.* 345: 1583-1592

377. Barter, P. J., M. Caulfield, M. Eriksson, S. M. Grundy, J. J. Kastelein, M. Komajda, J. Lopez-Sendon, L. Mosca, J. C. Tardif, D. D. Waters, C. L. Shear, J. H. Revkin, K. A. Buhr, M. R. Fisher, A. R. Tall, and B. Brewer 2007. Effects of torcetrapib in patients at high risk for coronary events. *N.Engl.J.Med.* 357: 2109-2122

378. Nissen, S. E., T. Tsunoda, E. M. Tuzcu, P. Schoenhagen, C. J. Cooper, M. Yasin, G. M. Eaton, M. A. Lauer, W. S. Sheldon, C. L. Grines, S. Halpern, T. Crowe, J. C. Blankenship, and R. Kerensky 2003. Effect of recombinant ApoA-I Milano on coronary atherosclerosis in patients with acute coronary syndromes: a randomized controlled trial. *JAMA* 290: 2292-2300

379. Nicholls, S. J., E. M. Tuzcu, I. Sipahi, P. Schoenhagen, T. Crowe, S. Kapadia, and S. E. Nissen 2006. Relationship between atheroma regression and change in lumen size after infusion of apolipoprotein A-I Milano. *J.Am.Coll.Cardiol.* 47: 992-997

380. Tardif, J. C., J. Gregoire, P. L. L'Allier, R. Ibrahim, J. Lesperance, T. M. Heinonen, S. Kouz, C. Berry, R. Basser, M. A. Lavoie, M. C. Guertin, and J. Rodes-Cabau 2007. Effects of reconstituted high-density lipoprotein infusions on coronary atherosclerosis: a randomized controlled trial. *JAMA* 297: 1675-1682

381. Libby, P. 2006. Inflammation and cardiovascular disease mechanisms. *Am.J.Clin.Nutr.* 83: 456S-460S

382. Cuchel, M. and D. J. Rader 2006. Macrophage reverse cholesterol transport: key to the regression of atherosclerosis? *Circulation* 113: 2548-2555

383. Heinecke, J. W. 2012. The not-so-simple HDL story: A new era for quantifying HDL and cardiovascular risk? *Nat.Med.* 18: 1346-1347

384. Wang, X., H. L. Collins, M. Ranalletta, I. V. Fuki, J. T. Billheimer, G. H. Rothblat, A. R. Tall, and D. J. Rader 2007. Macrophage ABCA1 and ABCG1, but not SR-BI, promote macrophage reverse cholesterol transport in vivo. *J.Clin.Invest* 117: 2216-2224

385. Khera, A. V., M. Cuchel, M. Llera-Moya, A. Rodrigues, M. F. Burke, K. Jafri, B. C. French, J. A. Phillips, M. L. Mucksavage, R. L. Wilensky, E. R. Mohler, G. H. Rothblat, and D. J. Rader 2011. Cholesterol efflux capacity, high-density lipoprotein function, and atherosclerosis. *N.Engl.J.Med.* 364: 127-135

386. Yvan-Charvet, L., M. Ranalletta, N. Wang, S. Han, N. Terasaka, R. Li, C. Welch, and A. R. Tall 2007. Combined deficiency of ABCA1 and ABCG1 promotes foam cell accumulation and accelerates atherosclerosis in mice. *J.Clin.Invest* 117: 3900-3908

387. Westerterp, M., A. J. Murphy, M. Wang, T. A. Pagler, Y. Vengrenyuk, M. S. Kappus, D. J. Gorman, P. R. Nagareddy, X. Zhu, S. Abramowicz, J. S. Parks, C. Welch, E. A. Fisher, N. Wang, L. Yvan-Charvet, and A. R. Tall 2013. Deficiency of ATP-binding cassette transporters A1 and G1 in macrophages increases inflammation and accelerates atherosclerosis in mice. *Circ.Res.* 112: 1456-1465

388. Joseph, S. B., E. McKilligin, L. Pei, M. A. Watson, A. R. Collins, B. A. Laffitte, M. Chen, G. Noh, J. Goodman, G. N. Hagger, J. Tran, T. K. Tippin, X. Wang, A. J. Lusis, W. A. Hsueh, R. E. Law, J.

L. Collins, T. M. Willson, and P. Tontonoz 2002. Synthetic LXR ligand inhibits the development of atherosclerosis in mice. *Proc.Natl.Acad.Sci.U.S.A* 99: 7604-7609

389. Naik, S. U., X. Wang, J. S. Da Silva, M. Jaye, C. H. Macphee, M. P. Reilly, J. T. Billheimer, G. H. Rothblat, and D. J. Rader 2006. Pharmacological activation of liver X receptors promotes reverse cholesterol transport in vivo. *Circulation* 113: 90-97

390. Levin, N., E. D. Bischoff, C. L. Daige, D. Thomas, C. T. Vu, R. A. Heyman, R. K. Tangirala, and I. G. Schulman 2005. Macrophage liver X receptor is required for antiatherogenic activity of LXR agonists. *Arterioscler.Thromb.Vasc.Biol.* 25: 135-142

391. Nakaya, K., J. Tohyama, S. U. Naik, H. Tanigawa, C. MacPhee, J. T. Billheimer, and D. J. Rader 2011. Peroxisome proliferator-activated receptor-alpha activation promotes macrophage reverse cholesterol transport through a liver X receptor-dependent pathway. *Arterioscler.Thromb.Vasc.Biol.* 31: 1276-1282

392. Li, A. C., C. J. Binder, A. Gutierrez, K. K. Brown, C. R. Plotkin, J. W. Pattison, A. F. Valledor, R. A. Davis, T. M. Willson, J. L. Witztum, W. Palinski, and C. K. Glass 2004. Differential inhibition of macrophage foam-cell formation and atherosclerosis in mice by PPARalpha, beta/delta, and gamma. *J.Clin.Invest* 114: 1564-1576

393. Rayner, K. J., F. J. Sheedy, C. C. Esau, F. N. Hussain, R. E. Temel, S. Parathath, J. M. van Gils, A. J. Rayner, A. N. Chang, Y. Suarez, C. Fernandez-Hernando, E. A. Fisher, and K. J. Moore 2011. Antagonism of miR-33 in mice promotes reverse cholesterol transport and regression of atherosclerosis. *J.Clin.Invest* 121: 2921-2931

394. Horie, T., K. Ono, M. Horiguchi, H. Nishi, T. Nakamura, K. Nagao, M. Kinoshita, Y. Kuwabara, H. Marusawa, Y. Iwanaga, K. Hasegawa, M. Yokode, T. Kimura, and T. Kita 2010. MicroRNA-

33 encoded by an intron of sterol regulatory element-binding protein 2 (Srebp2) regulates HDL in vivo. *Proc.Natl.Acad.Sci.U.S.A* 107: 17321-17326

395. Rayner, K. J., C. C. Esau, F. N. Hussain, A. L. McDaniel, S. M. Marshall, J. M. van Gils, T. D. Ray, F. J. Sheedy, L. Goedeke, X. Liu, O. G. Khatsenko, V. Kaimal, C. J. Lees, C. Fernandez-Hernando, E. A. Fisher, R. E. Temel, and K. J. Moore 2011. Inhibition of miR-33a/b in non-human primates raises plasma HDL and lowers VLDL triglycerides. *Nature* 478: 404-407

396. Sun, D., J. Zhang, J. Xie, W. Wei, M. Chen, and X. Zhao 2012. MiR-26 controls LXR-dependent cholesterol efflux by targeting ABCA1 and ARL7. *FEBS Lett.* 586: 1472-1479

397. Ramirez, C. M., A. Davalos, L. Goedeke, A. G. Salerno, N. Warrier, D. Cirera-Salinas, Y. Suarez, and C. Fernandez-Hernando 2011. MicroRNA-758 regulates cholesterol efflux through posttranscriptional repression of ATP-binding cassette transporter A1. *Arterioscler.Thromb.Vasc.Biol.* 31: 2707-2714

398. Kim, J., H. Yoon, C. M. Ramirez, S. M. Lee, H. S. Hoe, C. Fernandez-Hernando, and J. Kim 2012. MiR-106b impairs cholesterol efflux and increases Abeta levels by repressing ABCA1 expression. *Exp.Neurol.* 235: 476-483

399. Zhang, Y., I. Zanotti, M. P. Reilly, J. M. Glick, G. H. Rothblat, and D. J. Rader 2003. Overexpression of apolipoprotein A-I promotes reverse transport of cholesterol from macrophages to feces in vivo. *Circulation* 108: 661-663

400. Moore, R. E., M. Navab, J. S. Millar, F. Zimetti, S. Hama, G. H. Rothblat, and D. J. Rader 2005. Increased atherosclerosis in mice lacking apolipoprotein A-I attributable to both impaired reverse cholesterol transport and increased inflammation. *Circ.Res.* 97: 763-771

401. Alexander, E. T., G. L. Weibel, M. R. Joshi, C. Vedhachalam, M. Llera-Moya, G. H. Rothblat, M. C. Phillips, and D. J. Rader 2009. Macrophage reverse cholesterol transport in mice expressing ApoA-I Milano. *Arterioscler.Thromb.Vasc.Biol.* 29: 1496-1501

402. Navab, M., G. M. Anantharamaiah, S. T. Reddy, S. Hama, G. Hough, V. R. Grijalva, A. C. Wagner, J. S. Frank, G. Datta, D. Garber, and A. M. Fogelman 2004. Oral D-4F Causes Formation of Pre-beta High-Density Lipoprotein and Improves High-Density Lipoprotein-Mediated Cholesterol Efflux and Reverse Cholesterol Transport From Macrophages in Apolipoprotein E-Null Mice. *Circulation*

403. Amar, M. J., W. D'Souza, S. Turner, S. Demosky, D. Sviridov, J. Stonik, J. Luchoomun, J. Voogt, M. Hellerstein, D. Sviridov, and A. T. Remaley 2010. 5A apolipoprotein mimetic peptide promotes cholesterol efflux and reduces atherosclerosis in mice. *J.Pharmacol.Exp.Ther.* 334: 634-641

404. Bielicki, J. K., H. Zhang, Y. Cortez, Y. Zheng, V. Narayanaswami, A. Patel, J. Johansson, and S. Azhar 2010. A new HDL mimetic peptide that stimulates cellular cholesterol efflux with high efficiency greatly reduces atherosclerosis in mice. *J.Lipid Res.* 51: 1496-1503

405. Uehara, Y., S. Ando, E. Yahiro, K. Oniki, M. Ayaori, S. Abe, E. Kawachi, B. Zhang, S. Shioi, H. Tanigawa, S. Imaizumi, S. Miura, and K. Saku 2013. FAMP, a novel apoA-I mimetic peptide, suppresses aortic plaque formation through promotion of biological HDL function in ApoE-deficient mice. *J.Am.Heart Assoc.* 2: e000048

406. Zhang, Y., J. R. Da Silva, M. Reilly, J. T. Billheimer, G. H. Rothblat, and D. J. Rader 2005. Hepatic expression of scavenger receptor class B type I (SR-BI) is a positive regulator of macrophage reverse cholesterol transport in vivo. *J.Clin.Invest* 115: 2870-2874

407. Kozarsky, K. F., M. H. Donahee, J. M. Glick, M. Krieger, and D. J. Rader 2000. Gene transfer and hepatic overexpression of the HDL receptor SR-BI reduces atherosclerosis in the cholesterol-fed LDL receptor-deficient mouse. *Arterioscler.Thromb.Vasc.Biol.* 20: 721-727

408. Covey, S. D., M. Krieger, W. Wang, M. Penman, and B. L. Trigatti 2003. Scavenger receptor class B type I-mediated protection against atherosclerosis in LDL receptor-negative mice involves its expression in bone marrow-derived cells. *Arterioscler.Thromb.Vasc.Biol.* 23: 1589-1594

409. Trigatti, B., H. Rayburn, M. Vinals, A. Braun, H. Miettinen, M. Penman, M. Hertz, M. Schrenzel, L. Amigo, A. Rigotti, and M. Krieger 1999. Influence of the high density lipoprotein receptor SR-BI on reproductive and cardiovascular pathophysiology. *Proc.Natl.Acad.Sci.U.S.A* 96: 9322-9327

410. Zanotti, I., M. Pedrelli, F. Poti, G. Stomeo, M. Gomaraschi, L. Calabresi, and F. Bernini 2011. Macrophage, but not systemic, apolipoprotein E is necessary for macrophage reverse cholesterol transport in vivo. *Arterioscler.Thromb.Vasc.Biol.* 31: 74-80

411. Tanigawa, H., J. T. Billheimer, J. Tohyama, Y. Zhang, G. Rothblat, and D. J. Rader 2007. Expression of cholesteryl ester transfer protein in mice promotes macrophage reverse cholesterol transport. *Circulation* 116: 1267-1273

412. Navab, M., S. T. Reddy, B. J. Van Lenten, G. M. Anantharamaiah, and A. M. Fogelman 2009. The role of dysfunctional HDL in atherosclerosis. *J.Lipid Res.* 50 Suppl: S145-S149

413. Van, L. S., F. Spillmann, M. Lorenz, M. Meloni, F. Jacobs, M. Egorova, V. Stangl, G. B. De, H. P. Schultheiss, and C. Tschope 2009. Vascular-protective effects of high-density lipoprotein include the downregulation of the angiotensin II type 1 receptor. *Hypertension* 53: 682-687

414. Garner, B., A. R. Waldeck, P. K. Witting, K. A. Rye, and R. Stocker 1998. Oxidation of high density lipoproteins. II. Evidence for direct reduction of lipid hydroperoxides by methionine residues of apolipoproteins AI and AII. *J.Biol.Chem.* 273: 6088-6095

415. Fluiter, K., H. Vietsch, E. A. Biessen, G. M. Kostner, T. J. van Berkel, and W. Sattler 1996. Increased selective uptake in vivo and in vitro of oxidized cholesteryl esters from high-density lipoprotein by rat liver parenchymal cells. *Biochem.J.* 319 (Pt 2): 471-476

416. Cockerill, G. W., K. A. Rye, J. R. Gamble, M. A. Vadas, and P. J. Barter 1995. High-density lipoproteins inhibit cytokine-induced expression of endothelial cell adhesion molecules. *Arterioscler.Thromb.Vasc.Biol.* 15: 1987-1994

417. Bursill, C. A., M. L. Castro, D. T. Beattie, S. Nakhla, d. van, V, A. K. Heather, P. J. Barter, and K. A. Rye 2010. High-density lipoproteins suppress chemokines and chemokine receptors in vitro and in vivo. *Arterioscler.Thromb.Vasc.Biol.* 30: 1773-1778

418. Nobecourt, E., F. Tabet, G. Lambert, R. Puranik, S. Bao, L. Yan, M. J. Davies, B. E. Brown, A. J. Jenkins, G. J. Dusting, D. J. Bonnet, L. K. Curtiss, P. J. Barter, and K. A. Rye 2010. Nonenzymatic glycation impairs the antiinflammatory properties of apolipoprotein A-I. *Arterioscler.Thromb.Vasc.Biol.* 30: 766-772

419. Tolle, M., A. Pawlak, M. Schuchardt, A. Kawamura, U. J. Tietge, S. Lorkowski, P. Keul, G. Assmann, J. Chun, B. Levkau, M. van der Giet, and J. R. Nofer 2008. HDL-associated lysosphingolipids inhibit NAD(P)H oxidase-dependent monocyte chemoattractant protein-1 production. *Arteriosclerosis Thrombosis and Vascular Biology* 28: 1542-1548

420. Nicholls, S. J., G. J. Dusting, B. Cutri, S. Bao, G. R. Drummond, K. A. Rye, and P. J. Barter 2005. Reconstituted high-density lipoproteins inhibit the acute pro-oxidant and proinflammatory

vascular changes induced by a periarterial collar in normocholesterolemic rabbits. *Circulation* 111: 1543-1550

421. Kimura, T., H. Tomura, C. Mogi, A. Kuwabara, A. Damirin, T. Ishizuka, A. Sekiguchi, M. Ishiwara, D. S. Im, K. Sato, M. Murakami, and F. Okajima 2006. Role of scavenger receptor class B type I and sphingosine 1-phosphate receptors in high density lipoprotein-induced inhibition of adhesion molecule expression in endothelial cells. *J.Biol.Chem.* 281: 37457-37467

422. Wu, B. J., K. Chen, S. Shrestha, K. L. Ong, P. J. Barter, and K. A. Rye 2013. High-density lipoproteins inhibit vascular endothelial inflammation by increasing 3beta-hydroxysteroid-Delta24 reductase expression and inducing heme oxygenase-1. *Circ.Res.* 112: 278-288

423. Norata, G. D., E. Callegari, M. Marchesi, G. Chiesa, P. Eriksson, and A. L. Catapano 2005. High-density lipoproteins induce transforming growth factor-beta2 expression in endothelial cells. *Circulation* 111: 2805-2811

424. Kimura, T., H. Tomura, K. Sato, M. Ito, I. Matsuoka, D. S. Im, A. Kuwabara, C. Mogi, H. Itoh, H. Kurose, M. Murakami, and F. Okajima 2010. Mechanism and role of high density lipoprotein-induced activation of AMP-activated protein kinase in endothelial cells. *J.Biol.Chem.* 285: 4387-4397

425. Tabet, F., A. T. Remaley, A. I. Segaliny, J. Millet, L. Yan, S. Nakhla, P. J. Barter, K. A. Rye, and G. Lambert 2010. The 5A apolipoprotein A-I mimetic peptide displays antiinflammatory and antioxidant properties in vivo and in vitro. *Arterioscler.Thromb.Vasc.Biol.* 30: 246-252

426. Cheng, A. M., P. Handa, S. Tateya, J. Schwartz, C. Tang, P. Mitra, J. F. Oram, A. Chait, and F. Kim 2012. Apolipoprotein A-I attenuates palmitate-mediated NF-kappaB activation by reducing Toll-like receptor-4 recruitment into lipid rafts. *PLoS.One.* 7: e33917

427. Okura, H., S. Yamashita, T. Ohama, A. Saga, A. Yamamoto-Kakuta, Y. Hamada, N. Sougawa, R. Ohyama, Y. Sawa, and A. Matsuyama 2010. HDL/Apolipoprotein A-I Binds to Macrophage-Derived Progranulin and Suppresses its Conversion into Proinflammatory Granulins. *Journal of Atherosclerosis and Thrombosis* 17: 568-577

428. Carpintero, R., L. Gruaz, K. J. Brandt, A. Scanu, D. Faille, V. Combes, G. E. Grau, and D. Burger 2010. HDL interfere with the binding of T cell microparticles to human monocytes to inhibit pro-inflammatory cytokine production. *PLoS.One.* 5: e11869

429. Murphy, A. J., K. J. Woollard, A. Suhartoyo, R. A. Stirzaker, J. Shaw, D. Sviridov, and J. P. Chin-Dusting 2011. Neutrophil activation is attenuated by high-density lipoprotein and apolipoprotein A-I in in vitro and in vivo models of inflammation. *Arterioscler.Thromb.Vasc.Biol.* 31: 1333-1341

430. Murphy, A. J., K. J. Woollard, A. Hoang, N. Mukhamedova, R. A. Stirzaker, S. P. McCormick, A. T. Remaley, D. Sviridov, and J. Chin-Dusting 2008. High-density lipoprotein reduces the human monocyte inflammatory response. *Arterioscler.Thromb.Vasc.Biol.* 28: 2071-2077

431. Mills, C. D. 2012. M1 and M2 Macrophages: Oracles of Health and Disease. *Crit Rev.Immunol.* 32: 463-488

432. Feig, J. E., J. X. Rong, R. Shamir, M. Sanson, Y. Vengrenyuk, J. Liu, K. Rayner, K. Moore, M. Garabedian, and E. A. Fisher 2011. HDL promotes rapid atherosclerosis regression in mice

and alters inflammatory properties of plaque monocyte-derived cells. *Proc.Natl.Acad.Sci.U.S.A* 108: 7166-7171

433. Sanson, M., E. Distel, and E. A. Fisher 2013. HDL induces the expression of the M2 macrophage markers arginase 1 and Fizz-1 in a STAT6-dependent process. *PLoS.One.* 8: e74676

434. Aharoni, S., M. Aviram, and B. Fuhrman 2013. Paraoxonase 1 (PON1) reduces macrophage inflammatory responses. *Atherosclerosis* 228: 353-361

435. Rosenblat, M., N. Volkova, and M. Aviram 2011. Injection of paraoxonase 1 (PON1) to mice stimulates their HDL and macrophage antiatherogenicity. *Biofactors* 37: 462-467

436. Rosenblat, M., N. Volkova, J. Ward, and M. Aviram 2011. Paraoxonase 1 (PON1) inhibits monocyte-to-macrophage differentiation. *Atherosclerosis* 219: 49-56

437. Rosenblat, M., S. Ward, N. Volkova, T. Hayek, and M. Aviram 2012. VLDL triglycerides inhibit HDL-associated paraoxonase 1 (PON1) activity: in vitro and in vivo studies. *Biofactors* 38: 292-299

438. Gomaraschi, M., L. Calabresi, G. Rossoni, S. Iametti, G. Franceschini, J. A. Stonik, and A. T. Remaley 2008. Anti-inflammatory and cardioprotective activities of synthetic high-density lipoprotein containing apolipoprotein A-I mimetic peptides. *J.Pharmacol.Exp.Ther.* 324: 776-783

439. Imaizumi, S., V. Grijalva, M. Navab, B. J. Van Lenten, A. C. Wagner, G. M. Anantharamiah, A. M. Fogelman, and S. T. Reddy 2010. L-4F differentially alters plasma levels of oxidized fatty acids resulting in more anti-inflammatory HDL in mice. *Drug Metab Lett.* 4: 139-148

440. Patel, S., B. G. Drew, S. Nakhla, S. J. Duffy, A. J. Murphy, P. J. Barter, K. A. Rye, J. Chin-Dusting, A. Hoang, D. Sviridov, D. S. Celermajer, and B. A. Kingwell 2009. Reconstituted high-density lipoprotein increases plasma high-density lipoprotein anti-inflammatory properties and cholesterol efflux capacity in patients with type 2 diabetes. *J.Am.Coll.Cardiol.* 53: 962-971

441. Tolani, S., T. A. Pagler, A. J. Murphy, A. E. Bochem, S. Abramowicz, C. Welch, P. R. Nagareddy, S. Holleran, G. K. Hovingh, J. A. Kuivenhoven, and A. R. Tall 2013. Hypercholesterolemia and reduced HDL-C promote hematopoietic stem cell proliferation and monocytosis: studies in mice and FH children. *Atherosclerosis* 229: 79-85

442. Murphy, A. J., M. Akhtari, S. Tolani, T. Pagler, N. Bijl, C. L. Kuo, M. Wang, M. Sanson, S. Abramowicz, C. Welch, A. E. Bochem, J. A. Kuivenhoven, L. Yvan-Charvet, and A. R. Tall 2011. ApoE regulates hematopoietic stem cell proliferation, monocytosis, and monocyte accumulation in atherosclerotic lesions in mice. *J.Clin.Invest* 121: 4138-4149

443. Yvan-Charvet, L., T. Pagler, E. L. Gautier, S. Avagyan, R. L. Siry, S. Han, C. L. Welch, N. Wang, G. J. Randolph, H. W. Snoeck, and A. R. Tall 2010. ATP-binding cassette transporters and HDL suppress hematopoietic stem cell proliferation. *Science* 328: 1689-1693

444. Suc, I., I. Escargueil-Blanc, M. Troly, R. Salvayre, and A. Negre-Salvayre 1997. HDL and ApoA prevent cell death of endothelial cells induced by oxidized LDL. *Arterioscler.Thromb.Vasc.Biol.* 17: 2158-2166

445. Sugano, M., K. Tsuchida, and N. Makino 2000. High-density lipoproteins protect endothelial cells from tumor necrosis factor-alpha-induced apoptosis. *Biochem.Biophys.Res.Commun.* 272: 872-876

446. Nofer, J. R., B. Levkau, I. Wolinska, R. Junker, M. Fobker, A. von Eckardstein, U. Seedorf, and G. Assmann 2001. Suppression of endothelial cell apoptosis by high density lipoproteins (HDL) and HDL-associated lysosphingolipids. *J.Biol.Chem.* 276: 34480-34485

447. de Souza, J. A., C. Vindis, A. Negre-Salvayre, K. A. Rye, M. Couturier, P. Therond, S. Chantepie, R. Salvayre, M. J. Chapman, and A. Kontush 2010. Small, dense HDL 3 particles attenuate apoptosis in endothelial cells: pivotal role of apolipoprotein A-I. *J.Cell Mol.Med.* 14: 608-620

448. de Souza, J. A., C. Vindis, B. Hansel, A. Negre-Salvayre, P. Therond, C. V. Serrano, S. Chantepie, R. Salvayre, E. Bruckert, M. J. Chapman, and A. Kontush 2008. Metabolic syndrome features small, apolipoprotein A-I-poor, triglyceride-rich HDL3 particles with defective anti-apoptotic activity. *Atherosclerosis* 197: 84-94

449. Riwanto, M., L. Rohrer, B. Roschitzki, C. Besler, P. Mocharla, M. Mueller, D. Perisa, K. Heinrich, L. Altwegg, E. A. von, T. F. Luscher, and U. Landmesser 2013. Altered activation of endothelial anti- and proapoptotic pathways by high-density lipoprotein from patients with coronary artery disease: role of high-density lipoprotein-proteome remodeling. *Circulation* 127: 891-904

450. Terasaka, N., N. Wang, L. Yvan-Charvet, and A. R. Tall 2007. High-density lipoprotein protects macrophages from oxidized low-density lipoprotein-induced apoptosis by promoting efflux of 7-ketocholesterol via ABCG1. *Proc.Natl.Acad.Sci.U.S.A* 104: 15093-15098

451. Li, D., Y. Zhang, J. Ma, W. Ling, and M. Xia 2010. Adenosine monophosphate activated protein kinase regulates ABCG1-mediated oxysterol efflux from endothelial cells and protects against hypercholesterolemia-induced endothelial dysfunction. *Arterioscler.Thromb.Vasc.Biol.* 30: 1354-1362

452. Terasaka, N., M. Westerterp, J. Koetsveld, C. Fernandez-Hernando, L. Yvan-Charvet, N. Wang, W. C. Sessa, and A. R. Tall 2010. ATP-binding cassette transporter G1 and high-density lipoprotein promote endothelial NO synthesis through a decrease in the interaction of caveolin-1 and endothelial NO synthase. *Arterioscler.Thromb.Vasc.Biol.* 30: 2219-2225

453. Radojkovic, C., A. Genoux, V. Pons, G. Combes, H. de Jonge, E. Champagne, C. Rolland, B. Perret, X. Collet, F. Terce, and L. O. Martinez 2009. Stimulation of Cell Surface F-1-ATPase Activity by Apolipoprotein A-I Inhibits Endothelial Cell Apoptosis and Promotes Proliferation. *Arteriosclerosis Thrombosis and Vascular Biology* 29: 1125-U214

454. Kimura, T., K. Sato, E. Malchinkhuu, H. Tomura, K. Tamama, A. Kuwabara, M. Murakami, and F. Okajima 2003. High-density lipoprotein stimulates endothelial cell migration and survival through sphingosine 1-phosphate and its receptors. *Arterioscler.Thromb.Vasc.Biol.* 23: 1283-1288

455. Kruger, A. L., S. Peterson, S. Turkseven, P. M. Kaminski, F. F. Zhang, S. Quan, M. S. Wolin, and N. G. Abraham 2005. D-4F induces heme oxygenase-1 and extracellular superoxide dismutase, decreases endothelial cell sloughing, and improves vascular reactivity in rat model of diabetes. *Circulation* 111: 3126-3134

456. Werner, N., S. Junk, U. Laufs, A. Link, K. Walenta, M. Bohm, and G. Nickenig 2003. Intravenous transfusion of endothelial progenitor cells reduces neointima formation after vascular injury. *Circ.Res.* 93: e17-e24

457. Tamagaki, T., S. Sawada, H. Imamura, Y. Tada, S. Yamasaki, A. Toratani, T. Sato, S. Komatsu, N. Akamatsu, M. Yamagami, K. Kobayashi, K. Kato, K. Yamamoto, K. Shirai, K. Yamada, T. Higaki, K. Nakagawa, H. Tsuji, and M. Nakagawa 1996. Effects of high-density lipoproteins

on intracellular pH and proliferation of human vascular endothelial cells. *Atherosclerosis* 123: 73-82

458. Grewal, T., D. de, I, M. F. Kirchhoff, F. Tebar, J. Heeren, F. Rinninger, and C. Enrich 2003. High density lipoprotein-induced signaling of the MAPK pathway involves scavenger receptor type BI-mediated activation of Ras. *J.Biol.Chem.* 278: 16478-16481

459. Miura, S., M. Fujino, Y. Matsuo, A. Kawamura, H. Tanigawa, H. Nishikawa, and K. Saku 2003. High density lipoprotein-induced angiogenesis requires the activation of Ras/MAP kinase in human coronary artery endothelial cells. *Arterioscler.Thromb.Vasc.Biol.* 23: 802-808

460. Seetharam, D., C. Mineo, A. K. Gormley, L. L. Gibson, W. Vongpatanasin, K. L. Chambliss, L. D. Hahner, M. L. Cummings, R. L. Kitchens, Y. L. Marcel, D. J. Rader, and P. W. Shaul 2006. High-density lipoprotein promotes endothelial cell migration and reendothelialization via scavenger receptor-B type I. *Circulation Research* 98: 63-72

461. Feng, Y. M., M. Van Eck, E. Van Craeyveld, F. Jacobs, V. Carlier, S. Van Linthout, M. Erdel, M. Tjwa, and B. De Geest 2009. Critical role of scavenger receptor-BI-expressing bone marrow-derived endothelial progenitor cells in the attenuation of allograft vasculopathy after human apo A-I transfer. *Blood* 113: 755-764

462. Zhang, Q., H. Yin, P. Liu, H. Zhang, and M. She 2010. Essential role of HDL on endothelial progenitor cell proliferation with PI3K/Akt/cyclin D1 as the signal pathway. *Exp.Biol.Med.(Maywood.)* 235: 1082-1092

463. van der Vorst, E. P., L. Z. Vanags, L. L. Dunn, H. C. Prosser, K. A. Rye, and C. A. Bursill 2013. High-density lipoproteins suppress chemokine expression and proliferation in human vascular smooth muscle cells. *FASEB J.* 27: 1413-1425

464. Ramet, M. E., M. Ramet, Q. Lu, M. Nickerson, M. J. Savolainen, A. Malzone, and R. H. Karas 2003. High-density lipoprotein increases the abundance of eNOS protein in human vascular endothelial cells by increasing its half-life. *Journal of the American College of Cardiology* 41: 2288-2297

465. Landmesser, U., B. Hornig, and H. Drexler 2004. Endothelial function - A critical determinant in atherosclerosis? *Circulation* 109: 27-33

466. Zeiher, A. M., V. Schachlinger, S. H. Hohnloser, B. Saurbier, and H. Just 1994. Coronary atherosclerotic wall thickening and vascular reactivity in humans. Elevated high-density lipoprotein levels ameliorate abnormal vasoconstriction in early atherosclerosis. *Circulation* 89: 2525-2532

467. Li, X. P., S. P. Zhao, X. Y. Zhang, L. Liu, M. Gao, and Q. C. Zhou 2000. Protective effect of high density lipoprotein on endothelium-dependent vasodilatation. *Int.J.Cardiol.* 73: 231-236

468. Yuhanna, I. S., Y. Zhu, B. E. Cox, L. D. Hahner, S. Osborne-Lawrence, P. Lu, Y. L. Marcel, R. G. Anderson, M. E. Mendelsohn, H. H. Hobbs, and P. W. Shaul 2001. High-density lipoprotein binding to scavenger receptor-BI activates endothelial nitric oxide synthase. *Nat.Med.* 7: 853-857

469. Assanasen, C., C. Mineo, D. Seetharam, I. S. Yuhanna, Y. L. Marcel, M. A. Connelly, D. L. Williams, M. Llera-Moya, P. W. Shaul, and D. L. Silver 2005. Cholesterol binding, efflux, and a PDZ-interacting domain of scavenger receptor-BI mediate HDL-initiated signaling. *J.Clin.Invest* 115: 969-977

470. Kocher, O., A. Yesilaltay, C. Cirovic, R. Pal, A. Rigotti, and M. Krieger 2003. Targeted disruption of the PDZK1 gene in mice causes tissue-specific depletion of the HDL Receptor SR-BI and altered lipoprotein metabolism. *J.Biol.Chem.* 278: 52820-52825

471. Nofer, J. R., G. M. van der, M. Tolle, I. Wolinska, L. K. von Wnuck, H. A. Baba, U. J. Tietge, A. Godecke, I. Ishii, B. Kleuser, M. Schafers, M. Fobker, W. Zidek, G. Assmann, J. Chun, and B. Levkau 2004. HDL induces NO-dependent vasorelaxation via the lysophospholipid receptor S1P3. *J.Clin.Invest* 113: 569-581

472. Drew, B. G., N. H. Fidge, G. Gallon-Beaumier, B. E. Kemp, and B. A. Kingwell 2004. High-density lipoprotein and apolipoprotein AI increase endothelial NO synthase activity by protein association and multisite phosphorylation. *Proc.Natl.Acad.Sci.U.S.A* 101: 6999-7004

473. Silver, D. L., N. Wang, X. Xiao, and A. R. Tall 2001. High density lipoprotein (HDL) particle uptake mediated by scavenger receptor class B type 1 results in selective sorting of HDL cholesterol from protein and polarized cholesterol secretion. *J.Biol.Chem.* 276: 25287-25293

474. Noor, R., U. Shuaib, C. X. Wang, K. Todd, U. Ghani, B. Schwindt, and A. Shuaib 2007. High-density lipoprotein cholesterol regulates endothelial progenitor cells by increasing eNOS and preventing apoptosis. *Atherosclerosis* 192: 92-99

475. Mineo, C., H. Deguchi, J. H. Griffin, and P. W. Shaul 2006. Endothelial and antithrombotic actions of HDL. *Circ.Res.* 98: 1352-1364

476. Uittenbogaard, A., P. W. Shaul, I. S. Yuhanna, A. Blair, and E. J. Smart 2000. High density lipoprotein prevents oxidized low density lipoprotein-induced inhibition of endothelial nitric-oxide synthase localization and activation in caveolae. *Journal of Biological Chemistry* 275: 11278-11283

477. Blair, A., P. W. Shaul, I. S. Yuhanna, P. A. Conrad, and E. J. Smart 1999. Oxidized low density lipoprotein displaces endothelial nitric-oxide synthase (eNOS) from plasmalemmal caveolae and impairs eNOS activation. *J.Biol.Chem.* 274: 32512-32519

478. Yeh, M., A. L. Cole, J. Choi, Y. Liu, D. Tulchinsky, J. H. Qiao, M. C. Fishbein, A. N. Dooley, T. Hovnanian, K. Mouilleseaux, D. K. Vora, W. P. Yang, P. Gargalovic, T. Kirchgessner, J. Y. Shyy, and J. A. Berliner 2004. Role for sterol regulatory element-binding protein in activation of endothelial cells by phospholipid oxidation products. *Circ.Res.* 95: 780-788

479. Gharavi, N. M., N. A. Baker, K. P. Mouillesseaux, W. Yeung, H. M. Honda, X. Hsieh, M. Yeh, E. J. Smart, and J. A. Berliner 2006. Role of endothelial nitric oxide synthase in the regulation of SREBP activation by oxidized phospholipids. *Circ.Res.* 98: 768-776

480. Ou, Z., J. Ou, A. W. Ackerman, K. T. Oldham, and K. A. Pritchard, Jr. 2003. L-4F, an apolipoprotein A-1 mimetic, restores nitric oxide and superoxide anion balance in low-density lipoprotein-treated endothelial cells. *Circulation* 107: 1520-1524

481. Li, X. A., L. Guo, J. L. Dressman, R. Asmis, and E. J. Smart 2005. A novel ligand-independent apoptotic pathway induced by SR-BI and suppressed by eNOS and HDL. *J.Biol.Chem.* 280: 19087-19096

482. Doggen, C. J. M., N. L. Smith, R. N. Lemaitre, S. R. Heckbert, F. R. Rosendaal, and B. M. Psaty 2004. Serum lipid levels and the risk of venous thrombosis. *Arteriosclerosis Thrombosis and Vascular Biology* 24: 1970-1975

483. Deguchi, H., N. M. Pecheniuk, D. J. Elias, P. M. Averell, and J. H. Griffin 2005. High-density lipoprotein deficiency and dyslipoproteinemia associated with venous thrombosis in men. *Circulation* 112: 893-899

484. Pajkrt, D., P. G. Lerch, T. vanderPoll, M. Levi, M. Illi, J. E. Doran, B. Arnet, A. vandenEnde, J. W. tenCate, and S. J. H. vanDeventer 1997. Differential effects of reconstituted high-density lipoprotein on coagulation, fibrinolysis and platelet activation during human endotoxemia. *Thrombosis and Haemostasis* 77: 303-307

485. Calkin, A. C., B. G. Drew, A. Ono, S. J. Duffy, M. V. Gordon, S. M. Schoenwaelder, D. Sviridov, M. E. Cooper, B. A. Kingwell, and S. P. Jackson 2009. Reconstituted high-density lipoprotein attenuates platelet function in individuals with type 2 diabetes mellitus by promoting cholesterol efflux. *Circulation* 120: 2095-2104

486. Li, D. Y., S. Weng, B. C. Yang, D. S. Zander, T. Saldeen, W. W. Nichols, S. Khan, and J. L. Mehta 1999. Inhibition of arterial thrombus formation by apoA1 Milano. *Arteriosclerosis Thrombosis and Vascular Biology* 19: 378-383

487. Murphy, A. J., N. Bijl, L. Yvan-Charvet, C. B. Welch, N. Bhagwat, A. Reheman, Y. Wang, J. A. Shaw, R. L. Levine, H. Ni, A. R. Tall, and N. Wang 2013. Cholesterol efflux in megakaryocyte progenitors suppresses platelet production and thrombocytosis. *Nat.Med.* 19: 586-594

488. Fleisher, L. N., A. R. Tall, L. D. Witte, and P. J. Cannon 1983. Effects of high-density lipoprotein and the apoprotein of high-density lipoprotein on Prostacyclin synthesis by endothelial cells. *Advances in Prostaglandin Thromboxane and Leukotriene Research* 11: 475-480

489. Vinals, M., J. Martinez-Gonzalez, J. J. Badimon, and L. Badimon 1997. HDL-induced prostacyclin release in smooth muscle cells is dependent on cyclooxygenase-2 (Cox-2). *Arteriosclerosis Thrombosis and Vascular Biology* 17: 3481-3488

490. Escudero, I., J. Martinez-Gonzalez, R. Alonso, P. Mata, and L. Badimon 2003. Experimental and interventional dietary study in humans on the role of HDL fatty acid composition in PGI(2) release and Cox-2 expression by VSMC. *European Journal of Clinical Investigation* 33: 779-786

491. Liu, D., L. Ji, X. Tong, B. Pan, J. Y. Han, Y. Huang, Y. E. Chen, S. Pennathur, Y. Zhang, and L. Zheng 2011. Human apolipoprotein A-I induces cyclooxygenase-2 expression and prostaglandin I-2 release in endothelial cells through ATP-binding cassette transporter A1. *Am.J.Physiol Cell Physiol* 301: C739-C748

492. Zhang, Q. H., X. Y. Zu, R. X. Cao, J. H. Liu, Z. C. Mo, Y. Zeng, Y. B. Li, S. L. Xiong, X. Liu, D. F. Liao, and G. H. Yi 2012. An involvement of SR-B1 mediated PI3K-Akt-eNOS signaling in HDL-induced cyclooxygenase 2 expression and prostacyclin production in endothelial cells. *Biochem.Biophys.Res.Commun.* 420: 17-23

493. Nicholls, S. J., B. Cutri, S. G. Worthley, P. Kee, K. A. Rye, S. Bao, and P. J. Barter 2005. Impact of short-term administration of high-density lipoproteins and atorvastatin on atherosclerosis in rabbits. *Arteriosclerosis Thrombosis and Vascular Biology* 25: 2416-2421

494. Griffin, J. H., K. Kojima, C. L. Banka, L. K. Curtiss, and J. A. Fernandez 1999. High-density lipoprotein enhancement of anticoagulant activities of plasma protein S and activated protein C. *Journal of Clinical Investigation* 103: 219-227

495. MacCallum, P. K., J. A. Cooper, J. Martin, D. J. Howarth, T. W. Meade, and G. J. Miller 2000. Haemostatic and lipid determinants of prothrombin fragment F1.2 and D-dimer in plasma. *Thrombosis and Haemostasis* 83: 421-426

496. Deguchi, H., S. Yegneswaran, and J. H. Griffin 2004. Sphingolipids as bioactive regulators of thrombin generation. *Journal of Biological Chemistry* 279: 12036-12042

497. Eren, M., C. A. Painter, J. B. Atkinson, P. J. Declerck, and D. E. Vaughan 2002. Age-dependent spontaneous coronary arterial thrombosis in transgenic mice that express a stable form of human plasminogen activator inhibitor-1. *Circulation* 106: 491-496

498. Norata, G. D., C. Banfi, A. Pirillo, E. Tremoli, A. Hamsten, A. L. Catapano, and P. Eriksson 2004. Oxidised-HDL3 induces the expression of PAI-1 in human endothelial cells. Role of p38MAPK activation and mRNA stabilization. *British Journal of Haematology* 127: 97-104

499. Brill, A., A. Yesilaltay, S. F. De Meyer, J. Kisucka, T. A. Fuchs, O. Kocher, M. Krieger, and D. D. Wagner 2012. Extrahepatic high-density lipoprotein receptor SR-BI and apoA-I protect against deep vein thrombosis in mice. *Arterioscler.Thromb.Vasc.Biol.* 32: 1841-1847

500. Brodde, M. F., S. J. Korporaal, G. Herminghaus, M. Fobker, T. J. van Berkel, U. J. Tietge, H. Robenek, E. M. Van, B. E. Kehrel, and J. R. Nofer 2011. Native high-density lipoproteins inhibit platelet activation via scavenger receptor BI Role of negatively charged phospholipids. *Atherosclerosis*

501. Rinninger, F., M. Brundert, R. M. Budzinski, J. C. Fruchart, H. Greten, and G. R. Castro 2003. Scavenger receptor BI (SR-BI) mediates a higher selective cholesteryl ester uptake from LpA-I compared with LpA-I:A-II lipoprotein particles. *Atherosclerosis* 166: 31-40

502. Freedman, D. S., J. D. Otvos, E. J. Jeyarajah, J. J. Barboriak, A. J. Anderson, and J. A. Walker 1998. Relation of lipoprotein subclasses as measured by proton nuclear magnetic resonance spectroscopy to coronary artery disease. *Arteriosclerosis Thrombosis and Vascular Biology* 18: 1046-1053

503. Asztalos, B. F., L. A. Cupples, S. Demissie, K. V. Horvath, C. E. Cox, M. C. Batista, and E. J. Schaefer 2004. High-density lipoprotein subpopulation profile and coronary heart disease prevalence in male participants of the Framingham Offspring Study. *Arterioscler.Thromb.Vasc.Biol.* 24: 2181-2187

504. Asztalos, B. F., D. Collins, L. A. Cupples, S. Demissie, K. V. Horvath, H. E. Bloomfield, S. J. Robins, and E. J. Schaefer 2005. Value of high-density lipoprotein (HDL) subpopulations in predicting recurrent cardiovascular events in the Veterans Affairs HDL Intervention Trial. *Arterioscler.Thromb.Vasc.Biol.* 25: 2185-2191

505. Asztalos, B. F., D. Collins, K. V. Horvath, H. E. Bloomfield, S. J. Robins, and E. J. Schaefer 2008. Relation of gemfibrozil treatment and high-density lipoprotein subpopulation profile with cardiovascular events in the Veterans Affairs High-Density Lipoprotein Intervention Trial. *Metabolism* 57: 77-83

506. Oram, J. F. and A. M. Vaughan 2006. ATP-Binding cassette cholesterol transporters and cardiovascular disease. *Circ.Res.* 99: 1031-1043

507. Yoshikawa, M., N. Sakuma, T. Hibino, T. Sato, and T. Fujinami 1997. HDL3 exerts more powerful anti-oxidative, protective effects against copper-catalyzed LDL oxidation than HDL2. *Clin.Biochem.* 30: 221-225

508. Ashby, D. T., K. A. Rye, M. A. Clay, M. A. Vadas, J. R. Gamble, and P. J. Barter 1998. Factors influencing the ability of HDL to inhibit expression of vascular cell adhesion molecule-1 in endothelial cells. *Arterioscler.Thromb.Vasc.Biol.* 18: 1450-1455

509. Vaisar, T., P. Mayer, E. Nilsson, X. Q. Zhao, R. Knopp, and B. J. Prazen 2010. HDL in humans with cardiovascular disease exhibits a proteomic signature. *Clinica Chimica Acta* 411: 972-979

510. Ansell, B. J., M. Navab, S. Hama, N. Kamranpour, G. Fonarow, G. Hough, S. Rahmani, R. Mottahedeh, R. Dave, S. T. Reddy, and A. M. Fogelman 2003. Inflammatory/antiinflammatory properties of high-density lipoprotein distinguish patients from control subjects better than high-density lipoprotein cholesterol levels and are favorably affected by simvastatin treatment. *Circulation* 108: 2751-2756

511. Huszar, D., M. L. Varban, F. Rinninger, R. Feeley, T. Arai, V. Fairchild-Huntress, M. J. Donovan, and A. R. Tall 2000. Increased LDL cholesterol and atherosclerosis in LDL receptor-deficient mice with attenuated expression of scavenger receptor B1. *Arterioscler.Thromb.Vasc.Biol.* 20: 1068-1073

512. Van, E. M., M. Hoekstra, R. B. Hildebrand, Y. Yaong, D. Stengel, J. K. Kruijt, W. Sattler, U. J. Tietge, E. Ninio, T. J. Van Berkel, and D. Pratico 2007. Increased oxidative stress in scavenger receptor BI knockout mice with dysfunctional HDL. *Arterioscler.Thromb.Vasc.Biol.* 27: 2413-2419

513. Patel, P. J., A. V. Khera, K. Jafri, R. L. Wilensky, and D. J. Rader 2011. The anti-oxidative capacity of high-density lipoprotein is reduced in acute coronary syndrome but not in stable coronary artery disease. *J.Am.Coll.Cardiol.* 58: 2068-2075

514. Natarajan, P., K. K. Ray, and C. P. Cannon 2010. High-density lipoprotein and coronary heart disease: current and future therapies. *J.Am.Coll.Cardiol.* 55: 1283-1299

515. Saemann, M. D., M. Poglitsch, C. Kopecky, M. Haidinger, W. H. Horl, and T. Weichhart 2010. The versatility of HDL: a crucial anti-inflammatory regulator. *Eur.J.Clin.Invest* 40: 1131-1143

516. Tolle, M., T. Huang, M. Schuchardt, V. Jankowski, N. Prufer, J. Jankowski, U. J. Tietge, W. Zidek, and M. van der Giet 2012. High-density lipoprotein loses its anti-inflammatory capacity by accumulation of pro-inflammatory-serum amyloid A. *Cardiovasc.Res.* 94: 154-162

517. Holzer, M., R. Birner-Gruenberger, T. Stojakovic, D. El-Gamal, V. Binder, C. Wadsack, A. Heinemann, and G. Marsche 2011. Uremia alters HDL composition and function. *J.Am.Soc.Nephrol.* 22: 1631-1641

518. Patel, P. J., A. V. Khera, R. L. Wilensky, and D. J. Rader 2013. Anti-oxidative and cholesterol efflux capacities of high-density lipoprotein are reduced in ischaemic cardiomyopathy. *Eur.J.Heart Fail.* 15: 1215-1219

519. Morgantini, C., A. Natali, B. Boldrini, S. Imaizumi, M. Navab, A. M. Fogelman, E. Ferrannini, and S. T. Reddy 2011. Anti-inflammatory and antioxidant properties of HDLs are impaired in type 2 diabetes. *Diabetes* 60: 2617-2623

520. Armitage, J. Niacin causes serious unexpected side effects but no wothwhile benefits, for patients who are at increased risk of heart attacks and strokes. 2013.

Ref Type: Online Source

521. Schwartz, G. G., A. G. Olsson, M. Abt, C. M. Ballantyne, P. J. Barter, J. Brumm, B. R. Chaitman, I. M. Holme, D. Kallend, L. A. Leiter, E. Leitersdorf, J. J. McMurray, H. Mundl, S. J. Nicholls, P. K. Shah, J. C. Tardif, and R. S. Wright 2012. Effects of dalcetrapib in patients with a recent acute coronary syndrome. *N.Engl.J.Med.* 367: 2089-2099

522. Nissen, S. E., J. C. Tardif, S. J. Nicholls, J. H. Revkin, C. L. Shear, W. T. Duggan, W. Ruzyllo, W. B. Bachinsky, G. P. Lasala, and E. M. Tuzcu 2007. Effect of torcetrapib on the progression of coronary atherosclerosis. *N.Engl.J.Med.* 356: 1304-1316

523. Shao, B., S. Pennathur, and J. W. Heinecke 2012. Myeloperoxidase targets apolipoprotein A-I, the major high density lipoprotein protein, for site-specific oxidation in human atherosclerotic lesions. *J.Biol.Chem.* 287: 6375-6386

524. Zheng, L. M., B. Nukuna, M. L. Brennan, M. J. Sun, M. Goormastic, M. Settle, D. Schmitt, X. M. Fu, L. Thomson, P. L. Fox, H. Ischiropoulos, J. D. Smith, M. Kinter, and S. L. Hazen 2004. Apolipoprotein A-I is a selective target for myeloperoxidase-catalyzed oxidation and functional impairment in subjects with cardiovascular disease. *Journal of Clinical Investigation* 114: 529-541

525. Zheng, L., M. Settle, G. Brubaker, D. Schmitt, S. L. Hazen, J. D. Smith, and M. Kinter 2005. Localization of nitration and chlorination sites on apolipoprotein A-I catalyzed by myeloperoxidase in human atheroma and associated oxidative impairment in ABCA1-dependent cholesterol efflux from macrophages. *J.Biol.Chem.* 280: 38-47

526. Shao, B., G. Cavigiolio, N. Brot, M. N. Oda, and J. W. Heinecke 2008. Methionine oxidation impairs reverse cholesterol transport by apolipoprotein A-I. *Proc.Natl.Acad.Sci.U.S A* 105: 12224-12229

527. Wu, Z., M. A. Wagner, L. Zheng, J. S. Parks, J. M. Shy, III, J. D. Smith, V. Gogonea, and S. L. Hazen 2007. The refined structure of nascent HDL reveals a key functional domain for particle maturation and dysfunction. *Nat.Struct.Mol.Biol.* 14: 861-868

528. Huang, Y. and et al. 2014. An abundant dysfunctional apolipoprotein A1 in human atheroma. *Nature Medicine* advance online publication:

529. Didonato, J. A., Y. Huang, K. S. Aulak, O. Even-Or, G. Gerstenecker, V. Gogonea, Y. Wu, P. L. Fox, W. H. Tang, E. F. Plow, J. D. Smith, E. A. Fisher, and S. L. Hazen 2013. Function and distribution of apolipoprotein A1 in the artery wall are markedly distinct from those in plasma. *Circulation* 128: 1644-1655

530. Kar, S., M. A. Patel, R. K. Tripathy, P. Bajaj, U. V. Suvarnakar, and A. H. Pande 2012. Oxidized phospholipid content destabilizes the structure of reconstituted high density lipoprotein particles and changes their function. *Biochim.Biophys.Acta* 1821: 1200-1210

531. Berrougui, H., S. Loued, and A. Khalil 2012. Purified human paraoxonase-1 interacts with plasma membrane lipid rafts and mediates cholesterol efflux from macrophages. *Free Radic.Biol.Med.* 52: 1372-1381

532. Rosenblat, M., R. Karry, and M. Aviram 2006. Paraoxonase 1 (PON1) is a more potent antioxidant and stimulant of macrophage cholesterol efflux, when present in HDL than in lipoprotein-deficient serum: relevance to diabetes. *Atherosclerosis* 187: 74-81

533. Roghani, A. and V. I. Zannis 1988. Alterations of the glutamine residues of human apolipoprotein AI propeptide by in vitro mutagenesis. Characterization of the normal and mutant protein forms. *Biochemistry* 27: 7428-7435

534. Kypreos, K. E., K. W. Van Dijk, Z. A. van Der, L. M. Havekes, and V. I. Zannis 2001. Domains of apolipoprotein E contributing to triglyceride and cholesterol homeostasis in vivo. Carboxyl-terminal region 203-299 promotes hepatic very low density lipoprotein-triglyceride secretion. *J.Biol.Chem.* 276: 19778-19786

535. Matz, C. E. and A. Jonas 1982. Micellar complexes of human apolipoprotein A-I with phosphatidylcholines and cholesterol prepared from cholate-lipid dispersions. *J.Biol.Chem.* 257: 4535-4540

536. Dobiasova, M. and M. Schutzova 1986. Cold labelled substrate and estimation of cholesterol esterification rate in lecithin cholesterol acyltransferase radioassay. *Physiol Bohemoslov.* 35: 319-327

537. O K, J. S. Hill, X. Wang, and P. H. Pritchard 1993. Recombinant lecithin:cholesterol acyltransferase containing a Thr123-->Ile mutation esterifies cholesterol in low density lipoprotein but not in high density lipoprotein. *J.Lipid Res.* 34: 81-88

538. Williamson, R., D. Lee, J. Hagaman, and N. Maeda 1992. Marked reduction of high density lipoprotein cholesterol in mice genetically modified to lack apolipoprotein A-I. *Proc.Natl.Acad.Sci.U.S.A* 89: 7134-7138

539. Thorngate, F. E., P. G. Yancey, G. Kellner-Weibel, L. L. Rudel, G. H. Rothblat, and D. L. Williams 2003. Testing the role of apoA-I, HDL, and cholesterol efflux in the atheroprotective action of low-level apoE expression. *J.Lipid Res.* 44: 2331-2338

540. Fielding, C. J. and P. E. Fielding 1996. Two-dimensional nondenaturing electrophoresis of lipoproteins: applications to high-density lipoprotein speciation. *Methods Enzymol.* 263: 251-259

541. Greenfield, N. and G. D. Fasman 1969. Computed circular dichroism spectra for the evaluation of protein conformation. *Biochemistry* 8: 4108-4116

542. Kateifides, A. K. Analysis of the pathway of biogenesis of HDL by mutations of apolipoprotein A-I. 2011. University of Crete, Greece. 2011.

Ref Type: Thesis/Dissertation

543. Luo, J., Z. L. Deng, X. Luo, N. Tang, W. X. Song, J. Chen, K. A. Sharff, H. H. Luu, R. C. Haydon, K. W. Kinzler, B. Vogelstein, and T. C. He 2007. A protocol for rapid generation of recombinant adenoviruses using the AdEasy system. *Nat.Protoc.* 2: 1236-1247

544. Vezeridis, A. M. Molecular mechanisms of a dominant form of type III hyperlipoproteinemia and the biogenesis of apolipoprotein E-containing high density lipoprotein. 2009. Boston University, U.S.A.

Ref Type: Thesis/Dissertation

545. Hoffer, M. J., S. Niththyananthan, R. P. Naoumova, M. S. Kibirige, R. R. Frants, L. M. Havekes, and G. R. Thompson 1996. Apolipoprotein E1-Hammersmith (Lys146-->Asn;Arg147-->Trp), due to a dinucleotide substitution, is associated with early manifestation of dominant type III hyperlipoproteinaemia. *Atherosclerosis* 124: 183-189

546. Holleboom, A. G., J. A. Kuivenhoven, C. C. van Olden, J. Peter, A. W. Schimmel, J. H. Levels, R. M. Valentijn, P. Vos, J. C. Defesche, J. J. Kastelein, G. K. Hovingh, E. S. Stroes, and C. E. Hollak 2011. Proteinuria in early childhood due to familial LCAT deficiency caused by loss of a disulfide bond in lecithin:cholesterol acyl transferase. *Atherosclerosis* 216: 161-165

547. Maruyama, T., S. Yamashita, Y. Matsuzawa, H. Bujo, K. Takahashi, Y. Saito, S. Ishibashi, K. Ohashi, F. Shionoiri, T. Gotoda, N. Yamada, and T. Kita 2004. Mutations in Japanese subjects with primary hyperlipidemia--results from the Research Committee of the Ministry of Health and Welfare of Japan since 1996--. *J.Atheroscler.Thromb.* 11: 131-145

548. He, T. C., S. Zhou, L. T. da Costa, J. Yu, K. W. Kinzler, and B. Vogelstein 1998. A simplified system for generating recombinant adenoviruses. *Proc.Natl.Acad.Sci.U.S.A* 95: 2509-2514

549. Miller, K. R., J. Wang, M. Sorci-Thomas, R. A. Anderson, and J. S. Parks 1996. Glycosylation structure and enzyme activity of lecithin:cholesterol acyltransferase from human plasma, HepG2 cells, and baculoviral and Chinese hamster ovary cell expression systems. *J.Lipid Res.* 37: 551-561

550. Chong, K. S., M. Jahani, S. Hara, and A. G. Lacko 1983. Characterization of lecithin-cholesterol acyltransferase from human plasma. 3. Chemical properties of the enzyme. *Can.J.Biochem.Cell Biol.* 61: 875-881

551. Fotakis, P., I. Tiniakou, A. K. Kateifides, C. Gkolfinopoulou, A. Chroni, E. Stratikos, V. I. Zannis, and D. Kardassis 2013. Significance of the hydrophobic residues 225-230 of apoA-I for the biogenesis of HDL. *J.Lipid Res.* 54: 3293-3302

552. Arakawa, R. and S. Yokoyama 2002. Helical apolipoproteins stabilize ATP-binding cassette transporter A1 by protecting it from thiol protease-mediated degradation. *J.Biol.Chem.* 277: 22426-22429

553. Rothblat, G. H., M. Llera-Moya, V. Atger, G. Kellner-Weibel, D. L. Williams, and M. C. Phillips 1999. Cell cholesterol efflux: integration of old and new observations provides new insights. *J.Lipid Res.* 40: 781-796

554. Fielding, C. J. and P. E. Fielding 2001. Cellular cholesterol efflux. *Biochim.Biophys.Acta* 1533: 175-189

555. Francone, O. L., P. V. Subbaiah, A. van Tol, L. Royer, and M. Haghpassand 2003. Abnormal phospholipid composition impairs HDL biogenesis and maturation in mice lacking Abca1. *Biochemistry* 42: 8569-8578

556. Hassan, H. H., M. Denis, D. Y. Lee, I. Iatan, D. Nyholt, I. Ruel, L. Krimbou, and J. Genest 2007. Identification of an ABCA1-dependent phospholipid-rich plasma membrane apolipoprotein A-I binding site for nascent HDL formation: implications for current models of HDL biogenesis. *J.Lipid Res.* 48: 2428-2442

557. Lyssenko, N. N., M. Hata, P. Dhanasekaran, M. Nickel, D. Nguyen, P. S. Chetty, H. Saito, S. Lund-Katz, and M. C. Phillips 2012. Influence of C-terminal alpha-helix hydrophobicity and aromatic amino acid content on apolipoprotein A-I functionality. *Biochim.Biophys.Acta* 1821: 456-463

558. Biedzka-Sarek, M., J. Metso, A. Kateifides, T. Meri, T. S. Jokiranta, A. Muszynski, J. Radziejewska-Lebrecht, V. Zannis, M. Skurnik, and M. Jauhiainen 2011. Apolipoprotein A-I exerts bactericidal activity against Yersinia enterocolitica serotype O:3. *J.Biol.Chem.* 286: 38211-38219

559. Liu, T., M. Krieger, H. Y. Kan, and V. I. Zannis 2002. The effects of mutations in helices 4 and 6 of apoA-I on scavenger receptor class B type I (SR-BI)-mediated cholesterol efflux suggest that formation of a productive complex between reconstituted high density lipoprotein and SR-BI is required for efficient lipid transport. *J.Biol.Chem.* 277: 21576-21584

560. Woollett, L. A. and D. K. Spady 1997. Kinetic parameters for high density lipoprotein apoprotein AI and cholesteryl ester transport in the hamster. *J.Clin.Invest* 99: 1704-1713

561. Hoffer, M. J., S. Niththyananthan, R. P. Naoumova, M. S. Kibirige, R. R. Frants, L. M. Havekes, and G. R. Thompson 1996. Apolipoprotein E1-Hammersmith (Lys146-->Asn;Arg147-->Trp), due to a dinucleotide substitution, is associated with early manifestation of dominant type III hyperlipoproteinaemia. *Atherosclerosis* 124: 183-189

562. Vezeridis, A. M., K. Drosatos, and V. I. Zannis 2011. Molecular etiology of a dominant form of type III hyperlipoproteinemia caused by R142C substitution in apoE4. *J.Lipid Res.* 52: 45-56

563. Vezeridis, A. M., K. Drosatos, and V. I. Zannis 2010. Molecular etiology of a dominant form of type III hyperlipoproteinemia caused by R142C substitution in apoE4. *J.Lipid Res.*

564. Horie, Y., S. Fazio, J. R. Westerlund, K. H. Weisgraber, and S. C. Rall, Jr. 1992. The functional characteristics of a human apolipoprotein E variant (cysteine at residue 142) may explain its association with dominant expression of type III hyperlipoproteinemia. *J.Biol.Chem.* 267: 1962-1968

565. Drosatos, K., D. Sanoudou, K. E. Kypreos, D. Kardassis, and V. I. Zannis 2007. A dominant negative form of the transcription factor c-Jun affects genes that have opposing effects on lipid homeostasis in mice. *J.Biol.Chem.* 282: 19556-19564

566. Salinelli, S., J. Y. Lo, M. P. Mims, E. Zsigmond, L. C. Smith, and L. Chan 1996. Structure-function relationship of lipoprotein lipase-mediated enhancement of very low density lipoprotein binding and catabolism by the low density lipoprotein receptor. Functional importance of a properly folded surface loop covering the catalytic center. *J.Biol.Chem.* 271: 21906-21913

567. Medh, J. D., S. L. Bowen, G. L. Fry, S. Ruben, M. Andracki, I. Inoue, J. M. Lalouel, D. K. Strickland, and D. A. Chappell 1996. Lipoprotein lipase binds to low density lipoprotein receptors and induces receptor-mediated catabolism of very low density lipoproteins in vitro. *J.Biol.Chem.* 271: 17073-17080

568. Wetterau, J. R., L. P. Aggerbeck, S. C. Rall, Jr., and K. H. Weisgraber 1988. Human apolipoprotein E3 in aqueous solution. I. Evidence for two structural domains. *J.Biol.Chem.* 263: 6240-6248

569. Dong, L. M., C. Wilson, M. R. Wardell, T. Simmons, R. W. Mahley, K. H. Weisgraber, and D. A. Agard 1994. Human apolipoprotein E. Role of arginine 61 in mediating the lipoprotein preferences of the E3 and E4 isoforms. *J.Biol.Chem.* 269: 22358-22365

570. Dong, L. M. and K. H. Weisgraber 1996. Human apolipoprotein E4 domain interaction. Arginine 61 and glutamic acid 255 interact to direct the preference for very low density lipoproteins. *J.Biol.Chem.* 271: 19053-19057

571. Mahley, R. W., K. H. Weisgraber, and Y. Huang 2006. Apolipoprotein E4: a causative factor and therapeutic target in neuropathology, including Alzheimer's disease. *Proc.Natl.Acad.Sci.U.S.A* 103: 5644-5651

572. Cash, J. G., D. G. Kuhel, J. E. Basford, A. Jaeschke, T. K. Chatterjee, N. L. Weintraub, and D. Y. Hui 2012. Apolipoprotein E4 impairs macrophage efferocytosis and potentiates apoptosis by accelerating endoplasmic reticulum stress. *J.Biol.Chem.* 287: 27876-27884

573. Hofmann, S. M., D. Perez-Tilve, T. M. Greer, B. A. Coburn, E. Grant, J. E. Basford, M. H. Tschop, and D. Y. Hui 2008. Defective lipid delivery modulates glucose tolerance and metabolic response to diet in apolipoprotein E-deficient mice. *Diabetes* 57: 5-12

574. Kuhel, D. G., E. S. Konaniah, J. E. Basford, C. McVey, C. T. Goodin, T. K. Chatterjee, N. L. Weintraub, and D. Y. Hui 2013. Apolipoprotein E2 accentuates postprandial inflammation and diet-induced obesity to promote hyperinsulinemia in mice. *Diabetes* 62: 382-391

575. Kothapalli, D., I. Fuki, K. Ali, S. A. Stewart, L. Zhao, R. Yahil, D. Kwiatkowski, E. A. Hawthorne, G. A. FitzGerald, M. C. Phillips, S. Lund-Katz, E. Pure, D. J. Rader, and R. K. Assoian 2004. Antimitogenic effects of HDL and APOE mediated by Cox-2-dependent IP activation. *J.Clin.Invest* 113: 609-618

576. Moore, Z. W., B. Zhu, D. G. Kuhel, and D. Y. Hui 2004. Vascular apolipoprotein e expression and recruitment from circulation to modulate smooth muscle cell response to endothelial denudation. *Am.J.Pathol.* 164: 2109-2116

577. Moore, Z. W. and D. Y. Hui 2005. Apolipoprotein E inhibition of vascular hyperplasia and neointima formation requires inducible nitric oxide synthase. *J.Lipid Res.* 46: 2083-2090

578. Hui, D. Y. and J. E. Basford 2005. Distinct signaling mechanisms for apoE inhibition of cell migration and proliferation. *Neurobiol.Aging* 26: 317-323

579. Getz, G. S. and C. A. Reardon 2009. Apoprotein E as a lipid transport and signaling protein in the blood, liver, and artery wall. *J.Lipid Res.* 50 Suppl: S156-S161

580. Swertfeger, D. K. and D. Y. Hui 2001. Apolipoprotein E receptor binding versus heparan sulfate proteoglycan binding in its regulation of smooth muscle cell migration and proliferation. *J.Biol.Chem.* 276: 25043-25048

581. Stannard, A. K., D. R. Riddell, S. M. Sacre, A. D. Tagalakis, C. Langer, E. A. von, P. Cullen, T. Athanasopoulos, G. Dickson, and J. S. Owen 2001. Cell-derived apolipoprotein E (ApoE) particles inhibit vascular cell adhesion molecule-1 (VCAM-1) expression in human endothelial cells. *J.Biol.Chem.* 276: 46011-46016

582. Sacre, S. M., A. K. Stannard, and J. S. Owen 2003. Apolipoprotein E (apoE) isoforms differentially induce nitric oxide production in endothelial cells. *FEBS Lett.* 540: 181-187

583. Ishigami, M., D. K. Swertfeger, N. A. Granholm, and D. Y. Hui 1998. Apolipoprotein E inhibits platelet-derived growth factor-induced vascular smooth muscle cell migration and proliferation by suppressing signal transduction and preventing cell entry to G1 phase. *J.Biol.Chem.* 273: 20156-20161

584. Zhu, B., C. A. Reardon, G. S. Getz, and D. Y. Hui 2002. Both apolipoprotein E and immune deficiency exacerbate neointimal hyperplasia after vascular injury in mice. *Arterioscler.Thromb.Vasc.Biol.* 22: 450-455

585. Zhu, Y., A. Kodvawala, and D. Y. Hui 2010. Apolipoprotein E inhibits toll-like receptor (TLR)-3- and TLR-4-mediated macrophage activation through distinct mechanisms. *Biochem.J.* 428: 47-54

586. Bisgaier, C. L., O. P. Sachdev, L. Megna, and R. M. Glickman 1985. Distribution of Apolipoprotein-A-Iv in Human-Plasma. *Journal of Lipid Research* 26: 11-25

587. Lagrost, L., P. Gambert, M. Boquillon, and C. Lallemant 1989. Evidence for High-Density Lipoproteins As the Major Apolipoprotein A-Iv-Containing Fraction in Normal Human-Serum. *Journal of Lipid Research* 30: 1525-1534

588. Duverger, N., N. Ghalim, G. Ailhaud, A. Steinmetz, J. C. Fruchart, and G. Castro 1993. Characterization of apoA-IV-containing lipoprotein particles isolated from human plasma and interstitial fluid. *Arterioscler.Thromb.* 13: 126-132

589. Weinberg, R. B. and M. S. Spector 1985. Structural-Properties and Lipid-Binding of Human Apolipoprotein A-Iv. *Journal of Biological Chemistry* 260: 4914-4921

590. Aalto-Setala, K., C. L. Bisgaier, A. Ho, K. A. Kieft, M. G. Traber, H. J. Kayden, R. Ramakrishnan, A. Walsh, A. D. Essenburg, and J. L. Breslow 1994. Intestinal expression of human

apolipoprotein A-IV in transgenic mice fails to influence dietary lipid absorption or feeding behavior. *J.Clin.Invest* 93: 1776-1786

591. Cohen, R. D., L. W. Castellani, J. H. Qiao, B. J. Van Lenten, A. J. Lusis, and K. Reue 1997. Reduced aortic lesions and elevated high density lipoprotein levels in transgenic mice overexpressing mouse apolipoprotein A-IV. *J.Clin.Invest* 99: 1906-1916

592. Ostos, M. A., M. Conconi, L. Vergnes, N. Baroukh, J. Ribalta, J. Girona, J. M. Caillaud, A. Ochoa, and M. M. Zakin 2001. Antioxidative and antiatherosclerotic effects of human apolipoprotein A-IV in apolipoprotein E-deficient mice. *Arteriosclerosis Thrombosis and Vascular Biology* 21: 1023-1028

593. Zannis, V. I., H. Y. Kan, A. Kritis, E. E. Zanni, and D. Kardassis 2001. Transcriptional regulatory mechanisms of the human apolipoprotein genes in vitro and in vivo. *Curr.Opin.Lipidol.* 12: 181-207

594. Duverger, N., G. Tremp, J. M. Caillaud, F. Emmanuel, G. Castro, J. C. Fruchart, A. Steinmetz, and P. Denefle 1996. Protection against atherogenesis in mice mediated by human apolipoprotein A-IV. *Science* 273: 966-968

595. Vowinkel, T., M. Mori, C. F. Krieglstein, J. Russell, F. Saijo, S. Bharwani, R. H. Turnage, W. S. Davidson, P. Tso, D. N. Granger, and T. J. Kalogeris 2004. Apolipoprotein A-IV inhibits experimental colitis. *Journal of Clinical Investigation* 114: 260-269

596. Recalde, D., M. A. Ostos, E. Badell, A. L. Garcia-Otin, J. Pidoux, G. Castro, M. M. Zakin, and D. Scott-Algara 2004. Human apolipoprotein A-IV reduces secretion of proinflammatory cytokines and atherosclerotic effects of a chronic infection mimicked by lipopolysaccharide. *Arteriosclerosis Thrombosis and Vascular Biology* 24: 756-761

597. Zeiher, A. M., H. Drexler, H. Wollschlager, and H. Just 1991. Modulation of coronary vasomotor tone in humans. Progressive endothelial dysfunction with different early stages of coronary atherosclerosis. *Circulation* 83: 391-401

598. Kuvin, J. T., A. R. Patel, M. Sidhu, W. M. Rand, K. A. Sliney, N. G. Pandian, and R. H. Karas 2003. Relation between high-density lipoprotein cholesterol and peripheral vasomotor function. *Am.J.Cardiol.* 92: 275-279

599. Bisoendial, R. J., G. K. Hovingh, J. H. Levels, P. G. Lerch, I. Andresen, M. R. Hayden, J. J. Kastelein, and E. S. Stroes 2003. Restoration of endothelial function by increasing high-density lipoprotein in subjects with isolated low high-density lipoprotein. *Circulation* 107: 2944-2948

600. Nakou, M., G. Bertsias, I. Stagakis, M. Centola, I. Tassiulas, M. Hatziapostolou, I. Kritikos, G. Goulielmos, D. T. Boumpas, and D. Iliopoulos 2010. Gene network analysis of bone marrow mononuclear cells reveals activation of multiple kinase pathways in human systemic lupus erythematosus. *PLoS One* 5: e13351

601. Hirsch, H. A., D. Iliopoulos, A. Joshi, Y. Zhang, S. A. Jaeger, M. Bulyk, P. N. Tsichlis, L. Shirley, X, and K. Struhl 2010. A transcriptional signature and common gene networks link cancer with lipid metabolism and diverse human diseases. *Cancer Cell* 17: 348-361

Role of the hydrophobic and charged residues in the 218–226 region of apoA-I in the biogenesis of HDL[1]

Panagiotis Fotakis,*,† Andreas K. Kateifides,*,† Christina Gkolfinopoulou,§ Dimitra Georgiadou,§ Melissa Beck,*,† Katharina Gründler,* Angeliki Chroni,§ Efstratios Stratikos,§ Dimitris Kardassis,† and Vassilis I. Zannis[2],*

Whitaker Cardiovascular Institute,* Boston University School of Medicine, Boston, MA 02118; Department of Biochemistry,† University of Crete Medical School, Heraklion, Crete, Greece 71110; and National Center for Scientific Research "Demokritos",§ Athens, Greece 15310

Abstract **We investigated the significance of hydrophobic and charged residues 218–226 on the structure and functions of apoA-I and their contribution to the biogenesis of HDL. Adenovirus-mediated gene transfer of apoA-I[L218A/L219A/V221A/L222A] in apoA-I$^{-/-}$ mice decreased plasma cholesterol and apoA-I levels to 15% of wild-type (WT) control mice and generated pre-β- and α4-HDL particles. In apoA-I$^{-/-}$ × apoE$^{-/-}$ mice, the same mutant formed few discoidal and pre-β-HDL particles that could not be converted to mature α-HDL particles by excess LCAT. Expression of the apoA-I[E223A/K226A] mutant in apoA-I$^{-/-}$ mice caused lesser but discrete alterations in the HDL phenotype. The apoA-I[218–222] and apoA-I[E223A/K226A] mutants had 20% and normal capacity, respectively, to promote ABCA1-mediated cholesterol efflux. Both mutants had ∼65% of normal capacity to activate LCAT in vitro. Biophysical analyses suggested that both mutants affected in a distinct manner the structural integrity and plasticity of apoA-I that is necessary for normal functions. We conclude that the alteration of the hydrophobic 218–222 residues of apoA-I disrupts apoA-I/ABCA1 interactions and promotes the generation of defective pre-β particles that fail to mature into α-HDL subpopulations, thus resulting in low plasma apoA-I and HDL. Alterations of the charged 223, 226 residues caused milder but discrete changes in HDL phenotype.—** Fotakis, P., A. K. Kateifides, C. Gkolfinopoulou, D. Georgiadou, M. Beck, K. Gründler, A. Chroni, E. Stratikos, D. Kardassis, and V. I. Zannis. **Role of the hydrophobic and charged residues in the 218–226 region of apoA-I in the biogenesis of HDL.** ***J. Lipid Res.*** 54: **3281–3292.**

Supplementary key words apolipoprotein A-I mutations • pre-β and α-HDL particles • dyslipidemia • LCAT

ApoA-I is the major protein component of HDL and plays an essential role in the biogenesis, maturation, and the functions of HDL (1–3). The biogenesis and remodeling of HDL occurs extracellularly and requires ABCA1, LCAT, and several other proteins (4). HDL biogenesis occurs predominantly in the liver and, to a lesser extent, in extrahepatic tissues (5, 6). The crucial role of apoA-I, ABCA1, and LCAT for the biogenesis of HDL has been established by naturally occurring mutations in these proteins in humans with low HDL levels (7–9).

In previous studies, systematic mutagenesis and gene transfer of human apoA-I mutants in apoA-I-deficient (apoA-I$^{-/-}$) mice disrupted specific steps along the pathway of the biogenesis of HDL and generated discrete lipid and lipoprotein phenotypes (10). The phenotypes generated included inhibition of the formation of HDL (1); generation of unstable intermediates (11, 12); inhibition of the activation of LCAT (13); and increase in plasma cholesterol or increase in both plasma cholesterol and triglycerides (14). The previous studies also showed that apoA-I-deletion mutants that lack residues 220–231 have diminished capacity to promote ABCA1-mediated cholesterol efflux and fail to cross-link with ABCA1 and to synthesize spherical HDL (1, 15)

In the present study, we investigated the role of four hydrophobic (L218, L219, V221, L222) and two charged

This work was supported by National Institutes of Health Grant HL-48739, General Secretariat of Research and Technology of Greece Grant Synergasia 09SYN-12-897 (to D.K. and A.C.), and Ministry of Education of Greece Grant Thalis MIS 377286 (to D.K., A.C., and E.S.). D. Georgiadou was supported by the graduate fellowship program of the National Center for Scientific Research Demokritos. P. Fotakis has been supported by pre-doctoral training Fellowship HERACLEITUS II by the European Union and Greek national funds through the Operational Program "Education and Lifelong Learning" of the National Strategic Reference Framework (NSRF).

Manuscript received 28 March 2013 and in revised form 27 August 2013.

Published, JLR Papers in Press, August 29, 2013
DOI 10.1194/jlr.M038356

Abbreviations: ANS, 8-anilino-1-naphthalene-sulfonate; apoA-I[218–222], the apoA-I carrying the L218A/L219A/V221A/L222A mutations; apoA-I[E223A/K226A], the apoA-I carrying the E223A/K226A mutations apoA-I$^{-/-}$, apoA-I-deficient; apoA-I$^{-/-}$ × apoE$^{-/-}$, apoA-I and apoE double-deficient; CD, circular dichroism; cpt-cAMP, 8-(4-chlorophenylthio) adenosine 3′:5′-cyclic monophosphatase; DMPC, dimyristoyl-L-α-phosphatidylcholine; EM, electron microscopy; FPLC, fast-protein liquid chromatography; GdnHCl, guanidine hydrochloride; HEK293, human embryonic kidney 293; HTB-13, SW 1783 human astrocytoma; pfu, plaque-forming unit; POPC, β-oleoyl-γ-palmitoyl-L-α-phosphatidylcholine; rHDL, reconstituted HDL; WMF, wavelength of maximum fluorescence; WT, wild-type.

[1] See referenced companion article, *J. Lipid Res.* 2013, 54: 3293–3302.

[2] To whom correspondence should be addressed.
e-mail: vzannis@bu.edu

The online version of this article (available at http://www.jlr.org) contains supplementary data in the form of two tables, three figures, and methods.

(E223, K226) residues, located within or in the vicinity of the 220–231 region, on the biogenesis of HDL and the properties of apoA-I. The rationale for the alteration of these residues that reside within the 222–226 domain was based on the significance of this region for the structure of apoA-I. The crystal structure at 3.2 Å resolution of a truncated, lipid-free form of apoA-I [Δ(1–43)] that lacks the amino terminal domain indicated that, with the exception of the 220–227 region, apoA-I consists of a nearly continuous amphipathic α-helical sequence that is punctuated by small or pronounced kinks (16, 17). Most recently the three-dimensional structure of a dimeric truncated form of lipid-free apoA-I[Δ(185–243)] was determined at 2.2 A^{o} resolution (18). The structure showed that the N-terminal domain stabilizes the apoA-I dimer in solution and forces it to an antiparallel configuration that is similar to the configuration that the two apoA-I monomers assume when bound to discoidal HDL particles (16–19). In this configuration, it was proposed that the unstructured loop consisting of residues 220–227 allows helices 10 of each monomer to register in antiparallel orientation relative to the other.

In the present study, physicochemical studies and in vitro experiments determined how the mutations affected the structure of apoA-I and the ability of the mutant proteins to promote ABCA1-mediated cholesterol efflux and to activate LCAT. Adenovirus-mediated gene transfer of the apoA-I[218–222] mutant in apoA-I$^{-/-}$ × apoE$^{-/-}$ mice led to the formation of only pre-β-HDL particles and a small number of discoidal HDL particles. In contrast to previous studies (11–13), this defect, observed for the first time, could not be corrected by coexpression of the apoA-I[218–222] mutant and LCAT. Expression of the apoA-I[E223A/K226A] mutant in apoA-I$^{-/-}$ mice caused small alterations in the apoA-I structure and the HDL phenotype, suggesting that these residues also contribute to the efficient formation of HDL.

In addition to the drastic effect of the L218A/L219A/V221A/L222A mutations on the biogenesis of HDL, the mutants also inhibited the ability of lipid-free apoA-I to promote transendothelial transport (20), as well as its bactericidal activity against Gram-negative bacteria (21), indicating the importance of the 218–222 residues for the functions of apoA-I.

EXPERIMENTAL PROCEDURES

Materials

Materials not mentioned in this section have been obtained from sources described previously (2, 14).

Methods

Generation of adenoviruses expressing the wild-type and the mutant apoA-I forms and human LCAT. The apoA-I gene lacking the BglII restriction site that is present at nucleotide position 181 of the genomic sequence relative to the ATG codon of the gene was cloned into the pCDNA3.1 vector to generate the pCDNA3.1-apoA-I(ΔBglII) plasmid as described (12). This plasmid was used as a template to introduce the apoA-I mutations apoA-I[218–222] and apoA-I[E223A/K226A] using the QuickChange® XL mutagenesis kit (Stratagene, Santa Clara, CA) and the mutagenic primers shown in supplementary Table I. The recombinant adenoviruses were packaged in 911 cells, amplified in human embryonic kidney 293 (HEK293) cells, purified, and titrated as described (12).

The human LCAT cDNA in the pENTR221 vector was a gift of Dr. J. A. Kuivenhoven (University of Amsterdam). The LCAT cDNA was amplified using primers that contained restriction sites for BglII and EcoRV, respectively, at the 5′ and 3′ ends, as shown in supplementary Table I. The LCAT cDNA was digested with BglII and EcoRV and cloned into the corresponding sites of the pAdTrack-CMV vector. The recombinant adenovirus was constructed, purified, and titrated as described (12).

ApoA-I production, purification, and use for functional and physicochemical studies. Wild-type (WT) apoA-I, apoA-I[218–222] mutant, and apoA-I[E223A/K226A] mutant protein were obtained from the culture media of HTB-13 cells grown in roller bottles following infection with adenoviruses expressing the corresponding proteins. For protein production, the culture medium was collected every 24 h, dialyzed against 25 mM ammonium bicarbonate, and lyophilized. For the purification of WT apoA-I and apoA-I[E223A/K226A] mutant, the lyophilized medium was resuspended in 0.01M Tris (pH 8), filtered, and passed through a 5 ml HiTrap Q HP column (GE Healthcare). The proteins were eluted with linear gradient of 1M NH_4CO_3 in the Tris buffer, as described previously (1). The apoA-I[218–222] mutant was purified with the same procedure under denaturing conditions (8M urea) to facilitate the dissociation of apoA-I from other proteins that coelute with mutant apoA-I under native conditions. The purity of the apoA-I preparation was assessed by SDS-PAGE, and fractions greater than 95% pure were pooled.

ABCA1-dependent cholesterol efflux and LCAT assays. ABCA1-dependent efflux of cholesterol was measured in cultures of J774 macrophages in which expression of ABCA1 was induced by a cAMP analog using WT and mutant apoA-I forms as cholesterol acceptors. The J774 mouse macrophages were labeled with 0.3 μCi/ml [^{14}C]cholesterol ([4-^{14}C]cholesterol, 0.04 mCi/ml of specific activity 50 mCi/mmol; Perkin-Elmer Life Sciences) for 24 h and then treated with 0.3 mM cpt-cAMP [8-(4-chlorophenylthio)-cAMP] for 24 h. Cholesterol efflux was determined as described previously (1).

LCAT was purified as described (14) from the culture medium of human HTB13 cells infected with an adenovirus expressing the human LCAT cDNA (22). The reconstituted HDL (rHDL) particles used as the substrate contained cholesterol, and [^{14}C] cholesterol, β-oleoyl-γ-palmitoyl-L-α-phosphatidylcholine (POPC), and apoA-I. rHDL was prepared by the sodium cholate dialysis method as described previously (23). rHDL particles without ^{14}C-cholesterol containing mutant forms of apoA-I were prepared with the same procedure to measure their size by electron microscopy (EM). The size of these particles was determined from the negatives of the EM images. The enzymatic reactions and the derivation of the apparent V_{max} and K_m were carried out as described previously (13).

Physicochemical measurements. Derivation of far-UV spectra, thermal and chemical denaturation profiles, and 8-anilino-1-naphthalene-sulfonate (ANS) fluorescence spectra of the WT apoA-I, apoA-I[218–222] mutant, and apoA-I[E223A/K226A] mutant are described in the supplementary methods.

Animal studies. ApoA-I$^{-/-}$ (ApoA1^{tm1Unc}) C57BL/6J mice (24) were purchased from Jackson Laboratories (Bar Harbor,

ME). Mice deficient for apoA-I$^{-/-}$ and apoE$^{-/-}$ were a gift of Dr. Fayanne Thorngate and Dr. David Williams (25) or were obtained by crossing apoA-I$^{-/-}$ with apoE$^{-/-}$ (26). The mice were maintained on a 12 h light/dark cycle and standard rodent chow. All procedures performed on the mice were in accordance with National Institutes of Health guidelines and followed a protocol (AN-14219.2012.10) approved by the Institutional Animal Care and Use Committee (IACUC). ApoA-I$^{-/-}$ or apoA-I$^{-/-}$ × apoE$^{-/-}$ mice, 6–8 weeks of age, were injected via the tail vein with 1–2 × 10^9 pfu of recombinant adenovirus per animal. The animals were euthanized four days after injection following a four-hour fast. Five to six mice were used for each set of experiments. Determination of plasma lipids and apoA-I levels, fractionation of plasma by fast-protein liquid chromatography (FPLC), and density gradient ultracentrifugation EM of HDL and two-dimensional gel electrophoresis of plasma are as described (1, 2, 27 and supplementary methods).

Statistics. Statistical analyses were performed by two-tailed Student *t*-test with equal variance.

RESULTS

Expression of the apoA-I transgene following adenovirus infection

Total hepatic RNA was isolated from the livers of apoA-I$^{-/-}$ four days after infection with adenoviruses expressing the WT apoA-I, apoA-I[218–222] mutant, and apoA-I [E223A/K226A] mutant. The relative expression of the WT and the mutant apoA-I transgenes was determined by qPCR as described in the Experimental Procedures. This analysis showed that the expression of WT and the apoA-I [218–222] mutant were comparable, whereas the expression of apoA-I[E223A/K226A] was approximately 165% of that of WT apoA-I (supplementary Table II).

Plasma lipid and apoA-I levels and FPLC profiles

Plasma lipids and apoA-I were determined four days after infection of apoA-I$^{-/-}$ mice with adenoviruses expressing the WT and the two apoA-I mutants. It was found that the apoA-I[218–222] mutant decreased plasma cholesterol and apoA-I levels to approximately 15% as compared with WT apoA-I. The plasma apoA-I levels of the apoA-I[E223A/K226A] mutant were not statistically different from those of WT apoA-I, whereas the plasma cholesterol levels were significantly lower (62% as compared with WT apoA-I) (**Fig. 1A**, B). The plasma triglycerides of the apoA-I[E223A/K226A] mutant were slightly increased as compared with wild-type apoA-I ($P < 0.05$) (supplementary Table II). FPLC analysis of plasma from apoA-I$^{-/-}$ mice infected with the recombinant adenovirus expressing either WT apoA-I or the two apoA-I mutants showed that in all cases cholesterol was distributed in the HDL region and that the HDL cholesterol peak of the apoA-I[218–222] mutant was greatly diminished (Fig. 1C).

Fractionation of plasma, EM analysis, and two-dimensional electrophoresis of plasma of apoA-I$^{-/-}$ mice expressing the WT and the mutant forms of apoA-I

Fractionation of plasma by density gradient ultracentrifugation and subsequent analysis of the resulting fractions by SDS-PAGE showed that the WT apoA-I was equally distributed in the HDL2 and HDL3 region and that the apoA-I[E223A/K226A] and apoA-I[218–222] mutants were predominantly distributed in the HDL3 and, to a lesser extent, the HDL2 region (**Fig. 2A**, B). The apoA-I[218–222] mutant was characterized by low levels of apoA-I and increased levels of mouse apoE that floated in the HDL2/HDL3 (Fig. 2C and supplementary Fig. I-A, B) and in the VLDL/IDL/LDL region.

Analysis of the HDL fractions 6 and 7 obtained following density gradient ultracentrifugation by EM showed that the WT apoA-I as well as the two apoA-I mutants (apoA-I[E223A/K222A] and apoA-I[218–222]) generated spherical particles (Fig. 2D–F). Two-dimensional gel electrophoresis of plasma showed that WT apoA-I formed normal pre-β- and α-HDL subpopulations (Fig. 2G); the apoA-I[E223A/K226A] mutant formed predominantly α2, α3, and α4 and had increased amount of pre-β subpopulations (Fig. 2H); and the apoA-I[218–222] mutant formed only pre-β, α4, and α3 subpopulations (Fig. 2I).

To clarify whether the HDL particles observed in Fig. 2F originate from the apoA-I[218–222] mutant or mouse apoE that float in the HDL region (Fig. 2C and supplementary Fig. I-A, B), we performed adenovirus-mediated gene transfer in apoA-I$^{-/-}$ × apoE$^{-/-}$ mice, which lack both mouse apoA-I and apoE. Analysis of relative expression of the WT and the mutant apoA-I transgenes by qPCR showed that the expression of WT apoA-I and apoA-I[218–222] mutant were comparable (supplementary Table II). Separation of the plasma by density gradient ultracentrifugation and SDS-PAGE analysis of the fractions showed that WT apoA-I was distributed predominantly in the HDL2/HDL3 region (**Fig. 3A**). EM analysis of the fractions 6 and 7 obtained by density gradient ultracentrifugation of the plasma showed that WT apoA-I generated spherical particles (Fig. 3B). Two-dimensional gel electrophoresis showed that the plasma of mice expressing WT apoA-I contained the normal pre-β- and α-HDL subpopulations (Fig. 3C). SDS-PAGE analysis of plasma fractions obtained from mice expressing the apoA-I[218–222] mutant showed the presence of small amounts of the mutant protein in the HDL3 region (Fig. 3D). The L218A/L219A/V221A/L222A mutations in apoA-I resulted in a great increase in plasma apoA-IV that floated in the IDL/LDL/HDL2/HDL3 region (Fig. 3D and supplementary Fig. II) and the presence of apoB-48 in the HDL region (Fig. 3E). The apoA-I[218–222] mutant generated few discoidal particles as well as particles corresponding in size to VLDL (48.5 ± 15 nm), IDL (28.8 ± 3 nm), and LDL (20.2 ± 2.5 nm) (Fig. 3F). The appearance of the LDL- and IDL-sized particles is also supported by the presence of apoB-48 in fractions 6 and 7 used for the EM analysis (Fig. 3E). The plasma of mice expressing the apoA-I[218–222] mutant contained only pre-β-HDL particles (Fig. 3G). The relative migration of the particles generated by WT apoA-I and the apoA-I[218–222] mutant was established by two-dimensional gel electrophoresis of mixtures of the plasmas containing these two apoA-I forms (Fig. 3H).

Previous studies have shown that the low HDL levels and the abnormal HDL phenotypes of some natural apoA-I

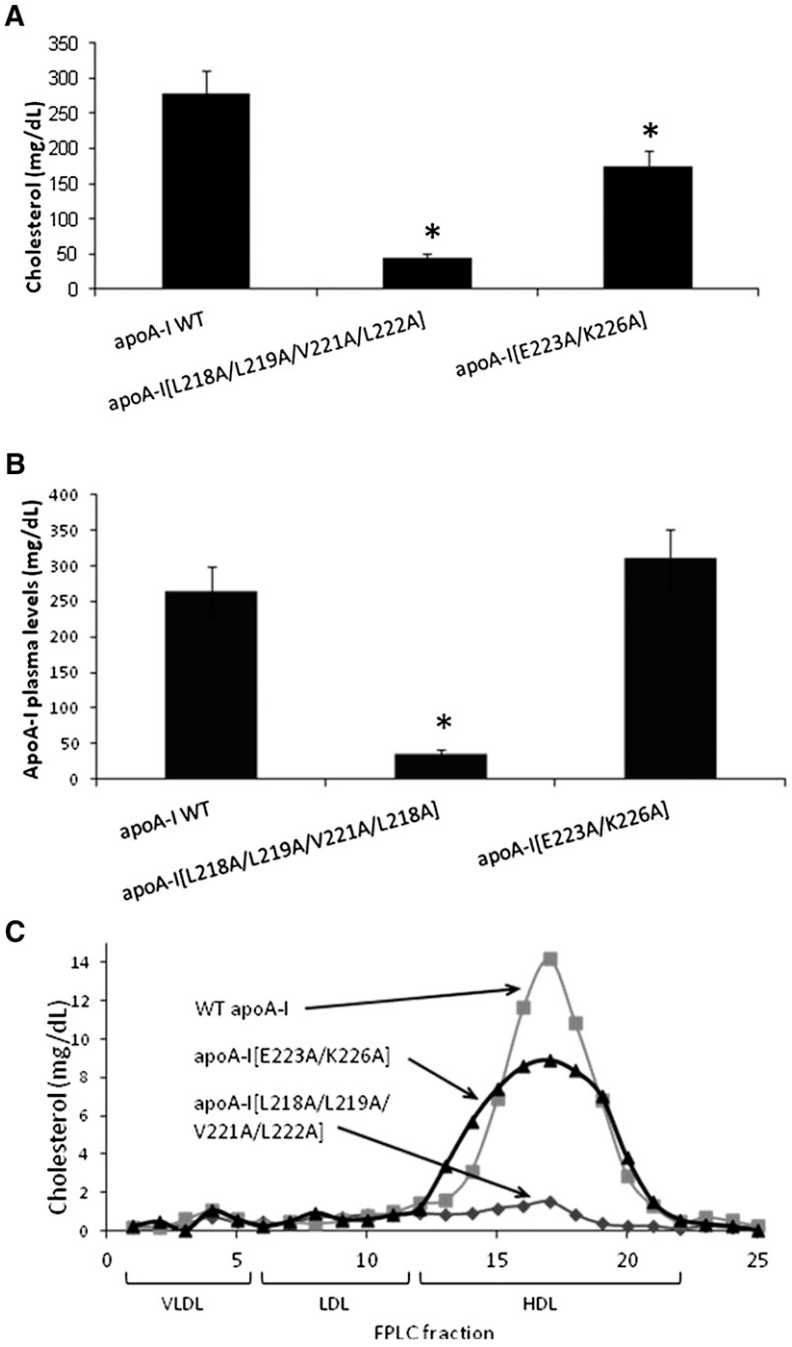

Fig. 1. Plasma cholesterol levels, plasma apoA-I levels, and plasma FPLC profiles four days after infection of apoA-I$^{-/-}$ mice with apoA-I-expressing adenoviruses. Plasma cholesterol (A), plasma apoA-I (B), and plasma FPLC cholesterol profiles (C) of mice infected with adenovirus expressing WT apoA-I, apoA-I[218–222] mutant, or apoA-I[E223A/K226A] mutant as indicated. *$P < 0.05$ compared to apoA-I WT.

mutants could be corrected by excess LCAT (11–13). To assess the potential insufficiency of LCAT that led to the generation of discoidal particles observed in Fig. 3F, we carried out gene transfer of both the apoA-I[218–222] mutant and LCAT in apoA-I$^{-/-}$ × apoE$^{-/-}$ mice. The lipid parameters and the expression levels of the transgene are shown in supplementary Table II. The FPLC profiles of plasma obtained from mice expressing WT apoA-I, apoA-I[218–222] mutant, or apoA-I[218–222] mutant in the presence of LCAT are shown in **Fig. 4A**. This comparative analysis showed that in all cases the great majority of cholesterol was distributed in the VLDL/IDL region. In the case of WT apoA-I, a small amount of cholesterol was distributed in the HDL region, whereas the apoA-I[218–222] mutant did not have an HDL cholesterol peak (Fig. 4A). Coexpression of the apoA-I[218–222] mutant and LCAT had a small effect on the HDL cholesterol peak, but it generated a pronounced cholesterol shoulder in the VLDL/IDL/LDL region (Fig. 4A). Density gradient ultracentrifugation of plasma followed by SDS-PAGE analysis of the fractions showed that a small amount of the mutant apoA-I was found in the HDL3. In addition, the plasma concentration of mouse apoA-IV increased, and the protein shifted toward the VLDL/IDL/LDL region (Fig. 4B). EM analysis of the HDL fraction obtained by density gradient ultracentrifugation showed the presence of small number of spherical HDL particles, along with larger particles corresponding in size to LDL and IDL (Fig. 4C). The appearance

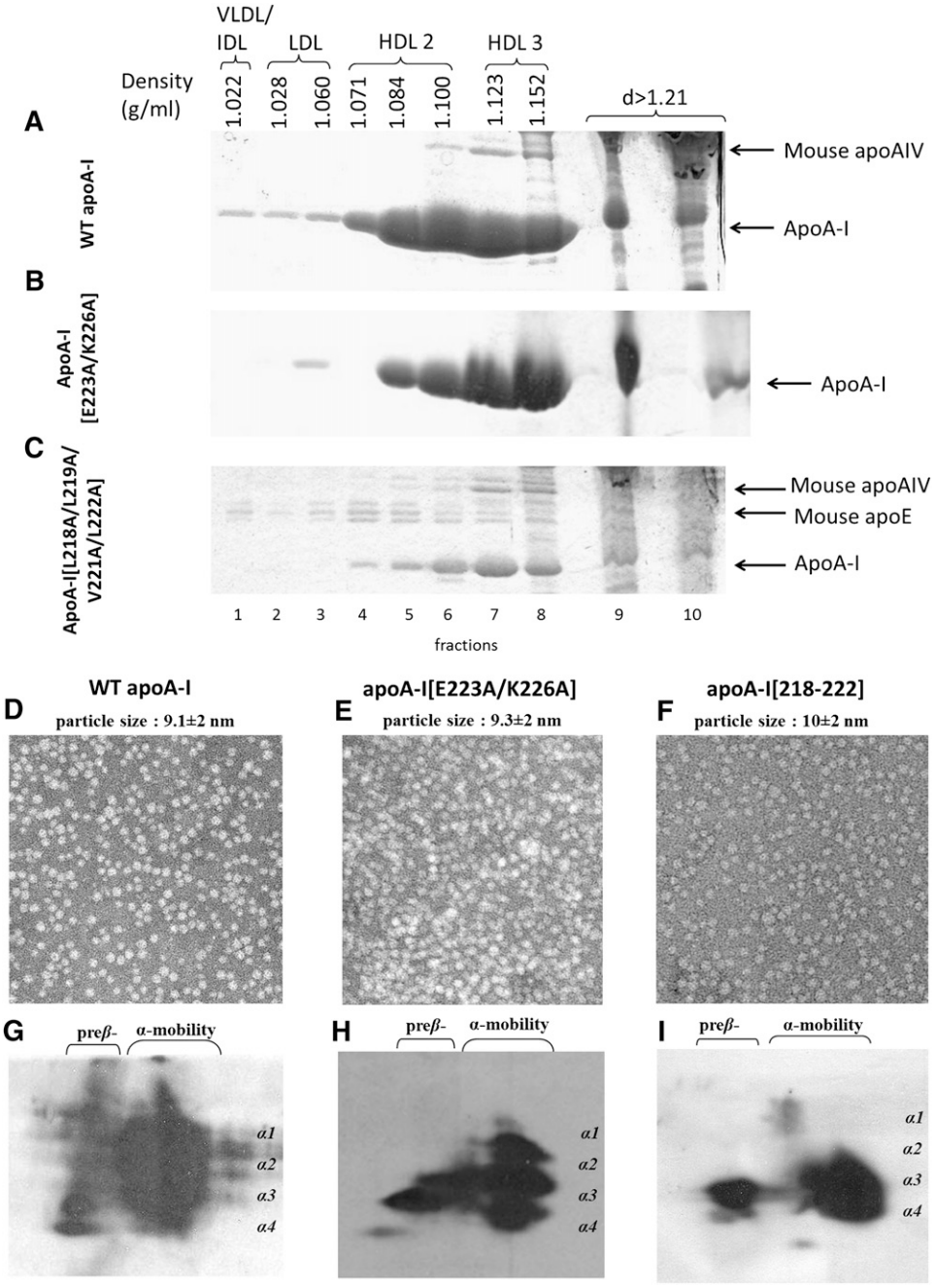

Fig. 2. Analysis of plasma of apoA-I$^{-/-}$ mice infected with adenoviruses expressing the WT apoA-I (A), apoA-I[E223A/K226A] mutant (B), or the apoA-I[218–222] mutant (C) by density gradient ultracentrifugation and SDS-PAGE. EM analysis of HDL fractions 6 and 7 obtained from apoA-I$^{-/-}$ mice expressing the WT apoA-I (D), the apoA-I[E223A/K226A] mutant (E), or the apoA-I[218–222] mutant (F) following density gradient ultracentrifugation of plasma. The photomicrographs were taken at 75,000× magnification and enlarged three times. Two-dimensional gel electrophoresis of plasma of apoA-I$^{-/-}$ mice infected with adenoviruses expressing the WT apoA-I (G), the apoA-I[E223A/K226A] mutant (H), and the apoA-I[218–222] mutant (I).

of the LDL- and IDL-sized particles is also supported by the presence of apoB-48 in fractions 6 and 7 used for the EM analysis (Fig. 4D). It is possible that the LDL- and IDL-sized particles might arise by initial formation of apoA-IV-containing HDL (28) and subsequent fusion of such HDL particles with apoB-containing lipoproteins (Fig. 4C, D). Two-dimensional gel electrophoresis showed that the plasma of mice coexpressing the apoA-I[218–222] mutant and LCAT contained only small amount of pre-β- and α4-HDL particles (Fig. 4E).

Comparative analysis of the in vitro functions of WT apoA-I, apoA-I[218–222] mutant, and apoA-I[E223A/K226A] mutant

The secretion of WT and mutant forms of apoA-I in the culture medium of HTB-13 cells following infection of the

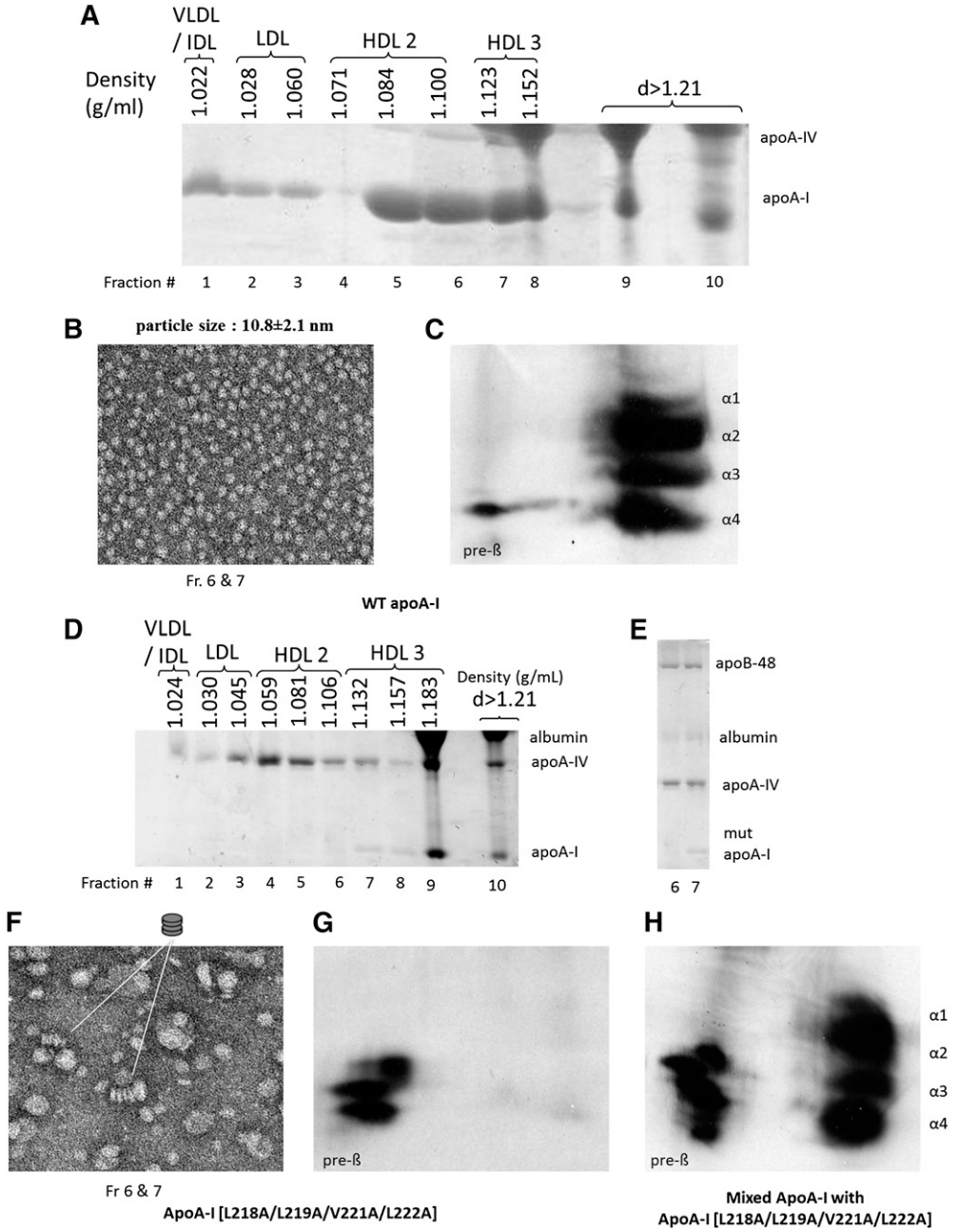

Fig. 3. Analysis of plasma of apoA-I$^{-/-}$ × apoE$^{-/-}$ mice infected with adenoviruses expressing WT apoA-I (A) or apoA-I[218–222] mutant (D) by density gradient ultracentrifugation and SDS-PAGE. EM analysis of HDL fractions 6 and 7 obtained from apoA-I$^{-/-}$ × apoE$^{-/-}$ mice expressing the WT apoA-I (B) or apoA-I[218–222] mutant (F) following density gradient ultracentrifugation of plasma as indicated. The photomicrographs were taken at 75,000× magnification and enlarged three times. E: SDS gel electrophoresis showing lipoprotein composition of fractions 6 and 7. These fractions were used for EM analysis in F. Two-dimensional gel electrophoresis of plasma of apoA-I$^{-/-}$ × apoE$^{-/-}$ mice infected with adenoviruses expressing WT apoA-I (C), apoA-I[L218–222] mutant (G), or mixture of samples obtained from mice expressing WT apoA-I and apoA-I[218–222] mutant (H).

cells with recombinant adenoviruses expressing the corresponding proteins was assessed as described previously (29). This analysis showed that the apoA-I[218–222] and apoA-I[E223A/K226A] mutants were secreted at comparable levels in the culture medium of the adenovirus-infected cells. To interpret the observed defects in HDL biogenesis that resulted from the apoA-I mutations, we purified WT apoA-I, as well as the apoA-I[218–222] and the apoA-I[E223A/K226A] mutants, from the culture media of HTB-13 cells grown in roller bottles and studied their properties in vitro. It was found that the ability of the apoA-I[218–222] mutant to promote ABCA1-mediated cholesterol efflux and to activate LCAT, were 20% and 66%, respectively, as compared with the WT control. The ability of the apoA-I[E223A/K226A] mutant to promote ABCA1-mediated cholesterol efflux was slightly increased

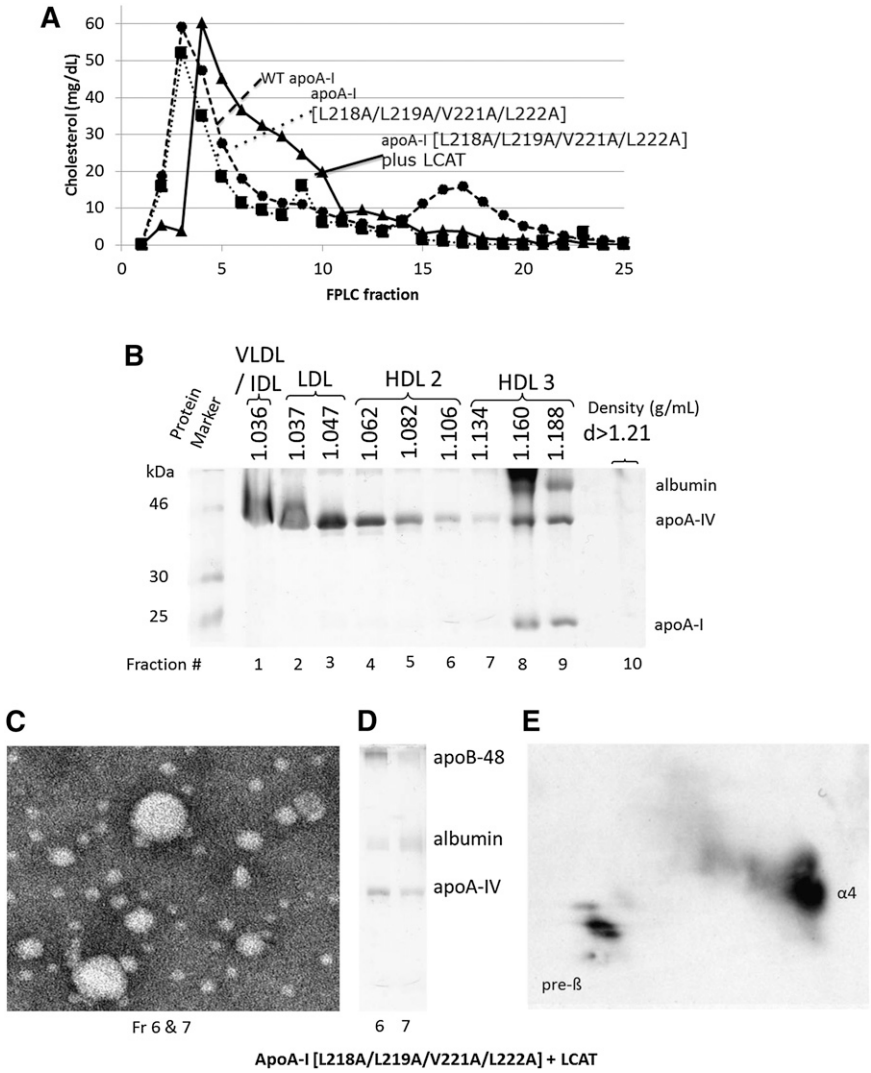

Fig. 4. Analyses of plasma of apoA-I$^{-/-}$ × apoE$^{-/-}$ mice infected with adenoviruses expressing the WT apoA-I or the apoA-I[218–222] mutant alone or in combination with human LCAT. A: Plasma FPLC profiles of mice expressing WT apoA-I or the apoA-I[218–222] mutant alone or in combination with LCAT as indicated. B: SDS-PAGE of fractions obtained by density gradient ultracentrifugation from mice expressing the apoA-I[218–222] mutant and LCAT. C: EM analysis of the HDL corresponding to fractions 6 and 7 of B. D: The photomicrograph was taken at 75,000× magnification and enlarged three times. SDS gel electrophoresis showing apolipoprotein composition of fractions 6 and 7 used for EM analysis in C. E: Two-dimensional gel electrophoresis of plasma of apoA-I$^{-/-}$ × apoE$^{-/-}$ mice infected with adenoviruses expressing the apoA-I[218–222] mutant and LCAT.

compared with that of WT apoA-I, and its ability to activate LCAT was 65% of the WT control (**Fig. 5A**, B).

Effect of the L218A/L219A/V221A/L222A and E223A/K226A mutations on the α-helical content, thermal unfolding, chemical unfolding, and hydrophobic surface exposure of apoA-I

To test whether the functional changes of the two apoA-I mutants are accompanied by changes in the structure and conformation of the protein, we used an array of biophysical assays to evaluate the effects of these mutations (**Fig. 6**). Circular dichroism (CD) measurements indicated 7% and 4.2% loss of helical content for the apoA-I[218–222] mutant and the apoA-I[E223A/K226A] mutant, respectively (Fig. 6A and **Table 1**). Thermal unfolding of apoA-I followed by CD measurements showed that the apoA-I[218–222] mutant had a much more cooperative unfolding transition, indicating a more compact structure for this mutant protein, whereas the apoA-I[E223A/K226A] mutant had a slightly less cooperative unfolding transition, indicating a slightly less compact structure for this mutant (Fig. 6B and Table 1). The chemical unfolding profile of the apoA-I[218–222] mutant, probed by intrinsic tryptophan fluorescence, was identical to that of the WT protein, whereas the chemical unfolding of the apoA-I [E223A/K226A] mutant was less cooperative than the WT apoA-I (Fig. 6C and Table 1). Overall, the apoA-I[E223A/K226A] mutant appears to be thermodynamically destabilized and is quite distinct from the apoA-I[218–222] mutant. Finally, the ANS fluorescence measurements indicated

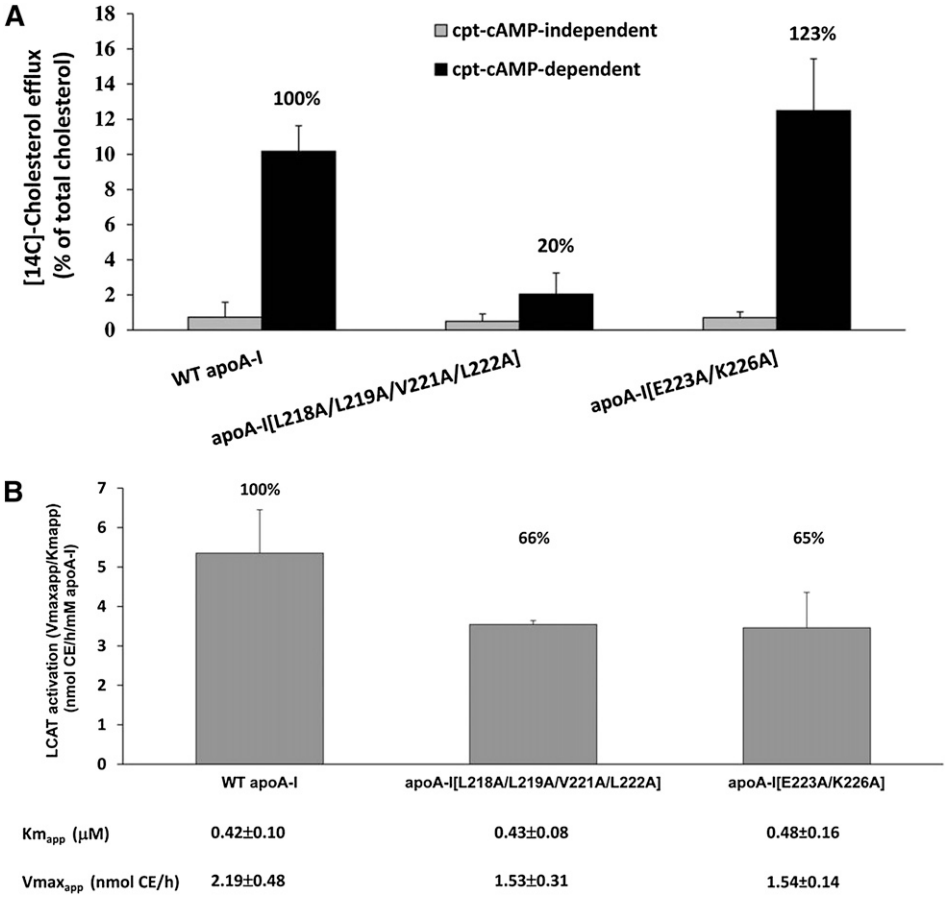

Fig. 5. A: ABCA1-mediated cholesterol efflux from J774 mouse macrophages treated with cpt-cAMP using WT apoA-I, apoA-I[218–222] mutant, and apoA-I[E223A/K226A] mutant as cholesterol acceptor. The ABCA1 independent and ABCA1-mediated efflux is shown. The ABCA1-mediated cholesterol efflux by WT apoA-I is set to 100%. B: LCAT activation capacity of WT apoA-I, apoA-I[218–222] mutant, and the apoA-I[E223A/K226A] mutant. Experiments were performed as described in the Experimental Procedures. The data represent the average from two independent experiments in triplicate.

that the apoA-I[218–222] mutant had a 40% reduction of hydrophobic surface exposure to the solvent, whereas the apoA-I[E223A/K226A] mutant had a 160% increase in the hydrophobic surface exposure to the solvent (Fig. 6D and Table 1).

DISCUSSION

Rationale for selection of the mutations

Lipid-free or minimally lipidated apoA-I promotes ABCA1-mediated cholesterol efflux and thus serves as an acceptor of cellular phospholipid and cholesterol (1, 30, 31). Lipid-bound apoA-I is a physiological activator of LCAT (31). The functional interactions between apoA-I and ABCA1 are important for cholesterol efflux and the biogenesis of HDL (1, 32, 33). To identify the specific C-terminal residues of apoA-I that are required for correct interactions with ABCA1 and/or LCAT that lead to the formation of mature α-HDL particles, we introduced two sets of mutations that span the 218–226 region of apoA-I. The properties of the apoA-I[218–222] and apoA-I[E223A/K226A] mutants thus generated were studied by in vitro experiments and adenovirus-mediated gene transfer.

L218A/L219A/V221A/L222A and E223A/K226A mutations alter the functional and physicochemical properties of apoA-I

The in vitro experiments showed that, compared with WT apoA-I, the capacity of the apoA-I[218–222] mutant to promote ABCA1-mediated cholesterol efflux and to activate LCAT was 20% and 66%, respectively. The capacity of the apoA-I[E223A/K226A] mutant to promote ABCA1-mediated cholesterol efflux was slightly increased compared with that of the WT control, and the capacity to activate LCAT was 65% of the WT control. The changes in the physicochemical properties of the apoA-I[218–222] mutant included a 7% decrease in its α-helical content, a more cooperative thermal unfolding transition (yet an identical chemical unfolding transition), and a 40% reduction of hydrophobic surfaces exposed to the solvent. The higher cooperativity observed during the thermal denaturation of this mutant suggests a more compact and stable structure, which may appear at odds with the lack of any observed stabilization during the chemical denaturation. The two methods, however, report on different aspects of the conformational change that follows protein denaturation (overall secondary structure versus

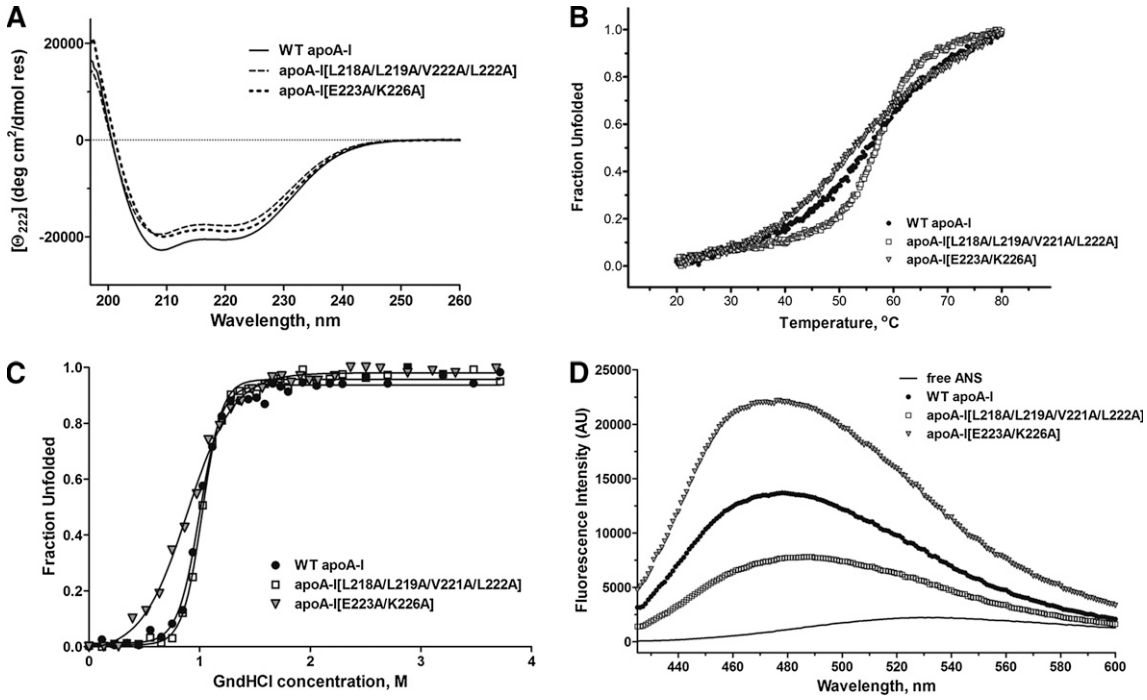

Fig. 6. Far-UV CD spectra of WT apoA-I, apoA-I[218–222] mutant, and apoA-I[E223A/K226A] mutant obtained at 25°C. A: Thermal denaturation profiles of WT apoA-I, apoA-I[218–222] mutant, and apoA-I[E223A/K226A] mutant determined by changes in molar ellipticity at 222 nm. B: Samples were denatured by increasing the temperature up to 80°C. Experimental points are depicted as dots. C: Chemical denaturation profile of WT apoA-I, apoA-I[218–222] mutant, and apoA-I[E223A/K226A] mutant. The intrinsic fluorescence signal of tryptophan of apoA-I was monitored while titrating with Gnd-HCl. The solid line represents nonlinear regression to a simple Boltzmann model. The experimental points are depicted as dots. D: ANS fluorescence spectra obtained in the presence of 50 μg/ml WT apoA-I, apoA-I[218–222] mutant, apoA-I[E223A/K226A] mutant, and buffer alone.

the immediate environment of the tryptophan residues). In apoA-I, all of the tryptophan residues are located in the N-terminal moiety of the molecule, and therefore, the lack of changes during chemical denaturation suggest that the thermodynamic stability of this domain is not affected by the mutation. Conversely, the altered thermal denaturation profile can be explained by localized changes in the folding and stability of the C-terminal moiety of the protein where the mutated residues are or to changes in the interactions between the C-terminal and N-terminal domain that primarily affect the stability of the C-terminal domain. However, since the two methods of denaturation use different mechanisms to unfold the protein, the possibility that the stabilization seen during

TABLE 1. Calculated biophysical parameters for WT and mutant apoA-I forms

Mutation	Circular Dichroism	Thermal Denaturation				Chemical Denaturation			ANS Binding
ApoA-I	α-Helix	T_m (°C)	Slope	Cooperativity Index (n)	ΔH (kcal/mol)	ΔG_D^o (kcal/mol)	$D_{1/2}$ (M)	m^c (kcal mol^{-2})	Fold Increase[a]
WT	60.0 ± 1.5	55.6 ± 0.4	8.3 ± 0.4	6.4 ± 0.2	25.9 ± 1.5	6.3 ± 0.4	1.01 ± 0.02	6.3 ± 0.4	6.0 ± 0.4
L218A/L219A/V221A/L222A	52.7 ± 1.6[b]	56.1 ± 0.8	4.6 ± 0.2[b]	9.7 ± 0.6[b]	46.4 ± 2.4[b]	6.6 ± 0.4	1.00 ± 0.03	6.4 ± 0.4	3.5 ± 0.2[b]
E223A/K226A	55.8 ± 1.1[c]	53.4 ± 0.2[b]	10.4 ± 1.4[d]	5.3 ± 0.7[b]	21.01 ± 2.2[e]	2.5 ± 0.2[b]	0.88 ± 0.02[f]	2.8 ± 0.1[b]	9.6 ± 0.5[b]

Values are means ± SD from three or four experiments. Parameters obtained from the indicated measurements are as follows: "α-helix" is the percentage of α-helical content of the protein as calculated from the molecular ellipticity of the protein sample at 222 nm; "T_m" is middle point of the thermal denaturation transition (melting temperature); "slope" is the calculated slope of the linear component of the thermal denaturation transition, around the melting temperature; "n" is an indicator of the cooperativity of the thermal unfolding transition and is calculated using the Hill equation n = (log 81) / log ($T_{0.9}$ / $T_{0.1}$), where $T_{0.9}$ and $T_{0.1}$ are the temperatures where the unfolding transition reaches a fractional completion of 0.9 and 0.1; "ΔH" is the relative enthalpy change during the thermal denaturation; "ΔG_D^o" is the relative change in Gibbs free-energy during the chemical denaturation; "$D_{1/2}$" is the guanidine HCl concentration at which the midpoint of chemical denaturation is achieved; "m" is the slope at the midtransition point of chemical denaturation; and "fold increase" is the increase in ANS fluorescence in the presence of the protein relative to free ANS in the same buffer.

[a] Fold increase in signal compared with unbound ANS.
[b] $P < 0.0001$.
[c] $P < 0.005$.
[d] $P < 0.05$.
[e] $P = 0.001$.
[f] $P < 0.0005$.

the thermal denaturation is dependent on the particular unfolding pathway utilized during heat denaturation should not be ruled out.

Finally, although the four mutated amino acids in the apoA-I[218–222] mutants correspond to ~5% of total hydrophobic amino acids of the protein, introduction of the mutations resulted in a 40% reduction of hydrophobic surface exposure, indicating that the residues L218/L219/V221/L222 give rise to almost half of the exposed hydrophobic sites of apoA-I. Taken as a whole, these findings suggest that the apoA-I[218–222] mutant greatly affects the structural integrity and conformational plasticity of apoA-I, effects that may at least partially underlie the observed changes in its in vitro and in vivo functions. The changes in the physicochemical properties of the apoA-I[E223A/K226A] mutant included a 4.2% decrease in its α-helical content, a less cooperative thermal and chemical unfolding, and a 160% increase in the hydrophobic surface exposed to the solvent. These changes indicate that this mutant is thermodynamically destabilized and distinct from the apoA-I[218–222] mutant.

Ability of the apoA-I[218–222] and apoA-I[E223A/K226A] mutants to promote biogenesis of HDL

Adenovirus-mediated gene transfer of the WT apoA-I and apoA-I[218–222] mutant in apoA-I$^{-/-}$ mice showed that, at comparable levels of gene expression, the plasma cholesterol and apoA-I levels of mice expressing apoA-I[218–222] mutant were greatly reduced as compared with WT apoA-I. The plasma cholesterol reduction was due to the great decrease in the HDL cholesterol levels as determined by FPLC fractionation. Density gradient ultracentrifugation of plasma showed that, compared with WT apoA-I, the apoA-I[218–222] mutant was mainly distributed in the HDL3 fraction and its quantity was greatly reduced. The HDL fraction also contained substantial amount of mouse apoE and some apoA-IV.

A sensitive analysis that can detect abnormalities in the pathway of HDL biogenesis is the two-dimensional gel electrophoresis of plasma. This analysis showed that the apoA-I[218–222] mutant when expressed in apoA-I$^{-/-}$ mice generated pre-β- and α4-HDL particles. Such particles were shown previously to undergo fast catabolism by the kidney (11, 34). The ability of the apoA-I[218–222] mutant to form HDL particles was also assessed by EM analysis of the HDL fractions obtained by density gradient ultracentrifugation of plasma. This analysis showed the presence of spherical HDL particles.

We showed recently that apoE- or apoA-IV-containing HDL particles can be formed following a pathway similar to that used for the generation of apoA-I-containing HDL particles (28, 35). Since the HDL fractions 6 and 7 analyzed by EM contained both apoA-I[218–222] mutant and mouse apoE, we considered the possibility that the observed spherical HDL particles in Fig. 2F might represent a mixture of apoA-I- and apoE-containing HDL.

To address this question, we performed gene transfer of the apoA-I[218–222] mutant in double-deficient (apoA-I$^{-/-}$ × apoE$^{-/-}$) mice, which lack the two endogenous mouse apolipoproteins. Density gradient ultracentrifugation showed that the plasma of these mice contained only small amounts of apoA-I in the HDL3 and the lipoprotein-free ($d \geq 1.21$ g/ml) fractions. EM analysis showed the presence of few discoidal HDL as well as spherical particles corresponding in size to LDL and IDL. This is compatible with the presence of apoB-48 and apoA-IV in the HDL density range. Two-dimensional gel electrophoresis of plasma showed that it contained only pre-β-HDL. These data indicated that in apoA-I$^{-/-}$ × apoE$^{-/-}$ mice, the apoA-I[218–222] mutant caused a defective lipidation of apoA-I, possibly due to defective apoA-I/ABCA1 interaction, which resulted in the generation of only pre-β-HDL particles that could not be converted to mature α-HDL particles. Previous studies showed that C-terminal deletion mutants that remove the 220-231 region of apoA-I prevented the biogenesis of normal α-HDL particles but allowed the formation of pre-β-HDL particles (1, 15). Similar pre-β-HDL particles have been found in the plasma of ABCA1-deficient mice and humans carrying ABCA1 mutations that are characterized by HDL deficiency (36–38).

It appears that in apoA-I$^{-/-}$ mice, the diminished interactions between ABCA1 and the apoA-I[218–222] mutant observed in vitro give the opportunity to the mouse apoE to compete more effectively for the ABCA1 binding site (3) and thus to be lipidated. This will lead to the formation of spherical apoE-containing HDL particles that float in the HDL2/HDL3 regions (Fig. 2C, F and supplementary Fig. I). Through unknown mechanisms, the formation of apoE-containing HDL appears to partially stabilize the limited number of nascent HDL particles that contain the apoA-I[218–222] mutant. In the absence of both apoA-I and apoE in the double-deficient mice, there is limited lipidation of the apoA-I[218–222] mutant, as evidenced by the low amount of apoA-I that floats in the HDL region and the formation of few discoidal HDL particles (Fig. 3F, G). The absence of apoE in this case appears to have a major destabilizing effect on any nascent HDL particle formed that contains the apoA-I[218–222] mutant. This explains the low apoA-I and HDL levels and the formation of few discoidal HDL particles associated with this mutant. Furthermore, the absence of apoE allows formation of apoA-IV-containing HDL particles in mice expressing the apoA-I[218–222] mutant that appear to interact with apoB-containing lipoproteins and shift their flotation in the HDL density range.

To explain why α4-HDL particles are formed in the apoA-I$^{-/-}$-deficient mice expressing the apoA-I[218–222] mutant, we explored the possibility of changes in ABCA1 protein or mRNA levels in these mouse models. Previous in vitro experiments had shown that, in THP-1 cells, apoA-I protects ABCA1 from proteasome-mediated degradation (39). However, the in vivo animal experiments in the present study did not show significant changes in ABCA1 mRNA or protein levels in apoA-I$^{-/-}$ or apoA-I$^{-/-}$ × apoE$^{-/-}$ mice without any treatment or following gene transfer of either the WT apoA-I or the apoA-I[218–222] mutant (supplementary Fig. III).

The gene transfer studies with the apoA-I[E223A/K226A] mutant showed that, at similar level of gene expression, the plasma apoA-I levels and the EM profile were comparable to those of WT apoA-I. The HDL was shifted toward the HDL3 region and the total HDL cholesterol levels for this mutant were two thirds of that obtained from apoA-I$^{-/-}$ mice expressing WT apoA-I. Slight differences were also observed in the two-dimensional pattern of this mutant, including increased ratio of pre-β- to α-HDL particles and decreased α1-HDL particles. The in vitro experiments showed that the apoA-I[E223A/K226A] mutant is thermodynamically destabilized, has normal capacity to activate ABCA1, and has a modest reduction (65%) in its capacity to activate LCAT. Overall, the data suggest that the apoA-I[E223A/K226A] mutant had small but distinct effects on the properties of apoA-I and the biogenesis of HDL.

In previous studies, we showed that, when expressed in mouse models, naturally occurring point mutations in apoA-I insufficiently activate LCAT and lead to the accumulation of discoidal HDL particles in plasma. In this category belongs the apoA-I variants apoA-I[R151C]$_{Paris}$ and apoA-I[R160L]$_{Oslo}$ as well as the bioengineered mutants apoA-I[R149A] and apoA-I[R160V/H162A] (11, 13). Other naturally occurring apoA-I variants, such as apoA-I[L141R]$_{Piza}$ and apoA-I[L159R]$_{Finland}$ mutants, when expressed in mouse models, were characterized by very low levels of HDL cholesterol, few HDL particles, and the presence of pre-β- and α4-HDL particles in plasma (12). A characteristic feature of these two categories of mutants, which are associated with low plasma HDL levels, is that the abnormal HDL phenotype could be corrected in vivo by gene transfer of human LCAT (11–13). The phenotype produced by the apoA-I[218–222] mutant is distinct from all previously described phenotypes and cannot be corrected by overexpression of LCAT. In addition, the mutant protein had reduced capability to promote the ABCA1-mediated cholesterol efflux. Although other interpretations are possible, the in vivo and in vitro data suggest that the interaction of the apoA-I[218–222] mutant with ABCA1 results in defective lipidation, which leads to the generation of pre-β-HDL particles that are not a good substrate for LCAT. If this interpretation is correct, one can envision a very precise initial orientation of the apoA-I ligand within the binding site of ABCA1 (3), similar to that described before for enzyme substrate interactions. A precise fit of the apoA-I ligand into the ABCA1 binding site will allow its correct lipidation. The nascent particle thus formed can then undergo cholesterol esterification by LCAT, which leads to the formation of mature α-HDL particles. In contrast, incorrectly lipidated apoA-I becomes a poor substrate of LCAT.

Clinical implications

The apoA-I[218–222] mutant generated a unique aberrant HDL phenotype that has not been observed previously. The hallmark of this phenotype is low HDL levels, formation of pre-β-HDL and discoidal HDL that do not mature to spherical α-HDL particles, and the presence of IDL- and LDL-sized particles in the HDL region that are enriched in apoA-IV and apoB-48. Phenotypes generated by mutagenesis of apoA-I can facilitate the identification of similar phenotypes that may exist in the human population. Such phenotypes may serve in the diagnosis, prognosis, and potential treatment of specific dyslipidemias.

Panagiotis Fotakis, Andreas Kateifides, and Melissa Beck have been students of the graduate program "The Molecular Basis of Human Disease" of the University of Crete Medical School. The authors thank Gayle Forbes for technical assistance. She passed away on September 21, 2013. This article is dedicated to her memory.

REFERENCES

1. Chroni, A., T. Liu, I. Gorshkova, H. Y. Kan, Y. Uehara, A. von Eckardstein, and V. I. Zannis. 2003. The central helices of apoA-I can promote ATP-binding cassette transporter A1 (ABCA1)-mediated lipid efflux. Amino acid residues 220–231 of the wild-type apoA-I are required for lipid efflux in vitro and high density lipoprotein formation in vivo. *J. Biol. Chem.* **278:** 6719–6730.
2. Liu, T., M. Krieger, H. Y. Kan, and V. I. Zannis. 2002. The effects of mutations in helices 4 and 6 of apoA-I on scavenger receptor class B type I (SR-BI)-mediated cholesterol efflux suggest that formation of a productive complex between reconstituted high density lipoprotein and SR-BI is required for efficient lipid transport. *J. Biol. Chem.* **277:** 21576–21584.
3. Hassan, H. H., M. Denis, D. Y. Lee, I. Iatan, D. Nyholt, I. Ruel, L. Krimbou, and J. Genest. 2007. Identification of an ABCA1-dependent phospholipid-rich plasma membrane apolipoprotein A-I binding site for nascent HDL formation: implications for current models of HDL biogenesis. *J. Lipid Res.* **48:** 2428–2442.
4. Zannis, V. I., A. Chroni, K. E. Kypreos, H. Y. Kan, T. B. Cesar, E. E. Zanni, and D. Kardassis. 2004. Probing the pathways of chylomicron and HDL metabolism using adenovirus-mediated gene transfer. *Curr. Opin. Lipidol.* **15:** 151–166.
5. Singaraja, R. R., M. Van Eck, N. Bissada, F. Zimetti, H. L. Collins, R. B. Hildebrand, A. Hayden, L. R. Brunham, M. H. Kang, J. C. Fruchart, et al. 2006. Both hepatic and extrahepatic ABCA1 have discrete and essential functions in the maintenance of plasma high-density lipoprotein cholesterol levels in vivo. *Circulation.* **114:** 1301–1309.
6. Chung, S., J. K. Sawyer, A. K. Gebre, N. Maeda, and J. S. Parks. 2011. Adipose tissue ATP binding cassette transporter A1 contributes to high-density lipoprotein biogenesis in vivo. *Circulation.* **124:** 1663–1672.
7. Kiss, R. S., N. Kavaslar, K. Okuhira, M. W. Freeman, S. Walter, R. W. Milne, R. McPherson, and Y. L. Marcel. 2007. Genetic etiology of isolated low HDL syndrome: incidence and heterogeneity of efflux defects. *Arterioscler. Thromb. Vasc. Biol.* **27:** 1139–1145.
8. Cohen, J. C., R. S. Kiss, A. Pertsemlidis, Y. L. Marcel, R. McPherson, and H. H. Hobbs. 2004. Multiple rare alleles contribute to low plasma levels of HDL cholesterol. *Science.* **305:** 869–872.
9. Frikke-Schmidt, R., B. G. Nordestgaard, G. B. Jensen, and A. Tybjaerg-Hansen. 2004. Genetic variation in ABC transporter A1 contributes to HDL cholesterol in the general population. *J. Clin. Invest.* **114:** 1343–1353.
10. Zannis, V. I., E. E. Zanni, A. Papapanagiotou, D. Kardassis, and A. Chroni. 2006. ApoA-I functions and synthesis of HDL: insights from mouse models of human HDL metabolism. *In* High-Density Lipoproteins. From Basic Biology to Clinical Aspects. Wiley-VCH, Weinheim. 237–265.
11. Koukos, G., A. Chroni, A. Duka, D. Kardassis, and V. I. Zannis. 2007. Naturally occurring and bioengineered apoA-I mutations that inhibit the conversion of discoidal to spherical HDL: the abnormal HDL phenotypes can be corrected by treatment with LCAT. *Biochem. J.* **406:** 167–174.
12. Koukos, G., A. Chroni, A. Duka, D. Kardassis, and V. I. Zannis. 2007. LCAT can rescue the abnormal phenotype produced by the natural ApoA-I mutations (Leu141Arg)Pisa and (Leu159Arg)FIN. *Biochemistry.* **46:** 10713–10721.

13. Chroni, A., A. Duka, H. Y. Kan, T. Liu, and V. I. Zannis. 2005. Point mutations in apolipoprotein a-I mimic the phenotype observed in patients with classical lecithin:cholesterol acyltransferase deficiency. *Biochemistry.* **44:** 14353–14366.
14. Chroni, A., H. Y. Kan, K. E. Kypreos, I. N. Gorshkova, A. Shkodrani, and V. I. Zannis. 2004. Substitutions of glutamate 110 and 111 in the middle helix 4 of human apolipoprotein A-I (apoA-I) by alanine affect the structure and in vitro functions of apoA-I and induce severe hypertriglyceridemia in apoA-I-deficient mice. *Biochemistry.* **43:** 10442–10457.
15. Chroni, A., G. Koukos, A. Duka, and V. I. Zannis. 2007. The carboxy-terminal region of apoA-I is required for the ABCA1-dependent formation of alpha-HDL but not prebeta-HDL particles in vivo. *Biochemistry.* **46:** 5697–5708.
16. Borhani, D. W., D. P. Rogers, J. A. Engler, and C. G. Brouillette. 1997. Crystal structure of truncated human apolipoprotein A-I suggests a lipid-bound conformation. *Proc. Natl. Acad. Sci. USA.* **94:** 12291–12296.
17. Borhani, D. W., J. A. Engler, and C. G. Brouillette. 1999. Crystallization of truncated human apolipoprotein A-I in a novel conformation. *Acta Crystallogr. D Biol. Crystallogr.* **55:** 1578–1583.
18. Mei, X., and D. Atkinson. 2011. Crystal structure of C-terminal truncated apolipoprotein A-I reveals the assembly of high density lipoprotein (HDL) by dimerization. *J. Biol. Chem.* **286:** 38570–38582.
19. Segrest, J. P., L. Li, G. M. Anantharamaiah, S. C. Harvey, K. N. Liadaki, and V. Zannis. 2000. Structure and function of apolipoprotein A-I and high-density lipoprotein. *Curr. Opin. Lipidol.* **11:** 105–115.
20. Ohnsorg, P. M., L. Rohrer, D. Perisa, A. Kateifides, A. Chroni, D. Kardassis, V. I. Zannis, and A. von Eckardstein. 2011. Carboxyl terminus of apolipoprotein A-I (ApoA-I) is necessary for the transport of lipid-free ApoA-I but not prelipidated ApoA-I particles through aortic endothelial cells. *J. Biol. Chem.* **286:** 7744–7754.
21. Biedzka-Sarek, M., J. Metso, A. Kateifides, T. Meri, T. S. Jokiranta, A. Muszynski, J. Radziejewska-Lebrecht, V. Zannis, M. Skurnik, and M. Jauhiainen. 2011. Apolipoprotein A-I exerts bactericidal activity against Yersinia enterocolitica serotype O:3. *J. Biol. Chem.* **286:** 38211–38219.
22. Amar, M. J., R. D. Shamburek, B. Vaisman, C. L. Knapper, B. Foger, R. F. Hoyt, Jr., S. Santamarina-Fojo, H. B. Brewer, Jr., and A. T. Remaley. 2009. Adenoviral expression of human lecithin-cholesterol acyltransferase in nonhuman primates leads to an antiatherogenic lipoprotein phenotype by increasing high-density lipoprotein and lowering low-density lipoprotein. *Metabolism.* **58:** 568–575.
23. Matz, C. E., and A. Jonas. 1982. Micellar complexes of human apolipoprotein A-I with phosphatidylcholines and cholesterol prepared from cholate-lipid dispersions. *J. Biol. Chem.* **257:** 4535–4540.
24. Williamson, R., D. Lee, J. Hagaman, and N. Maeda. 1992. Marked reduction of high density lipoprotein cholesterol in mice genetically modified to lack apolipoprotein A-I. *Proc. Natl. Acad. Sci. USA.* **89:** 7134–7138.
25. Thorngate, F. E., P. G. Yancey, G. Kellner-Weibel, L. L. Rudel, G. H. Rothblat, and D. L. Williams. 2003. Testing the role of apoA-I, HDL, and cholesterol efflux in the atheroprotective action of low-level apoE expression. *J. Lipid Res.* **44:** 2331–2338.
26. Zhang, S. H., R. L. Reddick, J. A. Piedrahita, and N. Maeda. 1992. Spontaneous hypercholesterolemia and arterial lesions in mice lacking apolipoprotein E. *Science.* **258:** 468–471.
27. Chroni, A., H. Y. Kan, A. Shkodrani, T. Liu, and V. I. Zannis. 2005. Deletions of helices 2 and 3 of human apoA-I are associated with severe dyslipidemia following adenovirus-mediated gene transfer in apoA-I-deficient mice. *Biochemistry.* **44:** 4108–4117.
28. Duka, A., P. Fotakis, D. Georgiadou, A. Kateifides, K. Tzavlaki, L. von Eckardstein, E. Stratikos, D. Kardassis, and V. I. Zannis. 2013. ApoA-IV promotes the biogenesis of apoA-IV-containing HDL particles with the participation of ABCA1 and LCAT. *J. Lipid Res.* **54:** 107–115.
29. Kateifides, A. K., I. N. Gorshkova, A. Duka, A. Chroni, D. Kardassis, and V. I. Zannis. 2011. Alteration of negatively charged residues in the 89 to 99 domain of apoA-I affects lipid homeostasis and maturation of HDL. *J. Lipid Res.* **52:** 1363–1372.
30. Rothblat, G. H., M. Llera-Moya, V. Atger, G. Kellner-Weibel, D. L. Williams, and M. C. Phillips. 1999. Cell cholesterol efflux: integration of old and new observations provides new insights. *J. Lipid Res.* **40:** 781–796.
31. Fielding, C. J., and P. E. Fielding. 2001. Cellular cholesterol efflux. *Biochim. Biophys. Acta.* **1533:** 175–189.
32. Wang, N., D. L. Silver, P. Costet, and A. R. Tall. 2000. Specific binding of ApoA-I, enhanced cholesterol efflux, and altered plasma membrane morphology in cells expressing ABC1. *J. Biol. Chem.* **275:** 33053–33058.
33. Remaley, A. T., J. A. Stonik, S. J. Demosky, E. B. Neufeld, A. V. Bocharov, T. G. Vishnyakova, T. L. Eggerman, A. P. Patterson, N. J. Duverger, S. Santamarina-Fojo, et al. 2001. Apolipoprotein specificity for lipid efflux by the human ABCAI transporter. *Biochem. Biophys. Res. Commun.* **280:** 818–823.
34. Timmins, J. M., J. Y. Lee, E. Boudyguina, K. D. Kluckman, L. R. Brunham, A. Mulya, A. K. Gebre, J. M. Coutinho, P. L. Colvin, T. L. Smith, et al. 2005. Targeted inactivation of hepatic Abca1 causes profound hypoalphalipoproteinemia and kidney hypercatabolism of apoA-I. *J. Clin. Invest.* **115:** 1333–1342.
35. Kypreos, K. E., and V. I. Zannis. 2007. Pathway of biogenesis of apolipoprotein E-containing HDL in vivo with the participation of ABCA1 and LCAT. *Biochem. J.* **403:** 359–367.
36. Daniil, G., A. A. Phedonos, A. G. Holleboom, M. M. Motazacker, L. Argyri, J. A. Kuivenhoven, and A. Chroni. 2011. Characterization of antioxidant/anti-inflammatory properties and apoA-I-containing subpopulations of HDL from family subjects with monogenic low HDL disorders. *Clin. Chim. Acta.* **412:** 1213–1220.
37. Francone, O. L., P. V. Subbaiah, A. van Tol, L. Royer, and M. Haghpassand. 2003. Abnormal phospholipid composition impairs HDL biogenesis and maturation in mice lacking Abca1. *Biochemistry.* **42:** 8569–8578.
38. Asztalos, B. F., M. E. Brousseau, J. R. McNamara, K. V. Horvath, P. S. Roheim, and E. J. Schaefer. 2001. Subpopulations of high density lipoproteins in homozygous and heterozygous Tangier disease. *Atherosclerosis.* **156:** 217–225.
39. Arakawa, R., and S. Yokoyama. 2002. Helical apolipoproteins stabilize ATP-binding cassette transporter A1 by protecting it from thiol protease-mediated degradation. *J. Biol. Chem.* **277:** 22426–22429.

Significance of the hydrophobic residues 225–230 of apoA-I for the biogenesis of HDL[1] [S]

Panagiotis Fotakis,[*,†] Ioanna Tiniakou,[†] Andreas K. Kateifides,[*,†] Christina Gkolfinopoulou,[§] Angeliki Chroni,[§] Efstratios Stratikos,[§] Vassilis I. Zannis,[2,3,*,†] and Dimitris Kardassis[2,†]

Whitaker Cardiovascular Institute,* Boston University School of Medicine, Boston, MA 02118; Department of Biochemistry,[†] University of Crete Medical School, Heraklion, Crete, Greece 71110; and National Center for Scientific Research "Demokritos",[§] Athens, Greece 15310

Abstract **We studied the significance of four hydrophobic residues within the 225–230 region of apoA-I on its structure and functions and their contribution to the biogenesis of HDL. Adenovirus-mediated gene transfer of an apoA-I[F225A/V227A/F229A/L230A] mutant in apoA-I$^{-/-}$ mice decreased plasma cholesterol, HDL cholesterol, and apoA-I levels. When expressed in apoA-I$^{-/-}$ × apoE$^{-/-}$ mice, approximately 40% of the mutant apoA-I as well as mouse apoA-IV and apoB-48 appeared in the VLDL/IDL/LDL. In both mouse models, the apoA-I mutant generated small spherical particles of pre-β- and α4-HDL mobility. Coexpression of the apoA-I mutant and LCAT increased and shifted the-HDL cholesterol peak toward lower densities, created normal αHDL subpopulations, and generated spherical-HDL particles. Biophysical analyses suggested that the apoA-I[225–230] mutations led to a more compact folding that may limit the conformational flexibility of the protein. The mutations also reduced the ability of apoA-I to promote ABCA1-mediated cholesterol efflux and to activate LCAT to 31% and 66%, respectively, of the WT control. Overall, the apoA-I[225–230] mutations inhibited the biogenesis of-HDL and led to the accumulation of immature pre-β- and α4-HDL particles, a phenotype that could be corrected by administration of LCAT.**—Fotakis, P., I. Tiniakou, A. K. Kateifides, C. Gkolfinopoulou, A. Chroni, E. Stratikos, V. I. Zannis, and D. Kardassis. **Significance of the hydrophobic residues 225–230 of apoA-I for the biogenesis of HDL.** ***J. Lipid Res.*** **2013.** 54: **3293–3302.**

Supplementary key words apolipoprotein A-I mutations • high density lipoprotein biogenesis • pre-β- and α-HDL particles • dyslipidemia

Previous studies by us showed the overall importance of the 220–231 region of apoA-I for apoA-I/ABCA1 interactions and the biogenesis of HDL but did not identify the apoA-I residues involved (1, 2). Other studies also showed the importance of the C-terminal region for the structure of apoA-I (3–5) as well as for other functions of apoA-I (6, 7). In the preceding article, we investigated the role of the hydrophobic residues L218, L219, V221, and L222 and the charged residues E223 and K226 on the structure and functions of apoA-I and their contribution to the biogenesis of HDL (8). These studies showed that substitution of the hydrophobic residues L218, L219, V221, and L222 of apoA-I by alanines inhibits the biogenesis and maturation of HDL and generates a phenotype that cannot be corrected by LCAT. Expression of E223 and K226 caused fewer but discrete alterations in the HDL phenotype.

The rationale for the present study was that the 225–230 region of apoA-I contains four additional hydrophobic residues that may be equally significant for its structure and functions. For this reason, we used gene transfer in two mouse models as well as biochemical and biophysical analyses to study the impact of substitutions of residues F225, V227, F229, and L230 by alanines on the structure and functions of apoA-I and their impact on the biogenesis of HDL. In vitro experiments showed that the apoA-I[225–230] mutations affected the structure of apoA-I, diminished its capacity to promote ABCA1-mediated cholesterol efflux, and decreased moderately its ability to activate LCAT. Gene transfer of the apoA-I mutant in apoA-I$^{-/-}$ and apoA-I$^{-/-}$ × apoE$^{-/-}$ mice resulted in the reduction

This work was supported by National Institutes of Health Grant HL-48739; General Secretariat of Research and Technology of Greece Grant Synergasia 09SYN-12-897 (to D.K. and A.C.); and Ministry of Education of Greece Grant Thalis MIS 377286 (to D.K., A.C., and E.S.). P. Fotakis has been supported by pre-doctoral training Fellowship HERACLEITUS II by the European Union and Greek national funds through the Operational Program "Education and Lifelong Learning" of the National Strategic Reference Framework (NSRF).

Manuscript received 27 August 2013 and in revised form 9 October 2013.

Published, JLR Papers in Press, October 12, 2013
DOI 10.1194/jlr.M043489

Abbreviations: ANS, 8-anilino-1-naphthalene-sulfonate; CD, circular dichroism; DMPC, dimyristoyl-L-α-phosphatidylcholine; EM, electron microscopy; FPLC, fast-protein liquid chromatography; GdnHCl, guanidine hydrochloride; HEK293, human embryonic kidney 293; HTB-13, SW 1783 human astrocytoma; POPC, β-oleoyl-γ-palmitoyl-L-α-phosphatidylcholine; WMF, wavelength of maximum fluorescence; WT, wild-type.

[1] See referenced companion article, *J. Lipid Res.* 2013, 54: 3281–3292.

[2] V. I. Zannis and D. Kardassis contributed equally to this work.

[3] To whom correspondence should be addressed.
e-mail: vzannis@bu.edu

[S] The online version of this article (available at http://www.jlr.org) contains supplementary data in the form of one table, three figures, and methods.

of plasma apoA-I and HDL levels and led to the formation of spherical particles with pre-β- and α4-HDL electrophoretic mobility. In contrast to the apoA-I[218–222] mutant described in the preceding article (8), the defective HDL phenotype caused by the 225–230 mutations could be corrected by coexpression of the apoA-I mutant and human LCAT.

MATERIALS AND METHODS

Materials

Materials not mentioned in the experimental procedures have been obtained from sources described previously (9, 10).

Generation of adenoviruses expressing the wild-type and mutant apoA-I forms

The apoA-I gene lacking the BglII restriction site, which is present at nucleotide position 181 of the genomic sequence relative to the ATG codon of the gene, was cloned into the pCDNA3.1 vector to generate the pCDNA3.1-apoA-I(ΔBglII) plasmid as described (11). This plasmid was used as a template to introduce the apoA-I mutations F225A/V227A/F229A/L230A using the QuickChange® XL mutagenesis kit (Stratagene, Santa Clara, CA) and the mutagenic primers shown in supplementary Table I. Recombinant adenoviruses expressing the WT and the mutant apoA-I were constructed using the Ad-Easy-1 system in which the recombinant adenovirus construct is generated in bacteria BJ-5183 (purchased from Stratagene) (12). The recombinant adenovirus was packaged in 911 cells, amplified in human embryonic kidney 293 (HEK 293) cells, purified, and titrated as described (11).

ApoA-I production, purification, ABCA1-dependent cholesterol efflux and LCAT assays, physicochemical measurements, animal studies, and statistics were described in the preceding article (8).

RESULTS

Secretion of the WT and the apoA-I[225–230] mutant in the culture media of cells

The secretion of WT and mutant form of apoA-I in the culture medium of HTB-13 cells expressing the WT and the mutant apoA-I form was assessed by SDS-PAGE analysis of the culture media. As shown in supplementary Fig. I, both the WT and the apoA-I[225–230] mutant were secreted at comparable levels in the culture medium of the apoA-I-expressing cells.

Expression of the apoA-I transgenes following adenovirus infection

Total hepatic RNA was isolated from the livers of apoA-I$^{-/-}$ or apoA-I$^{-/-}$ × apoE$^{-/-}$ mice four days post infection with adenoviruses expressing the WT apoA-I and the apoA-I[225–230] mutant. qRT-PCR analysis of the apoA-I mRNA levels showed that the expression of the apoA-I[225–230] mutant was comparable to WT apoA-I in apoA-I$^{-/-}$ × apoE$^{-/-}$ mice but slightly elevated in apoA-I$^{-/-}$ mice (**Table 1**).

Plasma lipid and apoA-I levels and FPLC profiles

Plasma lipids and apoA-I levels were determined four days post infection of apoA-I$^{-/-}$ or apoA-I$^{-/-}$ × apoE$^{-/-}$ mice with adenoviruses expressing the WT and the mutant apoA-I form. It was found that in apoA-I$^{-/-}$ mice the apoA-I[225–230] mutant decreased plasma cholesterol and apoA-I levels to 23% and 34%, respectively, as compared with WT apoA-I. Plasma triglycerides were not affected by the apoA-I mutations (Table 1). Fast-protein liquid chromatography (FPLC) analysis of plasma from apoA-I$^{-/-}$ mice infected with the recombinant adenovirus expressing either WT apoA-I or the apoA-I[225–230] mutant showed that all the cholesterol was distributed in the HDL region and that the HDL cholesterol peak of the apoA-I[225–230] mutant was greatly diminished (**Fig. 1A**).

Fractionation of plasma of apoA-I$^{-/-}$ mice expressing the WT apoA-I or the apoA-I[225–230] mutant, EM analysis, and two-dimensional electrophoresis

Fractionation of plasma by density gradient ultracentrifugation and subsequent analysis of the resulting fractions by SDS-PAGE showed that both the WT apoA-I and the apoA-I[225–230] mutant were predominantly distributed in the HDL3 region and to a lesser extent in the HDL2 region (Fig. 1B, C). Compared with WT apoA-I, the quantity of the apoA-I[225–230] mutant was greatly reduced (Fig. 1B, C). Flotation of other apolipoproteins in the VLDL/LDL/IDL/HDL region was not observed when the WT apoA-I and the apoA-I[225–230] mutant were expressed in apoA-I$^{-/-}$ mice.

TABLE 1. Plasma lipids, apoA-I, and hepatic mRNA levels of apoA-I$^{-/-}$ or apoA-I$^{-/-}$ × apoE$^{-/-}$ mice expressing WT and the mutant form of apoA-I as indicated

Treatment	None	WT ApoAI	ApoA-I[225–230]	ApoA-I[225–230] + LCAT
ApoAI $^{-/-}$ mice				
ApoA-Ih mRNA levels (%)	Nondetectable	100 ± 15[a]	130 ± 10[b]	80 ± 10
Plasma apoA-Ih protein (mg/dl)	Nondetectable	173 ± 63	59 ± 17[c]	149 ± 43
Plasma cholesterol (mg/dl)	27 ± 8	182 ± 82[d]	41 ± 12[d,e]	297 ± 69[d]
Plasma triglycerides (mg/dl)	34 ± 14	39 ± 15	42 ± 14	48 ± 21
ApoAI $^{-/-}$ × apoE $^{-/-}$ mice				
ApoA-Ih mRNA levels (%)	Nondetectable	100 ± 21[a]	140 ± 50	90 ± 30
TC (mg/dl)	337 ± 107	520 ± 85	377 ± 90	778 ± 103[d,e]
TG (mg/dl)	58 ± 23	680 ± 290[d]	35 ± 22[e]	87 ± 65[e]

Values are means ± SD based on analysis of 5–8 mice per experiment.

[a] Expression of WT apoA-I in the apoA-I$^{-/-}$ or apoA-I$^{-/-}$ × apoE$^{-/-}$ was set to 100%. Expression of LCAT was also confirmed by RT-PCR. Statistical significant differences at $P < 0.05$ were calculated between untreated mice and mice expressing the WT apoA-I and the apoA-I[F225A/V227A/F229A/L230A] in either the apoA-I$^{-/-}$ or apoA-I$^{-/-}$ × apoE$^{-/-}$ mouse background and are indicated as follows: [b]$P \leq 0.05$ relative to WT apoA-I control; [c]$P \leq 0.05$ relative to WT apoA-I control; [d]$P \leq 0.05$ relative to the untreated control; [e]$P \leq 0.05$ relative to WT apoA-I control.

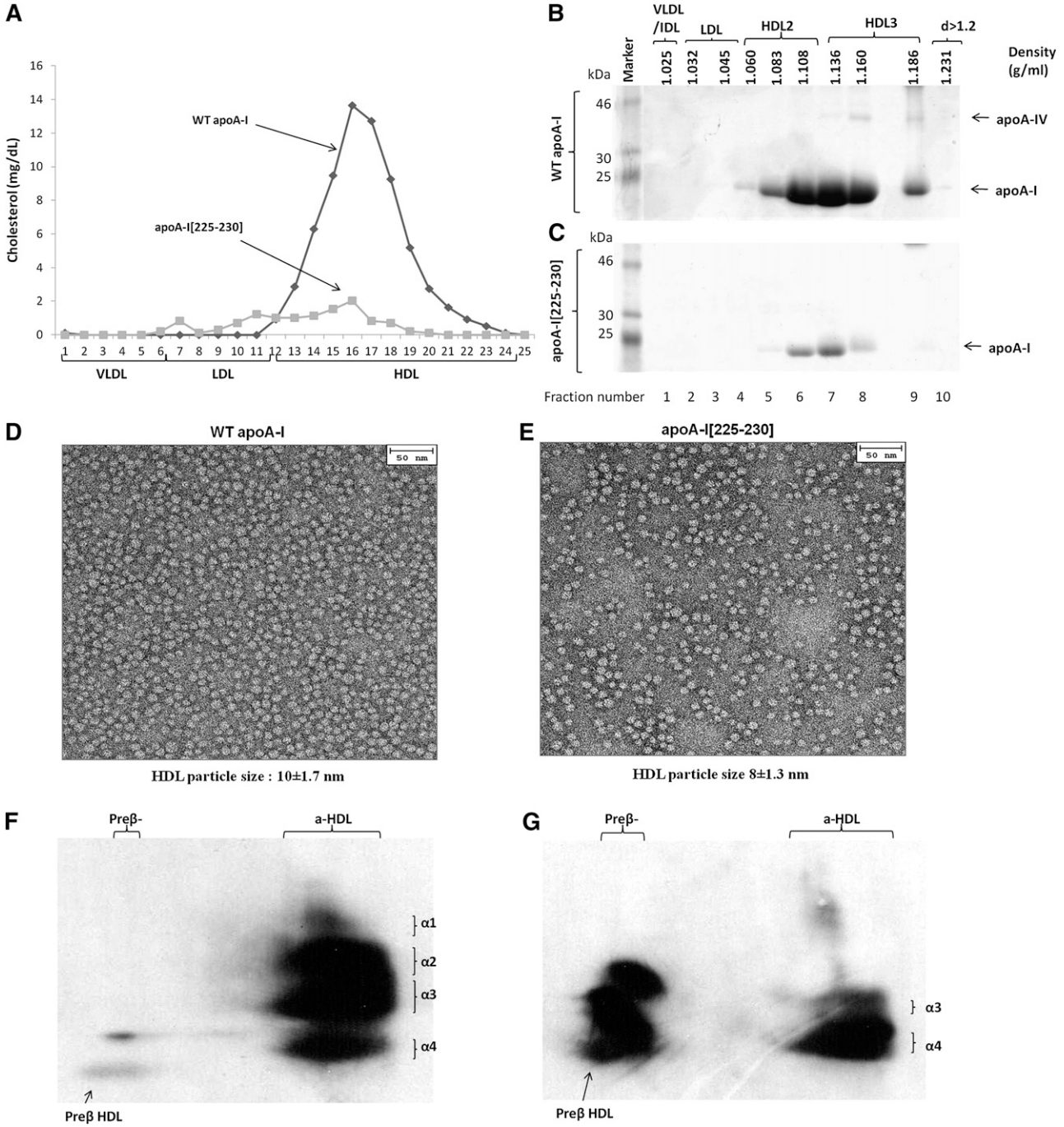

Fig. 1. Analysis of plasma of apoA-I$^{-/-}$ mice infected with adenoviruses expressing the WT apoA-I or apoA-I[225–230] by FPLC (A) and by density gradient ultracentrifugation and SDS-PAGE (B, C). EM analysis of HDL fractions 6 and 7 obtained from apoA-I$^{-/-}$ mice expressing the WT apoA-I (D) or apoA-I[225–230] mutant (E) following density gradient ultracentrifugation of plasma as indicated. The photomicrographs in this as well as in Figs. 2 and 3 were taken at 75,000× magnification and enlarged three times. The average diameter of the particles in this as well as in Figs. 2 and 3 was determined by measuring the diameter of 200 individual particles. Two-dimensional gel electrophoresis of plasma of apoA-I$^{-/-}$ mice infected with adenoviruses expressing WT apoA-I (F) or apoA-I[225–230] mutant (G).

Analysis of the HDL fractions 6 and 7 obtained following density gradient ultracentrifugation by EM showed that both the WT apoA-I and the apoA-I[225–230] mutant generated spherical particles (Fig. 1D, E). The diameters of the particles were 10 ± 1.7 nm for the WT apoA-I and 8 ± 1.3 for the apoA-I[225–230] mutant. Two-dimensional gel electrophoresis of plasma showed that WT apoA-I formed normal pre-β and α1, α2, α3, α4-HDL subpopulations (Fig. 1F), whereas the apoA-I[225–230] mutant formed predominantly pre-β and α4 subpopulations (Fig. 1G).

To assess how apoE deficiency affects HDL biogenesis, we also performed gene transfer experiments in apoA-I$^{-/-}$ × apoE$^{-/-}$ mice, which lack both mouse apoA-I and apoE. The plasma cholesterol and triglyceride levels of mice expressing the apoA-I[225–230] mutant were comparable to those of the noninfected apoA-I$^{-/-}$ × apoE$^{-/-}$ mice (Table 1).

In contrast, the plasma cholesterol levels of the mice expressing the WT apoA-I were increased 1.5-fold compared with the uninfected apoA-I$^{-/-}$ × apoE$^{-/-}$ mice, and the apoA-I expressing mice developed hypertriglyceridemia. The difference in the plasma cholesterol levels between apoA-I$^{-/-}$ × apoE$^{-/-}$ mice expressing WT apoA-I and the apoA-I[225–230] mutant can be explained by the corresponding FPLC analyses of the plasmas. This analysis showed that in apoA-I$^{-/-}$ × apoE$^{-/-}$ mice expressing the WT apoA-I, approximately two thirds of the cholesterol was found in the VLDL/IDL region and the remaining in the HDL region. In contrast, in mice expressing the apoA-I[225–230] mutant, the great majority of the cholesterol (>90%) was found in the VLDL/IDL region and the remaining in the LDL region. There was no appreciable HDL cholesterol peak in the HDL region (**Fig. 2A**). All triglycerides were found in the VLDL/IDL region (Fig. 2B).

Fractionation of the plasma by density gradient ultracentrifugation showed that WT apoA-I was distributed predominantly in the HDL2/HDL3 region, with small amounts in the VLDL/IDL/LDL region (Fig. 2C). Similar analysis for the apoA-I[225–230] mutant showed that apoA-I and mouse apoA-IV were distributed in all lipoprotein fractions and that the VLDL/IDL/LDL/HDL2 fractions were enriched with mouse apoB-48 (Fig. 2D). EM analysis of the fractions 6 and 7 obtained by density gradient ultracentrifugation of the plasma showed that both the WT apoA-I and the apoA-I mutant generated spherical particles that differed in size (Fig. 2E, F). The diameter of the particles were 9.2 ± 1.9 nm for the WT apoA-I and 7 ± 2.3 for the apoA-I[225–230] mutant. Larger spherical particles corresponding in size to IDL and LDL were observed in the HDL density fractions of apoA-I$^{-/-}$ × apoE$^{-/-}$ mice expressing the apoA-I[225–230] mutant. The appearance of the IDL- and LDL-sized particles coincides with the presence of apoB-48 in fractions 6 and 7 used for the EM analysis (Fig. 2D). Two-dimensional gel electrophoresis showed that the plasma of mice expressing WT apoA-I contained the normal pre-β and α−HDL subpopulations (Fig. 2G), whereas the plasma of mice expressing the apoA-I[F225A/V227A/F229A/L230A] mutant contained predominantly (∼70%) pre-β, smaller amounts of (∼30%) of α4-HDL, and few α3-HDL particles (Fig. 2H). The relative migration of the particles generated by WT apoA-I and the apoA-I[225–230] mutant in apoA-I$^{-/-}$ and apoA-I$^{-/-}$ × apoE$^{-/-}$ mice were established by two-dimensional gel electrophoresis of mixtures of the plasmas containing these two apoA-I forms (supplementary Fig. II-A, B).

To assess whether the defective phenotype of the apoA-I[225–230] mutant can be corrected by LCAT, we carried out gene transfer of both the apoA-I[225–230] mutant and LCAT in apoA-I$^{-/-}$ and apoA-I$^{-/-}$ × apoE$^{-/-}$ mice. In apoA-I$^{-/-}$, the coexpression of the apoA-I[225–230] mutant and LCAT increased plasma cholesterol without changing the plasma triglyceride levels (Table 1). The FPLC analysis of the plasma showed that the increase in plasma cholesterol was accompanied by a dramatic increase in the HDL cholesterol peak and its shift toward the lower densities (**Fig. 3A**). In double-deficient mice, the coexpression of the apoA-I[225–230] mutant with LCAT caused a 2.3-fold increase in plasma cholesterol compared with noninfected mice, without any significant change in plasma triglycerides (Table 1). The FPLC analysis showed that the increase in plasma cholesterol was associated with the generation of a cholesterol shoulder that extended from VLDL to HDL (Fig. 3B). Density gradient ultracentrifugation of plasma in apoA-I$^{-/-}$ mice coexpressing the apoA-I[225–230] mutant and LCAT showed that the major proportion of apoA-I was distributed mainly in the HDL2 region and a smaller amount in the VLDL/IDL/LDL and HDL3 regions. Mouse apoE was distributed predominantly in the VLDL/IDL/LDL region and to a lesser extend in the HDL2 region. Mouse apoA-IV floated in all lipoprotein fractions (Fig. 3C). The identity of the apoA-IV and apoE bands was confirmed by western blotting (data not shown). In apoA-I$^{-/-}$ × apoE$^{-/-}$ mice expressing both the apoA-I[225–230] mutant and LCAT, both apoA-I and apoA-IV were distributed in all lipoprotein fractions. ApoB-48 was present predominantly in the VLDL/IDL/LDL and HDL2 region and to a lesser extent in the HDL3 region (Fig. 3D). Electron microscopy of the HDL fractions 6 and 7 obtained from the plasma of apoA-I$^{-/-}$ mice coexpressing the apoA-I[225–230] mutant and LCAT showed the presence of spherical particles of 11 ± 3.1 nm diameter (Fig. 3E). Similar analysis of the HDL fractions 6 and 7 of plasma of apoA-I$^{-/-}$ × apoE$^{-/-}$ mice coexpressing the apoA-I[225–230] mutant and LCAT also showed the presence of spherical particles of 10.3 ± 2.8 nm diameter as well as a greater proportion of the larger particles that correspond in size to VLDL/IDL/LDL size (Fig. 3F). Two-dimensional gel electrophoresis of plasma of both apoA-I$^{-/-}$ and apoA-I$^{-/-}$ × apoE$^{-/-}$ mice showed that the coexpression of the apoA-I[225–230] mutant with LCAT restored the normal pre-β and α-HDL subpopulations and generated αHDL size subpopulations with larger size (Fig. 3G, H).

Comparative analysis of the in vitro functions and physicochemical properties of the WT apoA-I and the apoA-I[225–230] mutant

The WT apoA-I and the apoA-I[225–230] mutant were purified from the culture media of HTB-13 cells expressing the corresponding proteins and used for in vitro functional and physicochemical studies. The functional studies showed that the ability of this mutant to promote ABCA1-mediated cholesterol efflux and to activate LCAT was 31% and 66%, respectively, as compared with the WT control (**Fig. 4A**, B).

Circular dichroism (CD) measurements indicated 7.6% loss of helical content in the apoA-I[225–230] mutant (**Table 2** and supplementary Fig. III-A). Thermal unfolding followed by the CD signal showed that the F225A/V227A/F229A/L230A mutations caused a more cooperative unfolding transition as compared with WT apoA-I (Table 2 and supplementary Fig. III-B). In contrast, the chemical unfolding profile of the mutant, probed by the intrinsic tryptophan fluorescence, was similar to that of the WT apoA-I (Table 2 and supplementary Fig. III-C). Finally, the ANS fluorescence measurements showed that

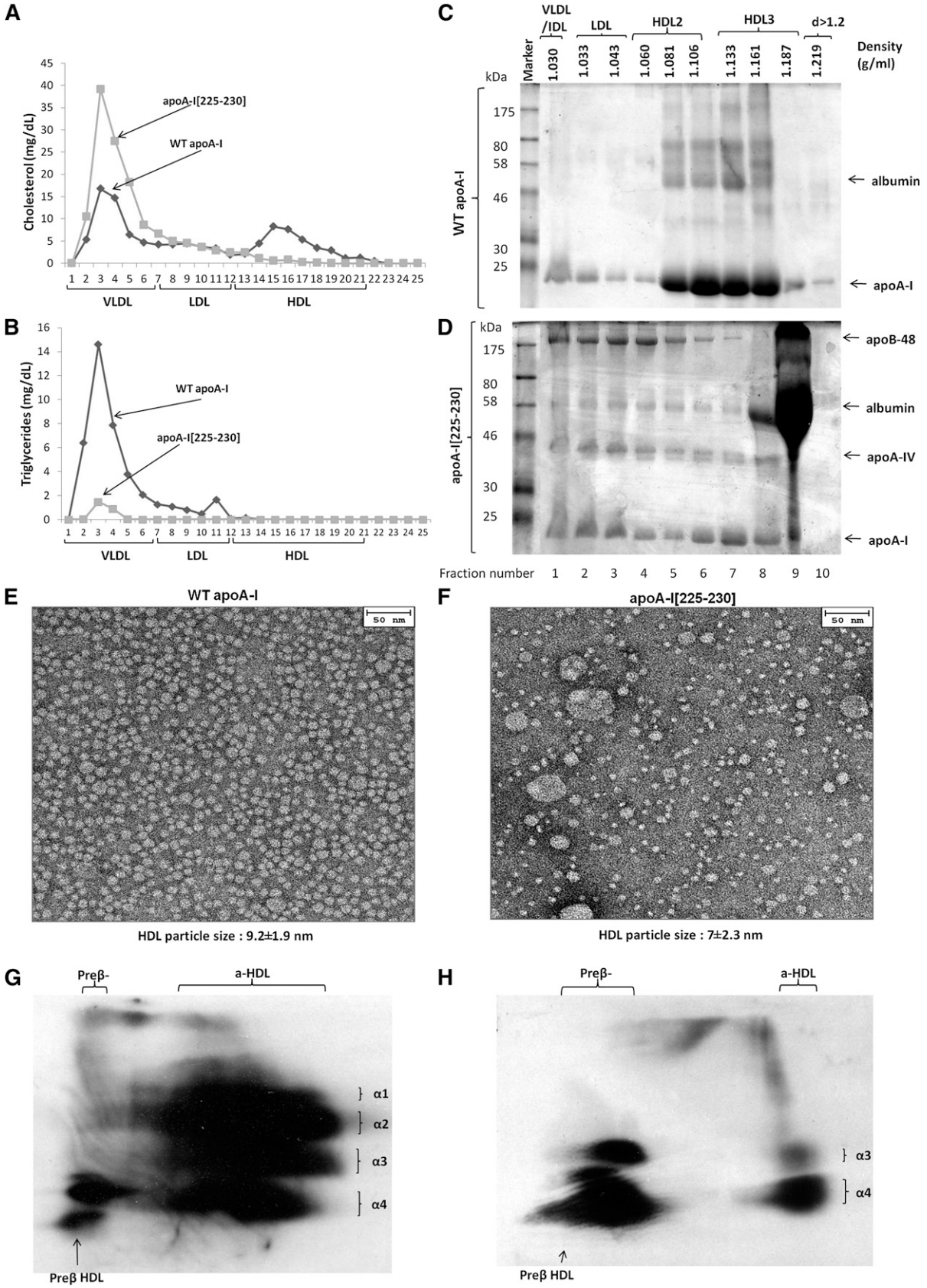

Fig. 2. Analysis of plasma of apoA-I$^{-/-}$ × apoE$^{-/-}$ mice infected with adenoviruses expressing the WT apoA-I or apoA-I[225–230] mutant by FPLC (A, B) and by density gradient ultracentrifugation and SDS-PAGE (C, D). EM analysis of HDL fractions 6 and 7 obtained from apoA-I$^{-/-}$ × apoE$^{-/-}$ mice expressing the WT apoA-I (E) or apoA-I[225–230] mutant (F) following density gradient ultracentrifugation of plasma as indicated. Two-dimensional gel electrophoresis of plasma of apoA-I$^{-/-}$ × apoE$^{-/-}$ mice infected with adenoviruses expressing WT apoA-I (G) or apoA-I[225–230] mutant (H).

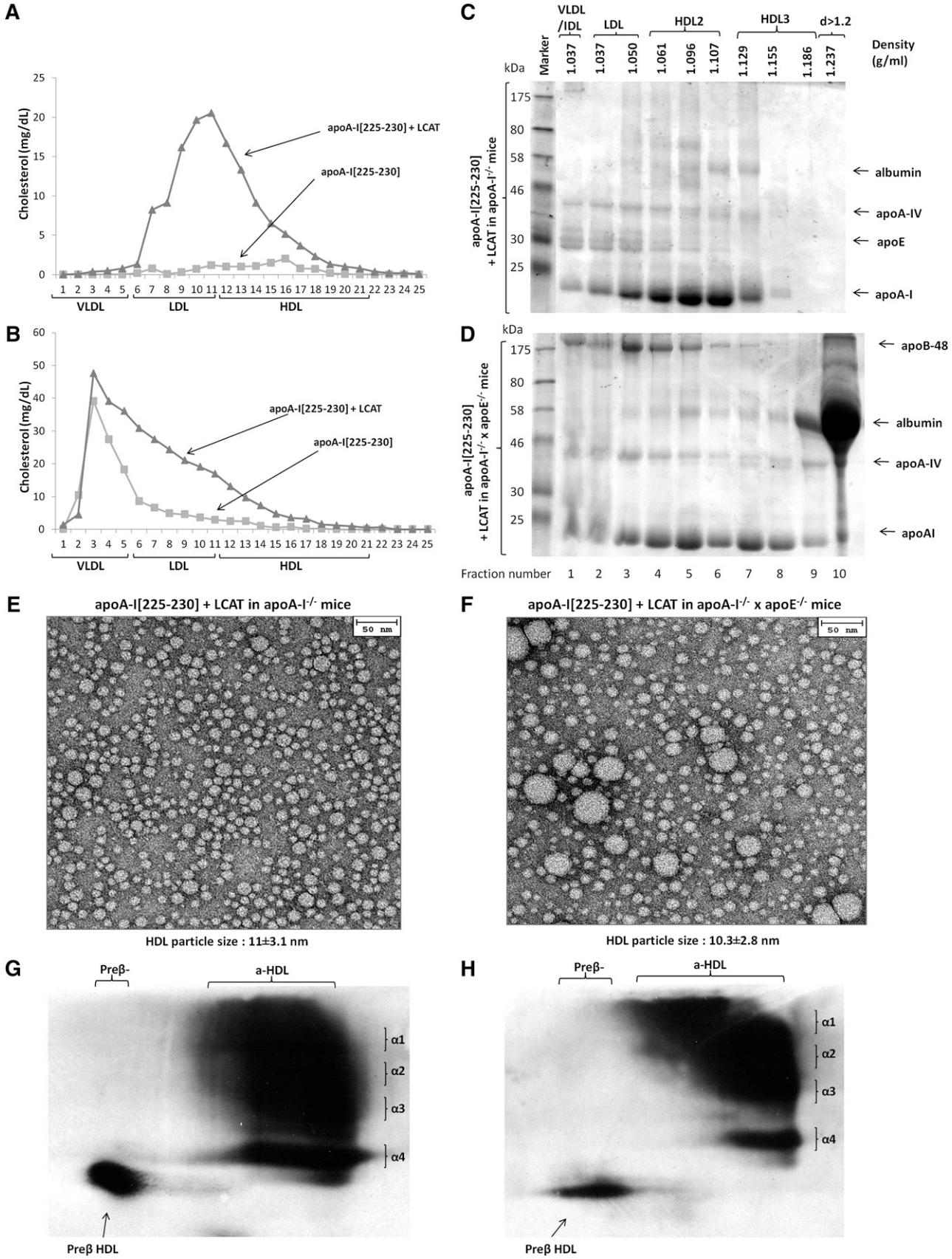

Fig. 3. Analyses of plasma of apoA-I$^{-/-}$ (A,C,E,G) or apoA-I$^{-/-}$ × apoE$^{-/-}$ mice (B, D, F, H) infected with adenoviruses expressing the apoA-I[225–230] mutant in combination with human LCAT. Plasma FPLC profiles of mice expressing the apoA-I[225–230] mutant alone or the apoA-I[225–230] mutant in combination with human LCAT in apoA-I$^{-/-}$ (A) or apoA-I$^{-/-}$ × apoE$^{-/-}$ background (B). SDS-PAGE of fractions obtained by density gradient ultracentrifugation from apoA-I$^{-/-}$ (C) or apoA-I$^{-/-}$ × apoE$^{-/-}$ mice (D) mice expressing the apoA-I[225–230]

the F225A/V227A/F229A/L230A mutations caused a 41% reduction of hydrophobic surface exposure to the solvent (Table 2 and supplementary Fig. III-D).

DISCUSSION

F225A/V227A/F229A/L230A mutations alter the functional and physicochemical properties of apoA-I

The functional assays probed two well-characterized properties of lipid-free and lipoprotein-bound apoA-I, which are its ability to promote ABCA1-mediated cholesterol efflux and to activate LCAT, respectively (1, 13, 14). The decreased capacity of the apoA-I[225–230] mutant to promote ABCA1-mediated cholesterol efflux (31% of the WT control) is expected to influence its capacity to form HDL in vivo. The reduction in the ability of the apoA-I mutant to activate LCAT was modest (65% of WT control). However, previous studies showed that the capacity of reconstituted HDL containing an apoA-I mutant to activate LCAT in vitro does not always predict their ability to affect LCAT activation in vivo (15, 16).

The physicochemical analysis of the apoA-I[225–230] mutant suggested that the mutations lead to a more compact folding that may limit the conformational flexibility of the protein. The observed 7.6% decrease in the protein's α-helical content indicated that the structural changes brought about by the mutations extend beyond the limited area of the location of the mutations. Thermodynamic stability analysis indicated that the mutation also resulted in a protein that is thermodynamically stabilized and presents a more cooperative unfolding transition and compact structure. This was only evident during thermal unfolding and not during chemical denaturation. Since, however, the chemical denaturation reports only on the local environment of the tryptophan residues of the protein, which are all located on the N-terminal region of apoA-I, this observation suggests that the structural repercussions brought about by the mutations may be limited to the C-terminal region of apoA-I where the mutation resides. In either case, a more cooperative thermal transition signifies a more compact structure with reduced conformational flexibility, a property that is necessary for lipid association. A recent, related study involving different amino acid substitutions within the 225–236 region of apoA-I explored the effects of the aromatic and hydrophobic residues F225, F229, A232, and Y236 on the cholesterol efflux capacity and the ability of apoA-I to solubilize phospholipids and form HDL particles by cell cultures. It was concluded that both functions were similar to those of WT apoA-I when the overall hydrophobicity of apoA-I was not affected by the mutations in residues F225, F229, A232, and Y236. However, both functions were impeded by a factor of three by substitution of the aromatic amino acids that decreased the hydrophobicity of apoA-I (17). Another important finding of the present study is that although F225/V227/F229/L230 represent ~5% of total hydrophobic amino acids of apoA-I, their substitution by alanines resulted in a 41% reduction in the ANS fluorescence, indicating that these residues constitute a major solvent-exposed hydrophobic patch on the surface of apoA-I. Overall, our findings suggest that the F225A/V227A/F229A/L230A mutations greatly affect the structural integrity and conformational flexibility of apoA-I, effects that may at least partially underlie the observed changes in its in vitro and in vivo functions.

225–230 mutations are associated with abnormalities in the biogenesis and maturation of HDL

In previous studies, systematic mutagenesis and gene transfer of human apoA-I mutants in apoA-I-deficient mice disrupted specific steps along the pathway of the biogenesis of HDL and generated discrete HDL phenotypes (16). These phenotypes were characterized by low HDL levels, preponderance of immature HDL subpopulations, or accumulation of discoidal HDL particles in plasma (1, 10, 11, 15, 18, 19).

To obtain a clearer picture how the apoA-I mutations affected different steps of the biogenesis and maturation of HDL in the presence or absence of the endogenous mouse apoE, gene transfer studies were carried out in apoA-I$^{-/-}$ mice that lack mouse apoA-I and in apoA-I$^{-/-}$ × apoE$^{-/-}$ mice that lack both mouse apoA-I and apoE.

The studies in apoA-I$^{-/-}$ mice showed that the expression of the apoA-I[225–230] mutant was associated with a great reduction in the plasma cholesterol and apoA-I levels, despite the fact that the expression of the mutant transgene was higher than that of the WT apoA-I transgene. The reduction in plasma apoA-I was associated with a great decrease in the HDL cholesterol levels as determined by FPLC fractionation of the plasma and was further confirmed by density gradient ultracentrifugation of plasma, which showed reduction in the quantity of the apoA-I[225–230] mutant.

Potential abnormalities in the HDL phenotype in apoA-I$^{-/-}$ mice resulting from the expression of the apoA-I[225–230] mutant were verified by two-dimensional gel electrophoresis of plasma that showed the formation of pre-β- and α4-HDL particles. Accumulation of such particles is indicative of defective maturation of HDL due to insufficiency of mouse LCAT (11, 18). The LCAT insufficiency may originate from fast catabolism of the nascent HDL particles along with the endogenous LCAT bound to them (11). Fast catabolism of the nascent HDL particles by the kidney has been described previously (18, 20).

The plasma of both of apoA-I$^{-/-}$ and apoA-I$^{-/-}$ × apoE$^{-/-}$ mice expressing the apoA-I[225–230] mutant contained predominantly pre-β- and, to a lesser extent, α4-HDL particles, thus reaffirming the concept that the apoA-I[225–230] mutations affected the biogenesis of HDL. An unexpected finding was that the expression of the apoA-I[225–230] mutant in apoA-I$^{-/-}$ × apoE$^{-/-}$ mice resulted in the flotation of the mutant protein in all density fractions, along with mouse apoA-IV and apoB-48. The

mutant and human LCAT. EM analysis of HDL fractions 6 and 7 obtained from apoA-I$^{-/-}$ (E) or apoA-I$^{-/-}$ × apoE$^{-/-}$ (F) mice expressing the apoA-I[225–230] mutant and human LCAT following density gradient ultracentrifugation of plasma as indicated. Two-dimensional gel electrophoresis of plasma of apoA-I$^{-/-}$ (G) or apoA-I$^{-/-}$ × apoE$^{-/-}$ (H) mice expressing the apoA-I[225–230] mutant and human LCAT .

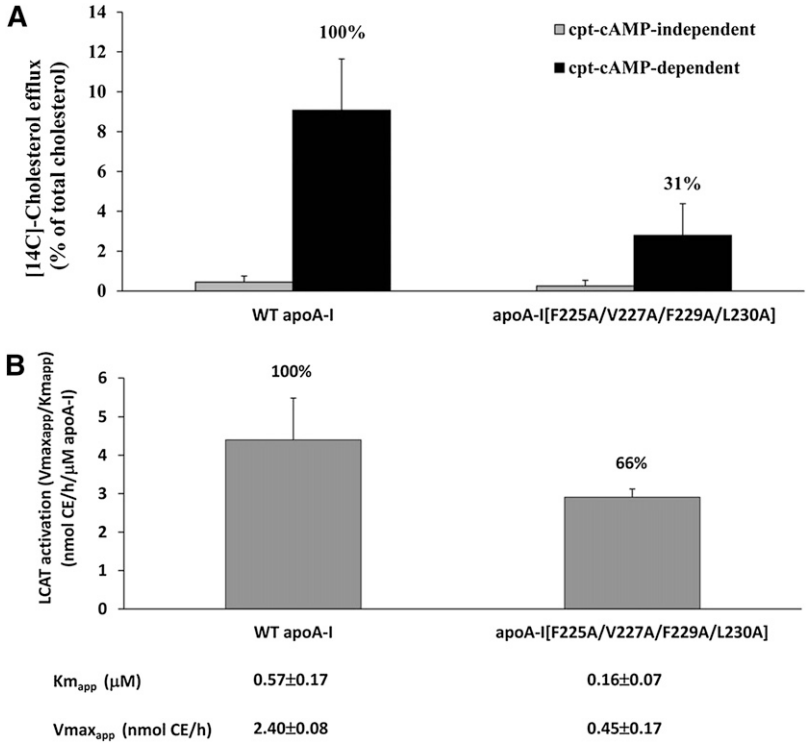

Fig. 4. ABCA1-mediated cholesterol efflux from J774 mouse macrophages treated with cpt-cAMP using WT apoA-I and the apoA-I[225–230] mutant as cholesterol acceptors (A). LCAT activation capacity of WT apoA-I and the apoA-I[225–230] mutant. Experiments were performed as described in Materials and Methods. The data represent the average from two independent experiments performed in triplicate (B).

presence of apoB-48 in the higher density fractions affected the particle composition of the HDL fraction by enriching it with larger particles corresponding in size to VLDL, IDL, and LDL. Previous studies showed that apoA-IV can also generate apoA-IV containing HDL particles (21). It is thus possible that apoA-IV containing HDL may fuse with apoB-48 containing particles and pull them toward the higher density regions.

LCAT corrects the aberrant HDL phenotype caused by the apoA-I[225–230] mutations

In previous studies, we have shown that naturally occurring or bioengineered point mutations in apoA-I when expressed in mouse models activate LCAT insufficiently and in some instances may lead to the accumulation of discoidal HDL particles in plasma (18, 19). Other mutations lead to very low levels of HDL cholesterol and accumulation

TABLE 2. Calculated biophysical parameters for WT apoA-I and the apoA-I [F225A/V227A/F229A/L230A] mutant

Mutation	Helicity	Thermal Denaturation			Chemical Denaturation	ANS Binding
ApoA-I	α-Helix	T_m (°C)	Slope[a]	Cooperativity Index (n)	$D_{1/2}$ (M)	Fold Increase[b]
WT	59.3 ± 0.5	56.0 ± 0.5	7.8 ± 0.1	6.3 ± 0.4	1.02 ± 0.06	10.2 ± 0.5
F225A/V227A/F229A/L230A	51.7 ± 0.3[c]	57.8 ± 0.2[d]	4.0 ± 0.0[c]	11.4 ± 0.4[e]	1.01 ± 0.03	6.0 ± 0.4[c]

Values are means ± SD of 3–4 experiments. Parameters obtained from the indicated measurements are as follows: α-helix is the % α-helical content of the protein as calculated from the molecular ellipticity of the protein sample at 222 nm; T_m, is middle point of the thermal denaturation transition (melting temperature); slope is the calculated slope of the linear component of the thermal denaturation transition, around the melting temperature; cooperativity index n is an indicator of the cooperativity of the thermal unfolding transition and is calculated using the Hill equation the Hill equation $n = (\log 81)/\log(T_{0.9}/T_{0.1})$, where $T_{0.9}$ and $T_{0.1}$ are the temperatures at which the unfolding transition has reached a fractional completion of 0.9 and 0.1; $D_{1/2}$ is the guanidine HCl concentration at which the midpoint of the chemical denaturation is achieved; fold increase is the increase in ANS fluorescence in the presence of the protein relative to free ANS in the same buffer.

[a] Slope is calculated from the fit of thermal denaturation curve to a Boltzman sigmoidal model curve using the equation $[\Theta]_{222}$ = Bottom + ((Top − Bottom) / (1 = exp((Tm − X) / Slope))). X describes the temperature, and slope describes the steepness of the curve, with a larger value denoting a shallow curve.

[b] Fold-increase in signal compared with unbound ANS.

[c] $P < 0.0001$.

[d] $P < 0.05$.

[e] $P < 0.001$.

of premature pre-β- and α4-HDL particles in plasma (11). A characteristic feature of these mutations is that the low HDL levels and the abnormal HDL phenotype could be corrected in vivo by gene transfer of LCAT (11, 18, 19). The preceding article showed that substitutions of residues L218, L219, V221, and L222 by alanines led to the generation of a unique and previously undetected low HDL phenotype that was characterized by the formation of only pre-β-HDL particles and could not be converted to spherical particles by excess LCAT (8). Since the changes in the structure and the functions of the apoA-I[225–230] and the apoA-I[218–222] mutant had several similarities, we carried out experiments to determine whether the aberrant HDL phenotype generated by the apoA-I[225–230] mutations could be corrected by LCAT. These experiments showed that coexpression of the LCAT and the apoA-I[225–230] mutant in apoA-I$^{-/-}$ mice restored the HDL cholesterol peak of the FPLC profile and shifted it toward lower densities (compare Fig. 1A with Fig. 3A). It also increased apoA-I levels and shifted its distribution to lower densities (compare Fig. 1B with Fig. 3C). Finally, it promoted the appearance of mouse apoE predominantly in the lower densities and of apoA-IV in all lipoprotein fractions (compare Fig. 1B with Fig. 3C).

Similar experiments in double-deficient mice showed that the coexpression of the LCAT and the apoA-I[225–230] mutant created a cholesterol shoulder that extended from VLDL to HDL as determined by FPLC analysis (Fig. 3B). The distribution of the mutant apoA-I, apoA-IV and apoB-48 in different densities was similar to that observed in mice expressing the apoA-I mutant alone (Fig. 3D). In both mouse models, the LCAT treatment created normal pre-β and α−HDL subpopulations and generated spherical HDL particles of a larger size. Thus, the observed LCAT insufficiency caused by the apoA-I[225–230] mutations could be reversed by treatment with LCAT.

The ability of LCAT to restore aberrant HDL phenotype caused by genetic or environmental factors may have important clinical implications for the correction of HDL abnormalities in humans. An abnormality that persisted in apoA-I$^{-/-}$ × apoE$^{-/-}$ mice expressing the apoA-I[225–230] mutant was the presence of VLDL-, IDL-, and LDL-sized particles in the HDL fractions.

The present study in combination with the preceding study (8) shows the essential role of eight hydrophobic residues present in the 218–230 region of apoA-I for the structure and function of apoA-I and its ability to form HDL. The two studies enhance our understanding of the complex factors that contribute to the correct extracellular assembly, maturation, and proteomic composition of HDL. Future studies are required to identify by existing and new assays how the aberrant forms of HDL identified in these and previous studies (1, 2, 10, 11, 15, 18, 19) affect different functions of HDL that are required for protection from atherosclerosis and other diseases.

Panagiotis Fotakis, Ioanna Tiniakou, and Andreas Kateifides have been students of the graduate program "The Molecular Basis of Human Disease" of the University of Crete Medical School. The authors thank Gayle Forbes and Dr. Arnold vonEckardstein (University of Zurich) for technical assistance.

REFERENCES

1. Chroni, A., T. Liu, I. Gorshkova, H. Y. Kan, Y. Uehara, A. Von Eckardstein, and V. I. Zannis. 2003. The central helices of ApoA-I can promote ATP-binding cassette transporter A1 (ABCA1)-mediated lipid efflux. Amino acid residues 220-231 of the wild-type ApoA-I are required for lipid efflux in vitro and high density lipoprotein formation in vivo. *J. Biol. Chem.* **278:** 6719–6730.
2. Chroni, A., G. Koukos, A. Duka, and V. I. Zannis. 2007. The carboxy-terminal region of apoA-I is required for the ABCA1-dependent formation of alpha-HDL but not prebeta-HDL particles in vivo. *Biochemistry.* **46:** 5697–5708.
3. Borhani, D. W., D. P. Rogers, J. A. Engler, and C. G. Brouillette. 1997. Crystal structure of truncated human apolipoprotein A-I suggests a lipid-bound conformation. *Proc. Natl. Acad. Sci. USA.* **94:** 12291–12296.
4. Borhani, D. W., J. A. Engler, and C. G. Brouillette. 1999. Crystallization of truncated human apolipoprotein A-I in a novel conformation. *Acta Crystallogr. D Biol. Crystallogr.* **55:** 1578–1583.
5. Mei, X., and D. Atkinson. 2011. Crystal structure of C-terminal truncated apolipoprotein A-I reveals the assembly of high density lipoprotein (HDL) by dimerization. *J. Biol. Chem.* **286:** 38570–38582.
6. Ohnsorg, P. M., L. Rohrer, D. Perisa, A. Kateifides, A. Chroni, D. Kardassis, V. I. Zannis, and A. von Eckardstein. 2011. Carboxyl terminus of apolipoprotein A-I (ApoA-I) is necessary for the transport of lipid-free ApoA-I but not prelipidated ApoA-I particles through aortic endothelial cells. *J. Biol. Chem.* **286:** 7744–7754.
7. Biedzka-Sarek, M., J. Metso, A. Kateifides, T. Meri, T. S. Jokiranta, A. Muszyński, J. Radziejewska-Lebrecht, V. Zannis, M. Skurnik, and M. Jauhiainen. 2011. Apolipoprotein A-I exerts bactericidal activity against Yersinia enterocolitica serotype O:3. *J. Biol. Chem.* **286:** 38211–38219.
8. Fotakis, P., A. Kateifides, C. Gkolfinopoulou, D. Georgiadou, M. Beck, K. Grundler, A. Chroni, E. Stratikos, D. Kardassis, and V. I. Zannis. 2013. Role of the hydrophobic and charged residues in the 218 to 226 region of apoA-I in the biogenesis of HDL. *J. Lipid Res.* Epub ahead of print. August 29, 2013; doi:10.1194/jlr.M038356.
9. Liu, T., M. Krieger, H. Y. Kan, and V. I. Zannis. 2002. The effects of mutations in helices 4 and 6 of ApoA-I on scavenger receptor class B type I (SR-BI)-mediated cholesterol efflux suggest that formation of a productive complex between reconstituted high density lipoprotein and SR-BI is required for efficient lipid transport. *J. Biol. Chem.* **277:** 21576–21584.
10. Chroni, A., H. Y. Kan, K. E. Kypreos, I. N. Gorshkova, A. Shkodrani, and V. I. Zannis. 2004. Substitutions of glutamate 110 and 111 in the middle helix 4 of human apolipoprotein A-I (apoA-I) by alanine affect the structure and in vitro functions of apoA-I and induce severe hypertriglyceridemia in apoA-I-deficient mice. *Biochemistry.* **43:** 10442–10457.
11. Koukos, G., A. Chroni, A. Duka, D. Kardassis, and V. I. Zannis. 2007. LCAT can rescue the abnormal phenotype produced by the natural ApoA-I mutations (Leu141Arg)Pisa and (Leu159Arg)FIN. *Biochemistry.* **46:** 10713–10721.
12. Luo, J., Z. L. Deng, X. Luo, N. Tang, W. X. Song, J. Chen, K. A. Sharff, H. H. Luu, R. C. Haydon, K. W. Kinzler, et al. 2007. A protocol for rapid generation of recombinant adenoviruses using the AdEasy system. *Nat. Protoc.* **2:** 1236–1247.
13. Rothblat, G. H., M. de la Llera-Moya, V. Atger, G. Kellner-Weibel, D. L. Williams, and M. C. Phillips. 1999. Cell cholesterol efflux: integration of old and new observations provides new insights. *J. Lipid Res.* **40:** 781–796.
14. Fielding, C. J., V. G. Shore, and P. E. Fielding. 1972. A protein cofactor of lecithin:cholesterol acyltransferase. *Biochem. Biophys. Res. Commun.* **46:** 1493–1498.
15. Chroni, A., H. Y. Kan, A. Shkodrani, T. Liu, and V. I. Zannis. 2005. Deletions of helices 2 and 3 of human apoA-I are associated with severe dyslipidemia following adenovirus-mediated gene transfer in apoA-I-deficient mice. *Biochemistry.* **44:** 4108–4117.
16. Zannis, V. I., E. E. Zanni, A. Papapanagiotou, D. Kardassis, and A. Chroni. 2006. ApoA-I functions and synthesis of HDL: insights

from mouse models of human HDL metabolism. *In* High-Density Lipoproteins. From Basic Biology to Clinical Aspects. C. J. Fielding, editor. Wiley-VCH, Weinheim. 237–265.

17. Lyssenko, N. N., M. Hata, P. Dhanasekaran, M. Nickel, D. Nguyen, P. S. Chetty, H. Saito, S. Lund-Katz, and M. C. Phillips. 2012. Influence of C-terminal α-helix hydrophobicity and aromatic amino acid content on apolipoprotein A-I functionality. *Biochim. Biophys. Acta.* **1821:** 456–463.
18. Koukos, G., A. Chroni, A. Duka, D. Kardassis, and V. I. Zannis. 2007. Naturally occurring and bioengineered apoA-I mutations that inhibit the conversion of discoidal to spherical HDL: the abnormal HDL phenotypes can be corrected by treatment with LCAT. *Biochem. J.* **406:** 167–174.
19. Chroni, A., A. Duka, H. Y. Kan, T. Liu, and V. I. Zannis. 2005. Point mutations in apolipoprotein A-I mimic the phenotype observed in patients with classical lecithin:cholesterol acyltransferase deficiency. *Biochemistry.* **44:** 14353–14366.
20. Timmins, J. M., J. Y. Lee, E. Boudyguina, K. D. Kluckman, L. R. Brunham, A. Mulya, A. K. Gebre, J. M. Coutinho, P. L. Colvin, T. L. Smith, et al. 2005. Targeted inactivation of hepatic Abca1 causes profound hypoalphalipoproteinemia and kidney hypercatabolism of apoA-I. *J. Clin. Invest.* **115:** 1333–1342.
21. Duka, A., P. Fotakis, D. Georgiadou, A. Kateifides, K. Tzavlaki, L. von Eckardstein, E. Stratikos, D. Kardassis, and V. I. Zannis. 2013. ApoA-IV promotes the biogenesis of apoA-IV-containing HDL particles with the participation of ABCA1 and LCAT. *J. Lipid Res.* **54:** 107–115.

ApoA-IV promotes the biogenesis of apoA-IV-containing HDL particles with the participation of ABCA1 and LCAT[S]

Adelina Duka,* Panagiotis Fotakis,*,§ Dimitra Georgiadou,† Andreas Kateifides,*,§ Kalliopi Tzavlaki,§ Leonard von Eckardstein,* Efstratios Stratikos,† Dimitris Kardassis,§ and Vassilis I. Zannis[1],*,§

Molecular Genetics,* Boston University School of Medicine, Boston, MA; National Centre for Scientific Research "Demokritos,"† Athens, Greece; Department of Biochemistry,§ University of Crete Medical School, Heraklion, Greece

Abstract The objective of this study was to establish the role of apoA-IV, ABCA1, and LCAT in the biogenesis of apoA-IV-containing HDL (HDL-A-IV) using different mouse models. Adenovirus-mediated gene transfer of apoA-IV in apoA-I$^{-/-}$ mice did not change plasma lipid levels. ApoA-IV floated in the HDL2/HDL3 region, promoted the formation of spherical HDL particles as determined by electron microscopy, and generated mostly α- and a few pre-β-like HDL subpopulations. Gene transfer of apoA-IV in apoA-I$^{-/-}$ × apoE$^{-/-}$ mice increased plasma cholesterol and triglyceride levels, and 80% of the protein was distributed in the VLDL/IDL/LDL region. This treatment likewise generated α- and pre-β-like HDL subpopulations. Spherical and α-migrating HDL particles were not detectable following gene transfer of apoA-IV in ABCA1$^{-/-}$ or LCAT$^{-/-}$ mice. Coexpression of apoA-IV and LCAT in apoA-I$^{-/-}$ mice restored the formation of HDL-A-IV. Lipid-free apoA-IV and reconstituted HDL-A-IV promoted ABCA1 and scavenger receptor BI (SR-BI)-mediated cholesterol efflux, respectively, as efficiently as apoA-I and apoE.[JLR] Our findings are consistent with a novel function of apoA-IV in the biogenesis of discrete HDL-A-IV particles with the participation of ABCA1 and LCAT, and may explain previously reported anti-inflammatory and atheroprotective properties of apoA-IV.—Duka, A., P. Fotakis, D. Georgiadou, A. Kateifides, K. Tzavlaki, L. von Eclardstein, E. Stratikos, D. Kardassis, and V. I. Zannis. **ApoA-IV promotes the biogenesis of apoA-IV-containing HDL particles with the participation of ABCA1 and LCAT. *J. Lipid Res.* 2013.** 54: **107–115.**

Supplementary key words apolipoprotein A-IV • lipoproteins • genetically altered mice • lecithin:cholesterol acyltransferase • ATP binding cassette transporter A1

ApoA-IV (Mr = 46 kDa) is a major component of HDL and chylomicrons in rats (1). Similar to apoA-I and apoE, apoA-IV contains repeated units mainly of 22 residues long that are organized in amphipathic α-helices (2, 3) and have been implicated in lipid binding. In humans and the majority of animal species, apoA-IV is synthesized primarily by the intestine and, to a lesser extent, by the liver, and is found in plasma, the lymph chylomicrons, and the cerebrospinal fluid (3–5). An exception is the rabbit, where both the liver and the intestine are major sites of apoA-IV mRNA synthesis (6). Following synthesis in the intestine, apoA-IV is incorporated into chylomicrons, secreted into the lymph, and reaches the plasma (4). Hydrolysis of the triglycerides of chylomicrons by lipoprotein lipase in plasma causes dissociation of apoA-IV and its redistribution in either in HDL or the d>1.21 g/ml fraction (4). ApoA-IV mRNA and protein synthesis in mammals is controlled by hormonal (7) and nutritional factors (8). Plasma apoA-IV levels increase following a fat meal (4, 9) and under conditions of hypertriglyceridemia (10). In rats under fasting conditions, 50% of plasma apoA-IV is produced by the intestine (11). In humans, apoA-IV has two common alleles, designated apoA-IV-1 and apoA-IV-2, that result from a Q360H substitution, and a few rare alleles that follow Mendelian inheritance and may affect plasma lipid levels (12).

The in vitro and in vivo properties of apoA-IV have been investigated extensively, and various potential physiological functions have been suggested. These include a role in lipid absorption, secretion, metabolism (4), and food uptake (13–15), and protective functions against inflammatory diseases (16, 17) and atherosclerosis (17–19). ApoA-IV

This work was supported by Grant HL-48739 from the National Institutes of Health. Its contents are solely the responsibility of the authors and do not necessarily represent the official views of the National Institutes of Health or other granting agencies. P. Fotakis has been supported by pre-doctoral training Fellowship HERAKLEITOS II of the Greek Ministry of National Education. D. Georgiadou was supported by the graduate fellowship program of the National Center for Scientific Research "Demokritos".

Manuscript received 3 July 2012 and in revised form 5 November 2012.

Published, JLR Papers in Press, November 6, 2012
DOI 10.1194/jlr.M030114

Abbreviations: DMPC, dimyristoyl-L-α-phosphatidyl-choline; EM, electron microscopy; FPLC, fast-protein liquid chromatography; SR-BI, scavenger receptor BI; WT, wild type.

[1] To whom correspondence should be addressed.
e-mail: vzannis@bu.edu

[S] The online version of this article (available at http://www.jlr.org) contains supplementary data in the form of two figures, two tables, and supplemanary Methods.

has structural (2, 3) and several functional similarities with apoA-I and apoE. Thus lipid-free apoA-IV promotes cholesterol efflux from cells (20–22), and rHDL-A-IV particles activate LCAT (23). ApoA-IV was also shown to bind saturably to cell surface sites (21, 24), as well as to hepatic cell membranes (25), to potentiate the apoCII-mediated activation of lipoprotein lipase (26) and the activity of cholesteryl ester transfer protein (27). Furthermore, apoA-IV was reported to have anti-oxidant (28) and anti-inflammatory (16, 29) properties, and similarly to apoA-I (30), and apoE (31), may also play some role in the development of Alzheimer's disease (32). A difference between apoA-IV and apoA-I or apoE exists on the contribution of the C-terminal domain of these proteins to the solubilization of dimyristoyl-L-α-phosphatidyl-choline (DMPC) phospholipids (33, 34). In the case of apoA-I and apoE, deletion of the C-terminal domain drastically reduced the ability of the truncated forms to solubilize DMPC phospholipids and to associate with preformed HDL (35, 36). In the case of apoA-IV, deletion of the 44 C-terminal residues increased its ability to solubilize DMPC phospholipids (34). Subsequent studies showed that deletion of the C-terminal residues 333–343 strongly increased the rate of association of truncated apoA-IV with DMPC phospholipids, and this enhancement required residues 11–20 of the truncated apoA-IV (37). The reduced capacity of the full-length apoA-IV to associate with phospholipids was attributed to intramolecular interactions of C- and N-terminal regions that contain residues F334 and F335, and W12 and F15, respectively (33). In cell culture studies, lipid secretion and the size of secreted lipoprotein particles increased dramatically with the deletion of the 344–354 region that contains three EQQQ motifs and one EQVQ motif in human apoA-IV (38). Increased lipid secretion was also observed in newborn swine, where apoA-IV lacks the EQQQ sequences, suggesting that these sequences modulate chylomicron packaging and secretion (38).

Studies with transgenic mice showed that overexpression of apoA-IV in the intestine did not affect the intestinal absorption of cholesterol and triglycerides and fat-soluble vitamins or the clearance of chylomicrons. It also did not cause weight gain and did not alter feeding behavior in transgenic mice as compared with control mice (15). Similar conclusions regarding lipid absorption and weight gain were reached by the study of apoA-IV-deficient mice (14). Previous studies had implicated apoA-IV as a satiety factor (13). The transgenic mice expressing the mouse apoA-IV gene mostly in the intestine had reduced levels of atherosclerotic lesions in response to atherogenic diets (19). The lipid profiles of these mice were similar, but not identical to those of the control wild-type (WT) mice (15). Plasma isolated from the mouse apoA-IV-transgenic mice had increased endogenous cholesterol esterification rates, and their HDL, isolated following fat feeding, promoted more efficiently cholesterol efflux from cholesterol-loaded human monocytes, as compared with HDL obtained from WT mice (19). Reduced atherosclerotic lesions were also observed in transgenic mice expressing human apoA-IV mainly in the intestine in an apoE-deficient background. Injection of lipopolysaccharide into these human apoA-IV-transgenic mice in an apoE-deficient background resulted in fewer atherosclerotic lesions than in apoE-deficient mice. The protective effect of apoA-IV in this case was attributed to its antioxidant properties (17) and the stronger Th1 response of the lymphocytes in the presence of apoA-IV. Lymphocytes isolated from human apoA-IV × apoE$^{-/-}$ transgenic mice produced lower levels of proinflammatory cytokines as compared with apoE$^{-/-}$ mice (29). The anti-inflammatory properties of apoA-IV were also manifested by intraperitoneal injection of the recombinant protein in WT and apoA-IV-deficient mice. This treatment delayed the onset and reduced the severity of the inflammation associated with experimentally induced colitis in rats (16). Reduced atherosclerosis was also observed in transgenic mice overexpressing the apoA-IV gene in the liver of either normal or apoE-deficient mice under the control of the hepatic control region of the apoE/apoC-I gene cluster (18).

The origin and the metabolic fate and the physiological significance of apoA-IV that resides on the HDL particle are not fully understood. Here we show that apoA-IV participates in the biogenesis of apoA-IV-containing HDL (HDL-A-IV) particles using the same pathway that is utilized by apoA-I and apoE. The HDL-A-IV particles formed may explain, at least partially, the previously reported anti-inflammatory and atheroprotective functions of apoA-IV.

EXPERIMENTAL PROCEDURES

Materials

Materials not mentioned in the experimental procedures have been obtained from sources described previously (39).

Methods

Generation of an adenovirus expressing the human apoA-IV. The apoA-IV cDNA was generated by RT-PCR of human mRNA using 5′ and 3′ primers contained restriction sites for Bgl-II and EcoRV, respectively. The apoA-IV cDNA was digested with Bgl-II and EcoRV and cloned into the corresponding sites of the pAdTrack-CMV vector. The recombinant adenoviruses were constructed and purified using the Ad-Easy-1 system where the adenovirus construct is generated in bacteria BJ-5183 (Agilent Technologies; Santa Clara, CA) as described (39). Correct clones were propagated in RecA DH5α cells (Invitrogen; Carlsbad, CA). The recombinant adenoviral vectors were linearized with PacI and used to transfect 911 cells. Following large-scale infection of HEK293 cell cultures with virus-containing cell lysates, the recombinant adenoviruses were purified by two consecutive Caesium chloride ultracentrifugation steps, dialyzed, and titrated (39).

Cholesterol efflux measurements. ATP-binding cassette transporter (ABC) A1-mediated cholesterol efflux measurements by lipid-free apoA-IV using HEK293-EBNA cells was performed as described (39). Net efflux was calculated by subtracting the efflux obtained in the untransfected cells from that of the ABCA1-transfected cells (40). Scavenger receptor BI (SR-BI)-mediated cholesterol efflux by reconstituted HDL-A-IV (rHDL-A-IV) using CHO ldlA[mSR-BI] cells was performed as described (39, 41, 42). Net efflux was calculated by subtracting the efflux

obtained in the parent IdlA CHO cells from that of ldlA[mSR-BI] CHO cells.

Animal studies, plasma lipids, fractionation of plasma, two-dimensional gel electrophoresis, electron microscopy, and apoA-IV mRNA analyses. ApoA-I$^{-/-}$ (ApoA1^{tm1Unc}) C57BL/6J mice (43) were purchased from Jackson Laboratories (Bar Harbor, ME). Mice deficient for apoA-I and apoE were a gift of Dr. Fayanne Thorngate and Dr. David Williams (44). Mice deficient in ABCA1 (45) (purchased from Jackson Laboratories) were provided by Dr. Mike Filtzerald. Mice deficient for LCAT were a gift of Dr. Santa-Marina Fojo (46). The mice were maintained on a 12 h light/dark cycle and standard rodent chow. All procedures performed on the mice were in accordance with National Institutes of Health guidelines and following an approved IACUC protocol. Mice, 6–8 weeks of age, were injected via the tail vein with 0.5 to 1.5×10^9 pfu of recombinant adenovirus per animal. Four days postinjection, following a 4 h fast, blood was drawn and the livers were collected for further analyses.

The fractionation of plasma by fast-protein liquid chromatography (FPLC) and density gradient ultracentrifugation, the two-dimensional gel electrophoresis of plasma, the cholesterol and triglyceride measurements, the electron microscopy (EM) of the HDL fractions, and the apoA-IV mRNA quantification were performed as described (47). For details, please see the Supplementary Methods.

Statistics

Statistical analyses were performed by two-tailed Student's-*t* test with equal variance.

RESULTS

In vitro properties of apoA-IV

We have generated a recombinant adenovirus expressing apoA-IV and used it to study its in vivo and in vitro properties.

ApoA-IV secreted in the culture medium of adenovirus-infected HTB-13 grown on a large scale was purified and used to study its cholesterol efflux potential and its physicochemical properties. As shown in **Fig. 1A**, the ABCA1-mediated cholesterol efflux to lipid-free apoA-IV, which represents the first step in the biogenesis of HDL, was comparable to that of lipid-free apoA-I and apoE. Similarly the SR-BI-mediated cholesterol efflux of rHDL-A-IV was comparable to those of rHDL, containing apoA-I or apoE (Fig. 1B).

Recombinant ApoA-IV had structural and thermodynamic properties that were reminiscent of apoA-I and apoE. Circular dichroism measurements revealed a significant helical content of 41.4%, albeit reduced compared with apoA-I and apoE (48, 49). Upon mixing with egg yolk phosphatidyl-choline, recombinant apoA-IV readily formed HDL-like particles with increased helical content of 46.7% (supplementary Fig. I A,B and Table I). Thermal denaturation of apoA-IV revealed a single limited-cooperativity transition with a T_m of 45.6°C (supplementary Fig. II A). The thermal denaturation of apoA-IV was largely reversible, inasmuch as the protein recovered more than 95% of its secondary structure after cooling (supplementary Fig. II A,B). rHDL-A-IV particles were significantly more stable versus thermal denaturation (T_m = 61.4°C) and exhibited

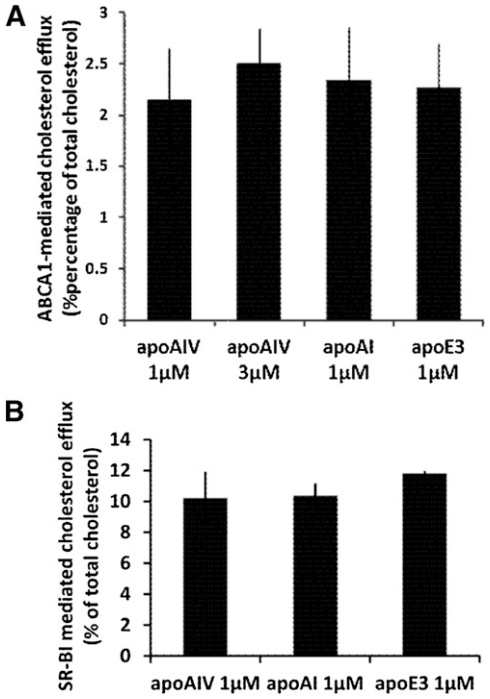

Fig. 1. A: ABCA1-mediated cholesterol efflux from HEK293 EBNA-T cells transfected with an ABCA1-expressing plasmid using human apoA-I, apoE, and apoA-IV as cholesterol acceptors. Cholesterol efflux was determined as described in Experimental Procedures. The concentration of the acceptor apoA-IV in the medium was 1 μM or 3 μM and the concentration of apoA-I and apoE was 1 μM as indicated. The net efflux was calculated by subtracting the efflux obtained in the untransfected HEK293 EBNA-T cells from that of ABCA1-transfected cells. The difference in the net efflux promoted by apoA-IV, apoA-I, or apoE3 was not statistically significant. B: SR-BI-mediated cholesterol efflux from IdlA[mSR-BI] CHO cell line expressing the murine SR-BI (42), using rHDL-containing human apoA-I, apoE3, and apoA-IV as cholesterol acceptors. The concentration of each acceptor apolipoprotein bound to rHDL in the medium was 1 μM. The net efflux was calculated by subtracting the efflux obtained in the untransfected IdlA CHO cells from that of IdlA [mSR-BI] CHO cells. Values are the means ± SE from three experiments performed in duplicate. The difference in the net efflux promoted by rHDL-A-IV, rHDL-A-I, and rHDL-E3 was not statistically significant.

a limited-cooperativity nonreversible transition (supplementary Table I and Fig. II A,B). Chemical denaturation of apoA-IV revealed single-step transition with limited cooperativity that lacked the intermediate described for the thermal denaturation of apoE (49). Chemical denaturation of rHDL-A-IV showed a highly noncooperative transition (supplementary Fig. II C,D). Overall, biophysical analysis of recombinant apoA-IV suggests extensive conformational changes upon lipid binding similar to those described for other apolipoproteins. Furthermore, this analysis suggests that although apoA-IV has structural and thermodynamic properties similar to those of apoA-I and apoE, it still retains a unique structural and thermodynamic profile that may be consistent with distinct functional roles.

Effect of apoA-IV on lipid and lipoprotein profiles and the generation of HDL-A-IV

The changes in the lipid and lipoprotein profiles as a result of hepatic expression of apoA-IV were studied in

different mouse models by adenovirus-mediated gene transfer 4 days postinfection. Gene transfer of apoA-IV in apoA-I$^{-/-}$ mice did not significantly alter total plasma lipid levels or the cholesterol and triglyceride FPLC profiles (**Fig. 2A, B**; **Fig. 3A, B**,, and supplementary Table II). The distribution of apoA-IV to different lipoprotein fractions was determined by density gradient ultracentrifugation of plasma followed by SDS-PAGE of the resulting fractions. This analysis showed that apoA-IV was distributed predominantly to HDL3 and, to a lesser extent, to the HDL2 fraction (**Fig. 4A**). EM of the HDL fractions showed that hepatic expression of apoA-IV promoted the formation of spherical particles (Fig. 4E). Two-dimensional gel electrophoresis of plasma showed that apoA-IV generated predominantly α-HDL particles with smaller amount of pre-β-like particles (Fig. 4I).

A different picture was obtained by adenovirus mediated gene transfer of apoA-IV in apoA-I$^{-/-}$ × apoE$^{-/-}$ double-deficient mice. Hepatic apoA-IV expression in these mice increased plasma cholesterol to levels greater than those of the uninfected controls and induced hypertriglyceridemia (Fig. 2A, B). FPLC analysis showed that all the cholesterol and triglycerides were found in the VLDL/IDL region (Fig. 3A, B). SDS-PAGE analyses of the lipoprotein fractions separated by density gradient ultracentrifugation of plasma, showed that the observed dyslipidemia was associated with distribution of the majority (80%) of apoA-IV in the VLDL/IDL/LDL region and to a lesser extend to the HDL2/HDL3 region (Fig. 4B). The apoA-IV fractions that float in the VLDL/IDL/LDL region also contain large amounts of apoB-48 (data not shown). EM showed formation of spherical HDL (Fig. 4F) and two-dimensional gel electrophoresis of plasma showed predominantly the formation of α-HDL and a small amount of pre-β-like HDL particles (Fig. 4J). The findings shown in Fig. 4A, B, E, F, I, and J suggest strongly that apoA-IV participates in the generation of HDL-A-IV particles. The findings shown in Fig. 3A, B and Fig. 4A, B show for the first time that in the absence of both apoE and apoA-I, apoA-IV has increased affinity for triglyceride-rich lipoproteins and that this increased affinity is associated with the induction of hypertriglyceridemia.

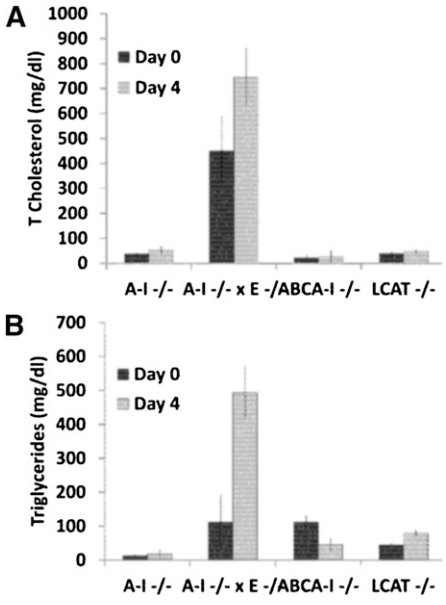

Fig. 2. Changes in the plasma cholesterol (A) and triglyceride (B) levels caused by expression of human apoA-IV in different mouse models (apoA-I$^{-/-}$, apoA-I$^{-/-}$ × apoE$^{-/-}$, ABCA1$^{-/-}$, and LCAT$^{-/-}$ mice).

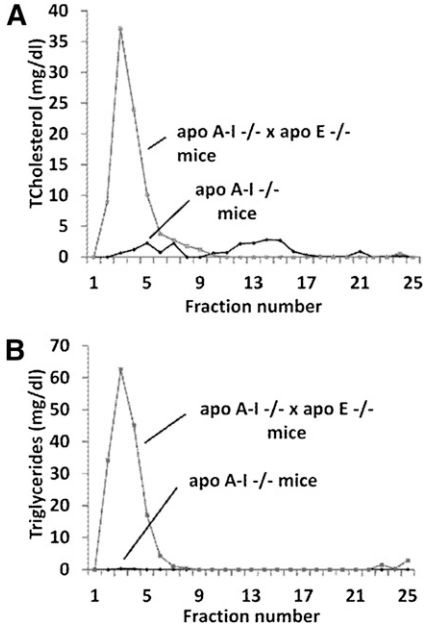

Fig. 3. FPLC profiles of total cholesterol (A) and triglycerides (B) of apoA-I$^{-/-}$ and apoA-I$^{-/-}$ × apoE$^{-/-}$ mice 4 days post-infection with adenoviruses expressing the human apoA-IV as indicated.

ABCA1 and LCAT are required for the biogenesis of HDL-A-IV

The next task was to determine the role of ABCA1 and LCAT in the biogenesis of HDL-A-IV. Adenovirus-mediated gene transfer of apoA-IV in ABCA1$^{-/-}$ mice failed to form HDL particles. The density gradient ultracentrifugation did not show the presence of apoA-IV in the HDL region (Fig. 4C), and the EM analysis of the HDL fractions, combined with the two-dimensional gel electrophoresis of plasma, failed to demonstrate formation of HDL particles (Fig. 4G, K).

A similar picture emerged from adenovirus-mediated gene transfer of apoA-IV in LCAT$^{-/-}$ mice. Following gene transfer, apoA-IV was not present in the HDL fractions (Fig. 4D). HDL particles were not detected by EM (Fig. 4H), and the two-dimensional gel electrophoresis of the plasma showed the formation of two types of particles with pre-β-like mobility (Fig. 4L). The relationship of these particles with α-HDL particles formed in apoA-I$^{-/-}$ mice expressing apoA-IV was established by mixing experiments (Fig. 4M).

The role of LCAT in the biogenesis of apoA-IV-containing HDL was also explored by coexpression of apoA-IV and LCAT in apoA-I$^{-/-}$ mice. This treatment increased the plasma HDL cholesterol levels as determined by FPLC

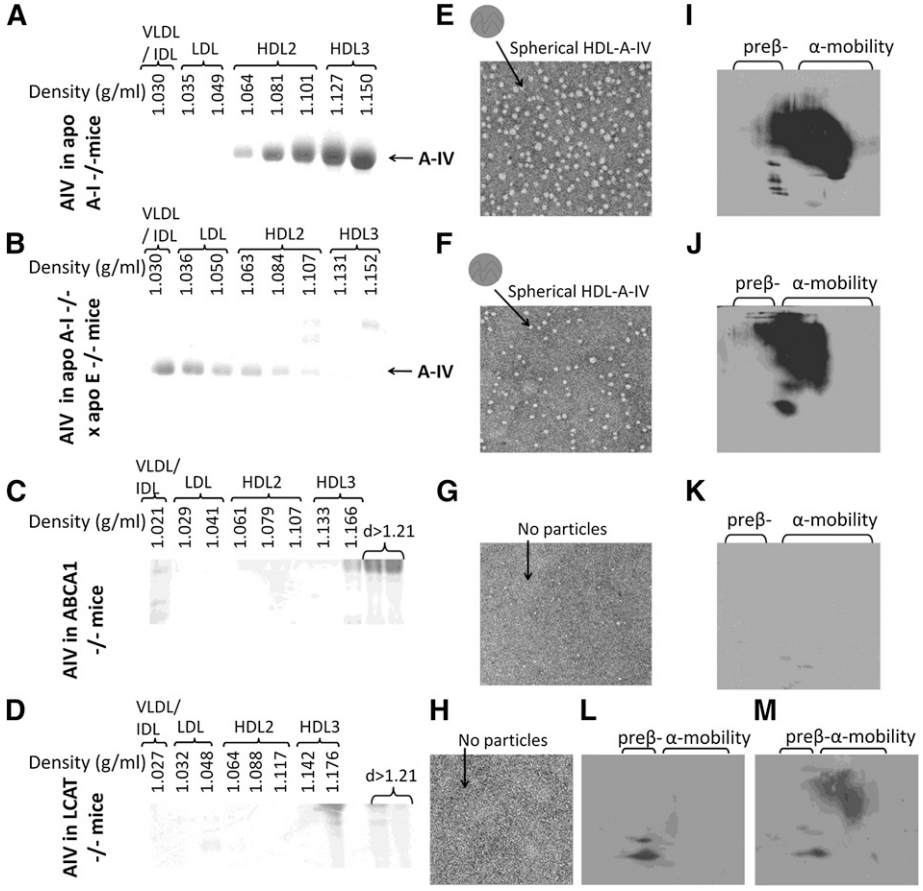

Fig. 4. Analyses of plasma of apoA-I$^{-/-}$, apoA-I$^{-/-}$ × apoE$^{-/-}$, ABCA1$^{-/-}$, and LCAT$^{-/-}$ mice infected with the adenovirus expressing the human apoA-IV by density gradient ultracentrifugation and SDS-PAGE, EM, and two-dimensional gel electrophoresis. A–D: SDS-PAGE analysis of density gradient ultracentrifugation fractions. E–H: EM pictures of HDL fractions 6–7 obtained from mice expressing human apoA-IV following density gradient ultracentrifugation of plasma, as indicated. The photomicrographs were taken at 75,000× magnification and enlarged three times. I–M: Analysis of plasma obtained from mice expressing the human apoA-IV following two-dimensional gel electrophoresis and Western blotting. A, E, I: Analyses of apoA-I$^{-/-}$ mice. B, F, J: Analyses of apoA-I$^{-/-}$ × apoE$^{-/-}$ mice. C, G, K: Analyses of ABCA1$^{-/-}$ mice. D, H, L, M: Analyses of LCAT$^{-/-}$ mice.

(**Fig. 5A**). It also promoted the flotation of apoA-IV in the HDL2 and HDL3 region (Fig. 5B) and generated spherical HDL-A-IV particles (Fig. 5C). The LCAT treatment also increased the concentration of the mouse apoE in the HDL2 fraction (Fig. 5B).

The overall pathway of the biogenesis and the potential functions of HDL-A-IV are depicted in Fig. 5D.

DISCUSSION

Role of apoA-IV, ABCA1, and LCAT in the biogenesis of HDL-A-IV

Although the functions of the intestinally delivered apoA-IV have been extensively studied during the past 35 years, there is limited information on the physiological significance and the functions of apoA-IV synthesized by the liver. Earlier studies showed that when ApoA-IV is purified from plasma by immunoprecipitation, immunoaffinity, gel filtration, or nondenaturing gradient gel electrophoresis, it is found on the HDL density fraction (50–52), but it dissociates from lipoproteins following ultracentrifugation of plasma (53). This raises the question whether apoA-IV-containing HDL particles originate from the transfer of apoA-IV that is displaced from chylomicrons to the surface of a preformed HDL molecule that contains apoA-I and in some instances other apolipoproteins. An alternative possibility is that HDL-A-IV particles are synthesized de novo by the liver.

Clues pertinent to this question were obtained from studies of transgenic mice expressing the apoA-IV gene under the control of its natural promoter or a heterologous hepatic promoter (15, 17, 19). Transgenic mice carrying the apoA-IV gene under the control of the common apoA-I/apoCIII/apoA-IV promoter and enhancer (54) express apoA-IV predominantly in the intestine and to a lesser extend in the liver (15). When the plasma of these transgenic mice was fractionated by gel filtration, the majority of apoA-IV was distributed in the same HDL fractions where apoA-I was also found (15). Such localization of apoA-IV reinforces the concept that lipid-free apoA-IV originating from chylomicrons or secreted by the liver

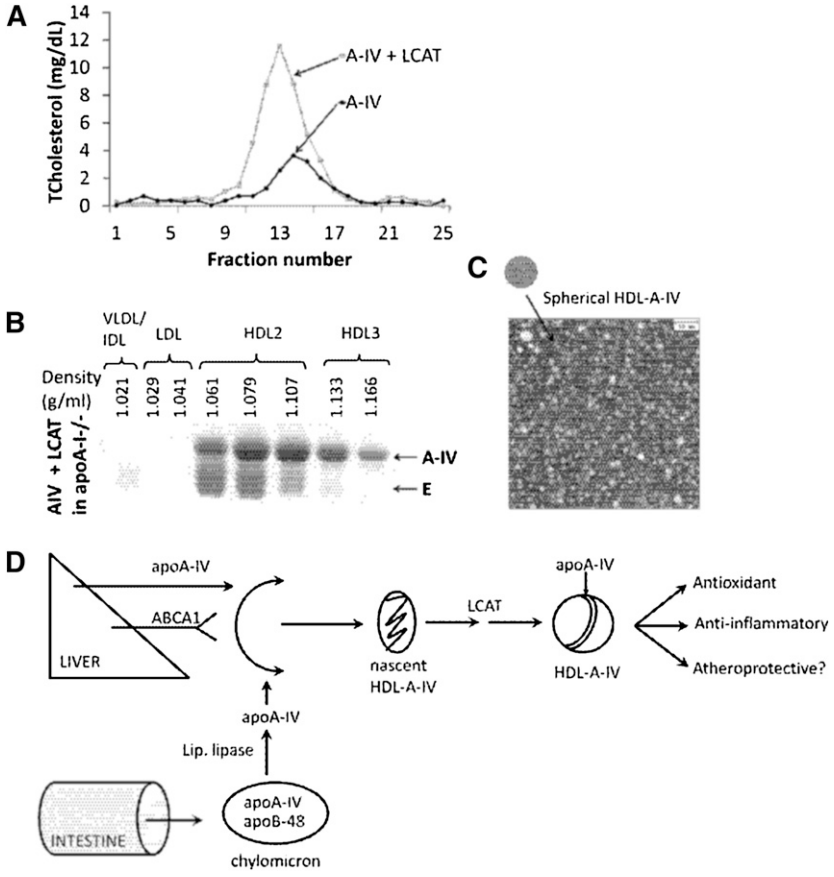

Fig. 5. Analysis of plasma from apoA-I$^{-/-}$ mice coinfected with 10^9 pfu adenovirus expressing human apoA-IV and 5×10^8 pfu adenovirus expressing human LCAT. A: FPLC profiles. B: SDS-PAGE of the fractions isolated by density gradient gel electrophoresis. C: EM analysis of the HDL2 fractions shown in B. D: Schematic representation of the pathway of biogenesis and the putative beneficial functions of HDL-A-IV.

may contribute in the de novo synthesis of HDL-A-IV particles.

We have shown previously that de novo synthesis of HDL particles containing apoA-I or apoE is initiated by interactions of the lipid-poor apolipoproteins with the ABCA1 lipid transporter. These functional interactions catalyze the transfer of phospholipids and subsequently cholesterol from intracellular membrane pools to lipid-free apoA-I or apoE leading to the formation of minimally lipidated particles which are gradually converted to discoidal particles (39, 47, 55, 56). Subsequent esterification of the cholesterol of the nascent pre-β and discoidal particles by LCAT generates the spherical HDL particles present in the plasma that can be visualized by EM (55, 56). In the present study the ability of apoA-IV to promote de novo formation of HDL-A-IV particles was established by adenovirus mediated gene transfer in four different mouse models. To ensure that pro-inflammatory conditions resulting from adenovirus over expression were not reached, we monitored the plasma transamimase levels during the experiments. Gene transfer of apoA-IV in apoA-I$^{-/-}$ mice showed that apoA-IV expressed in the liver was distributed in the HDL fraction of plasma. EM showed the presence of spherical particles and two-dimensional gel electrophoresis showed α-migrating HDL particles and pre-β-like HDL particles. To exclude the possibility that the spherical HDL particles observed in these experiments did not originate from apoE, we performed gene transfer experiments in apoA-I and apoE double-deficient mice. These studies also showed the formation of spherical HDL particles and pre-β-like and α-migrating HDL particles. These findings are consistent with in vivo interactions of lipid-free apoA-IV with ABCA1. As shown in Fig. 1A and documented in previous studies (20), lipid free apoA-IV promotes ABCA1 mediated cholesterol efflux to the same extend as lipid free apoA-I and apoE. The functional interactions of lipid-free apoA-IV with ABCA1 in vivo are expected to lipidate apoA-IV and lead to the generation of nascent HDL-A-IV particles. These particles may subsequently mature to spherical HDL-A-IV that can interact functionally with SR-BI. As shown in Fig. 1B, rHDL-A-IV promotes SR-BI mediated cholesterol efflux to similar extend as rHDL-A-I or rHDL-E (41, 57).

The requirement of ABCA1 and LCAT for the formation of HDL-A-IV was established by adenovirus-mediated gene transfer of apoA-IV in ABCA1- and LCAT-deficient mice, respectively. In these experiments, as expected, deficiency in ABCA1 prevented the formation of nascent or mature HDL-A-IV particles. The absence of LCAT also appears to prevent the formation of nascent or mature HDL-A-IV particles. It is possible that in the absence of LCAT, nascent HDL-A-IV particles formed by initial interactions

of lipid-free apoA-IV with ABCA1 are susceptible to fast catabolism. This interpretation is supported by coexpression of apoA-IV and LCAT in LCAT$^{-/-}$ mice. This treatment increased the HDL cholesterol peak and the plasma apoA-IV levels, promoted the formation of spherical HDL-A-IV particles and resulted in the distribution of apoA-IV in the HDL2 and HDL3 regions. Fast catabolism of pre-β-apoA-I-containing HDL particles by the kidney has been described previously (58).

Effect of apoA-IV on lipid and lipoprotein profiles in different mouse models

The experiments described above also showed that following gene transfer in apoA-I$^{-/-}$ mice, apoA-IV was distributed in the HDL2 and HDL3 regions and the mice had normal triglycerides. In contrast following gene transfer of apoA-IV in the apoA-I$^{-/-}$ × apoE$^{-/-}$ mice, 80% of apoA-IV was distributed in the VLDL/IDL region where apoB is also found and the mice developed hypertriglyceridemia. This implies that deficiency for both apoA-I and apoE increased the affinity of apoA-IV for apoB-containing lipoprotein particles and this might have triggered the hypertriglyceridemia.

Is there a role for HDL-A-IV in atheroprotection?

Numerous previous studies have indicated that the conventional apoA-I-containing HDL particles promote cholesterol efflux (42, 59), prevent oxidation of LDL (60), and inhibit expression of proinflammatory cytokines by macrophages (61), as well as expression of adhesion molecules by endothelial cells (62). HDL inhibits cell apoptosis (63) and promotes endothelial cell proliferation and migration (64). HDL stimulates release of NO from endothelial cells, thus promoting vasodilation (65). Other studies have also indicated that several beneficial effects of HDL on the arterial wall cells are mediated through signaling mechanisms mediated by SR-BI or other cell surface proteins (65–67). Owing to these properties, the conventional apoA-I-containing HDL particles are thought to protect the endothelium and inhibit several steps in the cascade of events that lead to the pathogenesis of atherosclerosis and various other human diseases.

The ability of apoA-IV to form discrete populations of HDL-A-IV particles reported in this study provides the basis for exploring further the previously reported atheroprotective functions of apoA-IV. Such functions were demonstrated in mouse models expressing apoA-IV in the intestine or the liver (15, 17, 19) as well as of apoA-IV knock-out mice (14).

Overall, the present study establishes that apoA-IV has the capacity to promote the de novo biogenesis of discrete HDL-A-IV particles. The formation of these particles requires the functions of ABCA1 and LCAT. Further work is required to establish whether the generation of HDL-A-IV by the liver is responsible, at least partially, for the previously reported anti-inflammatory and atheroprotective functions of apoA-IV (16–19, 29).

A. Kateifides and P. Fotakis are students in the graduate program "The Molecular Basis of Human Disease" of the University of Crete Medical School. The authors thank Gayle Forbes for technical assistance.

REFERENCES

1. Swaney, J. B., H. Reese, and H. A. Eder. 1974. Polypeptide composition of rat high density lipoprotein: characterization by SDS-gel electrophoresis. *Biochem. Biophys. Res. Commun.* **59:** 513–519.
2. Li, W. H., M. Tanimura, C. C. Luo, S. Datta, and L. Chan. 1988. The apolipoprotein multigene family: biosynthesis, structure, structure-function relationships, and evolution. *J. Lipid Res.* **29:** 245–271.
3. Karathanasis, S. K., I. Yunis, and V. I. Zannis. 1986. Structure, evolution, and tissue-specific synthesis of human apolipoprotein AIV. *Biochemistry.* **25:** 3962–3970.
4. Green, P. H. R., R. M. Glickman, J. W. Riley, and E. Quinet. 1980. Human apolipoprotein-A-IV. Intestinal origin and distribution in plasma. *J. Clin. Invest.* **65:** 911–919.
5. Utermann, G., and U. Beisiegel. 1979. Apolipoprotein-A-IV: protein occurring in human mesenteric lymph chylomicrons and free in plasma. Isolation and quantification. *Eur. J. Biochem.* **99:** 333–343.
6. Lenich, C., P. Brecher, S. Makrides, A. Chobanian, and V. I. Zannis. 1988. Apolipoprotein gene expression in the rabbit: abundance, size, and distribution of apolipoprotein mRNA species in different tissues. *J. Lipid Res.* **29:** 755–764.
7. Apostolopoulos, J. J., M. J. La Scala, and G. J. Howlett. 1988. The effect of triiodothyronine on rat apolipoprotein A-I and A-IV gene transcription. *Biochem. Biophys. Res. Commun.* **154:** 997–1002.
8. Weinberg, R. B., C. Dantzker, and C. S. Patton. 1990. Sensitivity of serum apolipoprotein A-IV levels to changes in dietary-fat content. *Gastroenterology.* **98:** 17–24.
9. Go, M. F., G. Schonfeld, B. Pfleger, T. G. Cole, N. L. Sussman, and D. H. Alpers. 1988. Regulation of intestinal and hepatic apoprotein synthesis after chronic fat and cholesterol feeding. *J. Clin. Invest.* **81:** 1615–1620.
10. Verges, B., D. Rader, J. Schaefer, L. Zech, M. Kindt, T. Fairwell, P. Gambert, and H. B. Brewer, Jr. 1994. In vivo metabolism of apolipoprotein A-IV in severe hypertriglyceridemia: a combined radiotracer and stable isotope kinetic study. *J. Lipid Res.* **35:** 2280–2291.
11. Windmueller, H. G., and A. L. Wu. 1981. Biosynthesis of plasma apolipoproteins by rat small intestine without dietary or biliary fat. *J. Biol. Chem.* **256:** 3012–3016.
12. Lohse, P., and H. B. J. Brewer. 1991. Genetic polymorphism of apolipoprotein A-IV. *Curr. Opin. Lipidol.* **2:** 90–95.
13. Fujimoto, K., K. Fukagawa, T. Sakata, and P. Tso. 1993. Suppression of food intake by apolipoprotein A-IV is mediated through the central nervous system in rats. *J. Clin. Invest.* **91:** 1830–1833.
14. Weinstock, P. H., C. L. Bisgaier, T. Hayek, K. Aalto-Setala, E. Sehayek, L. Wu, P. Sheiffele, M. Merkel, A. D. Essenburg, and J. L. Breslow. 1997. Decreased HDL cholesterol levels but normal lipid absorption, growth, and feeding behavior in apolipoprotein A-IV knockout mice. *J. Lipid Res.* **38:** 1782–1794.
15. Aalto-Setala, K., C. L. Bisgaier, A. Ho, K. A. Kieft, M. G. Traber, H. J. Kayden, R. Ramakrishnan, A. Walsh, A. D. Essenburg, and J. L. Breslow. 1994. Intestinal expression of human apolipoprotein A-IV in transgenic mice fails to influence dietary lipid absorption or feeding behavior. *J. Clin. Invest.* **93:** 1776–1786.
16. Vowinkel, T., M. Mori, C. F. Krieglstein, J. Russell, F. Saijo, S. Bharwani, R. H. Turnage, W. S. Davidson, P. Tso, D. N. Granger, et al. 2004. Apolipoprotein A-IV inhibits experimental colitis. *J. Clin. Invest.* **114:** 260–269.
17. Ostos, M. A., M. Conconi, L. Vergnes, N. Baroukh, J. Ribalta, J. Girona, J. M. Caillaud, A. Ochoa, and M. M. Zakin. 2001. Antioxidative and antiatherosclerotic effects of human apolipoprotein A-IV in apolipoprotein E-deficient mice. *Arterioscler. Thromb. Vasc. Biol.* **21:** 1023–1028.
18. Duverger, N., G. Tremp, J. M. Caillaud, F. Emmanuel, G. Castro, J. C. Fruchart, A. Steinmetz, and P. Denefle. 1996. Protection against atherogenesis in mice mediated by human apolipoprotein A-IV. *Science.* **273:** 966–968.
19. Cohen, R. D., L. W. Castellani, J. H. Qiao, B. J. Van Lenten, A. J. Lusis, and K. Reue. 1997. Reduced aortic lesions and elevated high density lipoprotein levels in transgenic mice overexpressing mouse apolipoprotein A-IV. *J. Clin. Invest.* **99:** 1906–1916.
20. Remaley, A. T., J. A. Stonik, S. J. Demosky, E. B. Neufeld, A. V. Bocharov, T. G. Vishnyakova, T. L. Eggerman, A. P. Patterson, N. J.

Duverger, S. Santamarina-Fojo, et al. 2001. Apolipoprotein specificity for lipid efflux by the human ABCAI transporter. *Biochem. Biophys. Res. Commun.* **280:** 818–823.
21. Steinmetz, A., R. Barbaras, N. Ghalim, V. Clavey, J. C. Fruchart, and G. Ailhaud. 1990. Human apolipoprotein-A-IV binds to apolipoprotein-A-I/apolipoprotein-A-II receptor-sites and promotes cholesterol efflux from adipose-cells. *J. Biol. Chem.* **265:** 7859–7863.
22. Gomaraschi, M., W. E. Putt, S. Pozzi, S. Iametti, A. Barbiroli, F. Bonomi, E. Favari, F. Bernini, G. Franceschini, P. J. Talmud, et al. 2010. Structure and function of the apoA-IV T347S and Q360H common variants. *Biochem. Biophys. Res. Commun.* **393:** 126–130.
23. Steinmetz, A., and G. Utermann. 1985. Activation of lecithin: cholesterol acyltransferase by human apolipoprotein A-IV. *J. Biol. Chem.* **260:** 2258–2264.
24. Savion, N., and A. Gamliel. 1988. Binding of apolipoprotein A-I and apolipoprotein A-IV to cultured bovine aortic endothelial cells. *Arteriosclerosis.* **8:** 178–186.
25. Weinberg, R. B., and C. S. Patton. 1990. Binding of human apolipoprotein-A-IV to human hepatocellular plasma membranes. *Biochim. Biophys. Acta.* **1044:** 255–261.
26. Goldberg, I. J., C. A. Scheraldi, L. K. Yacoub, U. Saxena, and C. L. Bisgaier. 1990. Lipoprotein ApoC-II activation of lipoprotein-lipase. Modulation by apolipoprotein-A-IV. *J. Biol. Chem.* **265:** 4266–4272.
27. Main, L. A., T. Ohnishi, and S. Yokoyama. 1996. Activation of human plasma cholesteryl ester transfer protein by human apolipoprotein A-IV. *Biochim. Biophys. Acta.* **1300:** 17–24.
28. Qin, X. F., D. K. Swertfeger, S. Q. Zheng, D. Y. Hui, and P. Tso. 1998. Apolipoprotein AIV: a potent endogenous inhibitor of lipid oxidation. *Am. J. Physiol.* **274:** H1836–H1840.
29. Recalde, D., M. A. Ostos, E. Badell, A. L. Garcia-Otin, J. Pidoux, G. Castro, M. M. Zakin, and D. Scott-Algara. 2004. Human apolipoprotein A-IV reduces secretion of proinflammatory cytokines and atherosclerotic effects of a chronic infection mimicked by lipopolysaccharide. *Arterioscler. Thromb. Vasc. Biol.* **24:** 756–761.
30. Lewis, T. L., D. Cao, H. Lu, R. A. Mans, Y. R. Su, L. Jungbauer, M. F. Linton, S. Fazio, M. J. LaDu, and L. Li. 2010. Overexpression of human apolipoprotein A-I preserves cognitive function and attenuates neuroinflammation and cerebral amyloid angiopathy in a mouse model of Alzheimer disease. *J. Biol. Chem.***285:** 36958–36968.
31. Holtzman, D. M., K. R. Bales, T. Tenkova, A. M. Fagan, M. Parsadanian, L. J. Sartorius, B. Mackey, J. Olney, D. McKeel, D. Wozniak, et al. 2000. Apolipoprotein E isoform-dependent amyloid deposition and neuritic degeneration in a mouse model of Alzheimer's disease. *Proc. Natl. Acad. Sci. USA.* **97:** 2892–2897.
32. Cui, Y., M. Huang, Y. He, S. Zhang, and Y. Luo. 2011. Genetic ablation of apolipoprotein A-IV accelerates Alzheimer's disease pathogenesis in a mouse model. *Am. J. Pathol.* **178:** 1298–1308.
33. Tubb, M. R., R. A. Silva, K. J. Pearson, P. Tso, M. Liu, and W. S. Davidson. 2007. Modulation of apolipoprotein A-IV lipid binding by an interaction between the N and C termini. *J. Biol. Chem.* **282:** 28385–28394.
34. Pearson, K., H. Saito, S. C. Woods, S. Lund-Katz, P. Tso, M. C. Phillips, and W. S. Davidson. 2004. Structure of human apolipoprotein A-IV: a distinct domain architecture among exchangeable apolipoproteins with potential functional implications. *Biochemistry.* **43:** 10719–10729.
35. Laccotripe, M., S. C. Makrides, A. Jonas, and V. I. Zannis. 1997. The carboxyl-terminal hydrophobic residues of apolipoprotein A-I affect its rate of phospholipid binding and its association with high density lipoprotein. *J. Biol. Chem.* **272:** 17511–17522.
36. Li, X., K. Kypreos, E. E. Zanni, and V. Zannis. 2003. Domains of apoE required for binding to apoE receptor 2 and to phospholipids: implications for the functions of apoE in the brain. *Biochemistry.* **42:** 10406–10417.
37. Pearson, K., M. R. Tubb, M. Tanaka, X. Q. Zhang, P. Tso, R. B. Weinberg, and W. S. Davidson. 2005. Specific sequences in the N and C termini of apolipoprotein A-IV modulate its conformation and lipid association. *J. Biol. Chem.* **280:** 38576–38582.
38. Lu, S., Y. Yao, X. Y. Cheng, S. Mitchell, S. Y. Leng, S. M. Meng, J. W. Gallagher, G. S. Shelness, G. S. Morris, J. Mahan, et al. 2006. Overexpression of apolipoprotein A-IV enhances lipid secretion in IPEC-1 cells by increasing chylomicron size. *J. Biol. Chem.* **281:** 3473–3483.
39. Chroni, A., T. Liu, I. Gorshkova, H. Y. Kan, Y. Uehara, A. von Eckardstein, and V. I. Zannis. 2003. The central helices of apoA-I can promote ATP-binding cassette transporter A1 (ABCA1)-mediated lipid efflux. Amino acid residues 220–231 of the wild-type apoA-I are required for lipid efflux in vitro and high density lipoprotein formation in vivo. *J. Biol. Chem.* **278:** 6719–6730.
40. Fitzgerald, M. L., A. J. Mendez, K. J. Moore, L. P. Andersson, H. A. Panjeton, and M. W. Freeman. 2001. ATP-binding cassette transporter A1 contains an NH2-terminal signal anchor sequence that translocates the protein's first hydrophilic domain to the exoplasmic space. *J. Biol. Chem.* **276:** 15137–15145.
41. Chroni, A., T. J. Nieland, K. E. Kypreos, M. Krieger, and V. I. Zannis. 2005. SR-BI mediates cholesterol efflux via its interactions with lipid-bound ApoE. Structural mutations in SR-BI diminish cholesterol efflux. *Biochemistry.* **44:** 13132–13143.
42. Gu, X., K. Kozarsky, and M. Krieger. 2000. Scavenger receptor class B, type I-mediated [3H]cholesterol efflux to high and low density lipoproteins is dependent on lipoprotein binding to the receptor. *J. Biol. Chem.* **275:** 29993–30001.
43. Williamson, R., D. Lee, J. Hagaman, and N. Maeda. 1992. Marked reduction of high density lipoprotein cholesterol in mice genetically modified to lack apolipoprotein A-I. *Proc. Natl. Acad. Sci. USA.* **89:** 7134–7138.
44. Thorngate, F. E., P. G. Yancey, G. Kellner-Weibel, L. L. Rudel, G. H. Rothblat, and D. L. Williams. 2003. Testing the role of apoA-I, HDL, and cholesterol efflux in the atheroprotective action of low-level apoE expression. *J. Lipid Res.* **44:** 2331–2338.
45. McNeish, J., R. J. Aiello, D. Guyot, T. Turi, C. Gabel, C. Aldinger, K. L. Hoppe, M. L. Roach, L. J. Royer, J. de Wet, et al. 2000. High density lipoprotein deficiency and foam cell accumulation in mice with targeted disruption of ATP-binding cassette transporter-1. *Proc. Natl. Acad. Sci. USA.* **97:** 4245–4250.
46. Sakai, N., B. L. Vaisman, C. A. Koch, R. F. Hoyt, Jr., S. M. Meyn, G. D. Talley, J. A. Paiz, H. B. Brewer, Jr., and S. Santamarina-Fojo. 1997. Targeted disruption of the mouse lecithin:cholesterol acyltransferase (LCAT) gene. Generation of a new animal model for human LCAT deficiency. *J. Biol. Chem.* **272:** 7506–7510.
47. Vezeridis, A. M., A. Chroni, and V. I. Zannis. 2011. Domains of apoE4 required for the biogenesis of apoE-containing HDL. *Ann. Med.* **43:** 302–311.
48. Gorshkova, I. N., K. Liadaki, O. Gursky, D. Atkinson, and V. I. Zannis. 2000. Probing the lipid-free structure and stability of apolipoprotein A-I by mutation. *Biochemistry.* **39:** 15910–15919.
49. Chroni, A., S. Pyrpassopoulos, A. Thanassoulas, G. Nounesis, V. I. Zannis, and E. Stratikos. 2008. Biophysical analysis of progressive C-terminal truncations of human apolipoprotein E4: insights into secondary structure and unfolding properties. *Biochemistry.* **47:** 9071–9080.
50. Bisgaier, C. L., O. P. Sachdev, L. Megna, and R. M. Glickman. 1985. Distribution of apolipoprotein-A-IV in human plasma. *J. Lipid Res.* **26:** 11–25.
51. Lagrost, L., P. Gambert, M. Boquillon, and C. Lallemant. 1989. Evidence for high-density lipoproteins as the major apolipoprotein A-IV-containing fraction in normal human-serum. *J. Lipid Res.* **30:** 1525–1534.
52. Duverger, N., N. Ghalim, G. Ailhaud, A. Steinmetz, J. C. Fruchart, and G. Castro. 1993. Characterization of apoA-IV-containing lipoprotein particles isolated from human plasma and interstitial fluid. *Arterioscler. Thromb.* **13:** 126–132.
53. Weinberg, R. B., and M. S. Spector. 1985. Structural properties and lipid-binding of human apolipoprotein A-IV. *J. Biol. Chem.* **260:** 4914–4921.
54. Zannis, V. I., H. Y. Kan, A. Kritis, E. E. Zanni, and D. Kardassis. 2001. Transcriptional regulatory mechanisms of the human apolipoprotein genes in vitro and in vivo. *Curr. Opin. Lipidol.* **12:** 181–207.
55. Kypreos, K. E., and V. I. Zannis. 2007. Pathway of biogenesis of apolipoprotein E-containing HDL in vivo with the participation of ABCA1 and LCAT. *Biochem. J.* **403:** 359–367.
56. Zannis, V. I., A. Chroni, and M. Krieger. 2006. Role of apoA-I, ABCA1, LCAT, and SR-BI in the biogenesis of HDL. *J. Mol. Med.* **84:** 276–294.
57. Liadaki, K. N., T. Liu, S. Xu, B. Y. Ishida, P. N. Duchateaux, J. P. Krieger, J. Kane, M. Krieger, and V. I. Zannis. 2000. Binding of high density lipoprotein (HDL) and discoidal reconstituted HDL to the HDL receptor scavenger receptor class B type I. Effect of lipid association and APOA-I mutations on receptor binding. *J. Biol. Chem.* **275:** 21262–21271.
58. Miettinen, H. E., H. Gylling, T. A. Miettinen, J. Viikari, L. Paulin, and K. Kontula. 1997. Apolipoprotein A-IFin. Dominantly inherited hypoalphalipoproteinemia due to a single base substitution in the apolipoprotein A-I gene. *Arterioscler. Thromb. Vasc. Biol.* **17:** 83–90.

59. Nakamura, K., M. A. Kennedy, A. Baldan, D. D. Bojanic, K. Lyons, and P. A. Edwards. 2004. Expression and regulation of multiple murine ATP-binding cassette transporter G1 mRNAs/isoforms that stimulate cellular cholesterol efflux to high density lipoprotein. *J. Biol. Chem.* **279:** 45980–45989.
60. Navab, M., S. Y. Hama, G. M. Anantharamaiah, K. Hassan, G. P. Hough, A. D. Watson, S. T. Reddy, A. Sevanian, G. C. Fonarow, and A. M. Fogelman. 2000. Normal high density lipoprotein inhibits three steps in the formation of mildly oxidized low density lipoprotein: steps 2 and 3. *J. Lipid Res.* **41:** 1495–1508.
61. Okura, H., S. Yamashita, T. Ohama, A. Saga, A. Yamamoto-Kakuta, Y. Hamada, N. Sougawa, R. Ohyama, Y. Sawa, and A. Matsuyama. 2010. HDL/apolipoprotein A-I binds to macrophage-derived progranulin and suppresses its conversion into proinflammatory granulins. *J. Atheroscler. Thromb.* **17:** 568–577.
62. Cockerill, G. W., K. A. Rye, J. R. Gamble, M. A. Vadas, and P. J. Barter. 1995. High-density lipoproteins inhibit cytokine-induced expression of endothelial cell adhesion molecules. *Arterioscler. Thromb. Vasc. Biol.* **15:** 1987–1994.
63. Nofer, J. R., B. Levkau, I. Wolinska, R. Junker, M. Fobker, A. von Eckardstein, U. Seedorf, and G. Assmann. 2001. Suppression of endothelial cell apoptosis by high density lipoproteins (HDL) and HDL-associated lysosphingolipids. *J. Biol. Chem.* **276:** 34480–34485.
64. Seetharam, D., C. Mineo, A. K. Gormley, L. L. Gibson, W. Vongpatanasin, K. L. Chambliss, L. D. Hahner, M. L. Cummings, R. L. Kitchens, Y. L. Marcel, et al. 2006. High-density lipoprotein promotes endothelial cell migration and reendothelialization via scavenger receptor-B type I. *Circ. Res.* **98:** 63–72.
65. Mineo, C., I. S. Yuhanna, M. J. Quon, and P. W. Shaul. 2003. High density lipoprotein-induced endothelial nitric-oxide synthase activation is mediated by Akt and MAP kinases. *J. Biol. Chem.* **278:** 9142–9149.
66. Terasaka, N., M. Westerterp, J. Koetsveld, C. Fernandez-Hernando, L. Yvan-Charvet, N. Wang, W. C. Sessa, and A. R. Tall. 2010. ATP-binding cassette transporter G1 and high-density lipoprotein promote endothelial NO synthesis through a decrease in the interaction of caveolin-1 and endothelial NO synthase. *Arterioscler. Thromb. Vasc. Biol.* **30:** 2219–2225.
67. Okajima, F., K. Sato, and T. Kimura. 2009. Anti-atherogenic actions of high-density lipoprotein through sphingosine 1-phosphate receptors and scavenger receptor class B type I. *Endocr. J.* **56:** 317–334.